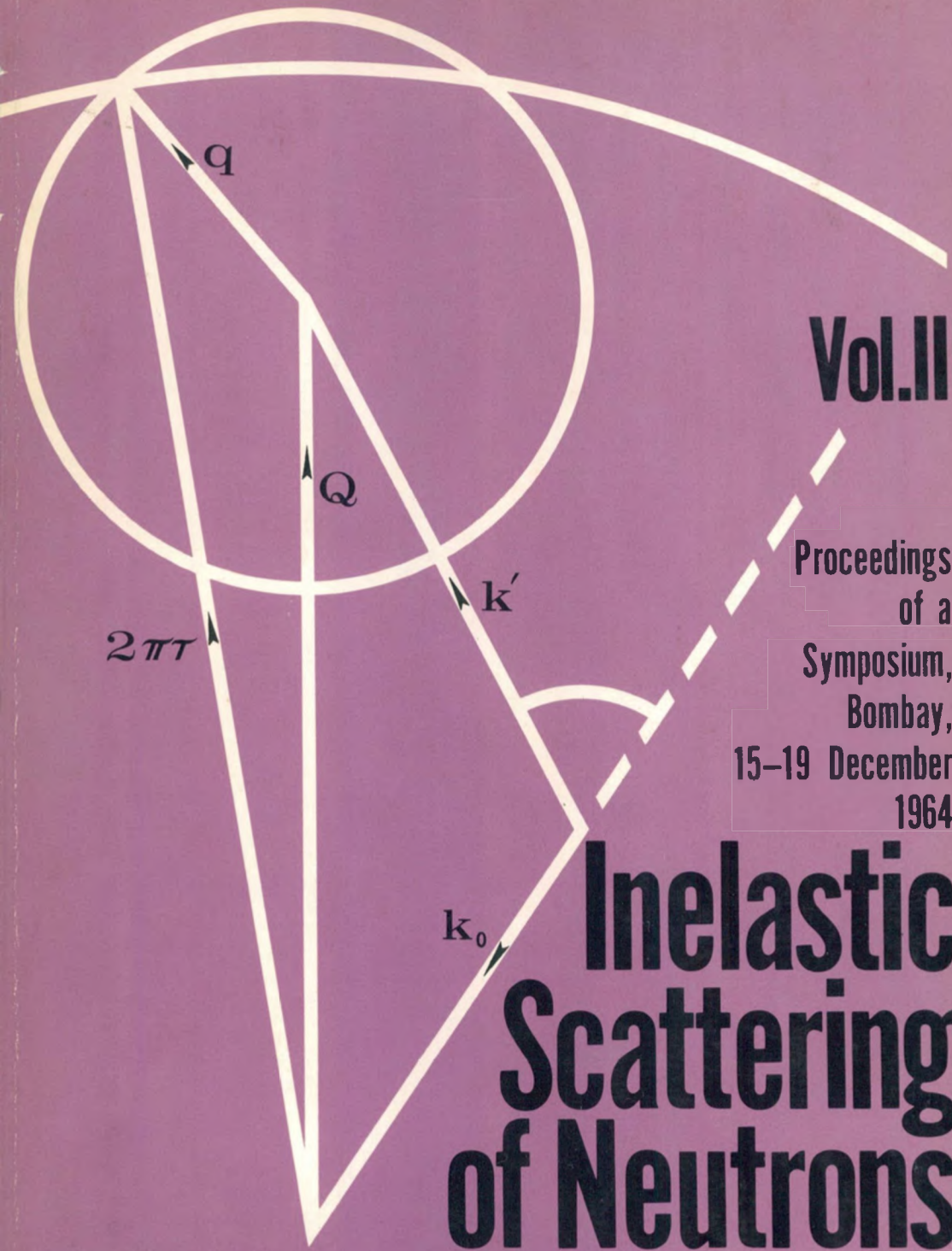

Vol. II

Proceedings of a Symposium, Bombay, 15–19 December 1964

Inelastic Scattering of Neutrons

INTERNATIONAL ATOMIC ENERGY AGENCY, VIENNA, 1965

INELASTIC SCATTERING OF NEUTRONS

VOL. II

The following States are Members of the International Atomic Energy Agency:

AFGHANISTAN
ALBANIA
ALGERIA
ARGENTINA
AUSTRALIA
AUSTRIA
BELGIUM
BOLIVIA
BRAZIL
BULGARIA
BURMA
BYELORUSSIAN SOVIET SOCIALIST REPUBLIC
CAMBODIA
CAMEROON
CANADA
CEYLON
CHILE
CHINA
COLOMBIA
CONGO, DEMOCRATIC REPUBLIC OF
COSTA RICA
CUBA
CZECHOSLOVAK SOCIALIST REPUBLIC
DENMARK
DOMINICAN REPUBLIC
ECUADOR
EL SALVADOR
ETHIOPIA
FINLAND
FRANCE
FEDERAL REPUBLIC OF GERMANY
GABON
GHANA
GREECE
GUATEMALA
HAITI
HOLY SEE
HONDURAS
HUNGARY
ICELAND
INDIA
INDONESIA
IRAN
IRAQ
ISRAEL
ITALY
IVORY COAST
JAPAN
REPUBLIC OF KOREA
KUWAIT
LEBANON
LIBERIA
LIBYA
LUXEMBOURG
MADAGASCAR
MALI
MEXICO
MONACO
MOROCCO
NETHERLANDS
NEW ZEALAND
NICARAGUA
NIGERIA
NORWAY
PAKISTAN
PARAGUAY
PERU
PHILIPPINES
POLAND
PORTUGAL
ROMANIA
SAUDI ARABIA
SENEGAL
SOUTH AFRICA
SPAIN
SUDAN
SWEDEN
SWITZERLAND
SYRIA
THAILAND
TUNISIA
TURKEY
UKRAINIAN SOVIET SOCIALIST REPUBLIC
UNION OF SOVIET SOCIALIST REPUBLICS
UNITED ARAB REPUBLIC
UNITED KINGDOM OF GREAT BRITAIN AND NORTHERN IRELAND
UNITED STATES OF AMERICA
URUGUAY
VENEZUELA
VIET-NAM
YUGOSLAVIA

The Agency's Statute was approved on 23 October 1956 by the Conference on the Statute of the IAEA held at United Nations Headquarters, New York; it entered into force on 29 July 1957. The Headquarters of the Agency are situated in Vienna. Its principal objective is "to accelerate and enlarge the contribution of atomic energy to peace, health and prosperity throughout the world".

Printed by the IAEA in Austria
June 1965

PROCEEDINGS SERIES

INELASTIC SCATTERING OF NEUTRONS

PROCEEDINGS OF THE SYMPOSIUM ON
INELASTIC SCATTERING OF NEUTRONS
HELD AT BOMBAY, 15-19 DECEMBER 1964

In two volumes

VOL.II

INTERNATIONAL ATOMIC ENERGY AGENCY
VIENNA, 1965

Symposium on Inelastic Scattering of Neutrons, Bombay, 15 - 19 December 1964.
Proceedings ... held by the International Atomic Energy Agency ... Vienna, the Agency, 1965.
2 vols. (IAEA Proceedings series)

539.171.4

INELASTIC SCATTERING OF NEUTRONS,
IAEA, VIENNA, 1965
STI/PUB/92

FOREWORD

The general technique of using neutron interactions - and in particular the inelastic scattering of neutrons - to study the dynamics of matter, and the interatomic forces which determine dynamics, is now well established. This area of physics research is of increasing interest to developing countries as well as to many advanced research centres of the world. Three international symposia have already been devoted to the subject of neutron inelastic scattering: the first was held in Stockholm in 1957; the second and third were convened by the IAEA in Vienna in October 1960, and in Chalk River, Canada, in September 1962. In view of continuing and expanding activity in this field, the IAEA convened the present Symposium at Bombay from 15 to 19 December 1964 on the invitation of the Government of India and the Indian Atomic Energy Commission.

A total of 66 papers representing 15 countries and 1 international organization were presented at Bombay. The meeting concentrated on experimental results and interpretation rather than on equipment and techniques; thus neutron inelastic scattering has "come of age" and is indeed now fully established as a versatile and powerful research tool.

Gratitude is expressed to authors of papers, chairmen of sessions, and discussion participants for their contributions to the success of the Bombay Symposium.

EDITORIAL NOTE

The papers and discussions incorporated in the proceedings published by the International Atomic Energy Agency are edited by the Agency's editorial staff to the extent considered necessary for the reader's assistance. The views expressed and the general style adopted remain, however, the responsibility of the named authors or participants.

For the sake of speed of publication the present Proceedings have been printed by composition typing and photo-offset lithography. Within the limitations imposed by this method, every effort has been made to maintain a high editorial standard; in particular, the units and symbols employed are to the fullest practicable extent those standardized or recommended by the competent international scientific bodies.

The affiliations of authors are those given at the time of nomination.

The use in these Proceedings of particular designations of countries or territories does not imply any judgement by the Agency as to the legal status of such countries or territories, of their authorities and institutions or of the delimitation of their boundaries.

The mention of specific companies or of their products or brand-names does not imply any endorsement or recommendation on the part of the International Atomic Energy Agency.

CONTENTS OF VOL. II

DYNAMICS OF LIQUIDS

MOLECULAR DYNAMICS

EXPERIMENTAL METHODS

DYNAMICS OF LIQUIDS

LIQUID DYNAMICS

K. - E. LARSSON
ROYAL INSTITUTE OF TECHNOLOGY, STOCKHOLM, SWEDEN

Abstract — Résumé — Аннотация — Resumen

LIQUID DYNAMICS. The neutron scattering results obtained from liquids may be divided into at least two classes: (a) those obtained from simple liquids such as liquid metals and condensed noble gases such as argon and (b) those obtained from polyatomic liquids such as the liquid hydrocarbons

From an analysis of the quasi-elastically and inelastically scattered spectrum for the simple liquids very direct information is obtained on the local order of the atomic arrangements as a function of time. The existence of interference scattering in the inelastic scattering region clearly indicates that local order is maintained in the simple liquids for a length of time of the order of 10^{-12} s or longer, allowing a development of vibratory motions of periods shorter than 10^{-12} s.

The studies of the more complex hydrogenous liquids have led to an increased insight into the relaxational phenomena in these liquids. Applying the principle of division of the scattered neutron spectrum into an inelastic and a quasi-elastic part, one obtains from the analysis of the inelastic part detailed information about the rotational, librational and vibrational levels in the molecule as well as in the intermolecular hydrogen bonds. The analysis of the quasi-elastic peak leads in several cases to a determination of a self-diffusion coefficient typical for the proton motion. It is also possible to derive a mean lifetime for the hydrogen bond or for a hindered rotation in some cases. The nature of diffusive motions in the hydrogenous H-bonded liquids is also rather clearly illustrated as a kind of step-wise rotational motion hindered by the H-bond. There seems to exist a universal limiting relaxation time of about 10^{-12} s in all the hydrogenous liquids investigated at temperatures such that the viscosity of the liquid is of the order of 1 cP or smaller. From a comparison with the ultrasonic data on glycerol it seems clear that the neutron does not observe all the existing relaxational effects present in glycerol but rather selects those mechanisms which occur on the right time scale of 10^{-11} to 10^{-13} s.

It seems that conglomerates of molecules, the size of which is strongly temperature dependent, may very well exist for the case of glycerol. In such cases the true diffusion mechanism seems to be a very complicated one occurring on various time scales of which the neutron experiments give information only on the faster parts. The neutron studies appear, however, as a good complement to the ultrasonic, dielectric and proton resonance methods of investigating relaxational phenomena in liquids.

If the technique of exchanging the proton against a deuteron is applied to the hydrogenous samples a considerable increase is gained in the amount of information obtained from the neutron data. This will be exemplified for glycerol which has been investigated both in a partially, $C_3H_5(OD)_3$, and fully, $C_3D_5(OD)_3$, deuterated form.

DYNAMIQUE DES LIQUIDES. Les données obtenues par la diffusion des neutrons dans les liquides peuvent se diviser pour le moins en deux catégories: a) données obtenues pour des liquides simples, tels que métaux liquides et gaz rares condensés comme l'argon; b) données obtenues pour des liquides polyatomiques tels que les hydrocarbures liquides.

En analysant le spectre de diffusion quasi élastique et inélastique pour les liquides simples, on obtient des renseignements directs sur l'ordre local des arrangements atomiques en fonction du temps. L'existence d'une diffusion d'interférence dans la région de diffusion inélastique montre clairement que dans les liquides simples, l'ordre local se maintient pendant une durée de l'ordre de 10^{-12} s ou davantage, ce qui permet l'apparition de mouvements vibratoires de périodes inférieures à 10^{-12} s.

Les études sur les liquides hydrogénés plus complexes ont permis de mieux comprendre les phénomènes de relaxation dans ces liquides. En appliquant le principe de la division du spectre des neutrons diffusés en une partie inélastique et une partie quasi élastique, on constate que l'analyse de la partie inélastique fournit des renseignements détaillés sur les niveaux de rotation, de libration et de vibration dans la molécule et les liaisons intermoléculaires par l'hydrogène. L'analyse du pic quasi élastique permet dans plusieurs cas de déterminer un coefficient d'autodiffusion typique pour le mouvement des protons. Il est également possible d'établir dans certains cas une valeur moyenne de la durée de vie pour la liaison par l'hydrogène ou pour une rotation inhibée. La nature des mouvements de diffusion dans les liquides hydrogénés à liaisons par l'hydrogène peut être assez

exactement représentée comme une sorte de mouvement rotatoire échelonné et inhibé par ces liaisons. Il semble qu'il existe un temps de relaxation limitatif universel d'environ 10^{-12} s dans tous les liquides hydrogénés étudiés à des températures telles que leur viscosité soit de l'ordre de 1 cP ou inférieure à cet ordre de grandeur. Une comparaison avec les données relatives à la glycérine obtenues à l'aide d'ultrasons fait apparaître nettement que le neutron ne subit pas tous les effets de relaxation se produisant dans la glycérine, mais de préférence ceux qui se manifestent à l'échelle de temps appropriée de 10^{-11} à 10^{-13} s.

L'existence de conglomérats de molécules, dont la dimension dépendrait étroitement de la température, semble parfaitement possible dans le cas de la glycérine. Le véritable mécanisme de diffusion représente alors probablement un processus fort complexe qui s'opère à diverses échelles du temps et au sujet duquel les expériences au moyen des neutrons ne fournissent de renseignements que sur les phases les plus rapides. Il apparaît toutefois que les études à l'aide des neutrons complètent fort bien les méthodes qui permettent d'étudier les phénomènes de relaxation dans les liquides au moyen de méthodes de résonance (ultrasons, diélectriques et protons).

En appliquant aux échantillons hydrogénés la technique fondée sur le remplacement du proton par un deutéron, on parvient à augmenter considérablement la somme des connaissances pouvant être déduites des données obtenues au moyen des neutrons. L'auteur cite, à titre d'exemple, la glycérine qu'il a étudiée sous une forme partiellement deutérée, $C_3H_5(OD)_3$, et entièrement deutérée, $C_3D_5(OD)_3$.

ДИНАМИКА ЖИДКОСТЕЙ. Результаты рассеяния нейтронов на жидкостях можно подразделить по крайней мере на две категории: a) результаты, полученные на простых жидкостях, например жидких металлах, и конденсированных инертных газах, например аргоне, и b) результаты, полученные на многоатомных жидкостях, например жидких углеводородах.

В результате анализа спектра квазиупругого и неупругого рассеяния на простых жидкостях получены очень ясные данные о локальном порядке расположения атомов как функции времени. Наличие интерференционного рассеяния в области неупругого рассеяния свидетельствует о том, что локальный порядок сохраняется в простых жидкостях в течение порядка 10^{-12} сек или более, что делает возможным колебательные движения с периодом менее 10^{-12} сек.

Изучение более сложных гидрогенных жидкостей позволило лучше понять явления релаксации в этих жидкостях. Если применить принцип деления спектра рассеянных нейтронов на неупругую и квазиупругую части, то оказывается, что анализ неупругой части дает подробную информацию относительно вращательного, вибрационного и колебательного уровней в молекуле, а также в межмолекулярных водородных связях. Анализ квазиупругого пика в ряде случаев дает возможность определить коэффициент самодиффузии, типичный для движения протонов. В некоторых случаях можно также определить среднее время существования водородной связи или стесненного вращения. Также довольно убедительно показывается характер диффузионных движений в гидрогенных жидкостях с водородными связями, как одного из видов ступенчатого вращательного движения, стесненного водородной связью. Для всех исследованных гидрогенных жидкостей при таких температурах, когда вязкость жидкости составляет порядка 1 сантипауза или менее, существует, по-видимому, универсальное предельное время релаксации, составляющее примерно 10^{-12} сек. Сравнение с ультразвуковыми данными по глицерину показывает, что нейтрон выявляет не все эффекты релаксации, существующие в глицерине, а лишь те механизмы, которые происходят в диапазоне $10^{-11}-10^{-13}$ сек.

Представляется, что в глицерине вполне могут существовать конгломераты молекул, размер которых в значительной степени зависит от температуры. В таких случаях истинный механизм диффузии является, по-видимому, очень сложным и происходит в различные промежутки времени. Нейтронные эксперименты позволяют получить данные только о более быстрой части этих механизмов. Однако нейтронные исследования являются хорошим дополнением ультразвукового и диэлектрического методов, а также метода протонного резонанса при исследовании явлений релаксации в жидкостях.

Если в отношении гидрогенных образцов применить метод замены протона дейтроном, то по нейтронным данным можно получить значительно больше информации. Это видно на примере глицерина, который исследовался как в частично, так и в полностью дейтеризованном виде, т.е. в виде $C_3H_5(OD)_3$ и $C_3D_5(OD)_3$ соответственно.

DINÁMICA DE LOS LÍQUIDOS. Los resultados logrados por dispersión de neutrones en líquidos pueden dividirse al menos en dos clases: a) los obtenidos con líquidos simples, tales como los metales líquidos y los *gases nobles como* el argón, condensados, y b) los obtenidos con líquidos poliatómicos, tales como los hidrocarburos líquidos.

El análisis del espectro de dispersión cuasielástica e inelástica en los líquidos simples permite obtener información muy directa sobre el orden local de los ajustes atómicos en función del tiempo. La existencia de interferencias en la región de dispersión inelástica indica claramente que el orden local se mantiene en los líquidos simples durante un lapso de unos 10^{-12} s o mayor, lo que es compatible con la existencia de movimientos vibratorios de período inferior a 10^{-12} s.

El estudio de los líquidos hidrogenados, que son más complejos, ha permitido profundizar los conocimientos que se poseen sobre los fenómenos de relajación en dichos líquidos. Cuando se aplica el principio de la división del espectro de dispersión neutrónica en una parte elástica y en otra cuasielástica, el análisis de la parte inelástica proporciona información detallada sobre los niveles de rotación, oscilación y vibración en la molécula y en los enlaces hidrógeno intermoleculares. El análisis del pico cuasielástico permite a veces determinar un coeficiente de autodifusión característico para el movimiento protónico. En algunos casos, también es posible deducir el período del enlace hidrógeno o de una rotación restringida. La naturaleza de los movimientos de difusión en los líquidos hidrogenados con enlaces hidrógeno se explica asimismo bastante claramente como una especie de movimiento rotacional gradual restringido por el enlace hidrógeno. Parece existir un tiempo límite de relajación universal de unos 10^{-12} s en todos los líquidos hidrogenados que se han investigado a temperaturas tales que su viscosidad es del orden de 1 cP o menor. De la comparación con los datos relativos al glicerol, obtenidos con ayuda de ultrasonidos, se desprende que los neutrones no se ajustan a todos los efectos de relajación existentes en el glicerol, sino que seleccionan los mecanismos que se verifican en el lapso, propicio para ellos, de 10^{-11} a 10^{-13} s.

Al parecer, en el glicerol pueden muy bien existir conglomerados de moléculas cuyo tamaño depende estrechamente de la temperatura. En tales casos, el verdadero mecanismo de difusión parece ser muy complicado y se desarrolla a ritmos diferentes; los experimentos de dispersión sólo proporcionan informaciones sobre los más rápidos. De todas formas, los estudios con ayuda de neutrones parecen constituir un buen complemento de los métodos ultrasónicos, dieléctricos y de resonancia protónica utilizados para el estudio de los fenómenos de relajación en los líquidos.

Si se aplica a sustancias hidrogenadas, la técnica de sustituir protones por deuterones amplía considerablemente la información que proporcionan los neutrones. A este respecto se cita el ejemplo del glicerol, que se ha investigado en sus formas parcial y completamente deuteradas, esto es, $C_3H_5(OD_3)$ y $C_3D_5(OD_3)$.

1. INTRODUCTION

It is possible to approach the problem of liquid dynamics from two directions: (a) either the liquid is considered as a disordered solid, and the solid-state ideas are transferred to the liquid field, or (b) the liquid is considered as a condensed gas and the gas aspects are supposed to be dominating. Both aspects may be fruitful to apply to the liquid dynamic problem. One or the other aspect dominates depending upon the temperature of the liquid and upon the time scale of observation. The experimental studies of fluctuation and transport phenomena of liquids range from the classical studies of diffusion and viscosity covering time periods of minutes and hours to relaxational studies by ultrasonics, proton resonance measurements, dielectric measurements and neutron scattering studies, altogether covering time ranges from 10^{-6} to $<10^{-13}$ s. In Raman and infrared spectroscopy an instantaneous picture is obtained of the energy transitions between various energy levels caused by rotational and vibrational motions of complex molecules in liquids. The intermolecular bonds in liquids often manifest themselves in the appearance of extra broad energy levels and the close collisions lead to a broadening and smearing out of sharp spectral lines for various reasons.

The liquids may be divided into a number of classes but from the dynamical point of view it seems proper to talk about (a) monatomic li-

quids and (b) molecular liquids. The vast majority of liquids belong to class (b) and most of the experimental information has been gained with molecular liquids. From the theoretical point of view the molecular liquids present a many-body problem of formidable complexity, whereas the simpler monatomic liquids, such as liquified noble gases and liquid metals, are somewhat simpler to handle theoretically. Thus the current models for liquid dynamics may be tested most simply in the neutron scattering results on these simpler fluids. In spite of this the neutron studies of the complex liquids offer a tool to deepen our understanding not only of the liquid dynamics but also of the neutron scattering method itself, clearly demonstrating its limitation and possibilities.

2. THE NEUTRON SCATTERING METHOD

The slow neutron scattering process happens to offer a very interesting time scale to the observing scientist. If the momentum transfer in the scattering process is $\hbar\vec{\kappa}$, where $\vec{\kappa} = \vec{k} - \vec{k}_0$ and $\vec{k}$ and $\vec{k}_0$ are scattered and ingoing wave vectors respectively, it follows from the uncertainty relation that the interaction range or observation range of a neutron is $\Delta x \geq 1/|\kappa|$. On the other hand, simple fluctuation theory predicts that in a time t a particle in a liquid diffuses a distance $(\Delta x^2)^{\frac{1}{2}} = (2Dt)^{\frac{1}{2}}$, where D is the self-diffusion coefficient of the molecules of the liquid. Identifying the two values of Δx one may see that the observation time of the neutron which would be necessary to feel the motion of the particle over the distance Δx is

$$t_{obs} \geq 1/2D\kappa^2 \tag{1}$$

If $D \simeq 10^{-5}$ cm^2/s and $0.1 < \kappa^2 < 10$ Å^{-2} in a typical neutron scattering experiment one may see that 5×10^{-11} s $> t_{obs} > 5 \times 10^{-13}$ s. If on the other hand one imagines that the slow neutron is interacting with a heavier molecule, say a mass of M = 100, its average speed $\bar{v}$ during interaction would be about 10^4 cm/s, so that its interaction time, $t_{int} = \Delta x/\bar{v} \geq 1/\kappa\bar{v}$, would be in the range 13×10^{-12} s $> t_{int} > 0.3 \times 10^{-12}$ s. Obviously the neutron will thus see the motions occuring on a time scale $\leq t_{int}$. If diffusion of a molecule occurs without any time delay the neutron would see the diffusive motion, so that a sharp ingoing neutron line would appear broadened due to the uncertainty in position of the scatterer. If on the other hand, the diffusive process would be delayed by the presence of neighbours the diffusive line-broadening will be observed only if the delay time is $\leq t_{int}$. If one also imagines that the nucleus with which the neutron is interacting is vibrating or rotating within the bond in the molecule or within an intermolecular bond, such as a proton in an H-bond, the neutron will also register the energy transfers in the vibrating-rotating system. Such energy transfers often occur with lifetimes τ of the order of 10^{-12} s in liquids, and therefore many periods of a damped oscillation might be felt by the neutron and registered as relatively sharp lines or bands in an inelastically scattered spectrum. Between the two regions of small diffusive and relatively large (rotational, vibrational) energy transfers there also exists a region which corresponds to hindered translations (damped oscillations) of the centre of gravity of the molecule. The

reason such oscillations should exist is simply that the oscillating molecule is caught in a cage created by neighbours oscillating in a like manner.

Various hypotheses regarding the mean lifetime τ_0 of such an oscillatory centre of gravity in a cage of neighbours [1, 2, 3, 4] and also regarding the period of diffusion [5] have been invented. In a solid-like model the relaxation time τ_0 is so long that the vibrational period $\tau = 1/\nu_{osc}$ is $\ll \tau_0$. Also in such a model the time τ_1 spent by the molecule in a diffusive or translational state is assumed short in comparison to τ_0. In one case it has also been assumed that because of the ever changing walls of the cage within which a molecule is enclosed, the molecule also performs a slight diffusive motion during the translational or oscillatory period. Because of the existence of a residential time τ_0 there should exist a frequency distribution $f(\omega)$ similar to the one defined for solids although the physical meaning is not so clear in the liquid case because of the strong damping and anharmonicity [6]. Other solid-like models have been created, such as the stochastic model in which the oscillatory motions of the centre of gravity of the molecules are similar to the phonons in a solid with the addition of a damping and with the assumption that low frequency modes, $\omega < \omega'$, may not be transmitted through the liquid but rather degenerate into diffusive modes [7]. No serious theoretical attempts have so far been made to describe the differential scattering cross-section of a vibrating-rotating system performing hindered translations and diffusion like a complex molecule. Yet considerable experimental effort has gone into the study of liquids like H_2, H_2O, D_2O, CH_4, C_5H_{12}, $C_3H_5(OH)_3$, $C_3H_5(OD)_3$, $C_3D_5(OD)_3$, $C_{17}H_{35}COOH$, CH_3OH, C_2H_5OH etc. [8]. In the following, the results obtained on such liquids exemplify what sort of information is obtainable from neutron scattering data.

In some of the liquids mentioned, like D_2O and $C_3D_5(OD)_3$, there should exist interference scattering resulting from the atomic short-range order within the molecule and possibly also collective scattering caused by the ordering effect of the intermolecular hydrogen bonds. In accordance with the picture of propagating more or less strongly damped waves in the liquid, there should exist around each molecule or atom in the liquid regions over which strong correlations in the molecular motions would persist. Within such a correlation range of a few atomic distances the atomic and molecular order should have such a mean lifetime that collective scattering should appear. In this modified sense it should be possible to regard and treat the interference scattering in a liquid like that in a polycrystal.

The analysis of such coherent scattering from complex liquids is, however, exceedingly difficult. It appears much simpler to study coherent scattering phenomena in monatomic liquids of which some are 100% coherent scatterers, such as liquid tin [9], lead [10] and aluminium [11]. Somewhat more difficult to interpret are the results measured on mixed coherently and incoherently scattering simple liquids like liquid argon [12, 13] and liquid sodium [14, 15]. A few examples of results obtained on coherently scattering simple liquids are given.

3. TREATMENT OF NEUTRON SCATTERING DATA

The neutron scattering data obtained from liquids may be of three kinds, namely total scattering data σ_s, angular distribution studies $d\sigma/d\Omega$ and finally the energy-analysed angular distribution $d^2\sigma/d\Omega d\omega$. In this review we concentrate on the last two observable quantities. The choice of proper ingoing neutron energy is very important as is illustrated by the following consideration.

Let us assume that the liquid would scatter as an incoherent solid such that $d^2\sigma/d\Omega d\omega$ may be given by the phonon expansion formula [16] with only the first few terms (n = 0, 1, 2, 3) retained. Let us assume that the experimental resolution function is of Gaussian shape and that the equivalent Debye temperature of the liquid is 50°K which corresponds to a Debye-Waller factor $2W = 3$ if the square of the momentum transfer $\kappa^2 = 15$ Å^{-2}, if the mass of the scatterer is M = 92 and if the temperature of the sample is 293°K. If we now consider four ingoing neutron wavelengths, namely $\lambda = 1.13$ Å corresponding to an energy of E = 64 meV and a resolution width $\Delta\lambda/\lambda = 8\%$, $\lambda = 1.5$ Å corresponding to $E \simeq 36$ meV and $\Delta\lambda/\lambda = 5\%$, $\lambda = 2.25$ Å corresponding to $E \simeq 16$ meV and $\Delta\lambda/\lambda = 5\%$, and finally $\lambda = 4$ Å corresponding to $E \simeq 5$ meV and $\Delta\lambda/\lambda = 4\%$, we observe (Fig. 1) that it is not possible to resolve the elastic peak unless the ingoing neutron energy is low. The fact that too high neutron energies give only the gas model result is well known, but for the sake of clarity it is nevertheless mentioned here. Of course a higher resolution would give the central peak resolved even at the higher neutron energies, but for intensity reasons such high resolutions are not practical in many cases. If one therefore wants to study broadening effects of the central quasi-elastic peak, very low ingoing neutron energies are preferable. This means that the inelastic scattering will be mainly observed only in energy gain. If particular attention is to be paid to very high energy transfers, $\omega > 15 \times 10^{13}$ rad/s (E > 0.1 eV), only an energy loss experiment with higher ingoing energy will solve the experimental problem.

There are essentially two or three different ways to treat the neutron data.

(a) One basic idea in the detailed treatment of neutron scattering data is that the observed intensity distribution, which more or less directly reflects the cross-section $d^2\sigma/d\Omega dE$, may be divided into a quasi-elastic and an inelastic part. The ideal situation would be one which allowed a direct comparison of all the observed intensity with a theoretically obtained $d^2\sigma/d\Omega d\omega$, thus including both quasi-elastic and inelastic scattering caused by both diffusive, hindered translational, hindered rotational and internal vibrational motions and energy transfers. As such a situation does not exist one has to resort to simplified ideas and approximate formulas.

If cold neutrons of 4 to 5-Å wavelength are used as ingoing neutrons, broadenings of the quasi-elastic line in a range 3×10^{-5} to 8×10^{-4} eV may usually be analysed with normal resolution values of $d\lambda/\lambda\,(dt/t)$ down to the region of 1.5%. Larger broadenings up to a few millivolts may be analysed with somewhat higher ingoing energy, such as the example of $\lambda = 2.25$ Å or E = 16 meV given in Fig. 1 (for which the assumed resolution broadening is 1.6 meV). Examples of scattering results obtained with the full cold

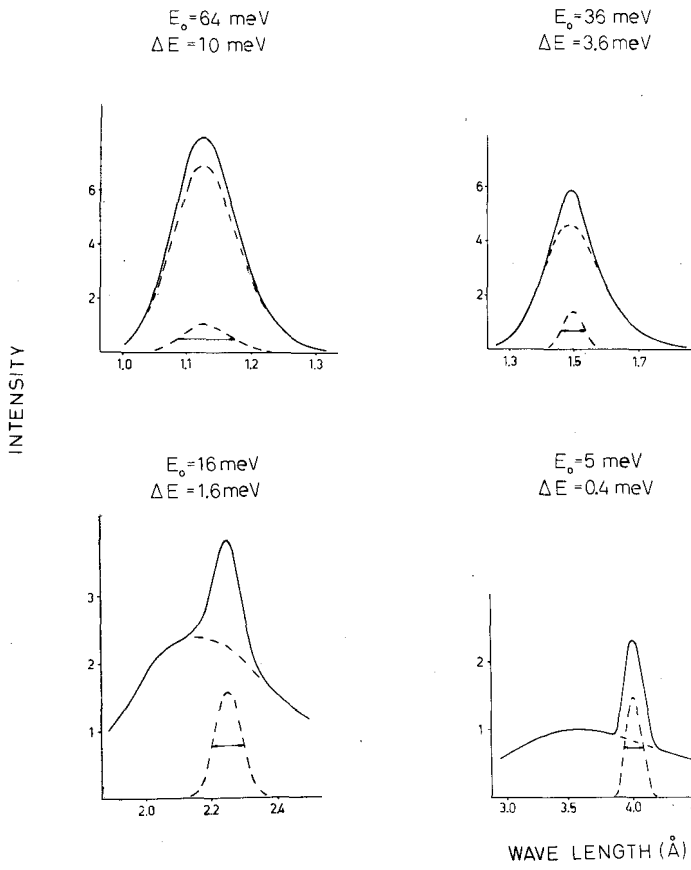

Fig. 1

Illustration of the importance of making the correct choice of ingoing energy E_0 when the resolution is given by instrumental properties.
It is seen that only when E_0= 16 and 5 meV is the elastic peak resolved and a study of its width possible.

neutron spectrum and with neutrons of wavelength 2.25 Å impinging on glycerol, pentane and liquid aluminium as well as results gained when a reduced cold neutron spectrum is scattered from liquid argon are shown in Fig. 2. It is observed that a separate analysis of the quasi-elastic peak is impossible for the full cold neutron spectrum and for too large broadenings but that larger widths obtained at higher temperatures or larger κ-values may be analysed from the observations with neutrons of shorter wavelength. The argon results of Fig. 2 exemplify a case of a loosely bound liquid where none or very little inelastic scattering is observed. The results on liquid aluminium exemplify a case where no quasi-elastic scattering appears at all.

The isolated quasi-elastic peak may be used for a direct comparison with various cross-section predictions or it may be used to derive one

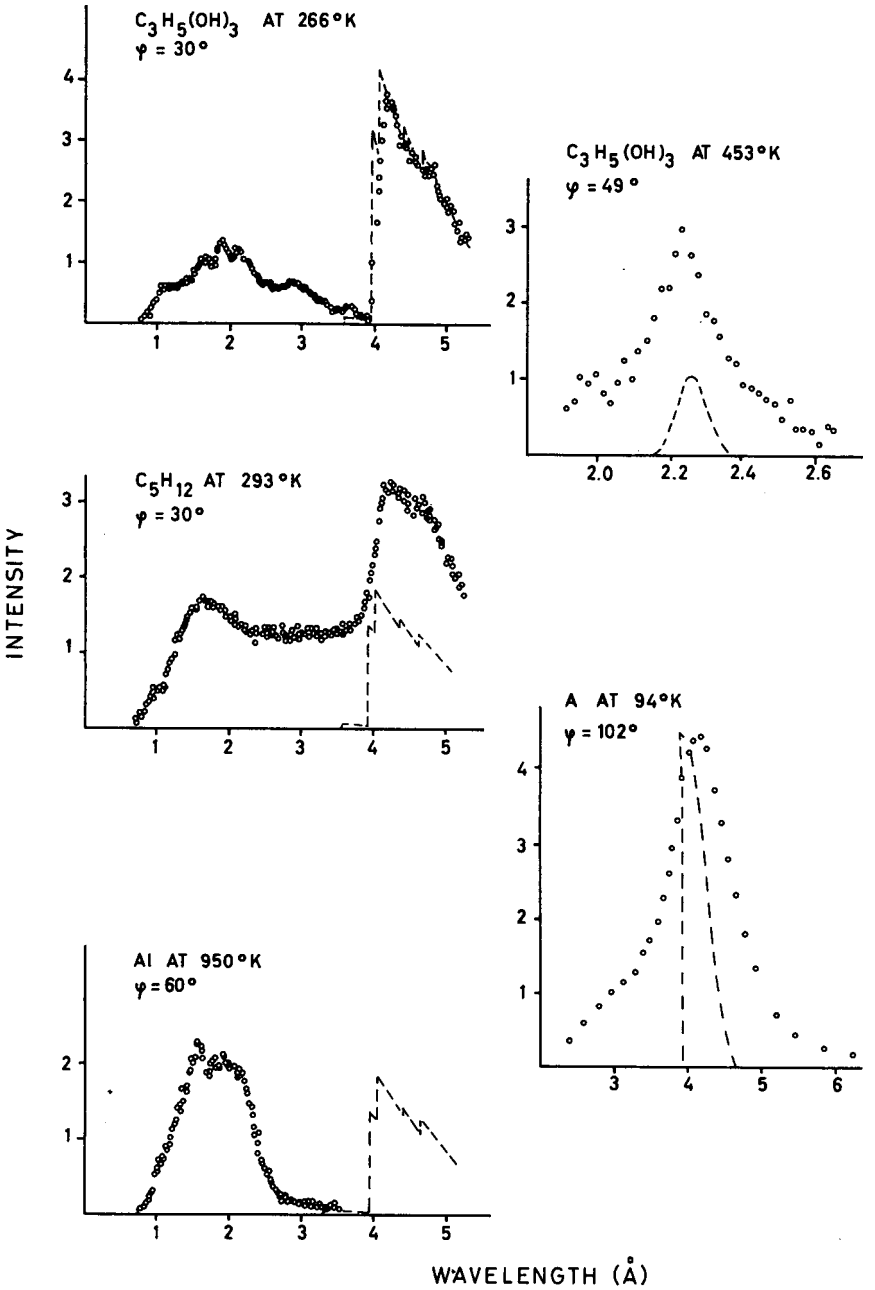

Fig. 2

Examples of scattered neutron spectra from liquids
with various ingoing neutron energies and spectral distributions.

quantity, the width ΔE. Definite predictions of the full width at half maximum are given by a number of liquid models, the most important of which have been

(i) The simple diffusion model [17]

$$\Delta E = 2\hbar D\kappa^2 \tag{2}$$

(ii) The jump diffusion model [1]

$$\Delta E = \frac{2\hbar}{\tau_0}\left(1 - \frac{e^{-2W}}{1 + D\kappa^2\tau_0}\right) \tag{3}$$

(iii) The modified jump diffusion model [4]

$$\Delta E = \frac{2\hbar}{\tau_0}\left(1 + \kappa^2 D_0\tau_0 - \frac{e^{-2W}}{1 + \kappa^2 D\tau_0}\right). \tag{4}$$

Here D is the total self-diffusion coefficient and D_0 is a smaller diffusion coefficient describing the slow continuous motion of the vibrating particle during the residential time τ_0 . D_0 is, at least at higher viscosities, much smaller than D.

(iv) Further possibilities to obtain theoretical line width values for comparison with the observed widths are obtained from numerical computations with formulas developed by SCHOFIELD [2] and EGELSTAFF and SCHOFIELD [3] which for larger κ-values give a width

$$\Delta E = \sqrt{2\ln 2}\,\sqrt{(D/\tau)}\hbar\kappa, \tag{5}$$

where τ is of the character of a delay time before the simple diffusive spreading of an atom occurs.

(v) The stochastic model of a monatomic liquid developed by RAHMAN, SINGWI and SJÖLANDER [7] may be used to calculate the cross-section from which the width of the quasi-elastic peak is obtained. The value of the ratio $(\omega'/\omega_D)^3$ appearing in their formulas gives the delay time $t_d = (MD/kT)(\omega_D/\omega')^3$ before diffusion sets in. ω_D is the Debye frequency and $\omega' \leq \omega_D$.

(vi) The simple diffusion model corrected for interference scattering [18]

$$\Delta E = \hbar(\overline{\omega^2_{coh}})^{\frac{1}{2}}, \tag{6}$$

where $\overline{\omega^2_{coh}} = [\kappa^2/(1 + \gamma(\kappa))]\,[k_B T/M]$. Here $(1 + \gamma(\omega))$ is the Fourier transform of the pair correlation function for the liquid and M is the mass of the scattering atom.

Instead of measuring the width of the quasi-elastic peak, this isolated intensity distribution may also be compared directly with the computed cross-section formulas of (a) Vineyard, (b) Singwi-Sjölander, (c) Oskotskii, (d) Egelstaff and Schofield, or (e) Rahman, Singwi and Sjölander. Essentially

all these models describe a scale of variation of the atomic motion between a continuous diffusion by small and frequent collisions and a solid-like oscillatory behaviour.

In case the quasi-elastic peak has been isolated there remains an inelastically scattered spectrum to be analysed. As has been shown,a generalized frequency distribution $f(\omega)$ corresponding to the distribution of normal modes in a solid might be derived from the inelastic neutron spectrum [6, 19]. The best way of obtaining this is to study the scattered distribution $(\vec{k}/\vec{k}_0)S(\kappa,\omega)$ for various ingoing neutron energies and scattering angles and then to obtain $f(\omega)$ from values of $\lim_{\kappa\to 0}\left(\frac{S(\kappa,\omega)}{\kappa^2}\right)_{\omega=\text{const.}}$. The scattered and ingoing wave vectors are $\vec{k}$ and $\vec{k}_0$, respectively. This method has been described in detail by EGELSTAFF [6, 20].

In case the experimenter cannot cover a big enough region of points in (κ,ω)-space because of technical reasons, another and approximate method may be used to derive a $f(\omega)$. This method consists in making use of the phonon-expansion formula developed for a solid and to retain only the first (one-phonon) term [21]. To approach the limit $\kappa \to 0$, the measurement is made at a small angle of observation. In this case $f(\omega)$ is obtained from

$$f(\omega) \sim S(\kappa,\omega)\,\frac{\omega}{\kappa^2}\,\frac{1}{1 \pm \coth(\hbar\omega/2kT)}\,e^{2W} \tag{7}$$

where the plus sign refers to energy loss and the minus sign to energy gain experiments. Most often e^{2W} must be put equal to one, as the Debye-Waller factor is not known.

Parameters gained from such an analysis of the data are the diffusion coefficient D which is obtained from the slope of the line-width curve $\Delta E = f(\kappa)$ at the origin if $6D\tau_0 >> \langle r^2\rangle$, where $\langle r^2\rangle$ is the rms deviation of the vibrating atom from the origin (the Debye-Waller factor is $2W = (\langle r^2\rangle/6)\kappa^2$), the relaxation or correlation time τ_0 which is obtained from the line-width curve for large κ-values if the curve saturates because then $\Delta E = 2\hbar/\tau_0$ and the frequency distribution $f(\omega)$. Such an analysis is of interest for the case of complex liquids like water (H_2O), glycerine ($C_3H_5(OH)_3$), pentane (C_5H_{12}) etc.

(b) A different approach to the problem of data treatment is to make use of the very general definition of the cross-section [22]

$$\frac{d^2\sigma}{d\Omega d\omega} = a^2\,\frac{k}{k_0}\,\frac{1}{2\pi}\int\int e^{i(\vec{\kappa}\cdot\vec{r}-\omega t)}\;G(\vec{r},t)\,d\vec{r}\,dt. \tag{8}$$

If the ingoing neutron spectrum is very narrow, such that the energy spread may be neglected, the observed intensity distribution is essentially identical with $d^2\sigma/d\Omega d\omega$. Therefore a double Fourier transform over κ- and ω-space of the observed intensity gives $G(\vec{r},t)$. As an integration over all κ- and ω-space must be made, the measurement should cover a wide range of κ,ω-values. If the scattering atom scatters incoherently or if only so large κ-values are considered that $(1+\gamma(\kappa))$ is essentially constant, it is possible to derive the rms-deviation of an atom from the origin $\rho(t)$ from one single Fourier transform of the data

$$F_s(\kappa, t) = \exp(-\kappa^2 \rho(t)) = 2 \int_0^\infty \cos \beta\tau \; S_s(\alpha, \beta) d\beta, \tag{9}$$

where $\alpha = \hbar^2\kappa^2/2Mk_BT$, $\beta = \hbar\omega/k_BT$ and $\tau = (k_BT/\hbar)t$ and $S(\alpha, \beta)$ is the dimensionless scattering law in the symmetric form. $S(\alpha, \beta)$ is related to the cross-section Eq. (8) through

$$\frac{d^2\sigma}{d\Omega d\omega} = \frac{k}{k_0} \left(\langle |a|^2 \rangle S_s(\vec{\kappa}, \omega) + |\langle a \rangle|^2 S_d(\vec{\kappa}, \omega) \right) \tag{10}$$

for the general case with a mixed coherent (S_d and $|\langle a \rangle|^2$) and mixed incoherent (S_s and $\langle |a|^2 \rangle$) scatterer. a is the scattering length and $S_{s,d}$ are the self and distinct parts of the scattering function $S(\kappa, \omega)$. The relation between $S(\kappa, \omega)$ and $S(\alpha, \beta)$ follows from

$$e^{-\beta/2} S(\alpha, \beta) = k_B T \cdot S(\kappa, \omega) \tag{11}$$

Equation (9) for $F_s(\kappa, t)$ results if the self-correlation function for an atom is Gaussian with a width function $\rho(t)$

$$G_s(r, t) = \frac{\exp(-r^2/\rho(t))}{(\pi\rho(t))^{3/2}} \tag{12}$$

The function $\rho(t)$ gives a very clear picture of what happens to an atom in the liquid as time proceeds.

(c) When the scattering nuclei have a considerable coherent scattering length the analysis of the data is very complicated. In the case of a polycrystal treated as a harmonic oscillator, cross-section formulas were worked out at an early stage of development [23, 24]. Inelastic neutron scattering was shown to occur only if the condition

$$2\pi\tau_{hkl} - q < \kappa < 2\pi\tau_{hkl} + q \tag{13}$$

is fulfilled. Here $q (q = 2\pi/\lambda)$ is the phonon wave number and $\tau_{hkl} = 1/d_{hkl}$ where d_{hkl} is the distance between the lattice planes h, k and l. In a liquid there are no lattice planes of ideally infinite extension but one may at least for a simple monatomic liquid imagine regions around each atom within which a strong local order exists such that a sort of local "lattice planes" of small extension exist. If it is also assumed that damped phonons exist, such that a q-vector may be defined in the liquid, then it should be expected that coherently scattered neutron intensity would occur only if

$$\kappa + q > 2\pi\tau > \kappa - q. \tag{14}$$

In a liquid the distribution of τ-vectors should be continuous rather than discrete. If these basic assumptions are made it is possible to define a coherent cross-section for the liquid [11, 25]

$$\left(\frac{d^2\sigma}{d\Omega d\omega}\right)_{coh} = \left(\frac{d^2\sigma}{d\Omega d\omega}\right)_{incoh} \cdot Z, \tag{15}$$

where Z is a structure factor given by

$$Z = \frac{2\pi^2}{q\kappa} \cdot \int_{\tau_{min.}}^{\tau_{max.}} \tau(1+\gamma(\tau))\, d\tau \qquad (16)$$

Here $(1+\gamma(\tau))$ is equivalent to the normal liquid structure factor $(1+\gamma(\kappa))$ with κ replaced by τ.

The small energy transfer region corresponding to quasi-elastic scattering was early treated by the convolution approximation which describes the coherent cross-section as a product of the incoherent cross-section and the liquid structure factor $(1+\gamma(\kappa))$. The validity of this approximation has, however, been shown to be rather limited.

Other approaches to the problem of analysing the coherent scattering of neutrons were recently presented by RAHMAN [26] and by SINGWI in [27]. Rahman showed that a time-delayed convolution approximation may describe an observed scattering cross-section. Few systematic attempts have, however, been made to interpret the coherent quasi-elastic and inelastic neutron scattering, which may certainly give much important information about correlation ranges and local order in liquids [27].

4. SOME EXPERIMENTAL RESULTS AND THEIR INTERPRETATION

In the following a few examples are given on experimental results on liquids which have been most intensively investigated. Only results related to the above discussion have been selected.

(a) Water

Water was one of the substances first investigated by the neutron scattering technique [28-36]. Investigations of the width of the quasi-elastic line at room temperature indicated that there exists a delay time τ_0 of magnitude 1.5×10^{-12}s (Fig. 3). During this average time a spectrum of hindered translation (motions of the centre of gravity) and hindered intermolecular rotations of the OH group in the H-bond is developed as was shown by the derived frequency spectrum $f(\omega)$. The hindered rotations cover a broad band centred round $\omega \sim 10^{14}$ rad/s corresponding to about 70 meV (Fig. 4), whereas the hindered translations of the H_2O molecule and of the OH group are observed in a region $\omega < 6 \times 10^{13}$ rad/s or $E < 45$ meV. A comparison between the spectra scattered from H_2O and D_2O showed that the 70-meV peak was shifted to an energy which is nearly $\sqrt{2}$ towards lower ω-values than it should be if the proton were performing harmonic vibrations or rotations in the interatomic potential, whereas the low energy part of the spectrum did not shift, which verifies the identification made. A Fourier analysis of water data has given a partial result for the width $\rho(t)$ of the assumed Gaussian spreading behaviour of a molecule (Fig. 5). It is found from the figure that the asymptotic diffusive behaviour $\rho(t) \to Dt$ does not occur at room temperature until a delay time of the order of $(1-2) \times 10^{-12}$s has elapsed, in excellent agreement with the value of τ_0 derived from the line-width data of Fig. 3.

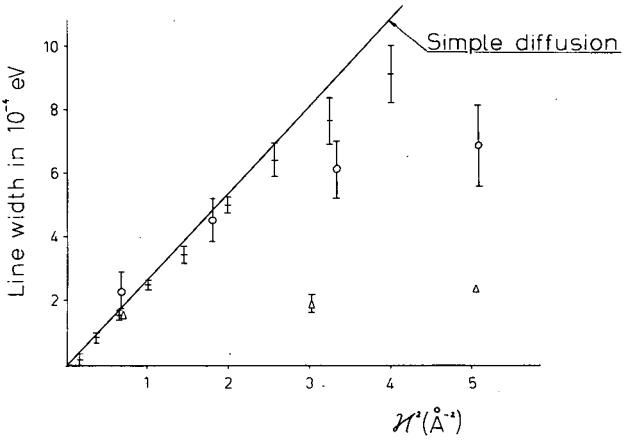

Fig. 3

Line widths of the quasi-elastic peak of water observed at three different laboratories

+ Sakamoto
Δ Stiller
O Larsson

(b) Glycerine, pentane and oleic acid

A substance which was investigated in much detail is glycerine which has the formula

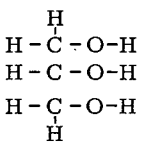

Further complex liquids investigated in relatively great detail [35, 37] are pentane

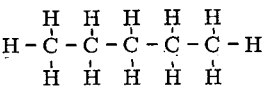

and oleic acid $C_{17}H_{33}COOH$. Glycerine shows a strong variation of viscosity and consequently also of the diffusion constant with temperature. Furthermore the glycerine molecule is, like water, bound to neighbouring molecules by hydrogen bonds. There might also exist internal molecular H-bonds. Already from the study of glycerine as well as of the hydrocarbons, of which pentane is an example, certain facts are known from ultrasonic studies, proton magnetic resonance studies, dielectric studies, and Raman and infrared spectroscopy. Also measurements of the coefficient of viscosity η have been made from which the self-diffusion coefficient D may be obtained by use of Eyrings theory

$$D = k_B T / 2r\eta, \tag{17}$$

where r is the molecular radius.

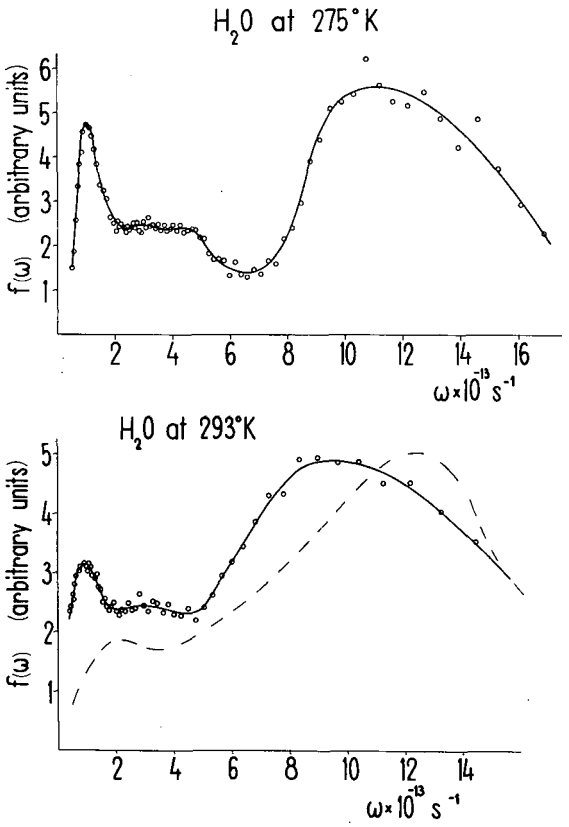

Fig. 4

Generalized frequency distributions obtained from neutron spectra of water at two different temperatures and at two different laboratories using different methods of analysis.

It is known that the long molecules show rotational isomerism, which means that the molecule may exist in several different steric forms obtained by a partial rotation of a CH_2 group round a C - C bond. As the different forms have different potential energy the shift from one form to the other is associated with an energy difference or activation energy E_0 which by Raman spectroscopy for pentane and other substances is found to be ~ 0.5 kcal/mole [38]. By successive rotations about neighbouring linkages, multiples of this value may occur such that 0.5, 2×0.5, 3×0.5 kcal/mole would appear as possible energy barriers to isomeric rotations.

It is also known [39] from infrared spectroscopy that CH_2 rocking motions occur in a carbon chain which in pentane shows up in a band at 6-800 cm^{-1}, corresponding to $\omega \simeq (11-15) \times 10^{13}$ rad/s. Furthermore skeletal vibrations exist which are sensitive to the length of the carbon chain [40]. The higher energy proton vibrations are difficult to observe in a neutron scattering experiment.

Energy transfers between quantum levels of all these motions should appear in the inelastically scattered neutron spectrum and some of the mo-

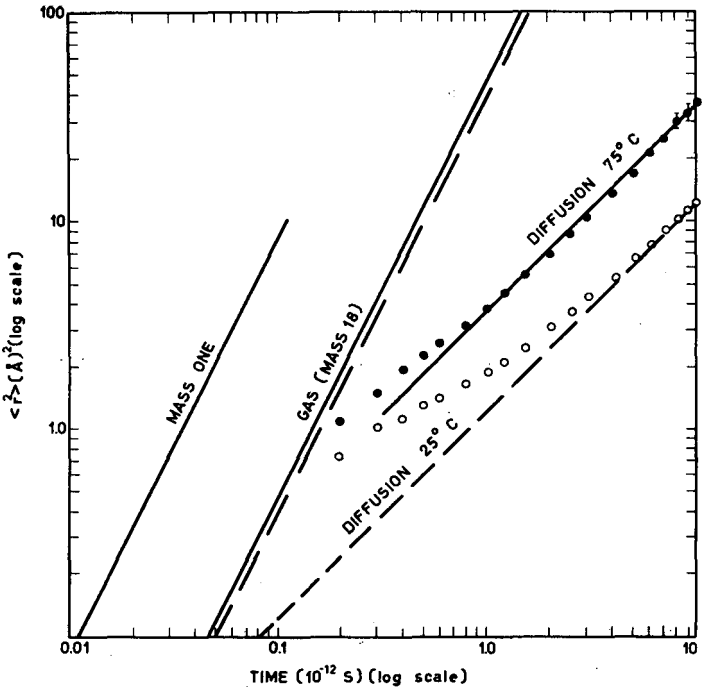

Fig. 5

The rms deviation of the scattering proton in water as a function of time
○ - - - 25°C
● —— 75°C

tions might cause broadening of the quasi-elastic line because all these motions involve changes of the proton positions. Torsional oscillations of an OH-group in an H-bond as seen in the H_2O spectrum at ($\omega \simeq 10 \times 10^{13}$ rad/s) (70 meV) should also appear in the glycerine spectrum. There is thus good reason to believe that the observed neutron spectrum would be a complicated mixture of intramolecular and intermolecular energy transitions.

By sending in the full cold neutron spectrum with its sharp cut-off at 4 Å, neutron spectra were obtained from glycerine, oleic acid and pentane at a series of temperatures. Approximate generalized frequency distributions $f(\omega)$ were obtained by the phonon expansion technique (compare Eq.(7)). Examples of the results are given in Fig. 6. For glycerine $f(\omega)$ is given both in the solid glass state and in the liquid state, for oleic acid both in the solid and in the liquid state and for pentane only in the liquid state. It is seen that the spectra show considerable similarities. In the liquid state and sometimes also in the solid state peaks appear at $\omega \simeq 1.3$, 2.7 and 4×10^{13} rad/s. Similarly, broad intensity maxima seem to appear at $\omega \simeq 6$ and $(13\text{-}14) \times 10^{13}$ rad/s in the two long molecules C_5H_{12} and $C_{17}H_{33}COOH$. In glycerine a broad intensity maximum appears at $\omega \simeq (10\text{-}11) \times 10^{13}$ rad/s, where the hindered rotation band appears in water. In all substances there is a faint indication of an intensity maximum for $\omega \simeq (0.5\text{-}0.9) \times 10^{13}$ rad/s.

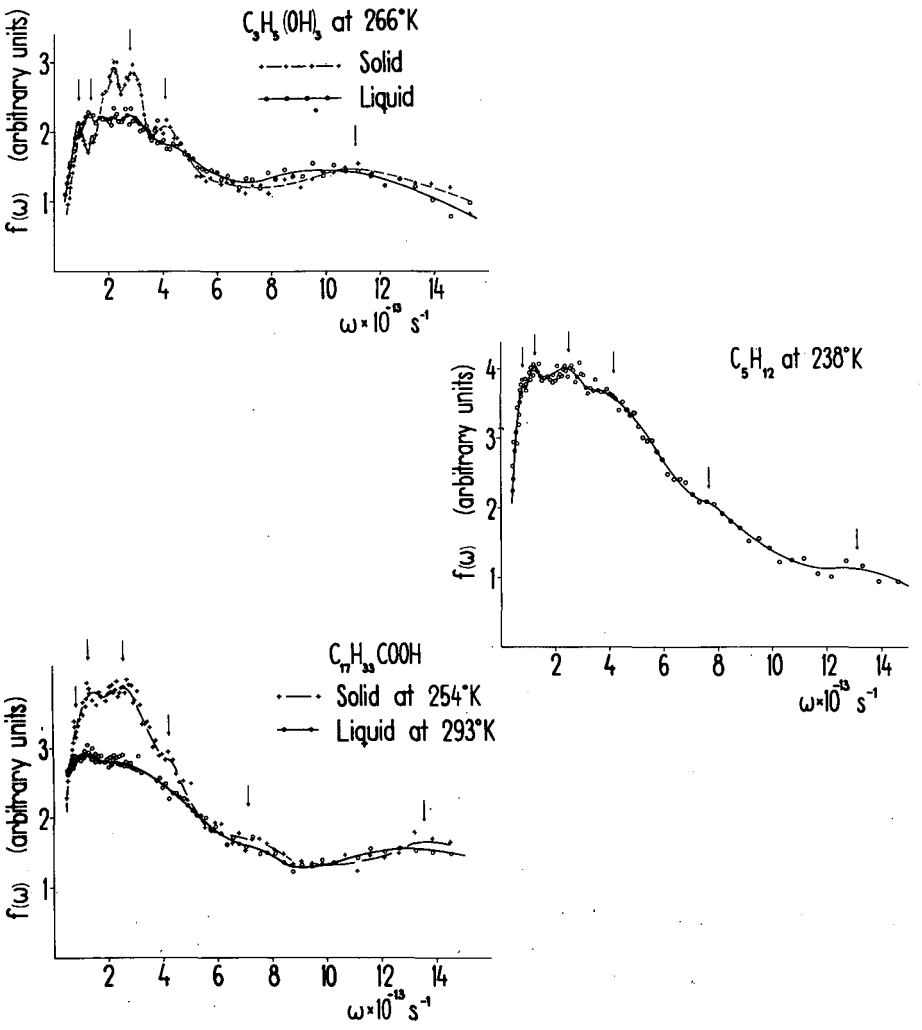

Fig. 6

Generalized frequency distributions obtained from glycerine, pentane and oleic acid in solid and liquid phases

The band at $\omega \simeq (13\text{–}14) \times 10^{13}$ rad/s may very well correspond to CH_2 rocking vibration. The faint band at $\omega = 4$ may well be some kind of skeletal vibration involving some motion of the protons bound to the carbon atom. It is believed that the two main peaks at $\omega \simeq 1.3$ and 2.7×10^{13} rad/s are due to partial rotations of CH_2 groups (rotational isomerism) and finally the faint peak at $\omega \simeq (0.5\text{–}0.9) \times 10^{13}$ rad/s is believed to be due to oscillatory motions of the centre of gravity of the molecule in its cage of neighbours.

Measurements perfomed on partially deuterated glycerine $C_3H_5(OD)_3$ (Fig. 7) showed that in glycerine the assignment of the peaks at $\omega = 1.4$, 2.7 and 4×10^{13} rad/s due to protons bound to carbon atoms is correct, as well as the interpretation that the broad maximum at $\omega \simeq 10 \times 10^{13}$ rad/s is due to

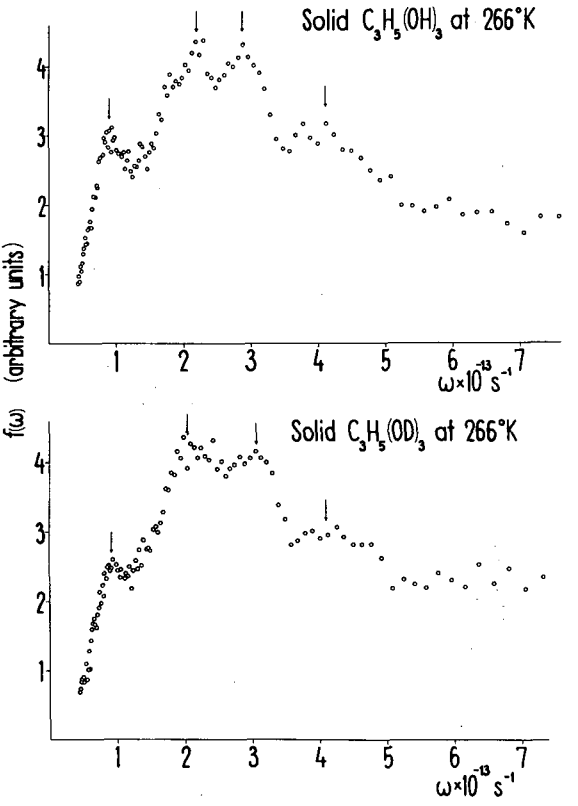

Fig. 7

The low-frequency part of the frequency spectra obtained from natural and partially deuterated glycerine in the glass state

the proton in the OH group. The scattering from the deuterons is not visible from a thin (0.2-mm thick) sample; only the scattering from the protons is registered.

It is also of interest to note that when the temperature is strongly increased such that the viscosity of the medium comes into the region of 1 cP a pronounced peak appears at $\omega \simeq (0.5\text{-}0.9)\times 10^{13}$ rad/s (Fig. 8). Such an effect could result from a strong diffusive component (not shown) in $f(\omega)$ for small ω which could make the peak appear more intense. One may also compare the results with those obtained on water and with the predictions of the stochastic model by Rahman, Singwi and Sjölander, which may be applied only to the motion of the centre of gravity of the molecule.

It should be noted that with the interpretation given here almost all of $f(\omega)$ refers to motions within the molecule. Only the small peak at $(0.5\text{-}0.9)\times 10^{13}$ rad/s in pentane, oleic acid and glycerine and the hindered rotation peak at 10×10^{13} rad/s in glycerine are assumed to correspond to intermolecular degrees of freedom.

The analysis of the quasi-elastic peak has given line-width data $\Delta E = f(\kappa^2)$ of which some examples are given in Fig. 9. The larger line widths of gly-

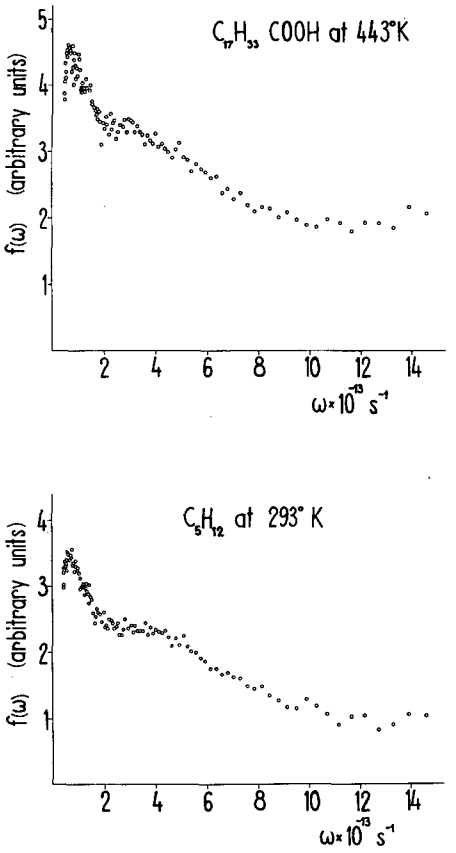

Fig. 8

Shape of the frequency distributions in oleic acid and pentane at high temperatures (close to the boiling points)

cerine at 453°K were obtained with a crystal spectrometer and 2.25-Å ingoing neutron wavelength, all other data being obtained from cold neutron measurements. It is important to notice that line broadenings were observed even in the solid phase for glycerine and oleic acid showing that the broadening is at least in some cases not caused by true diffusive motions but probably by partial rotational jumps over an angle of 120° of CH_2 groups. This explanation is in conformity with the assignment of peaks in the frequency distribution f(ω). As shown by the figure the line-width curves show the typical saturation character even for the low viscosity case of glycerol at 453°K, where $\eta = 0.021$ p. From the tangent at the origin to the line-width curves values of D are derived and from the saturation value of ΔE for large κ-values one obtains values of τ_0. It is observed (Fig. 10) that the D-values thus obtained for glycerine show two regions: one region for $T < 400$°K, where one derives an activation energy E_0 by assuming

$$D = D_0 e^{-E_0/kT} \tag{18}$$

of 3 kcal/mole, and another region for T > 400°K where the average value of E_0 = 7.5 kcal/mole. This value of E_0 for the temperature range 450 > T

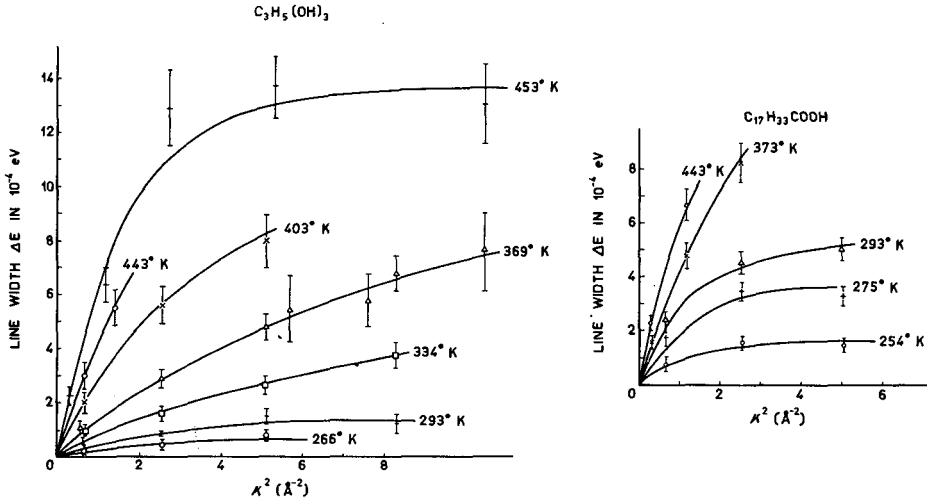

Fig. 9

Observed line widths in glycerine and oleic acid in solid and liquid phases
(Solid glycerine at 266°K and solid oleic acid at 254 and 275°K)

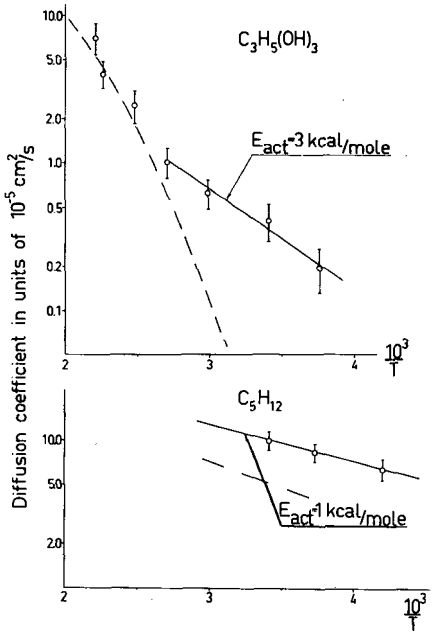

Fig. 10

"Diffusion coefficients" derived from observations
of the type illustrated in Fig. 9

> 400°K is in agreement with direct measurement [41] of the average activation energy for viscosity in this range, assuming $\eta = \eta_0(T)\ e^{E_0/kT}$. Also the absolute value of D agrees with the value calculated from the measured η-value and the Eyring formula (Eq. (17)).

The values of τ_0 derived from the line-width curves show an interesting variation (Fig. 11). The relaxation times all decrease with increasing

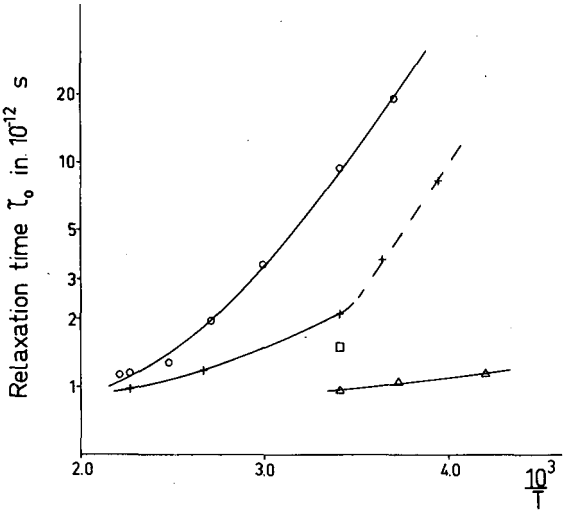

Fig. 11

Relaxation times for the scattering protons in water, glycerine, oleic acid and pentane.

□ H_2O
○ $C_3H_5(OH)_3$
\+ $C_{17}H_{33}COOH$
△ C_5H_{12}

temperature and seem to more or less saturate at $\tau_0 = 10^{-12}$s when the viscosity comes into the region of 0.01 P. Let us now assume that in the case of glycerine the line broadening for large κ-values is caused by a rotational jump of a CH_2OH group round a C–C bond [42] such that τ_0 is considered as a mean lifetime of a hydrogen bond which has to be broken to allow the rotation of the considered group. It is then logical to assume that

$$\tau_0 = \tau_{hr}\ e^{E_0/kT}, \tag{19}$$

where τ_{hr} is the inverse value of the hindered rotation frequency $\omega_{hr} = (10\text{–}11) \times 10^{13}$ rad/s. If the observed values of ω_{hr} and the value of τ_0 are used one obtains for E_0 a value of 3 kcal/mole in the temperature region $T < 400$°K and 2.5 kcal/mole for $T > 400$°K. The value of 3 kcal/mole is in excellent agreement with the value obtained separately from the D-value at small κ-values and equal to the energy of an H-bond. If it is assumed that the neutron is really observing the motion of the whole glycerine molecule for $T > 400$°K, it is natural to assume that three H-bonds have to be broken

to allow a diffusion of the molecule. The energy necessary to break three bonds each of an energy of 2.5 kcal/mole would be 7.5 kcal/mole, in excellent agreement with the observed activation energy for the diffusion constant for T > 400°K. Such a conclusion would also mean that the viscosity η could be described by

$$\eta = c \cdot e^{3E_0/kT} = c \cdot \tau_0^3 \qquad (20)$$

This makes a strong test of this analysis as η is measured quite separately with classical methods. As seen in Fig. 12 where the measured η is given

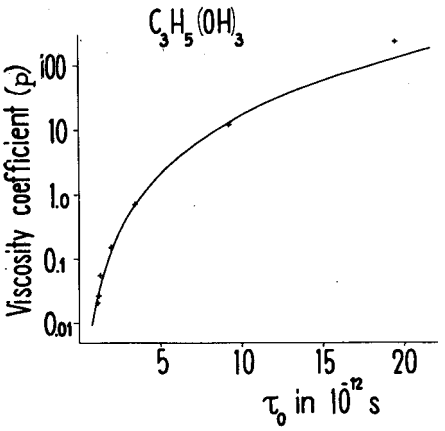

Fig. 12

Observed viscosity as a function of observed relaxation time
Full curve corresponds to the relation $\eta = 1.74 \times 10^{34}\ \tau_0^3$.

as a function of the measured τ_0, a good fit is obtained with a calculated $\eta = c \cdot \tau_0^3$ curve which strongly supports these ideas.

One may say that in the case of glycerine the line broadening is caused by an intramolecular rotation, which is hindered by the intermolecular binding potential.

In the case of pentane and liquid oleic acid it is reasonable to assume that the line broadening is caused by the partial rotation of a CH_2 group. In these cases the situation is never reached that the calculated D-value reaches the observed "neutron value". The uncertainty in the D-values is too large to permit a closer analysis but an activation energy of the order of 1 kcal/mole is obtained from the temperature variation of the D-values. This is in reasonable agreement with the value of 0.45 kcal/mole obtained in Raman spectroscopic measurements for the basic activation energy for formation of rotational isomers.

If it is assumed that the CH_2 groups perform hindered rotation round a C-C axis during an average time τ_0 and thereafter jump to another position (a new rotational isomeric state is formed) with an activation energy of $nE_0 \simeq n \times 0.45$ kcal/mole, it would be possible to calculate the hindered rotational frequencies ω_{hr} from

$$\tau_0 = \frac{2\pi}{\omega_{hr}} e^{nE_0/kT}, \tag{21}$$

As τ_0 for pentane and high temperature oleic acid is $\sim 10^{-12}$s this gives for n = 1, 2, 3 and 4 the frequencies 1.4, 2.9, 6.4 and 13.8×10^{13} rad/s, respectively. It is noticed that the first two values happen to coincide rather well with the observed peaks in $f(\omega)$ at $\omega = 1.3$ and 2.7×10^{13} rad/s. In pentane and oleic acid faint peaks are also observed at $\omega = (6-7) \times 10^{13}$ and $\omega = (13-14) \times 10^{13}$ rad/s, respectively.

The D-values obtained in this way for pentane, oleic acid and glycerine for T < 400°K are not true diffusion constants but rather a measure of proton transport by rotational motions within a molecule. The fact that the neutron is observing internal molecular motions and not intermolecular motions is demonstrated, if the line-width data are plotted on a reduced scale (Fig. 13).

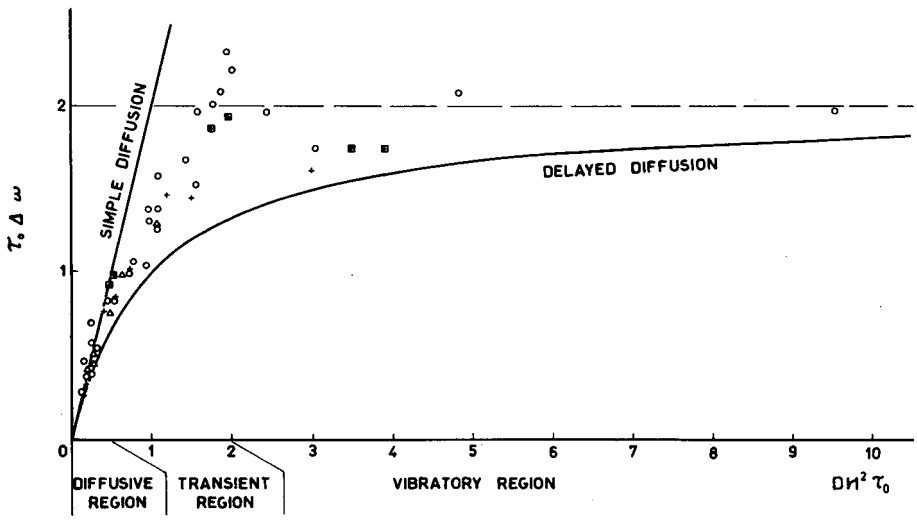

Fig. 13

Generalized line-width curve.

○ $C_3H_5(OH)_3$
\+ $C_{17}H_{33}COOH$
⊞ $C_{17}H_{33}COOH$ (solid)
△ C_5H_{12}

Instead of plotting $\Delta E = \hbar\Delta\omega$ versus κ^2 one plots $\Delta\omega\tau_0$ versus $D\kappa^2\tau_0$, both quantities being dimensionless. In this reduced plot all the measured points fall along one single curve. It is also found that the experimental values obtained from solid oleic acid and glycerol in the glass state fall along the same curve as those values obtained from the liquid state of glycerol, pentane and oleic acid. In order to understand this plot it is worth while to compare it with a discussion given by de GENNES [18]. Neglecting the possible vibrational motions of the scattering atoms he gives a similar reduced plot of the width $\Delta\omega$ of the expected scattered neutron distribution measured in units of a correlation frequency Ω_0 as a function of the variable

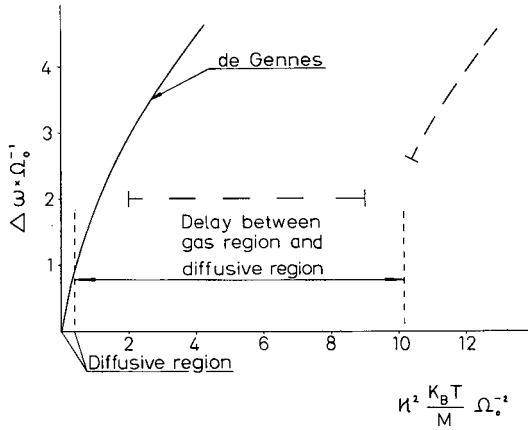

Fig. 14

General line-width curve predicted by de Gennes
neglecting the vibratory motion of atoms compared to the experimental line-width curve

$(\kappa^2 k_B T/M\ \Omega_0^2)^{\frac{1}{2}} \cdot \Omega_0^{-1}$ appears as a correlation time for velocities of atoms in the medium (Fig. 14). In the case of simple Langevin diffusion we have

$$k_B T/M = D/t_\beta, \tag{22}$$

where t_β is a very short delay time before diffusion sets in. It is a measure of the collision time itself. In the simple Langevin case we should expect that $\Omega_0^{-1} = t_\beta$. Thus $\kappa^2 k_B T/M\ \Omega_0^2 = \kappa^2 D t_\beta$ for Langevin diffusion. As $k_B T/M = \bar{v}^2$ ($\bar{v}$ calculated from the most probable energy $E_0 = \frac{1}{2} k_B T$) it is seen that

$$\kappa^2 \frac{k_B T}{M} = \kappa^2 \bar{v}^2 \simeq \frac{1}{t_{obs}^2}, \tag{23}$$

where t_{obs} is the neutron observation time. We thus see that the abscissa is t_β/t_{obs}. When $t_\beta/t_{obs} < 1$ the neutron observes diffusion behaviour and when $t_\beta/t_{obs} > 1$ the neutron observes gas behaviour.

In the hydrogenous liquids we are now dealing with there exists a long delay period τ_0 during which the observed particle performs vibratory motions (the flat position of Fig. 13). In this case $\Omega_0^{-1} = \tau_0$. The fact that not all modes of motion are diffusive is considered if in Eq. (20) above a delay time $f t_\beta$ ($f > 1$) is accepted

$$k_B T/fM = D/f t_\beta. \tag{24}$$

This leads to $\kappa^2 k_B T/M\ \Omega_0^2 \rightarrow \kappa^2 [D/(f t_\beta)]\ \tau_0^2$. But $f t_\beta$ is just τ_0 so that the abscissa $\kappa^2 k_B T/M\ \Omega_0^2$ reduces to $\kappa^2 D \tau_0$ which has been used in Fig. 13. $1/\kappa^2 D$ has the meaning of the neutrons interaction time t_{obs} and the abscissa as before means τ_0/t_{obs}. The following facts are found:

(i) If $\kappa^2 D \tau_0 < 0.5$ diffusive behaviour is observed. As for high temperature liquids $\tau_0 \simeq 10^{-12}$ s we find that only for times longer than 2×10^{-12} s is pure diffusive behaviour observed.

(ii) If $0.5 < D\kappa^2\tau_0 < 2$ there exists a transient region in which both diffusive and vibratory motion are participating. Actually the average of the observed variation of $\Delta\omega\tau_0$ in this region may be described by $\Delta E = 0.9\hbar D\kappa^2 + 0.4\hbar/\tau_0$. One may see that a diffusive as well as a vibratory term is present. Most of the cold neutron studies fall in this region. If $\tau_0 = 10^{-12}$ s this transient region corresponds to a time range between 2×10^{-12} and 5×10^{-13} s.

(iii) If $2 < D\kappa^2\tau_0 <$ at least 10, a flat region exists in which $\Delta\omega\tau_0 \simeq 2$ which means $\Delta E = 2\hbar/\tau_0$, the saturation value for vibratory behaviour when the correlation or residence time is τ_0. For a high temperature liquid with $\tau_0 \sim 10^{-12}$ s this corresponds to a time region between 10^{-13} and 5×10^{-13} s.

(iv) Only if $D\kappa^2\tau_0 >$ at least 10 is the typical gas behaviour possible. As the limiting value of τ_0 for high temperature liquids seems to be $\sim10^{-12}$ s one may see that the neutron is still observing vibratory behaviour when its interaction time is only 10^{-13} s. $1/D\kappa^2 \simeq t_{obs} \simeq \sqrt{M/k_B T\kappa^2} = 1/\bar{v}\kappa$ has to be $< 10^{-13}$ s before only the gas behaviour is observed. This is to be compared with observations on liquid sodium (Fig. 18) where the gas-like behaviour of the atoms in this liquid is approached for times of the order of 10^{-13} s.

The fact that the experimental results for the proton motion in the solid and the liquid phases agree in magnitude means that the same mechanism for motion is observed in both cases and must be of intramolecular origin. This mechanism is probably the partial rotational motions just discussed.

Probably the very general curve of Fig. 13 has a considerable range of validity. Such a general line-width behaviour should be expected for all substances and for solids, liquids and gases. The only feature that would be expected to vary is the length of the plateau giving a measure of the degree of solid-like behaviour (compare Fig. 14). In a solid it would be long; in an associated liquid shorter; in an almost ideal liquid, such as for instance liquid argon, it might be almost non-existent and in a gas it should disappear.

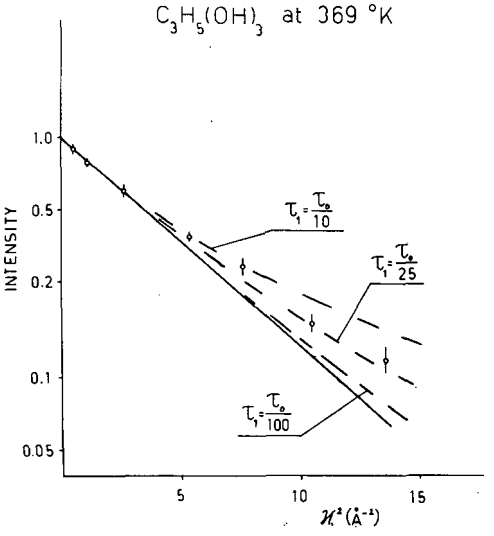

Fig. 15

Angular distribution $d\sigma/d\Omega$ of quasi-elastically scattered neutrons in glycerol. The dashed lines were calculated by use of Eq. (25).

Angular distribution measurements $d\sigma/d\Omega$ including the integration of scattered intensity over only the quasi-elastic peak may give interesting information. Such measurements may for instance be performed with a crystal monochromator to select for instance 2.25-Å wavelength, the scattered spectrum being energy analysed by the time-of-flight technique. The quasi-elastic peak is then easily separated and its area may be plotted versus κ^2. Such a procedure will to a certain extent be able to select between various models. This is exemplified by an experiment of this type performed on glycerine at 369°K (Fig. 15). It is found that the observed intensity may not be described by a straight line, $\ln I = <r^2/6>\kappa^2$, as it should if the quasi-elastic peak described the harmonic hindered rotation of an OH proton in the hydrogen bond. Apparently the finite lifetime of the proton in its vibratory position must play a role. If it is assumed that the jump diffusion model may be used to describe rotational jumps it should be possible to fit the observed points with the integrated formula $d\sigma/d\Omega = \oint (d^2\sigma/d\Omega d\omega)d\omega$. If this integration is performed on the Singwi-Sjölander jump diffusion cross-section [1] one obtains

$$\frac{d\sigma}{d\Omega} \sim \frac{e^{-2W}}{1+(\tau_1/\tau_0)} \left(\frac{\tau_1}{\tau_0} e^{2W} \cdot b + c\right) \frac{1}{[f+(f^2-4b_g^2)^{\frac{1}{2}}]^{\frac{1}{2}}+[f-(f^2-4b_g^2)^{\frac{1}{2}}]^{\frac{1}{2}}}, \quad (25)$$

where

$$b = 1+\kappa^2 D_1\tau_1 - e^{-2W}$$

$$c = 1+\kappa^2 D_1\tau_1 + 2(\tau_1/\tau_0) + (\tau_1/\tau_0)^2 \cdot e^{2W}$$

$$f = (1+\kappa^2 D_1\tau_1)^2 + (\tau_1/\tau_0)^2 + 2(\tau_1/\tau_0)\cdot e^{-2W}$$

$$g = (\tau_1/\tau_0)^2, \quad D_1\tau_1 = D\tau_0\,[1+(\tau_1/\tau_0)]$$

τ_1 = average time spent in the diffusive jump. The value of the Debye-Waller factor $2W = (<r^2>/6)\kappa^2$ is obtained from the slope of the measured curve at $\tau_0 = 2\times 10^{-12}$ s; it is possible to calculate $d\sigma/d\Omega$ for various values of τ_1. As will be seen in the figure τ_1 appears as a rather sensitive parameter such that in this particular case a fit is obtained to the measured intensity distribution for $\tau_1 = \tau_0/25 = (8\pm 3)\times 10^{-14}$ s. It is interesting to note that this value of τ_1 is also found for all the other temperatures in the range 369-453°K. This value comes very close to the inverse value of the hindered rotation frequency which is $2\pi \times 10^{-14}$ s. The flip-over of a CH_2OH group occurs very rapidly. It also should be noticed that this is a typical non-Gaussian behaviour of the angular distribution.

To connect the neutron relaxation times τ_0 to other relaxation studies on liquid glycerine the results on dielectric [43] and ultrasonic [44] relaxation time studies are given in Fig. 16. It is found that the dielectric relaxation time is more than two orders of magnitude longer than τ_0 at room temperature and the ultrasonic relaxation time is about one order of magnitude larger. On the other hand both curves intersect the neutron curve in the temperature region $T > 400$°K. This behaviour may be understood if the dielectric relaxation time is associated with the mean lifetime of a cluster of molecules whereas the ultrasonic is associated with the relaxation of one single molecule returning by diffusion to the position it had before the compressional wave was applied.

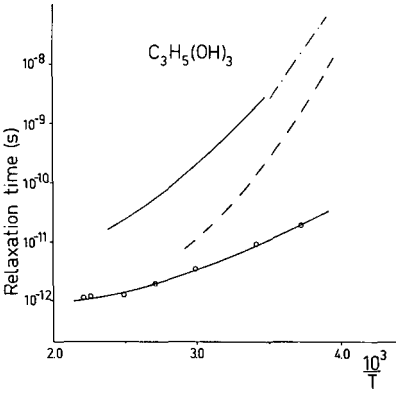

Fig. 16

Relaxation times in glycerine obtained by nuclear magnetic, dielectric and ultrasonic relaxation studies compared to the neutron data

—— NMR
—·— Dielectric
- - - Ultrasonic
•——• Neutron data

(c) Liquid sodium

As exemplified above the neutron scattering picture obtained from molecular liquids is indeed very complex. The results obtained from liquid metals are considerably easier to handle. In this case it is to be expected that the derivation of the intermediate scattering function $F_s(\kappa, t)$ and even of $G_s(r, t)$ and $G_d(r, t)$ might be possible and fruitful.

It is interesting to compare two experiments performed on liquid sodium: one which [14] used cold ingoing neutrons $E \sim 5$ meV and the previously described separation method to analyse the data, and the other [15] which used neutrons of 25- 70- and 100-meV energy combined with a derivation of $F_s(\kappa, t)$ and thus of the interesting width function $\rho(t)$. Both investigations were performed at temperatures between 100 and 200°C. The main results of the cold neutron experiments are:

(i) A fit of the Egelstaff-Schofield cross-section formula [3] to the quasi-elastic peak at such low κ-values (scattering angles of 30°, 45° and 60° so that $(1+\gamma(\kappa))$ is small) gave numerical values for the parameter c which may be interpreted as equivalent to, although not identical with, the delay time τ_0 before diffusion begins. Values obtained for c were in the region $(1 - 1.5) \times 10^{-12}$ s.

(ii) An attempt to use the cross-section based on the convolution approximation [17] to interpret data obtained at larger κ-values (75° and 90° scattering angles) showed that no good fit to the data could be obtained.

(iii) By comparing the inelastically scattered spectra from the solid and the liquid phases it was shown that the difference is very small. It was shown that the inelastically scattered spectrum could relatively well be described by the one-phonon incoherent cross-section formula using an earlier calculated frequency spectrum.

In conclusion one might say that this experiment clearly demonstrated the solid-like character of liquid sodium.

In the other experiments as many as eight scattering angles between 16.3° and 84.7° were used together with the three higher ingoing neutron energies mentioned above. A large region of energy-momentum space (ω,κ) was thus covered and a Fourier transform involving integration over the ω co-ordinate of the data without involving too long extrapolations of the observed cross-section values is made to give the intermediate scattering function which in the Gaussian approximation directly gives the width function $\rho(t)$. It is interesting to notice the form of the cross-section (or the scattering law $S(\kappa,\omega)$) as a function of κ (Fig. 17). It is seen that for κ-values lower than 6 $Å^{-1}$ and for ω-values lower than about 10^{13} rad/s there is a pronounced coherence effect causing peaks to occur for those κ-values where the liquid structure factor $(1+\gamma(\kappa))$ had its maxima. This structure factor

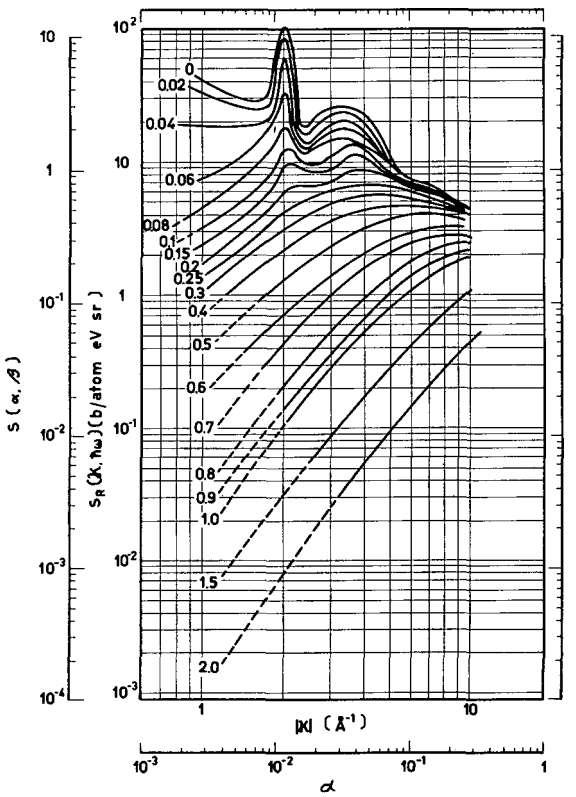

Fig. 17

Scattering law for sodium at 100°C

$\beta = \hbar\omega/0.0321 = (E - E_0)/k_BT$

$\alpha = \hbar^2\kappa^2/2Mk_BT$

$M = 23\ m_n$

$k_BT = 0.0321$ eV

flattens out at $\kappa \simeq 5$ or 6 Å^{-1}. For larger κ-values the interference contribution to the scattering is small and therefore only those larger κ-values are considered in the determination of $\rho(t)$. This is equivalent to restricting the observation range of the neutron $\Delta x > 1/\kappa$ to relatively small values and therefore $\rho(t)$ is not obtained in the long time region where the diffusive motions should occur. The values of $\rho(t)$ thus obtained are given in Fig. 18.

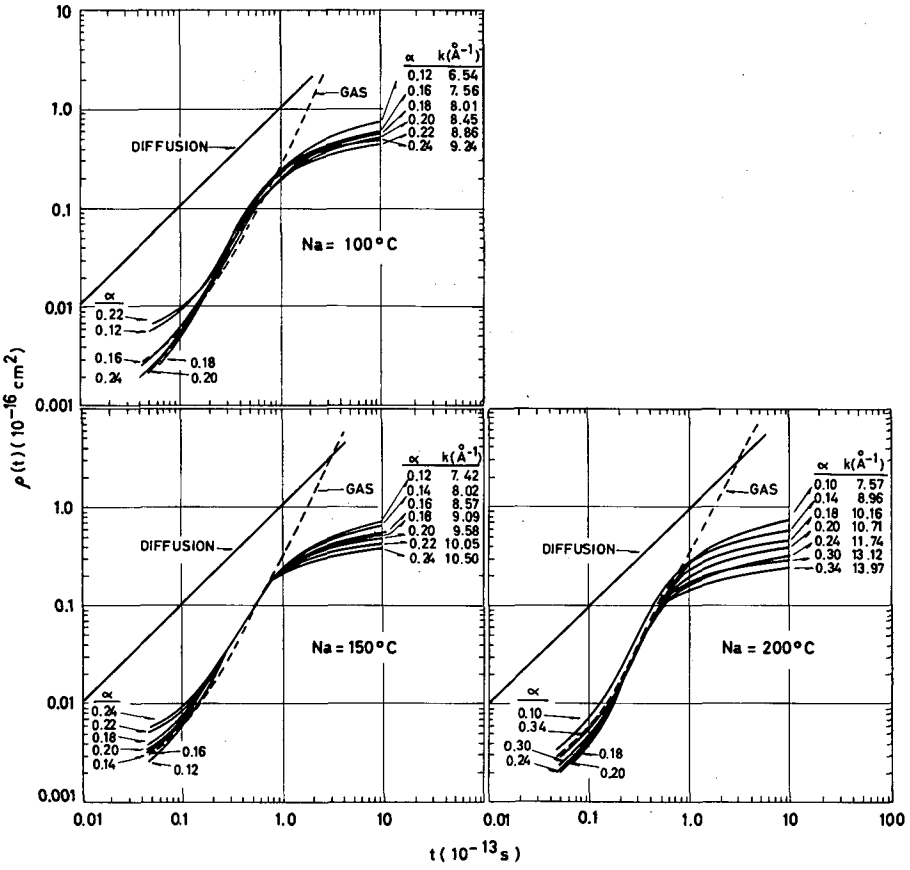

Fig. 18

Time-dependent width functions $\rho(t)$ for sodium obtained by Fourier transformation of the scattering law assuming a Gaussian for the self-correlation function

—— Experiment $e^{(-\kappa^2/4)\rho(t)} \exp = 2\int_0^\infty \cos(\beta\tau) S(\alpha,\beta) d\beta$

- - - Gas $\rho(t) = \hbar^2/2Mk_BT + (2k_BT/M)t^2$

—— Diffusing atom $\rho(t) = 4Dt$

$\alpha = \hbar^2 k^2/2Mk_BT$; $\tau = (k_BT/\hbar)t$

The important features of this $\rho(t)$ function are:

(i) For times $t < 10^{-13}$ s it shows the expected gas-like behaviour. The atom spreads out from the origin as $\langle r^2 \rangle = (vt)^2$. In a time region between

10^{-13} and at least 10^{-12} s it flattens out and shows a typical solid-like behaviour. The value of $<r^2> = \rho(t)$ in this region determines a Debye-Waller factor. It is found that in 10^{-12} s the atoms have spread out an average distance of only 0.87 Å which is small compared to the nearest-neighbour distance 3.83 Å. The atom finds itself still within the cage of neighbours after this time and diffusive behaviour is not expected until a longer time has elapsed.

(ii) The fact that the various $\rho(t)$ curves obtained for different κ-values do not agree in the "solid-like" region $10^{-13} < t \leq 10^{-12}$ s indicates that here the Gaussian approximation may not be quite correct. On the other hand the coincidence of the curves in the "gas-like" region $t < 10^{-13}$ s shows that here the Gaussian model is correct, a fact already proved theoretically [17, 19].

In conclusion it is interesting to note that both the cold neutron experiment and the higher energy neutron experiment indicate the same fact: there is a delay before diffusion sets in which is at least of the order of 10^{-12} s. During this time a solid-like behaviour develops, a fact which to a certain extent justifies the use of approximate formulas like the phonon expansion formula. The slight upward slope of the $\rho(t)$ curve indicates, however, that the multiphonon terms might be of importance as it is just the difference $\rho(t) - \rho(\infty)$ which in the form of a series expansion gives rise to the phonon terms.

(d) Coherently scattering monatomic liquids

Experiments have been performed on liquid tin [9], lead [10] and aluminium [11] which more or less clearly showed the existence of coherent, collective scattering also in the case of a liquid.

Experiments on liquid lead were performed with various ingoing neutron energies and at various κ-values such that a double Fourier transform could be made of the data. In this case, as well as for the sodium experiment described above, no corrections were performed for the finite width of the primary neutron "line". The resulting $G_s(r, t)$ and $G_d(r, t)$ function showed the expected smearing out with increasing time. From the width of $G_s(r, t)$ a $\rho_s(t)$ function was derived and from the width of the first peak in $G_d(r, t)$ a $\rho_d(t)$ width function was obtained. It was shown that $\rho_s(t)$ exhibited a behaviour similar to the one obtained above for sodium whereas $\rho_d(t)$ starting from a larger finite value at $t = 0$ after a time of the order of 3×10^{-13} s almost coincided with $\rho_s(t)$. A non-diffusive and more solid-like behaviour for more than 10^{-12} s was established for liquid lead.

The experiment on liquid tin using 6.25-Å neutrons showed that there possibly exists a coherent selection rule $\kappa + q \geq 2\pi\tau \geq \kappa - q$ in the liquid as well as in the solid polycrystalline case, in accordance with the theoretical outlines given by the Eqs. (13) and (14).

A similar experiment on liquid aluminium [11] showed very definitely that the inelastically scattered spectrum from the liquid is almost identical with the spectrum obtained from the polycrystalline solid. This indicates that round each atom of the liquid there exists a region of a radius of several atomic distances, a correlation range, within which collective, coupled vibrations similar to the phonons exist.

(e) Liquid argon

Of particular interest are the neutron scattering experiments performed on liquid argon. Such scattering experiments have been performed both in the liquid and in the polycrystalline, solid phase [12, 13]. The results obtained from the liquid phase indicate clearly the existence of collective scattering effects. This is shown both in the variation of the width of the quasi-elastic peak which shows the typical wavy character predicted by de GENNES [18] and in the inelastically scattered spectra, which when plotted versus κ for constant ω show the typical broad peaks also observed directly in liquid sodium. No values of the correlation time τ_0 have been obtained experimentally for liquid argon but computations have shown [27] that probably there is no plateau in the width function $\rho(t)$ for this case. The shape of the calculated generalized frequency distribution shows that a deviation from simple Langevin diffusion exists but is small. These measurements and calculations indicate that liquid argon rather closely approximates an ideal liquid although the deviations are large enough to give rise to a certain solid-like behaviour. (See [45] for a detailed report on argon.)

4. CONCLUSION

Several other interesting neutron experiments have been performed on liquids and it is interesting to note that in none of the cases studied so far has one found a simple diffusive behaviour of the liquid following directly upon the gas behaviour for short times $t < 10^{-13}$ s. There seems to exist a universal minimum delay time of $\sim 10^{-12}$ s in the condensed state due to the high value of the density of the liquid as compared to a gas. During this time a solid-like vibratory behaviour develops. The neutron scattering method also appears valuable in the study of intermolecular and intramolecular motions of molecules in complex liquids. Details of the hydrogen bond mechanism may be studied by the neutron technique. A connection to other experimental techniques is obtained by a method similar to that of the Raman and infrared spectra and the inelastically scattered neutron spectra, and a connection to ultrasonic and dielectric relaxation studies may be established via the studies of the relaxation phenomena causing the width of the quasi-elastically scattered neutron spectrum.

REFERENCES

[1] SINGWI, K. S. and SJÖLANDER, A., Phys. Rev. 119 (1960) 863-71.
[2] SCHOFIELD, P., "Fluctuation, relaxation and resonance in magnetic systems", Scottish University Summer School 1961, (TER HAAR, D., Ed.) Edinburgh & London (1962) 207-17.
[3] EGELSTAFF, P. A. and SCHOFIELD, P., Nucl. Sci. Engng 12 (1962) 260-70.
[4] OSKOTSKII, V. S., Soviet Phys. - Sol. State 5 (1963) 789-91.
[5] EGELSTAFF, P. A., Adv. Phys. 11 (1962) 203-32.
[6] EGELSTAFF, P. A., Inelastic Scattering of Neutrons in Solids and Liquids, IAEA, Vienna (1961) 25-38.
[7] RAHMAN, A., SINGWI, K. S. and SJÖLANDER, A., Phys. Rev. 126 (1962) 997-1004.

[8] INTERNATIONAL ATOMIC ENERGY AGENCY, Inelastic Scattering of Neutrons in Solids and Liquids, IAEA, Vienna (1961) 642 pp. and 2 vols. (1963) 809 pp.
[9] COCKING, S.J. and GUNER, Z., Inelastic Scattering of Neutrons in Solids and Liquids I IAEA, Vienna (1963) 237-48.
[10] BROCKHOUSE, B.N. and POPE, N.K., Phys. Rev. Lett. 3 (1959) 259-62.
[11] LARSSON, K.-E., DAHLBORG, U. and JOVIC, D., "Collective atomic motions in liquid aluminium studied by cold neutron scattering", these Proceedings II.
[12] DASANNACHARYA, B.A. and RAO, K.R., Neutron scattering from liquid argon, unpublished report (1964).
[13] KROÓ, N., BORGONOVI, G., SKÖLD, K. and LARSSON, K.-E., Phys. Rev. Lett. 12 (1964) 721-22.
[14] COCKING, S.J., Inelastic Scattering of Neutrons in Solids and Liquids I IAEA, Vienna (1963) 227-36.
[15] RANDOLPH, P.D., Phys. Rev. 134 5A (1964) 1238-48.
[16] SJÖLANDER, A., Ark. Fys. 14 (1958) 315-71.
[17] VINEYARD, G.H., Phys. Rev. 110 (1958) 999-1010.
[18] de GENNES, P.G., Physica 25 (1959) 825-39.
[19] RAHMAN, A., SINGWI, K.S. and SJÖLANDER, A., Phys. Rev. 126 (1962) 986-96.
[20] EGELSTAFF, P.A., Inelastic Scattering of Neutrons in Solids and Liquids I IAEA, Vienna (1963) 65-80.
[21] LARSSON, K.-E. and DAHLBORG, U., Reactor Sci. Techn. 16 (1962) 81-89.
[22] VAN HOVE, L., Phys. Rev. 95 (1954) 249-62.
[23] WEINSTOCK, R., Phys. Rev. 65 (1944) 1-20.
[24] EGELSTAFF, P.A., AERE, Rpt. N/R 1164, Harwell (1953).
[25] EGELSTAFF, P.A., AERE, Rpt. N/R 4101, Harwell (1962).
[26] RAHMAN, A., Correlations in motion of atoms in liquid argon, unpublished report.
[27] SINGWI, K. and FELDMANN, G., "Coherent scattering of slow neutrons by liquid sodium", these Proceedings II.
[28] BROCKHOUSE, B.N., Nuovo Cim., 9 (Suppl.) Serie X, (1958) 45-71.
[29] BROCKHOUSE, B.N., Phys. Rev. Lett. 2 (1959) 287-89.
[30] SAKAMOTO, N., BROCKHOUSE, B.N., JOHNSON, R.H. and POPE, N.K., Conf. on Magnetism and Neutron Diffraction, Kyoto (Sept. 1961).
[31] HUGHES, D.J., PALEVSKY, H., KLEY, W. and TUNKELO, E., Phys. Rev. 119 (1960) 872-82.
[32] LARSSON, K.-E., HOLMRYD, S. and OTNES, K., Inelastic Scattering of Solids and Liquids in Neutrons, IAEA, Vienna (1961) 329-41.
[33] STILLER, H., "Proton motions in acid aqueous solutions", these Proceedings II.
STILLER, H. and DANNER, H.R., Inelastic Scattering of Neutrons in Solids and Liquids, IAEA, Vienna (1961) 363-73.
[34] BAJORIK, A., GOLIKOV, V.V., ZUKOVSKAYA, L., SHAPIRO, F.L., SHKATULA, A. and JANIK, E.A., Inelastic Scattering of Neutrons in Solids and Liquids I IAEA, Vienna (1963) 383-88.
[35] LARSSON, K.-E. and DAHLBORG, U., Inelastic Scattering of Neutrons in Solids and Liquids I IAEA, Vienna (1963) 317-40.
[36] EGELSTAFF, P.A., HAYWOOD, B.C. and THORSON, I.M., Inelastic Scattering of Neutrons in Solids and Liquids I IAEA, Vienna (1963) 343-56.
[37] LARSSON, K.-E. and DAHLBORG, U., Physica 30 (1964) 1561-99.
[38] SHEPPARD, N. and SZASZ, G.J., J. Chem. Phys. 17 (1949) 86-92.
[39] RASMUSSEN, R.S., J. Chem. Phys. 16 (1948) 712-27.
[40] SAN-ICHERO MIGUSHIMA and TAKEHIKO SIMANOUTI, J. Amer. chem. Soc. 71 (1949) 1320-24.
[41] MOHAMMAD NASEEM and MAZHAR MAHMOOD OURASHI, Pakistan J. Sci. industr. Res. 1 (1958) 197-206.
[42] LARSSON, K.-E. and SINGWI, K.S., Phys. Lett. 3 (1962) 145-47.
[43] Mc DUFFIE, G.E., Jr., and LITOWITZ, T., J. Chem. Phys. 37 (1962) 1699-1705.
[44] PICIRELLI, R. and LITOWITZ, T., J. acoust. Soc. Amer. 29 (1957) 1009-20.
[45] KROÓ, N., BORGONOVI, G., SKÖLD, K. and LARSSON, K.-E., "Inelastic scattering of cold neutrons by condensed argon", these Proceedings II.

DISCUSSION

J.A. JANIK: Could you tell us how you obtain the widths of your quasi-elastic peaks? Obviously the widths obtained from scattered neutron spectra depend to a large extent on the method by which you subtract the low-energy part of the phonon spectrum.

K.-E. LARSSON: We use a number of methods. For example: (a) we compare the top corner of the "beryllium break" with a calculated spectrum. The latter is obtained as a folding of a Lorentzian, a Gaussian and the spectrum EdE with all its details; (b) we measure the width from the half-height of the "beryllium break" to the top and multiply by two; (c) we assume that the cold neutron spectrum is a step-function spectrum, in which case the wing at the bottom of the "beryllium break" must be the same as the rounding off at the top. All the methods give comparable results.

J.J. RUSH: I am interested in the way in which you have determined the activation energy for reorientation of the glycerol molecules. Is there enough information available on the structure of glycerol to calculate a barrier to reorientation, using some average of the observed torsional frequency band and the moment of inertia of the rotating group (assuming perhaps an average cosine potential for the reorientation)? Also, do you have any idea of the average angle through which the molecule flips in breaking the hydrogen bonds?

K.-E. LARSSON: We are still looking for basic explanations to account for our data, and I am therefore unable to give a satisfactory answer to your questions at present.

W. GLÄSER: In the case of solid oleic acid, is the line width of the quasi-elastic peak large compared with the rotational level spacing? If not, you should see discrete lines.

K.-E. LARSSON: The line width of the quasi-elastic peak in the solid state is of the order 0.2 - 0.5 meV. Therefore the level distances for rotational motions ought to be of the order of 0.1 meV or smaller, in order to be considered as building up the quasi-elastic peak. This value might be too small for a level distance.

G. VENKATARAMAN: What technique was used for measuring the intensity of the quasi-elastic peak?

K.-E. LARSSON: A crystal monochromator was used to produce an ingoing wavelength of 2 - 3 Å. The scattered spectrum was analysed by a time-of-flight technique. The only cases used were those in which very simple separation of the quasi-elastic "line" from the broad inelastic spectrum was possible.

A KINETIC DESCRIPTION OF THE VAN HOVE CORRELATION FUNCTIONS

M. NELKIN*, J. M. J. VAN LEEUWEN** AND S. YIP*
CORNELL UNIVERSITY, ITHACA, N. Y., UNITED STATES OF AMERICA

Abstract — Résumé — Аннотация — Resumen

A KINETIC DESCRIPTION OF THE VAN HOVE CORRELATION FUNCTIONS. The Van Hove density correlation function $G(r, t)$ for a classical fluid is written as the integral over momenta of an appropriate one-particle distribution function $F(r, \vec{p}, t)$. A similar procedure gives the self-correlation function $G_S(r, t)$ in terms of a different distribution function $F_S(r, \vec{p}, t)$. It is shown that for moderately dense gases these distribution functions can be calculated from kinetic equations. The kinetic equations are derived from density series expansions of $F(r, \vec{p}, t)$ and $F_S(r, \vec{p}, t)$. For times short compared to the time between collisions the density series can be used directly. For longer times it is necessary to sum an infinite series of terms in order to properly account for the effects of multiple collisions. The summation of the most dominant terms can be carried out in terms of the solution to an integral equation. In the lowest order this equation has the form of a linearized Boltzmann equation including corrections for incomplete collisions. If these corrections are neglected the appropriate equation for $F(r, \vec{p}, t)$ becomes the linearized Boltzmann equation as used in the theory of sound propagation in gases. The appropriate equation for $F_S(r, \vec{p}, t)$ becomes the neutron transport equation. Since these equations are known to have the correct hydrodynamic limit, the long-wavelength behaviour of $G(r, t)$ and $G_S(r, t)$ is thus explicitly derived.

The kinetic equations are directly applicable only to dilute systems; however, they are suitable for a systematic study of dynamical correlations. The essential difference between the two equations is the collisional invariants. In the equation determining $F(r, \vec{p}, t)$ the invariants are particle number, momentum and energy, whereas in the equation determining $F_S(r, \vec{p}, t)$ only the particle number is an invariant. Because the degeneracy of the zero eigenvalue of the associated collision operators in the two cases is different, the hydrodynamic equations appropriate to $G(r, t)$ and $G_S(r, t)$ do not have the same form. The consequences of the two descriptions are demonstrated by model calculations in the context of simple relaxation approximations. The $G_S(r, t)$ calculation leads to a correlation function with non-Gaussian effects which are qualitatively similar to but more pronounced than those calculated by Rahman in liquid argon from molecular dynamics. More refined treatment of the collision integral is now being considered. The $G(r, t)$ calculation shows the expected effects of thermal diffusion and damped sound wave propagation at long wavelengths, and deviates from the conventional hydrodynamic description at short wavelengths.

DESCRIPTION CINÉTIQUE DES FONCTIONS DE CORRÉLATION DE VAN HOVE. La fonction de corrélation de densité de van Hove $G(r, t)$ pour un fluide classique est exprimée par une intégration sur les quantités de mouvements d'une fonction appropriée de distribution à une particule $F(r, \vec{p}, t)$. Par un procédé analogue, on obtient la fonction d'autocorrélation $G_S(r, t)$ exprimée à l'aide d'une autre fonction de distribution $F_S(r, \vec{p}, t)$. Les auteurs montrent que pour des gaz de densité moyenne, ces fonctions de distribution peuvent être calculées à partir d'équations cinétiques. Ces dernières sont établies par des développements en série, selon la densité, de $F(r, \vec{p}, t)$ et $F_S(r, \vec{p}, t)$. Pour des temps courts par rapport aux intervalles entre les chocs, les séries ainsi obtenues peuvent être utilisées directement. Pour des temps plus longs, il faut faire la somme d'une série infinie de termes de manière à tenir compte des effets de chocs multiples. La sommation des termes prédominants peut se ramener à la solution d'une équation intégrale. Dans l'ordre inférieur, cette équation a la forme d'une équation de Boltzmann linéarisée, corrigée pour tenir compte des chocs incomplets. Lorsque ces corrections sont négligées, l'équation appropriée relative à $F(r, \vec{p}, t)$ devient l'équation de Boltzmann linéarisée telle qu'elle

* Work of these authors supported by the United States Atomic Energy Commission under contract AT(30-1)-3326.

** Present address: National Bureau of Standards, Washington, D. C. On leave from the Catholic University of Nijmegen, Netherlands. The work of this author was supported in part by the United States Air Force through the Air Force Office of Scientific Research under grant 324-63.

est employée dans la théorie de la propagation du son dans les gaz. L'équation appropriée relative à $F_S(r, \vec{p}, t)$ devient l'équation de transport des neutrons. Comme on sait que ces équations tendent vers la limite hydrodynamique correcte, on obtient ainsi explicitement le comportement de $G(r, t)$ et $G_S(r, t)$ pour les grandes ondes.

Les équations cinétiques ne s'appliquent directement qu'aux systèmes dilués; cependant, elles conviennent à une étude systématique des corrélations dynamiques. La différence essentielle entre les deux équations est constituée par les invariants de choc. L'équation qui détermine $F(r, \vec{p}, t)$ comporte les invariants suivants: nombre de particules, quantité de mouvement et énergie; en revanche, dans l'équation qui détermine $F_S(r, \vec{p}, t)$, seul le nombre de particules ne varie pas. Comme, dans les deux cas, la valeur propre zéro des opérateurs de choc associés accuse une dégénérescence différente, les équations hydrodynamiques appropriées à $G(r, t)$ et $G_S(r, t)$ n'ont pas la même forme. Les conséquences de ces deux descriptions sont mises en évidence par les calculs à l'aide d'un modèle dans le contexte des approximations de relaxation simples. Le calcul de $G_S(r, t)$ aboutit à une fonction de corrélation ayant des effets non-gaussiens qui sont qualitativement similaires aux effets que Rahman a calculés pour l'argon liquide en se fondant sur la dynamique des molécules, mais sont plus prononcés que ces effets. Les auteurs étudient maintenant la possibilité de soumettre l'intégrale de choc à un traitement plus fin. Le calcul de $G(r, t)$ indique les effets prévus de diffusion thermique et de propagation d'ondes acoustiques amorties pour les grandes ondes, et s'écarte de la description hydrodynamique classique pour les ondes courtes.

КИНЕТИЧЕСКОЕ ОПИСАНИЕ ФУНКЦИЙ КОРРЕЛЯЦИИ ВАН ГОВЕ. Функция корреляции плотности Ван Гове $G(r, t)$ для классической жидкости выражается в виде интеграла по всем моментам соответствующей функции распределения одной частицы $F(r, \vec{p}, t)$. В результате применения аналогичного метода выводится функция самокорреляции $G_s(r, t)$ в рамках функции различного распределения $F_s(r, \vec{p}, t)$. Показывается, что для средних по своей плотности газов эти функции распределения можно рассчитывать из кинетических уравнений. Кинетические уравнения выводятся из расширений ряда плотностей функций $F(r, \vec{p}, t)$ и $F_s(r, \vec{p}, t)$. Для периодов, краткосрочных по сравнению со временем между столкновениями, ряд плотностей можно использовать непосредственно. Для более продолжительных периодов необходимо суммировать бесконечные ряды членов с целью надлежащего учета эффектов многократных столкновений. Суммирование наиболее часто встречающихся членов можно проводить в рамках решения применительно к интегральному уравнению. При наименьшем порядке это уравнение имеет форму линеаризированного уравнения Больцмана, включающего поправки на неполные столкновения. Если пренебречь этими поправками, то соответствующее уравнение для $F(r, \vec{p}, t)$ становится линеаризированным уравнением Больцмана в том виде, в котором оно используется в теории распространения звука в газах. Соответствующее уравнение для $F_s(r, \vec{p}, t)$ становится уравнением для переноса нейтронов. Поскольку известно, что эти уравнения имеют правильный гидродинамический предел, поэтому легко выводится длинноволновая характеристика $G(r, t)$ и $G_s(r, t)$.

Кинетические уравнения непосредственно применимы только к разбавленным системам. Однако они пригодны для систематического изучения динамических корреляций. Существенным различием между этими двумя уравнениями является наличие противоречивых инвариантных величин. В уравнении, определяющем $F(r, \vec{p}, t)$, инвариантами являются количество частиц, импульс и энергия, в то время как в уравнении, определяющем $F_s(r, \vec{p}, t)$, только количество частиц является инвариантом. Ввиду того, что в этих двух случаях снижение нулевого собственного значения связанных операторов столкновения не одинаково, гидродинамические уравнения, соответствующие $G(r, t)$ и $G_s(r, t)$ не имеют одинаковой формы. Значения этих двух описаний демонстрируются расчетами моделей в плане простых приближений ослабления. В результате расчета $G_s(r, t)$ выводится функция корреляции с негауссовыми эффектами, которые подобны в качественном отношении, но более выразительны, чем эффекты, рассчитанные Раманом при изучении молекулярной динамики в жидком аргоне. В настоящее время изучается вопрос о более усовершенствованной обработке интеграла столкновений. Расчет $G(r, t)$ свидетельствует о наличии предполагаемых эффектов тепловой диффузии и распространении затухающих звуковых волн при большой длине волн, и такой расчет отличается от обычного гидродинамического описания при малой длине волны.

DESCRIPCION CINETICA DE LAS FUNCIONES DE CORRELACION DE VAN HOVE. La función de correlación de Van Hove de la desnidad $G(r, t)$ de un fluido clásico se expresa como la integral, a lo largo de impulsos, de una función apropiada de distribución de una sola partícula $F(r, \vec{p}, t)$. Por un procedimiento análogo se obtiene la función de autocorrelación $G_S(r, t)$ a partir de una función de distribución diferente $F_S(r, \vec{p}, t)$. Se demuestra que, en el caso de gases moderadamente densos, estas funciones de distribución pueden calcularse

sobre la base de ecuaciones cinéticas, que se obtienen por desarrollo en serie, en fonción de la densidad, de $F(r, \vec{p}, t)$ y de $F_S(r, \vec{p}, t)$. Para intervalos breves en comparación con el tiempo que media entre los choques, puede utilizarse directamente la serie en función de la densidad. Tratándose de intervalos prolongados es preciso sumar una serie infinita de términos para tener debidamente en cuenta los efectos de los choques múltiples. La suma de los términos predominantes puede efectuarse por resolución de una ecuación integral. En el término de orden inferior, ésta asume la forma de una ecuación linealizada de Boltzmann que comprende las correcciones para tener en cuenta los choques incompletos. Si se desprecian estas correcciones, la ecuación correspondiente a $F(r, \vec{p}, t)$ pasa a ser la ecuación de Boltzmann linealizada tal como se utiliza en la teoría de la propagación del sonido en los gases. La ecuación correspondiente a $F_S(r, \vec{p}, t)$ pasa a ser la ecuación de transporte neutrónico. Como se sabe que estas ecuaciones tienen el límite hidrodinámico correcto, se deduce explícitamente el comportamiento de $G(r, t)$ y $G_S(r, t)$ para grandes longitudes de onda.

Las ecuaciones cinéticas sólo se pueden aplicar directamente a los sistemas diluidos; no obstante, se prestan al estudio sistemático de las correlaciones dinámicas. La diferencia esencial entre las dos ecuaciones son los términos invariables de choque. En la ecuación determinante de $F(r, \vec{p}, t)$, los términos invariables son el número de partículas, el impulso y la energía, mientras que en la ecuación determinante de $F_S(r, \vec{p}, t)$, sólo hay un término de esa clase, a saber, el número de partículas. Como la degeneración del valor propio cero de los operadores de choque asociados es diferente en uno y otro caso, las ecuaciones hidrodinámicas correspondientes a $G(r, t)$ y $G_S(r, t)$ no presentan la misma forma. Las consecuencias de una y otra descripción se ponen de manifiesto por cálculos realizados a base de modelos en el marco de aproximaciones por relajación simple. Del cálculo basado en $G_S(r, t)$ se deduce una función de correlación con efectos no gaussianos que son cualitativamente análogos a los calculados por Rahman para el argón líquido a partir de la dinámica molecular, pero más pronunciados. Los autores están estudiando un tratamiento más depurado de la integral de choque. El cálculo basado en $G(r, t)$ pone en evidencia los efectos previstos de difusión térmica y de propagación amortiguada de ondas sonoras para grandes longitudes de onda, y difiere de la expresión hidrodinámica clásica para pequeñas longitudes de onda.

I. INTRODUCTION

It is generally recognized that the linear response of a system to an external disturbance can be expressed in terms of time-dependent correlation functions in the equilibrium ensemble [1]. If the disturbance is sufficiently slowly varying in space and time, the response is expressible in terms of linear phenomenological equations [2], and the only properties of the system which enter are certain thermodynamic derivatives and transport coefficients. In particular for a one-component classical fluid, the response to a density disturbance [3] is determined by the heat conductivity κ, the shear viscosity η and the second or bulk viscosity ξ. There is general agreement [1] as to the correct expressions of these quantities in terms of correlation functions.

The Van Hove correlation function $G(r, t)$ can be considered in terms of propagation of the density impulse associated with localizing an atom at the origin at time zero. The slow space and time variation of $G(r, t)$ is determined by the behaviour of the double Fourier transform $S(k, \omega)$ for small k and ω. In the limit of small k and ω it is reasonable to calculate $S(k, \omega)$ from the Fourier transformed linearized hydrodynamic equations. The associated hydrodynamic limit of $S(k, \omega)$ has been considered by many authors [4, 5, 6]. The basic idea is that the response to a small density disturbance should obey the same equations whether this disturbance is externally induced or occurs as an equilibrium fluctuation. The basic validity of this idea has been known for a long time from the observation of the Brillouin-

Mandelshtam doublet in the frequency spectrum of light scattered by a liquid [7].

In neutron scattering, however, we are dealing with much more rapid space and time variation. We can no longer assume that the hydrodynamic equations are applicable either to $G(r, t)$ or to the response to an externally induced density disturbance of high frequency and short wavelength. In order to study this problem we need a more detailed kinetic description which is applicable to more rapid phenomena and which goes to the correct hydrodynamic limit. It is an open question whether the response to an external disturbance and to a spontaneous fluctuation remains the same in the kinetic regime.

In trying to understand this problem for simple liquids, we are limited both by a lack of theoretical understanding and by a lack of relevant experimental information. On the theoretical side we have no generally valid kinetic equation for liquids. Experimentally, the response to an external density disturbance can be studied through the propagation of ultrasonic or hypersonic waves. Modern techniques allow these phenomena to be studied up to frequencies of the order of 10^{10} s^{-1}, but there is no information yet available concerning dispersion or deviations from classical sound absorption in monatomic liquids. The response to spontaneous density fluctuation is given by $S(k, \omega)$ as measured by light scattering [7] or neutron scattering. There are not as yet any scattering experiments in simple liquids which can be directly compared with existing or with feasible sound absorption experiments.

In order to understand better the behaviour of $S(k, \omega)$ in the kinetic regime, we have investigated the case of a dilute monatomic gas including the effects of binary collisions. For this case, the propagation of sound for an arbitrary ratio of wavelength to mean free path is known to be described by the linearized Boltzmann equation [8] (i.e. the linearization for small departures from equilibrium of the equation originally proposed by Boltzmann for the kinetic theory of gases). There is experimental information on the propagation of sound in the kinetic regime [9], and there is an extensive literature on approximate methods of solution of the linearized Boltzmann equation [10]. The basic conclusion of the present work is that the same linearized Boltzmann equation for the propagation of sound in gases is applicable to the calculation of $S(k, \omega)$. This is true as long as the effects of incomplete collisions can be ignored.

In section II, we summarize a derivation [11] of kinetic equations appropriate for $G(r, t)$ and $G_s(r, t)$ in a moderately dense classical gas. The formulation is quite general and systematically allows for the effects of incomplete collisions as well as for the inclusion of statistical correlations at zero time. If these effects are neglected the resulting kinetic equations reduce to the linearized Boltzmann equation in the case of $G(r, t)$ and the neutron transport equation in the case of $G_s(r, t)$. In section III we discuss the differences between these two equations. The equation for $G_s(r, t)$ has a collision integral which conserves only particle number, and leads to a hydrodynamic limit which is described by simple diffusion. The collision integral in the equation for $G(r, t)$ conserves energy and momentum as well as particle number, and the associated hydrodynamic limit is described

by the processes of sound wave propagation and heat diffusion. In section IV we consider single-relaxation-time kinetic models which allow analytic solutions of the kinetic equations. These solutions give us a semi-quantitative understanding of the behaviour of $S(k, \omega)$ and $S_s(K, \omega)$ as we go from the hydrodynamic limit (small k) to the free particle limit (large k). Finally in section V we give some general discussion of our results.

II. DERIVATION OF KINETIC EQUATIONS

The Van Hove density correlation functions for an isotropic fluid are

$$G(r, t) = \frac{1}{n} \sum_{i,j} \langle \delta(\vec{q}_i - \vec{q}) \delta(\vec{q}_j(t) - \vec{q}') \rangle, \tag{2.1}$$

$$G_s(r, t) = \frac{1}{n} \sum_{i} \langle \delta(\vec{q}_i - \vec{q}) \delta(\vec{q}_i(t) - \vec{q}') \rangle, \tag{2.2}$$

where n is the equilibrium density, $r = |\vec{q} - \vec{q}'|$, $\vec{q}_i$ and $\vec{q}_i(t)$ are the positions of the i-th molecule initially and at time t, and indices i and j run over all the particles in the system. When these expressions are treated classically, the ensemble average $\langle\ \rangle$ implies

$$G(r, t) = \frac{1}{n} \sum_{i,j} \int dx^N \varphi_1 \ldots \varphi_N \frac{e^{-\beta U}}{Q_N} \delta(\vec{q}_i - \vec{q}) e^{tL} \delta(\vec{q}_j - \vec{q}'), \tag{2.3}$$

where we have assumed an equilibrium distribution appropriate to a canonical ensemble, and

$$\varphi_j = \varphi(p_j) = (\beta / 2\pi m)^{3/2} e^{-\beta p_j^2 / 2m}, \tag{2.4}$$

with $\beta^{-1} = T_0$, the equilibrium temperature in energy units, m is the particle mass, and $\vec{p}_j$ is the momentum of the j-th molecule. The vector $x^N = (x_1 \ldots x_N)$, defined in γ-space, specifies the phase of the system whereas $x_j = (\vec{q}_j, \vec{p}_j)$, defined in μ-space, specifies the phase of the molecule. The potential energy of the system, assuming two-body additive forces, is

$$U(q^N) = \sum_{i<j} \Phi(q_{ij}), \tag{2.5}$$

where $q_{ij} = |\vec{q}_i - \vec{q}_j|$ and Φ is the pair potential. Other symbols in Eq. (2.3) to be defined are the configuration integral

$$Q_N = \int dq^N e^{-\beta U(q^N)}, \tag{2.6}$$

and the Liouville operator

$$L = L^0 + L^1, \tag{2.7}$$

$$L^0 = \sum_i \frac{1}{m} \vec{p}_i \cdot \vec{\nabla}_{q_i}, \tag{2.8}$$

$$L^1 = \sum_{i<j} (\vec{\nabla}_{p_j} - \vec{\nabla}_{p_i}) \cdot \vec{\nabla}_{q_i} V(q_{ij}). \tag{2.9}$$

In using the Koopman time-displacement operator exp(tL) to study the evolution of a system there will appear certain symmetries between the momentum and position of a particle. We can exploit this property by introducing an obvious generalization of the Van Hove functions,

$$f(xx';t) = \frac{1}{n} \sum_{i,j} \langle \delta(x_i - x)\, \delta(x_j(t) - x') \rangle, \tag{2.10}$$

$$f_s(xx';t) = \frac{1}{n} \sum_i \langle \delta(x_i - x)\delta(x_i(t) - x') \rangle. \tag{2.11}$$

It is clear that analogous to $G(r,t)$ f gives the expected number of molecules at the phase point x' at time t, given initially that there was a molecule at x. Once we have a description of f, $G(r,t)$ is immediately determined by integrations,

$$G(r,t) = \int d^3p\, d^3p'\, f(xx';t). \tag{2.12}$$

Normalization of the momentum-impulse function is

$$\int dx'\, f(xx';t) = N\varphi(p), \tag{2.13}$$

which implies

$$\int d^3r\, G(r,t) = N \tag{2.14}$$

and N is the total number of molecules in the system. Correspondingly, in the case of the self-correlation function

$$G_s(r,t) = \int d^3p\, d^3p'\, f_s(xx';t), \tag{2.15}$$

$$\int dx' f_s(xx';t) = \varphi(p), \tag{2.16}$$

$$\int d^3r G_s(r,t) = 1. \tag{2.17}$$

It is not feasible to evaluate the ensemble average $\langle\ \rangle$ directly from the explicit expression (2.3). However, a systematic reduction of this many-body problem can be achieved by using the Ursell expansion [12] of exp(tL). Thus,

$$e^{tL}\delta(x_j - x') = \left[u_t(j) + \sum_{j_1}{}' u_t(jj_1) + \ldots + \frac{1}{(\ell-1)!}\sum_{j_1\ldots j_\ell}{}' u_t(jj_1\ldots j_\ell) + \ldots\right]\delta(x_j - x'), \tag{2.18}$$

where

$$u_t(1) = e^{tL(1)} = e^{tL^0(1)}, \tag{2.19}$$

$$u_t(12) = e^{tL(12)} - e^{tL^0(12)}, \tag{2.20}$$

$$u_t(123) = e^{tL(123)} - e^{t[L(12)+L^0(13)]} - e^{t[L(13)+L^0(2)]} - e^{t[L(23)+L^0(1)]} + 2e^{tL^0(123)}, \tag{2.21}$$

etc.

The prime over each summation sign indicates that the summation indices must not equal j and that they must also not equal each other. Equation (2.18) describes the evolution of the phase of the j-th molecule in the system during time interval t in terms of the evolution of successively larger clusters of molecules. In the leading term molecule j moves freely, and in the next term j interacts dynamically with only one other molecule, and so on. Substituting Eq. (2.18) into Eq. (2.10) we see that for a given term only the phases of the molecules in the set $(jj_1\ldots j_\ell)$ and the phase of the i-th molecule, if i is not already contained in the set, need be considered. The dependence upon all other molecules is eliminated by integration. In analysing the evolution of a cluster two basically different types of interparticle correlation effects should be distinguished. Consider, for example, the case where i is a member of $(jj_1\ldots j_\ell)$; then calling all such contributions in Eq. (2.10) f_a, we find

$$f_a(xx';t) = \frac{1}{n}\sum_{\ell}\frac{1}{\ell!}\int dx^\ell \varphi_1\ldots\varphi_\ell n(1\ldots\ell)\sum_{i,j=1}^{\ell}\delta(x_i - x)u_t(1\ldots\ell)\delta(x_j - x'), \tag{2.22}$$

where

$$n(1\ldots\ell) = \frac{N(N-1)\ldots(N-\ell+1)}{Q_N}\int d^3q_{\ell+1}\ldots d^3q_N e^{-\beta U(q^N)} \tag{2.23}$$

is the usual ℓ-particle distribution function in equilibrium theory. In each cluster each molecule initially has a Maxwellian momentum distribution and is spatially correlated to all the other molecules in the cluster according to $n(1\ldots\ell)$. We shall speak of these molecules as being statistically correlated. The dynamical interactions among the molecules in the cluster which take place during time interval t are described by $u_t(1\ldots\ell)$. So the molecules are also dynamically correlated after time t. In the present treatment, statistical and dynamical effects appear separately; thus they can be treated with different approximations.

For a sufficiently dilute gas all statistical effects can be ignored. The function $n(1\ldots\ell)$ is then replaced by n^ℓ and Eq. (2.22) then becomes a density series. The expression in wavelength-frequency space is ($V = N/n$ is the system volume)

$$f_a(kz\vec{p}\vec{p}') = \frac{1}{V}\int_0^\infty dt\, e^{-zt}\int d^3q\, d^3q'\, e^{i\vec{k}\cdot(\vec{q}-\vec{q}')}\, f_a(xx';t)$$

$$= \frac{1}{V}\sum_{\ell=1}^{\infty}\frac{n^{\ell-1}}{\ell!}\int dx^\ell \varphi_1\ldots\varphi_\ell \sum_{i,j=1}^{\ell} e^{-i\vec{k}\cdot\vec{q}_i}\,\delta(\vec{p}_i-\vec{p})u_z(1\ldots\ell)e^{i\vec{k}\cdot\vec{q}_j}\,\delta(\vec{p}_j-\vec{p}')$$

$$\equiv \sum_{\ell=0}^{\infty} n^\ell f_a^\ell(kz\vec{p}\vec{p}'), \tag{2.24}$$

which may be interpreted as describing the propagation of a disturbance characterized by wave vector k and frequency z. In this case the molecules are dynamically correlated but not statistically correlated. Aside from f_a the remaining contributions to Eq. (2.10) are simple to evaluate in the absence of statistical effects. The function $f(xx';t)$ now becomes

$$f(kz\vec{p}\vec{p}') = z^{-1}n\delta(\vec{k})\varphi(p)\varphi(p') + f_a(kz\vec{p}\vec{p}') \tag{2.25}$$

and the first few terms in $f_a(kz\vec{p}\vec{p}')$ are

$$f_a^0(kz\vec{p}\vec{p}') = \varphi(p)\delta(\vec{p}-\vec{p}')(z - i\vec{k}\cdot\vec{v})^{-1}, \tag{2.26}$$

$$f_a^1(kz\vec{p}\vec{p}') = \frac{1}{2V}\int dx_1dx_2\varphi_1\varphi_2\sum_{i,j=1}^{2}\delta(\vec{p}_i-\vec{p})e^{i\vec{k}\cdot\vec{q}_i}\;B(12)e^{i\vec{k}\cdot\vec{q}_j}(z - i\vec{k}\cdot\vec{v}_j)^{-1}\,\delta(\vec{p}_j-\vec{p}'), \tag{2.27}$$

$$f_a^2(kz\vec{p}\vec{p}') = \frac{1}{2V}\int dx_1dx_2dx_3\varphi_1\varphi_2\varphi_3\sum_{i=1}^{3} e^{-i\vec{k}\cdot\vec{q}_i}\,\delta(\vec{p}_i-\vec{p})\,[\,B(12)B(13)$$

$$+ B(13)B(12) + B(23)B(12) + B(23)B(13)\,]e^{i\vec{k}\cdot\vec{q}_1}\,\delta(\vec{p}_1-\vec{p}')(z - i\vec{k}\cdot\vec{v}_1)^{-1}, \tag{2.28}$$

where $\vec{v} = \vec{p}/m$,

$$u_z(ij) = \int_0^\infty dt\, e^{-zt} u_t(ij) = B(ij)[z - L^0(ij)]^{-1}, \tag{2.29}$$

and

$$B(ij) = [z - L^0(ij)]^{-1} L^1(ij)[1 + B(ij)]. \tag{2.30}$$

In writing Eq. (2.28) we have made a binary collision expansion of the Ursell operator $u_z(123)$ and retained only the most dominant terms at long times (or small z). This means that collision sequences which contain a cycle, B(12)B(13)B(23), or repeated collision, B(12)B(13)B(12), have less singular behaviour at small z and in the present approximation have been ignored. The binary collision kernel B(ij) obtained from an expansion of $u_z(1 \ldots i \ldots j \ldots \ell)$ is still a ℓ-body operator. However, the molecules, except for i and j, only stream freely and this effect does not appear in the analysis when their initial spatial correlation is ignored. Hence binary collision expansions of different u_z operators all give the same B(ij).

For very short time behaviour the density series given in Eq. (2.24) can be used directly [13]. At long times the series diverges as successively higher terms contain contributions proportional to higher inverse powers of z. Thus if a description is to be valid for both short and long times the density series must be summed to all orders. Such a summation can be carried out in the above approximation of considering only collision sequences which contain no cycles or repeated collisions. In equilibrium theory a connected graph with no cycles is called a Cayley tree [12], and so we may call our approximation the Cayley-tree approximation. Using this approximation and ignoring statistical correlation we have reduced a many-body problem to one wherein only binary effects are present. It is at this level that we are able to derive kinetic equations for f and f_s.

The operator B(ij) acts on the relative separation of molecules i and j as well as their momenta. The spatial effects of this operator can be exhibited more explicitly by its k-space representation,

$$(\vec{k}_i' \vec{k}_j' | B(ij) | \vec{k}_i \vec{k}_j) = \frac{1}{V} \int d^3q_i\, d^3q_j\, e^{-i(\vec{k}_i' \cdot \vec{q}_i + \vec{k}_j' \cdot \vec{q}_j)}\, B(ij)\, e^{i(\vec{k}_i \cdot \vec{q}_i + \vec{k}_j \cdot \vec{q}_j)} \tag{2.31}$$

which is an operator only in momentum space. Combining Eqs. (2.25), (2.26) and (2.27) we then have

$$f_a(kz\vec{p}\vec{p}') = \varphi(p)\delta(\vec{p} - \vec{p}')(z - i\vec{k}\cdot\vec{v})^{-1} + n\int d^3p_1 d^3p_2 \varphi_1\varphi_2[\delta(\vec{p}_1 - \vec{p})(\vec{k}O|B(12)|\vec{k}O)$$

$$+ \delta(\vec{p}_2 - \vec{p})(O\vec{k}|B(12)|\vec{k}O)]\delta(\vec{p}_1 - \vec{p}')(z - i\vec{k}\cdot\vec{v}_1)^{-1}$$

$$+ n^2\int d^3p_1 d^3p_2 d^3p_3 \varphi_1\varphi_2\varphi_3\{\delta(\vec{p}_1 - \vec{p})(\vec{k}O|B(13)|\vec{k}O)(\vec{k}O|B(12)|\vec{k}O)$$

$$+ \delta(\vec{p}_2 - \vec{p})(\vec{k}O|B(23)|\vec{k}O)(O\vec{k}|B(12)|\vec{k}O)$$

$$+ \delta(\vec{p}_3 - \vec{p})[(O\vec{k}|B(13)|\vec{k}O)(\vec{k}O|B(12)|\vec{k}O)$$

$$+ (O\vec{k}|B(23)|\vec{k}O)(O\vec{k}|B(12)|\vec{k}O)]\}\delta(\vec{p}_1 - \vec{p}')(z - i\vec{k}\cdot\vec{v}_1)^{-1} + \ldots \tag{2.32}$$

It can be shown [11] that this series can be reproduced to all orders in the density by iterating the integral equation,

$$f_a(kz\vec{p}\vec{p}') = \varphi(\vec{p})\delta(\vec{p} - \vec{p}')(z - i\vec{k}\cdot\vec{v})^{-1} + n\int d^3p_1 d^3p_2 \delta(\vec{p} - \vec{p}_1)$$

$$[(\vec{k}O|B(12)|\vec{k}O)\varphi_2 f_a(kz\vec{p}_1\vec{p}') + (\vec{k}O|B(12)|O\vec{k})\varphi_1 f_a(kz\vec{p}_2\vec{p}')]. \tag{2.33}$$

Since the momentum $\vec{p}'$ is superfluous the same physical content is given by

$$(z - i\vec{k}\cdot\vec{v}_1)F(kz\vec{p}_1) = \varphi(p_1) + n\int d^3p_2(z - i\vec{k}\cdot\vec{v}_1)$$

$$[(\vec{k}O|B(12)|\vec{k}O)\varphi_2 F(kz\vec{p}_1) + (\vec{k}O|B(12)|O\vec{k})\varphi_1 F(kz\vec{p}_2)], \tag{2.34}$$

where

$$F(kz\vec{p}) = \int d^3p' f_a(kz\vec{p}\vec{p}'). \tag{2.35}$$

Equation (2.34) is a kinetic equation in Fourier space. The collision integral is non-Markoffian because of incomplete collisions and is also non-local because of the finite extent of the molecules. Ignoring these effects we can transform the integral to give

$$(z - i\vec{k}\cdot\vec{v}_1)F(kz\vec{p}_1) = \varphi(p_1) + n\int d^3p_2 v_{12} b db d\epsilon(\varphi_2' F_1' + \varphi_1' F_2' - \varphi_2 F_1 - \varphi_1 F_2), \tag{2.36}$$

where (b, ϵ) are the usual impact variables for a binary collision $v_{12} = |\vec{v}_1 - \vec{v}_2|$, and the prime denotes that the function has the velocity after the collision. Equation (2.36) is just the linearized Boltzmann equation appropriately transformed, with initial condition, $F(r,\vec{p},t=0) = \delta(\vec{r})\varphi(p)$. For the self-correlation function we have

$$(z - i\vec{k}\cdot\vec{v}_1)F_s(kz\vec{p}_1) = \varphi(p_1) + n\int d^3p_2 v_{12} b db d\epsilon [\varphi(p_2')F_s(kz\vec{p}_1') - \varphi(p_2)F_s(kz\vec{p}_1)], \tag{2.37}$$

which is the neutron transport equation with the same initial condition. From Eqs. (2.36) and (2.37) we have the initial conditions for $G(r,t)$ and $G_s(r,t)$,

$$G(r,0) = n + \delta(\vec{r}), \tag{2.38}$$

$$G_s(r,0) = \delta(\vec{r}). \tag{2.39}$$

III. COLLISIONAL INVARIANTS AND HYDRODYNAMICAL BEHAVIOUR

The only difference in our descriptions of $G(r,t)$ and $G_s(r,t)$ lies in the collisional integrals in the kinetic equations. For times short compared to the mean free time the dominant effects are those due to molecular streaming. In the limiting case both G and G_s can be calculated from the free molecule result,

$$F(kz\vec{p}) = F_s(kz\vec{p}) = \varphi(p)(z - i\vec{k}\cdot\vec{v})^{-1}. \tag{3.1}$$

At the opposite extreme of large times, collision effects dominate and the two correlation functions can be expected to exhibit markedly different behaviour. It has been widely recognized that $G(r,t)$ has a hydrodynamic limit for slowly varying disturbances [4, 5, 6]. This limit exists for any classical one-component fluid and is characterized by the irreversible processes of damped sound wave propagation and heat conduction. On the other hand, the corresponding limit for $G_s(r,t)$ is simple diffusion. Thus the long-wavelength spectrum associated with $G(r,t)$ consists of a central peak and two equally displaced peaks (the Brillouin doublet) while that for G_s has a Lorentzian shape. In this section we shall discuss the hydrodynamical limits of our kinetic equations briefly and emphasize that such characteristic behaviour of the correlation functions is a direct consequence of the structure of the collision integrals.

From the two kinetic equations it is clear that in the one description the disturbances propagate with collisions which conserve particle number, momentum and energy, whereas in the other only the particle number is conserved. This observation is easily demonstrated using kinematical transformations well known in the kinetic theory of gases [14]. If $J(F)$ and $J_s(F_s)$ are the collision integrals in Eqs. (2.36) and (2.37), respectively, then

$$\int d^3v_1 d^3v_2 v_{12} b db d\epsilon \begin{pmatrix} 1 \\ \vec{v} \\ v^2 \end{pmatrix} J(F) = 0 \tag{3.2}$$

and

$$\int d^3v_1 d^3v_2 v_{12} b db d\epsilon \; J_s(F_s) = 0. \tag{3.3}$$

In other words the zero eigenvalue of the collision operator corresponding to $J(F)$ is five-fold degenerate whereas that corresponding to $J_s(F_s)$ is non-degenerate. From Eq. (2.36) one obtains a set of conservation equations

$$\begin{aligned} &\frac{\partial}{\partial t} Z(r, t) + \nabla_\mu C_\mu(r, t) = 0, \\ &\frac{\partial}{\partial t} C_\mu(r, t) + \nabla_\nu P_{\mu\nu}(r, t) = 0, \\ &\frac{\partial}{\partial t} E(r, t) + \nabla_\mu Q_\mu(r, t) = 0, \end{aligned} \tag{3.4}$$

and initial conditions

$$\begin{aligned} Z(r, 0) &= \delta(\vec{r}), \\ C_\mu(r, 0) &= 0, \\ E(r, 0) &= \frac{3}{\beta m} \delta(\vec{r}), \end{aligned} \tag{3.5}$$

where Greek subscripts denote Cartesian components and

$$\begin{pmatrix} Z \\ C_\mu \\ P_{\mu\nu} \\ E \\ Q_\mu \end{pmatrix} = \int d^3v \, F(r\vec{v}t) \begin{pmatrix} 1 \\ v_\mu \\ v_\mu v_\nu \\ v^2 \\ v_\mu v^2 \end{pmatrix}. \tag{3.6}$$

In order to use the hydrodynamic equations additional expressions must be found for $P_{\mu\nu}$ and Q_μ, which within a constant factor, are just the pressure tensor and heat flux vector. A number of approximations common in fluid dynamics can be used here. For example, in the ideal gas approximation $P_{\mu\nu}$ is diagonal and Q_μ vanishes and the result is the Euler equations. This leads to a delta function for $S(k, \omega)$, aside from a term proportional to $\delta(\vec{k})$ with $\omega = ck$, where c is the adiabatic sound speed for a monatomic ideal gas, $c = (5/3\ m)$. A more realistic approximation is to use Newton and Fourier laws for $P_{\mu\nu}$ and Q_μ which then results in the Navier-Stokes equations.

One can show [15] in this case that for small k, $S(k, \omega)$ indeed gives a three-component spectrum; the width of the central component depends upon the coefficient of thermal conductivity κ while the width of the displaced components depends on κ as well as on η and ξ, the shear and bulk viscosities. Thus we see in the long wavelength limit the dynamical processes which characterize the system response to a microscopic density disturbance are precisely those which determine the transport properties of the system.

Applying similar considerations to Eq. (2.37) one has only the conservation equation

$$\frac{\partial}{\partial t} G_s(r, t) + \nabla_\mu W_\mu(r, t) = 0, \tag{3.7}$$

where

$$W_\mu(r, t) = \int d^3v \, v_\mu F_s(r\vec{v}t). \tag{3.8}$$

Higher order velocity-moment equations can be written down but it is clear that in these equations there will be contributions due to $J_s(F_s)$. The problem is identical to that encountered in neutron transport theory. In the approximation that the current and density are simply related by a Fick's rule, Eq. (3.7) becomes the diffusion equation and $S_s(k, \omega)$ is a Lorentzian whose width depends on the diffusion coefficient D [16].

The approach of Eqs. (2.36) and (2.37) to their hydrodynamic limits can be studied systematically as an expansion in the relative change in macroscopic variables over the distance of a mean free path [8]. This is the well-known Chapman-Enskog method for calculating transport coefficients from kinetic equations. The method can be applied directly to Eqs. (2.36) and (2.37) but because it is designed specifically for the evaluation of transport coefficients little can be said from such an analysis about the system response to moderately rapid space-time variations. One therefore needs to seek explicit solutions of Eqs. (2.36) and (2.37) in the kinetic region. Although these initial value problems are already well-defined, detailed calculations using specific two-body potentials have not yet been carried through. In the next section we discuss model calculations which are useful in understanding dynamical correlation effects in the region where the wavelengths are of the same order as the mean free path.

IV. SINGLE-RELAXATION-TIME KINETIC MODELS FOR $G(r, t)$ and $G_s(r, t)$

The basis of the Chapman-Enskog development is the assumption that collision effects dominate so that the zeroth order solution is obtained by simply ignoring the effects of free molecular flow. When wavelengths and mean free path are comparable there is no reason to believe that this is a reasonable assumption. However, the difficulty is avoided if appropriate simplification of the collision integrals can be found which enables exact solution of the resulting equation. Kinetic models for which this is possible

have been considered by BOHM and GROSS [17] and by BHATNAGAR, GROSS and KROOK [18]. Subsequent literature on this approach is quite extensive.

The kinetic models to be used for the calculation of $G(r,t)$ and $G_s(r,t)$ can be systematically developed from Eqs. (2.36) and (2.37) [10, 19]. We shall summarize the essential points in the derivation. One assumes that there exists a complete set of eigenfunctions $\{\psi_i\}$ of the linear operator $J(F)$

$$J(\psi_i) = \lambda_i \psi_i$$

with eigenvalues λ_i. Except for the case of Maxwell molecules ($\Phi(r) \sim 1/r^4$) the explicit forms of ψ_i and λ_i are not known. However, certain properties of $J(F)$ can be demonstrated for arbitrary central force interaction. For example, it has already been mentioned that the eigenvalue $\lambda = 0$ is five-fold degenerate as a consequence of the conservation of particle, momentum and energy. The corresponding orthogonal eigenfunctions ψ_i, $i = 1 \ldots 5$, are proportional to 1, v_μ, and $v^2/v_0^2 - 3/2$, with $v_0^2 = 2/\beta m$. All other eigenvalues must be negative since the kinetic equation is irreversible. One then has

$$F(r\vec{v}t) = \sum_n a_n(r,t)\varphi(v)\psi_n(\vec{v}), \tag{4.1}$$

$$a_n(r,t) = \frac{\int d^3v \psi_n(\vec{v}) F(r\vec{v}t)}{\int d^3v \varphi(v) \psi_n^2(\vec{v})}, \tag{4.2}$$

and upon inserting Eq. (4.1) into $J(F)$ one finds

$$J(F) = \sum_n a_n \lambda_n \psi_n \tag{4.3}$$

A kinetic model is obtained if all the non-zero eigenvalues are assumed to have the same value, $-\lambda$. In this approximation the collision integral can be rearranged as

$$\begin{aligned} J_{BGK}(F) &= -\lambda F(r\vec{v}t) + \lambda\varphi(v) \sum_{n=1}^{5} a_n(r,t)\psi_n(\vec{v}) \\ &= -\lambda F(r\vec{v}t) + \lambda\varphi(v) \left[Z(r,t) + \frac{2}{v_0^2} n\vec{v}\cdot\vec{q}(r,t) + n\left(\frac{v^2}{v_0^2} - \frac{3}{2}\right)\tau(r,t) \right] \end{aligned} \tag{4.4}$$

where we have written $n\vec{q}(r,t) = \vec{C}(r,t)$, and $E(r,t) = \frac{3}{2} v_0^2 [Z(r,t) + n\tau(r,t)]$. In this form the local density is $n + Z(r,t)$, the local velocity is $\vec{q}(r,t)$ and the local temperature is $T(r,t) = T_0[1 + \tau(r,t)]$. A similar approximation of Eq. (2.37) yields

$$J_{BG}(F_s) = -\lambda_s F_s(r\vec{v}t) + \lambda_s \varphi(v) G_s(r,t). \tag{4.5}$$

The constants λ and λ_s are model parameters yet to be determined. Since they are average eigenvalues, in principle they can be computed if the eigenvalue spectra are known. This is possible only in the case of J(F) for Maxwell molecules, so that in practice additional conditions are required. In each case, the parameter has the interpretation of the average rate at which the molecules approach local equilibrium, and an estimate of this relaxation frequency can be obtained by requiring the kinetic description to predict certain transport coefficients correctly.

Kinetic descriptions of $G(r,t)$ and $G_s(r,t)$ based on Eqs. (4.4) and (4.5) have been considered recently. On account of the simplicity of the models exact solutions for the wavelength-frequency components of the correlation functions have been obtained. The results are applicable to dilute fluids for arbitrary ratios of wavelength to mean free path. For the self-correlation function it is found that [20]

$$S_s(k,\omega) = \frac{1}{2\pi}\int_{-\infty}^{\infty} dt\, e^{-i\omega t} \int d^3r G_s(r,t) = \frac{1}{\pi\lambda_s}\,\frac{U(xy)[1-U(xy)] - V^2(xy)}{[1-U(xy)]^2 + V^2(xy)}, \tag{4.6}$$

where

$$x = -\omega/kv_0, \qquad y = \lambda_s/kv_0,$$

$$U(xy) = \pi^{\frac{1}{2}} y u(xy), \qquad V(xy) = \pi^{\frac{1}{2}} y v(xy),$$

$$u(xy) + iv(xy) = \frac{i}{\pi}\int_{-\infty}^{\infty} ds (x + iy - s)^{-1} e^{-s^2}.$$

The parameter y is a measure of the wavelength of the disturbance as compared to the collision mean free path. In the limit of small and large y one has respectively

$$S_s(k,\omega) \xrightarrow[y\to 0]{} (kv_0\pi^{\frac{1}{2}})^{-1} \exp[-\omega^2/k^2v_0^2] \xrightarrow[y \gg 1]{} \frac{1}{\pi}\,\frac{Dk^2}{\omega^2 + (Dk^2)^2}, \tag{4.7}$$

which are just the free molecule and simple diffusion results appropriate to large and small momentum transfer. The diffusion coefficient D is given by $v_0^2/2\lambda_s$. In Fig. 1 we plot some typical numerical results for $S_s(k,\omega)$. Away from the hydrodynamic region the line shape is seen to be narrower than the simple diffusion result. It should be observed that the kinetic description represents a non-Gaussian calculation, in spite of the fact that the mean square displacement predicted is identical to that given by a simple Langevin equation with damping constant λ_s. For comparison Gaussian approximation results are also given in the same figure. It is of some interest to study the non-Gaussian behaviour from the ratio of spatial moments. We can define

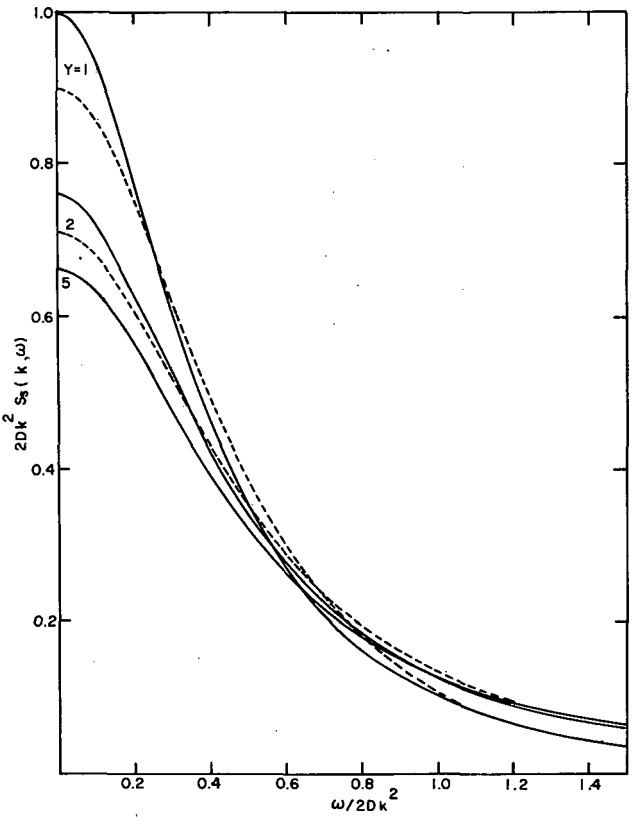

Fig. 1

Deviations of response function $2D\ k^2 S_s(k, \omega)$ from simple diffusion line shape as a function of $\omega/2D\ k^2$ (solid curves). Also shown are the Gaussian approximation results of Singwi and Sjölander (dashed curves), Phys. Rev. 119 (1960) 863.

$$\alpha_n(t) = \frac{\langle r^{2n} \rangle}{C_n \langle r^2 \rangle^n} - 1, \tag{4.8}$$

where $C_n = 1, 3, 5 \ldots (2n+1)/3^n$. The function $\alpha_n(t)$ would be zero for all times if $G_s(r, t)$ were Gaussian. In Fig. 2. we show α_2, α_3 and α_4 [21]. It can be seen that the deviation increases with increasing n with the maximum showing a tendency to shift to larger times. The same qualitative behaviour has been observed in Rahman's calculations [22] for liquid argon based on classical equations of motion. The non-Gaussian effects in Rahman's calculations are smaller, but it is not known whether this is because he uses a realistic interatomic potential or because he calculates for a high density system. It is of interest to obtain a better physical understanding of the similarities and differences between these two calculations.

For the case of the density correlation function the solution again involves the functions U(x, y) and V(x, y), where y is now defined with λ_s re-

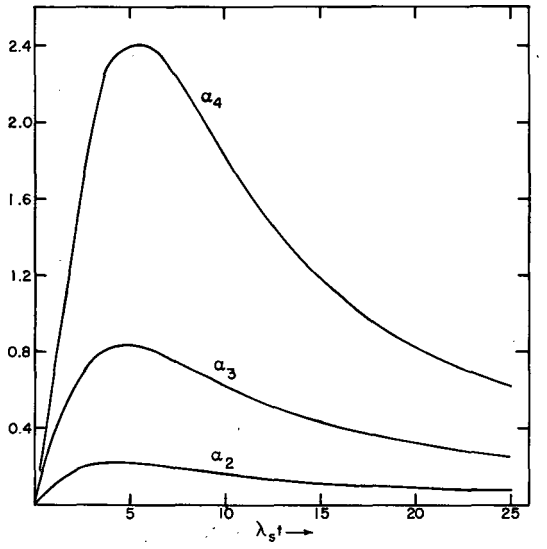

Fig. 2

The non-Gaussian behaviour of the single-relaxation-time kinetic model as a function of $\lambda_s t$. If $G_s(r, t)$ were Gaussian, α_2, α_3 and α_4 would vanish identically.

placed by λ [23]. The expression is considerably more complicated and will not be displayed here. In Fig. 3 we show how $S(k,\omega)$ varies for different ratios of wavelength to mean free path. At long wavelengths it is evident that the adiabatic propagation of pressure disturbances and the diffusion of thermal disturbances give rise to well separated peaks. For $y \geqslant 5$ the location of the displaced component is given by the adiabatic sound speed, $(5/6)^{\frac{1}{2}} v_0$. The corresponding intensity ratio of the central peak to displaced peaks is also characterized by the ideal, monatomic gas value of $(C_p - C_v)/C_p$, C_p and C_v being the usual specific heats at constant pressure and volume.

Since the kinetic results are applicable when the wavelengths become comparable to mean free path, the range of validity of the hydrodynamic equations can be examined in the present approximation. KADANOFF and MARTIN [5] have derived an expression for $S(k, \omega)$ from a set of linearized hydrodynamic equations appropriate to a one-component fluid,

$$S_{KM}(k, \omega) = \left(1 - \frac{C_v}{C_p}\right) \frac{D_T k^2}{\omega^2 + (D_T k^2)^2} + \frac{C_v}{C_p} \frac{c^2 k^4 \Gamma}{(\omega^2 - c^2 k^2)^2 + (\omega k^2 \Gamma)^2}$$

$$- \left(1 - \frac{C_v}{C_p}\right) \frac{D_T k^2 (\omega^2 - c^2 k^2)}{(\omega^2 - c^2 k^2)^2 + (\omega k^2 \Gamma)^2}, \qquad (4.9)$$

where c is the sound speed, $D_T = \kappa/mnC_p$, $\Gamma = \frac{(4\eta/3 + \xi)}{mn} + D_T\left(\frac{C_p}{C_v} - 1\right)$, κ is the thermal conductivity, η is the shear viscosity and ξ is the second or bulk viscosity. Equation (4.9) is an approximate result valid at long wave-

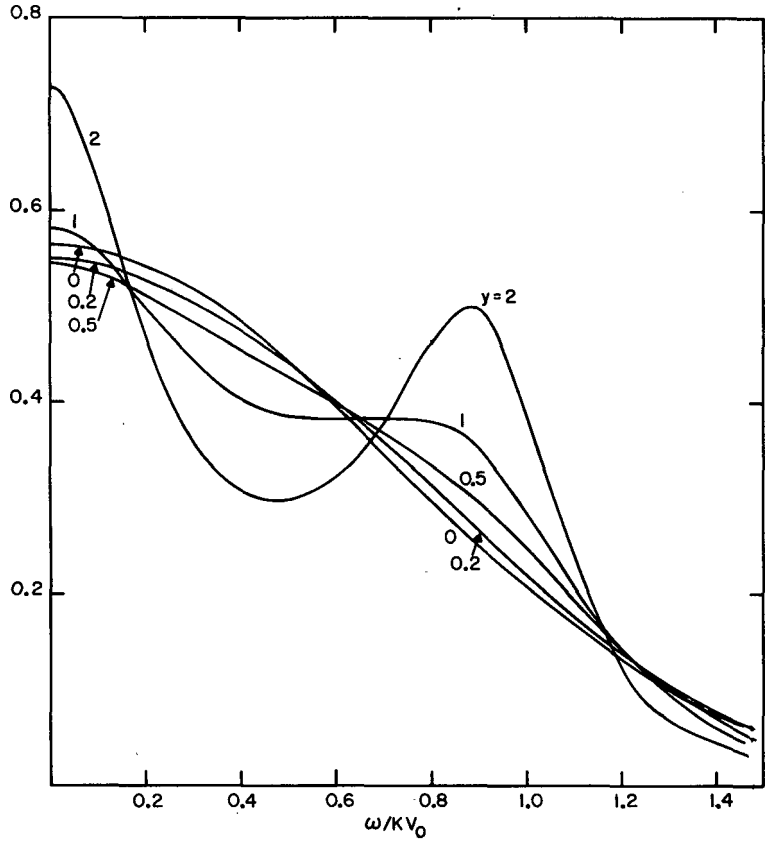

Fig. 3

Variations of response function $(kv_0/\pi)S(k, \omega)$ for various ratios (ratio = $2\pi\sqrt{2}$ y) of wavelength to mean free path.

lengths. To compare with our calculations we use the exact expression as derived from the same hydrodynamic equations [24]

$$S_H(k, \omega) = \frac{\frac{C_v}{C_p} c^2 k^4 \omega^2 D_\ell + c^2 k^6 D_T \left[\left(1 - \frac{C_v}{C_p}\right) c^2 + \frac{C_p}{C_v} k^2 D_\ell D_T \right]}{k^4 \left[\omega^2 \left(D_\ell + \frac{C_p}{C_v} D_T \right) - c^2 k^2 D_T \right]^2 + \omega^2 \left[\omega^2 - c^2 k^2 - \frac{C_p}{C_v} k^4 D_\ell D_T \right]^2}, \quad (4.10)$$

$$D_\ell = \left(\frac{4}{3}\eta + \xi\right)/mn. \quad (4.11)$$

A comparison of $S_H(K, \omega)$ with $S(k, \omega)$ is shown in Fig. 4, where we have used the following: $C_v/C_p = 3/5$, $c = (5/6)^{\frac{1}{2}} v_0$, $\xi = 0$, $\kappa = 5nmv_0^2 C_p/6\lambda$, and $\eta = nmv_0^2/2\lambda$. If included, S_{KM} would lie intermediate to the two curves shown. It appears that for $y \lesssim 1$ the hydrodynamic description is not appropriate, a conclusion not unexpected since one is certainly in the kinetic region.

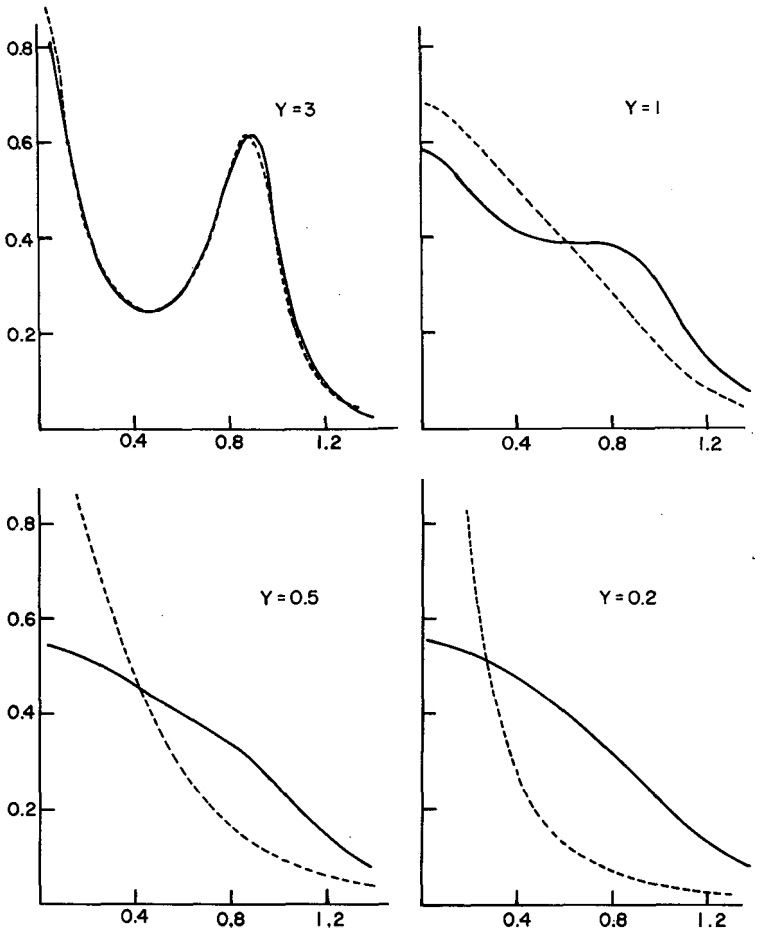

Fig. 4.

Comparison of $(kv_0/\pi)S(k, \omega)$ (solid curves) and $(kv_0/\pi)S_H(k, \omega)$ (dashed curves).

The kinetic results for $S(k,\omega)$ and $S_s(k,\omega)$ also provide a test of Vineyard's convolution approximation [16]. However, the comparison is meaningful only if the parameters λ and λ_s can be specified in an internally consistent way. One approach is to adjust these constants such that appropriate transport coefficients calculated from the kinetic models are in agreement with measurements. For argon at 0°C and one atmosphere, λ is 3.14×10^9 s^{-1} or 4.81×10^9 s^{-1} depending on whether the thermal conductivity or the shear viscosity [25] is used. The discrepancy arises because the stress tensor and the heat flux vector are different velocity moments and therefore should have different decay rates. In the single-relaxation-time approximation this difference is explicitly neglected, so that the ratio of κ to ηC_p is 5/3 instead of 5/2 for monatomic gases. We can obtain an average value for λ using the same relative proportions as found in the classical sound absorption

coefficient. One then has $\lambda = 4.1 \times 10^9$ s^{-1}. From the measured diffusion coefficient [25] λ_s is found to be 3.66×10^9 s^{-1}. Thus λ and λ_s differ by roughly 10%. Neglecting this difference we show in Fig. 5 a comparison

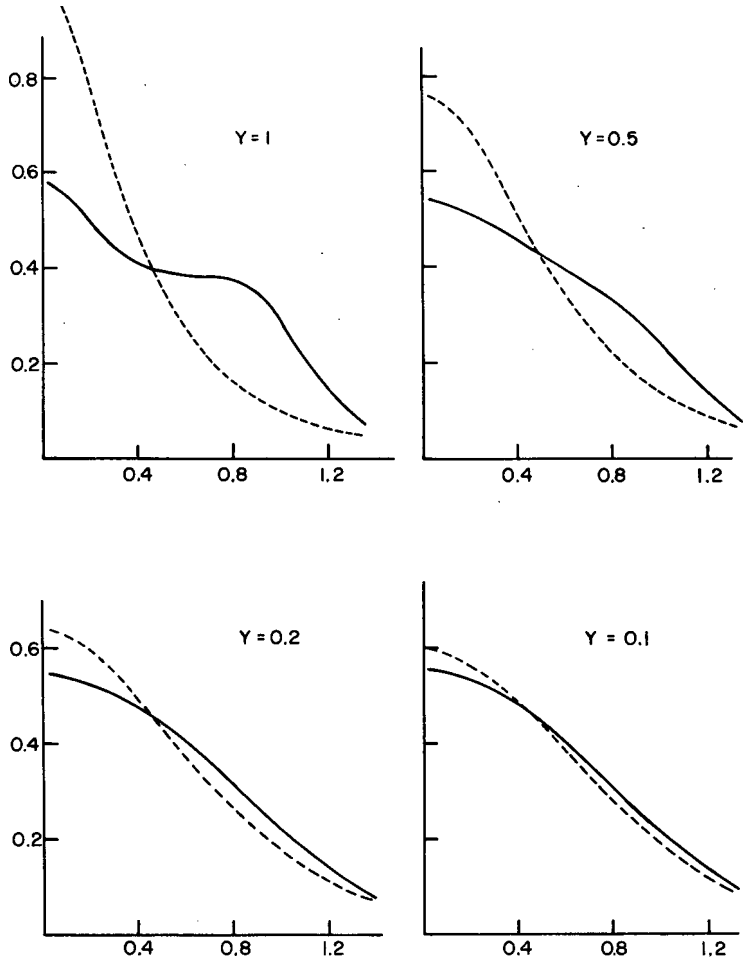

Fig. 5

Comparison of $(kv_0/\pi)S(k,\omega)$ and $(kv_0/\pi)S_s(k,\omega)$ as calculated in the single-relaxation-time approximation assuming λ and λ_s are the same (solid and dashed curves respectively).

of $S(k,\omega)$ and $S_s(k,\omega)$ at the same values of y. The results are identical at y = 0, and at large y the central peak of S is similar in shape to S_s, in particular both widths are the same in the hydrodynamic limit if $\lambda = \lambda_s$. At intermediate values of y where the sound peak in S is less well developed, S is considerably broader. One may conclude that in dilute gases Vineyard's convolution approximation would lead to too narrow a spectrum for wavelengths comparable to or less than the mean free path. For very long wave-

lengths this approximation even gives the wrong line shape as is already well known.

V. DISCUSSION

We have derived kinetic equations for the calculation of Van Hove's correlation functions, and in so doing a connection between slow-neutron (and light) scattering and the theory of irreversible processes is established. The approach is different from VINEYARD's [26] generalization of the B-B-G-K-Y hierarchy equations for molecular distribution functions. For dilute systems it is shown that $G(\mathbf{r}, t)$ can be calculated from an equation for single densities without calculating any two-particle distribution functions. The density correlation function $G(\mathbf{r}, t)$ is given by two parts which in general should be calculated separately. When statistical effects are ignored, one of the two parts is simply the equilibrium density and is of no further interest. The other part is the zeroth velocity moment of the solution to the linearized Boltzmann equation provided effects due to incomplete collisions and finite extent of the molecules are neglected. The self-correlation function $G_s(\mathbf{r}, t)$, in the same approximation, is given by the zeroth velocity moment of the solution to the neutron transport equation. If incomplete collisions are taken into account the equations become non-Markoffian. A different non-Markoffian kinetic equation which can be used to calculate $G_s(\mathbf{r}, t)$ has recently been derived by NOSSAL [27]. It has been recognized that to account properly for short-time behaviour a description should include memory effects. Rahman's molecular dynamics calculations for liquid argon give a momentum correlation function which becomes negative at intermediate times. This will not occur in a kinetic description without memory effects. In liquid argon it is not likely that this behaviour is due to incomplete collisions, but is due rather to oscillations in the attractive force field of neighbouring molecules, which is not a binary collision effect. It should be noted that an equation for the calculation of the momentum correlation function $\langle \vec{p} \cdot \vec{p}(t) \rangle$ can be derived from the results of section II. One has

$$\langle \vec{p} \cdot \vec{p}(t) \rangle = \int d^3p \, d^3p' \, \vec{p} \cdot \vec{p}' \, \Psi(\vec{p}\vec{p}'; t), \tag{5.1}$$

$$\Psi(\vec{p}\vec{p}'; t) = n \int d^3q \, d^3q' \, f_s(xx'; t). \tag{5.2}$$

The equation for $\Psi(\vec{p}\vec{p}'; t)$ turns out to be the space-independent form of the neutron transport equation if non-local effects in the collision are ignored.

Thus far the kinetic descriptions of $G(\mathbf{r}, t)$ and $G_s(\mathbf{r}, t)$ have been explored only in the context of simple relaxation models. Interesting results are obtained if the calculations are performed directly with Eqs. (2.36) and (2.37) for a particular two-body potential. Attempts to carry out such a calculation are currently under way. In both cases, the kinetic equations can be put into the form

$$\left[\frac{\partial}{\partial t} + \vec{v}\cdot\vec{\nabla} + nK_0(v)\right] f(r\vec{v}t) = n\int d^3v' K_1(\vec{v},\vec{v}')f(r\vec{v}'t), \qquad (5.3)$$

where $K_0(v)$ and $K_1(\vec{v},\vec{v}')$ are known integrals of the differential cross-section. It can also be shown that K_1 depends only on the magnitude of $\vec{v}$ and $\vec{v}'$ and the angle between them. Since a given force law completely characterizes both calculations of S and S_s, a quantitative test of the convolution approximation can be thus obtained.

Comparison of kinetic and hydrodynamic calculations has shown that appreciable differences appear in the region $y \lesssim 1$. Presumably one can extend the range of applicability of the hydrodynamic equations by introducing fequency-dependent transport coefficients and dispersion effects in the sound speed. A question arises as to whether in so doing it is appropriate to use Eq. (4.9), which differs significantly from Eq. (4.10) in the kinetic region even when constant transport coefficients are used. It should be remembered that the validity of the hydrodynamic equations is not limited by the applicability of the kinetic equation from which they can be derived. The hydrodynamic equations can be applied to dense fluids as long as the appropriate values of the parameters are used. On the other hand, the hydrodynamic description is restricted to small k. While Eqs. (4.9) and (4.10) should be useful in analysing the Doppler shifts in light scattering experiments, they are less likely to be appropriate for interpreting slow neutron scattering data.

From our kinetic calculations for a dilute system, it appears qualitatively reasonable to apply the hydrodynamic Eq. (4.10) to slow neutron scattering by liquids for the smallest obtainable momentum transfers ($k \sim 2\times10^7$ cm^{-1}). In doing this we find that the frequency distribution $S(k,\omega)$ is much broader than that of $S_s(k,\omega)$. The thermal diffusivity in liquids is much larger than the atomic diffusion coefficient (for argon at 90°K, $D_T/D \sim 50$ [28]). Thus the central peak of $S(k,\omega)$ is much broader than $S_s(k,\omega)$. The presence of the unresolved sound wave peaks will accentuate this difference. This is a qualitatively striking result since near the first diffraction maximum, de Gennes narrowing effect [4] occurs, and $S(k,\omega)$ is narrower than $S_s(k,\omega)$. Since the fraction of incoherent scattering in argon can be varied by varying the isotopic composition, the observation of this strikingly different behaviour of $S(k,\omega)$ and $S_s(k,\omega)$ for $k \sim 2\times10^7$ cm^{-1} as compared to $k \sim 2\times10^8$ cm^{-1} may be experimentally feasible.

The kinetic equations considered in the present work are valid only for dilute systems. To extend the description to moderately dense fluids additional effects should be taken into consideration. Among these are the dynamical effects of triple collisions and the statistical effects of spatial correlation. Using Eq. (2.25) we have been able to justify approximately the introduction of the equilibrium pair distribution function in the collision integral. The result is similar in character to Enskog's modification of the Boltzmann equation for dense gases [14].

In summary we have established the relationship between kinetic theory and inelastic neutron scattering for classical monatomic fluids in the range of low density where the kinetic theory is very well understood. The extension to moderate densities is feasible, difficult, and of considerable

current theoretical interest. It is not yet clear whether this approach will eventually lead to quantitative predictions which can be compared with inelastic neutron scattering experiments.

ACKNOWLEDGEMENTS

We wish to thank R. C. Desai and I. Herbst for communicating results of their calculations prior to publication. One of us (J. M. J. V. L.) gratefully acknowledges a grant from the Netherlands Organization for the Advancement of Pure Research.

REFERENCES

[1] LUTTINGER, J. M., Phys. Rev. 135 (1964) A1505.
[2] deGROOT, S. R. and MAZUR, P., Non-Equilibrium Thermodynamics, North Holland, Amsterdam (1962).
[3] HERZFELD, K. F. and LITOVITZ, T. A., Absorption and Dispersion of Ultrasonic Waves, Academic Press, N. Y. (1959).
[4] De GENNES, P. G., Physica 25 (1959) 825; Inelastic Scattering of Neutrons in Solids and Liquids, IAEA Vienna (1961) 239-48.
[5] KADANOFF, L and MARTIN, P. C., Ann. Phys. (N. Y.) 24 (1963) 419.
[6] MORI, H., Prog. theor. Phys. 28 (1962) 763.
[7] PECORA, R., J. Chem. Phys. 40 (1964) 1604.
[8] UHLENBECK, G. E. and FORD, G. W., Lectures in Statistical Mechanics, Amer. math. Soc., Providence (1963).
[9] GREENSPAN, M., J. Acoust. Soc. Amer. 22 (1950) 568.
[10] GROSS, E. P., in Rarefied Gas Dynamics (DeVIENNE, F. M., Ed.) Pergamon Press, London (1960) 139.
[11] VAN LEEUWEN, J. M. J. and YIP, S., to be published.
[12] UHLENBECK, G.E. and FORD, G. W., Studies in Statistical Mechanics I (de BOER, J. and UHLENBECK, G. E. Eds.) North Holland, Amsterdam (1960) part B
[13] MAZO, R. M. and ZEMACH, A. C., Phys. Rev. 109 (1958) 1564.
[14] CHAPMAN, S. and COWLING, T. G., The Mathematical Theory of Non-Uniform Gases (2nd ed.) Cambridge University Press, London (1960).
[15] LANDAU, L. D. and LIFSHITZ, E. M., Electrodynamics of Continuous Media, Pergamon Press, London (1960) Chap. XIV.
[16] VINEYARD, G. H., Phys. Rev. 110 (1958) 999.
[17] BOHM, D. and GROSS, E. P., Phys. Rev. 75 (1949) 1851.
[18] BHATNAGAR, P. F., GROSS, E. P. and KROOK, M., Phys. Rev. 94 (1954) 511.
[19] GROSS, E. P. and JACKSON, E. A., Phys. Fluids 2 (1959) 432.
[20] NELKIN, M. and GHATAK, A., Phys. Rev. 135 (1964) A4.
[21] DESAI, R. C., private communication.
[22] RAHMAN, A , to appear in Phys. Rev.
[23] YIP, S. and NELKIN, M., Phys. Rev. 135 (1964) A1241.
[24] HERBST, I., private communication.
[25] HIRSCHFELDER, CURTISS and BIRD, Molecular Theory of Gases and Liquids, John Wiley, N. Y. (1955).
[26] VINEYARD, G. H , Phys. Fluids 3 (1960) 339.
[27] NOSSAL, R. J., Phys. Rev. 135 (1964) A1579.
[28] UHLIR, A., J. Chem. Phys. 20 (1952) 463; NAGHIZADEH, J. and RICE, S. A., J. Chem. Phys. 36 (1961) 2710.

DISCUSSION

P. EGELSTAFF: What is the shape of $\int S(k,\omega)\,d\omega$ according to your model? After all, this function has a large effect on the positions of the peaks in $S(k,\omega)$ plotted as a function of ω.

S. YIP: The integral is unity for all k, and follows from the fact that in this model the particles are statistically uncorrelated at equilibrium.

A. SJÖLANDER: Do you really have to go beyond the ordinary Boltzmann equation to get the kind of curves you have shown us, i.e. a broadened sound peak and a diffusive central peak deviating from the macroscopic results?

S. YIP: No, the linearized Boltzmann equation will always give this type of line shape for small wavelengths.

THE SELF-CORRELATION FUNCTION OF REAL GASES

D. J. SIGMAR
INSTITUTE FOR THEORETICAL PHYSICS,
TECHNICAL UNIVERSITY OF VIENNA,
VIENNA, AUSTRIA

Abstract — Résumé — Аннотация — Resumen

THE SELF-CORRELATION FUNCTION OF REAL GASES. In the formal theory of inelastic scattering of neutrons, the self-correlation function has been worked out in terms of statistical averages of the derivatives of the N-body interaction-potential of the scatterer.

In the present paper, these averages are evaluated for real gases by means of a cluster-expansion related to that of Mayer-Ursell. This leads to certain non-linear types of clusters, which are investigated with respect to the topology of the graphs, their multiplicity (by combinatorial analysis) and their quadrature. As one expects, in view of the many-body problem, some of the clusters are not separable and have to be machine-integrated.

In this way, the self-correlation function $\gamma_s(\vec{\kappa}, t)$ is calculated for short times, including also the first non-Gaussian term. The cluster-expansion breaks off after the first interaction term, so that the results are valid for low density only. This still gives rise to very many different types of clusters, containing up to seven points, for each coefficient. The assumed potential is a general two-particle, hard-core type.

As Singwi et al. have shown, the long time behaviour of γ_s is determined by the time integral of the velocity auto-correlation:

$$\int_0^\infty < v_\kappa(0)\, v_\kappa(t) >_T dt.$$

To construct the integrand for all times, we can make use of our cluster-expansion for small t and adopt Langevin's diffusion theory for large t.

Numerical computations are under way.

FONCTION D'AUTOCORRÉLATION DES GAZ RÉELS. Dans la théorie formelle de la diffusion inélastique des neutrons, on a établi la fonction d'autocorrélation en se fondant sur les moyennes statistiques des dérivées du potentiel d'interaction à N corps du diffuseur.

L'auteur a évalué ces moyennes pour des gaz réels à l'aide d'un développement par amas en rapport avec celui de Mayer-Ursell. Il obtient ainsi des types d'amas non linéaires qu'il étudie du point de vue de la topologie des diagrammes, de leur multiplicité (par analyse combinatoire) et de leur quadrature. Comme on peut s'y attendre pour ce problème à plusieurs corps, certains amas ne sont pas séparables et doivent être intégrés au moyen d'un ordinateur.

De cette façon, la fonction d'autocorrélation $\gamma_s(\vec{\kappa}, t)$ est calculée pour des temps courts, y compris le premier terme non gaussien. Le développement par amas cesse de s'appliquer après le premier terme d'interaction, de sorte que les résultats ne sont valables que pour les faibles densités. On obtient encore de très nombreux types différents d'amas qui contiennent jusqu'à sept points, pour chaque coefficient. Le potentiel admis est du type général à deux particules et à cœur dur.

Comme Singwi et son équipe l'ont montré, le comportement à long terme de γ_s est déterminé par l'intégrale de temps de l'autocorrélation de vitesse:

$$\int_0^\infty < v_\kappa(0)\, v_\kappa(t) >_T dt$$

En vue de déterminer l'expression à intégrer pour toutes les valeurs temps, on peut utiliser le développement par amas proposé par l'auteur lorsque t est petit et adopter la théorie de la diffusion de Langevin lorsque t est grand.

On est en train de faire des calculs numériques.

ФУНКЦИЯ САМОКОРРЕЛЯЦИИ РЕАЛЬНЫХ ГАЗОВ. В формальной теории неупругого рассеяния нейтронов функция самокорреляции выведена в средне-статистических производных взаимодействие-потенциал N-тела рассеивателя.

В данном докладе эти средние значения определяются для реальных газов разложением на группы, связанным с методом Майера-Урселля. Это приводит к получению некоторых нелинейных типов групп, которые изучаются в отношении топологии граф, их многократности (методами комбинаторного анализа) и их квадратуры. Как предполагается в связи с проблемой многих тел, некоторые из групп неразделимы, и их необходимо интегрировать с помощью счетно-решающих машин.

Таким путем рассчитывается функция самокорреляции $\gamma_s(\vec{\kappa}, t)$ для коротких промежутков времени, в том числе и первый негауссовский член. Разложение на группы прерывается после первого члена, выражающего взаимодействие, так что результаты справедливы только для низкой плотности. Это тем не менее приводит к самым различным типам групп, в которых содержится до 7 точек для каждого коэффициента. В качестве потенциала предполагается обычная твердая сердцевина с двумя частицами.

Как показали Сингви и др., характеристика γ_s для продолжительного времени определяется временным интегралом по скорости-автокорреляции:

$$\int_0^\infty < v_K(0) v_K(t) >_T dt .$$

Для составления подинтегрального выражения для всех случаев мы можем использовать наше разложение на группы для небольших значений t и принять теорию диффузии Ланжевена для больших значений t.

Числовые подсчеты готовятся.

LA FUNCIÓN DE AUTOCORRELACION DE LOS GASES REALES. En la teoría formalista de la dispersión inelástica de neutrones, la función de autocorrelación se ha elaborado sobre la base de los promedios estadísticos de las derivadas del potencial de interacción (N cuerpos) del dispersor.

En la memoria, estos promedios se calculan para los gases reales según el procedimiento de un desarrollo en racimo, que guarda relación con la de Mayer-Ursell. Ello da origen a ciertos tipos no lineales de racimos, que se estudian en lo que respecta a la topología de los gráficos, a su multiplicidad (por análisis combinatorio) y a su cuadratura. Como es de esperar, dado el problema de la multiplicidad de cuerpos, algunos de los racimos no son separables y han de ser integrados con una calculadora electrónica.

De esta manera se calcula la función de autocorrelación $\gamma_s(\vec{\kappa}, t)$ para tiempos breves, incluido el primer término no gaussiano. El desarrollo en racimo cesa después del primer término de interacción, de forma que los resultados sólo son válidos para densidades bajas. Pero aun así aparecen en cada coeficiente muchos tipos diferentes de racimos que contienen hasta siete puntos. En cuanto al potencial, se admite la hipótesis de un núcleo rígido formado por dos partículas.

Como han demostrado Singwi y sus col., el comportamiento a largo plazo de γ_s viene determinado por la integral, respecto del tiempo, de la autocorrelación de la velocidad:

$$\int_0^\infty < v_K(0)\ v_K(t) >_T dt.$$

Con el fin de determinar el integrando correspondiente a cualquier tiempo, se puede recurrir al desarrollo en racimo cuando t es pequeño, y aceptar la teoría de la difusión de Langevin en los casos en que t es grande.

Se están realizando cálculos numéricos.

1. INTRODUCTION

SCHOFIELD [1], among others, has developed the formal theory for the inelastic scattering of neutrons in statistical media. In his work, to which we mainly refer, the self-correlation function

$$\gamma_s(\vec{\kappa}, t) \equiv \frac{1}{N}\left\langle \sum_{i=1}^{N} e^{-i\vec{\kappa}\cdot\vec{r}_i(0)} \; e^{i\vec{\kappa}\cdot\vec{r}_i(t)} \right\rangle_T \tag{1.1}$$

is finally expressed in classical thermal averages of derivatives of the interaction potential $V(\vec{r}_1, \vec{r}_2, \ldots \vec{r}_N)$. (The scatterer is supposed to consist of N spinless interacting atoms.) In Eq. (1.1) $\hbar\vec{\kappa}$ is the momentum transfer of the neutrons to the scattering system and $\vec{r}_i(t)$ the Heisenberg operator for the position of the i-th atom at time t.

$$\langle A \rangle_T \equiv \text{trace } (Ae^{-\mathcal{H}/kT})/\text{trace } e^{-\mathcal{H}/kT}$$

$$\mathcal{H} = \sum_{i=1}^{3N} \frac{p_i^2}{2m} + V(\vec{r}_1, \vec{r}_2, \ldots \vec{r}_N),$$

where $\mathcal{H}$ is the Hamiltonion operator of the scattering N-body system and T the temperature of the scatterer.

The transition from quantum thermal averages, as defined above, to classical ones,

$$(A)_T \equiv \int\int d^N\vec{p}\, d^N\vec{r}\, A(\vec{p}_j, \vec{r}_j)\, e^{-H/kT} \Big/ \int\int d^N\vec{p} d^N\vec{r}\, e^{-H/kT}, \tag{1.2}$$

H being the classical Hamiltonian of the system, is possible by means of an expansion in powers of $\hbar$. This was done in [1] so that only classical thermal averages have to be evaluated. In [1] it is shown that for an isotropic scattering system

$$\ln \gamma_s(\vec{\kappa}, t) = -\kappa^2\Gamma_1 + \kappa^4\Gamma_2 - \ldots, \tag{1.3}$$

where

$$\Gamma_1 = \frac{1}{2!}\frac{kT}{m} y^2 \left[1 + (1 - 2\bar{K}_x)\left(\frac{kTy}{\hbar}\right)^2 + O(y^4)\right] \tag{1.4}$$

and

$$\Gamma_2 = \frac{1}{4!} 4 \left(\frac{kT}{m}\right)^2 \left(\frac{kT}{\hbar}\right)^4 [(\bar{K}_x^2 - 3(\bar{K}_x)^2) y^8 + O(y^{10})]. \tag{1.5}$$

Here y^2 is a complex time variable defined by

$$y^2(t) \equiv t^2 - \frac{i\hbar t}{kT} \tag{1.6}$$

and

$$1 - 2\bar{K}_x = -\frac{1}{12}\frac{\hbar^2}{m(kT)^2}\left(\frac{\partial^2 V}{\partial x^2}\right)_T + O(\hbar^4)$$

$$\bar{K}_x^2 - 3(\bar{K}_x)^2 = \frac{\hbar^4}{4m^2}\left\{\frac{1}{48}\frac{1}{(kT)^4}\left[\left(\left(\frac{\partial^2 V}{\partial x^2}\right)^2\right)_T - \left(\frac{\partial^2 V}{\partial x^2}\right)_T^2\right] - \frac{1}{80}\frac{1}{(kT)^3}\left(\frac{\partial^4 V}{\partial x^4}\right)_T\right\} + O(\hbar^6).$$

(In Eq. (26) of Ref. [1], i.e. the last equation shown above, there is an omission of the term $1/(kT)^3$.) By $\partial^2 V/\partial x^2$ we mean $(\partial^2/\partial x_1^2)V(\vec{r}_1, \vec{r}_2, \ldots \vec{r}_N)$, with $\vec{r}_1 = (x_1, y_1, z_1)$.

In this paper we calculate $(\partial^2 V/\partial x^2)_T$, $((\partial^2 V/\partial x^2)^2)_T$ and $(\partial^4 V/\partial x^4)_T$ for real gases of a very general class. From this, then, we derive the self-correlation function γ_s to a certain approximation.

2. ADOPTED MODEL OF THE REAL GAS

We assume the gas to consist of N atoms (mass m), which interact through two-body forces with potential $\phi(r)$. For the following calculations we need not specify the function $\phi(r)$. It might be a Lennard-Jones or a hard-core potential or any other short-range-type potential.

$$V(\vec{r}_1, \vec{r}_2, \ldots \vec{r}_i, \vec{r}_j, \ldots \vec{r}_N) = \sum_{i<j} \phi(|\vec{r}_i - \vec{r}_j|). \tag{2.1}$$

(We note that in dense systems three-body forces should also play a role.)

3. THERMAL AVERAGES

As the quantities A in question here happen to be $\vec{p}$-independent, we obtain from Eqs. (1.2) and (2.1)

$$(A)_T = \int d^N\vec{r}\, A(\vec{r}_1, \vec{r}_2, \ldots \vec{r}_N) \exp\left(-\beta\sum_{i<j}\phi_{ij}\right) \Big/ \int d^N\vec{r} \exp\left(-\beta\sum_{i<j}\phi_{ij}\right). \tag{3.1}$$

Here $\phi_{ij} \equiv \phi(r_{ij}) = \phi(|\vec{r}_i - \vec{r}_j|)$ and $\beta = 1/kT$. Our method consists in calculating

$$\int d^N\vec{r}\, A(\vec{r}_j) \exp\left(-\beta\sum\phi_{ij}\right)$$

by means of a special cluster expansion, originating from the well-known Ursell-Mayer one [2]. The denominator in Eq. (3.1) can be taken over from the virial theory of real gases.

4. CALCULATION OF $(\partial^2 V/\partial x_1^2)_T$

Here

$$A(\vec{r}_j) \equiv \frac{\partial^2}{\partial x_1^2} V(\vec{r}_1, \vec{r}_2, \ldots \vec{r}_N) \equiv V_{11} .$$

4.1. V_{11}

$$V_{11} = \frac{\partial^2}{\partial x_1^2} \sum \phi(r_{ki}) = \frac{\partial^2}{\partial x_1^2} \sum_{k=2}^{N} \phi(r_{k1}) = \sum_{k=2}^{N} \left[\phi''_{k1} \left(\frac{\partial r_{k1}}{\partial x_1} \right)^2 + \phi'_{k1} \frac{\partial^2 r_{k1}}{\partial x_1^2} \right],$$

where

$$\phi_{k1} \equiv \phi(r_{k1})$$

$$r_{k1} = |\vec{r}_k - \vec{r}_1|$$

$$\frac{\partial r_{k1}}{\partial x_1} = -\frac{x_k - x_1}{r_{k1}} \equiv -\cos\vartheta_k$$

$$\frac{\partial^2 r_{k1}}{\partial x_1^2} = \frac{\sin^2\vartheta_k}{r_{k1}}$$

hence

$$V_{11} = \sum_{k=2}^{N} \left(\phi''_{k1} \cos^2\vartheta_k + \phi'_{k1} \frac{\sin^2\vartheta_k}{r_{k1}} \right) \equiv \sum_{k=2}^{N} a_{k1} . \tag{4.1}$$

The quantities a_{k1}, thus defined, are functions of $\vec{r}_k - \vec{r}_1$ only. With $\phi(r_{k1})$ given, ϕ''_{k1} and ϕ'/r_{k1} are known functions.

4.2. $(V_{11})_T$

It follows that

$$(V_{11})_T \propto \int \frac{d^N\vec{r}}{v^N} \sum_{k=2}^{N} a_{k1} \exp\left(-\beta \sum_{i<j} \phi_{ij} \right),$$

where v is the volume of the gas. Following Ursell-Mayer, we introduce the everywhere-bounded quantities

$$f(r_{ij}) \equiv f_{ij} \equiv \exp(-\beta\phi_{ij}) - 1, \tag{4.2}$$

so that

$$\exp\left(-\beta \sum_{i<j} \phi_{ij} \right) = \prod_{i<j} (1 + f_{ij}) = 1 + \sum_{i<j} f_{ij} + \sum_{i<j} \sum_{i'<j'} f_{ij} f_{i'j'} + \ldots$$

In what follows, we keep only the first two terms of this expansion. Higher order terms of f_{ij} products give rise to very many more terms in the following cluster expansion, but these can be managed principally. For numerical results, they must be taken into account partially, depending on the density Nv_0/v, v_0 being hard sphere volume. We then have

$$(V_{11})_T \propto \int \frac{d^N \vec{r}}{v^N} \sum_{k=2}^{N} a_{k1} \left(1 + \sum_{\substack{i<j \\ i=1}}^{N} f_{ij} + \ldots\right) = \sum_{k=2}^{N} \int d\tau_N a_{k1} + \sum_{k=2}^{N} \sum_{i<j} \int d\tau_N a_{k1} f_{ij} + \ldots \quad (4.3)$$

where $d\tau_N = d^N \vec{r}/v^N$. These are "cluster integrals", for only if the points $\vec{r}_k, \vec{r}_1, \vec{r}_i$ and $\vec{r}_j$ are clustered together are the integrands non-zero.

4.3. *Notation for cluster integrals*

To treat the sums properly, we adopt the following graph notation for the cluster integrals.

$\int d\tau_N f_{ij}$ i —— j

$\int d\tau_N a_{k1}$ 1 —— k

$\int d\tau_N a_{k1} f_{ij}$ 1 —— k, i —— j

$\int d\tau_N a_{k1} f_{1j}$ 1 < k, j

$\int d\tau_N a_{k1} f_{ki}$ 1 > k, i

$\int d\tau a_{k1} f_{k1}$ 1 == k

etc.

The numerical value of each type of cluster integral is, of course, independent of particular values of i, j and k. We see that in one graph two points are connected by more than one line. This non-linearity complicates the counting problem, as will be seen.

4.4. *Counting of cluster integrals*

For Eq. (4.3) the counting is easy

$$\sum_{k=2}^{N} \int d\tau_N a_{k1} = (N-1) \times [k\text{—}1]; \qquad \nu_2 = N - 1 \quad (4.4.1)$$

(ν_i is the number of graphs in Σa_{k1} with i points.)

$$\sum_{k=2}^{N}\sum_{i<j}\int d\tau_N\, a_{k1} f_{ij} = n_2 \times \left[1 \text{---} k\right] + n_3' \times \left[\begin{array}{l} 1 \\ j \end{array}\!\!<\!\!\begin{array}{l} \\ k \end{array}\right] + n_3'' \times \left[\begin{array}{l} 1 \\ i \end{array}\!\!>\!\!\begin{array}{l} \\ k \end{array}\right] + n_4 \times \left[\begin{array}{l} 1\text{---}k \\ i\text{---}j \end{array}\right] \tag{4.4.2}$$

(n_i is the number of graphs in $\Sigma\, a_{ki} f_{ij}$ with i points.)

n_2

$$n_2 = N - 1 \tag{4.4.3}$$

n_3' and n_3''

With k, j = 2, 3, ... N, the question is, how many possibilities k-j are there. Since k-j and j-k have to be counted separately, this is the number of variations of N-1 elements in pairs of two.

$$n_3' = \frac{(N-1)!}{[(N-1)-2]!} = (N-1)(N-2). \tag{4.4.4}$$

Likewise,

$$n_3'' = \frac{(N-1)!}{[(N-1)-2]!} = (N-1)(N-2) \tag{4.4.5}$$

n_4

At first sight the equation for n_4 should be

$$\frac{(N-1)!}{[(N-1)-3]!} = (N-1)(N-2)(N-3)$$

(triple variations k-i-j). But this would mean the occurence of both 1, k, i, j and 1, k, j, i. Yet in $\sum_{i<j} f_{ij}, f_{ji}$ does not occur at all, so

$$n_4 = \tfrac{1}{2}(N-1)(N-2)(N-3). \tag{4.4.6}$$

An illustration for N = 4 is

$$\sum_k \sum_{i<j} a_{k1} f_{ij} = (a_{21} + a_{31} + a_{41})(f_{21} + f_{31} + f_{41} + f_{32} + f_{43} + f_{42}).$$

There is no term f_{12}, f_{13} etc. For the counting to be correct, the following condition is necessary and this condition may serve as a check: In

$$\sum_{k=2}^{N} a_{k1} \sum_{\substack{i=1 \\ i<j}}^{N} f_{ij}$$

there are $(N-1)\binom{N}{2} = \frac{N-1}{2}[N(N-1)]$ terms. The same number should re-

sult by adding the above multiplicities of the graphs, namely,

$$n_2 + n_3' + n_3'' + n_4 = (N-1) + 2(N-1)(N-2) + \tfrac{1}{2}(N-1)(N-2)(N-3)$$

$$= \frac{N-1}{2}\,[2 + 4(N-2) + (N-2)(N-3)]$$

$$= \frac{N-1}{2}\,[N(N-1)]\,.$$

Thus we obtain from Eqs. (4.3) and (4.4.1)-(4.4.6)

$$(V_{11})_T \propto (N-1) \times [k \text{——} 1] + (N-1) \times [k \text{===} 1]$$

$$+ (N-1)(N-2) \times \left[\begin{array}{c} 1 \\ /\ \backslash \\ k \quad j \end{array}\right] + (N-1)(N-2) \times \left[\begin{array}{c} k \\ /\ \backslash \\ 1 \quad i \end{array}\right]$$

$$+ \tfrac{1}{2}(N-1)(N-2)(N-3) \times [\overset{1}{i} \text{===} \overset{k}{j}] + \ldots \tag{4.5}$$

5. CALCULATION OF $(V_{11}^2)_T$

$$V_{11} = \partial^2 V / \partial x_1^2\,.$$

From Eq. (4.1)

$$V_{11} = \sum_{k=2}^{N} a_{k1},$$

we obtain

$$(V_{11}^2)_T \propto \int d\tau_N \sum_{\ell,k=2}^{N} a_{k1} a_{\ell 1} \left(1 + \sum_{i<j} f_{ij} + \ldots\right) \tag{5.1}$$

5.1. Investigation of $\sum_{\ell,k} a_{k1}\, a_{\ell 1}$

Here two types of graph occur

$$\left[\begin{array}{c} 1 \\ /\ \backslash \\ k \quad \ell \end{array}\right] \quad \text{and} \quad k \text{===} 1.$$

As in section 4.4. we obtain

$$\nu_3 = (N-1)(N-2) \text{ and } \nu_2 = (N-1) \tag{5.2}$$

for these graphs, respectively. To check this, we observe that in $\sum_{\ell,k=2}^{N} a_{k1} a_{\ell 1}$ there are $(N-1)^2$ terms, and $\nu_3 + \nu_2 = (N-1)^2$ also.

5.2. Cluster types

In $\Sigma\, a_{k1} a_{\ell 1} f_{ij}$ there are the following topological possibilities of combining $\wedge$ with ---:

(a) 5 clusters:  n_5

(b) 4 clusters: 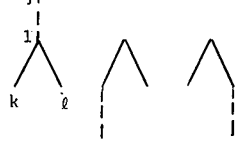 $n'_4\, n''_4\, n'''_4$

(c) 3 clusters:  $n'_3\, n''_3\, n'''_3$

Combinations of $=$ with ---:

(d) 4 clusters: 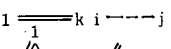 m_4 (5.3)

(e) 3 clusters: 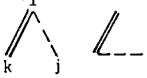 $m'_3\, m''_3$

(f) 2 clusters:  m_2

Here we have introduced the numbers m_i of graphs, belonging to $=$. The n_i belong to $\wedge$.

5.3. Counting

By the same arguments as those in section 4.4., one finds

$$
\begin{aligned}
n_5 &= \tfrac{1}{2}\,(N-4)\,(N-3)\,(N-2)\,(N-1)\\
n'_4 &= n''_4 = n'''_4 = (N-1)\,(N-2)\,(N-3)\\
n'_3 &= n''_3 = n'''_3 = (N-1)\,(N-2)\\
m_4 &= \tfrac{1}{2}\,(N-3)\,(N-2)\,(N-1)\\
m'_3 &= m''_3 = (N-1)\,(N-2)\\
m_2 &= (N-1).
\end{aligned}
\qquad (5.4)
$$

From Eqs. (5.1) - (5.4) $(V_{11}^2)_T$ can be found

$$(V_{11}^2)_T = (N-1)(N-2) \times$$ 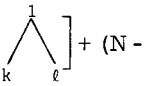
$$+ (N-1) \times$$ 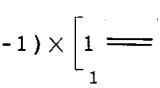
$$+ \tfrac{1}{2}(N-4)(N-3)(N-2)(N-1) \times$$ 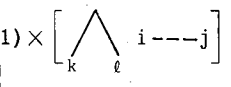
$$+ (N-1)(N-2)(N-3) \times$$ 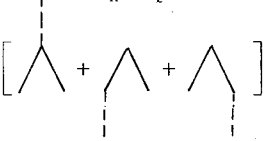
$$+ (N-1)(N-2) \times$$ 
$$+ \tfrac{1}{2}(N-3)(N-2)(N-1) \times$$ 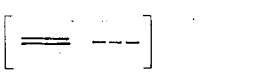
$$+ (N-1)(N-2) \times$$ 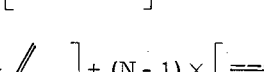
$$+ (N-1) \times$$
.

As a check, in $\sum_{\ell,k=2} a_{k1}a_{\ell 1} \sum_{i=1,i<j}^{N} f_{ij}$, there are

$$(N-1)^2 \binom{N}{2} = \frac{N-1}{2}\left[N(N-1)^2\right] = \frac{N-1}{2}\left[N^3 - 2N^2 + N\right]$$

terms. Likewise

$$\sum_{i=3}^{5} n_i + \sum_{i=2}^{4} m_i = \frac{N-1}{2}\left[N^3 - 2N^2 + N\right].$$

6. CALCULATION OF $\left(\frac{\partial^4 V}{\partial x_1^4}\right)_T$

6.1. $(V_1^4)_T$

One could of course differentiate $V(\vec{r}_1 \ldots \vec{r}_N) = \sum_{i<j} \phi(r_{ij})$ four times. But $(\partial^4 V/\partial x_1^4)_T \equiv (V_{1111})_T$ is by definition an integral over $(d\vec{r}_1)$. So we prefer to perform a partial integration first. Generally,

$$\left(\frac{\partial V}{\partial x_1} A\right)_T = kT \left(\frac{\partial}{\partial x_1} A\right)_T . \tag{6.1}$$

Proof:

$$(A)_T \propto \int d^N\vec{r}\; A(\vec{r}_1 \ldots \vec{r}_N) \exp[-\beta V(\vec{r}_1 \ldots \vec{r}_N)]$$

$$\left(\frac{\partial V}{\partial x_1} A\right)_T \propto \int d^N\vec{r}\, \frac{\partial V}{\partial x_1}\, A\, e^{-\beta V}$$

$$-\frac{\partial}{\partial x_1}(A\, e^{-\beta V}) + \frac{\partial A}{\partial x_1}\, e^{-\beta V} = \beta A \frac{\partial V}{\partial x_1} e^{-\beta V}$$

$$-\int d^N\vec{r}\, \frac{\partial}{\partial x_1}(A\, e^{-\beta V}) + \left(\frac{\partial A}{\partial x_1}\right)_T = \beta \left(A \frac{\partial V}{\partial x_1}\right)_T .$$

The first integral vanishes (surface term). Let $A = (\partial V/\partial x_1)^3$ in Eq. (6.1). $\partial V/\partial x_1 \equiv V_1$. Then

$$(V_1 V_1^3)_T = kT \left(\frac{\partial}{\partial x_1} V_1^3\right)_T = 3\,kT\, (V_1^2 V_{11})_T$$

$$= 3\; kT\; kT \left(\frac{\partial}{\partial x_1} [V_1\, V_{11}]\right)_T = 3\,(kT)^2\, (V_{11}^2 + V_1\, V_{111})_T$$

$$= 3\,(kT)^2\, (V_{11}^2)_T + 3\,(kT)^3\, (V_{1111})_T .$$

Hence

$$3\,(kT)^3\, (V_{1111})_T = (V_1^4)_T - 3\,(kT)^2\, (V_{11}^2)_T . \qquad (6.2)$$

Since we already know $(V_{11}^2)_T$, only the calculation of $(V_1^4)_T$ remains.

$$V_1 = \frac{\partial V}{\partial x_1} = \frac{\partial}{\partial x_1} \sum_{i<k} \phi(r_{ki}) = \sum_{k=2}^{N} \phi'(r_{k1})\, (-\cos\vartheta_k)$$

where $\cos\vartheta_k = (x_k - x_1)/r_{k1}$ (see section 4.1.). If

$$-\phi'(r_{k1}) \cos\vartheta_k \equiv b_{k1}; \qquad b_{k1} = b_{k1}(\vec{r}_k - \vec{r}_1) \qquad (6.3)$$

then

$$V_1^4 = \sum_{k,\ell,m,n=2}^{N} b_{k1} b_{\ell 1} b_{m1} b_{n1}$$

and

$$(V_1^4)_T \propto \int d\tau_N \sum_{k,\ell,m,n} b_{k1} b_{\ell 1} b_{m1} b_{n1} \left(1 + \sum_{i<j} f_{ij} + \ldots\right). \qquad (6.4)$$

6.2. $\int d\tau_N \sum b_{k1} b_{\ell 1}\, b_{m1}\, b_{n1}$

6.2.1. Cluster types

In this sum, there are the following cluster types. (Now 1 —— k stands for $\int d\tau_N\, b_{k1}$!)

(a) 5 clusters  ν_5

(b) 4 clusters 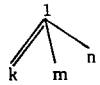 ν_4

(c) 3 clusters  ν_3''  ν_3'

(d) 2 clusters  ν_2.

6.2.2. The counting of non-linear graphs

We demonstrate what we mean on this graph:  It consists of i = 3 points (the fourth labelled with 1 is always the same) and R = 4 lines. The lines occur in groups, namely one group ($n_1 = 1$) with $r_1 = 2$ lines and two groups ($n_2 = 2$) with $r_2 = 1$ line. (Of course, $\sum_j n_j r_j = R$.) Let ν be the number of possible graphs, characterized by (i, R, n_j, r_j).

(a) If it were a linear graph (only single lines),

$$\nu = \bar{n} = (N-1)(N-2)\ldots(N-i) \tag{6.5}$$

(k, m, n = 2, 3, ... N; variations in groups of i.)

(b) Because there are double lines in  , ν is larger than $\bar{n}$. Remember, 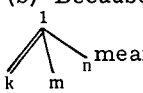 means $\int b_{k1} b_{k1} b_{m1} b_{n1} d\tau_N$. Now this product also originates from $b_{k1}\, b_{m1}\, b_{n1}\, b_{k1}$ etc. So we get

$$\nu = \bar{\bar{n}}\, \bar{n} \tag{6.6}$$

with

$$\bar{\bar{n}} = \frac{R!}{(r_1!)^{n_1}(r_2!)^{n_2}\ldots n_1!\, n_2!\ldots} \tag{6.7}$$

(i) There are R! possible arrays of $k, \ell, m, n \ldots$,
(ii) But permutations of the r_j lines within a group do not count and there are n_j such groups to which this applies.
(iii) Permutations of whole groups with equal number of lines do not count: $1/n_j!$

In this formula $\nu = \bar{n}\,\bar{\bar{n}}$, all clusters of equal (i, R, n_j, r_j) are contained, e.g.

For 

, this yields

$$\nu = \bar{n}\,\bar{\bar{n}} = (N-1)(N-2)(N-3)\frac{4!}{2\cdot 1\cdot 1\cdot 2} = 6(N-1)(N-2)(N-3).$$

This result. we could have obtained in a more direct way, too:

(i) With $k = \ell$, you get $(N-1)(N-2)(N-3) = \bar{n}$ different 

(ii) also $\bar{n}$ such clusters 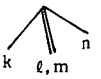

(iii) and $\bar{\bar{n}}$ such clusters 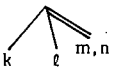

(iv) Each of them also occurs with k, ℓ or ℓ, m or m, n having changed places: ℓ, k; m, ℓ; n, m. This means a factor 2 and from (i), (ii) and (iii) a total

$$\nu = 6\,\bar{n} = 6(N-1)(N-2)(N-3).$$

We now apply Eqs. (6.5), (6.6) and (6.7) to the clusters in section 6.2.1. and obtain

$$\nu_5 = (N-1)(N-2)(N-3)(N-4)$$

$$\nu_4 = 6(N-1)(N-2)(N-3)$$

ν_3' : $i = 2$, $R = 4$, $n_1 = 1$, $r_1 = 3$, $n_2 = 1$, $r_2 = 1$

$$\nu_3' = \frac{4!}{3!\,1\cdot 1\cdot 1}(N-1)(N-2) = 4(N-1)(N-2)$$

(6.8)

ν_3'' : $i = 2$, $R = 4$, $n_1 = 2$, $r_1 = 2$, $n_2 = 0$

$$\nu_3'' = \frac{4!}{2^2\cdot 2!}(N-1)(N-2) = 3(N-1)(N-2)$$

$$\nu_2 = N - 1.$$

Combining the Eqs. (6.8) and section 6.2.1., we obtain

$$\int d\tau_N \sum_{k,\ell,m,n} b_{k1}\, b_{\ell 1}\, b_{m1}\, b_{n1}$$

$$= (N-1)(N-2)(N-3)(N-4) \times \Big[\begin{smallmatrix} & 1 & \\ k & \ell & m & n \end{smallmatrix} \Big] + 6(N-1)(N-2)(N-3) \times \Big[\begin{smallmatrix} & 1 & \\ k & m & n \end{smallmatrix} \Big]$$

$$+4(N-1)(N-2) \times \Big[\begin{smallmatrix} & 1 & \\ k & & n \end{smallmatrix} \Big] + 3(N-1)(N-2) \times \Big[\begin{smallmatrix} & 1 & \\ \ell & & m \end{smallmatrix} \Big] + (N-1) \times \Big[1 \equiv k \Big].$$

(6.9)

To check this, we find that in $\sum b_{k1}\, b_{\ell 1}\, b_{m1}\, b_{n1}$, there are $(N-1)^4 = (N-1)[N^3 - 3N^2 + 3N - 1]$ terms. In Eq. (6.9), there are

$$(N-1)[(N-2)(N-3)(N-4) + 6(N-2)(N-3) + 7(N-2) + 1]$$

$$= (N-1)[N^3 - 3N^2 + 3N - 1].$$

6.3. $\int d\tau_N \sum b_{k1}\, b_{\ell 1}\, b_{m1}\, b_{n1} \sum f_{ij}$.

6.3.1. Cluster types

(The numbers 1), 2) ... below the clusters refer to the multiplicities to be found below.)

(a) 4 clusters $1 \equiv k$ $i \text{---} j$ 3 clusters $\begin{smallmatrix} & 1 & \\ k & & j \end{smallmatrix}$ 2) $\begin{smallmatrix} & 1 & \\ k & & i \end{smallmatrix}$ 3)

1)

2 clusters $1 \equiv k$

4)

(b_1) 5 clusters $\begin{smallmatrix} & 1 & \\ k & & n \end{smallmatrix}$ $i \text{---} j$ 4 clusters $\begin{smallmatrix} & 1 & \\ k & & n \\ & j & \end{smallmatrix}$ 6) $\begin{smallmatrix} & 1 & \\ k & & n \end{smallmatrix}$ $_j$ 7) $\begin{smallmatrix} j & & \\ 1 & & \\ k & & n \end{smallmatrix}$ 8)

5)

3 clusters $\begin{smallmatrix} & 1 & \\ k & & \ell \end{smallmatrix}$ 9) $\begin{smallmatrix} & 1 & \\ k & & \ell \end{smallmatrix}$ 10) $\begin{smallmatrix} & 1 & \\ k & & \ell \end{smallmatrix}$ 11)

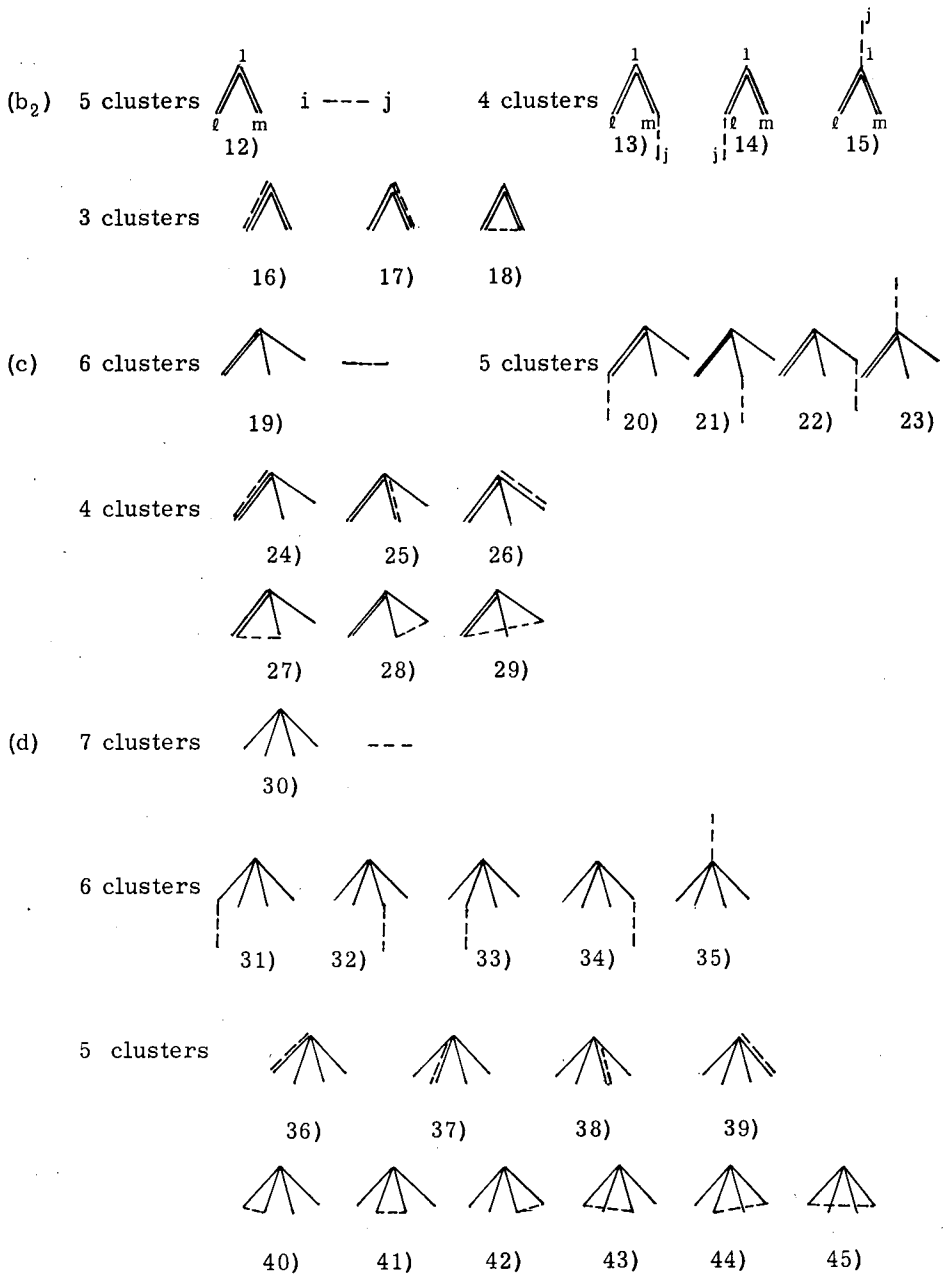

6.3.2. Counting

Using the experience of the foregoing chapters, we find the multiplicity of cluster numbers 1), 2) ... 45) as follows.

1): With k fixed, there are $\frac{1}{2}(N-2)(N-3)$ different $i---j$. There are N-1 values of k.
Result: $\frac{1}{2}(N-1)(N-2)(N-3)$

2): $(N-1)(N-2)$

3): $(N-1)(N-2)$

4): $(N-1)$

5): For each  , there are $\frac{1}{2}(N-3)(N-4)$ different $i---j$. There are $4(N-1)(N-2)$ different  .
Result: $2(N-1)(N-2)(N-3)(N-4)$

6), 7), 8): For each  , there are $N-3$ possible attached $n---j$; $4(N-1)(N-2)$ different  .
Result: $4(N-1)(N-2)(N-3)$

9), 10), 11): $4(N-1)(N-2)$

12):  fixed, $\frac{1}{2}(N-3)(N-4)$ possible $i---j$; $3(N-1)(N-2)$ 
Result: $\frac{3}{2}(N-1)(N-2)(N-3)(N-4)$

13), 14), 15): $3(N-1)(N-2)(N-3)$

16), 17), 18): $3(N-1)(N-2)$

19): For each  , there are $\frac{1}{2}(N-4)(N-5)$ $i---j$; $6(N-1)(N-2)(N-3)$ different 
Result: $3(N-1)(N-2)(N-3)(N-4)(N-5)$

20), 21), 22), 23): $6(N-1)(N-2)(N-3)(N-4)$

24), 25), 26), 27), 28), 29): $6(N-1)(N-2)(N-3)$

30): $\frac{1}{2}(N-5)(N-6)[(N-1)\ldots.(N-4)]$
Result: $\frac{1}{2}(N-1)(N-2)\ldots\ldots(N-6)$

31), 32), 33), 34), 35): $[(N-1)(N-2)\ldots(N-4)](N-5)$

36), 37), ... 45): (10 graphs): $(N-1)(N-2)(N-3)(N-4)$

6.3.3. Summary

$$\int d\tau_N \sum\sum b_{k1}\, b_{\ell 1}\, b_{m1} b_{n1}\, f_{ij}$$

$$= \tfrac{1}{2}(N-1)(N-2)(N-3) \times [\,1 \equiv k \;\; i \;---\; j] + (N-1)(N-2) \times \Big[\overset{1}{\underset{k \quad j}{\wedge}} + \overset{1}{\underset{k \quad j}{\wedge}} \Big]$$

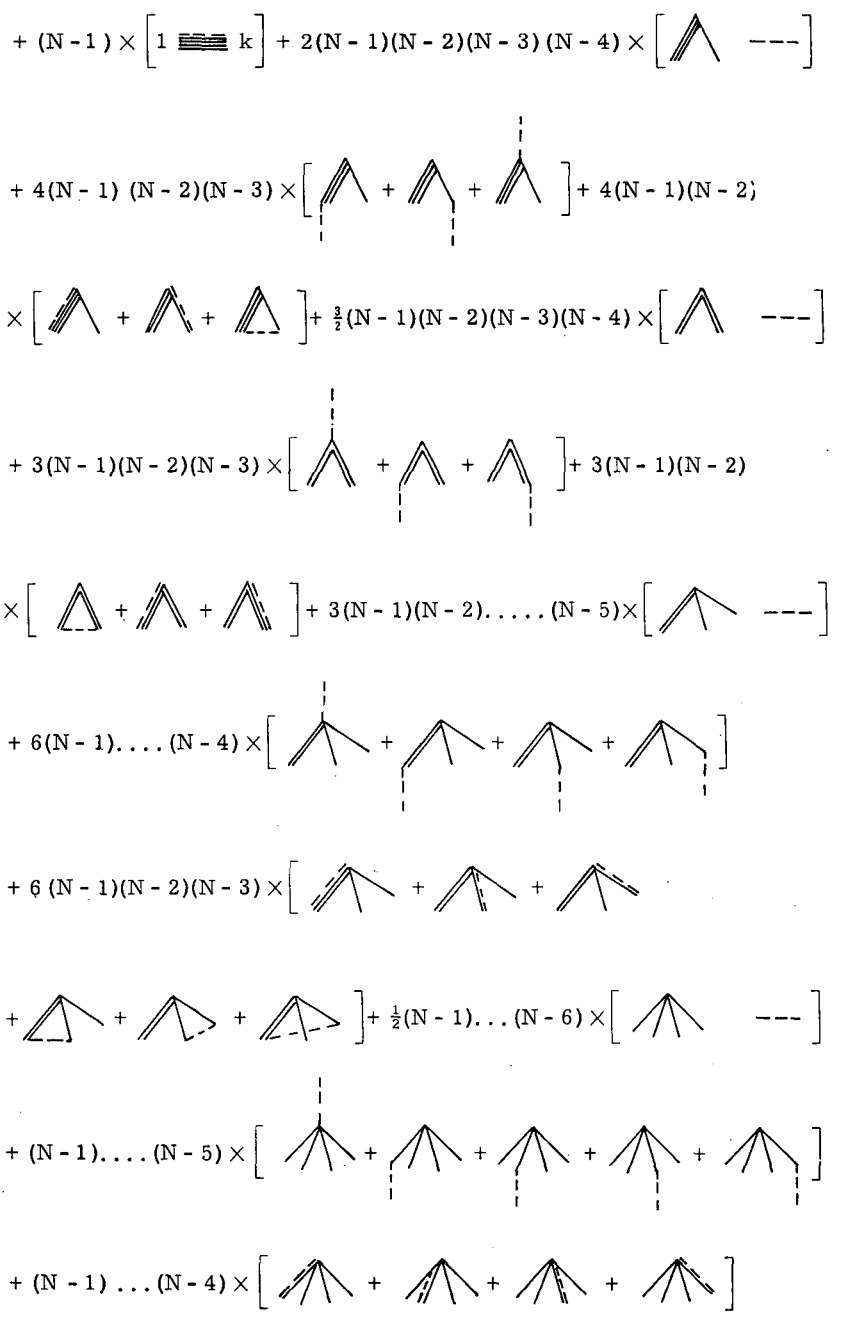
+ (N - 1) ×
1
k
+ 2(N - 1)(N - 2)(N - 3)(N - 4) ×
+ 4(N - 1) (N - 2)(N - 3) ×
+ 4(N - 1)(N - 2)
×
+ ³/₂(N - 1)(N - 2)(N - 3)(N - 4) ×
+ 3(N - 1)(N - 2)(N - 3) ×
+ 3(N - 1)(N - 2)
×
+ 3(N - 1)(N - 2). . . . . (N - 5) ×
+ 6(N - 1). . . . (N - 4) ×
+ 6 (N - 1)(N - 2)(N - 3) ×
+ ½(N - 1). . . (N - 6) ×
+ (N - 1). . . . (N - 5) ×
+ (N - 1) . . . (N - 4) ×

$$+(N-1)\ldots(N-4)\times\Big[$$ 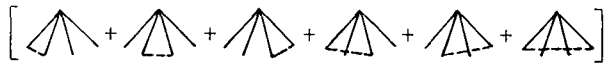 $$+\ldots \qquad (6.10)$$

This expression we call Eq. (6.10). Checking the number of terms we find that in

$$\sum_{k,\ell,m,n=2}^{N} b_{k1}b_{\ell 1}b_{m1}b_{n1} \sum_{i<j,i=1}^{N} f_{ij}$$

there are

$$(N-1)^4\binom{N}{2} = \frac{N-1}{2}[N^5 - 4N^4 + 6N^3 - 4N^2 + N]$$

terms. Adding up the number of graphs in (6.10) yields the same. From Eqs. (6.9) and (6.10) we obtain $(V_1^4)_T$ (see Eq. (6.4)) and by means of Eq. (6.2) finally $(V_{1111})_T$.

7. QUADRATURE OF THE GRAPHS

7.1. 1 ═══ k

In section 4.4. we had

$$1 \text{═══} k = \int d\tau_N \; a_{k1}f_{1k} = \int \frac{d^N\vec{r}}{V^N} a(\vec{r}_k - \vec{r}_1)\, f(r_{k1}) \qquad (7.1)$$

a_{k1} was defined in Eq. (4.1) as

$$a_{k1} = \phi''(r_{k1})\cos^2\vartheta_k + \frac{\phi'(r_{k1})}{r_{k1}}\sin^2\vartheta_k \qquad (7.2)$$

with $\cos\vartheta_k = (x_k - x_1)/r_{k1}$ and $f(r) = e^{-\beta\phi(r)} - 1$. Considering f, ϕ, ϕ', ϕ'/r and ϕ'' as integrable functions, we obtain from Eq. (7.1)

$$1 \text{═══} k = \int\int \frac{d\vec{r}_1\, d\vec{r}_k}{V^2} a(\vec{r}_k - \vec{r}_1) f(r_{k1})$$

Substituting $\vec{r}_k - \vec{r}_1 \equiv \vec{r}$ and $r_{k1} = r$,

$$1 \text{═══} k = \int \frac{d\vec{r}_1}{V} \int \frac{d\vec{r}}{V} f(r)\, a(\vec{r}) = \int \frac{d\vec{r}}{V} f(r)\, a(\vec{r})$$

With $a(\vec{r})$ from Eq. (7.2), one can introduce polar co-ordinates. Depending on ϕ, the radial part is elementary or not. In the latter case, numerical

computation is necessary. As previously mentioned, the values of the graphs apparently are independent of the naming of the subscripts.

7.2. 

$$\begin{array}{c}1\\ \diagdown\ \diagup\\ k\quad j\end{array} = \iiint \frac{d\vec{r}_1\, d\vec{r}_k\, d\vec{r}_j}{v^3}\, a_{k1} f_{j1}$$

We set $\vec{r}_j - \vec{r}_1 = \vec{r}$ and perform $\int d\vec{r}_j$, then we set $\vec{r}_k - \vec{r}_1 = \vec{r}'$ and perform $\int d\vec{r}_k$. The last integration $\int d\vec{r}_1$ simply yields v. In this way, we get

$$\begin{array}{c}1\\ \diagdown\ \diagup\\ k\quad j\end{array} = \int \frac{d\vec{r}}{v} f(r) \int \frac{d\vec{r}'}{v}\, a(\vec{r}')$$

7.3. 

This cluster can be treated similarly. (Start with $\int d\vec{r}_1$.) 1 —— k i ––– j falls into two parts from the beginning.

7.4. 

This type splits into products of three single integrals, to be treated by three successive substitutions $\vec{r}_k - \vec{r}_1 = \vec{r}$ etc..

7.5. 

These can also be separated or "reduced" to clusters of lower orders. (Start with $\int d\vec{r}_\ell$, then $\int d\vec{r}_1$.)

7.6. Closed triangles

$$\begin{array}{c}1\\ \diagdown\ \diagup\\ k\ \_\_\ \ell\end{array} = \int d\tau_N\, a_{k1} a_{\ell 1} f_{k\ell} = \iiint \frac{d\vec{r}_1\, d\vec{r}_k\, d\vec{r}_\ell}{v^3}\, a_{k1}\, a_{\ell 1}\, f_{k\ell}$$

This is the first irreducible cluster. Substitutions $\vec{r}_k - \vec{r}_1 = \vec{r}$, $\vec{r}_\ell - \vec{r}_1 = \vec{r}'$ do not work because of $f(r_{k\ell})$. Therefore, machine integration must be used. While, for a specific gas, the parameters of the potential ϕ can be inserted

numerically, in f(r) the temperature T is contained. So, the computation must be repeated for every value of T.

Fortunately, the number of closed triangle-graphs is small in our approximation. Summing up sections 4,5 and 6, one finds only four such clusters which do not vanish.

8. REMARKS ON THE CONVERGENCE OF THE CLUSTER EXPANSION

We had

$$(A)_T = \int \frac{d^N\vec{r}}{v^N} A\, e^{-\beta V} \Big/ \int \frac{d^N\vec{r}}{v^N} e^{-\beta V} \tag{8.1}$$

(v^N we have added for convenience.)
(We note, that the classical Maxwell-Boltzmann statistics have been used, indistinguishability not being taken into account. But the latter brings only a factor $1/N!$, which is cancelled in Eq. (8.1). Maxwell-Boltzmann statistics apply to the usual temperatures, as long as the thermal wavelength $\lambda \ll \sqrt[3]{v/N}$), The denominator

$$\int \frac{d^N\vec{r}}{v^N} e^{-\beta V} \equiv e^{N\alpha} \qquad (N \to \infty) \tag{8.2}$$

has been treated extensively in virial theory, which yields

$$\alpha = \sum_{\nu=1}^{\infty} \left(\frac{N}{v}\right)^{\nu} \beta_\nu(T),$$

β_ν being virial coefficients. The order of magnitude of β_ν is v_0^ν (v_0 being the hard-core volume), so

$$\left(\frac{N}{v}\right)^{\nu} \beta_\nu \simeq \left(\frac{N v_0}{v}\right)^{\nu} .$$

remains finite, when $N \to \infty$, $v \to \infty$; N/v = constant; and α exists as long as $Nv_0 < v$. (This is true for non-condensed gases.) For the problem of convergence of virial expansions, see [3].

With α finite,

$$e^{N\alpha} = \int \frac{d^N\vec{r}}{v} e^{-\beta V}$$

diverges for $\alpha > 0$, $N \to \infty$.

8.1. Behaviour of the numerator of Eq. (8.1)

For example, let $A(\vec{r}_1 \ldots \vec{r}_N) \equiv V_{11}(\vec{r}_1 \ldots \vec{r}_N)$. We found

$$\int \frac{d^N\vec{r}}{v^N} V_{11}\, e^{-\beta V}$$

$$= (N-1) \times \left[k \text{ —— } 1 + k \text{ ═══ } 1 \right] + (N-1)(N-2) \times \left[\begin{array}{c} 1 \\ \diagup\ \diagdown \\ k \quad j \end{array} + \begin{array}{c} 1 \\ \diagup \\ k \text{ - - - } j \end{array} \right]$$

$$+ \tfrac{1}{2}(N-1)(N-2)(N-3) \times \left[\begin{array}{l} i \text{ - - - } j \\ 1 \text{ —— } k \end{array} \right] + \ldots \qquad (8.3)$$

For $N \to \infty$, $N - i \simeq N$, $i = 1, 2 \ldots$

k —— $1 = \int \frac{d\vec{r}}{v} a(\vec{r}) \simeq \frac{v_0}{v}$, since $a(\vec{r})$ vanishes for $|\vec{r}| \gg r_0$; $r_0 \ldots$ hard core radius

k ═══ $1 = \int \frac{d\vec{r}}{v} a(\vec{r}) f(r) \simeq \frac{v_0}{v}$ for the same reason

$$\begin{array}{c} 1 \\ \diagup\ \diagdown \\ k \quad j \end{array} = \int \frac{d\vec{r}}{v} a(\vec{r}) \int \frac{d\vec{r}}{v} f(r) \simeq \frac{v_0^2}{v^2}, \qquad \begin{array}{c} 1 \\ \diagup \\ k \text{ - - - } j \end{array} \simeq \frac{v_0^2}{v^2}$$

$$\begin{array}{l} i \text{ - - - } j \\ 1 \text{ —— } k \end{array} = \int \frac{d\vec{r}}{v} f(r) \int \frac{d\vec{r}}{v} a(\vec{r}) \simeq \frac{v_0^2}{v^2}$$

Consequently, the last term in Eq. (8.3) diverges as

$$\lim_{N,v\to\infty} N^3 \frac{v_0^2}{v^2} = \lim N \frac{N^2 v_0^2}{v^2}$$

in spite of our assumption $(Nv_0/v)^2 \ll 1$. So the numerator diverges, too. But from physical reasons, we know that the entire fraction (Eq. (8.1)) will exist or be proportional to N, if A is an extensive quantity.

Similar arguments apply to $(V_{11}^2)_T$, $(V_{1111})_T$.

9. THE SELF-CORRELATION FUNCTION FOR LARGE TIMES

Until now, the underlying theory of Schofield, which made use of a Taylor series in t, limited the results to small times. For large times, we make use of a theory by RAHMAN et al. [4] and SINGWI et al. [5]. They have worked out the correlation function

$$\frac{1}{N} \left\langle \sum_i \exp[-i\vec{\kappa} \cdot \vec{r}(0)] \exp[i\vec{\kappa} \cdot \vec{r}(t)] \right\rangle_T$$

which they call F_s (Schofield's γ_s) in terms of velocity-correlation functions, valid for all values of t and get

$$\ln F_s(\vec{\kappa}, t) = -\kappa^2\left(-\frac{i\hbar t}{2m} + \gamma_1(t)\right) + \kappa^4\gamma_2(t) + O(\kappa^6) \tag{9.1}$$

where

$$\gamma_1(t) = \int_0^t (t - t_1)\langle v_\kappa(0)\, v_\kappa(t_1)\rangle_T\, dt_1 = \frac{1}{3}\int_0^t (t - t_1)\langle \vec{v}(0)\vec{v}(t_1)\rangle dt_1 \tag{9.2}$$

For our target being isotropic in space,

$$\langle v_\kappa(0)\, v_\kappa(t)\rangle_T = \frac{1}{3}\langle \vec{v}(0)\vec{v}(t)\rangle_T .$$

$$\gamma_2(t) = \int_0^t dt_1 \int_0^{t_1} dt_2 \ldots \int_0^{t_3} dt_4 \langle v_\kappa(t_4)\, v_\kappa(t_3)\, v_\kappa(t_2)\, v_\kappa(t_1)\rangle_T - \frac{1}{2}\gamma_1^2(t) \tag{9.3}$$

Here $v_\kappa(t)$ is a Heisenberg operator, v_κ being defined by $\vec{\kappa}\cdot\vec{v} \equiv \kappa \cdot v_\kappa$, $\vec{v} \equiv \vec{p}/m$, $\vec{p}$ being the momentum operator.

9.1. Schofield's expression

If we recall Schofield's expression (see Eqs. (1.3)-(1.6)), comparison yields

$$\left.\begin{aligned} \gamma_1(t) &= \Gamma_1(y^2) + \frac{i\hbar t}{2m} \\ \gamma_2(t) &= \Gamma_2(y^2) \end{aligned}\right\} \quad t \text{ small} \tag{9.4, 9.5}$$

Thus, we know $\gamma_1(t)$ and $\gamma_2(t)$ from our cluster expansion. By differentiating Eq. (9.2) twice, we also know

$$\frac{1}{3}\langle \vec{v}(0)\vec{v}(t)\rangle_T = \frac{d^2}{dt^2}\gamma_1(t) = \frac{d^2}{dt^2}\left(\Gamma_1 + \frac{i\hbar t}{2m}\right) \tag{9.6}$$

for $0 \leqslant t \leqslant t_0$, t_0 being the upper limit for Γ_1, Γ_2 to converge reasonably.

9.2. Rahman et al.

Now Rahman et al. show that for $t \to \infty$

$$\gamma_n(t) = D_n \cdot t - C_n$$

with

$$D_1 = \frac{1}{3}\int_0^\infty \langle \vec{v}(0)\vec{v}(t_1)\rangle_T\, dt_1 \tag{9.7}$$

$$C_1 = \frac{1}{3}\int_0^\infty t_1 \cdot \langle \vec{v}(0)\vec{v}(t_1)\rangle_T \, dt_1 \tag{9.8}$$

Besides, they indicate that for large t and not too large κ^2 ($\kappa^2 D_1 \tau \ll 1$, τ being the correlation time), γ_1 gives the dominant contribution to Eq. (9.1). The higher γ_n may be neglected in this case.

All one has to know is $\langle \vec{v}(0)\,\vec{v}(t)\rangle_T$ for all times in order to find $F_s(\vec{\kappa}, t)$ for large t.

From Eq. (9.6), we know the velocity auto-correlation for small t. For large t, however, it is known that quantum effects are not important any more [6]. Therefore, the classical calculation of $(\vec{v}(0)\vec{v}(t))_T$ for large t suffices, which can be done by means of Langevin's stochastic diffusion theory [6, 7, 8]. This leads to

$$\frac{1}{3}(\vec{v}(0)\vec{v}(t))_T = \frac{kT}{m} e^{-\eta t}; \qquad t_* \leqslant t \leqslant \infty, \tag{9.9}$$

where η is the viscosity and t_* the lower limit for the classical approximation to be valid (Condition: $t_* \gg \hbar/kT$).

9.3. Calculation of D_1

We split up the integral in Eq. (9.7) according to

$$D_1 = \int_0^{t_0} dt_1 (\text{Eq. (9.6)}) + \int_{t_*}^{\infty} dt_1 (\text{Eq. (9.9)}); \tag{9.10}$$

that means we use Eq. (9.6) as integrand in the first integral and Eq. (9.9) in the second. Of course, $t_0 \simeq t_*$ is desirable. This depends on how many clusters one calculates. From Eq. (9.6) it follows that

$$\frac{1}{3}\int_0^{t_0} dt_1 \langle \vec{v}(0)\vec{v}(t_1)\rangle_T = \Gamma_1'(y_0^2)\left(2t_0 - \frac{i\hbar}{kT}\right) + \frac{i\hbar}{2m}$$

where $y_0^2 \equiv y^2(t = t_0) = t_0^2 - (i\hbar t_0/kT)$ and $\Gamma_1' = (d/dy^2)\Gamma_1$. Here, we have used $\gamma_1'(0) = 0$, which comes from Eq. (9.2). If $t_0 \simeq t_*, y_0^2 \simeq t_0^2$ and

$$t_0 \gg \frac{\hbar}{kT} \quad \text{or} \quad \frac{t_0 kT}{\hbar} \gg 1 \tag{9.11}$$

From Eq. (9.9) one finds

$$\frac{1}{3}\int_{t_*}^{\infty} dt_1 \, (\vec{v}(0)\vec{v}(t))_T = \frac{kT}{m\eta} e^{-\eta t_*}$$

Hence, Eq. (9.10) becomes

$$D_1 = \Gamma_1'(t_0^2)\, 2t_0 + \frac{i\hbar}{2m} + \frac{kT}{m\eta}\, e^{-\eta t^*} \tag{9.12}$$

Γ_1 in Schofield's theory was given by

$$\Gamma_1(y^2) = \frac{1}{2}\frac{kT}{m} y^2 \left[1 - \frac{1}{12}\frac{\hbar^2}{m(kT)^2}(V_{11})_T \left(\frac{kTy}{\hbar}\right)^2 + \ldots\right] \tag{9.13}$$

Hence,

$$\frac{d\Gamma_1}{dy^2} = \frac{kT}{2m} - \frac{1}{24}\frac{\hbar^2}{m^2 kT}(V_{11})_T \frac{(kT)^2}{\hbar^2}\, 2y^2 + \ldots$$

$$\Gamma_1'(t_0^2) = \frac{kT}{2m} - \frac{\hbar^2}{12m^2 kT}(V_{11})_T \left(\frac{t_0 kT}{\hbar}\right)^2 \tag{9.14}$$

and from Eq. (9.12)

$$D_1 = 2t_0\left[\frac{kT}{2m} - \frac{\hbar^2}{12m^2 kT}(V_{11})_T\left(\frac{t_0 kT}{\hbar}\right)^2\right] + \frac{kT}{m\eta} e^{-\eta t^*} + i\frac{\hbar}{2m} \tag{9.15}$$

The imaginary part $\hbar/2m$ could be neglected because of Eq. (9.11), but for $\ln \gamma_s$ (see Eq. (9.1)), we just need $D_1 - (i\hbar/2m)$ which from Eq. (9.15) appears to be real.

9.4. Calculation of C_1

Similarly to Eq. (9.10), we write

$$C_1 = \int_0^{t_0} t_1 (\text{Eq. (9.6)})\, dt_1 + \int_{t^*}^{\infty} t_1 (\text{Eq. (9.9)})\, dt_1 \tag{9.16}$$

$$\int_0^{t_0} t_1 (\text{Eq. (9.6)})\, dt_1 = \int_0^{t_0} t_1 \gamma_1''(t_1)\, dt_1 = t_0\gamma_1'(t_0) - \gamma_1(t_0)$$

and with Eq. (9.4), one arrives at

$$\int_0^{t_0} t_1 (\text{Eq. (9.6)})\, dt_1 = t_0\Gamma_1'(y_0^2)\left(2t_0 - \frac{i\hbar}{kT}\right) + \frac{i\hbar t_0}{2m} - \Gamma_1(y_0^2) - \frac{i\hbar t_0}{2m}$$

Here, we can insert Eq. (9.11), i.e. $y_0^2 \simeq t_0^2$, $2t_0 - i\hbar/kT \simeq 2t_0$, Eq. (9.14) for $\Gamma_1'(y_0^2 = t_0^2)$, and Eq. (9.13) for $\Gamma_1(y_0^2 = t_0^2)$. Doing this, one gets

$$\int_0^{t_0} t_1(\text{Eq. (9.6)})\,dt_1 = t_0\left[\frac{kT}{2m} - \frac{\hbar^2}{12m^2kT}(V_{11})_T\left(\frac{kT\,t_0}{\hbar}\right)^2\right] 2t_0$$

$$- \frac{kTt_0^2}{2m}\left[1 - \frac{\hbar^2}{12\,m(kT)^2}(V_{11})_T\left(\frac{kTt_0}{\hbar}\right)^2\right]$$

$$= \frac{t_0^2kT}{2m}\left[1 - \frac{3\hbar^2}{12\,m(kT)^2}(V_{11})_T\left(\frac{kTt_0}{\hbar}\right)^2\right] \qquad (9.17)$$

$$\int_{t_*}^{\infty} t_1(\text{Eq. (9.9)})\,dt_1 = \frac{kT}{m}\int_{t_0}^{\infty} t_1\,e^{-\eta t_1}\,dt_1 = \frac{kT}{m\eta}\,e^{-\eta t_*}\left(t_* + \frac{1}{\eta}\right) \qquad (9.18)$$

Inserting Eqs. (9.17) and (9.18) in Eq. (9.16) yields

$$C_1 = \frac{t_0^2kT}{2m}\left[1 - \frac{3\hbar^2}{12\,m(kT)^2}(V_{11})_T\left(\frac{kTt_0}{\hbar}\right)^2\right] + \frac{kT}{m\eta}\left(t_* + \frac{1}{\eta}\right)e^{-\eta t_*} \qquad (9.19)$$

So we have found D_1 and C_1 in $\gamma_1(t) = t\,D_1 - C_1$ for $t \to \infty$. And Eq. (9.1) finally becomes

$$\ln \gamma_s(\vec{\kappa}, t) = -\kappa^2\left(-\frac{i\hbar t}{2m} + t\,D_1 - C_1\right); \quad t \to \infty.$$

10. CONCLUSIONS

For small times, the self-correlation function and also the velocity auto-correlation function of real gases can be calculated by means of cluster expansions of the thermal averages occurring in Schofield's theory. From this and with the help of Langevin's diffusion theory, used only in the long time range where it is valid, it is possible to find the diffusion constants D_1 and C_1 as defined in [4, 5], whence the self-correlation function for large times is also known.

ACKNOWLEDGEMENTS

I am grateful to H. Nowotny (of this Institute) for a critical reading of the manuscript and some very helpful discussions. I also wish to acknowledge the generous financial support of the Verband der Freunde der Technischen Hochschule in Vienna, which enabled me to attend this Symposium.

REFERENCES

[1] SCHOFIELD, P., Inelastic Scattering of Neutrons in Solids and Liquids, IAEA, Vienna (1961) 39-50.
[2] HUANG, K., Statistical Mechanics, John Wiley and Sons, Inc., N.Y. (1963).

[3] LEBOWITZ, J. and PENROSE, O., J. Math. Phys. 5 7 (1964).
[4] RAHMAN, A., SINGWI, K. and SJÖLANDER, A., Phys. Rev. 126 (1962) 986.
[5] SINGWI, K., SJÖLANDER, A. and RAHMAN, A., Inelastic Scattering of Neutrons in Solids and Liquids I IAEA, Vienna (1963) 215-25.
[6] VINEYARD, G., Phys. Rev. 110 (1958) 999.
[7] SCHOFIELD, P., in Fluctuation, Relaxation and Resonance in Magnetic Systems", (TER HAAR, D., Ed.) Oliver and Boyd (1962).
[8] GLAUBER, R., in Lectures in Theoretical Physics IV Interscience Publ. (1962).

DISCUSSION

K.S. SINGWI: You might be interested to know that Professor Nijboer at the Argonne National Laboratory recently performed the small-time expansion of the velocity autocorrelation function (expansion carried up to t^6), and the coefficients of expansion are to be calculated numerically for the case of liquid argon. As yet, no results are available.

D.J. SIGMAR: What potential was used?

K.S. SINGWI: It was a Lennard-Jones 6-12 potential.

S. YIP: As you know, the kinetic approach also gives a non-Gaussian result. It would be interesting to compare your numerical results with those obtained by solving the kinetic equation describing $G_S(r,t)$. The latter are being investigated by Desai at Cornell. In addition, Nussal at Michigan has investigated the quantum correction and the effect of a potential, so it would be interesting to compare your results with his.

COHERENT SCATTERING OF SLOW NEUTRONS BY LIQUID SODIUM*

K. S. SINGWI AND G. FELDMANN**
ARGONNE NATIONAL LABORATORY, ARGONNE, ILL.,
UNITED STATES OF AMERICA

Abstract — Résumé — Аннотация — Resumen

COHERENT SCATTERING OF SLOW NEUTRONS BY LIQUID SODIUM. This paper presents a calculation of the scattering law $S(\alpha,\beta)$ for liquid sodium at two different temperatures, based on a phenomenological theory of coherent scattering of slow neutrons by liquids developed earlier by one of us (K. S. S.). The main result of this paper is that for small values of β the peaks of $S(\alpha,\beta)$, which are characteristic of $1 + \Gamma(\vec{\kappa})$ curve, tend to disappear for large values of β, a result in agreement with Randolph's observations and which cannot be explained by the convolution approximation of Vineyard. Further, the calculated curves for $S(\alpha,\beta)$ suggest that precision experiments would be needed to determine the dispersion relation for "phonons" and the range of coherence R in a classical liquid.

DIFFUSION COHÉRENTE DES NEUTRONS LENTS PAR LE SODIUM LIQUIDE. Les auteurs présentent un mode de calcul de la loi de diffusion $S(\alpha,\beta)$ pour le sodium liquide à deux températures différentes; le calcul se fonde sur la théorie phénoménologique de la diffusion cohérente des neutrons lents par les liquides, proposée antérieurement par l'un des auteurs (K. S. S.). La conclusion essentielle du mémoire est que les pics de $S(\alpha,\beta)$, caractéristiques de la courbe $1 + \Gamma(\vec{\kappa})$, que l'on constate pour les petites valeurs de β, tendent à disparaître pour les grandes valeurs de β. Ce résultat, qui concorde avec les observations de Randolph, ne saurait être expliqué par l'approximation de convolution de Vineyard. En outre, il semble ressortir du calcul des courbes de $S(\alpha,\beta)$ que des expériences de précision seraient nécessaires pour déterminer le rapport de diffusion pour les « phonons» et la gamme de cohérence R dans un liquide classique.

КОГЕРЕНТНОЕ РАССЕЯНИЕ МЕДЛЕННЫХ НЕЙТРОНОВ НА ЖИДКОМ НАТРИИ. Дается расчет закона рассеяния $S(\alpha,\beta)$ для жидкого натрия при двух различных температурах, основанный на феноменологической теории когерентного рассеяния медленных нейтронов на жидкостях, разработанной ранее одним из авторов (К.С.С.). Основным результатом настоящей работы является то, что для небольших значений β пики $S(\alpha,\beta)$, характеризующие кривую $1+\Gamma(\vec{\kappa})$, сглаживаются при больших значениях β. Этот результат согласуется с наблюдениями Рандольфа и не может быть объяснен приближением свертки функций, предложенным Вайнярдом. Кроме того, рассчитанные кривые для $S(\alpha,\beta)$ показывают, что для определения дисперсионного соотношения для "фононов" и области когерентности R в классической жидкости необходимы точные эксперименты.

DISPERSIÓN COHERENTE DE NEUTRONES LENTOS EN EL SODIO LÍQUIDO. En la memoria se calcula la ley de dispersión $S(\alpha,\beta)$ para el sodio líquido a dos temperaturas diferentes, basándose en la teoría fenomenológica de la dispersión coherente de neutrones lentos en líquidos, formulada anteriormente por uno de los autores (K. S. S.). El resultado más importante de este trabajo es que los picos característicos de $S(\alpha,\beta)$, que se observan para valores reducidos de β y que constituyen un reflejo de los picos de la función $1 + \Gamma(\vec{\kappa})$, tienden a desaparecer para valores elevados de β, resultado que concuerda con las observaciones de Randolph y que no puede explicar la aproximación basada en la integral de convolución de Vineyard. Asimismo, las curvas calculadas para $S(\alpha, \beta)$ sugieren que serían necesarios experimentos de gran precisión para determinar la relación de dispersión de los « fonones» y el alcance de la coherencia R en un líquido clásico.

---

* Based on work performed under the auspices of the United States Atomic Energy Commission.

** Present address: Department of Physics, Harvard University, Cambridge, Mass., United States of America.

1. INTRODUCTION

In a paper [1], one of us (K. S. S.) proposed an extension of the convolution approximation of VINEYARD [2] to treat the coherent scattering of slow neutrons by a monatomic liquid. The intermediate scattering function $F(\vec{\kappa},t)$ can be written as

$$F(\vec{\kappa}, t) = (1 + \Gamma(\vec{\kappa}))F_s(\vec{\kappa}, t) + H(\vec{\kappa}, t), \tag{1}$$

where

$$H(\vec{\kappa}, t) = \frac{1}{N}\sum_{\alpha\neq\beta}^{<R} \langle \exp(i\vec{\kappa}\cdot\vec{R}_\alpha(0))\, \exp(-i\vec{\kappa}\cdot\vec{R}_\beta(t))\rangle_T$$

$$-\frac{1}{N}\sum_{\alpha\neq\beta}^{<R} \langle \exp(i\vec{\kappa}\cdot\vec{R}_\alpha(0))\, \exp(-i\vec{\kappa}\cdot\vec{R}_\beta(0))\rangle_T \langle \exp(i\vec{\kappa}\cdot\vec{R}_\beta(0))$$

$$\exp(-i\vec{\kappa}\cdot\vec{R}_\beta(t))\rangle_T, \tag{2a}$$

where $\vec{R}_\alpha(0)$ is the position vector of atom α at time 0 and $\vec{R}_\beta(t)$ is the position vector of atom β at time t and both are the usual Heisenberg operators. The sum in Eq. (2a) extends over all atoms β which lie within a sphere of radius R with atom α as the centre, and is to be understood in the following sense

$$\frac{1}{N}\sum_{\alpha\neq\beta}^{<R} \langle \exp(i\vec{\kappa}\cdot\vec{R}_\alpha(0))\exp(-i\vec{\kappa}\cdot\vec{R}_\beta(0))\rangle_T = \int e^{i\vec{\kappa}\cdot\vec{r}} g(\vec{r})\, \exp(-|\vec{r}|^2/R^2)d\vec{r}, \tag{2b}$$

$g(\vec{r})$ being the static pair correlation function. $\vec{\kappa}$ is the momentum transfer. In writing $F(\vec{\kappa}, t)$ in the form given by Eq. (1), it has been assumed that the convolution approximation is good for all atoms whose distance of separation is greater than a certain distance R, which is a parameter of the model. The correction term $H(\vec{\kappa}, t)$, which is supposed to take care of correlated motions of neighbouring atoms for short times, times of the order of 10^{-12} s or less, was evaluated as if the liquid behaved like a "quasi-harmonic" solid. To test how good or bad this model was, an explicit numerical calculation of the width of the "quasi-elastic" scattering as a function of momentum transfer $\vec{\kappa}$ was made for liquid argon near the triple point. The calculated width exhibited an oscillatory behaviour which for certain values of the parameters agreed reasonably well with the observations of BROCKHOUSE et al. [3] and those of LARSSON and co-workers [4]. This agreement gave us some confidence in our model.

In a second paper [5], the calculations of Ref. [1] were improved in several respects; in particular it was shown what role the coherence para-

meter R played in determining the width of the "quasi-elastic" scattering (whereas in [1] the case $R \to \infty$ was considered). Besides, a formula for the inelastic differential scattering cross-section in "one-phonon" approximation was derived without making any assumption regarding the existence of a reciprocal lattice vector in a liquid. The harmonic approximation was, however, used. This formula was used to calculate the scattering law $S(\alpha, \beta)$ for liquid argon near the triple point. It was also shown in Ref. [5] that in the limit $R \to \infty$ and $\vec{q} \ll \vec{\kappa}$, $\vec{q}$ being the wave number of the "phonon", our formula for coherent inelastic scattering reduced to that valid for a polycrystalline solid after appropriate modifications as introduced by EGELSTAFF [6] for the case of a liquid. The latter formula was used by KROÓ et al. [7] to analyse their scattering data, and which analysis led these authors to arrive at a dispersion relation for "phonons" in liquid argon.

A result of some significance which we arrived at in Ref. [5] for liquid argon is the following: the characteristic peaks of $S(\alpha, \beta)$ which occur for small values of β, and which are a reflection of the peaks of $1 + \Gamma(\vec{\kappa})$, tend to disappear for large values of β, a result which cannot be accounted for by the convolution approximation. Such a behaviour of $S(\alpha, \beta)$ has been observed by RANDOLPH [8] in his studies with liquid sodium. This led us to apply our model to liquid metals, and in this paper we present detailed numerical calculations of $S(\alpha, \beta)$ for liquid sodium as a function of α for various values of β. These curves for $S(\alpha, \beta)$ suggest the direction in which future experiments ought to be done and the accuracy needed if we were to determine a dispersion relation for "phonons" in a liquid and the range of coherence R.

It is worth mentioning here that the considerations of our model are more valid the closer the behaviour of a liquid is to that of a solid. And since in liquid metals experimental indications [8-11] are that, at least for times of interest in slow neutron scattering, the behaviour of the mean square displacement $\rho(t)$ of an atom resembles more that of a solid, these liquids offer a best testing ground for our model. Studies with liquid metals might, therefore, help in elucidating the nature of coherent scattering. And this has been the main motivation for this paper.

2. MATHEMATICAL FORMULAE

The mathematical framework was developed in Refs. [1] and [5] to which the reader is referred. We give below the relevant formulae needed for present calculations. The inelastic differential scattering cross-section in "one-phonon" approximation (for energy gain) is given by

$$\frac{d^2\sigma}{d\Omega d\omega} = \frac{N}{4\pi} \frac{k}{k_0} \sigma_{coh} \exp\left(-\frac{\hbar\omega}{2k_B T}\right) \exp(-\vec{\kappa}^2 \hat{a}) \coth\left(\frac{\hbar\omega}{2k_B T}\right) \frac{\vec{\kappa}^2 \hbar}{4M} \frac{1}{\omega^2} f(\omega)$$

$$\left[\frac{\sigma_{inc}}{\sigma_{coh}} + 1 + \Gamma(\vec{\kappa}) + \operatorname{sech}\left(\frac{\hbar\omega}{2k_B T}\right) \frac{1}{6} \frac{\omega^2}{c^2} L(R, \kappa, q)\right], \qquad (3)$$

where the function $L(R, \kappa, q)$ is defined by

$$L(R, \kappa, q) = \frac{3R}{q^2\kappa\sqrt{\pi}} \int_0^\infty k\,\Gamma(k)dk \frac{1}{2q} \int_{-q}^{+q} \left\{ \left[\exp\left(-\frac{R^2}{4}(\kappa - k + x)^2\right) \right.\right.$$

$$\left. - \exp\left(-\frac{R^2}{4}(\kappa + k + x)^2\right)\right] - \left[\exp\left(-\frac{R^2}{4}(\kappa - k)^2\right)\right.$$

$$\left.\left. - \exp\left(-\frac{R^2}{4}(\kappa + k)^2\right)\right]\right\} dx, \tag{4}$$

see Eqs. (45) and (46) of [5]. In the above equations the coherence parameter R has the same meaning as in Eq. (2) and q is the magnitude of the wave number of the "phonon" whose mean velocity is defined by c. The other symbols have their usual meaning. $f(\omega)$ is the generalized frequency distribution function given by the Fourier transform of the velocity autocorrelation function. $\Gamma(\vec{\kappa})$ is the Fourier transform of the static pair correlation function $g(\vec{r})$ of the liquid; $\exp(-\vec{\kappa}^2 a)$ is the usual Debye-Waller factor.

$f(\omega)$ can be assumed to consist of a sum of two functions $f_1(\omega)$ and $f_2(\omega)$, the former corresponding to the diffusive type of modes and the latter to the damped vibratory type of modes. For our purpose we can neglect $f_1(\omega)$ for two reasons: (a) Since the mean square displacement of a sodium atom is very much like that of a solid [8] for times $\sim 2\times 10^{-12}$ s, one would expect [12] to get an $f(\omega)$ such that the area under $f_1(\omega)$ is very small compared to the area under $f_2(\omega)$; and (b) Since we are interested here in values of energy transfers $\hbar\omega$ which are large compared to the width of $f_1(\omega)$, we can forget about the latter. For $f(\omega)$ we therefore assume the following simple form:

$$f(\omega) = \frac{4\omega^2}{\omega_m^3} e^{-2\omega/\omega_m}, \tag{5}$$

which is so chosen that it is normalized to unity and has a maximum for $\omega = \omega_m$; ω_m is a parameter which is adjusted to fit the experimental data.

Introducing the dimensionless variables

$$\alpha = \vec{\kappa}^2\hbar^2/2Mk_BT \tag{6}$$

and

$$\beta = \hbar\omega/k_BT, \tag{7}$$

and using Eq. (5) and assuming $\hbar\omega < 2k_BT$, we can write Eq. (3) in the following form:

$$\frac{1}{N}\frac{d^2\sigma}{d\Omega dE} = \left(\frac{E}{E_0}\right)^{\frac{1}{2}} \exp(-\hbar\omega/2k_BT) S_R(\vec{\kappa}, \hbar\omega), \tag{8}$$

where

$$S_R(\vec{\kappa}, \hbar\omega) = \frac{\sigma_{coh}}{4\pi k_B T} S(\alpha, \beta). \tag{9}$$

The scattering law $S(\alpha, \beta)$ is given by

$$S(\alpha, \beta) = \frac{4\alpha}{\beta_m^3} \exp(-2\beta/\beta_m) \exp(-\vec{\kappa}^2 a) \left[\frac{\sigma_{inc}}{\sigma_{coh}} + 1 + \Gamma(\vec{\kappa}) + \frac{1}{6} \beta^2 \left(\frac{k_B T}{c\hbar} \right)^2 L(R, \kappa, q) \right]. \tag{10}$$

In the above equations E_0 and E denote the initial and final neutron energies, respectively. Equation (8) is in the form used by RANDOLPH [8]. Following Egelstaff, $S(\alpha, \beta)$ is usually referred to as the scattering law. It is a dimensionless quantity depending on energy and momentum transfers and is characteristic of the scattering medium. The most important term in Eq. (10) is the one which contains $L(R, \kappa, q)$ and represents our correction to the convolution approximation. $S(\alpha, \beta)$ in the convolution approximation is given by Eq. (10) with $L(R, \kappa, q) = 0$.

3. RESULTS AND DISCUSSION OF $S(\alpha, \beta)$

The first thing we notice in Eq. (10) is that the correction to the convolution approximation depends on β, the mean velocity c of the "phonon" and the function $L(R, \kappa, q)$. The correction term has both the static and the dynamic character. $L(R, \kappa, q)$ as a function of κ for various values of R and q has an interesting behaviour.

In Fig. 1(a), the experimental values [13] of $1 + \Gamma(\vec{\kappa})$ for liquid sodium at T = 100°C are plotted, and in Fig. 1(b) the same for T = 325°C are plotted. Using these values the integrals in Eq. (4) have been evaluated numerically (using CDC 3600) for different values of the parameters R and q. For the sake of illustration, we have plotted in Fig. 2(a) the function $L(R, \kappa, q)$ for R = 12 Å for three different values of q for T = 100°C. Notice that as q becomes large, the function becomes comparatively much flatter from its behaviour for small q's. In Fig. 2(b) we have plotted $L(R, \kappa, q)$ for a given $q = 0.5$ Å^{-1} for three different values of R. Notice that $L(R, \kappa, q)$ is much less sensitive to the change in the values of R. All these characteristics of $L(R, \kappa, q)$ are, as we shall see, reflected in $S(\alpha, \beta)$.

To calculate $S(\alpha, \beta)$ we need to know the values of β_m and a. In the region of small $\vec{\kappa}$- and β-values where the correction term is negligible and where the Debye-Waller factor is approximately unity, β_m can be obtained by comparing the calculated $S(\alpha, \beta)$ with the observed one. In this way we arrived at a value of $\beta_m \simeq 0.28$ for T = 100°C. For a we have taken a value of 0.125 Å^2, which gives a reasonable overall fit with experimental $S(\alpha, \beta)$. $\sigma_{inc}/\sigma_{coh} = 1.85/1.55$ (see [8]). For a given β and q, the mean velocity of sound $c = \beta k_B T/\kappa q$ is fixed. In Figs. 3-6 we have plotted $S(\alpha, \beta)$ as a function of α for four different values of β for the values of the parameters shown. $S(\alpha, \beta)$ as calculated from the convolution approximation is also plotted. For two values of β, 0.08 and 0.2, $S(\alpha, \beta)$ was also calculated for a higher tem-

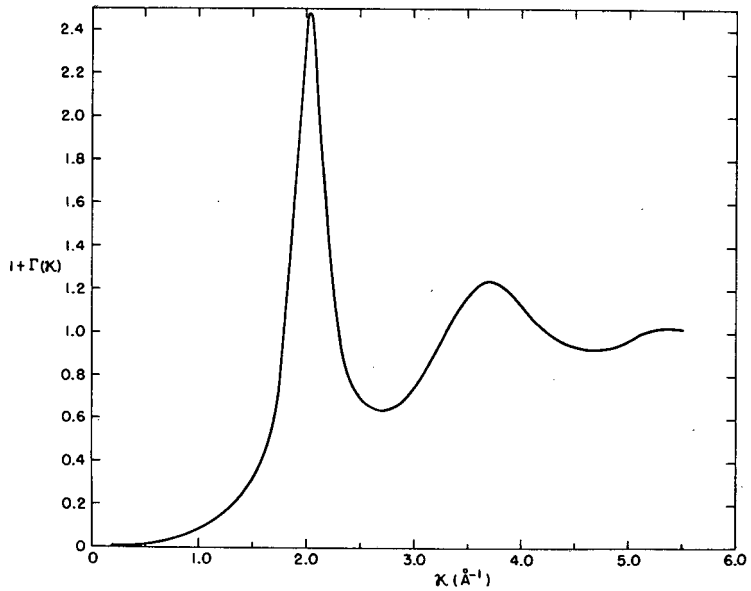

Fig. 1(a)

$1+\Gamma(\kappa)$ [13] versus $\kappa(\text{Å}^{-1})$ for liquid sodium at T = 100°C

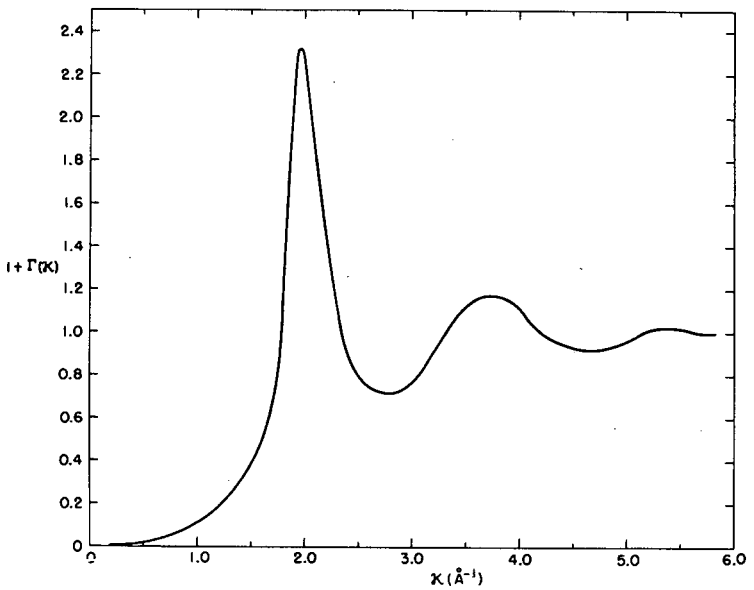

Fig. 1(b)

$1+\Gamma(\kappa)$ [13] versus $\kappa(\text{Å}^{-1})$ for liquid sodium at T = 325°C

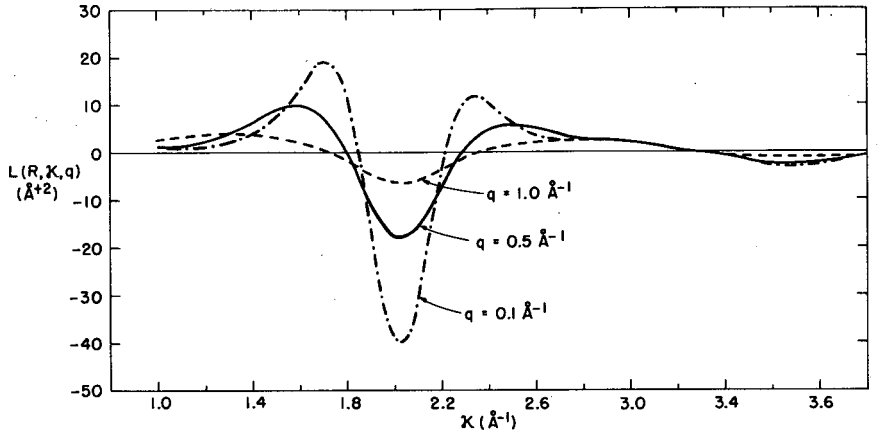

Fig. 2(a)

Function L(R, κ, q) in Å^{+2} versus κ(Å^{-1}) for liquid sodium at T = 100°C for R = 12 Å for three different values of q as shown

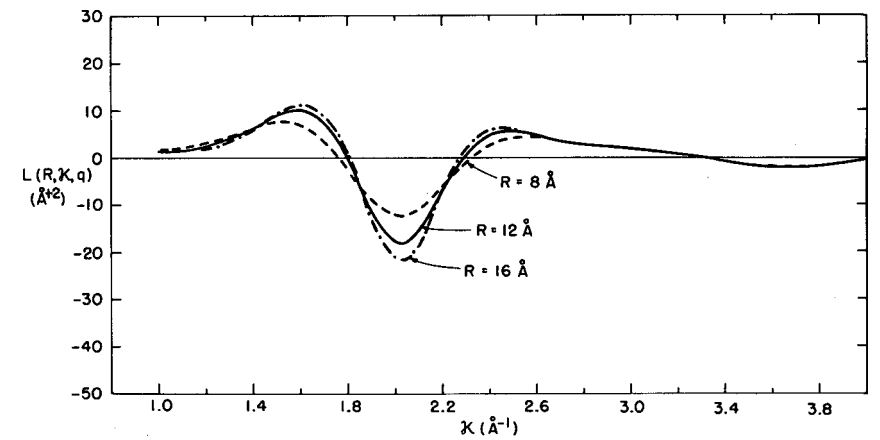

Fig. 2(b)

Function L(R, κ, q) in Å^{+2} versus κ(Å^{-1}) for liquid sodium at T = 100°C for q = 0.5 Å for three different values of R as shown

perature T = 325°C, and the results are shown in Figs. 3(a), 3(b), 3(c), 5(a), and 5(c). For T = 325°C we arbitrarily took a slightly higher value for a = 0.15 Å and for $\beta_m = 0.3$. The curves denoted by $\sigma_{inc} = 0$, correspond to the hypothetical case of sodium being a completely coherent scatterer; and have been drawn to illustrate what one should expect for the general shape of $S(\alpha, \beta)$ in the case of completely coherent liquid metals.

From an inspection of the curves in Figs. 3-6, the following general conclusions can be drawn:

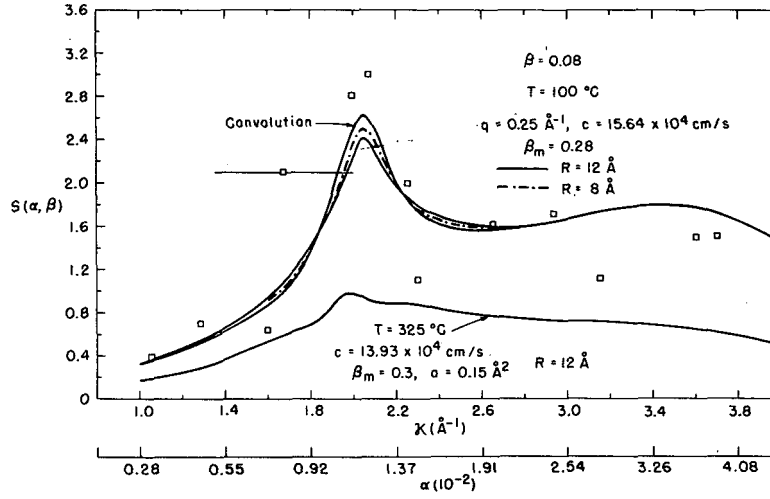

Fig. 3(a)

Scattering law $S(\alpha, \beta)$ as a function of α for $\beta = 0.08$ for the values of the parameters shown. The curve marked convolution is as calculated using the convolution approximation of Vineyard. The squares indicate the experimental points of RANDOLPH [8] for an energy gain experiment. The horizontal bar shows the magnitude of the experimental error involved. $S(\alpha, \beta)$ curve for T = 325°C for the values of the parameters shown is also plotted.

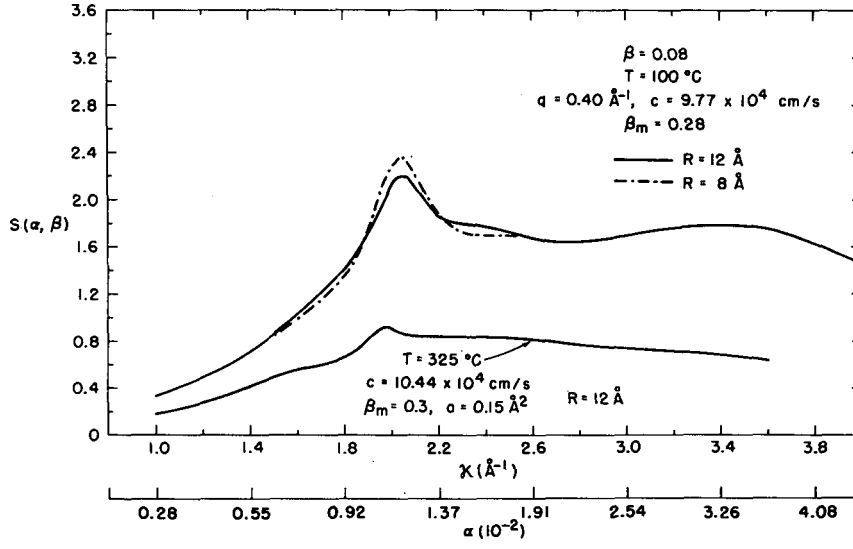

Fig. 3(b)

Scattering law $S(\alpha, \beta)$ as a function of α for $\beta = 0.08$ for the values of the parameters shown

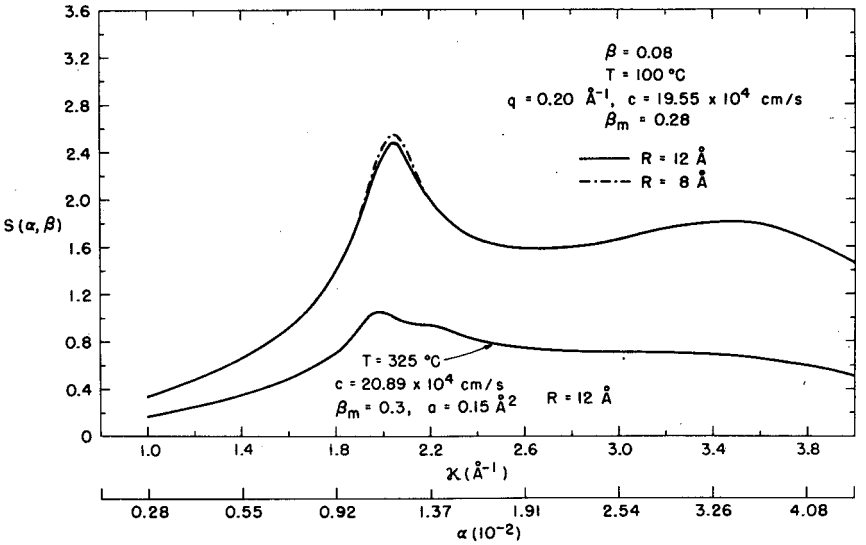

Fig. 3(c)

Scattering law $S(\alpha, \beta)$ as a function of α for $\beta = 0.08$ for the values of the parameter shown

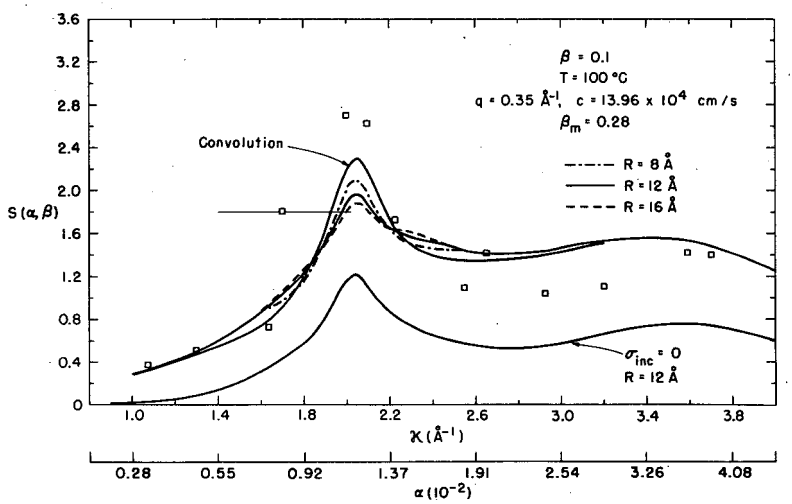

Fig. 4(a)

Scattering law $S(\alpha, \beta)$ as a function of α for $\beta = 0.1$ for the values of the parameters shown. The curve marked convolution is as calculated using the convolution approximation of Vineyard. The squares indicate the experimental points of RANDOLPH [8] for an energy gain experiment. The horizontal bar shows the magnitude of the experimental error involved. The curve for R = 16 Å approaches Randolph's smooth experimental curve of his Fig. 8 fairly closely. The curve marked $\sigma_{inc} = 0$ corresponds to the hypothetical case of sodium being a completely coherent scatterer.

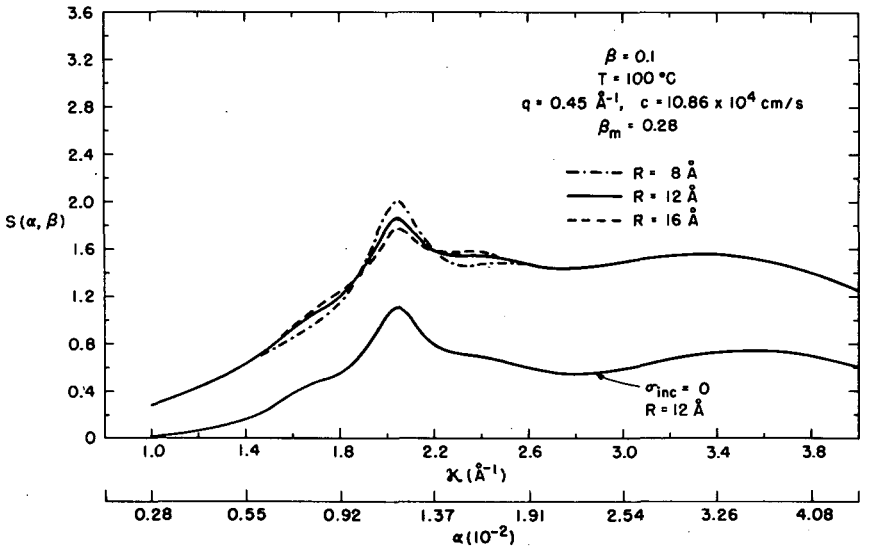

Fig. 4(b)

Scattering law $S(\alpha, \beta)$ as a function of α for $\beta = 0.1$ for the values of the parameters shown

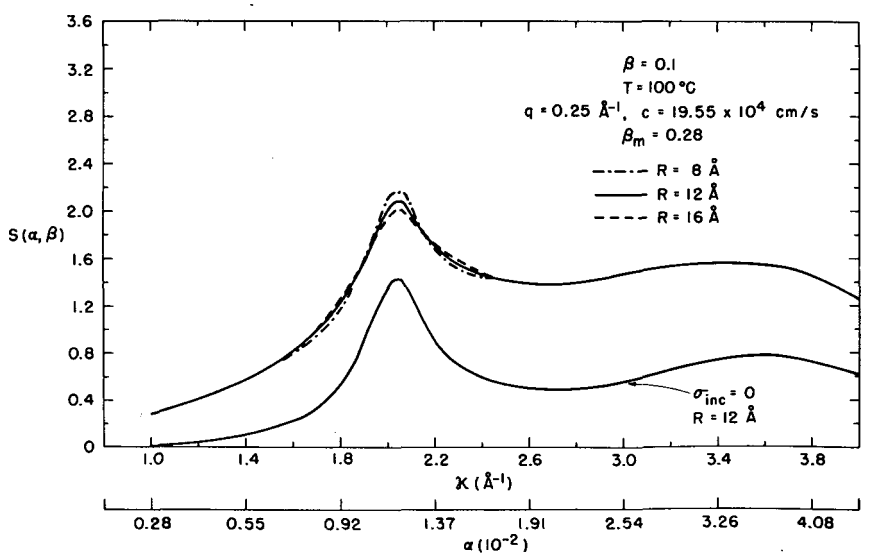

Fig. 4(c)

Scattering law $S(\alpha, \beta)$ as a function of α for $\beta = 0.1$ for the values of the parameters shown

(a) For small values of β and hence of energy transfer, the difference between the values of $S(\alpha, \beta)$ as given by our Eq. (10) and the convolution approximation is small. This difference is largest in the region of κ-values

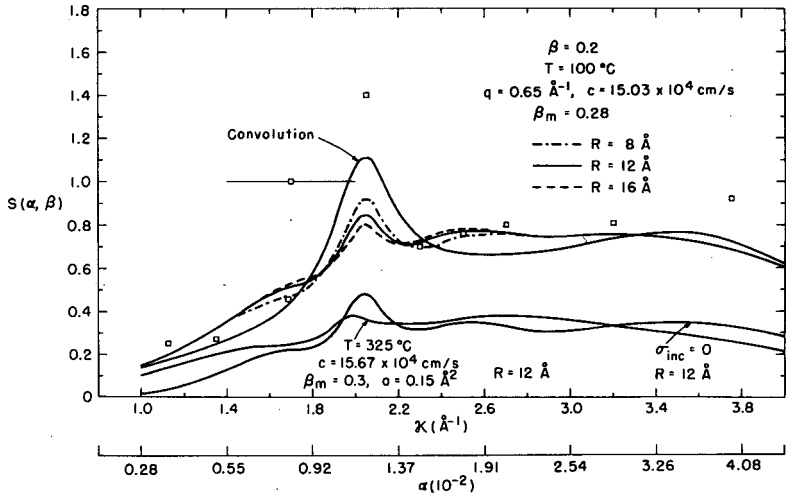

Fig. 5(a)

Scattering law $S(\alpha, \beta)$ as a function of α for $\beta = 0.2$ for the values of the parameters shown. The curves marked convolution are as calculated using the convolution approximation of Vineyard. The squares indicate the experimental points of RANDOLPH [8] for an energy gain experiment. The horizontal bar shows the magnitude of the experimental error involved. The curve for R = 16 Å approaches Randolph's smooth experimental curve of his Fig. 8 fairly closely. The curve marked $\sigma_{inc} = 0$ corresponds to the hypothetical case of sodium being a completely coherent scatterer. $S(\alpha, \beta)$ curve for T = 325°C is also plotted for the values of the parameters shown.

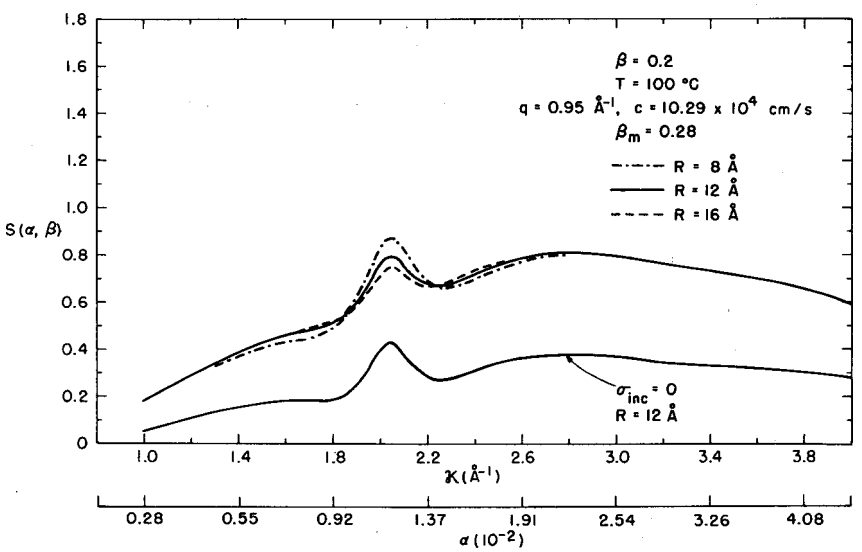

Fig. 5(b)

Scattering law $S(\alpha, \beta)$ as a function of α for $\beta = 0.2$ for the values of the parameters shown

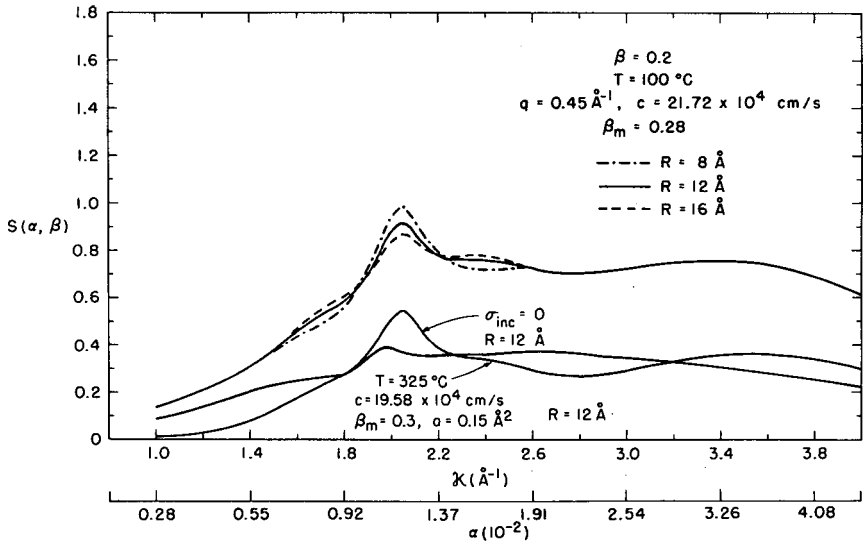

Fig. 5(c)

Scattering law $S(\alpha, \beta)$ as a function of α for $\beta = 0.2$ for the values of the parameters shown. $S(\alpha, \beta)$ curves for T = 325°C and for the hypothetical case $\sigma_{inc} = 0$ are also shown.

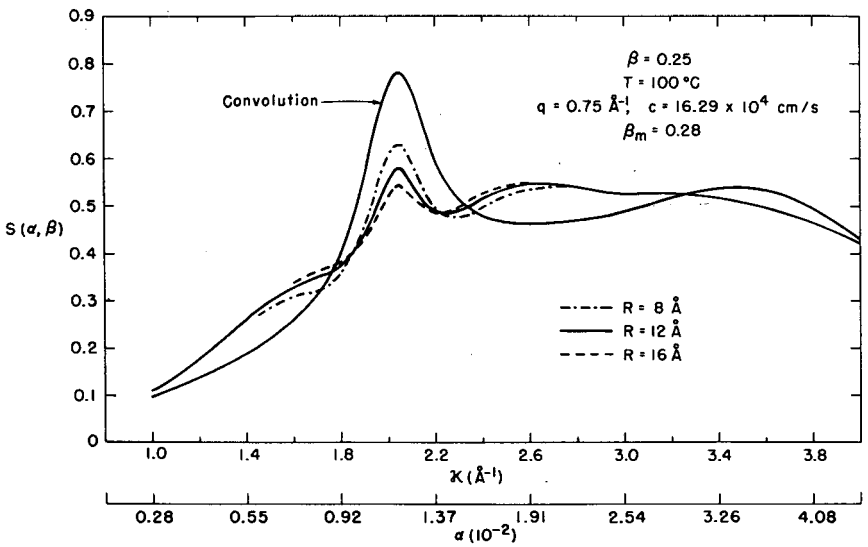

Fig. 6(a)

Scattering law $S(\alpha, \beta)$ as a function of α for $\beta = 0.25$ for the values of the parameters shown. The curve marked convolution is as calculated using the convolution approximation of Vineyard. The curve for R = 16 A approaches RANDOLPH's smooth experimental curve [8] of his Fig. 8 fairly closely.

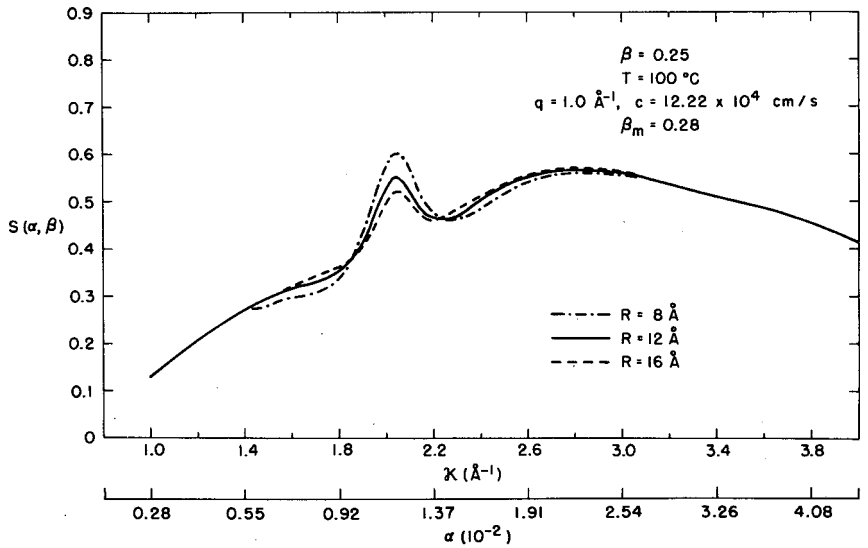

Fig. 6(b)

Scattering law $S(\alpha, \beta)$ as a function of α for $\beta = 0.25$ for the values of the parameters shown

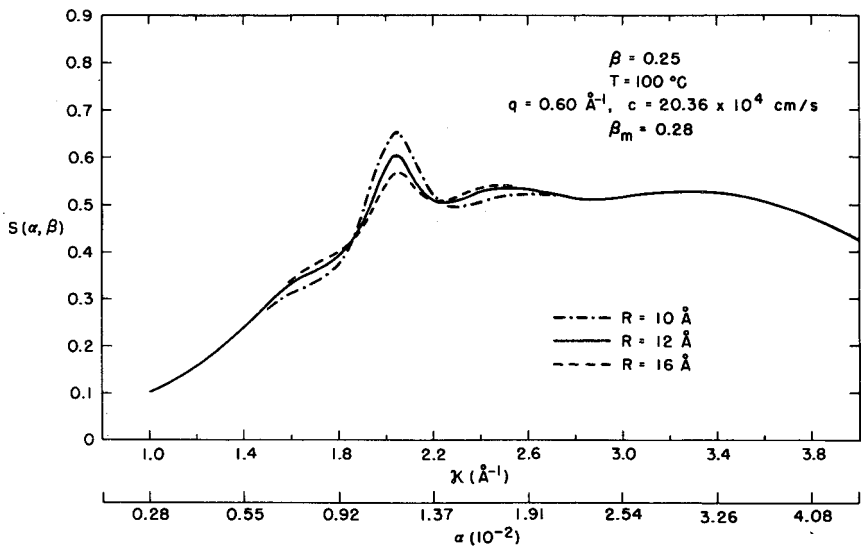

Fig. 6(c)

Scattering law $S(\alpha, \beta)$ as a function of α for $\beta = 0.25$ for the values of the parameters shown

corresponding to the main peak of $1 + \Gamma(\vec{\kappa})$. It, however, increases as the value of β increases. For large values of β ($\geqslant 0.2$), the detailed shape of $S(\alpha, \beta)$ is quite different from the one given by the convolution approximation.

In fact, for large values of the coherence parameter R for a given β (≥ 0.2), the main peak of $S(\alpha, \beta)$ tends to disappear.

(b) For temperatures far above the melting point, the main peak of $S(\alpha, \beta)$ (in the region $\kappa \simeq 2$ Å^{-1}) is almost non-existent even for $\beta = 0.08$; and the shape of $S(\alpha, \beta)$ is so much distorted that one can hardly discern the effect of $1 + \Gamma(\vec{\kappa})$ which was so clearly evident near the melting point.

(c) One would need fairly precision experiments to distinguish for a given β between $S(\alpha, \beta)$ curves for different values of R or for a given R between curves for different q's. Thus it would not be easy to determine a dispersion relation for "phonons".

4. COMPARISON WITH EXPERIMENT

In Figs. 3(a), 4(a), and 5(a), the squares denote the experimental points of Randolph (energy gain experiment) for T = 100°C. The horizontal bar for the point $|\vec{\kappa}| = 1.7$ Å^{-1} gives an idea of the magnitude of the error involved in the measurement of momentum transfer. Judging purely from these experimental points, $S(\alpha, \beta)$ as given by the convolution approximation is as good as that given by our Eq. (10). If, however, one compares Randolph's smooth curves (not shown) for the scattering law (Fig. 8 of Ref. [8]), one would see that his curves approach fairly closely our corresponding calculated curves for R = 16 Å and $c \simeq 15 \times 10^4$ cm/s. We do not know what criteria were used by Randolph to draw the smooth curves of his Fig. 8 through the points of his Fig. 5.

In spite of the poor precision of his experiments, Randolph was able to draw a general conclusion that for values of $\beta \geq 0.2$, the main peak of $S(\alpha, \beta)$ disappears which for small values of β is quite prominent. And for higher temperatures this seems to happen even for values of β smaller than 0.2 (see Fig. 10 of [8]). His conclusions thus seem to be in general agreement with our conclusions (a) and (b) of section 3.

For small values of $\vec{\kappa}$, the last term in the square brackets in Eq. (10) is negligible, in which case $\beta \sinh(\beta/2)\, S(\alpha, \beta)$ is proportional to $\beta^2 \exp(-2\beta/\beta_m)$ for $\beta \ll 1$. The function $\beta^2 \exp(-2\beta/\beta_m)$ is our generalized frequency distribution function. The value of $\beta_m \simeq 0.28$, which we have chosen for our computations, is approximately what one would obtain from Randolph's curve for $\alpha = 0.006$ of his Fig. 12.

The value of 15×10^4 cm/s for the mean velocity of sound which seems to give a reasonable fit with Randolph's data is of the right order of magnitude, when one remembers that the experimental value [14] for the longitudinal velocity of sound in liquid sodium at 100°C is 26×10^4 cm/s.

5. CONCLUSIONS

The scattering law $S(\alpha, \beta)$ as given by our Eq. (10) seems to be in reasonable agreement with experimental data hitherto known. It needs to be extended by taking "multiphonon" contribution into account. How good our Eq. (10) for $S(\alpha, \beta)$ is for other liquid metals still remains to be tested, though

there is no reason to believe that the latter would behave dynamically very differently from sodium. Precision measurements would be needed, as is clear from curves of Figs. 3-6, to determine the dispersion relation for "phonons" and the value for the coherence parameter R. It is also apparent that the most fruitful region of experimental investigation lies in the domain of $|\vec{\kappa}|$-values lying between 1.4 and 2.8 Å^{-1} where the coherent effects are most pronounced. A study of the temperature variation of $S(\alpha, \beta)$ is also interesting. Since the coherent effects depend on the nature of the function $L(R, \kappa, q)$, which in turn depends sensitively on the precise shape of the function $1 + \Gamma(\vec{\kappa})$, it is important that the latter should be studied experimentally very carefully. Hitherto, this fact has not been stressed.

Finally, let us remember that our theory is purely phenomenological. But until we have a rigorous mathematical theory of the liquid state, our approach should at least help in understanding the coherent neutron scattering data and in suggesting new experiments.

REFERENCES

[1] SINGWI, K. S., Phys. Rev., to be published.
[2] VINEYARD, G. H., Phys. Rev. 110 (1958) 999.
[3] BROCKHOUSE, B. N., BERGSMA, J., DASANNACHARYA, B. A. and POPE, N. K., in Inelastic Scattering of Neutrons in Solids and Liquids I IAEA, Vienna (1963) 189-201.
[4] KROÓ, N., BORGONOVI, G., SKÖLD, K. and LARSSON, K.-E., unpublished report.
[5] SINGWI, K. S., communicated to Phys. Rev.
[6] EGELSTAFF, P. A., AERE Rpt N/R 4101 (1962).
[7] KROÓ, N., BORGONOVI, G., SKÖLD, K and LARSSON, K.-E., Phys. Rev. Lett. 12 (1964) 721.
[8] RANDOLPH, P. D., Phys. Rev. 134 (1964) A1238.
[9] PALEVSKY, H., in Inelastic Scattering of Neutrons in Solids and Liquids I IAEA, Vienna (1963) 285.
[10] BROCKHOUSE, B. N and POPE, N. K., Phys. Rev. Lett. 3 (1959) 259.
[11] COCKING, S. J , in Inelastic Scattering of Neutrons in Solids and Liquids I IAEA, Vienna (1963) 227-36.
[12] RAHMAN, A., SINGWI, K. S. and SJÖLANDER, A., Phys. Rev. 126 (1962) 997.
[13] GINGRICH, N. S. and HEATON, L., J. Chem. Phys. 34 (1961) 873.
[14] TRELIN, Yu. S., VASILEV, I. N. and ROSHCHUPKIN, V. V., Soviet J. atomic Energy 9 (1960) 955.

DISCUSSION

K.-E. LARSSON: Within the correlation range R you are treating the liquid as a solid when you use the phonon description of the collective modes. I wonder what the true difference is between your treatment and the semi-crystalline treatment proposed by Dr. Egelstaff. What is the unit in your theory that takes up the momentum in the scattering process?

K.S. SINGWI: In our treatment we do not assume the existence of a reciprocal lattice vector in a liquid, which in itself is an improvement from a theoretical standpoint. The treatment also accounts for diffusion and enables one to get an idea of the range of coherence in a liquid. The unit is the mass of atoms contained in a sphere of approximate radius R.

N. KROÓ: In our argon measurements we have observed the disappearance of the first diffraction peak at higher energies, as in the case of the liquid sodium data. It should be added, however, that the same effect is apparently found in solid-phase results near the melting point.

INELASTIC SCATTERING OF COLD NEUTRONS BY CONDENSED ARGON

N. KROÓ*, G. BORGONOVI**, K. SKÖLD AND K.-E. LARSSON***
AB ATOMENERGI, STUDSVIK, SWEDEN

Abstract — Résumé — Аннотация — Resumen

INELASTIC SCATTERING OF COLD NEUTRONS BY CONDENSED ARGON. In recent years the question of the existence of collective modes of heat-motion in liquids has been put forward by different authors. To investigate this problem we have done neutron inelastic scattering measurements on liquid argon at 88°K temperature. As a comparison, solid, polycrystalline argon (80°K) was also studied. The experiment was carried out with the time-of-flight spectrometer at the Studsvik R2 reactor. The ingoing neutron energy was 5 meV and the scattered neutron spectra were analysed at nine angles between 60° and 100°.

The interference part of the scattering has been used to obtain information about the collective motions of atoms in the two phases. The meaning of average dispersion relations is discussed, and methods by which these functions can be obtained are described.

The results of such analysis are given for both the solid and liquid phase. Dispersion relations were obtained in both cases. The slopes of these curves at the origin are in good agreement with the sound velocities obtained by other methods.

The results on liquid argon can be taken as proof that the energy and momentum conservation relations were both active in the scattering process, and as a strong support to the idea of the existence of collective motions in a classical liquid.

DIFFUSION INÉLASTIQUE DES NEUTRONS FROIDS DANS L'ARGON CONDENSÉ. Au cours de ces dernières années, différents chercheurs se sont intéressés à la question de l'existence de modes collectifs d'agitation thermique dans les liquides. En vue d'étudier ce problème, les auteurs ont mesuré la diffusion inélastique des neutrons dans l'argon liquide à la température de 88°K. A titre de comparaison, ils ont également examiné l'argon polycristallin solide (80°K). L'expérience a été faite à l'aide du spectromètre à temps de vol du réacteur R2 de Studsvik. L'énergie des neutrons incidents était de 5 meV; les spectres des neutrons diffusés ont été analysés pour neuf angles différents compris entre 60 et 100°.

La partie de la diffusion due aux effets d'interférence a été utilisée pour obtenir des renseignements sur les mouvements collectifs des atomes dans les deux phases. Les auteurs examinent l'interprétation des relations de dispersion moyennes et décrivent les méthodes qui permettent d'établir ces fonctions.

Ils indiquent les résultats de cette analyse à la fois pour la phase solide et pour la phase liquide. Ils ont établi des courbes de dispersion pour les deux cas. Les pentes de ces courbes à l'origine concordent assez bien avec les vitesses du son obtenues par d'autres méthodes.

Les résultats relatifs à l'argon liquide attestent le fait que la relation de conservation de l'énergie et celle de conservation de la quantité de mouvement exercent toutes les deux une influence sur le processus de diffusion; ils confirment aussi nettement l'idée de l'existence de mouvements collectifs dans un liquide classique.

НЕУПРУГОЕ РАССЕЯНИЕ ХОЛОДНЫХ НЕЙТРОНОВ НА КОНДЕНСИРОВАННОМ АРГОНЕ. За последние годы вопрос о существовании коллективных форм теплового движения в жидкостях поднимался различными авторами. Для изучения этой проблемы мы провели измерения неупругого рассеяния нейтронов на жидком аргоне при температуре 88°К. Для сравнения изучался также твердый многокристаллический аргон (80°К). Эксперимент проводился на реакторе R2 в Студсвике с помощью спектрометра по времени пролета. Энергия входящих нейтронов составляла 5 мэв; анализы спектров рассеянных нейтронов проводились при 9 углах между 60° и 100°.

---

* IAEA fellow from the Central Research Institute for Physics, Budapest, Hungary.
** On leave from the Comitato Nazionale per l'Energia Nucleare, Ispra, Italy.
*** The Royal Institute of Technology, Stockholm, Sweden.

Интерференционная часть рассеяния использовалась для получения информации о коллективных движениях атомов в двух фазах. Рассматривается значение средних дисперсионных соотношений и описываются методы, при помощи которых могут быть получены эти функции.

Результаты такого анализа приводятся как для твердой, так и для жидкой фазы. В обоих случаях были получены дисперсионные соотношения. Наклоны этих кривых в начале хорошо согласуются со скоростями звука, полученными другими методами.

Результаты, полученные с жидким аргоном, могут служить доказательством того, что соотношения сохранения как импульса, так и энергии являются активными в процессе рассеяния, а также подтверждением концепции о существовании коллективных движений в классической жидкости.

DISPERSIÓN INELASTICA DE LOS NEUTRONES FRIOS EN EL ARGON CONDENSADO. En los últimos años, diversos investigadores han planteado la cuestión de la existencia de modos colectivos del movimiento térmico en los líquidos. A fin de estudiar este problema, los autores han efectuado mediciones de la dispersión inelástica de los neutrones en argón líquido a 88°K. A fines de comparación, se estudió también el comportamiento del argón sólido policristalino (80°K). El experimento se realizó con ayuda del espectrómetro de tiempo de vuelo instalado en el reactor R32 de Studsvik. La energía de los neutrones incidentes era de 5 meV, y se analizaron los espectros de los neutrones dispersos en nueve ángulos distintos, comprendidos entre 60° y 100°.

La interferencia observada en la dispersión se ha utilizado para obtener información acerca de los movimientos colectivos de los átomos en las dos fases. Los autores examinan el significado de las relaciones medias de dispersión, y describen los métodos por los que pueden obtenerse esas funciones.

Exponen también los resultados de tales análisis tanto para la fase sólida como para la fase líquida. En ambos casos se obtuvieron relaciones de dispersión. La pendiente de estas curvas, en su tramo inicial, se ajusta bastante bien a las velocidades del sonido determinadas por otros métodos.

Los resultados obtenidos con el argón líquido pueden considerarse como prueba de que las relaciones de conservación de la energía y del impulso intervienen activamente en el proceso de dispersión, y vienen en apoyo de la idea de la existencia de movimientos colectivos en un líquido clásico.

I. INTRODUCTION

The method of inelastic scattering of cold neutrons has been extensively applied to investigations of the dynamics of condensed matter. The previous investigations in the liquid phase have shown many features of the scattering to be similar to those observed in solids, especially in polycrystals [1]; it is well known for example from X-ray and elastic neutron scattering measurements that a certain amount of short range order remains in the liquid phase [2, 3].

To compare the dynamical behaviour of a solid and a simple liquid system, argon has been chosen for the present measurements.

II. THEORETICAL BACKGROUND

Argon, occurring in nature, is a mixture of different isotopes with different scattering lengths for neutrons. Therefore the scattering contains a coherent as well as an incoherent part. According to the measurements of HENSHAW [3] the nuclear coherent and incoherent scattering cross-sections are $\sigma_{coh} = 0.6$ b and $\sigma_{incoh} = 0.19$ b, respectively.

The general formulation of the scattering cross-section for thermal neutrons from an arbitrary system of atoms was given in 1954 by VAN HOVE [4] in the first Born approximation. He showed that the coherent and in-

coherent scattering cross-sections are directly related to the time-dependent correlation functions, namely

$$\frac{d^2\sigma_{coh}}{d\Omega d\omega} = \frac{\sigma_{coh}}{8\pi^2\hbar}\frac{k'}{k_0}\int \exp\, i(\vec{\kappa}\cdot\vec{r} - \omega t)G(\vec{r}, t)d\vec{r}dt \tag{1}$$

$$\frac{d^2\sigma_{inc}}{d\Omega d\omega} = \frac{\sigma_{inc}}{8\pi^2\hbar}\frac{k'}{k_0}\int \exp\, i(\vec{\kappa}\cdot\vec{r} - \omega t)G_s(\vec{r}, t)d\vec{r}dt. \tag{2}$$

This formulation shows that both the single-particle and the co-operative modes give contributions to the inelastic neutron scattering cross-section. In the present investigation only coherent scattering is discussed.

According to EGELSTAFF [5] the pair correlation function for a classical isotropic system can be written as

$$G_d(r, t) = g(r)F(r, t) \tag{3}$$

where $g(r)$ is the static pair correlation function and $F(r, t)$ is a function defined by Eq. (3) and describes the motions in the system. If we substitute Eq. (3) in Eq. (1) we get

$$\frac{d^2\sigma_{coh}}{d\Omega d\omega} = \frac{\sigma_{coh}}{8\pi^2\hbar}\frac{k'}{k_0}\left\{S_s(\kappa, \omega) + \int \gamma(\kappa - \kappa')R(\kappa', \omega)d\kappa'\right\} \tag{4}$$

with

$$S_s(\kappa, \omega) = \frac{1}{2\pi}\int \exp\, i(\kappa r - \omega t)G_s(r, t)\, d\vec{r}dt \tag{5}$$

$$R(\kappa, \omega) = \frac{1}{2\pi}\int \exp\, i(\kappa r - \omega t)F(r, t)d\vec{r}dt \tag{6}$$

and

$$\gamma(\kappa) = \int g(r)\exp\, i\,\kappa r d\vec{r}. \tag{7}$$

From Eq. (4) we can see that the "dynamical function" of the scattering system is always observed folded with the function, which depends on the structure of the scatterer.

A. Solids

Because in the solid phase $\gamma(\kappa)$ is a set of δ-functions Eq. (4) can be written as a sum. Looking only at the one-phonon part of the cross-section one can rely upon a formula derived by WEINSTOCK [6] for a microcrystal and extended by EGELSTAFF [7] to the polycrystalline case. This formula reads

$$\frac{d^2\sigma_{coh}}{d\Omega d\omega} = \frac{\sigma_{coh}}{4\pi}\frac{1}{2M}\frac{k'}{k_0}e^{-2W}\frac{\kappa^2}{\omega}\begin{Bmatrix} N+1 \\ N \end{Bmatrix} f(\omega)Z \tag{8}$$

and

$$Z = \sum_{\tau} \frac{\pi F_\tau}{2B\tau\kappa q} \ldots \tag{9}$$

In Eq.(8) M is the mass of the scattering nucleus, e^{-2W} is the Debye-Waller factor, $N = [\exp(\hbar\omega/k_B T)]^{-1}$ is the population factor for energy gain and N+1 is the corresponding population factor of energy loss of the neutron; $f(\omega)$ is the frequency distribution of the normal modes. In Eq.(9) Z is the polycrystalline (energy-dependent) structure factor, τ is the modulus of a reciprocal lattice vector, F_τ is the crystalline structure factor times the multiplicity of the proper plane, B is the volume per atom in the crystal and q is the modulus of the average phonon wave vector corresponding to the frequency ω. The limits within which contributions to Z are created from a certain set of planes, characterized by τ, are given by

$$\kappa(\Theta,\omega) - q(\omega) \leqq 2\pi\tau \leqq \kappa(\Theta,\omega) + q(\omega), \tag{10}$$

where Θ is the scattering angle. Therefore the cross-section will show discontinuities at the limits of the interval given by Eq.(10).

One can see that in order to calculate the coherent scattering cross-section one needs the frequency distribution of the normal modes and the average dispersion relation $q = q(\omega)$. Conversely, if τ is known one can determine the average dispersion relation from the position of the breaks in the observed coherent single-phonon cross-section. The meaning of this function and the method to evaluate it are discussed later.

B. Multiphonon corrections

From the phonon expansion formula of Eq.[8] it is known that the factor 2W governs the multiphonon intensity. Because of the small value of this factor ($2W = (0.0434\,\text{Å}^2)(\kappa^2\,\text{Å}^{-2})$) for solid argon at 80°K, the two-phonon and higher-phonon terms can be neglected in the incoherent cross-section.

As far as the coherent multiphonon cross-section is concerned, it is clear [7] that this contribution does not give rise to sharp breaks and therefore it does not affect our determination of the dispersion relation. Numerical calculations of the coherent two-phonon cross-section showed that the ratio of the two-phonon to the one-phonon term never exceeded 0.03 in the region of interest. These calculations were done in the Debye approximation using formulas derived by EGELSTAFF [7]. The higher phonon terms are still smaller and, besides, they may be represented by the incoherent approximation and may therefore be neglected.

C. Dispersion relations in isotropic systems

In a single crystal one can always determine the dispersion relations of the normal modes by studying the coherently and inelastically scattered

neutron spectra. Because both the energy and quasi-momentum conservation laws have to be fulfilled, resonances are observed in the one-phonon scattering which help determine the $\omega = \omega(q)$ relation.

In the polycrystalline case one cannot speak about the direction of τ caused by the isotropic distribution of the crystalline planes in the different grains. Therefore we cannot determine the $\omega = \omega(q)$ dispersion relation. We can instead define a function (scalar-scalar) which, for example, gives the connection between the energy and an average wave number (q) of the phonons in the crystal. If we had an isotropic medium, i.e. one dispersion curve, then Z in Eq.(8), as already mentioned, would be different from zero only in the $\kappa - q \leq 2\pi\tau \leq \kappa + q$ region, with sharp breaks at the two ends of the interval. At a fixed ω the distance between the two breaks would be $\Delta\kappa = 2q$ and the relation $\omega = \omega(q)$ could be determined. In the real case at a certain energy ω, since the constant energy surfaces in the Brillouin zone are not spheres, the corresponding q-values have a finite distribution. Therefore we cannot find sharp breaks in the coherent scattering picture, only some broad distribution in κ. But we can still define the average dispersion relation from the full width at half height of this distribution in the form

$$\omega = \omega(\Delta\kappa_{1/2}) = \omega(2q). \tag{11}$$

D. Liquids

In the liquid phase the long-range order existing in solids is replaced by a short range order only, as verified by the experimental studies of pair-distribution functions by X-rays and neutron diffraction. Also recent neutron inelastic scattering studies have clearly shown that vibratory motions may exist in a liquid as well as in a solid. Thus frequency spectra for the motions of the atoms in liquids have been derived from incoherent neutron scattering studies [9, 10]. Similarly it has been found that interference scattering is caused by a liquid as well as by a solid. This was shown from scattering studies on liquid metals like tin and aluminium [11, 12].

In the case of solid argon the mixture of the coherent and incoherent inelastic scattering does not cause any serious difficulties in the interpretation of the data. The reason for this is that the coherently scattered intensity is about one order of magnitude higher than the incoherent one in the region where the important breaks occur.

In the liquid case the situation may be entirely different, if the coherent inelastically scattered intensity does not show the same break structure as in the solid phase, and thus would be almost indistinguishable from the smooth incoherently scattered intensity. This difficulty may be expected to occur in liquid argon because of the high mobility and the weak binding of the spherical atoms. A diffusion broadening of the sharp breaks, which is of the same order of magnitude as the inelastic energy transfer itself, is expected. Moreover, the incoherent quasi-elastic scattering will show a similar broad distribution, overlapping any inelastic coherent scattering.

There is still a possibility left to draw conclusions about the collective motions in the liquid, namely by doing investigation around the well-pronounced first peak in $[1+\gamma(\kappa_0)]$. This function describes the angular distri-

bution of elastically scattered neutrons and can be interpreted as the result of broadening of the sharp Bragg peaks which exist in the solid phase.

With the above-mentioned similarities between the solid and liquid phases in mind it seems reasonable to extend the validity of Eq.(8) to the liquid phase with one modification. Instead of δ-functions in the angular distribution of the coherent elastically scattered neutrons there is now, as mentioned above, a smooth function with a few dominant peaks. The summation over the discrete τ-values should now be replaced by an integration over τ, [1] giving

$$Z(\kappa, q) \sim \frac{1}{\kappa, q} \int_{\kappa-q}^{\kappa+q} 2\pi\tau \, [1+\gamma(2\pi\tau)] \, d(2\pi\tau). \tag{12}$$

A decisive test of the existence of collective modes in a liquid would be to search for a dispersion relation. With the generalization of Eq.(8), expressed in Eq.(12), in mind, it seems consistent to apply the treatment described for the solid in section II.C to the liquid.

In this treatment the first diffraction peak at different energies ω should be broadened in κ, as determined by the relation between ω and q for the "quasi-phonons". This is expressed by the limits of integration in Eq.(12). It is seen that contributions to $Z(\kappa, \omega)$ originate from a region $(\kappa+q)-(\kappa-q)=2q$ and the width of this function is therefore a measure of q.

To obtain the width of the "dynamical function" from the total width of the broadened diffraction peak we might, as an approximation, take

$$2q = \Delta\kappa = [(\Delta\kappa_\omega)^2 - (\Delta\kappa_0)^2]^{1/2}, \tag{13}$$

where $\Delta\kappa_\omega$ is equal to the measured full width at half height of the first diffraction peak at energy ω. This formula is exact for the folding of Gaussians only.

The advantage of using Eq.(13) may be understood from the form of Eq. (4) expressing that the "dynamical function" can only be observed folded with a function depending on the structure of the scatterer. Being always around the well-pronounced first peak, the effect of this folding is about the same.

The method discussed above is concerned only with the interference part of the scattering. To perform the analysis we must first subtract the incoherent contribution from the observed data. If we have a model describing the incoherent scattering we can normalize the predicted cross-section to the measurement by taking data in a region of κ and ω where only incoherent scattering can occur. The cross-section, normalized in this way, can then be extrapolated to the region of κ and ω where interference scattering occurs. The form of the incoherent cross-section which was used is given here for reference:

$$\frac{d^2\sigma_{inc}}{d\Omega d\omega} = \frac{a^2_{inc}}{\pi} \frac{k'}{k_0} \frac{D\kappa^2}{(D\kappa^2)^2 + \omega^2}, \tag{14}$$

where D is the diffusion coefficient.

This is the cross-section which would be observed if the atomic motions could be described as simple diffusion only.

III. EXPERIMENTAL DETAILS

The experiment was carried out with the time-of-flight spectrometer at the Studsvik R2 reactor. A description of this instrument is given elsewhere [13]. The incident spectrum is centred around 4.1 Å with a wavelength spread of 7%. The scattered spectra are analysed by the conventional time-of-flight technique. The time resolution at 4 Å is 1.5%. The angular spread of the scattered beam is ±2°.

To study argon in both solid and liquid form a liquid nitrogen cooled cryostat was constructed in which it was possible to keep the sample at liquid nitrogen temperature and higher. Temperatures above the nitrogen boiling point were reached with the aid of a small electric heater attached to the bottom of the argon chamber. The sample container was made of aluminium in the form of a cylinder with diameter 6 cm and wall thickness 0.1 cm. The transmission for scattering of the liquid sample along a diameter was about 93%. The effect of the absorption was found negligible within the present accuracy.

Since the temperature region for the liquid phase of argon is only 5.5° the temperature of the liquid has to be kept constant and the temperature gradient over the sample not too large. By heating in a corner of the bottom of the container the convection in the liquid could be increased and the temperature gradient therefore decreased. It was found that with a constant current through the heater and the nitrogen container filled above a certain level the temperature was constant within 0.2°. The temperature difference between the top and bottom of the sample was less than 1°. In the case of a solid sample it was found that to keep the temperature constant within 0.1° it was sufficient to ensure that the nitrogen container was filled above a certain level. The temperature difference between top and bottom was in this case 0.2°. The temperature of the solid sample was (80 ± 0.2)°K. The liquid was kept at (88 ± 0.7)°K in a closed volume and thus under its own vapour pressure, which at this temperature is 1.2 atm. By having overpressure in the sample container we could avoid contamination of the sample with air. This could be a serious problem even with a relatively tight system, as the same sample should be used for weeks and impurities could thus accumulate. To avoid contamination of the solid sample we kept helium gas at 1.2 atm above the solid surface. To check that, despite the precautions mentioned above, there were no impurities in the sample and that the sample was solid or liquid, respectively, everywhere over the region covered by the beam, we evaporated the samples a few times and measured again at the same angle with a new sample. We could not, in any case, see any difference between the spectra scattered from the two different samples.

The data read out from the 1024 channel time-analyser in the form of a punched tape were sent to a computer by which certain standard corrections were performed for the energy-dependent detector efficiency, the energy-dependent removal of neutrons by the air between the sample and the detector and a conversion of the data from flight-time to energy scale. The flat back-

ground, determined by averaging over 50 channels in an energy region where the background was known to be flat, was subtracted at the same time. No effort was made to evaluate the absolute values of the cross-sections. Runs at different angles were normalized to each other with the help of a monitor placed in the beam between the chopper and the sample.

IV. RESULTS AND DISCUSSIONS

A. Solid argon

The temperature of the solid sample was (80.0 ± 0.2)°K which is 4°K below the melting point. The spectra of the scattered neutrons were analysed at nine scattering angles in the angular region between 60° and 100°. One of the results of the three-day runs, corrected as described in section III, is shown in Fig. 1.

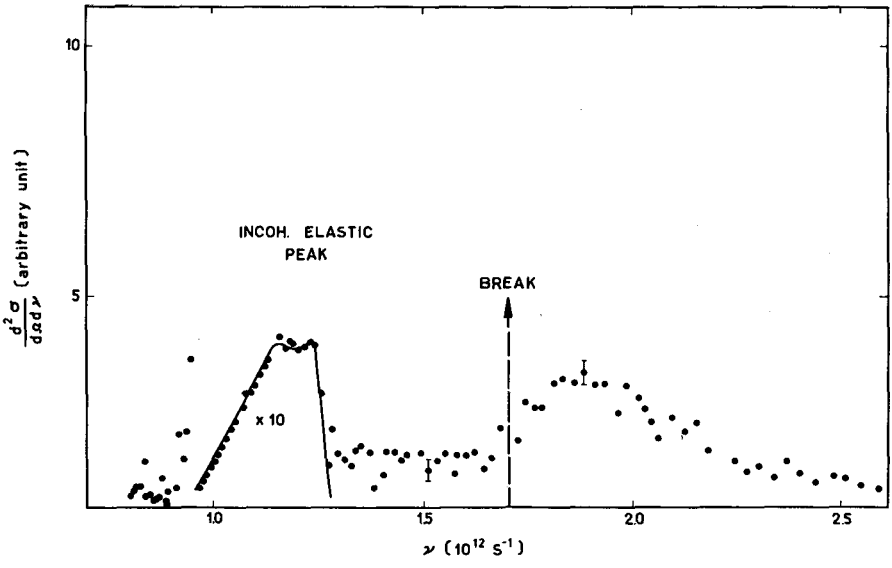

Fig. 1

Intensity-distribution of the neutrons scattered by solid argon at 60°

From the breaks, such as the one indicated by the arrow in the figure, we determined the average dispersion relation by the method described in section II.A. The result of this analysis is shown in Fig. 2. The straight line drawn in this figure is the result of a least square fit to the first eleven points.

The high value of the cross-section at small energy transfers appears in the measured data as well as in Eq. (9). One of the most obvious differences between the measured cross-sections and Eq. (8) is the low value of the experimental data at higher energies. This fact made it impossible to find breaks at higher energies. To investigate which factor in the cross-

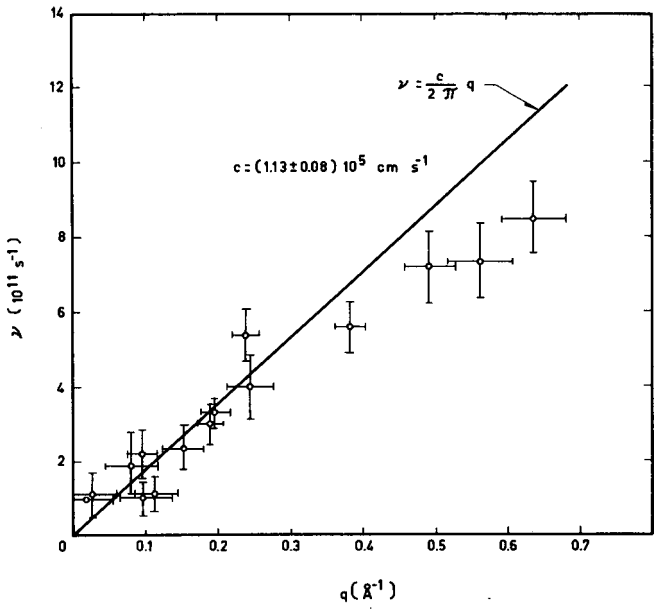

Fig. 2

Dispersion relation for solid argon

section is responsible for this disagreement it would be necessary to undertake a measurement of the frequency spectrum. Such an investigation has not yet been completed.

B. Liquid argon

The temperature of the liquid sample was (88 ± 0.7)°K and the liquid was kept under its own vapour pressure. The scattering angles were the same as in the measurement on the solid sample. One of the corrected spectra is shown in Fig. 3. Each spectrum represents three to four days' running time. Since in this case not only the inelastic but also the quasi-elastic part of the scattering is involved, it was necessary to study the intensity of the elastic scattering from the sample container. To this end runs were made with the sample container filled with He gas and cooled to liquid nitrogen temperature. In the analysis of the quasi-elastic scattering this extra scattering was corrected for.

The width of the quasi-elastic peak was studied as a function of κ. The cross-section at small ω was supposed to be Lorentzian in ω [14]. This assumption is in fact later shown to involve a slight oversimplification, but the exact shape of the quasi-elastic peak should not be too important in evaluating the width. To evaluate this quantity at the various scattering angles the incident spectrum was folded with Lorentzians of different widths. The full width at half height after folding was then plotted as a function of the width of the Lorentzian. In this way we obtained a calibration curve which helped us to find directly the proper width of the cross-section from the measured

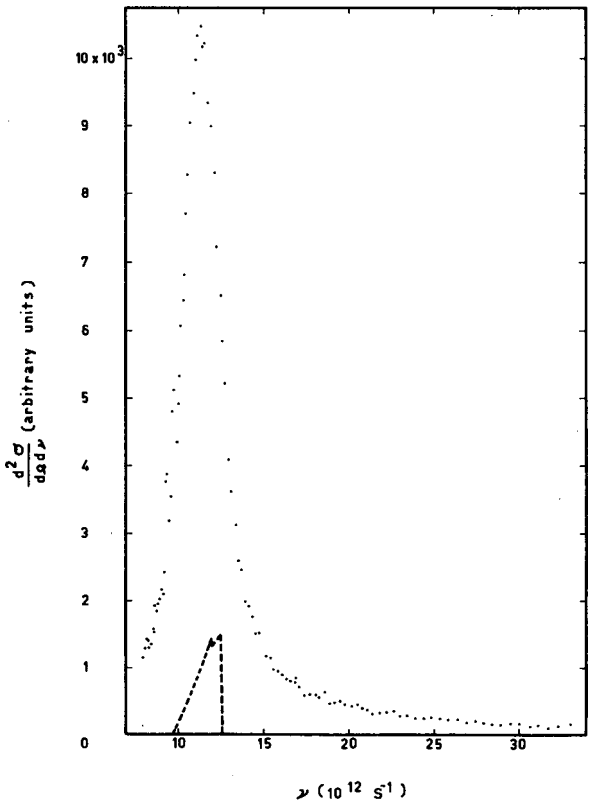

Fig.3

Intensity distribution of neutrons scattered by liquid argon at 79.5°

total width at a certain angle. The natural widths obtained in this way are plotted as a function of κ in Fig.4. Our results agree within the limits of error with those obtained by BROCKHOUSE et al.[15] with the sample at T = 84.5°K and under its own vapour pressure.

In Fig.5 is shown the result of such a folding of the incident spectrum with a Lorentzian, together with the observed spectrum scattered at 79.5°. The width of the Lorentzian was chosen to agree with the width of the quasi-elastic peak at this angle. It can be seen that the Lorentzian is incapable of explaining the scattering even for relatively small energy transfers. This shows that there is some meaning in trying to apply more elaborate models in which the possibility of collective modes is taken into account.

In order to correct for the incoherent part of the scattering a measurement was made at 27.5° at which the coherent contribution is small. Equation (14) was normalized and fitted to this measurement. After subtraction of this incoherent part of the scattering, the coherent intensity at fixed ω was plotted as a function of κ. To increase the statistical accuracy the channels were grouped together three and three. Such constant ω plots were performed for eleven different values. The intensity at constant ω is,

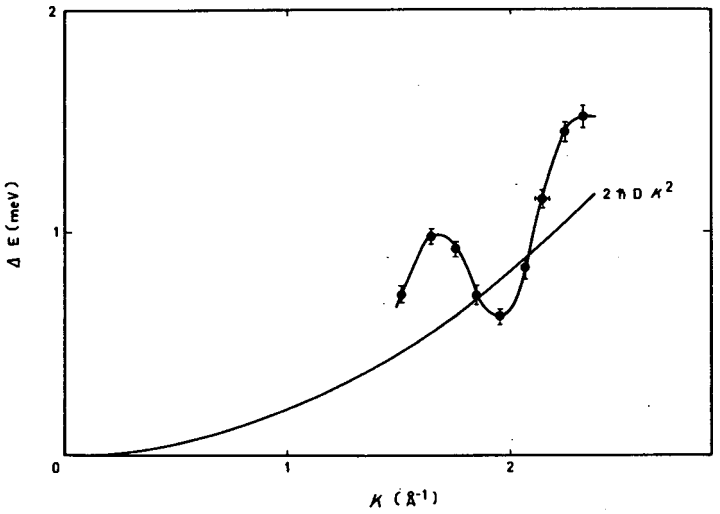

Fig. 4

Energy broadening of the quasi-elastic peak as a function of κ supposing it to be a Lorentzian

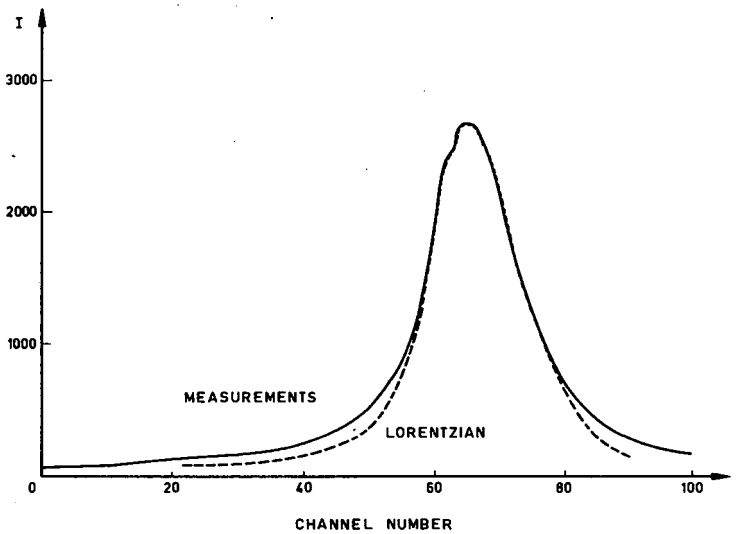

Fig. 5

Intensity distribution of neutrons scattered at 79.5°
The dotted line shows a Lorentzian folded with the ingoing spectrum. The width of the Lorentzian is chosen to give the same total width as that observed at 79.5°

according to Eq. (8), proportional to $\kappa^2 Z(\kappa)$. In order to obtain $Z(\kappa)$, the measured data (corrected for incoherent scattering) were divided by κ^2. Examples of the intensity per κ^2 as a function of κ are shown in Fig. 6. The widths in κ at half height were determined and interpreted in the way described in section II.D to yield a dispersion relation. The eleven pairs of ω

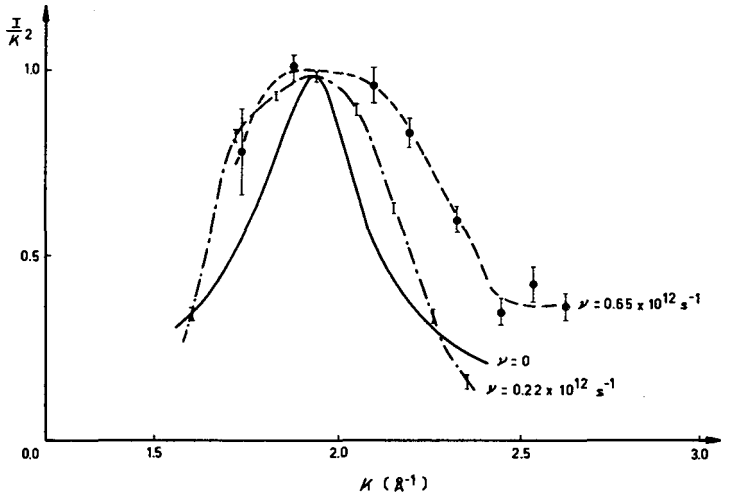

Fig. 6

Intensity distribution of the neutrons scattered by liquid argon at fixed ω-values

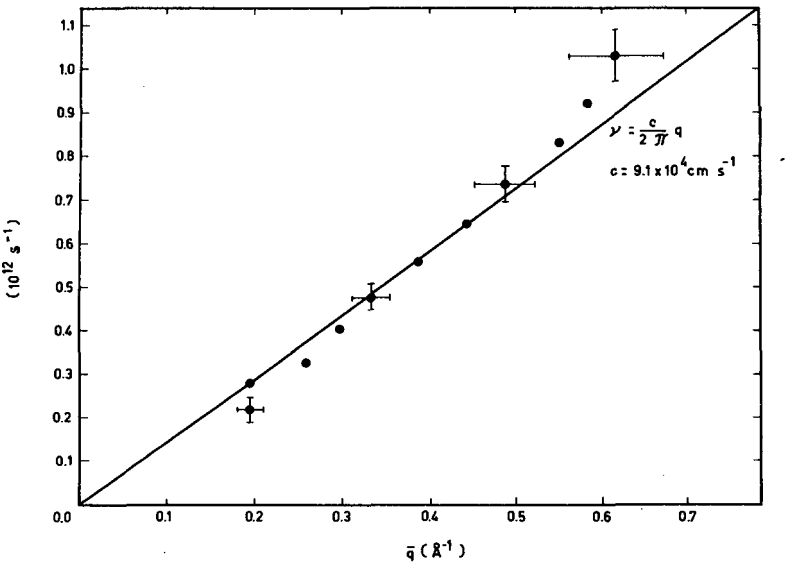

Fig. 7

Average dispersion relation for liquid argon

and q determined in this way are shown in Fig. 7, where a straight line corresponding to sound velocity $c = 9.1 \times 10^4$ cm s^{-1} is also drawn.

In the treatment of the data the following approximations have been made:

(1) The first diffraction peak is supposed to be a Gaussian in κ at all energies. This is not quite true, as can be seen in Fig. 6. This approximation is the basis of Eq. (13) by which $\Delta\kappa$ was evaluated.

(2) Because of the κ^2 factor in the cross-section the statistical accuracy is low at small κ. To overcome this difficulty we used only the intensity on the high κ-side of the first diffraction peak assuming the intensity per κ^2, i.e. Z, to be symmetric around this peak.

(3) The incoherent cross-section is approximated with a Lorentzian. Because a dispersion relation exists, the incoherent scattering is different from a Lorentzian which describes the simple diffusion scattering only. Because of the low intensity of the inelastic scattering at small κ-values, where the incoherent contribution to the scattering was normalized, we did not find it worthwhile to search for a more elaborate model. The smooth behaviour of any incoherent scattering in the region of the coherent peak is believed to give a small correction to the results.

(4) No effort has been made to correct for the contribution of higher phonon terms. In the solid case they could be neglected both in the coherent and incoherent scattering. Assuming that the form of the multiphonon cross-sections used for the solid are valid in the liquid phase too, the only difference in the multiphonon corrections should come from the difference in the Debye temperatures. Using Mott's relation [16] and $\Theta_{DS} = 81°K$ for the solid, one obtains in the liquid case $\Theta_{DL} = 47°K$, but according to the preliminary results of our incoherent scattering investigations the agreement of the Rahman-Singwi-Sjölander model with the measurements is the best with $\Theta_{DL} \sim 70°K$. Because the difference in the Debye temperatures is not too large and the data used in the determination of the dispersion relation cover only the lower part of the frequency spectrum, the multiphonon terms can be neglected within the experimental errors, since their maximum is in the high frequency region. They are furthermore believed to be smooth, monotonous functions of κ in the region of interest here.

Because of the many experimental difficulties it is clear that the results obtained by this analysis are of significance in a qualitative sense only. With this in mind no effort has been made to evaluate the errors introduced by the approximations, and the error bars given in Fig. 6 include the statistical uncertainties only.

V. CONCLUSIONS

These measurements on solid and liquid argon have served a dual purpose: (1) A method has been given to measure an average dispersion relation in a polycrystalline sample and (2) knowing the result for the polycrystalline case, it has been shown that a similar average dispersion law may be found in the liquid. The reason so much effort was devoted to the study of the average dispersion law for the polycrystal is that if in the liquid phase collective modes occur at all, they should produce neutron scattering effects similar to those observed in polycrystals. As already discovered in studies on liquid metals, such as aluminium [11] and tin [12], it is not possible to observe any individual effects of collective scattering like the single-phonon lines observed from single crystals.

It is natural to conceive the crystal lattice broken up into a microscopic mixture of crystallites of short mean life. Such a mixture would show a

scattering picture very similar to that obtained from a polycrystal. The difference between the scattering from the rapidly fluctuating microcrystalline structure of a liquid and the static polycrystalline system would be a broadening of each individual phonon line leading to a smearing out of the sharp cut-off's at $2\pi\tau = \kappa + q$ in the polycrystalline case. This lifetime effect may in the case of argon lead to an almost complete disappearance of the sharp cut-off's in the inelastic scattering picture since the measured broadening due to diffusion corresponds to about 1 meV (compare Fig. 4) whereas the value of the energy transfer at the position of the crystalline cut-off's is in the range 0-5 meV. In the scattered spectra it is then reasonable to expect a smooth intensity distribution for the coherent as well as for the incoherent scattering. As seen from a comparison between the scattered spectra from the polycrystalline and the liquid samples there are no breaks in the liquid case. This fact does not, however, mean that the coherence effects are absent. As has been shown it is possible to derive an average dispersion relation, which can be taken as a proof that the energy and quasi-momentum relations were both active in the scattering process. This observation is in agreement with the results of [11] where, however, the diffusion broadening is so small that sharp microcrystalline breaks are observable in the liquid as well as in the solid scattering.

That the randomness of the atomic motions caused by diffusion allows the existence of vibratory modes of motion may be understood from the following arguments: In a time t, a diffusing atom, on the average, moves a distance 6Dt. It is reasonable to expect that if this distance is small compared to the wavelength of the quasi-phonon, i.e.

$$\sqrt{6Dt} \ll \lambda = \frac{2\pi}{q} \tag{15}$$

the damping caused by diffusion is not too large and the quasi-phonon can exist. To a certain phonon wavelength λ belongs a frequency ν determined by the dispersion relation. The inverse value of ν gives the period τ_0 of the vibration. From the observed dispersion law (see Fig. 7) and the known value of D it is found that for the lowest measured point at $q = 0.2$ Å^{-1} the distance covered by diffusion during one vibration is of the order of 2 Å while the phonon wavelength is 30 Å. At the highest observed q-value we find that $\sqrt{6Dt\tau_0} \sim 1$Å, whereas λ has the value 10 Å. The condition in Eq. (15) is thus very well fulfilled and we conclude that, in spite of the diffusion motion, it is possible for an atom to participate in a damped periodic vibration over the whole region investigated. The validity, at a certain q, of the statement made above is, as can be seen from Eq. (15), dependent upon the ratio between the diffusion constant and the frequency at that particular q. If the frequency at any q is taken as proportional to the Debye temperature it is seen that the validity of Eq. (15) is determined by the ratio of D to Θ_D. An inspection of the values of these quantities for other elements shows that the condition in Eq. (15) is fulfilled by a great number of liquids.

One feature of the present observations that indicates a strong damping of the atomic vibrations in the polycrystalline as well as in the liquid case is that the coherently scattered intensity is unexpectedly low at the highest ν-values. For this reason we do not present any experimental points on the

dispersion curves in Figs. 2 and 7 for q-values above ~0.6 Å^{-1}. The reason for this damping might be that the anharmonicity of the shallow potential in which the argon atoms are moving is so large at the highest frequencies that these vibrations are very far from the simple periodic ones.

These measurements on liquid argon have given strong support to the idea of the existence of collective motions in a classical liquid.

ACKNOWLEDGEMENTS

The authors wish to thank Mr. A. Nyström for designing the cryostat, Mr. L. Karlon for vigorous technical assistance and Mr. B. Tollander for valuable help in the computer calculations. At the same time they would like to express their thanks to Dr. R. Pauli for his personal interest in this work. Two of the authors (Kroó and Borgonovi) are indebted to the AB Atomenergi for the hospitality shown to them. One of them (Kroó) would like to express his thanks to the International Atomic Energy Agency for a ten month scholarship and to AB Atomenergi for the two month extension which made it possible for him to take part in the completion of this work.

REFERENCES

[1] EGELSTAFF, P.A., AERE Rpt R4101 (1962).
[2] EISENSTEIN, A. and GINGRICH, N.S., Phys. Rev. 62 (1962) 261.
[3] HENSHAW, D.G., Phys. Rev. 105 (1957) 976.
[4] VAN HOVE, L., Phys. Rev. 95 (1954) 1374.
[5] EGELSTAFF, P.A., Inelastic Scattering of Neutrons in Solids and Liquids I IAEA, Vienna (1963) 203-14.
[6] WEINSTOCK, R., Phys. Rev. 65 (1944) 1.
[7] EGELSTAFF, P.A., AERE Rpt N/R 1164 (1953).
[8] SJÖLANDER, A., Ark. Fys. 17 (1958) 315.
[9] LARSSON, K.-E. and DAHLBORG, U., R. Sci. Tech. 16 (1962) 81; Inelastic Scattering of Neutrons in Solids and Liquids I IAEA, Vienna (1963) 317-40.
[10] EGELSTAFF, P.A., COCKING, S.J., ROYSTON, R. and THORSON, I., Inelastic Scattering of Neutrons in Solids and Liquids, IAEA, Vienna (1961) 309-20.
[11] LARSSON, K.-E., DAHLBORG, U. and JOVIC, D., Collective atomic motions in liquid aluminium studied by cold neutron scattering", these Proceedings II.
[12] COCKING, S.J. and GUNER, Z., Inelastic scattering of Neutrons in Solids and Liquids I IAEA, Vienna (1963) 237-48.
[13] HOLMRYD, S., SKÖLD, K., PILCHER, E. and LARSSON, K.-E., Nucl. Instrum. Meth. 27 (1964) 61.
[14] VINEYARD, G.H., Phys. Rev. 110 (1958) 999.
[15] BROCKHOUSE, B.N., BERGSMA, J., DASANNACHARYA, B.A. and POPE, N.K., Inelastic Scattering of Neutrons in Solids and Liquids I IAEA, Vienna (1963) 189-201.
[16] MOTT, N.F., Proc. roy. Soc. 146 (1934) 465.

DISCUSSION

B.A. DASANNACHARYA: I would like to present the figure below, in which the square of the width function for liquid argon is plotted against time. The dots are derived from experiments done at Chalk River and the solid line is fitted to the points at large time. It gives us a diffusion coefficient value

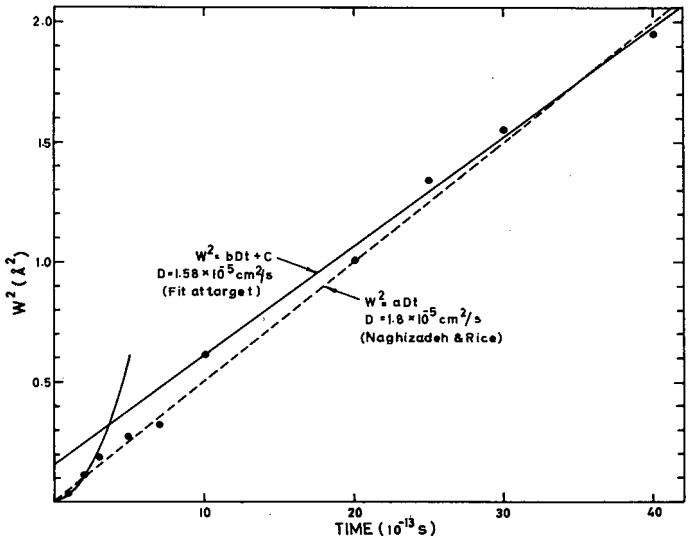

Fig. 1

Liquid argon at 84.5° K.

of 1.58 x 10^{-5} cm^2/s, which is in good agreement with the value obtained directly from the scattering function at small momentum transfers. The points at smaller times all lie below this line*.

N. KROÓ: I think that this figure represents a further argument in support of what we were trying to prove with our work. It is clear that the difference between your points and the width function for simple diffusion is not too great, but the fact that we were still able to see the dispersion of quasi-phonons is proof of the usefulness of our method.

G. VENKATARAMAN: It seems to me that there is considerable evidence in your experiments for collective motions in liquid argon. Is this reflected in the inelastic spectrum?

N. KROÓ: Yes, it is. The wings of the time-of-flight spectra are always above the Lorentzians, giving the same half-widths as the measured ones.

* For detailed results see Phys. Rev. (Jan. 1965).

COLLECTIVE ATOMIC MOTIONS IN LIQUID ALUMINIUM STUDIED BY COLD NEUTRON SCATTERING

K.-E. LARSSON
ROYAL INSTITUTE OF TECHNOLOGY, STOCKHOLM
AND
U. DAHLBORG AND D. JOVIC*
AB ATOMENERGI, STOCKHOLM, SWEDEN

Abstract — Résumé — Аннотация — Resumen

COLLECTIVE ATOMIC MOTIONS IN LIQUID ALUMINIUM STUDIED BY COLD NEUTRON SCATTERING. The neutron spectra scattered inelastically from polycrystalline and liquid aluminium have been studied by means of the cold neutron technique. The polycrystal was kept at 630°C and the liquid at 677°C. It is found that the approximate cross-section formulas based on the harmonic approximation but including the effect of coherence describe relatively well the high temperature results of the solid phase. The liquid scattering picture shows very strikingly the same characteristics as the polycrystalline one. Particularly it is observed that a low frequency cut-off exists in the liquid scattering picture, which may be understood only on the assumption of the existence of collective scattering from the liquid. The results imply that, at least over a region of dimensions of a few Ångström, a considerable local order is maintained for such a length of time that vibratory motions can develop. The results thus clearly demonstrate the existence of a frequency spectrum for the liquid atomic motions consisting of two parts of different nature, one of transversal nature, the other of longitudinal nature. The results also indicate that the frequency spectrum for the liquid state and that for the solid state at room temperature differ most markedly from each other in the high frequency region, a region within which the shortest range order is of decisive importance. On the other hand, the difference between the frequency spectra in the solid at high temperature and in the liquid differ only very slightly. The results imply that the diffusion in liquid aluminium is a slow process with a delay or relaxation time probably of the order of 10^{-12} s or greater, a result already obtained for other liquids by the neutron scattering technique.

MOUVEMENTS COLLECTIFS DES ATOMES DANS L'ALUMINIUM LIQUIDE, ÉTUDIÉS PAR LA DIFFUSION DES NEUTRONS FROIDS. Les auteurs ont étudié les spectres des neutrons diffusés inélastiquement par l'aluminium à l'état polycristallin et à l'état liquide au moyen de la méthode des neutrons froids en maintenant le polycristal à 630°C et le liquide à 677°C. Ils ont constaté que les formules approchées de la section efficace, fondées sur l'approximation harmonique mais tenant compte de l'effet de cohérence, décrivent assez bien les résultats obtenus à haute température en phase solide. Le schéma de diffusion des neutrons par le liquide présente manifestement les mêmes caractéristiques que la diffusion des neutrons par le polycristal. Les auteurs ont constaté notamment que la diffusion des neutrons par le liquide comportait une coupure à faible fréquence, que l'on ne peut expliquer qu'en admettant l'existence d'une diffusion des neutrons collective. Ces résultats laissent supposer que, pour le moins dans une région ayant des dimensions de quelques angströms, un ordre local considérable persiste pendant une durée suffisante pour permettre aux mouvements vibratoires de se développer. Ils montrent ainsi nettement que les mouvements atomiques d'un liquide donnent un spectre des fréquences comportant deux parties de caractère différent, l'une de caractère transversal et l'autre de caractère longitudinal. Ils indiquent en outre que les spectres des fréquences pour l'état liquide et pour l'état solide à la température ambiante diffèrent de façon très marquée l'un de l'autre dans la région des hautes fréquences où l'ordre du plus petit parcours revêt une importance décisive. En revanche, les spectres des fréquences pour le solide à haute température et pour le liquide n'accusent qu'une très faible différence. Il ressort de ces données que la diffusion dans l'aluminium liquide constitue un processus lent comportant probablement un retard ou temps de relaxation

---

* Visiting scientist from the Boris Kidrič Institute of Nuclear Science, Belgrade Yugoslavia, on an International Atomic Energy Agency fellowship.

de l'ordre de 10^{-12} s ou plus long; ce résultat a déjà été constaté pour d'autres liquides étudiés par la méthode de la diffusion des neutrons.

ИЗУЧЕНИЕ КОЛЛЕКТИВНЫХ ДВИЖЕНИЙ АТОМОВ В ЖИДКОМ АЛЮМИНИИ С ПОМОЩЬЮ РАССЕЯНИЯ "ХОЛОДНЫХ"НЕЙТРОНОВ. С помощью метода "холодных" нейтронов изучены нейтронные спектры, неупруго рассеянные от поликристаллического и жидкого алюминия. Температура нагрева поликристалла поддерживалась на уровне 630°С, а жидкости — на уровне 677°С. Обнаружено, что приблизительные формулы для сечения, основанные на аппроксимации гармониками, но включающие эффект когерентности, сравнительно хорошо показывают высокотемпературные результаты твердой фазы. При рассеянии в жидкости отчетливо проявляются те же самые характеристики, что и при рассеянии поликристалла. Особенно можно наблюдать, что завал на низкой частоте происходит при рассеянии в жидкости, что объясняется только на основе предположения о существовании коллективного рассеяния от жидкости. Результаты говорят о том, что по крайней мере за пределами области размеров в несколько ангстрем поддерживается значительный локальный порядок в течение такого промежутка времени, когда могут возникнуть вибрационные движения. Таким образом, результаты ясно доказывают существование спектра частот для движения атомов в жидкости, состоящего из двух частей различной природы, одна — поперечного характера, другая — продольного. Результаты также указывают на то, что частотный спектр в жидкости и спектр для твердого состояния при комнатной температуре наиболее заметно отличаются друг от друга в высокочастотной области — области, в которой величина самого малого порядка имеет решающее значение. С другой стороны, спектры частот в твердом состоянии при высокой температуре и в жидком состоянии различаются между собой лишь крайне незначительно. Результаты говорят о том, что диффузия в жидком алюминии происходит медленно, причем время задержки или ослабления составляет примерно 10^{-12} сек или более. Этот результат уже получен для других жидкостей с помощью метода рассеяния нейтронов.

ESTUDIO DE LOS MOVIMIENTOS COLECTIVOS DE ATOMOS EN EL ALUMINIO LIQUIDO POR DISPERSION DE NEUTRONES FRIOS. Los autores han estudiado los espectros de neutrones dispersos inelásticamente en aluminío policristalino y líquido, aplicando a tal efecto la técnica de neutrones fríos. El policristal se mantuvo a 630°C y el líquido a 677°C. Las fórmulas aproximadas de la sección eficaz, basadas en la aproximación armónica pero que incluyen el efecto de coherencia, describen en forma relativamente satisfactoria los resultados obtenidos a temperaturas elevadas en la fase sólida. La imagen de dispersión en el líquido presenta caracterís-ticas notablemente similares a las obtenidas en la fase policristalina. En especial, se observa en esa imagen una interrupción a baja frecuencia, que sólo se explica admitiendo la existencia de una dispersión colectiva en el líquido. Los resultados implican que, por lo menos para una región de algunos angstroms, se mantiene un grado considerable de orden durante tiempo suficiente para que puedan producirse movimientos vibratorios. Así, los resultados demuestran claramente que en el caso de los movimientos atómicos en el líquido existe un espectro de frecuencias, que consiste en dos partes de naturaleza diferente, una transversal y otra longitudinal. Indican asimismo que la mayor diferencia entre los espectros de frecuencia correspondientes al estado líquido y al estado sólido a temperatura ambiente se observa en la región de las frecuencias elevadas, donde las fuerzas de corto alcance adquieren una importancia decisiva. En cambio, los espectros de frecuencia del sólido a temperatura elevada sólo difieren muy ligeramente de los correspondientes al líquido. Los resultados indican que la difusión en el aluminio líquido es un proceso lento, caracterizado por un tiempo de retardo o relajación del orden de 10^{-12}s o mayor. El mismo resultado se obtuvo ya para otros líquidos por la técnica de dispersión de neutrones.

I. INTRODUCTION

Neutrons of an energy as low as 5 meV have proved to be a most sensitive tool to investigate microscopic fluctuation phenomena in solids and liquids [1, 2]. Particularly the research on the atomic or molecular motions in liquids have been of great importance, as so far very few methods have existed which have allowed the detailed study of the correlations of these motions among the particles. A considerable number of measurements have already been performed mainly on incoherently scattering liquids like the

hydrogenous water, glycerol, methane, alcohols etc. [1, 2, 3, 4, 5]. The reason for this choice of liquid samples invariably has been that hydrogen is an incoherent scatterer and the scattered neutron spectrum would in this simple case reveal all the motions of the scatterer, i.e. the proton, without any limitation. There is, however, a serious drawback with the complicated molecular liquids exemplified above, namely that not only are the protons dragged with the molecule as a whole in the motion of its centre of mass, but they are also performing a complicated motion between the molecules in existing hydrogen bonds and in the molecules to form a complex inelastically scattered neutron spectrum involving librational, rotational and vibrational motions. The motion of the centre of mass of the molecule is consequently hard to distinguish from the rest of the motions.

A liquid metal would not present this problem as it is a monatomic liquid. The inelastically scattered neutron spectrum would in this case correspond to the motions of the centre of mass of the metal nucleus. Another difficulty is, however, encountered: most metal nuclei are mixed coherent and incoherent scatterers. Therefore the interpretation of the scattered neutron spectra is very much complicated as the coherence may impose strong limitations on the collective scattering process. Very little is known about the extent to which coherence effects are operating in the liquid phase. A few experiments have been made which have aimed at the study of the possible coherent elastic or quasi-elastic scattering in liquid metals like lead [6]. Similarly studies on liquid tin have been reported, which have shown the existence of an inelastic neutron spectrum with similarities between the liquid and solid phases [7]. From the studies on liquid lead the time-displaced self-correlation function and the correlation function for the sphere of nearest neighbours was derived and it was found that for a time of the order of about 5×10^{-3} s the atoms move relatively little, which would mean that vibrations of frequencies larger than 2×10^{12} c/s may exist in the liquid. This would in turn mean that it would probably be meaningful to speak about pseudo-phonons in the liquid and about a frequency spectrum for these pseudo-phonons. This would be so because for liquids, the parent solid of which has a high Debye temperature, the frequencies in the frequency spectrum range up to high values, for example 9×10^{12} c/s for aluminium at room temperature [8]. Such a conclusion would also entail that, provided the nuclei have a coherent scattering cross-section, a nucleus and its nearest surrounding would produce interference effects in the scattering process. This would thus be a result of the slow diffusion in the liquid, which does not cause an appreciable change in the average position of an atom during a vibrational period and during the neutrons interaction time. It would thus be expected that strongly limiting conditions would be imposed on the inelastically scattered neutron spectrum due to coherence effects in the liquid as well as in the solid polycrystalline case.

On the basis of these ideas we undertook a study of the scattering of cold neutrons from polycrystalline and liquid aluminium at temperatures of 630 and 677°C respectively. The melting point of aluminium is 659.7°C. Aluminium is a practically pure coherent scatterer and should thus clearly show the coherence effects discussed above. Moreover, this substance has been thoroughly studied earlier by the neutron scattering technique at various higher temperatures [9].

II. THEORETICAL IDEAS ON THE CROSS-SECTION FOR COHERENT INELASTIC SCATTERING

As already pointed out above very few attempts exist to formulate a realistic and practically useful formula for the coherent inelastic scattering cross-section for slow neutrons. Already in 1944 WEINSTOCK [10] formulated this cross-section for a polycrystalline sample on the basis of the harmonic approximation. This general form is, however, not very practical for comparison to experimental results. At the price of sacrificing the generality of Weinstock's formula, EGELSTAFF [11] in 1953 derived a form for this cross-section which was more amenable to practical work. According to this formulation the polycrystalline coherent inelastic single-phonon cross-section may be given by

$$\frac{d^2\sigma_{coh}}{d\Omega d\omega} = a_{coh}^2 \cdot I \cdot \sum_{\tau} \frac{\pi F_\tau}{2 B\tau\kappa q} \tag{1}$$

with

$$I = \frac{\hbar}{2M} \frac{k'}{k} \frac{\kappa^2}{\omega} e^{-2W} \frac{f(\omega)}{\exp(\hbar\omega/k_B T)-1} \tag{2}$$

Here a_{coh} is the coherent scattering length
B is the volume per nucleus in the crystal
$\vec{\tau}$ is a reciprocal lattice vector
$\hbar\vec{\kappa}$ is the momentum transfer in the scattering process
$\vec{q}$ is the phonon wave vector
F_τ is the structure factor for the plane series specified by τ
M is the mass of the scattering nucleus
$\vec{k}$, $\vec{k'}$ are the ingoing and scattered wave vectors
$2W$ is the Debye-Waller factor
$\hbar\omega$ is the energy transfer in the scattering process
k_B is the Boltzmann constant
T is the absolute temperature
$f(\omega)$ is the frequency distribution of the normal modes.

Formally Eq. (2) describes the inelastic incoherent cross-section except for a numerical factor. Equation (1) therefore gives the coherent cross-section as the incoherent multiplied with a structure factor Z which is

$$Z_{solid} = \sum_{\tau} \frac{\pi F_\tau}{2B\tau\kappa q} \cdot \tag{3}$$

Formally this is similar to an application of a type of convolution approximation to the inelastic scattering [12]. To arrive at Eqs. (1) and (2) it was necessary to assume the Debye frequency distribution $f(\omega) = 3\omega^2/\omega_D^3$. Thus

the simple form of the structure factor Z, which is nothing but a result of an averaging process over the momentum conservation condition $\delta(\vec{\kappa} + \vec{q} - 2\pi\vec{\tau})$ in the polycrystalline cross-section, was obtained only by the use of the relation $\omega = cq$. Secondly the form given for Eq. (2) was shown to be valid only for the Debye frequency distribution. Without this last assumption Eq. (2) would have contained instead of $f(\omega)$ the factor $q^2\, dq/d\omega$. It is seen that if $\omega = cq$ we find for the last factor the value ω^2/c^3 which is proportional to $f(\omega)$ only if $f(\omega) \sim \omega^2$. The use of a general and more realistic frequency distribution in Eq. (2) will probably lead to an error which may be considerable for the large values of ω. Only for small values of ω may the true frequency distribution be realistically approximated by an ω^2-distribution. For larger values of ω the true dispersion relation deviates very much from $\omega = cq$. As a matter of fact $d\omega/dq$ may be equal to 0 for large q- or ω-values. This means that the expression I in Eq. (1), before the introduction of the assumption of a Debye spectrum, may reach values considerably higher than those calculated from Eq. (2).

By a suitable definition of average dispersion relations derived from the realistic shape of $f(\omega)$ it should, however, be possible to improve this situation. Such a definition was given by KROÓ et al. [13] in the form:

$$\int_0^{\omega} f(\omega)\, d\omega = 4\pi \int_0^{q} q^2 dq\,. \tag{4}$$

This relation establishes a connection $q = q(\omega)$ and it is seen that $f(\omega) = q^2 \frac{dq}{d\omega}$, as is generally required in the formulas derived by Egelstaff. The use of Eq. (4) should be most realistic for a rather isotropic substance. Using Eq. (4) and a frequency spectrum divided into a low frequency region describing waves of transversal nature and a high frequency region describing waves of longitudinal nature (compare the X-ray work of WALKER, [8]), two average dispersion relations are defined as follows:

$$q_{\text{transversal}} = \left[\frac{1}{4\pi} \int_0^{\omega} [f(\omega)]_{\text{transversal}}\, d\omega\right]^{\frac{1}{3}} \tag{5a}$$

$$q_{\text{longitudinal}} = \left[\frac{1}{4\pi} \int_0^{\omega} [f(\omega)]_{\text{longitudinal}}\, d\omega\right]^{\frac{1}{3}} \tag{5b}$$

The cross-section according to Eq. (1) may then be calculated separately for the longitudinal and transversal branches. The two results are then added.

Already for the case of a solid the theoretical basis for a cross-section calculation for a high temperature sample is relatively weak. In the case of a liquid the current theories [14] dealing with the possible coherence effects to be expected in the inelastic scattered neutron spectrum are very scarce. As was pointed out in the introduction there are several experimental facts speaking in favour of the existence of a very solid-like behaviour of a liquid

when seen on a time scale in the range of 10^{-12} s. Thus a frequency spectrum for the proton motions was derived from measurements on water both in the solid and in the liquid phase. The two frequency spectra were found identical over most of the spectral range investigated which was $0.5 \times 10^{13} < \omega < 15 \times 10^{13}$ rad/s [5]. In the case of a liquid, however, the frequency spectrum can hardly be imagined to have the same ideal definition as in a solid. The atomic vibrations must be strongly damped in the liquid and it is not appropriate to speak about phonons in the sense of freely propagating waves. Rather one may imagine a pseudo-phonon picture in the liquid as well as in the high temperature solid. As a matter of fact it was already shown for the case of aluminium at temperatures close to the melting point that the lifetime of the phonons are of the order of 10^{-12} s and the mean free paths only of the order of a few wavelengths [9].

It therefore suggests itself to develop for the liquid some sort of generalization of the formulas developed for the polycrystal [15]. It is well known from elastic X-ray and neutron scattering that the discrete structure factors F_τ, for the Bragg reflections in the solid, shift over to a continuous intensity, determining structure factor $1+\gamma(\kappa)$ in the liquid case with broad peaks close to the former sharp sets of Bragg planes. (For the shape of $1 + \gamma(\kappa)$ see Fig. 4.) It would consequently be logical to replace the summation over the discrete lattice planes in the structure factor Z, as given by Eq. (3), by an integration over a continuous distribution of "reflecting planes". The extension of these "planes" in the liquid could be just a few atomic distances wide. The discrete structure factor F_τ would simultaneously be replaced by the continuous liquid structure factor $1 + \gamma(\tau)$, where $\vec{\kappa}$ has been replaced by $\vec{\tau}$. We then have the transformation

$$Z = \sum_\tau \frac{\pi F_\tau}{2B\,\tau\kappa q} \longrightarrow \frac{\pi}{2} \int \frac{4\pi\tau^2\, d\tau\, (1+\gamma(\tau))}{\tau\kappa q} . \qquad (6)$$

In order to use the transformed structure factor of Eq. (6) certain limits of integration have to be established. To fix these, the existence of dispersion relations for the liquid have to be postulated. At least one experiment has been performed to establish the existence of a single phonon in a liquid [16]. This experiment was, however, negative. According to our opinion this is what may be expected: a liquid does not scatter like a single crystal. If there is any coherent scattering at all, it has to be derived from the coupled motion of atoms over a small region such as in a polycrystal. The dispersion relation thus must be originating from the strongly damped phonons confined to a small region of atoms in the liquid. If, however, a dispersion relation is postulated, a phonon wave vector is defined and the corresponding value or values of ω are also defined. Consequently $\vec{\kappa}$ is defined and also the limits of integration, which apparently are $\vec{\tau}_{max.} = \frac{\vec{\kappa}+\vec{q}}{2\pi}$ and $\vec{\tau}_{min.} = \frac{\vec{\kappa}-\vec{q}}{2\pi}$. The structure factor in the liquid case thus is

$$Z_{liquid} = \frac{2\pi^2}{q\kappa} \int_{\tau_{min.}}^{\tau_{max.}} \tau \left(1+\gamma(\tau)\right) d\tau \qquad (6')$$

In order to be reasonably realistic one has to assume the existence of at least two dispersion relations, one longitudinal and one transverse, which is degenerate, both in the polycrystalline case and in the liquid case. In the case of aluminium, which is relatively isotropic, this appears as a reasonable assumption. In the original formulas by Weinstock there enters into the cross-section the product $(\vec{e}_q \cdot \vec{e}_\kappa)^2$, where $\vec{e}_q$ is the polarization vector of the phonon and $\vec{e}_\kappa$ is a unit vector in the direction of $\vec{\kappa}$. In a very primitive approximation one might imagine the longitudinal and transverse phonons to be pure, i.e. with their polarization vectors parallel and at right angles to the propagation direction. This results in values for $(\vec{e}_q \cdot \vec{e}_\kappa)^2$ of $\cos^2 \Theta$ or $\sin^2 \Theta$ for the two cases respectively, where Θ is the angle between $\vec{q}$ and $\vec{\kappa}$. The value of Θ is easily found from the vector diagram of $\vec{\kappa}$, $\vec{q}$ and $\vec{\tau}$. The final structure factor for the liquid case would thus be

$$Z_{\text{liquid}} = \frac{2\pi^2}{q\kappa} \int_{\tau_{\text{min.}}}^{\tau_{\text{max.}}} \tau \left(1 + \gamma(\tau)\right) (\vec{e}_q \cdot \vec{e}_\kappa)^2 d\tau, \tag{7}$$

The results of the two calculations are finally added. The structure factor Z_{solid} is also taken with the $\sin^2 \Theta$ and $\cos^2 \Theta$ factors included.

The factor I defined in Eq. (2) is taken over to the liquid case without any changes. This involves the assumption of the existence of a frequency distribution in the liquid, which is a logical consequence of the postulation of a dispersion relation. A cross-section formula for the liquid case is thus created

$$\frac{d^2\sigma_{\text{coh}}}{d\Omega\, d\omega} = a_{\text{coh}}^2 \cdot I \cdot Z_{\text{liquid}} \tag{8}$$

Equations (1) and (8) were used by us for computations of expected single-phonon cross-sections for comparisons with the experimental results on high temperature solid and on liquid aluminium, respectively.

As the experiments were performed at high temperatures compared to the Debye temperature of aluminium, a considerable multiphonon contribution is expected. As was already shown in earlier work [9] the multiphonon cross-section in this coherent scattering case is very well described by the incoherent approximation, for which a convenient phonon expansion formula exists [17]. We have used the expansion

$$\left(\frac{d^2\sigma}{d\Omega\, d\omega}\right)_{\text{multiphonon}} = a^2 \frac{k'}{k} \exp\left[-2W - \frac{\hbar(\omega-\omega_0)}{2kT}\right] \sum_{n=2}^{\infty} \frac{(2W)^n}{n!} \bar{G}_n(\omega-\omega_0), \tag{9}$$

where

$$\bar{G}_n(\omega - \omega_0) = \frac{1.74}{(2\pi n)^{1/2}} \cdot \exp - \left[\frac{3.03}{2n} \left(\frac{\omega - \omega_0}{\omega_D}\right)^2\right]. \tag{10}$$

Here $\hbar(\omega - \omega_0)$ is the energy transfer in the scattering process and $\hbar\omega_D = k_B\Theta_D$, where Θ_D is the Debye temperature of the sample. Usually it is enough at the temperatures investigated to include the terms n = 2, 3, 4 and 5 to get a high accuracy.

III. EXPERIMENTAL METHOD AND ARRANGEMENT

The principle of the present neutron scattering arrangement is the same as has been used in a series of scattering experiments that have been performed at the Stockholm reactor.

The beryllium-filtered cold part of the Maxwellian reactor spectrum is sent into the aluminium sample and the scattered neutrons are analysed in energy at selected angles by the slow chopper time-of-flight technique [18]. For this experiment, which aims at a study of the inelastically scattered neutron spectrum, the question of the width of the ingoing spectrum is important. This question was considered in detail and in all calculations of theoretically expected spectra for comparison with the experiment. The cross-section calculated for a monochromatic ingoing neutron spectrum was folded with the ingoing cold neutron spectrum of the form $f(\lambda)\,d\lambda \sim \lambda^5\,d\lambda \sim \omega\,d\omega$. The calculated scattered neutron spectrum $I(\omega, \Omega)$ was thus given by

$$I(\omega, \Omega) = \text{const.} \int_0^{\omega_{max.}} \frac{d^2\sigma(\omega' \to \omega)}{d\Omega\, d\omega}\, \omega'\, d\omega', \qquad (11)$$

where $\omega_{max.}$ corresponds to 0.796×10^{13} rad/s or an energy of 5.2 meV. It was found insufficient to use approximate methods like a division of this spectrum into four parts to calculate the effect on the scattered spectrum of the ingoing one. The complicated foldings according to Eq. (11) were performed on an electronic computer. All calculations in this work including the incoherent and coherent one-phonon terms as well as the multiphonon expansion were performed according to Eq. (11).

The observations were performed at 20° and 60° angles of scattering with the aluminium sample in the polycrystalline case at a temperature of 630°C and in the liquid case at 677°C. The sample, which was rectangular with an area of 100 cm^2 and a thickness of 1.2 cm in the polycrystalline case and 1.7 cm in the liquid case, was oriented in the neutron beam such that it made an angle of 45° with the beam. This ensures that approximately the same area of the sample is seen through the chopper by the detector at the two angles of observation.

The containment of liquid aluminium for a long time is a serious problem as the walls of the container have to be thin in order to reduce background scattering from it. Our final arrangement consisted of a frame of ceramics which served as a holder for two plates of molybdenum of the area mentioned above. The aluminium was kept between the molybdenum plates, which hence constituted the main source of background. The thickness of the molybdenum plates in the polycrystalline case was 0.01 cm and in the liquid case 0.1 cm. The transmission of the plates for cold neutrons was 99% and about 90% respectively. Heating wires were wound round the ceramic frame and the

whole container was kept in a vacuum vessel at about 10^{-3} mm Hg. The polycrystalline sample consisted of about a hundred cubes to ensure that even if some preferred crystal orientation should have occurred in each piece, the total sample is a true polycrystalline one. The transmission for thermal neutrons of the aluminium was of the order of 90% for the polycrystalline sample and 86% for the liquid sample. The temperature was electronically regulated and measured by thermocouples to an accuracy of ± 3°C.

IV. EXPERIMENTAL RESULTS AND DISCUSSION

As all the present experiments were made at high sample temperatures a considerable background problem arises due to inelastic scattering from the sample holder. The relative importance of careful background studies are exemplified in Fig. 1, where the primary scattered neutron spectra for 60° angle of scattering are given for the polycrystalline as well as for the liquid case. Also shown in this figure are the backgrounds, which consist of various contributions, namely:

(a) A thermal neutron component which is peaked around flight-times of 450 μs/m or 25 meV. This is caused by incoherent inelastic scattering from the molybdenum container walls.

(b) A fast neutron component which is peaked at flight-times of 55 and 863 μs/m. Between these peaks the fast background is time-independent. The cause for this double peak is that the chopper transmits fast neutrons twice per revolution, a 0° and a 180° pulse. The energy at the position of the fast pulse is about 1.6 eV.

(c) A cold neutron component arising from the incoherent elastic scattering from the molybdenum container walls which is clearly visible as the lower curve for Fig. 1 for flight-times longer than 1000 μs/m.

(d) For flight-times longer than 1000 μs/m there is also an extra intensity created by the fact that the chopper transmits a smaller percentage of the inelastic scattered neutrons in the 180° pulse. From the transmission curve of the chopper [18] the expected value of the ratio between the intensities transmitted in the main 0° pulse to the 180° pulse is about six. This agrees very well with the observed ratio of the intensity at flight-times of 400 μs/m to the intensity at 1150 μs/m. As a result all the scattered intensity for flight-times longer than 1000 μs/m is explained as various kinds of backgrounds. The backgrounds were measured by the total scattering from the empty container plus the fast component from the aluminium itself. The backgrounds were taken at the temperatures of 630 and 677°C.

The data, carefully corrected for the various background effects, were then corrected for the chopper transmission function and the detector efficiency.

The corrected result of the four runs on solid and liquid aluminium is shown in Fig. 2. It is first of all striking to note that the observed scattered spectra from the solid and the liquid phases are almost identical. In the solid phase a well-defined frequency spectrum of the phonons exists and this observation hence indicates that a similar spectrum exists in the liquid. The spectrum obtained from the polycrystal contains two peaks of which the low energy peak mainly is built up of neutron energy exchange with transversal phonons and the high energy peak is a combination of neutron energy exchange

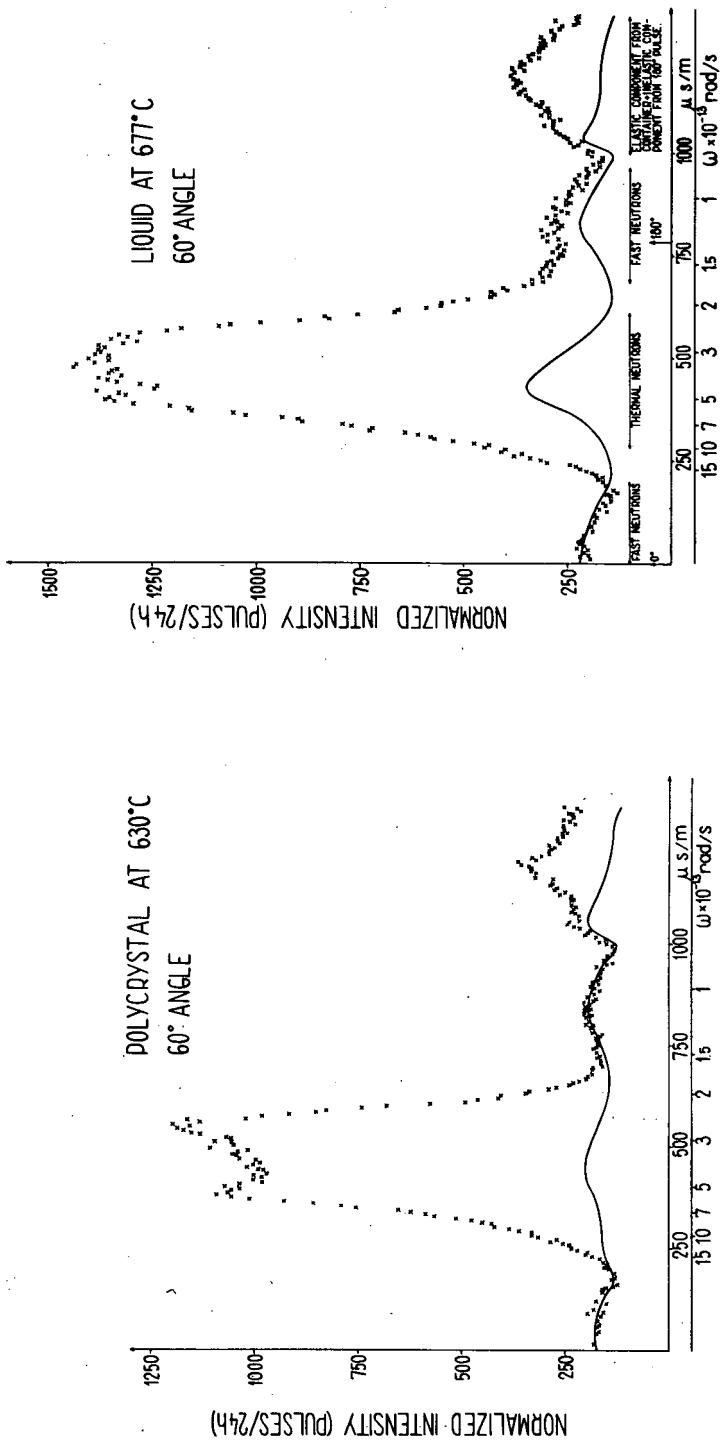

Fig. 1

Primary scattering data from solid and liquid aluminium at 60° angle of observation
The background level is also given and the origin of the various peaks in the background is indicated

with longitudinal phonons and multiple phonon interactions. It is a striking fact that the neutron distributions scattered from the liquid phase show exactly the same characteristics. The assumption of the existence of pseudo-phonons in the liquid phase mentioned in section II hence gets strong support.

The next question would then be if there is any possibility to establish a typical coherence phenomenon in the liquid. As it is to be expected that only the single-phonon interactions would reveal any coherence effects, the multiphonon contribution must be subtracted from the observed spectra. The fact that the multiphonon cross-section calculated on the basis of the incoherent approximation describes the observed multiphonon spectrum was shown earlier for various high temperatures of a single crystal of aluminium [9]. It is therefore obvious that the same formulas will describe the multiphonon contribution to the polycrystalline cross-section which was actually shown in the older series of measurements (Fig. 3). The normalization of the calculated multiphonon term to the experimentally observed data was in the present case made by fitting it to the high energy front of the observed spectrum as exemplified in Fig. 6. This procedure contains only a relatively small uncertainty factor as also shown by the older results of Fig. 3. Following this procedure the one-phonon term was isolated from the observed spectra. In order to calculate the multiphonon spectra we used, as explained in section II above, the Gaussian approximation [17] with a Debye temperature [9] of 327°K for the solid and 313°K for the liquid case. The Debye-temperature of 327°K corresponds to a decrease of 15% from the room temperature value and 313°K corresponds to a decrease of 20% from this value. The one-phonon term obtained in this way should contain some of the characteristics of the frequency spectrum. As a matter of fact, if the scattering process were an incoherent one, the one-phonon term would for a polycrystal be given by

$$\frac{d^2\sigma_{inc}}{d\Omega\, d\omega} = a_{inc}^2 \frac{\hbar}{2M} \frac{k'}{k} \frac{\kappa^2}{\omega} \frac{e^{-2W}}{\exp(\hbar\omega/k_B T)-1} f(\omega) \qquad (12)$$

and if it were a coherent one, the one-phonon term would be given by

$$\frac{d^2\sigma_{coh}}{d\Omega\, d\omega} = a_{coh}^2 \frac{\hbar}{2M} \frac{k'}{k} \frac{\kappa^2}{\omega} \frac{e^{-2W}}{\exp(\hbar\omega/k_B T)-1} f(\omega) \sum_{\tau} \frac{\pi F_\tau}{2B\tau\kappa q}, \qquad (13)$$

where the last formula is a very much simplified version of the expected true behaviour in the coherent case. These two cross-sections have to be folded with the ingoing spectrum before a comparison to the experiment may be performed as mentioned earlier in this section (Eq. (11)).

In order to calculate cross-sections according to Eq. (12) the frequency spectrum has to be known and if Eq. (13) is used the frequency spectrum and the dispersion relations have to be known. Fortunately f(ω) was derived from X-ray data for a room-temperature crystal of aluminium [8]. As no such study was made at our high sample temperature we had to rely upon an extra-

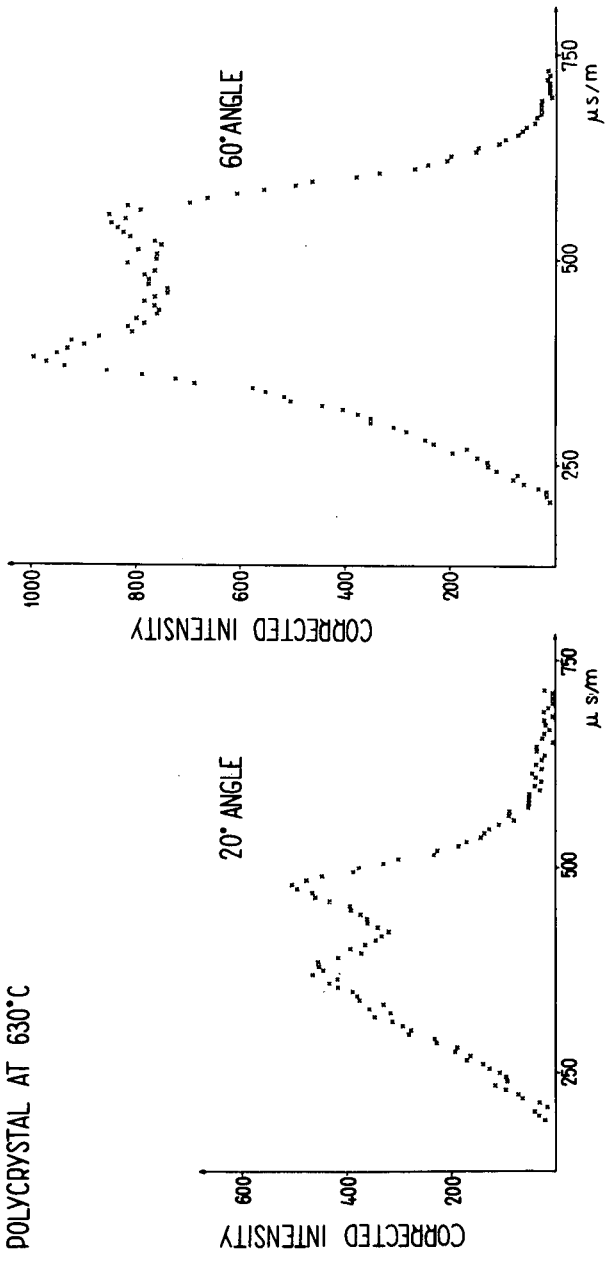
POLYCRYSTAL AT 630°C
20° ANGLE
60°ANGLE
CORRECTED INTENSITY
200
400
600
800
1000
250
500
750
μs/m

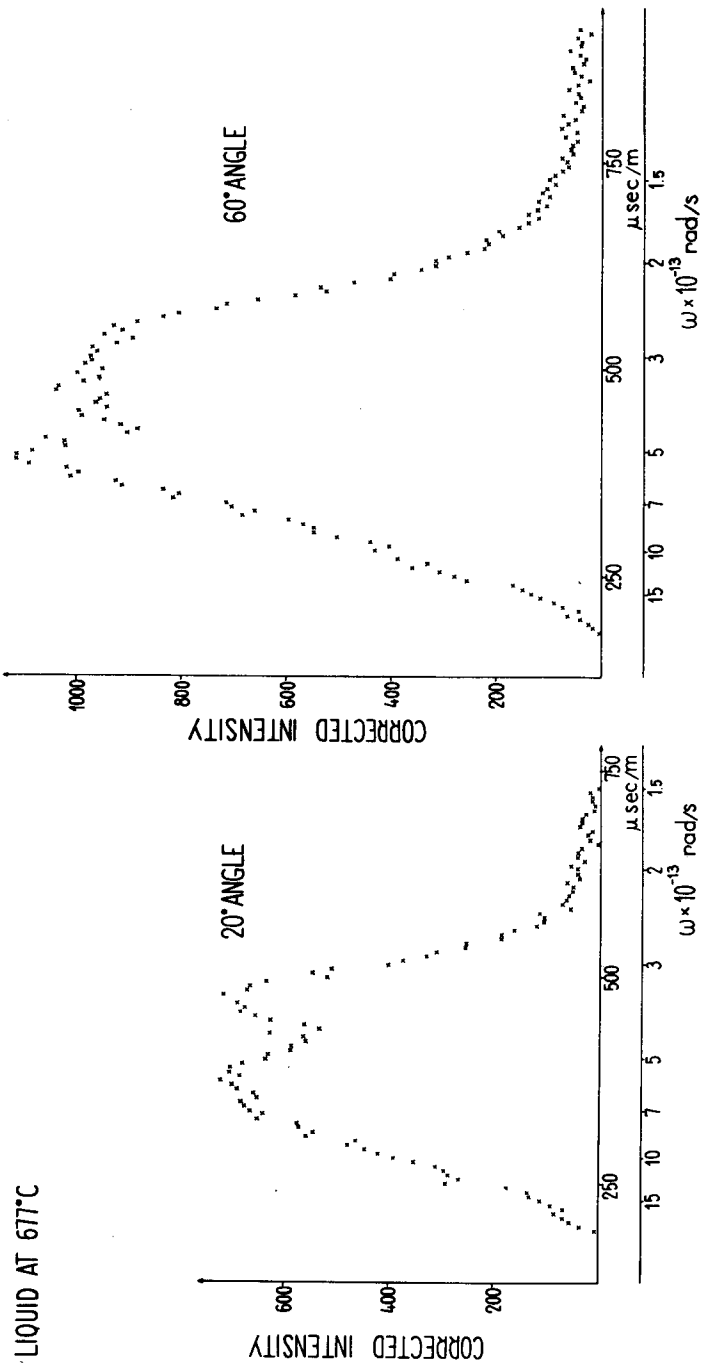

Fig. 2

Corrected scattered spectra of cold neutrons from polycrystalline aluminium at 630°C and from liquid aluminium at 677°C taken at 20° and 60° angle of observation

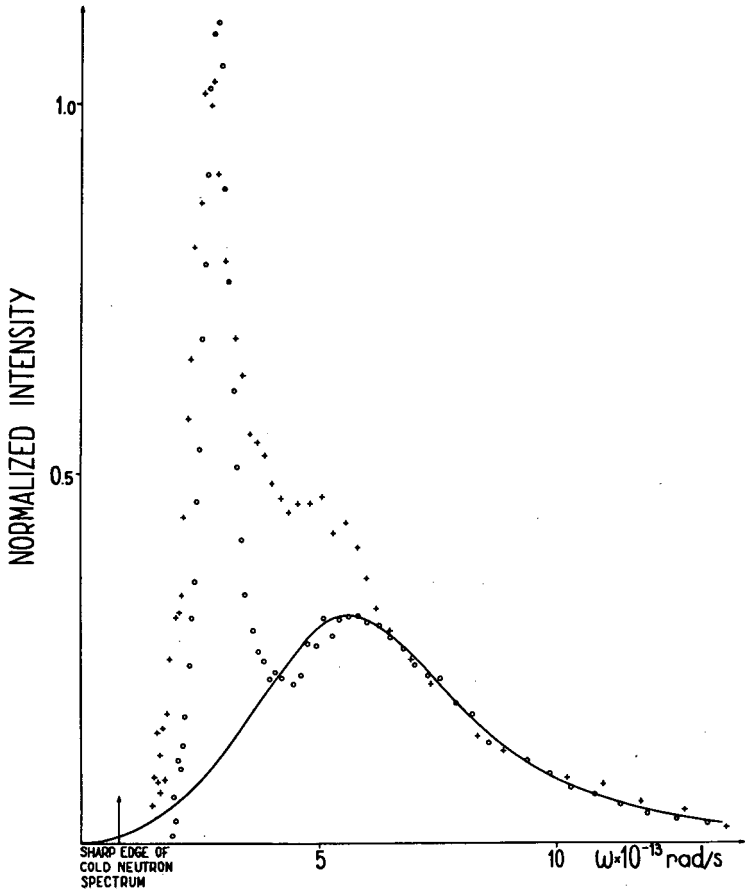

Fig. 3

Observed neutron spectra from a single crystal and a polycrystal of aluminium at 650°C and 50° angle of observation given in energy units
The observation on the single crystal shows a single-phonon peak and a well-isolated multiphonon spectrum, which is compared to a calculated multiphonon spectrum for a Debye temperature of 325°K. This observation was performed in 1959 (see Ref. [9]).

0 Single crystal 650°C
\+ Polycrystal 650°C
——— Multiphonon

polation of earlier experiences on the temperature variation of certain isolated phonons in aluminium from 300 to 800°K. Over this temperature interval we had found [9] that the frequencies drop by about 12%. We therefore assumed that all frequencies decrease by 15% in going from 300 to 903°K. As nothing else is known about the liquid phase we assumed a frequency spectrum of the same shape as for the solid but with a further decrease of the frequencies to 20%. As a matter of fact various values for the percental change of the vibratory frequencies were tried but it was found that the values of 15 and 20% respectively gave the best fit to the observed data. With these frequency

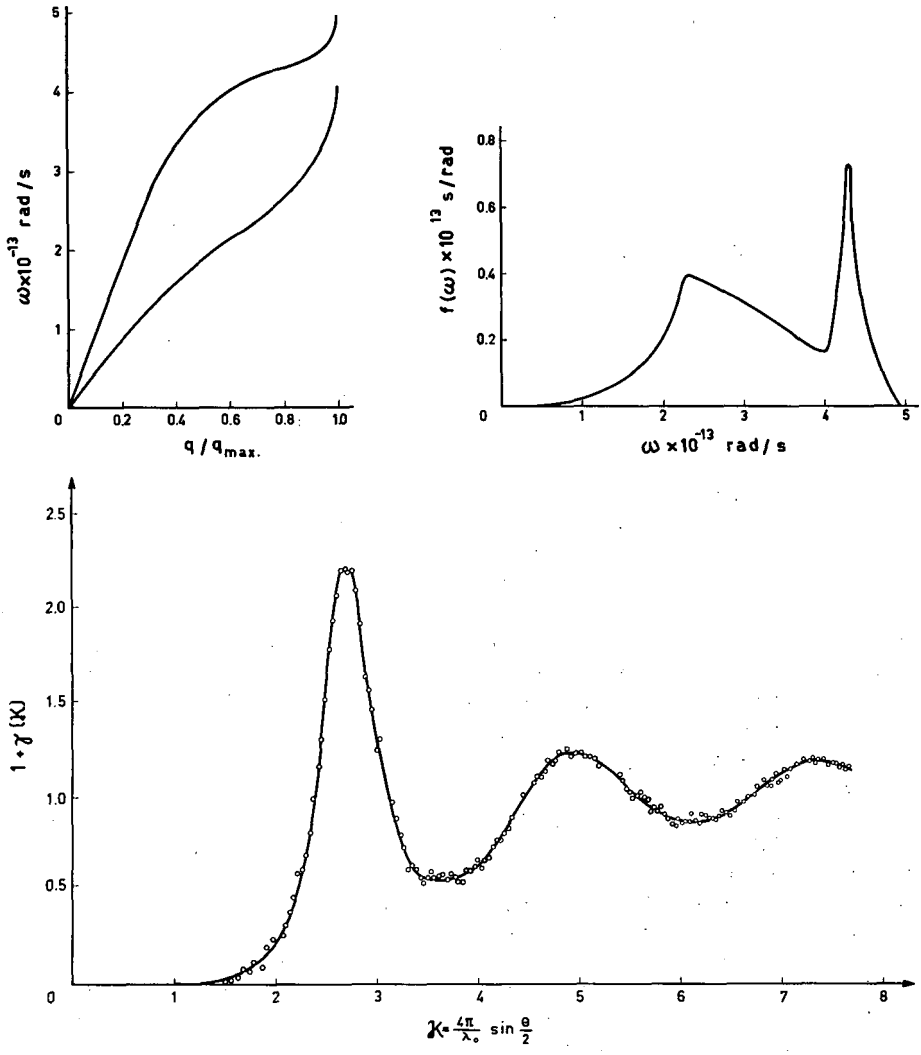

Fig. 4

The average dispersion relations, the frequency spectrum and the liquid structure factor $1 + \gamma(\kappa)$ used to calculate Z_{liquid}

spectra given it is easy to calculate average dispersion relations according to Eqs. (5a) and (5b), which was done for the solid as well as for the liquid case. As aluminium is a fairly isotropic substance the definition of average dispersion relations should be a reasonable procedure. The only justification we have to proceed in the same way for a solid and a liquid is our primary observation that the observed scattered neutron spectra look almost identical, even including a fairly sharp cut-off in the spectra on the low energy side (at flight-times of 500-700 μs in Fig. 2). Examples of the frequency spectrum and derived average dispersion relations which we used for the case of liquid

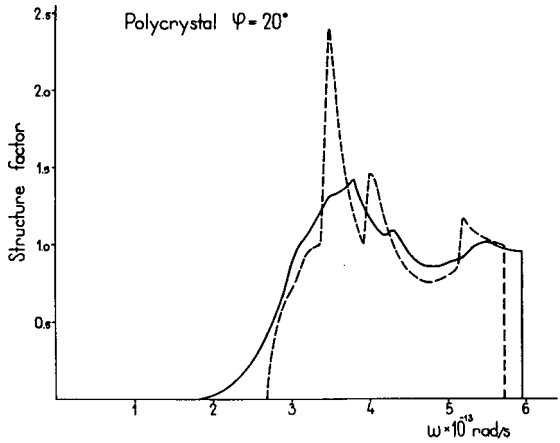

Fig. 5

Structure factor Z_{solid} calculated for a narrow ingoing spectrum (dashed line) $0.55 \leq \omega_0 \times 10^{-13} \leq 0.60$ rad/s and for the full cold spectrum (solid line) $0 \leq \omega_0 \times 10^{-13} \leq 0.80$ rad/s.

aluminium are given in Fig. 4, where also the structure factor $1 + \gamma(\tau)$ needed to calculate Z_{liquid} according to Eq. (6) is given. As mentioned in conjunction with Eq. (11) it was found necessary to integrate the cross-section formulas over the ingoing neutron spectrum before comparison to the experiment. In Fig. 5 the calculated structure factor is shown for two assumptions regarding the ingoing spectrum. It is seen that an integration over the whole ingoing spectrum is needed.

The final results of the calculations giving the best simultaneous fit to the data at 20° as well as at 60° are given in Fig. 6. Here the observed and calculated scattered neutron distributions are given on an absolute energy scale. The ingoing cold neutron spectrum thus shows its sharp edge at $\omega \simeq 0.8 \times 10^{13}$ råd/s. The multiphonon spectrum calculated according to Eq. (10) is fitted to the observed spectrum in the high frequency tail for $\omega > 8 \times 10^{13}$ rad/s. The calculated one-phonon term according to Eqs. (1) and (6) for the solid and liquid cases, respectively, is then added to the multiphonon term and the compounded result compared to the experiment.

As is quite clear from an examination of Fig. 6 the simple theoretical model describes the observed data reasonably well for the polycrystalline case. The most prominent discrepancy between the experimental result and the theoretical curve is that the experiment gives a higher intensity than is predicted theoretically for $5 < \omega < 8 \times 10^{13}$ rad/s. This corresponds to frequencies at the end of and above the high frequency branch. Perhaps this is an indication that new high frequencies are created by anharmonic effects in the crystal. It seems obvious that the frequency spectrum should range up to higher frequencies at this high temperature limit of 630°C. The creation of localized modes due to interstitial atoms might be a possible physical cause for the discrepancy. Possibly other changes of the frequency spectrum are the causes for the discrepancies over the main peak corresponding mostly to the transversal part of the frequency distribution. On the whole the agree-

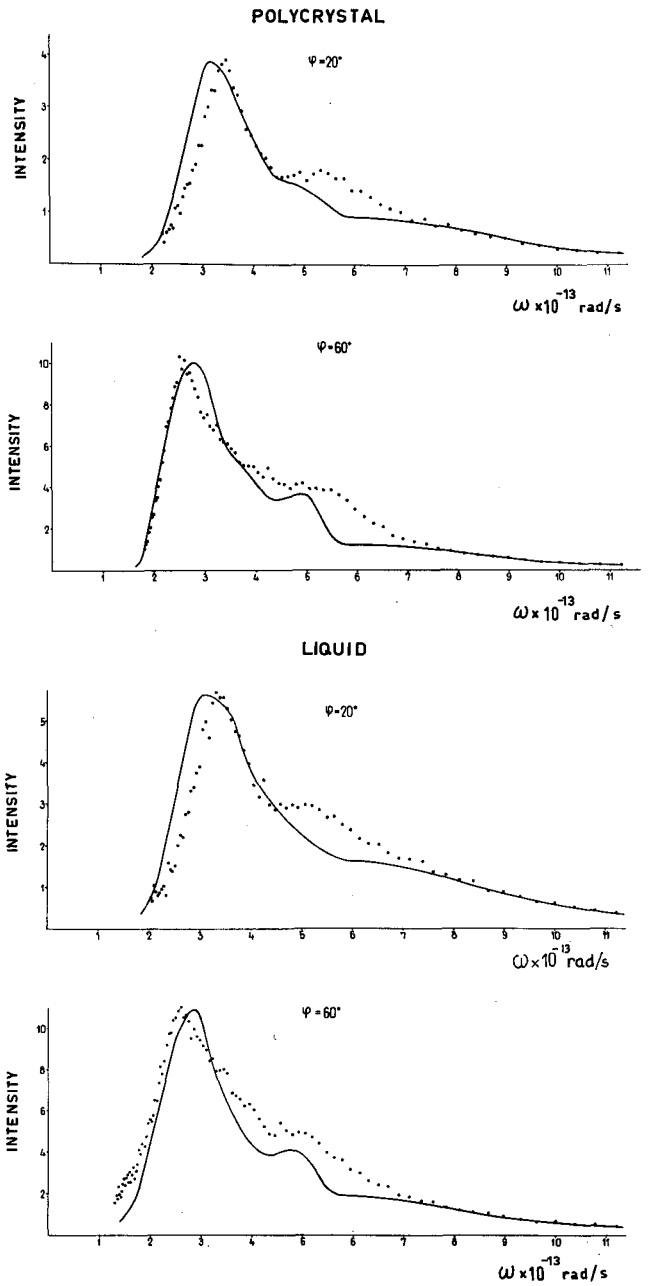

Fig. 6

Observed and calculated cross-sections for polycrystalline (630°C) and liquid (677°C) aluminium at 20° and 60° angles of observation

ment is reasonable and surprisingly good in view of the basic assumption of the harmonic approximation for the vibrational motions in the crystal.

As is also seen in Fig. 6 the overall agreement is not so good for the liquid case as for the solid. Larger discrepancies occur over the transversal part as well as at the high frequency end. A comparison with the cross-section predicted on the basis of the incoherent approximation (Eq.(12)) shows however the important fact that the observed low frequency cut-off at $\omega = 2$ or 3×10^{13} rad/s is much better reproduced by the coherent approximation (Eq.(6)) showing the existence of collective scattering in a liquid. Similarly to what is observed for the polycrystalline case the theory cannot predict the observed intensity distribution in the high frequency end of the spectrum for $4 \leq \omega \leq 7 \times 10^{13}$ rad/s. The main factor which damps the calculated intensity to low values in this frequency range is the $\cos^2 \Theta$ term in the structure factor, Z. If this factor is omitted in the calculations, which means that the effect of the polarization of the quasi-phonons is not taken into account, the predicted intensity distribution in this region is too high. Some intermediate value is better although not perfect as the predicted one-phonon distribution stops at $\omega \simeq 5 \times 10^{13}$ rad/s compared to the experimental value of $\omega \simeq 7 \times 10^{13}$ rad/s.

The conclusion of the analysis is hence that on the whole the coherent cross-section describes the observed neutron distribution relatively well both in the solid and the liquid cases and much better than does the incoherent cross-section. For the case of the liquid this means that during the short interaction times of the neutron with a nucleus (about 10^{-12} s) the rearrangements of the atoms caused by diffusion is so small that the atoms may be considered almost stationary. The neutron mainly interacts with the vibratory modes of motion, i.e. with the pseudo-phonons. As a certain local order exists among the atoms, as shown by the structure factor $1 + \gamma(\kappa)$, the condition for interference scattering is fulfilled and therefore the coherent cross-section describes the observed neutron data. It is to be stressed once more that the existence of a transversal part of the frequency spectrum for the liquid means that liquid aluminium shows a finite shear modulus. This is easily understood for the case of neutron scattering because the neutrons' interaction time is about 10^{-12} s which is exactly of the right order to observe vibratory modes having frequencies in the range 10^{12}- 10^{13} c/s. Obviously the relaxation time τ for diffusion is at least of the order of 10^{-12} s in the liquid, because otherwise the vibratory motions would not exist.

It is to be noted that the results just described also mean that in general it is not allowed to derive a frequency spectrum from an observed inelastically scattered one-phonon spectrum, using the incoherent approximation which describes only the self-motion of one particle, ignoring collective effects, when the scattering nucleus has a considerable coherent scattering length. Such a procedure would give a $f(\omega)$ that might be radically distorted by the effect of the structure factor. This statement holds true for the solid and liquid phases.

The implication of this result is that the momentum rule $\vec{k} - \vec{k}_0 = \vec{q} + 2\pi\vec{\tau}$ is valid for the liquid as well as for the solid. As $\hbar\vec{\tau}$ may be considered as the recoil momentum taken up by the whole lattice in the case of a perfect crystal, it would in the liquid case be equivalent to the recoil taken up by a group of atoms. From the present observation it is not possible to deter-

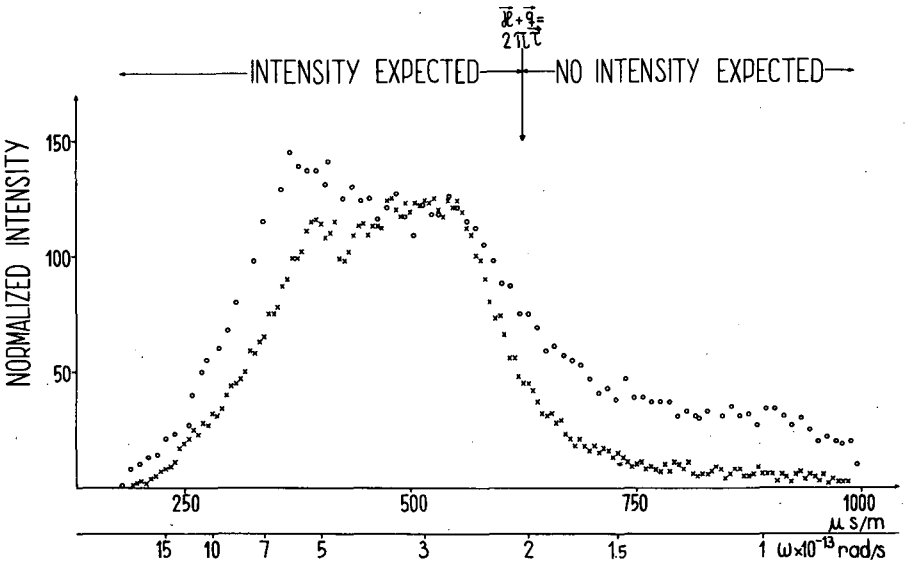

Fig. 7

Thick (o) and thin (x) sample observation on liquid aluminium
The thick sample observation is arbitrarily normalized to the thin sample observation at $\omega = 3$.
The data is given in time-of-flight scale as well as in energy scale

mine the size of the group. The size of this group would be determined by a correlation length or a mean free path of the phonons in the medium. The size of this correlation length would be of the order of a few interatomic distances. Also this size would decrease with temperature as shown by the fact that the liquid structure factor $1 + \gamma(\kappa)$ is smeared out at higher temperatures.

In performing scattering experiments of this kind the multiple scattering of the sample might be of outstanding importance. In an older series of experiments [9] the scattering from a single crystal of large dimensions was investigated. This crystal had a diameter of 6.5 cm and a length of 12 cm. At the end of the single-phonon study this crystal was melted and the neutron spectrum scattered from liquid aluminium was investigated at various angles of scattering. This liquid sample had a transmission for thermal neutrons of about 60%. In the present investigation the liquid sample had a transmission of 86%. The old observation with the thick sample was performed at 50° angle of observation and may be compared to the present thin sample observation at 60° angle of observation (Fig. 7). A striking difference is the high intensity observed at small energy transfers in the thick sample case beyond the "crystalline" cut-off at $2\pi\tau = \kappa + q$. As a matter of fact, if a thick sample is used one may erroneously draw the conclusion that there is no sharp low energy cut-off in the liquid case. Such a conclusion is, however, altogether false. Another difference between the thick and thin sample observation is the secondary peak growing up at neutron energies round $\omega = 5$ or 6×10^{13} rad/s as seen in Fig. 7. This extra peak corresponds to the start of a building up of a Maxwellian equilibrium spectrum. On the whole this

comparison shows that the multiple scattering causes a considerable smearing out of the true single scattering distribution. Samples ought to have about 90% transmission to be reasonably thin.

V. COMPARISON TO OTHER MEASUREMENTS

Very few other neutron scattering studies have been performed on liquid metals which gave results of the kind discussed in the present work. There are, however, to our knowledge two neutron scattering studies, which partly aim at a result similar to that we have obtained. The first one is the work of COCKING and GUNER [7] on liquid tin and by COCKING [19] on liquid sodium. Of these two liquids the sodium has about equal coherent and incoherent cross-sections, namely $\sigma_{coh} = 1.55$ b and $\sigma_{inc} = 1.85$ b. The results obtained by scattering of cold neutrons from sodium will therefore show a very involved nature. From the results it seems that the observed inelastic neutron distribution is relatively well described by the incoherent cross-section. This is understandable when one remembers firstly that sodium scatters incoherently to about 55% and secondly that the difference between the predictions of the coherent and incoherent formulas is not too big. The effect of a structure factor Z would in the case of sodium be rather small and difficult to observe.

Concerning the results on liquid tin the conclusions are different as expected, because it is an almost 100% coherent scatterer. The results obtained on liquid tin with 6.25-Å neutrons and scatter angles between 20° and 90° are reasonably similar to those we have found in aluminium. Cocking and Guner did observe a sharp low energy cut-off in polycrystalline tin at 210°C as expected but did not see the sharp cut-off in liquid tin at 240°C. We believe, however, that there are two reasons why such a cut-off was not seen in this case, namely:

(a) The Debye temperature of liquid tin at 240°C is probably of the order of 160°K. The temperature of the sample is more than three times this value. Therefore the multiphonon term is at least as important as in our case in order to produce extra intensity at the position of the expected cut-off at $\vec{\kappa} + \vec{q} = 2\pi\vec{\tau}$.

(b) As the diameter of the cylindrical sample was 3.75 cm and the scattering cross-section is 4.6 b the transmission of the sample for the once-scattered neutrons will be in the range between 54% and 100%, on the average about 70%. As illustrated in our Fig. 7 the multiple scattering effect under such circumstances is very important for creating intensity just at small energy transfers below the cut-off at $\vec{\kappa} + \vec{q} = 2\pi\vec{\tau}$.

We therefore believe that, if the scattering experiments on liquid tin were corrected for these effects, they would agree with our present results.

We have recently been informed that new measurements on liquid lead have been performed by Cocking (see Ref. [20]) in the form of thin samples, where the effects discussed above on aluminium have been clearly brought out. In this case ingoing neutrons with an energy of 2.2 meV were used.

The second work, of the same kind as the present one, was performed by COTTER [21]. He observed the cold neutron spectrum scattered at a 90° angle from liquid lead at 335°C. The result was a spectrum showing an

inelastically as well as a quasi-elastically scattered spectrum. A quasi-elastically scattered spectrum is expected at this angle of observation in liquid lead because the liquid structure factor, $1 + \gamma(\kappa)$, has a high value for κ in the range of 2 $Å^{-1}$. Cotter subtracted from his observed inelastically scattered spectrum a multiphonon term which he fitted to his observed spectrum on a basis similar to the one we have used in this work. In agreement with our observation he found a broad peak in the inelastic spectrum, which he, however, interpreted as a strongly broadened single-phonon peak. We have performed a study of both single-phonon peaks in a monocrystal and of the integrated single-phonon peaks in a polycrystal and in the liquid phase at nearly the same high temperatures. The result of this study is given in Fig. 7. The monocrystal was oriented in such a way that no single-phonon peak occurred in the energy region around the peak of the multiphonon spectrum, which is thus seen very clearly. It is seen that in the polycrystal as well as in the melted single crystal, i.e. in the liquid phase, the characteristic single-phonon peak has disappeared and instead a broad spectrum corresponding to an integration over all the single phonon peaks is observed. This shows that no single phonons may be observed in the liquid but merely the effect of the frequency spectrum, i.e. the frequency spectrum modified by a structure factor as explained above. We therefore believe that Cotter's interpretation of his liquid lead data is false. What was observed in the lead experiment by Cotter was simply the same type of intensity distribution as was observed by us in the present experiment and by Cocking and Guner for liquid tin. Lead is on the whole much more difficult to study with 4-Å cold neutrons than aluminium because the expected energy changes are so small. The reason for this is the very low Debye temperature, 96°K at room temperature. Long wavelength neutrons would be more suitable for such a study.

In conclusion it seems that the present experiment, as well as that of Cocking and Guner, shows that interference effects exist in the neutron scattering from a liquid as well as from a solid. The only difference between the solid and the liquid phases seems to be that smaller regions of atoms are responsible for the interference of the scattered neutron waves in the liquid. This is shown by the fact that when a single crystal is melted, the same neutron spectrum is scattered from the melt as from a melted polycrystal. Both of these scattered spectra show strong similarities to the spectrum observed from a polycrystal. Therefore the scattering mechanism in a liquid metal seems to be exactly analogous to that of a polycrystal. The existence of small regions of local order would create such a picture as explained above.

ACKNOWLEDGEMENTS

It is a pleasure for one of us (Jovic) to express his gratitude to the International Atomic Energy Agency in Vienna, which sponsored his stay in Sweden for ten months. His thanks are also due to the Swedish Atomic Energy Company for prolongation of his stay in Sweden for five months to participate in the completion of this work.

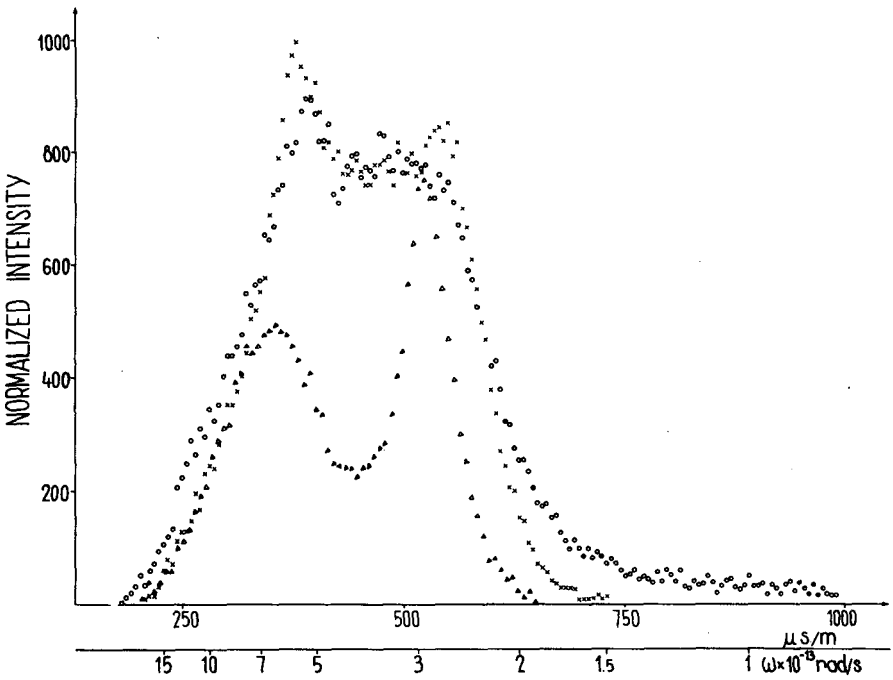

Fig. 8

Time-of-flight spectra of cold neutrons scattered from a single crystal at 650°C (Δ), from a polycrystal at 630°C (x) and from liquid aluminium at 677°C (o)

REFERENCES

[1] INTERNATIONAL ATOMIC ENERGY AGENCY, Inelastic Scattering of Neutrons in Solids and Liquids, IAEA, Vienna (1961) 651 pp.

[2] INTERNATIONAL ATOMIC ENERGY AGENCY, Inelastic Scattering of Neutrons in Solids and Liquids I and II IAEA, Vienna (1963).

[3] BROCKHOUSE, B. N., Nuovo Cim. 9 (Suppl.) Serie X (1958) 45;
BROCKHOUSE, B. N., Phys. Rev. Lett. 2 (1959) 287;
SAKAMOTO, M., BROCKHOUSE, B. N. JOHNSON, R. H. and POPE, N. K., Proc. Conf. on Magnetism and Neutron Diffraction (Kyoto, Sept. 1961).

[4] HUGHES, D. J. PALEVSKY, H., KLEY, W. and TUNKELO, W., Phys. Rev. 119 (1960) 872.

[5] LARSSON, K.-E. HOLMRYD, S. and OTNES, K., Inelastic Scattering of Neutrons in Solids and Liquids, IAEA, Vienna (1961) 329-41;
LARSSON, K.-E. and DAHLBORG, U., Reactor Sci. Techn. 16 (1962) 81;
LARSSON, K.-E. and DAHLBORG, U., Physica (in press, 1964).

[6] BROCKHOUSE, B. N. and POPE, N. K., Phys. Rev. Lett. 2 (1959) 287.

[7] COCKING, S. J. and GUNER, Z., Inelastic Scattering of Neutrons in Solids and Liquids I IAEA, Vienna (1962) 237-48.

[8] SQUIRES, G. L., Phys. Rev. 103 2 (1956) 304;
WALKER, C. B., Phys. Rev. 103 (1956) 547.

[9] LARSSON, K.-E., DAHLBORG, U. and HOLMRYD, S., Ark. Fys. 17 (1960) 369.

[10] WEINSTOCK, R., Phys. Rev. 65 (1944) 1.

[11] EGELSTAFE, P. A., *AERE Rpt. N/R 1164 (1953).*
[12] VINEYARD, G. H., Phys. Rev. 110 (1958) 999.
[13] KROÓ, N., BORGONOVI, G., SKÖLD, K. and LARSSON, K.-E., Inelastic scattering of cold neutrons by condensed argon, unpublished report; summary of the report, Phys. Rev. Lett. 12 (1964) 721-22.
[14] EGELSTAFF, P. A., Inelastic Scattering of Neutrons in Solids and Liquids I IAEA, Vienna (1963) 203-12.
[15] EGELSTAFF, P. A., AERE Rpt R4101 (1962).
[16] BROCKHOUSE, B. N., BERGSMA, I., DASANNACHARYA, B. A. and POPE, N. K., Inelastic Scattering of Neutrons in Solids and Liquids I IAEA, Vienna (1963) 189-201.
[17] SJÖLANDER, A., Ark. Fys. 17 (1958) 315.
[18] LARSSON, K.-E. DAHLBORG, U., HOLMRYD, S., OTNES, K. and STEDMAN, R., Ark. Fys. 16 (1959) 199.
[19] COCKING, S. I., Inelastic Scattering of Neutrons in Solids and Liquids I IAEA, Vienna (1963) 227-48.
[20] EGELSTAFF, P. A., private communication (1964).
[21] COTTER, M. I. Inelastic scattering of cold neutrons by solid and liquid lead, Doctor's dissertation at Forham University, N. Y. (1962).

THE VAN HOVE SCATTERING FUNCTION FOR WATER*

N. K. POPE AND R. NATION
ROYAL MILITARY COLLEGE, KINGSTON, ONTARIO, CANADA

Abstract — Résumé — Аннотация — Resumen

THE VAN HOVE SCATTERING FUNCTION FOR WATER. Measurements, using the Chalk River rotating crystal spectrometer at a resolution of 2×10^{-4} eV, of the energy distributions of neutrons scattered by water at 25 and 75°C have been reported previously. From the results the Van Hove scattering function, $S(Q, \epsilon)$, was formed for wave vector transfers in the range $0.4 \leq Q \leq 2.0$ Å^{-1} at 75°C and $0.4 \leq Q \leq 2.6$ Å^{-1} at 25°C. Since, for the smaller values of Q used, the energy distributions for fixed Q show quasi-elastic peaks of widths much less than the resolution of the spectrometer, the results were analysed without constructing a scattering function which had been corrected for resolution.

The previously reported $S(Q, \epsilon)$ have now been corrected for resolution. The correction has been carried out by assuming that $S(Q, \epsilon)$ can be represented by the quotient of a slowly varying function of ϵ and a Lorentz function. It is found that in the region of the quasi-elastic peak $S(Q, \epsilon)$ can be represented by the Lorentzian form $AW/(\epsilon^2 + W^2)$ where A is slightly Q-dependent and W deviates only slightly from the value DQ^2. D is a constant having values in good agreement with the values of the diffusion constant of water measured at the appropriate temperature.

The resolution-corrected $S(Q, \epsilon)$ have been used to construct the frequency spectra of the velocity autocorrelation function. No evidence has been found for a dip near the origin caused by a partial separation of diffusive modes of motion from other types of modes.

FONCTION DE DIFFUSION DE VAN HOVE POUR L'EAU. La distribution énergétique des neutrons diffusés par l'eau à 25 et 75°C avait été mesurée au moyen du spectromètre à cristal tournant de Chalk River ayant un pouvoir de résolution de $2 \cdot 10^{-4}$ eV; les résultats obtenus avaient déjà fait l'objet d'un article de revue. En partant de ces résultats, on avait déterminé la fonction de diffusion de Van Hove $S(Q, \epsilon)$ pour les transferts de vecteurs d'onde dans la gamme $0,4 \leq Q \leq 2,0$ Å^{-1} à 75°C et dans la gamme $0,4 \leq Q \leq 2,6$ Å^{-1} à 25°C. Etant donné que pour les faibles valeurs fixes de Q, la distribution énergétique présente des pics quasi élastiques de largeur très inférieure au pouvoir de résolution du spectromètre, on avait analysé les résultats sans établir de fonction de diffusion préalablement corrigée pour tenir compte du pouvoir de résolution.

La fonction $S(Q, \epsilon)$ indiquée dans cet article a fait maintenant l'objet d'une telle correction. A cette fin, les auteurs ont supposé que $S(Q, \epsilon)$ peut être représenté par le quotient d'une fonction à variations lentes de ϵ et d'une fonction de Lorentz. Ils ont constaté que dans la région du pic quasi élastique, $S(Q, \epsilon)$ peut être exprimé par la forme lorentzienne $AW/(\epsilon^2 + W^2)$ dans laquelle A dépend faiblement de Q, et W ne s'écarte que légèrement de la valeur DQ^2. D est une constante dont les valeurs concordent assez bien avec celles de la constante de diffusion de l'eau, mesurée à la température voulue.

La fonction $S(Q, \epsilon)$, corrigée pour tenir compte du pouvoir de résolution, a servi à établir les spectres de fréquence de la fonction d'autocorrélation de vitesse. Rien n'a permis de conclure à l'existence, au voisinage de l'origine, d'une dépression qui serait due à une séparation partielle entre les modes de mouvement de diffusion et les autres modes.

ФУНКЦИИ РАССЕЯНИЯ ВАН ГОВЕ ДЛЯ ВОДЫ. Об измерениях распределения энергии нейтронов, рассеянных на воде при температуре 25°C и 75°C, выполненных с помощью спектрометра с вращающимся кристаллом с разрешающей способностью $2 \cdot 10^{-4}$ эв в Чок-Ривер, сообщалось ранее. По результатам этих измерений была выведена функция рассеяния Ван Гове $S(Q, \epsilon)$ для перемещений волнового вектора в диапазоне $0,4 \leqslant Q \leqslant 2,0$ Å^{-1} при температуре 75 °C и в диапазоне $0,4 \leqslant Q \leqslant 2,6$ Å^{-1} при температуре 25°C. Поскольку при меньших взятых значениях Q распределение энергии для установленного Q дает квазиупругие пики с шириной,

* The research for this paper was supported (in part) by the Defence Research Board of Canada, Grant Number 9510-30.

которая значительно меньше разрешающей способности спектрометра, результаты анализировались без составления функции рассеяния, которая была исправлена для разрешающей способности.

Функция $S(Q,\epsilon)$, о которой сообщалось ранее, исправлена для разрешающей способности. Исправление производилось в предположении, что $S(Q,\epsilon)$ может быть представлена в виде отношения медленно изменяющейся функции ϵ и функции Лоренца. Исправленная для разрешающей способности функция $S(Q,\epsilon)$ использовалась для составления спектров автокорреляционной функции скорости. Установлено, что в области квазиупругого пика $S(Q,\epsilon)$ может быть представлена в форме Лоренца $Aw/\epsilon^2+w^2)$, где A – в незначительной степени зависит от Q, а w – только незначительно отклоняется от значения DQ^2. D – постоянная со значениями, хорошо согласующимися со значениями постоянной диффузии для воды, измеренными при соответствующей температуре.

Исправленная разрешающая $S(Q,\epsilon)$ использована для построения спектра автокорреляционной функции скорости. Не было обнаружено признаков провала кривой вблизи начала координат, обусловленного частичным отделением диффузионных видов движения от других видов.

LA FUNCIÓN DE DISPERSIÓN DE VAN HOVE CORRESPONDIENTE AL AGUA. Ya se conocen los resultados de las mediciones de la distribución energética de los neutrones dispersos por agua a 25°C y 75°C, efectuadas con el espectrómetro de cristal giratorio de Chalk River, quyo poder de resolución es de $2 \cdot 10^{-3}$ eV. Basándose en los resultados de esas mediciones se determinó la función de dispersión de Van Hove, $S(Q,\epsilon)$, correspondiente a transferencias de los vectores de onda en el intervalo $0{,}4 \leq Q \leq 2{,}0$ Å^{-1} a 75°C, y $0{,}4 \leq Q \leq 2{,}6$ Å^{-1} a 25°C. Dado que para los valores inferiores de Q utilizados, las distribuciones energéticas de Q constante presentan picos cuasielásticos de amplitud mucho menor que el poder de resolución del espectrómetro, los resultados se analizaron sin establecer una función de distribución corregida para tener en cuenta el poder resolutivo.

La función $S(Q,\epsilon)$ anteriormente dada a conocer ha sido objeto de una corrección de esa índole. A tal efecto, se ha supuesto que $S(Q,\epsilon)$ puede representarse por el cociente de una función de variación lenta de ϵ y de una función de Lorentz. Se comprueba que, en la región del pico cuasielástico, $S(Q,\epsilon)$ puede representarse por la forma lorentziana $AW/(\epsilon^2 + W^2)$, en la que A depende ligeramente de Q, y W sólo difiere poco del valor DQ^2; D es una constante cuyos valores concuerdan satisfactoriamente con los de la constante de difusión del agua medidos a la temperatura apropiada.

La función $S(Q,\epsilon)$, corregida en cuanto al poder resolutivo, se ha utilizado para establecer el espectro de frecuencias de la función de autocorrelación de la velocidad. En las proximidades del origen no se han observado indicios de inflexión debida a separación parcial entre los modos difusivos de movimiento y otros tipos de modos.

1. INTRODUCTION

The interpretation of thermal neutron scattering experiments on liquids is now carried out, almost universally, using the Van Hove formalism [1]. In this formalism, the partial differential scattering cross-section for the incoherent scattering of neutrons by an isotropic sample can be expressed in terms of the incoherent scattering function $S(Q,\epsilon)$* in the following way:

$$\frac{d^2\sigma}{d\Omega d\epsilon} = \frac{k'}{k_0} a_{inc}^2 S(Q,\epsilon). \tag{1.1}$$

This is the cross-section per atom of a monatomic system for the scattering of a neutron into a solid angle $d\Omega$ with wave vector transfer

$$\vec{Q} = \vec{k}_0 - \vec{k}' \tag{1.2}$$

* The Van Hove scattering function is usually considered to be a function of $\omega = \epsilon/\hbar$, say $s(Q,\omega)$ where $s(Q,\omega)d\omega = S(Q,\epsilon)d\epsilon$.

and energy transfer

$$\epsilon = E_0 - E', \tag{1.3}$$

where $\vec{k}_0$ and $\vec{k}'$ are the wave vectors of the incident and scattered neutrons, respectively, and E_0 and E' their respective energies. For an isotropic scatterer, the Van Hove space-time self-correlation function $G(r, t)$ [1] can be related to the scattering function by means of the so-called intermediate scattering function $i(Q, t)$ in the following way

$$i(Q, t) = \int_{\epsilon=-\infty}^{\epsilon=\infty} S(Q, \epsilon)\exp(i\epsilon t)\hbar)d\epsilon \tag{1.4}$$

and

$$G(r, t) = \frac{1}{2\pi^2} \int_{Q=0}^{Q=\infty} i(Q, t) \frac{\sin Qr}{Qr} Q^2 dQ. \tag{1.5}$$

$G(r, t)$ is, in general, complex. However, in the classical domain it is real and has a simple intuitive interpretation, namely, given a particle at the origin at time zero, $G(r, t)$ gives the probability of finding that particle at a distance r at a later time t. Thus, in principle, from measurements of the partial differential cross-section one can construct first the scattering function, then the intermediate scattering function and finally the self-correlation function. Unfortunately, it does not seem possible to find a monatomic liquid which scatters neutrons incoherently and is also easily handled. Water has therefore been studied extensively because most of the scattering is incoherent and it is easy to obtain good samples. However, the incoherent scattering is produced by protons in the water molecules, and analysis of the scattering leads in the first instance to information about the motion of these protons. It is hoped, nevertheless, to be able to deduce information about the centre-of-mass motion of the molecules.

The first experiments on water were carried out by BROCKHOUSE [2]. This work showed that the scattering contained a quasi-elastic component whose width is related to the diffusion of the atoms in the liquid. In a second series of experiments BROCKHOUSE [3] showed that although the width as a function of the temperature is a little smaller than the experimental coefficient of self-diffusion for water, it varies in a similar manner. A theoretical interpretation of these facts was given on the basis of the specific nature of the diffusive motions. A little later it was proposed by other workers, first by HUGHES et al. [4] at Brookhaven, that the quasi-elastic peak is not broadened, but split.

More recently, work has been carried out on water at 25 and 75°C by SAKAMOTO et al. [5] using the Chalk River rotating-crystal time-of-flight spectrometer with a slightly better resolution than that used by HUGHES et al. [4] (approximately 2×10^{-4} eV) and no evidence was found for the splitting of the quasi-elastic peak.

This data was used by POPE et al. [6] (see also BROCKHOUSE et al. [7]) to calculate the intermediate scattering function and the space-time self-correlation function of the protons in water. In these calculations the resolution correction for energy broadening was applied to the intermediate scattering function on account of the difficulty of applying the correction to the measured scattering function itself.

There are both practical and theoretical reasons for wishing to apply this resolution correction to the scattering function directly. In order to construct scattering functions for large ranges of the energy transfer ϵ, it is often necessary to combine series of measurements for fixed Q which have been broadened by different resolution functions. Theoretically, it is interesting to know the width of the quasi-elastic peak as a function of the magnitude of the wave vector transfer $\vec{Q}$ and the temperature in order to relate this broadening to the diffusive motions of the scattering atoms. Further, provided the scattering function has been corrected for resolution broadening, for those liquids which can be treated in the Gaussian approximation, it is possible to calculate the frequency spectrum of the velocity auto-correlation function, even for small energy transfers, by the method proposed by EGELSTAFF [8]. For these reasons, this paper is primarily concerned with the construction of a scattering function for water (corrected for energy resolution) from a measured scattering function and a measured resolution function. From the result, the width of the quasi-elastic peak is determined as a function of Q and the frequency distribution of the velocity correlation function is calculated. Previous determinations of the frequency spectra of water have been made by Egelstaff and collaborators and also by Larsson and collaborators. The present results, however, include a detailed investigation of the frequency spectra in the region corresponding to energy transfers of less than 10^{-3} eV.

2. THE RESOLUTION-CORRECTED SCATTERING FUNCTION FOR WATER

The calculations described in this paper are based on measurements of the scattering function for water and the corresponding energy resolution functions reported by SAKAMOTO et al. [5]. In this experiment the wavelength of the incident neutrons was 4.059 Å and about twenty wavelength distributions were taken at each temperature at angles of scattering ranging from 15° to 114° at 25°C and from 15° to 93° at 75°C. After applying corrections for backgrounds, removal of frame overlap and corrections for counter efficiency, the twenty measured distributions at each temperature were used to form a grid of values of the scattering function which is plotted in Fig. 1 for the available values of $\epsilon > -1.3\times10^{-3}$ eV. The grid points were taken at intervals in Q of 0.2 $Å^{-1}$ and in ϵ of 0.5×10^{-4} eV. In the region of energy transfers for which $\epsilon < -1.3\times10^{-3}$ eV the scattering function was approximated by the function $B(\epsilon)Q^2 + C(\epsilon)Q^4$. A Q-independent term $A(\epsilon)$ was interpreted as multiple scattering and discarded. The quasi-elastic peaks shown in Fig. 1 are broadened by resolution in ϵ. The resolution in ϵ for each Q was obtained from a series of measured distributions of the elastic

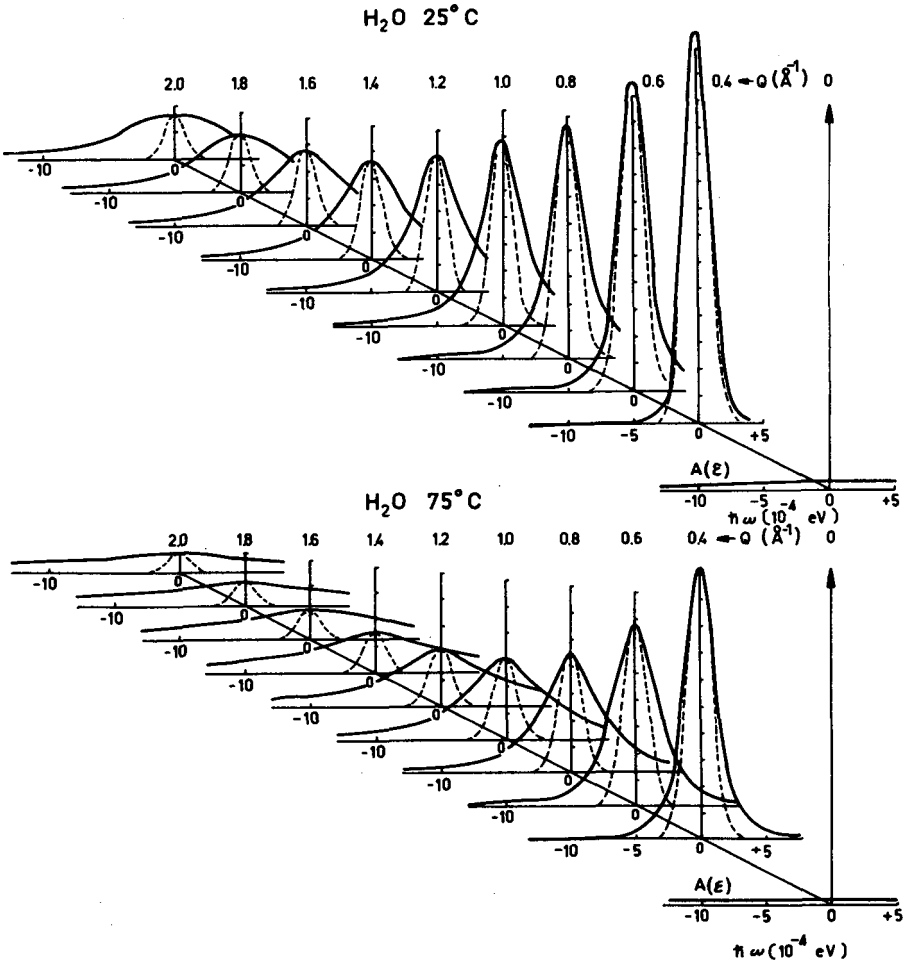

Fig. 1

The scattering function $S(Q, \epsilon)$ at small energy transfer for water at 25 and 75°C (SAKAMOTO et al. [5])
The resolution functions are shown as broken line curves.
The multiple scattering $A(\epsilon)$ which was subtracted is also shown.

incoherent scattering by vanadium metal and is shown in Fig. 1 by the broken lines.

From Fig. 1 it is seen that for small Q the widths of the energy distributions become comparable to the widths of the measured resolution functions. Under these conditions it becomes very difficult to apply resolution corrections. If $S'(Q, \epsilon)$ denotes energy distributions which have not been corrected for resolution and $R(Q, \epsilon)$ the resolution function, then $S(Q, \epsilon)$, the resolution-corrected scattering function, satisfies the equation

$$S'(Q, \epsilon) = \int_{-\infty}^{\infty} S(Q, \epsilon - \epsilon')R(Q, \epsilon')d\epsilon' \qquad (2.1)$$

If $S'(Q, \epsilon)$ and $R(Q, \epsilon)$ are suitably behaved functions defined on the infinite range $-\infty < \epsilon < \infty$, then the integral equation can be solved by the method of Fourier transforms for $S(Q, \epsilon)$. However, even under these conditions the solution for $S(Q, \epsilon)$ is not unique: for, any function which gives zero when folded with $R(Q, \epsilon)$ can be added to $S(Q, \epsilon)$ and the resulting function will also be a solution of the equation. In the present case, $S'(Q, \epsilon)$ has been measured over only part of the range of ϵ. Further, even over the range for which measurements are available the values of $S(Q, \epsilon)$ are not exact because of experimental error. Small errors in $S'(Q, \epsilon)$ can give rise to large errors in $S(Q, \epsilon)$ when the width of $R(Q, \epsilon)$ becomes very small. The basic philosophy adopted in the analysis has been to assume that no peaks or oscillations should occur in $S(Q, \epsilon)$ unless there is visible evidence for them in the uncorrected scattering function.

During the past few years, a number of unsuccessful attempts have been made to remove the resolution from the scattering functions shown in Fig. 1. These have all failed in that the corrected scattering functions contained fluctuations which were obviously spurious. These fluctuations arose probably because too much emphasis was placed on obtaining an exact representation of the measured scattering function and not enough attention was given to seeing that this lead to a proper form for the corrected scattering function.

In this paper, for the series of equally spaced values of Q, values of $S'(Q, \epsilon)$ at the equally spaced values of ϵ were used to find values of $S(Q, \epsilon)$. Values of $R(Q, \epsilon)$ were taken for the same values of Q and at the same spacings in ϵ. The increment in ϵ, 0.5×10^{-4} eV, is large compared to the width of the resolved peaks for small Q. Thus, it is not adequate to try to represent $S(Q, \epsilon)$ by a series of parabolas drawn through sets of three adjacent points and then to evaluate the integral in Eq. (2.1) by Simpson's rule. In the limit of small Q it is expected that $S(Q, \epsilon)$ should be inversely proportional to $\epsilon^2 + w^2$ where $w \to \hbar D Q^2$. It was, therefore, assumed that $S(Q, \epsilon)$ could be represented by $A(Q, \epsilon)/[(\epsilon - c)^2 + w^2]$ where $A(Q, \epsilon)$ is a slowing varying function of ϵ which can adequately be represented by a series of parabolas and c, also a function of Q, is a parameter to allow for the fact that the curves of $S'(Q, \epsilon)$ may be slightly off-centre. It was decided to find values of $A(Q, \epsilon)$ and hence $S(Q, \epsilon)$ for the values of Q and ϵ for which values of $S'(Q, \epsilon)$ were given. These values of $A(Q, \epsilon)$ were to be regarded as unknown parameters which are to be found by solving Eq. (2.1) for fixed Q with the assumption that the function $A(Q, \epsilon)$ can be represented by a series of parabolas joining each adjacent set of three points. After some rather simple but tedious analysis, Eq. (2.1) can be approximated by the set of linear equations

$$S'_n = \sum_m R_{n,m} A_{n+m-8} \qquad (2.2)$$

Here it is assumed that the values of ϵ used are numbered consecutively from some minimum value to the maximum value. S'_n and A_n are the values of $S'(Q, \epsilon)$ and $A(Q, \epsilon)$ for the n-th value of ϵ; the explicit Q-dependence is dropped. The factor 8 in the subscript of A_{n+m-8} arises because it has

been assumed that $R(Q, \epsilon)$ is represented by parabolas drawn through fifteen values R_n of $R(Q, \epsilon)$ and R_8 is the central value of the resolution function. Each $R_{n,m}$ is a constant times R_{16-m}, and the constant is a function of w, c, n, m and the spacing between adjacent points on the energy scale. The derivation of the expression for $R_{n,m}$ is given in the Appendix.

The problem is now reduced to solving a set of linear equations for the A_n. However, if r-values of S'_n are used the resulting r-equations contain r + 14 values of A_n. In order to solve these equations it is necessary to assume values for 14 of the A_n, seven corresponding to the lowest seven values of n and seven corresponding to the highest seven values of n. A solution of these equations was made in only one case, that for the cold water sample with $Q = 1$ Å^{-1}. The resulting values of $S(Q, \epsilon)$, S_n, are plotted

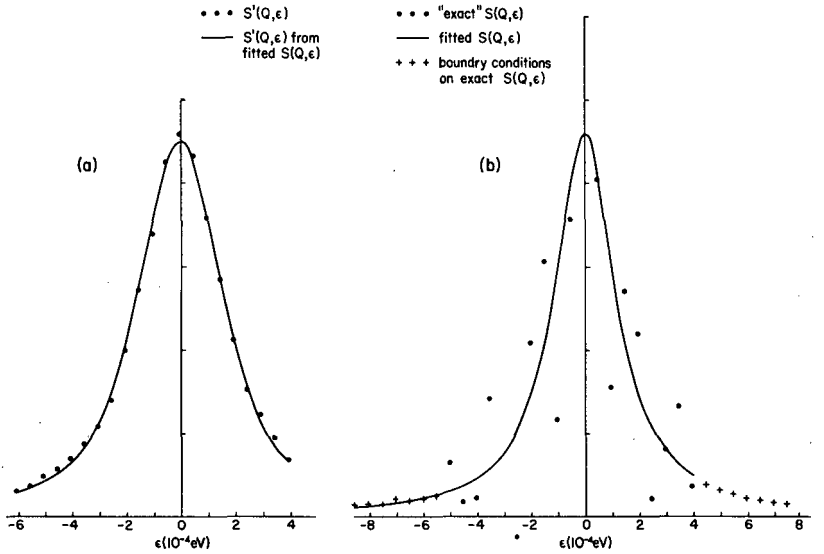

Fig. 2

(a) Measured scattering functions for water at T = 25°C for Q = 1 Å^{-1}.
The solid circles are the data of SAKAMOTO et al. [5].
The curve is calculated by assuming that the resolution-corrected scattering function is a Lorentz function.

(b) Resolution-corrected scattering functions.
The solid circles are obtained from the solid circles in (a).
The curve is a Lorentz function.

as solid circles in Fig. 2(b). It is seen that the values of S_n do not lie on a smooth curve and therefore are not a satisfactory solution to Eq. (2. 1). A plot of A_n as a function of ϵ showed that these points tended to lie on a straight line of almost zero slope. A straight line was, therefore, drawn through the points and a smooth set of A_n was read from the line. The resulting S_n lie on the smooth curve shown in Fig. 2(b). The corresponding S'_n lie on the smooth curve shown in Fig. 2(a). The solid circles are the original S'_n, and the two sets of S'_n are nearly equal to each other.

These considerations suggest that in order to obtain a smooth $S(Q, \epsilon)$ a simple analytic form containing a few unknown parameters should be taken for $A(Q, \epsilon)$. Best values for the parameters can then be determined so that the S'_n calculated from Eq. (2.2), using this $A(Q, \epsilon)$, are a best fit to the measured S'_n. Accordingly, it was assumed that $A(Q, \epsilon)$ could be written in the form

$$A(Q, \epsilon) = e^{\frac{1}{2}\beta\epsilon} \sum_{i=0}^{m} A_i(Q)\epsilon^{2i} \tag{2.3}$$

Here $\beta = 1/kT$; the $A_i(Q)$ are constants for given Q, and m is some small positive integer. The corresponding form for $S(Q, \epsilon)$ is given by

$$S(Q, \epsilon) = \frac{e^{\frac{1}{2}\beta\epsilon} \sum_{i=0}^{m} A_i(Q)\epsilon^{2i}}{(\epsilon - c)^2 + w(Q)^2} \tag{2.4}$$

The factor $e^{\frac{1}{2}\beta\epsilon}$ has been introduced to ensure that the expression for $S(Q, \epsilon)$ satisfies the principle of detailed balance. It is of little significance in the region of the quasi-elastic peak.

Equations (2.2) and (2.3) were used to calculate values of S'_n. It is seen that the calculated S_n are linear in the $A_i(Q)$ but non-linear in c and w. In order to avoid undue complication in the initial work the polynomial in ϵ^2 in Eqs. (2.3) and (2.4) was reduced to a constant $A_0(Q)$. Non-linear least squares fits were then carried out in order to find the best values of $A_0(Q)$, c and $w(Q)$ for each value of Q, for both samples of the water data. The values of w are plotted as functions of Q^2 in Fig. 3. A good fit to w is obtained by using the form

$$w(Q) = \hbar(DQ^2 + D'Q^4) \tag{2.5}$$

where, if a simple diffusion model is valid in the limit of small Q, D is the diffusion coefficient. The values of D obtained are 2.17×10^{-5} cm^2/s at 25°C and 6.23×10^{-5} cm^2/s at 75°C, which are to be compared with values of 2.13×10^{-5} cm^2/s and 6.27×10^{-5} cm^2/s, respectively, measured by SIMPSON and CARR [9]. $A_0(Q)$ can also be fitted quite well by a parabolic form of the type used to represent w. This result is in accordance with the general theoretical result that $S(Q, \epsilon)$ should be proportional to Q^2 for small Q.

The function $S(Q, \epsilon)$ has been plotted in Fig. 4 by drawing smooth curves through the values of S_n obtained by putting $c = 0$ and using the appropriate values of $A_0(Q)$ and $w(Q)$ in Eq. (2.4). The broken line curves, shown only for small values of Q, represent the measured scattering functions uncorrected for resolution but normalized, over the range $-0.023 < \epsilon < 0$ eV, to the same area as the corrected scattering functions $S(Q, \epsilon)$. The width at half maximum of the energy distribution for $Q = 0.4$ Å^{-1} for the 25°C sample is 1.09×10^{-5} eV, which is to be compared with a half width of the order of 1.4×10^{-4} eV for the corresponding resolution function.

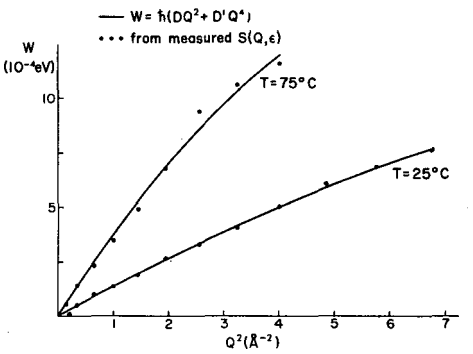

Fig. 3

The energy half-widths at half maximum of the scattering function for fixed Q plotted against Q^2. The curves shown were obtained by fitting the parameters D and D' to the data; D has the value 2.17×10^{-5} cm²/s for T = 25°C and 6.23×10^{-5} cm²/s for T = 75°C.

Figs. 5(a) and (b) give an indication of the accuracy of the analysis by comparing, for three values of Q, the data of SAKAMOTO et al. [5], shown as solid circles, with the calculated $S'(Q, \epsilon)$ obtained by using a constant $A_0(Q)$ for the polynomial in Eq. (2.3).

3. THE FREQUENCY DISTRIBUTION FUNCTION

In previous analysis of these scattering functions [6, 7] it has been shown that the intermediate scattering functions are, to a good approximation, Guassian in Q*. In this approximation it is customary to work with $f(\epsilon)$ and $g(\epsilon)$, the frequency spectra of the real and imaginary parts of the velocity auto-correlation function. It can be shown [8, 10] that

$$g(\epsilon) = \tfrac{1}{2}\beta\epsilon \coth(\tfrac{1}{2}\beta\epsilon) f(\epsilon) \tag{3.1}$$

$$f(0) = 2MD\beta/\pi\hbar \tag{3.2}$$

and

$$\lim_{Q \to 0} \epsilon^2 S(Q, \epsilon)/Q^2 = (\hbar^2/4M)\epsilon f(\epsilon)[1 + \coth(\tfrac{1}{2}\beta\epsilon)]. \tag{3.3}$$

This last relation has been used by Egelstaff and co-workers to construct the frequency spectra from the measured scattering functions by extrapolating $\epsilon^2 S(Q, \epsilon)/Q^2$ to small values of Q. The procedure has now been carried out for the water scattering functions in the regions of small energy transfers. In the region of $|\epsilon| < 13 \times 10^{-4}$ eV the scattering function was represented by

$$S(Q, \epsilon) = \frac{e^{\frac{1}{2}\beta\epsilon}[A_0(Q) + A_1(Q)\epsilon^2]}{\epsilon^2 + w^2} \tag{3.4}$$

* Here, note the small term $D'Q^4$ in Eq. (2.5).

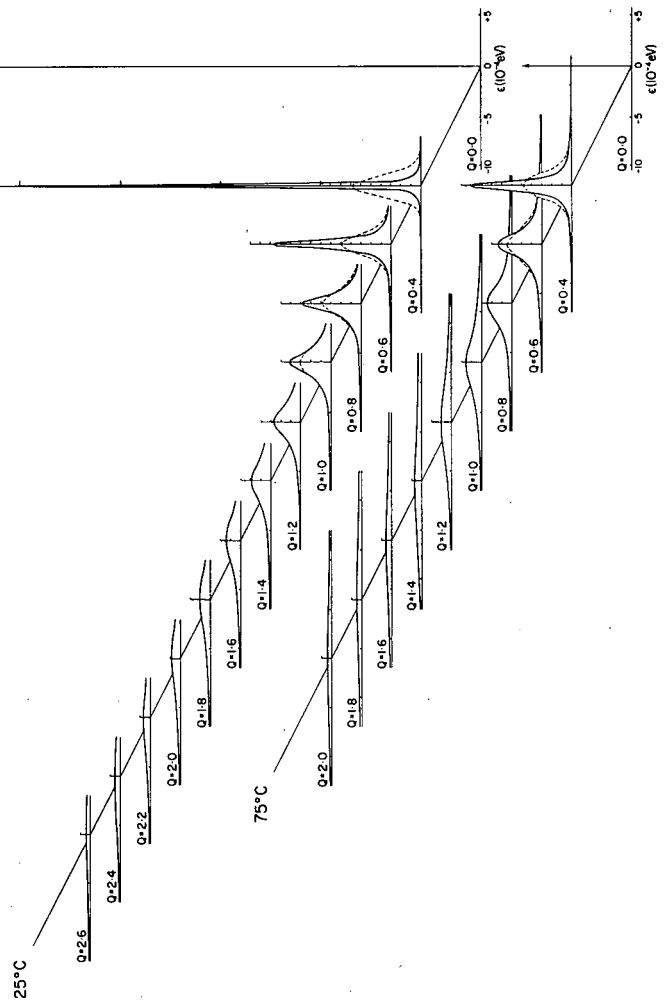

Fig. 4

The resolution-corrected scattering function at small energy transfer for water at 25 and 75°C. The broken-line curves shown for small Q represent the scattering function before the resolution-correction is applied.

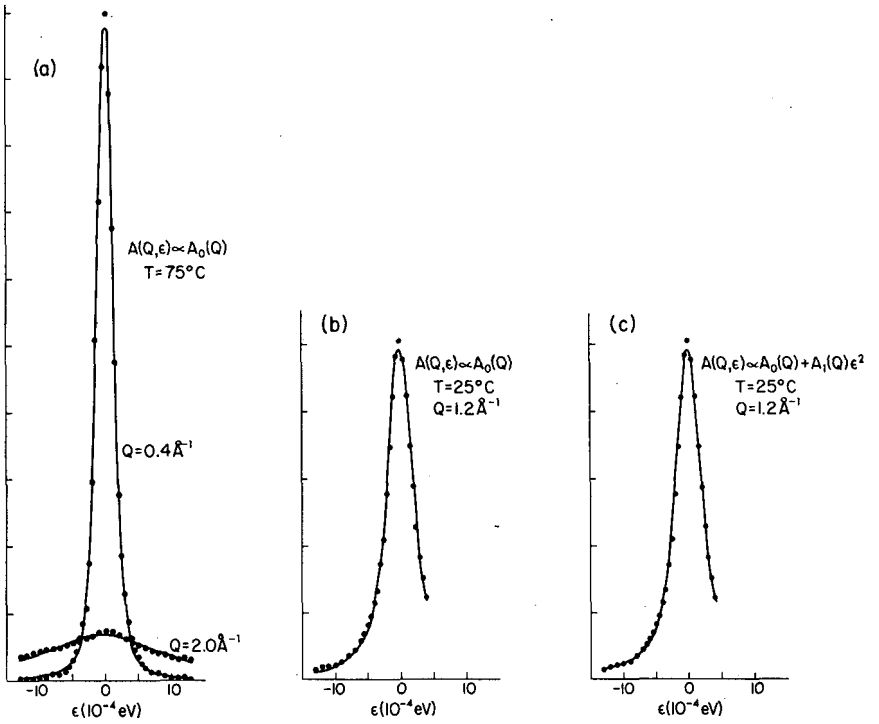

Fig. 5

Least-squares fits to the scattering function data, shown as solid circles, of SAKAMATO et al. [5]. The fits shown in (a) and (b) are calculated by assuming that the resolution-corrected scattering function is Lorentzian. (b) and (c) show the improvement in fit obtained by introducing an extra parameter $A_1(Q)$ into the representation of the scattering function.

and hence

$$\lim_{Q\to 0} \epsilon^2 S(Q, \epsilon)/Q^2 = e^{\frac{1}{2}\beta\epsilon}[B_0 + B_1\epsilon^2], \tag{3.5}$$

where

$$B_i = \lim_{Q\to 0} A_i(Q)/Q^2 \qquad i = 0 \text{ or } 1. \tag{3.6}$$

When $\epsilon < -13 \times 10^{-4}$ eV the original data of SAKAMOTO et al. [5] was corrected approximately for energy resolution broadening to give a representation of the form

$$S(Q, \epsilon) = B(\epsilon)Q^2 + C(\epsilon)Q^4 \tag{3.7}$$

and

$$\lim_{Q\to 0} \epsilon^2 S(Q, \epsilon)/Q^2 = \epsilon^2 B(\epsilon) \tag{3.8}$$

Best values for the coefficients $A_0(Q)$ and $A_1(Q)$ were determined for each value of Q at which $S'(Q, \epsilon)$ is given by using the previously determined values of c and w(Q) and carrying out linear least-squares fits. A typical

fit is shown in Fig. 5(c). The values of $A_0(Q)/Q^2$ and $A_1(Q)/Q^2$ are plotted against Q^2 in Figs. 6(a) and (b), respectively. The points of $A_0(Q)/Q^2$ at the two temperatures lie close to the straight lines shown and these straight lines have been extrapolated to zero Q^2 in order to determine the limiting value

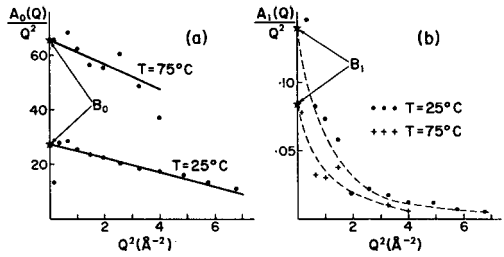

Fig. 6

Values of $1/Q^2$ times the scattering function parameters $A_0(Q)$ and $A_1(Q)$ plotted against Q^2. The limiting values B_0 of $A_0(Q)/Q^2$ are obtained by drawing straight lines through the data and extrapolating the lines to $Q^2 = 0$. The corresponding values of B_1 have been chosen to avoid discontinuities in the frequency spectra (see text).

B_0. Unfortunately, for the distributions at small Q, the data is not accurate enough to allow a precise determination of $A_1(Q)$. However it is possible to find a value of B_1 such that the two sections of the function $\lim_{Q\to 0} \epsilon^2 S(Q, \epsilon)/Q^2$ defined by Eqs. (3.5) and (3.8) join together smoothly. These values of B_1 for the two samples are shown in Fig. 6(b) and within the accuracy of the analysis they appear to lie on extrapolations of smooth curves drawn through the values of $A_1(Q)/Q^2$.

By combining the two sections, the function $\lim_{Q\to 0} \epsilon^2 S(Q, \epsilon)/Q^2$ has been constructed over the range $-0.023\ \text{eV} < \epsilon < 0\ \text{eV}$ and is plotted in Fig. 7 for the 25°C and the 75°C samples. By means of Eqs. (3.1) and (3.3) the frequency spectra have been constructed and are also shown in Fig. 7. All the curves were normalized according to Eq. (3.2) where the mass of the water molecule has been used for M.

The spectra of the 25°C sample show broad maxima in the region of 7×10^{-3} eV (60°K) and then increase steadily over the rest of the energy range shown. The same structure is not observed in the 75°C sample. RAHMAN et al. [11] have proposed an "ergodic" model for a liquid in which it would be possible for the frequency spectrum to exhibit a minimum for small values of ϵ corresponding to a partial separation of the frequency spectrum into a diffusive component and a vibrating component. No such minimum is observed.

The area under $f(\epsilon)$ for $0 < \epsilon < 0.023$ eV is 2.4 for the 25°C sample and 4.0 for the 75°C sample. As defined, the total area under $f(\epsilon)$ should be unity. The discrepancy arises no doubt from the presence of scattering associated with internal motions of the water molecules.

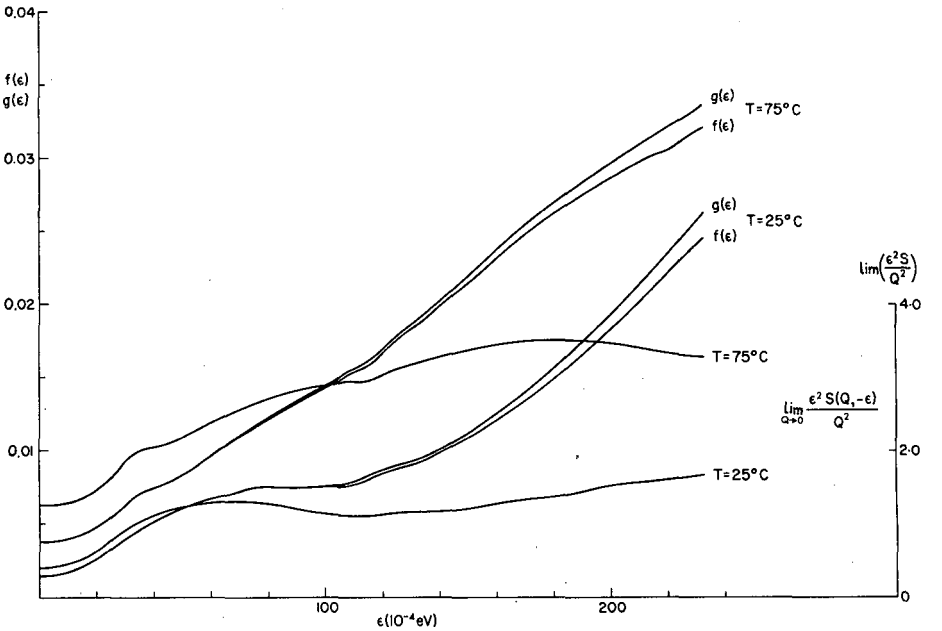

Fig. 7

The functions $\lim_{Q\to 0} \frac{\epsilon^2 S(Q-\epsilon)}{Q^2}$ and the real part $f(\epsilon)$ and the imaginary part $g(\epsilon)$ of the spectra of the velocity auto-correlation functions for water at 25 and 75°C.

$$f(0) = g(0) = 2M_{H_2O}D/\pi\kappa T\hbar$$

ACKNOWLEDGEMENTS

The authors wish to acknowledge the valuable assistance of Miss E. Baker and Miss S. Watson in numerical work.

APPENDIX

In this Appendix Eq. (2.2) is derived from Eq. (2.1). On dropping the explicit Q-dependence of the various quantities and inserting the proposed form for $S(Q, \epsilon)$ Eq. (2.1) becomes

$$S'(\epsilon) = \int_{\epsilon'=-7a}^{\epsilon'=7a} \frac{R(\epsilon')A(\epsilon-\epsilon')}{(\epsilon-\epsilon'-c)^2+w^2}\,d\epsilon'$$

In this equation, $a = 0.5\times10^{-4}$ eV is the spacing between the values of ϵ at which values of $S'(\epsilon)$, the measured scattering function, and $R(\epsilon)$, the mea-

sured values of the resolution function, are given. The quantities $A(\epsilon)$ and w are defined in the text. New variables X, X', C and W are introduced by the substitutions

$$\epsilon = a(X - X_0); \qquad \epsilon' = a(X' - 8)$$

$$c = aC; \qquad w = aW$$

Then if $-(X_0 - 1)a$ is the first value of ϵ used in $S'(\epsilon)$, $S(\epsilon)$ and $A(\epsilon)$, then the set of values of X corresponding to the set of values of ϵ used are the integers 1, 2, 3, 4, ... In the same way the set of values of X' corresponding to the set of values of ϵ' at which $R(\epsilon')$ is given, are the integers from 1 to 15 inclusive. In what follows when X or X' take on integral values, from 1 to 15 inclusive. In what follows when X or X' take on integral values, say n or m, the values of the corresponding functions will be denoted by a suffix notation, thus $S'[a(n - X_0)] = S'_n$ and $R[a(m - 8)] = R_m$. With these substitutions one has

$$S'_n = \frac{1}{a} \int_{X'=1}^{X'=15} \frac{R[a(X' - 8)]A[a(n - X_0 - X' + 8)]}{(n - X_0 - X' + 8 - C)^2 + W^2} dX'. \qquad (A.1)$$

In order to evaluate the integral, the range of integration of X' is broken up into seven segments 1-3, 3-5, ..., 13-15 and on each segment the numerator of the integrand is represented by the parabola passing through the values of the numerator at the end and mid-points of each segment, i.e. it is assumed that

$$R[a(X' - 8)]A[a(n - X_0 - X' + 8)] = \alpha_{s,n} X'^2 + \beta_{s,n} X' + \gamma_{s,n}; \quad s = 1, 2, \ldots, 7.$$

The coefficients $\alpha_{s,n}$, $\beta_{s,n}$, $\gamma_{s,n}$ are given by

$$2\alpha_{s,n} = R_{2s+1} A_{n-2s+7} - 2R_{2s} A_{n-2s+8} + R_{2s-1} A_{n-2s+9}$$

$$2\beta_{s,n} = (1 - 4s)R_{2s+1} A_{n-2s+7} + 8sR_{2s} A_{n-2s+8} - (1 + 4s)R_{2s-1} A_{n-2s+9}$$

$$\gamma_{s,n} = (2s^2 - s)R_{2s+1} A_{n-2s+7} + (1 - 4s^2)R_{2s} A_{n-2s+8} + (2s^2 + s)R_{2s-1} A_{n-2s+9}$$

Equation (A.1) can now be written

$$S'_n = \frac{1}{a} \sum_{s=1}^{s=7} \int_{X'=2s-1}^{X'=2s+1} \frac{\alpha_{s,n} X'^2 + \beta_{s,n} X' + \gamma_{s,n}}{(n - X_0 - X' + 8 - C)^2 + W^2} dX'$$

$$= \frac{1}{a} \sum_{s=1}^{s=7} \left[2 + \eta L_s + \frac{\eta^2 - W^2}{W} T_s \right] \alpha_s + (\tfrac{1}{2} L_s + \eta T_s / W)\beta_s + (T_s / W)\gamma_s. \qquad (A.2)$$

The following abbreviations have been used:

$$\eta = n - X_0 + 8 - C$$

$$L_s = \ln[(2s + 1 - \eta)^2 + W^2] - \ln[(2s - 1 - \eta)^2 + W^2]$$

$$T_s = \arctan[(2s + 1 - \eta)/W] - \arctan[(2s - 1 - \eta)/W].$$

If the values of α_s, β_s and γ_s are substituted in Eq. (A. 2) the result can be written in the form

$$S'_n = \sum_{m=1}^{m=15} R_{n,m} A_{n+m-8}$$

If z is defined by

$$z = n + m - X_0 - 8 - C$$

the coefficients $R_{n,m}$ are given by

$$R_{n,m} = \frac{1}{a}\left\{-2 + z \ln\left[\frac{(z+1)^2 + W^2}{(z-1)^2 + W^2}\right] + \frac{1 + W^2 - z^2}{W}\left[\arctan\frac{z+1}{W} - \arctan\frac{z-1}{W}\right]\right\} R_{16-m} \quad \text{for m even,}$$

$$R_{n,m} = \frac{1}{2a}\left\{4 - (z - 3/2)\ln\left[\frac{z^2+W^2}{(z-2)^2+W^2}\right] - (z + 3/2)\ln\left[\frac{(z+2)^2+W^2}{z^2+W^2}\right] - [W - (z+1)(z+2)/W]\left[\arctan\frac{z+2}{W} - \arctan\frac{z}{W}\right] - [W - (z-1)(z-2)/W]\left[\arctan\frac{z}{W} - \arctan\frac{z-2}{W}\right]\right\} R_{16-m}$$

$$\text{for } m = 3, 5, 7, \ldots, 13,$$

$$R_{n,1} = \frac{1}{2a}\left\{2 - (z + 3/2)\ln\left[\frac{(z+2)^2 + W^2}{z^2 + W^2}\right] - [W - (z+1)(z+2)/W]\left[\arctan\frac{z+2}{W} - \arctan\frac{z}{W}\right]\right\} R_{15}$$

$$R_{n,15} = \frac{1}{2a}\left\{2 - (z - 3/2)\ln\left[\frac{z^2+W^2}{(z-2)^2+W^2}\right] - [W - (z-1)(z-2)/W]\left[\arctan\frac{z}{W} - \arctan\frac{z-2}{W}\right]\right\} R_1.$$

REFERENCES

[1] VAN HOVE, L., Phys. Rev. 95 (1954) 249.
[2] BROCKHOUSE, B. N., Nuovo Cim. Suppl. 9 (1958) 45.
[3] BROCKHOUSE, B. N., Phys. Rev. Lett. 2 (1959) 287.
[4] HUGHES, D. J., PALEVSKY, H., KLEY, W. and TUNKELO, E., Phys. Rev. 119 (1960) 872.
[5] SAKAMOTO, M., BROCKHOUSE, B. N., JOHNSON, R. G. and POPE, N. K., J. phys. Soc. (Japan) Suppl. BII 17 (1962) 370.
[6] POPE, N. K., BROCKHOUSE, B. N., JOHNSON, R. G. and SAKAMOTO, M., Bull. Amer. phys. Soc. 7 (1962) 24.
[7] BROCKHOUSE, B. N., BERGSMA, J., DASANNACHARYA, B. A. and POPE, N. K., Inelastic Scattering of Neutrons in Solids and Liquids I IAEA, Vienna (1963) 189-201.
[8] EGELSTAFF, P. A., Inelastic Scattering of Neutrons in Solids and Liquids, IAEA, Vienna (1961) 25-37.
[9] SIMPSON, J. H. and CARR, H. Y., Phys. Rev. 111 (1960) 1201.
[10] RAHMAN, A., SINGWI, K. S. and SJÖLANDER, A., Phys. Rev. 126 (1962) 986.
[11] RAHMAN, A., SINGWI, K. S. and SJÖLANDER, A., Phys. Rev. 126 (1962) 997.

DISCUSSION

P. EGELSTAFF: I think that the absence of a dip near the origin of your frequency spectra may be related to the fact that you equate $S(Q,\epsilon)$ to $A_0(\epsilon^2 + W^2)$ plus small correction terms. In our experiments and in those of Professor Larsson's group, emphasis was placed upon the large ϵ region where this form is certainly not valid. Do you think that the apparent discrepancy in these results for the frequency spectra merely reflects this difference?

N. POPE: In principle, the method can be extended to the large ϵ region by replacing the constant $A_0(Q)$ by a polynomial of large enough order or by some other appropriate form. Our assumption is that this polynomial varies slowly over regions of the order of width of the resolution function - not that it is $A_0(Q)$ plus a small correction term. The latter result is a consequence of the input data we have used, namely the scattering function net in (Q,ϵ)-space prepared by Sakamoto et al. and the fact that we have used this form to analyse the data only over the small range $0 \leqslant \epsilon \leqslant 1.2$ meV. Thus I do not believe that the differences between these frequency spectra and yours are due to the form we have chosen for $S(Q,\epsilon)$.

COLD NEUTRON SCATTERING BY METHANE

B. A. DASANNACHARYA, G. VENKATARAMAN AND K. USHA DENIZ
ATOMIC ENERGY ESTABLISHMENT TROMBAY, BOMBAY, INDIA

Abstract — Résumé — Аннотация — Resumen

COLD NEUTRON SCATTERING BY METHANE. Preliminary measurements are reported on the scattering of 4.1-Å neutrons by liquid methane using a rotating crystal spectrometer. The quasi-elastic width follows the simple diffusion model up to $Q_0 = 1.5$ Å^{-1}. The inelastic parts of the distributions have been compared with an extension, to the liquid state, of Griffing's theory for gaseous methane. The calculations show that free rotational states, if they exist in the liquid state, can be seen as peaks in the scattered neutron spectra at small angles. Our distribution at 30° angle of scattering does not show any such peak. We conclude, therefore, consistent with spectroscopic measurements, that the rotational states should be split due to intermolecular interactions.

DIFFUSION DES NEUTRONS FROIDS PAR LE MÉTHANE. Les auteurs font état de mesures préliminaires de la diffusion des neutrons de 4,1 Å par le méthane liquide, faites au moyen d'un spectromètre à cristal tournant. La largeur quasi élastique reste conforme au modèle de diffusion simple jusqu'à $Q_0 = 1,5$ Å^{-1}. Les fractions inélastiques des distributions ont été comparées en étendant à la phase liquide la théorie de Griffing relative au méthane gazeux. Les calculs montrent que les états de rotation libre – si toutefois ils existent en phase liquide – devraient se manifester sous la forme de pics dans les spectres des neutrons diffusés à de petits angles. La distribution pour des angles de diffusion de 30° n'a présenté aucun pic de ce genre. Les auteurs en ont conclu, en s'appuyant sur des mesures spectrométriques, que les états de rotation se trouvent probablement fragmentés par suite d'interactions intermoléculaires.

РАССЕЯНИЕ ХОЛОДНЫХ НЕЙТРОНОВ НА МЕТАНЕ. Сообщаются предварительные результаты измерений рассеяния нейтронов с длиной волны 4,1 Å на жидком метане. Измерения были выполнены с помощью вращающегося кристаллического спектрометра. Квазиупругая ширина соответствует простой модели диффузии до $Q_0 = 1,5$ Å^{-1}. Было произведено сравнение неупругой части рассеяния с результатами распространения теории Гриффинга для газообразного метана на жидкое состояние. Расчеты показывают, что состояния свободного вращения, если они существуют в жидком состоянии, могут быть видны в виде пиков в спектрах рассеянных нейтронов при небольших углах. Наше распределение при угле рассеяния, составляющем 30° не дало такого пика. Поэтому в соответствии с данными спектроскопических измерений мы сделали вывод, что вращательные состояния должны быть расщеплены вследствие межмолекулярных взаимодействий.

DISPERSIÓN DE NEUTRONES FRÍOS EN EL METANO. Se presentan los resultados de mediciones preliminares relativas a la dispersión de neutrones de 4,1 Å en el metano líquido, efectuados con un espectrómetro de cristal giratorio. La amplitud cuasielástica se ajusta al modelo de difusión simple hasta el valor $Q_0 = 1,5$ Å^{-1}. La parte inelástica de las distribuciones se ha comparado con los resultados de extender al estado líquido la teoría de Griffing para el metano gaseoso. Los cálculos muestran que los estados de rotación libre, si existen en el estado líquido, pueden observarse como picos de los espectros de neutrones dispersos en pequeños ángulos. La distribución de la dispersión obtenida por los autores para un ángulo de 30° no presenta ninguno de estos picos. Concluyen, por lo tanto, de conformidad con las mediciones espectroscópicas, que los estados de rotación deben hallarse desdoblados como consecuencia de efectos intermoleculares.

I. INTRODUCTION

Several authors [1-4] have reported measurements on differential scattering of slow neutrons by liquid methane during the last few years. The earliest measurements were those of STILLER and HAUTECLER [1] who,

using a beryllium detector spectrometer, concluded that discrete levels characteristic of freely rotating molecules exist in the liquid state. Later measurements of HARKER and BRUGGER [2] suggest that the rotational mode is unchanged from its characteristics in the gas where the rotations are known to be free. Infrared absorption [5] and Raman scattering [6] studies from liquid methane have also been made. No discrete rotational levels are observable and the indications are that while the rotations are essentially free for the higher levels, hindering may occur in the lower levels. The situation regarding the existence of free rotations in liquid methane, thus, does not seem to be clear. We have therefore reinvestigated neutron scattering by liquid methane using cold neutrons, which have the advantage of revealing not only the rotational but also the translational effects. Preliminary results of our investigations are reported here.

II. THEORY

When slow neutrons are scattered by molecular systems they exchange energy with vibrational, rotational and translational degrees of freedom. The rotational part of the inelastic spectrum will be modified considerably by the translatory motions and it is important to know the extent of this effect. For this purpose we have developed a model which is essentially an extension of Griffing's work on gaseous methane.

As in all calculations of scattering by molecular systems, our starting point is the work of ZEMACH and GLAUBER [7]. Following the notation used by these authors, the partial differential cross-section per nucleus for incoherent scattering can be expressed as

$$\frac{d^2\sigma_{inc.}}{d\Omega d\epsilon} = \frac{a^2_{inc.,\nu}}{2\pi\hbar} \frac{k}{k_0} \int dt \exp(-i\epsilon t/\hbar)\ \chi_\nu^{vib.} \chi_\nu^{rot.} \chi_\nu^{trans.} \qquad (1)$$

where χ's are the intermediate scattering functions and $a_{inc.,\nu}$ is the incoherent scattering amplitude of the ν-th nucleus; otherwise the notation is the same as that of Zemach and Glauber. The intermediate scattering functions are given by

$$\chi_\nu^S = \sum_{Si} B_{Si}(T) \left\langle \sum_{Sf} \exp\left[\frac{i(E_{Si} - E_{Sf})t}{\hbar}\right] \left| \langle \psi_{Sf} \left| \exp - i\vec{K} \cdot \vec{S}_\nu \right| \psi_{Si} \rangle \right|^2 \right\rangle_\Omega \qquad (2)$$

Here S stands for vibration, rotation or translation, $\vec{S}_\nu$ denotes the appropriate co-ordinate and $B_{Si}(T)$ is the probability that the target molecule is in a given vibrational, rotational or translational initial state; $\langle \ldots\ldots \rangle_\Omega$ represents averaging over orientations and applies only to vibrations and rotations. In obtaining Eq. (1), the assumption is made that the average over molecular orientation of the product of rotational and vibrational factors is equal to the product of their averages.

In applying Eq. (1) to the case of liquid methane, we have made the assumption that the vibrations of the molecule are not excited either thermally

or by the neutrons and that the rotations are completely free. The intermediate scattering functions for vibration and rotations under these assumptions can then be readily written down from the works of KRIEGER and NELKIN [8] (Eq. (20)) and GRIFFING [9] (Eqs. (9) and (10)), respectively. We have further assumed that the translational motions are describable by the simple diffusion model. This probably is a fairly reasonable assumption for a spherical-top molecule like methane with weak intermolecular forces. For a classical liquid of this type

$$\chi_{\nu}^{\text{trans.}} = \exp(-D\kappa^2 |t|),$$

where D is the diffusion coefficient. The above expression for $\chi^{\text{trans.}}$ does not, however, lead to a cross-section which satisfies the detailed balance condition. On making the necessary modifications suggested by Schofield to take account of this, we have

$$\chi_{\nu}^{\text{trans.}} = \exp\left[-D\kappa^2\left(|t| - \frac{i\hbar}{2k_B T}\right)\right]$$

Upon introducing the appropriate expressions for the χ's in Eq. (1), we get (in the notation of Refs. [8] and [9]).

$$\frac{d^2\sigma_{\text{inc.}}}{d\Omega\, d\epsilon} = \frac{a^2_{\text{inc.},\nu}}{2\pi\hbar}\,\frac{k}{k_0}\,\exp(-\hbar\kappa^2\gamma_{\nu\nu})\sum_{jJ}\left[\frac{2D\kappa^2}{(D\kappa^2)^2 + [(\epsilon-\beta)/\hbar]^2}\exp\left(-\frac{\epsilon-\beta}{2k_B T}\right)\right]$$

$$\times\left[\frac{(2J+1)}{(2j+1)}\right]B_j(T)\sum_{n=|j-J|}^{j+J} j_n^2(\kappa b_\nu), \qquad (3)$$

where

$$\beta = \frac{\hbar^2}{2I}[j(j+1) - J(J+1)]\,.$$

In deriving the above expression, no account has been taken of any possible nuclear-spin correlations.

It is interesting to compare this with

$$\frac{d^2\sigma_{\text{inc.}}}{d\Omega\, d\epsilon} = \frac{a^2_{\text{inc.},\nu}}{2\pi\hbar}\,\frac{k}{k_0}\,\exp\left(-\frac{\epsilon}{2k_B T}\right)\frac{2D\kappa^2}{(D\kappa^2)^2 + (\epsilon/\hbar)^2},$$

the cross-section for a monatomic liquid in which the motions occur through simple diffusion. We observe that in the case of liquid methane there are additional Lorentzians (just as there are additional Gaussians for the case of gaseous methane) located at the energies corresponding to the various rotational transitions. The widths of the Lorentzians are governed by the momentum transfers involved. It is clear therefore that the rotational struc-

ture is best examined under conditions of small momentum transfer, i.e. using neutrons of low energy and small scattering angles. A comparison of experimental data with calculations based on Eq. (3) is discussed in a later section.

III. EXPERIMENTAL RESULTS

The experiments were carried out using the rotating crystal spectrometer at the Canada-India Reactor (CIR). This instrument gives bursts of neutrons of 4.1-Å wavelength (E_0 = 4.87 meV) produced by Bragg-reflecting beryllium-filtered neutrons from two sets of (111) planes of a spherical aluminium crystal rotating at 8000 rpm. The neutrons after being scattered by the sample, traverse a 3-m flight-path at the end of which they are detected in a set of six $B^{10}F_3$ counters 2 in in diameter and 18 in long, covering a total horizontal span of ~6.5°. The spectra are recorded in a 100-channel time analyser with 32-μs channel width. The energy resolution of the spectrometer at the incident energy is ~0.36 meV (i.e. $\Delta t/t$ ~3.6%).

A 1-mm thick sample at (97.5 ± 0.5)°K in the transmission geometry was used for all the measurements. The sample* was contained in an aluminium cassette with 0.75-mm walls. The time-of-flight distributions were taken at scattering angles of 30°, 37.5°, 45°, 60° and 90°, the duration of each run being roughly 48 h. Since the background is time-independent, it was recorded by stopping the crystal in an off-Bragg position and counting for one hour every day. The counts were then scaled suitably and distributed equally over the 100 channels after correcting for the duty cycle of the analyser. It is worth noting here that the background measured with a cadmium shutter in the monochromatic beam or just an empty container gives too low a value, especially if one uses samples with large scattering, as diffuse scattering from the samples is eliminated. Distributions taken with the empty container at 30° and 90° scattering angles showed that the cassette contribution was very small. No correction has therefore been applied for this. The final distributions after subtracting background and correcting for counter efficiency and air scattering are shown in Fig. 1 as solid circles. These distributions have been normalized so that the area of the raw data follow the measured diffraction pattern. There were about 400 counts per channel around the inelastic maximum (~700 μs/m). No distinct rotational structure is visible in the scattering patterns even at the smallest scattering angle. (This point is discussed in some detail later.) The 30° pattern also shows the resolution function. This was measured by wrapping the empty sample holder with a thin (~0.15-mm) sheet of polythene and observing the distribution of elastically scattered neutrons.

A run was also taken at 84°K at which temperature methane is in the solid state. The results after correction of this measurement, which was made at a scattering angle of 90°, are shown as open circles in Fig. 1. The distribution was normalized to the liquid distribution such that the integrated intensity in the raw data in the region of 600 to 800 μs/m was the same for the two patterns.

---

* C. P. grade methane gas supplied by Matheson Gas Co. was used in the experiments.

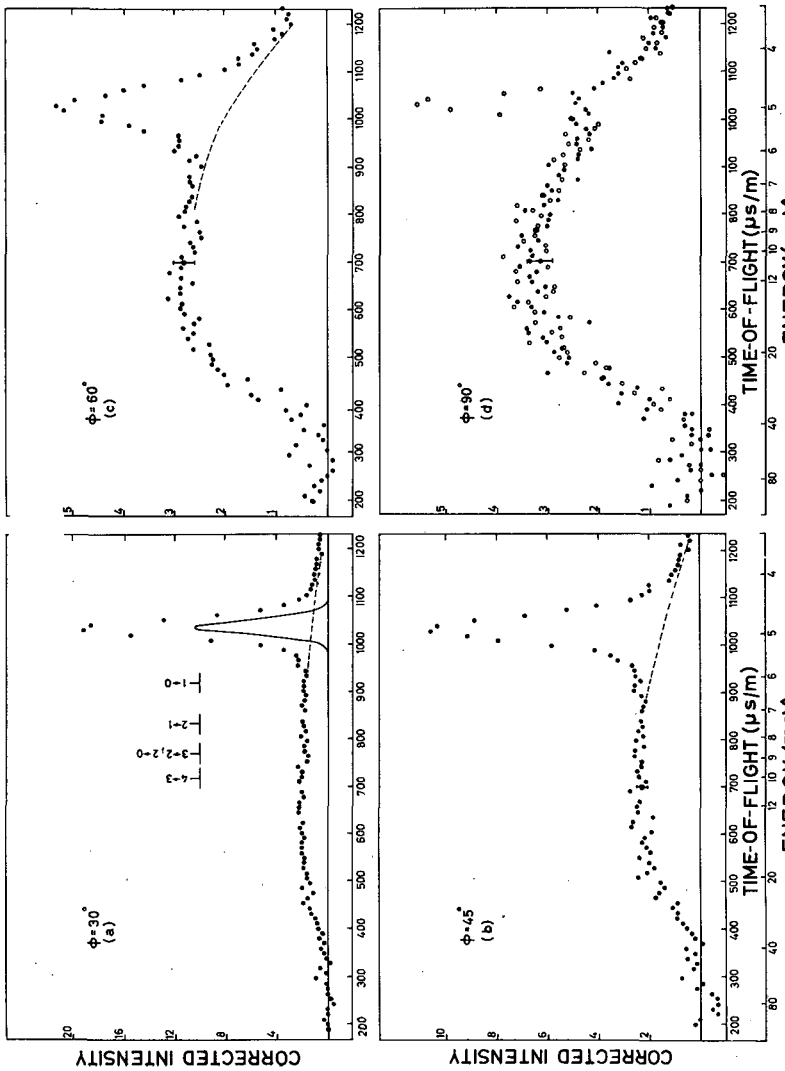

Fig. 1

Corrected time-of-flight distributions of 4.1-Å neutrons scattered by liquid methane at 97.5°K.
Open circles in (d) show the observed spectrum from solid methane at 84°K.

$\lambda_0 = 4.1$ Å
$E_0 = 4.87$ meV

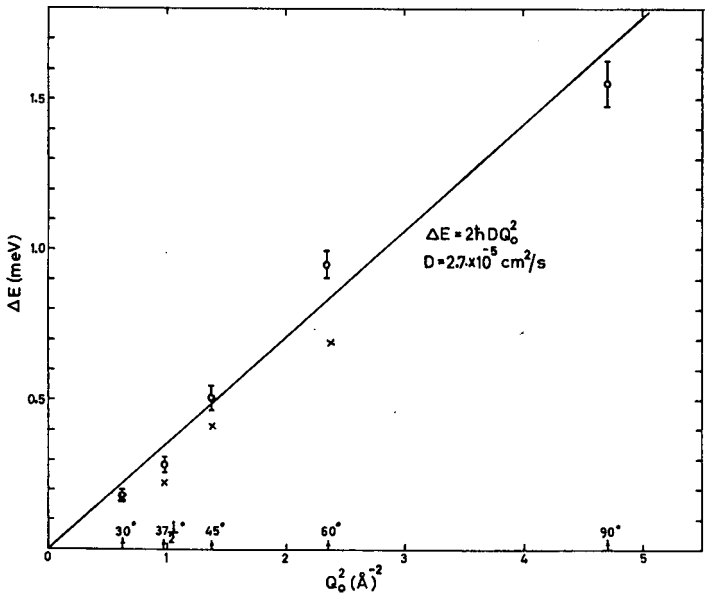

Fig. 2

Quasi-elastic width plotted as a function of square of the momentum transfer for liquid methane at 97.5°K

IV. DISCUSSION

As usual, the measured spectra for the liquid are seen to consist of a quasi-elastic and an inelastic part. The quasi-elastic part gives information about the diffusive behaviour of the molecules and the inelastic part, in this experiment, about the rotational motions. We shall first consider the quasi-elastic part of the distributions.

Quasi-elastic scattering

The quantity which one needs for comparison with theoretical models is the full width at half maximum of the quasi-elastic distribution. Now it can be seen from Fig. 1, that the quasi-elastic part can be separated from the inelastic with certainty only at small angles of scattering. This separation becomes increasingly difficult as the scattering angles become larger and is almost impossible at 90°. However, we have tried some approximate methods to get the value of the width and the results derived from these various methods are plotted in Fig. 2, as a function of Q^2. The widths have been derived under the assumption that the observed quasi-elastic distribution is a convolution of a Lorentzian distribution with a Gaussian resolution. The open circles at 30° and $37\frac{1}{2}$° are the full widths at half maximum without subtracting any contribution. The circles at higher angles have similarly been found but using only the energy loss side. The error bars indicate uncertainties from counting statistics only. This should give an upper limit

for the quasi-elastic width. The crosses show the widths found by assuming the dashed lines in Fig. 1 as the inelastic background. In this case, at all the angles, the full width at half maximum has been taken. This is probably the maximum inelastic contribution that one can subtract and so the crosses could be considered as the lower limit for the quasi-elastic width. There is probably still another method of finding this width when the temperature is very near the melting point. One could measure the spectra from the liquid and in the solid near the melting point. If the sample is a pure incoherent scatterer, one can get the quasi-elastic scattering by subtracting the properly normalized inelastic spectrum of the solid from the total spectrum of the liquid. This assumes that the inelastic spectra are the same in the solid and the liquid state near the melting point. We have not been able to do this because of the poor statistics of our data. The straight line shows the theoretical value of the width based on a simple diffusion model using the diffusion coefficient given by the measurements of NAGHIZADEH and RICE [10]. The agreement is fair.

Inelastic scattering

If the molecules of methane are rotating freely in the liquid state, then the scattered neutron distribution will show peaks corresponding to the various possible transitions, which will be spaced at intervals of twice the rotational constant for methane, i.e. at 1.3 meV. Assuming that the time-of-flight resolution (full width at half maximum) remains constant with time, the energy resolution changes from 0.36 meV at the incident energy to about 1.1 meV at 10 meV (i.e. the position of j = 4 to J = 3 transition). Thus we do not expect to see any discrete level in our experiments beyond 10 meV ($\sim$ 720 μs/m). So we concentrate our attention on lower energies. It is worth looking at the theoretical calculations first.

Results of the calculations of our model for 97.5°K are given in Fig. 3. In these calculations we have considered rotational states with j and $J \leqslant 10$ and spherical Bessel functions of order $\leqslant 8$. The following values were used for the other constants: $D = 2.7 \times 10^{-5}$ cm^2/s [10], $a_{\text{inc.},\nu} = 2.52 \times 10^{-12}$ cm, $\lambda_0 = 4.1$ Å, $b_\nu = 1.093 \times 10^{-8}$ cm and $I = 5.33 \times 10^{-40}$ g cm^2. Resolution effects have not been taken into account. As remarked earlier the inelastic part of the theoretical spectrum consists of a number of Lorentzians. This fact is easily observed at the smallest scattering angle, but with the increasing angle the Lorentzians get broadened and merge into each other.

Referring now to Fig. 1(a) we find that the inelastic part of the distribution does not show any structure. The expected positions of the various rotational peaks are marked by vertical lines, and the horizontal lines give the expected width, taking the resolution and diffusion broadening into account. It seems reasonable to assume that we should be able to observe at least the first few states. It is true that multiple scattering will tend to wash off the peaks to some extent but since we are using a small angle of scattering multiple scattering should not be very much. Therefore we feel that it should be possible to see at least some structure if discrete rotational levels were present.

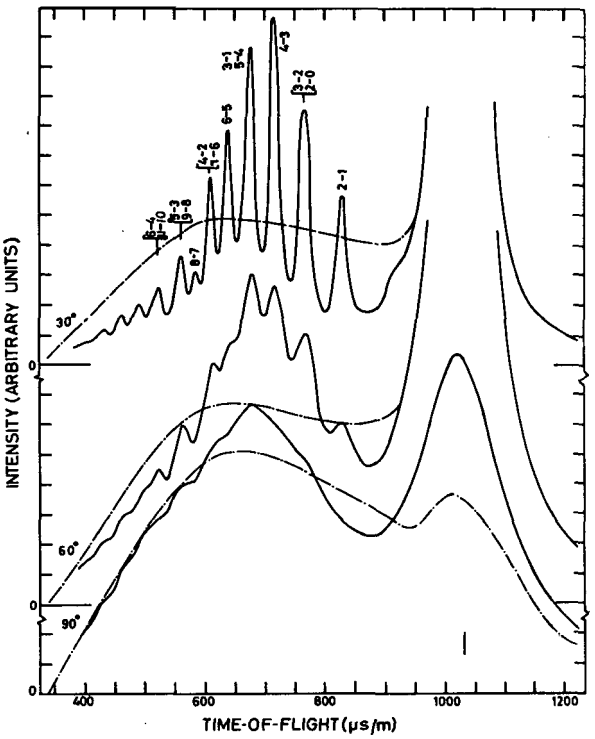

Fig. 3

Time-of-flight distributions of 4.1-Å neutrons scattered by liquid methane at 97.5°K for three different angles using our model

——— Calculated
——·—— Smooth curves through experimental data

For purposes of comparison, our experimental results are shown as dashed lines in Fig. 3. The pattern at 90° has been arbitrarily normalized and the same normalization has been used for other angles. It is seen that even though the agreement is poor as to details, the general trend of inelastic scattering is reproduced, in that the maximum in the inelastic scattering does not shift much with angle. This is an improvement over the Krieger-Nelkin theory which has been used often for explaining rotational effects. A Krieger-Nelkin calculation gives no quasi-elastic peak in the time-of-flight distribution and the inelastic peak shifts considerably from 90° to 30° scattering angle. For methane at 100°K the Krieger-Nelkin calculation gives a maximum at about 650 μs/m at ϕ = 90° which shifts to 900 μs/m at 30° angle of scattering. This shortcoming is removed in Griffing's work, but since his treatment is for the gaseous state the diffusive effects cannot be properly described.

In conclusion, our measurements are consistent with the spectroscopic experiments regarding the absence of discrete rotational levels. To explain the absence CRAWFORD et al. [6], found it necessary to assume that the

rotational levels are split as a result of intermolecular interactions. They were then able to account for their observed intensity by assuming broadened rotational lines at the positions of the free rotational levels. Calculations along these lines are in progress to see whether a broadening of the rotational levels, over and above the resolution, will give a better description of the experimental observations.

The inelastic spectrum for the solid methane near the melting point and the liquid are very similar to each other, as observed in other measurements. Our data are too limited to make further comments about the solid state.

V. SUMMARY

(i) The width of the quasi-elastic scattering from methane follows the curve given by the simple diffusion model up to $Q = 1.5$ Å^{-1}.

(ii) Inelastic scattering from rotational modes indicates that completely free rotational states cannot be observed in liquid methane for lower levels. It is not possible to conclude about the nature of higher levels (greater than $J \sim 3$) from our experiments since the resolution becomes poorer with increasing energy transfer. Measurements with better resolution and statistics are being done to confirm this conclusion.

(iii) A preliminary comparison of our experiments with an extension of Griffing's theory of the liquid state suggests that modifications might be necessary in order to get better agreement with theory. One possible modification is to introduce, in the rotational levels, a broadening arising from the removal of degeneracy of the rotational states.

ACKNOWLEDGEMENTS

We would like to thank Dr. C.L. Rao for providing us with the methane gas, Mr. T.U. Rao for technical help, Mr. P.K. Dayanidhi for computer calculations and the reactor maintenance personnel for help during the installation of the spectrometer.

REFERENCES

[1] STILLER, H. and HAUTECLER, S., Z. Phys. 166 (1962) 393.
[2] HARKER, Y.D. and BRUGGER, R.M., J. Chem. Phys., to be published.
[3] OTNES, K., MELLOR, J. and PALEVSKY, H., Bull. Amer. phys. Soc. 9 (1963) 421.
[4] WHITTEMORE, W.L., Nucl. Sci. Engng 18 (1964) 182.
[5] EWING, G.E., J. Chem. Phys. 40 (1964) 179.
[6] CRAWFORD, M.F., WELSH, H.L. and HARROLD, J.H., Canad. J. Phys. 30 (1952) 81.
[7] ZEMACH, A.C. and GLAUBER, R.J., Phys. Rev. 101 (1956) 118, 129.
[8] KRIEGER, T.J. and NELKIN, M.S., Phys. Rev. 106 (1957) 290.
[9] GRIFFING, G.W., Phys. Rev. 124 (1961) 1489.
[10] NAGHIZADEH, J. and RICE, S.A., J. Chem. Phys. 36 (1962) 2710.

DISCUSSION

B. DORNER: I would like to point out that Dr. Stiller found that, in the liquid state, the rotational level for L = 1 was split in two. This means that you have two peaks which are too small and too close to each other, thus making their analysis impossible. Moreover, Dr. Stiller's resolution was better than yours, by a factor of about 2.5.

B.A. DASANNACHARYA: As regards the splitting of the first level, if the lower (J = 1) level is at 0.95 meV, as suggested by Hautecler and Stiller, we should be able to see some structure, at least on the energy-loss side. However, no such effect is observed.

B. DORNER: In calculating the intensities of the expected lines, did you take into account the different spin configurations of CH_4?

B.A. DASANNACHARYA: We have not taken any spin correlation into account. Zemach and Glauber state that this correlation is small in the case of methane. However, we are making a more detailed investigation of the question.

H. PALEVSKY (Chairman): Dr. Otnes at Brookhaven has carried out a very extensive set of measurements on gaseous, liquid and solid methane and his results for the liquid are in essential agreement with those of the Indian group. Theoreticians in the United States have found that the effect of spin correlations is small. Dr. Otnes does not see any signs of distinct rotational transitions.

G. VENKATARAMAN: Perhaps I may comment on what Dr. Palevsky has just said regarding Otnes' measurements on liquid methane. In looking for rotational transitions it is important to use monochromatic incident neutrons, especially as the rotational levels are closely spaced. The use of a filtered spectrum is likely to wash out any possible structure in the inelastic distribution.

B.A. DASANNACHARYA: Yes, in methane the spacing between rotational transitions is ~ 1.3 meV and the spread in a beryllium filtered spectrum itself is larger than this.

R.E. SCHMUNK: I might add that Dr. Griffing at MTR (Materials Testing Reactor, Idaho, USA) is working on a liquid model for the scattering from liquid methane and, while this work is not yet finished, his results indicate a hindrance of the rotational modes.

K.-E. LARSSON: In your line-width representation you give a point at 90° scattering angle. Is it really possible to define a line broadening at this angle where the quasi-elastic peak has almost completely merged into the broad inelastic background?

B.A. DASANNACHARYA: It is not possible to define the line broadening at 90°, as pointed out in the text of the paper. However, the point can probably still be treated as an upper limit for quasi-elastic width.

RECENT MEASUREMENTS OF THE SCATTERING LAWS OF SOME HYDROGENOUS MODERATORS

W. GLÄSER, G. EHRET AND A. MERKEL
INSTITUT FÜR ANGEWANDTE KERNPHYSIK,
KERNFORSCHUNGSZENTRUM KARLSRUHE, FEDERAL REPUBLIC OF GERMANY

Abstract — Résumé — Аннотация — Resumen

RECENT MEASUREMENTS OF THE SCATTERING LAWS OF SOME HYDROGENOUS MODERATORS. The measurement of scattering laws for hydrogen-containing materials is of great importance as much for a better understanding of the thermalization of neutrons in such moderators as for a basic physical understanding of the dynamical behaviour of such systems.

With the rotating crystal time-of-flight technique double differential scattering cross-sections for benzene, zirconium hydride and ordinary water vapour have been measured.

These measurements have been performed with incident neutron energies between 0.018 and 0.06 eV and scattering angles between 20° and 140°. Measured Q-values cover the range from 0 to 15 $Å^{-1}$ (here $\hbar Q$ is the momentum transfer). Scattering law data have been extracted from the measured cross-sections and were extrapolated with the help of LEAP and ADDELT calculations to meet energy and momentum transfer values not accessible directly by the experiments.

In the cases of benzene and zirconium hydride also the generalized frequency distributions $p(\beta)$ were determined by the extrapolation method.

The results for water vapour are compared with theoretical calculations based on the Krieger-Nelkin theory and an improved theory of Griffing.

DÉTERMINATION DES LOIS DE DIFFUSION DE PLUSIEURS RALENTISSEURS HYDROGÉNÉS. La détermination des lois de diffusion pour les matières hydrogénées revêt une grande importance tant pour mieux comprendre le processus de thermalisation des neutrons dans ces ralentisseurs que pour déterminer les bases physiques du comportement dynamique de ces systèmes.

Les auteurs ont mesuré les sections efficaces différentielles de diffusion doubles pour le benzène, l'hydrure de zirconium et la vapeur d'eau ordinaire, par la méthode du temps de vol faisant appel à un cristal tournant.

Ils se sont servis de neutrons incidents d'une énergie comprise entre 0,018 et 0,06 eV et d'angles de diffusion allant de 20 à 140°. Les valeurs de Q mesurées couvrent la gamme comprise entre 0 et 15 $Å^{-1}$ ($\hbar Q$ étant le transfert de quantité de mouvement). Les auteurs ont extrait les données relatives aux lois de diffusion des sections efficaces mesurées et les ont extrapolées à l'aide de calculs LEAP et ADDELT pour saisir les valeurs du transfert d'énergie et du transfert de quantité de mouvement, auxquelles on n'a pas directement accès par voie expérimentale.

Dans les cas du benzène et de l'hydrure de zirconium aussi, ils ont établi les distributions de fréquence généralisées $p(\beta)$ par extrapolation. Ils comparent les résultats obtenus pour la vapeur d'eau aux calculs théoriques fondés sur la théorie de Krieger-Nelkin et une théorie améliorée de Griffing.

УСТАНОВЛЕНИЕ ЗАКОНОВ РАССЕЯНИЯ НА НЕКОТОРЫХ ВОДОРОДСОДЕРЖАЩИХ ЗАМЕДЛИТЕЛЯХ. Установление законов рассеяния на водородсодержащих материалах имеет большое значение как для лучшего понимания термализации нейтронов в таких замедлителях, так и для понимания физических основ динамического поведения таких систем.

С помощью метода измерения по времени пролета (вращающийся кристалл) были измерены двойные дифференциальные сечения рассеяния для бензола, циркониевого гидрида и паров обычной воды.

Эти измерения были осуществлены при энергиях бомбардирующих нейтронов от 0,018 до 0,06 эв и при углах рассеяния между 20 и 140°. Измеренные величины Q охватывают диапазон от 0 до 15 $Å^{-1}$ (здесь $\hbar Q$ — передача импульса). Данные о законе рассеяния были выведены из измеренных поперечных сечений и были экстраполированы с помощью расчетов LEAP

и ADDELT для получения значений передачи энергии и импульса, которые невозможно получить непосредственно экспериментальным путем.

Методом экстраполяции были определены также обобщенные распределения частот $p(\beta)$ для бензола и циркониевого гидрида.

Результаты для водяных паров сравниваются с теоретическими расчетами, основанными на теории Кригера-Нэлкина и на улучшенной теории Гриффинга.

RECIENTES COMPROBACIONES DE LAS LEYES DE DISPERSION EN ALGUNOS MODERADORES HIDROGENADOS. La comprobación experimental de las leyes de dispersión en lo que respecta a las sustancias hidrogenadas reviste considerable importancia porque contribuye a un mejor conocimiento del procesó de termalización de los neutrones en moderadores de ese tipo y de los fundamentos físicos del comportamiento dinámico de tales sistemas.

Empleando un espectrómetro de cristal rotatorio para medir tiempos de vuelo, se han determinado las secciones eficaces de dispersión diferencial doble correspondientes al benceno, hidruro de circonio y vapor de agua común.

Las mediciones se han efectuado con neutrones incidentes de energía comprendida entre 0, 018 y 0, 06 eV, y con ángulos de dispersión de 20 a 140°. Los valores medidos de Q abarcan de 0 a 15 $Å^{-1}$ (siendo $\hbar Q$ la transferencia del impulso). De las secciones eficaces medidas, se han deducido los datos relativos a las leyes de dispersión, los cuales se han extrapolado con ayuda de las claves de cómputo LEAP y ADDELT a fin de obtener los valores de la energía y del impulso que no pueden determinarse por vía experimental directa.

En el caso del benceno y del hidruro de circonio, también se determinaron por extrapolación las distribuciones de las frecuencias generalizadas $p(\beta)$.

Los resultados obtenidos para el vapor de agua se comparan con los datos calculados con arreglo a la teoría de Krieger-Nelkin y a la teoría perfeccionada de Griffing.

I. INTRODUCTION

The study of the scattering of low energy neutrons by many-particle systems yields valuable information on the dynamical behaviour of such systems. The most detailed quantity that can be measured experimentally is the double differential scattering cross-section $d^2\sigma/d\Omega dE$, which consists in the Fermi pseudo-potential approximation of two factors. One depends only on the properties of the neutron and the other, the so-called scattering law, depends only on the dynamical properties of the scatterer.

Often the scatterer is isotropic with respect to the incident neutron beam (polycrystalline solids, liquids and gases); in this case the scattering law can be written:

$$S(\alpha, \beta) = \frac{4k_BT}{\sigma_b} \left(\frac{E_0}{E}\right)^{1/2} e^{\beta/2} \frac{d^2\sigma}{d\Omega dE}, \tag{1}$$

where E_0 is the incident energy, E the scattered energy, σ_b the bound atom cross-section of the scattering atom, k_BT the temperature in energy units and $d\Omega$ the element of solid angle into which the neutrons are scattered. α and β have the following meaning:

$$\alpha = [E + E_0 - \sqrt{EE_0} \cos\theta]/A\, k_BT \tag{2}$$

where A is the ratio of the mass of the scattering nucleus to the mass of the neutron, and

$$\beta = (E - E_0)/k_BT. \tag{3}$$

The measurement of $S(\alpha, \beta)$ of moderator and reflector materials for all possible α- and β-values is desirable for a better description of the neutron thermalization process in reactors. The fine details of $S(\alpha, \beta)$ are not so important for thermalization studies; however, accurate measurements of $S(\alpha, \beta)$ also yield valuable information of more fundamental interest. Although the main aim of the present work was of the first kind we have tried to extract from the measured scattering laws physically interesting features. In section II of this paper a short description of the experimental arrangement and of the data processing is given; in section III the results on water vapour, benzene and zirconium hydride are described.

II. EXPERIMENTAL PROCEDURE AND METHODS OF DATA PROCESSING

1. *Apparatus*

The Karlsruhe rotating-crystal time-of-flight spectrometer described elsewhere [1] was used to produce the monoenergetic pulsed beams needed for the measurements to be described. The incident neutron energy was between 18 and 80 meV. The width at half-height of the beam incident on the scattering sample was 20 μs, time-of-flight resolution was 20 μs/m, and primary energy resolution was about 5% at 18 meV.

Nine detectors located at a distance of 2 m from the sample and arranged between 20° and 140° detected simultaneously the scattered neutrons. During the experiment the output of the detectors was handled by MIDAS (a multiple input data acquisition system using a Control Data 160-A computer) and was written on magnetic tape [2].

For the benzene measurements an arrangement installed at the reactor DIORIT was used. It was similar to the arrangement described above but had only six detectors and a conventional multichannel analyser.

2. *Scattering samples*

To get a reasonable amount of scattering from a small volume of H_2O vapour a temperature of 241°C and a pressure of 25 atm were chosen. The container was a cylinder made of aluminium, 5 cm in diameter with an active scattering zone 5 cm in length. The wall thickness of the container was 0.18 cm. Under the given conditions the density of vapour was 12 mg/cm^3 and the transmission about 90% for an incident energy of 18.2 meV. For the surface reaction of the aluminium with the water vapour producing $Al(OH)_3$ a correction of the order of 2% was made for the number of scattering molecules.

In the case of benzene, samples of 5 cm × 12 cm and 0.06 cm thickness were used. The containers used 0.05-cm thick aluminium windows.

In the early zirconium hydride measurements powder of $ZrH_{1.8}$ was used. Although a few runs at room temperature were made most were performed at 210°C. In the later experiments the sample was a hydrogenated plate of zirconium metal 0.05-cm thick, 4.5 cm × 7 cm in size, with the composition $ZrH_{1.1}$, which was easier to handle in heating.

The normal procedure for all the investigated substances was to make a run of several days for each incident energy and also a similar background run in which the sample was omitted. The latter run delivered all the data necessary for background corrections.

3. *Data processing*

The data processing cycle starts with a summation of the information written on magnetic type, using the CDC-160 A computer. Further processing was done on an IBM-7070 where, after the determination of detector sensitivity, the "scattering-law programme" was used to evaluate α, β, $S(\alpha,\beta)$ and $S(\alpha,\beta)/\alpha$ as well as the statistical errors caused by the number of collected counts. In this programme also smoothing of the raw data can be done if conditions make this advisable. Smoothing has been done mainly for background runs and the measurements at lowest energy.

In these calculations no general corrections for energy resolution and multiple scattering have been done. However, in the cases where the extrapolation method, to be described now, is used, a resolution correction for the elastic peak has been carried out.

To obtain the generalized frequency distribution $p(\beta)$ the S/α values were plotted against α on a semi-logarithmic scale and extrapolated to $\alpha = 0$. With $p(\beta)$ (Eq. (4)) estimated in this way a LEAP [3]

$$p(\beta) = \beta^2 \lim_{\alpha \to 0} S/\alpha \tag{4}$$

calculation was done to determine S/α again on the basis of a harmonic approximation for the motion of the scattering nuclei. In the range covered by the experiments essentially a phonon expansion is used, varied in the case of non-solids by folding with a simple diffusion model.

III. EXPERIMENTAL RESULTS

1. *Water vapour*

Runs with incident energies of 0.018 and 0.032 eV were made. The evaluated energy and momentum transfer ranges were $0 < \beta < 5$ and $0 < \alpha < 5$ ($T = 514°K$). The density of the vapour (12 mg/cm^3) should be small enough to suppress significant interaction between molecules.

A typical scattering curve is shown in Fig. 1. In this diagram the counting rates in five adjacent channels are smoothed and the background is subtracted. This smoothing process corresponds to the experimental resolution and therefore should not introduce serious errors. There is a slight structure in the curve. At the points indicated by the arrows are bands of energy transfer known from rotation spectra of H_2O. From the experimental data, scattering-law values $S(\alpha,\beta)$ have been derived. The values for one scattering angle obtained at different incident energies are plotted in Fig. 2. The lines are calculated with the KRIEGER-NELKIN theory [4] using an effective mass of $\overline{m}_r = 1.9$ determined from the Sachs-Teller mass tensor

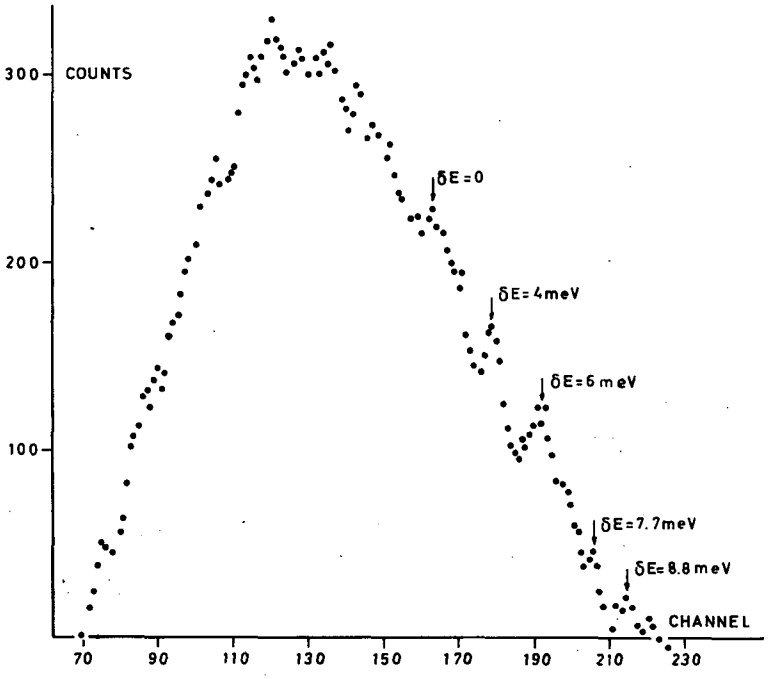

Fig. 1

Typical scattering distribution from H_2O vapour at 241°C and 25 atm.
$E_0 = 18.2$ meV; $\theta = 43.9°$

of the H_2O molecule. The assumptions of this theory, i.e. that the incident energy is large compared with the rotational level spacing and small compared with the vibrational levels of the molecule, are satisfied by the experiment. However the theory agrees with experiment only for large momentum transfer values. The overall agreement can be improved by using an effective mass of the order of four to five which also has been observed by HUGHES et al. [5] with cold neutrons. A good description of the experimental results was obtained also by approximating the H_2O molecule as a symmetric top with an effective moment of inertia $I = 1.96 \times 10^{-40}$ g cm^2 which is the average of the principal moments of inertia of the H_2O molecule. The squares in Fig. 2 were calculated in this way, considering only incoherent scattering from the protons. There have been attempts to treat the rotation of asymmetric tops in neutron scattering theory by quantum mechanics [6]. Unfortunately no numerical results for the double differential scattering cross-section of H_2O molecules are available so far from these calculations.

A set of $S(\alpha, \beta)$ curves for constant β as parameter is shown in Fig. 3.

2. Benzene

With the benzene samples described in section II measurements with incident energies of 0.025, 0.032 and 0.059 eV were made. The range of

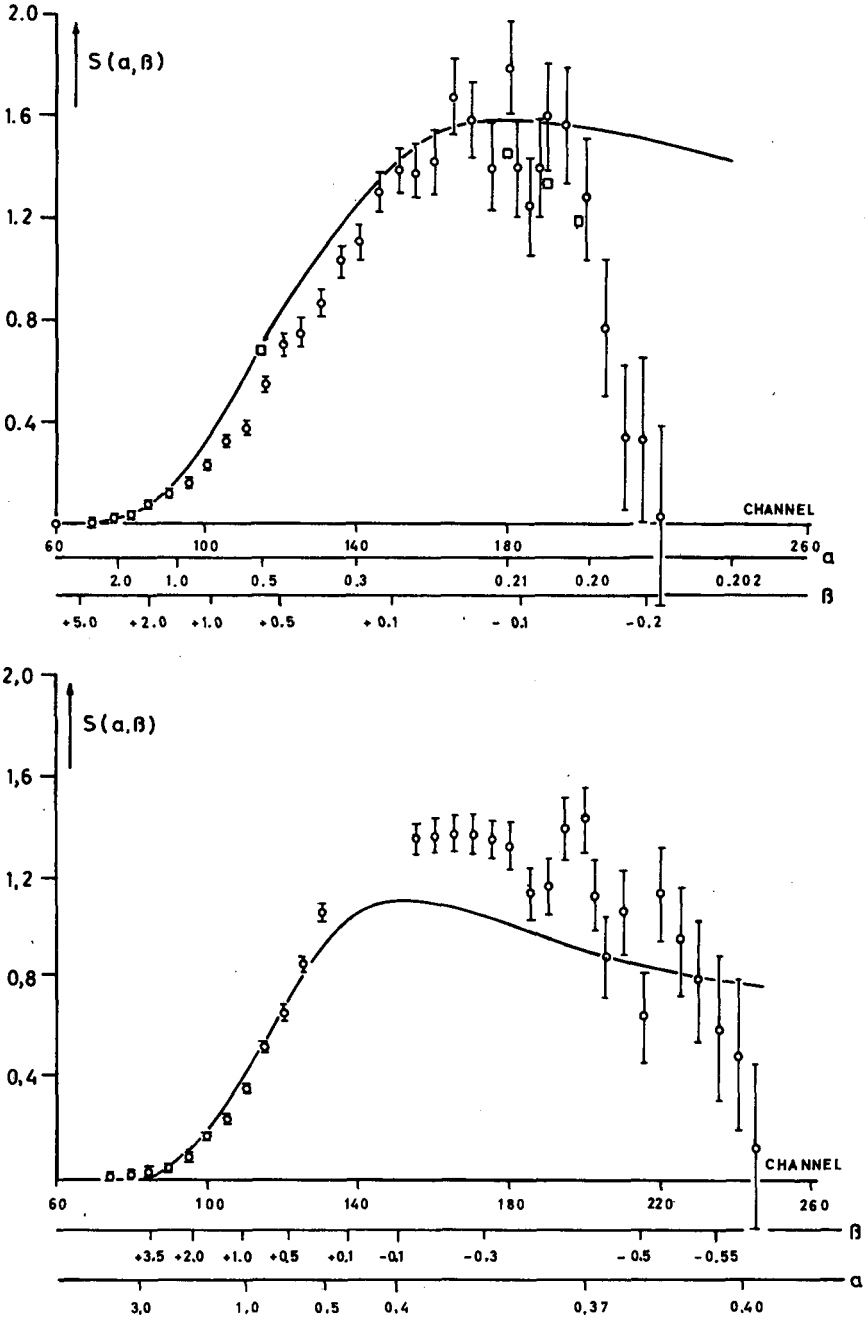

Fig. 2

S(α,β) for the detector at 43.9° at two incident energies
Above: $E_0 = 18.2$ meV
Below: $E_0 = 32.6$ meV

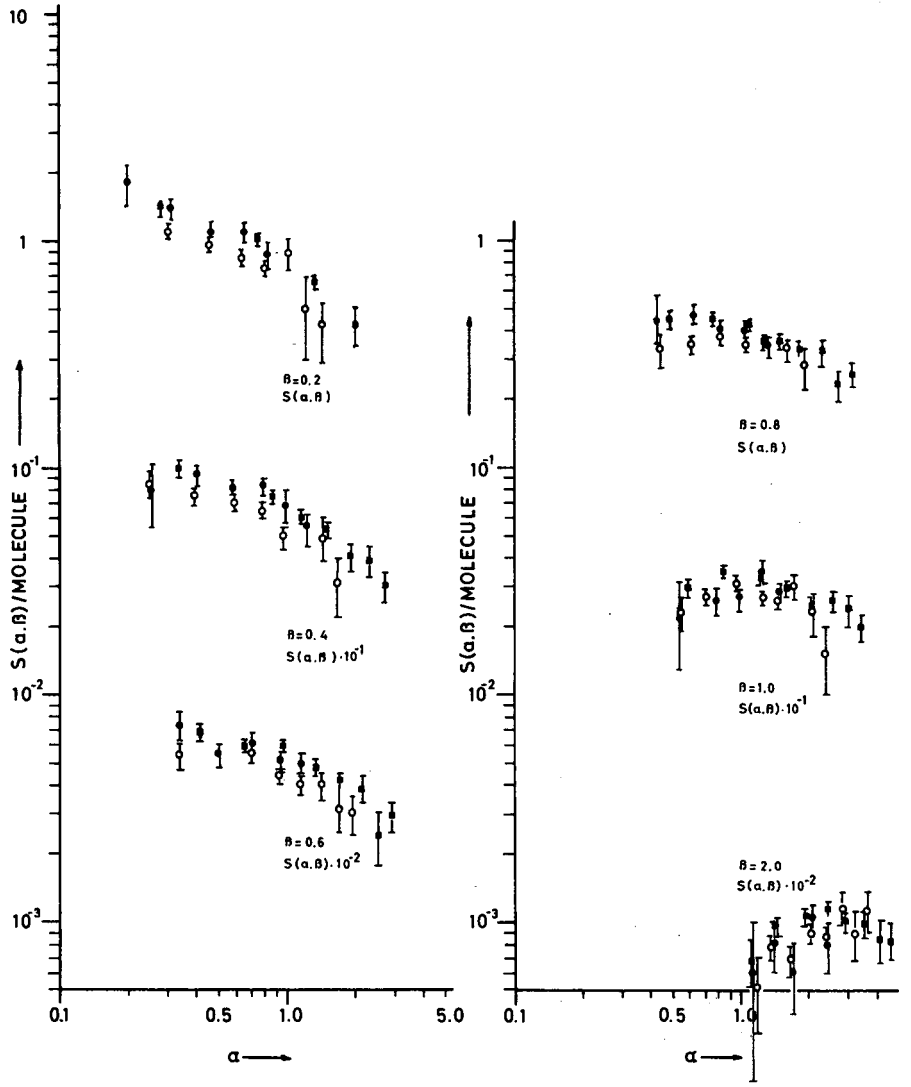

Fig. 3

A plot of S(α,β)/molecule using β as a parameter for H_2O vapour at 241°C and 25 atm
○, ● 18, 2 meV (two runs)
■ 32, 6 meV (one run)

α- and β-values covered was: $0 < \alpha < 12$, $0 < \beta < 3$ (T = 293°C). A few examples of $S(\alpha, \beta)$ values extracted from the measurements are plotted in Fig. 4. The solid lines are results from LEAP calculations. The effect of most of the high energy vibration not directly accessible in the present measurement is corrected for by an additional ADDELT calculation using the LEAP output and the known vibration frequencies. This contributes mainly to the Debye-Waller factor. The dashed lines are from a "benzene gas"

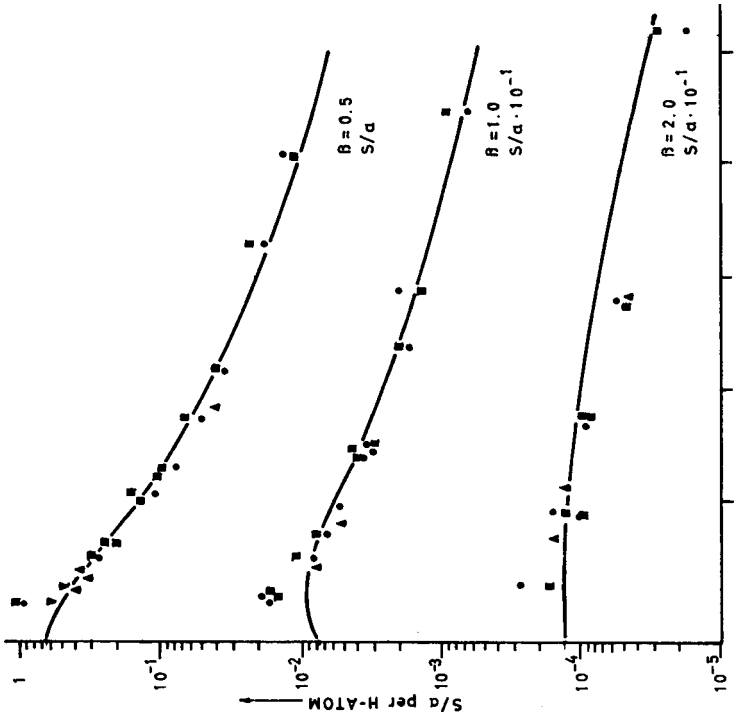

Fig. 5
Examples of extrapolation of benzene S/α values for α = 0
▲ = 25.1 meV ●, ■ = 59.2 meV
▼ = 31.5 meV

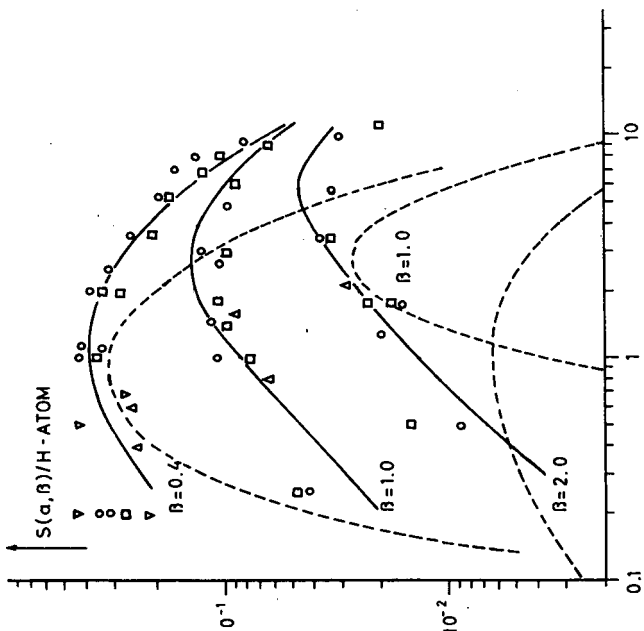

Fig. 4
A few examples of S(α,β) versus α for liquid benzene
△ = 25.1 meV □, ○ = 59.2 meV
▽ = 31.5 meV

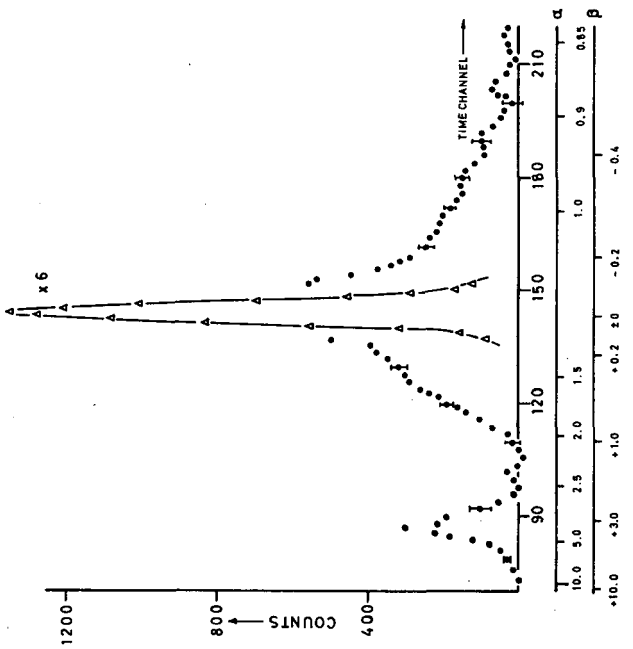

Fig. 7 -
Typical scattering distribution obtained with $ZrH_{1.1}$ at 210°C
Incident energy was 0,033 eV, scattering angle 77,1° and $E_0 = 32,6$ meV.

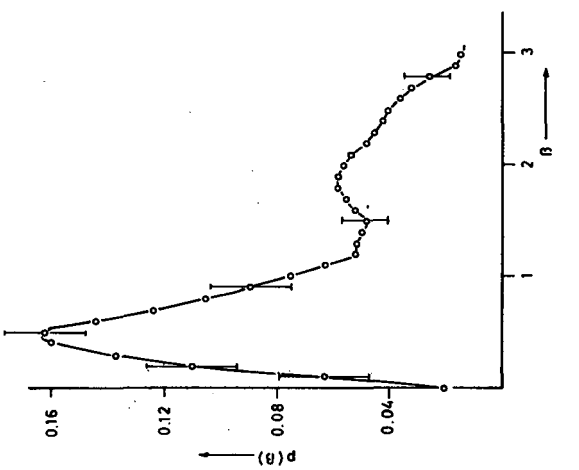

Fig. 6
The frequency distribution p(β) for benzene derived from measurements at 20°C

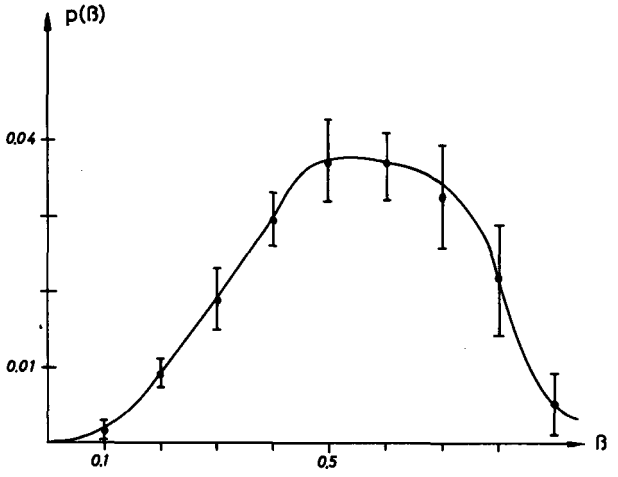

Fig. 8

Fitted low energy distribution p(ß) for zirconium hydride at 210°C

model described by BOFFI et al. [7]. In these curves only two terms in the phonon expansion are taken into consideration. Typical extrapolation curves S/α versus α for determining $(S/\alpha)_{\alpha=0}$ are shown in Fig. 5 and the resultant generalized frequency distribution $p(\beta)$ is given in Fig. 6. The indicated errors are the possible uncertainties in the extrapolation process. The $p(\beta)$ is in good agreement with results of infrared and Raman measurements. The high energy part of $p(\beta)$ ($\beta > 1$) is determined by the properties of the benzene ring, the lowest normal vibration of which is predicted to be at $\beta = 1.99$. This vibration, however, is inactive in infrared and Raman measurements. The broad peak of the distribution near $\beta = 2$ may be attributed to this vibration.

For lower energies the interaction between molecules contributes to the frequency spectrum. From Raman measurements in solid benzene [8] frequencies at about $\beta = 0.32$ and $\beta = 0.52$ are known. The broad peak centred at about $\beta = 0.48$ can be attributed to these motions and from theoretical analysis these are very probably caused by torsional vibrations of the benzene molecule in the field of its neighbours. For studying these motions in more detail a higher resolution than that used in the present measurements is necessary.

3. *Zirconium hydride*

Fig. 7 shows a typical scattering distribution obtained with the $ZrH_{1.1}$ plate at 210°C. Although the high energy peak makes the most important contribution to inelastic scattering, the main aim of the present work was to determine the contribution of the low energy acoustical modes. McREYNOLDS et al. [9] have carefully studied the high energy line using 4-Å neutrons, with higher accuracy than this work yields. Therefore we used the peak half-width of these authors in our data evaluation. As is expected from theory the low energy modes take only a few per cent of the

frequency distribution. We obtained the best fit with the S/α values using the distribution $p(\beta)$ shown in Fig. 8.

ACKNOWLEDGEMENTS

The authors are indebted to Professor K. H. Beckurts for advice and encouragement in the course of this work. F. Carvalho delivered invaluable help in the processing of the data. The technical assistance of Miss G. Zipf and H. D. Jünger is acknowledged.

REFERENCES

[1] CARVALHO, R. et al., Study Group Meeting on Research Reactor Experimental Techniques (Bucharest, Oct. 1964).
[2] KRÜGER, G. and DIMMLER, G., EANDC Conf. on Automatic Acquisition and Reduction of Nuclear Data, Gesellschaft für Kernforschung m.b.H., Karlsruhe (July 1964) 149.
[3] EGELSTAFF, P. A. and SCHOFIELD, P., Nucl. Sci. Engng. 12 (1962) 260.
[4] KRIEGER, T. J. and NELKIN, M. S., Phys. Rev. 106 (1957) 290.
[5] HUGHES, D. J. et al., Phys. Rev. 119 (1960) 872.
[6] VOLKIN, H. C., Phys. Rev. 113 (1959) 866.
[7] BOFFI, V. C., MOLINARI, V. G. and PARKS, D. E., Inelastic Scattering of Neutrons in Solids and Liquids I IAEA, Vienna (1963) 285-95.
[8] FRUHLING, A., Ann. Phys. 6 (1951) 401.
[9] McREYNOLDS, A. W. et al., General Atomics Rpt. GA-471, Chapter 3 (1958).

DISCUSSION

G. KOSÁLY: I should like to make two points. First, you stated in your oral presentation that the assumptions of the Sachs-Teller mass-tensor theory are satisfied by your experiment. However, I do not think that this is the case. High energy and high temperature are the validity conditions for the mass-tensor concept only as far as integral cross-sections are concerned. In the theory of the scattering law, the mass-tensor concept can be used only for high-momentum transfers, and this is just what you have found in your experiments. Secondly, you have used a "benzene gas" model described by Boffi et al. If I remember correctly, their effective mass is said not to be the same as that of Krieger and Nelkin. We looked into this matter and found that their true value for effective mass was 21 M, and not 15 M, as erroneously given in their paper, and this is just the value given by the Krieger-Nelkin formulation. Don't you think that the use of the true value might help to improve the theoretical curves?

W. GLÄSER: I do not believe that the effective mass exerts a strong influence on the curves I showed. Much more important at high α-values is the number of terms in the phonon expansion to be taken into account. At lower α-values the actual form of motion of the particles (for example, torsional vibrations) may be important.

PROTON MOTIONS IN ACID AQUEOUS SOLUTIONS

H. STILLER
KERNFORSCHUNGSANLAGE JÜLICH, FEDERAL REPUBLIC OF GERMANY
AND
CENTRE D'ÉTUDES DE L'ÉNERGIE NUCLÉAIRE, MOL, BELGIUM

(Presented by H. Hahn)

Abstract — Résumé — Аннотация — Resumen

PROTON MOTIONS IN ACID AQUEOUS SOLUTIONS. The incoherent scattering function, $S_{inc}(\vec{Q}, \omega)$, is measured for liquid and solid aqueous solutions of HF and NH_4F in the region $0.8\ Å^{-1} < Q < 1.6\ Å^{-1}$ and $-0.9\ meV < \hbar\omega < +1.2\ meV$. Discrete energy transfers, corresponding to frequencies of the order of $2 \times 10^{11}\ s^{-1}$, are found in all HF solutions and in the solid solution of NH_4F. The results are compared to earlier results obtained with water. The observed transitions are interpreted as fluctuations of protons between equivalent hydrogen bonding sites.

MOUVEMENT DES PROTONS DANS LES SOLUTIONS AQUEUSES D'ACIDES. La fonction de diffusion incohérente $S_{inc}(\vec{Q}, \omega)$ est mesurée pour des solutions aqueuses liquides et solides de HF et NH_4F dans les régions $0,8\ Å^{-1} < Q < 1,6\ Å^{-1}$ et $-0,9\ meV < \hbar\omega < 1,2\ meV$. Dans toutes les solutions de HF et dans la solution solide de NH_4F, on a observé des transferts d'énergie discontinus, correspondant à des fréquences de l'ordre de $2.10^{11} s^{-1}$. Les résultats sont comparés aux données obtenues antérieurement pour l'eau. L'auteur conclut que les transitions observées correspondent à des fluctuations de protons entre des points équivalents de liaison par l'hydrogène.

ДВИЖЕНИЯ ПРОТОНОВ В КИСЛОТНЫХ ВОДНЫХ РАСТВОРАХ. Функция некогерентного рассеяния $S_{inc}(\vec{Q}, \omega)$ измерена для жидких и твердых водных растворов HF и NH_4F в области $0{,}8\ Å^{-1} < Q < 1{,}6\ Å^{-1}$ и $-0{,}9$ мэв $< \hbar\omega < +1{,}2$ мэв. Во всех растворах HF и в твердом растворе NH_4F обнаружена дискретная передача энергии, соответствующая частотам порядка $2 \cdot 10^{11}$ сек $^{-1}$. Эти результаты сопоставляются с результатами, полученными ранее для воды. Наблюдаемые переходы рассматриваются как флуктуации протонов между положениями с эквивалентными водородными связями.

MOVIMIENTOS PROTÓNICOS EN SOLUCIONES ÁCIDAS ACUOSAS. Se ha medido la función de dispersión incoherente, $S_{inc}(\vec{Q}, \omega)$, para soluciones acuosas líquidas y sólidas de HF y de NH_4F en el intervalo $0,8\ Å^{-1} < Q < 1,6\ Å^{-1}$ y $-0,9\ meV < \hbar\omega < +1,2\ meV$. En todas las soluciones de HF y en la solución sólida de NH_4F se observan transferencias de energía discretas, correspondientes a frecuencias del orden de $2 \cdot 10^{11}\ s^{-1}$. Los resultados se comparan con otros datos obtenidos anteriormente para el agua. Las transiciones observadas se interpretan como fluctuaciones de protones entre puntos equivalentes de enlace hidrógeno.

INTRODUCTION

Several cold neutron experiments [1-4] have indicated small discrete energy transfers, of about 7×10^{-4} eV, in the scattering from water. The nature of these transitions is still unknown. The present experiments were carried out in view of the possibility that the observed energy transfers have their origin in motions of individual protons rather than in molecular motions. As the transitions then might be related to the bulk mobility of protons, an investigation with acid aqueous solutions was started, because it is known that the presence of OH_3 ions increases the proton mobility.

EXPERIMENTAL RESULTS

The experiments were performed at the BR 1 reactor in Mol, Belgium, by means of the beryllium-filtered detector technique, for which the measured quantity is [5]

$$N(E_0, \vec{Q}) \propto \int_{-\infty}^{\infty} R(E_0 - \epsilon)\, d\epsilon \int_{0}^{E_f} T(E')\, S(\vec{Q}, \epsilon - E')\, dE', \qquad (1)$$

where E_0 is the energy of the neutrons incident on the sample, E' the energy of the scattered neutrons, E_f the filter cut-off energy, $R(E_0 - \epsilon)$ the resolution function of the apparatus, $T(E')$ the filter transmission function, $S(\vec{Q}, \epsilon - E')$ the scattering function, $\hbar\vec{Q}$ the momentum transfer and $\epsilon - E' = \hbar\omega$. At $E_0 = E_f = 5.2$ meV the full width at half maximum of the resolution function was $(1.4 \pm 0.2) \times 10^{-4}$ eV. The filtered detector method was again chosen, because it turned out to be the only technique by which a resolution sufficient for the present purpose could be obtained with the available facilities.

The measurements were carried out for liquid solutions of 5, 10 and 25 wt.% HF in H_2O and of 5 wt.% NH_4F in H_2O and for solid aqueous solutions of 10 wt.% HF and 5 wt.% NH_4F. The liquid samples were at room temperature; the solid samples were at approximately -15°C. The samples were layers, a few tenths of a millimetre in thickness, giving transmissions between 75 and 80%. The layers were contained between thin sheets of magnesium inside an aluminium cylinder, through which passed a continuous flow of nitrogen gas. The solid samples were cooled by connecting the Mg container to a bath of dry ice and acetone.

Figure 1 shows results of earlier measurements [6] on H_2O and D_2O. As with all samples the main increases of $N(E_0)$ are the integrals of Eq. (1) over the elastic peak. Due to the presence of a second filter cut-off at $E_0 = 6.35$ meV the inelastic scattering appears more clearly on the energy gain side ($E_0 < E_f$). In H_2O discrete energy transfers do appear again, but the experimental conditions did not allow improvement of the resolution and the statistics were such that it is uncertain whether there are, in the energy region covered, two or only one such of transitions. In D_2O, on the other hand, no discrete, but only a continuous increase of $N(E_0)$ is observed. This observation rules out molecular rotations, unhindered with respect to some rotation axes, as an explanation for the transition [7]. In D_2O rotational frequencies should appear shifted by a factor of approximately $2^{-\frac{1}{2}}$; such a shift would have been observable in the experiment.

Figure 2 shows the results for the three liquid H_2O-HF solutions. In all three samples a peak in $S_{inc.}(Q, \omega)$ is observed on both sides of the elastic peak. This peak in inelastic scattering is much more pronounced than the one (or either one of the two) found in pure H_2O. Its intensity as well as the frequency, at which it appears, seem to be highest for the 10 wt.% solution. Figure 3 shows the dependence on the scattering angle ϕ for the 5 wt.% solution.

Figure 4 shows results for a liquid aqueous solution of 5 wt.% NH_4F. In contrast to the HF solutions a very large broadening of the elastic peak

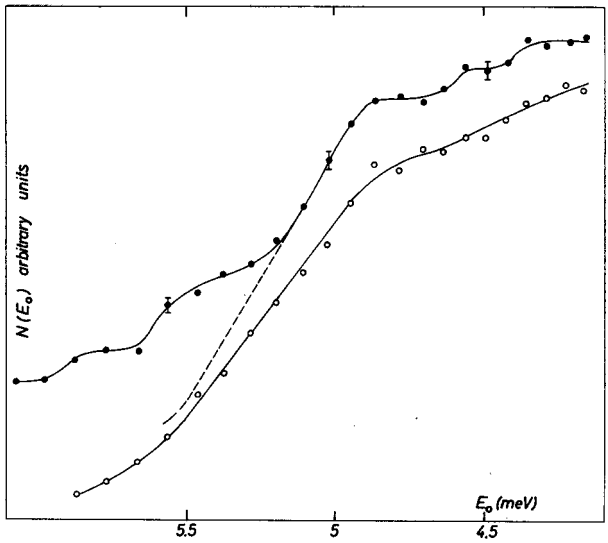

Fig. 1

Experimental results for H_2O and D_2O in the region -0.9 meV $< \hbar\omega < +1.1$ meV

● H_2O $\phi = 60°$
○ D_2O $\phi = 45°$

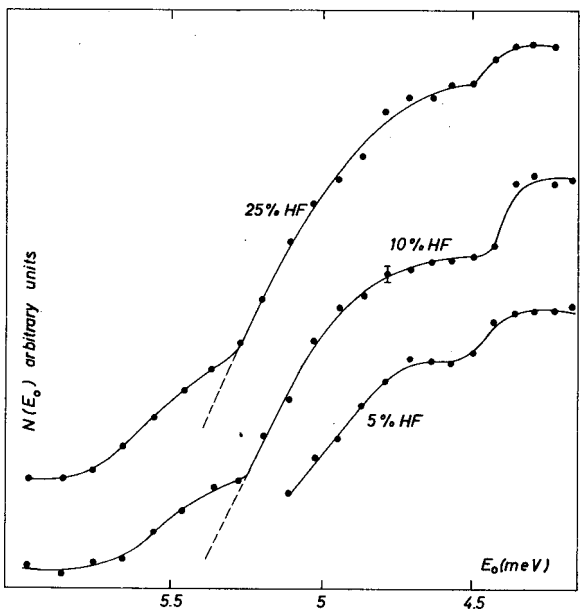

Fig. 2

Experimental results for three liquid HF-H_2O solutions
-0.8 meV $< \hbar\omega < +1.1$ meV

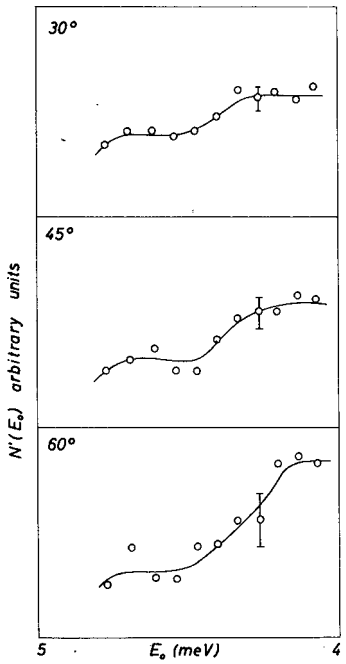

Fig. 3

The integrated peak of inelastic scattering in the 5 wt. % HF solution, observed in energy gain for three scattering angles $N'(E_0) = N(E_0)$ divided by the integrated elastic peak.

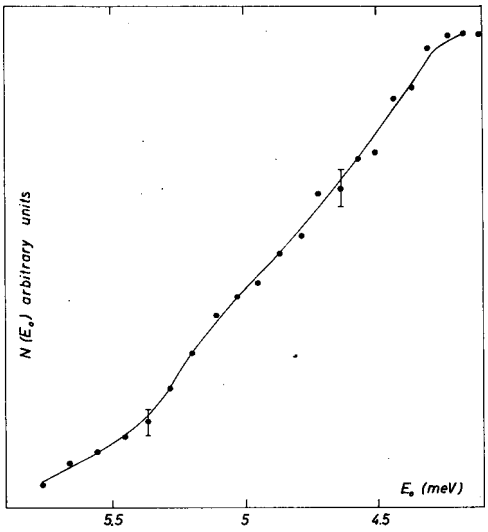

Fig. 4

Experimental results for a liquid aqueous solution of 5 wt. % NH_4F
-0.7 meV $< \hbar\omega < +1.2$ meV; $\phi = 60°$

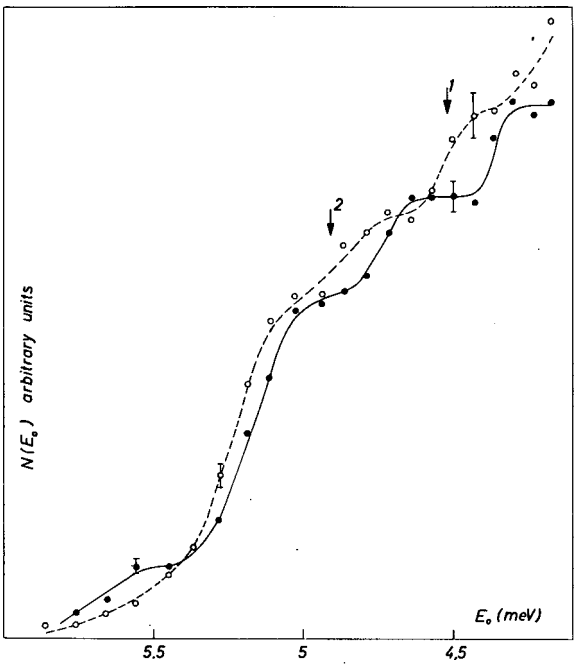

Fig. 5

Experimental results for solid aqueous solutions of 5 wt.% NH_4F and 10 wt.% HF
-0.7 meV $< \hbar\omega < +1.1$ meV

○ 5% NH_4F $\phi = 55°$
● 10% HF $\phi = 60°$

is observed; within this broadening no discrete increase can be detected. Preliminary measurements have indicated a similar behaviour for other NH_4F concentrations.

Figure 5 shows results for a solid aqueous solution of 10 wt.% HF and preliminary results for a solid solution of 5 wt.% NH_4F. For the HF solution there appear two discrete energy transfers with, taken together, even more intensity than at the one transfer observed for the same substance in the liquid state. The data may not allow a decision as to how well the lower increase, at $E_0 = (4.75 \pm 0.05)$ meV ($\hbar\omega = 0.45$ meV), is separated from the elastic peak, but the presence of inelastic scattering with a sharp fall-off in the region 4.65 meV $> E_0 >$ 4.40 meV cannot be doubted. For the NH_4F solution there appears again a large amount of apparently continuous inelastic scattering. Yet a discrete increase, indicated by arrow 1, is also seen. There is an indication of a second single increase, at the position of arrow 2; its existence cannot be established, however, within the statistics of the measurement.

The data, $N(E_0)\Delta E_0$, given in the figures are calculated from the measured $N(\theta)\Delta\theta$, where θ is the Bragg angle of a monochromizing Ther-

mica crystal. They are normalized to constant incident flux[1] and corrected for background, measured with the empty containers.

DISCUSSION

The most striking aspects of the experimental results are (i) that the discrete energy transfers appear in the HF solutions with much higher intensity than in water and (ii) that they also appear in solid solutions of HF and NH_4F. The different behaviour of the liquid NH_4F solution probably indicates that the presence of NH_3 molecules changes many parts of the internal dynamics of the liquid. Investigations with respect to this problem are in progress; we will, therefore, exclude this sample from the present discussion.

The fact that also the proton mobility, investigated for instance by conductivity, relaxation and nuclear magnetic resonance measurements, is increased in acid solutions suggests a relation between the transitions observed here and the motions of individual protons.

The anomalous proton mobility in aqueous substances is generally supposed to be a consequence of the structure of ice [8], which probably is retained within the short range order of water and also in many acid solutions. The structure is characterized by hydrogen bonds: each O-H arm is oriented towards a neighbouring oxygen atom, so that there is, in the absence of defects, one proton on each line connecting two neighbouring oxygens, in a distance of 0.99 Å from one and of 1.77 Å from the other. The lines connecting neighbouring oxygens form closed rings as indicated schematically (in one plane) in Fig. 6.

Within the lattice the sites marked in Fig. 6 by small open circles are obviously equivalent to the sites marked by solid points. This fact has been used to explain the high zero point entropy of ice [9]. Neutron diffraction measurements on heavy ice [10] have indeed shown that the protons are equally distributed on the two equilibrium positions. It seems, therefore, possible that they actually may fluctuate between the two sites; such fluctuations are assumed to be part of the mechanism of the proton mobility [8]. The transitions may occur quite frequently, if, for these, several protons are correlated. If for instance the six protons within the ring of Fig. 6 perform the transition simultaneously, then the process involves no effective dissociation. In acid solutions such correlations may not be strictly required, because here, as indicated in Fig. 7, the transitions may represent effectively only migrations of OH_3 ions. This provides one reason for the higher proton mobility in such solutions.

The strongest evidence for the occurrence of fluctuations between the two sites has been observations on the line widths of O-H and O-D stretching vibrations [11]. In infrared spectra of solid H_2O, D_2O and solutions of HOD in H_2O and D_2O the widths of the O-H vibration frequencies were found to be much larger than those of O-D vibrations. The widths appeared to depend exponentially on the mass. The comparison indicated for the state $\nu_{OH} = 3275\ cm^{-1}$ a mean lifetime of 4.2×10^{-11} s. If the transitions occur

[1] For details about the normalization see [5].

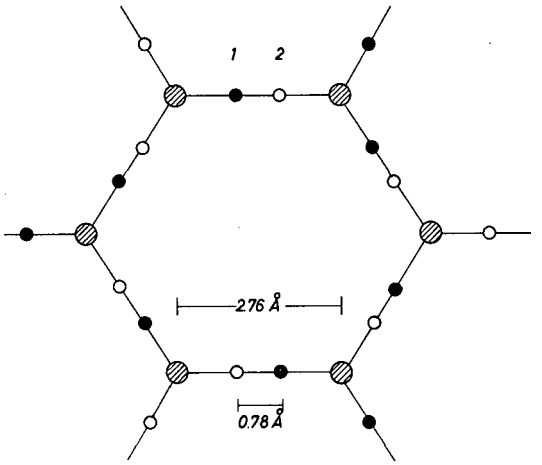

Fig. 6

Schematic representation of the ring structure of ice
The large shaded circles represent oxygen atoms, the solid points represent protons at sites 1. The small open circles indicate equivalent lattice sites (labelled 2) for the protons.

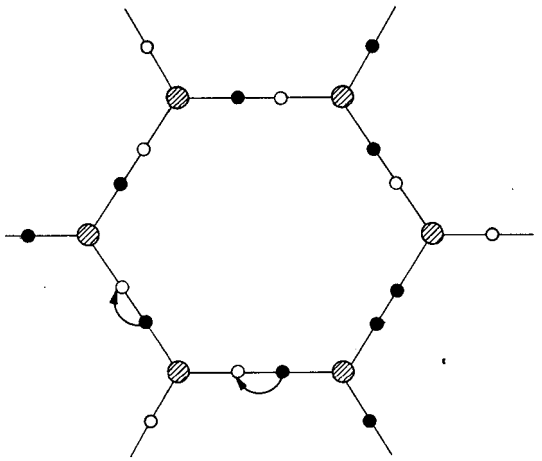

Fig. 7

The structure of Fig. 6 with one excess proton
The arrows indicate a mechanism for migration of the ionic state.

with such frequencies, a tunnel mechanism must be assumed. Such a mechanism is also suggested by the observed exponential mass dependence. The transitions are then associated with defined frequencies.

Unfortunately quantum mechanical calculations on the tunnel frequency [11, 12] are not very relevant in this case, for three reasons. In the first place the potential at the site momentarily not occupied by the proton is unknown. Secondly it is difficult to take into account the O-O vibrations, which may increase the transition frequency considerably [11]. Finally the actual

range of eventual correlations is unknown. It seems worthwhile, therefore, to describe the process more phenomenologically.

We consider a time, long compared to the period of the proton vibrations at the sites 1 and 2, but short compared to ω_0^{-1}, if ω_0 is the frequency of the transition between the two sites. For the case in which the proton is located at, say, position 1, at the beginning, the probability of finding it at time t at a position $\vec{r}$ between two neighbouring oxygens is given by the following equation:

$$\rho_s(\vec{r}, t) = \langle \rho_1(\vec{r}) \rangle \cos^2 \frac{\omega_0 t}{2} + \langle \rho_2(\vec{r}) \rangle \sin^2 \frac{\omega_0 t}{2}, \tag{2}$$

where $\langle \rho_1(\vec{r}) \rangle$ is the mean density distribution around site 1 and $\langle \rho_2(\vec{r}) \rangle$ the mean density distribution around site 2. In a first approximation we may set

$$\begin{aligned} \langle \rho_1(\vec{r}) \rangle &= \left(\frac{\alpha}{2\pi}\right)^{3/2} \exp\left[-\alpha(\vec{r} - \vec{R}_1)^2\right], \qquad \alpha = \frac{M\omega_1^2}{2k_B T} \\ \langle \rho_2(\vec{r}) \rangle &= \left(\frac{\beta}{2\pi}\right)^{3/2} \exp\left[-\beta(\vec{r} - \vec{R}_2)^2\right], \qquad \beta = \frac{M\omega_2^2}{2k_B T}, \end{aligned} \tag{3}$$

where M is the effective proton mass and ω_1 and ω_2 are the frequencies of the vibrational motions at the sites 1 and 2, respectively. $\vec{R}_1$ and $\vec{R}_2$ are the equilibrium positions. In ice one has $R = |\vec{R}_1 - \vec{R}_2| = 0.78$ Å.

From Eqs. (2) and (3) it follows that

$$\begin{aligned} G_s(\vec{r}, t) &= \frac{1}{N} \int d\vec{r}\,' \langle \rho_s(\vec{r}\,', 0)\, \rho_s(\vec{r}\,' + \vec{r}, t) \rangle \\ &= \frac{N^{-1}}{2(2\pi)^3} \int d\vec{r}\,' \Big\{ \alpha^{3/2} \exp\left[-\alpha(\vec{r}\,' - \vec{R}_1)^2\right] \Big(\alpha^{3/2} \exp\left[-\alpha(\vec{r}\,' - \vec{R}_1 + \vec{r})^2\right] \cos^2 \frac{\omega_0 t}{2} \\ &\quad + \beta^{3/2} \exp\left[-\beta(\vec{r}\,' - \vec{R}_2 + \vec{r})^2\right] \sin^2 \frac{\omega_0 t}{2} \Big) \\ &\quad + \beta^{3/2} \exp\left[-\beta(\vec{r}\,' - \vec{R}_2)^2\right] \Big(\beta^{3/2} \exp\left[-\beta(\vec{r}\,' - \vec{R}_2 + \vec{r})^2\right] \cos^2 \frac{\omega_0 t}{2} \\ &\quad + \alpha^{3/2} \exp\left[-\alpha(\vec{r}\,' - \vec{R}_1 + \vec{r})^2\right] \sin^2 \frac{\omega_0 t}{2} \Big) \Big\} \end{aligned}$$

With this self-correlation function one obtains, after averaging over all directions of $\vec{R}$,

$$S_{inc.}(\vec{Q},\omega) = \frac{N}{(2\pi)^2}\int G_s(\vec{r},t)\exp[i(\vec{Q}\cdot\vec{r} - \omega t)]\, d\vec{r}\, dt$$

$$= \frac{1}{32(2\pi)^5}\left\{\left(e^{-Q^2/2\alpha} + e^{-Q^2/2\beta} + 3\exp\left[-\frac{Q^2}{2}\left(\frac{1}{2\alpha}+\frac{1}{2\beta}\right)\right]\frac{\sin QR}{QR}\right)\delta(\omega)\right.$$

$$\left. + \left(e^{-Q^2/2\alpha} + e^{-Q^2/2\beta} - \exp\left[-\frac{Q^2}{2}\left(\frac{1}{2\alpha}+\frac{1}{2\beta}\right)\right]\frac{\sin QR}{QR}\right)[\delta(\omega-\omega_0)+\delta(\omega+\omega_0)]\right\} \quad (4a)$$

If the protons are correlated in the transition in a way as described above, one has $\omega_1 \simeq \omega_2$, i.e. $\alpha = \beta$, so that $S_{inc.}$ becomes

$$S_{inc.}(\vec{Q},\omega) = \frac{\exp[-Q^2/2\alpha]}{32(2\pi)^5}\left\{\delta(\omega)\left[2+3\frac{\sin QR}{QR}\right]\right.$$

$$\left. + [\delta(\omega-\omega_0)+\delta(\omega+\omega_0)]\left[2-\frac{\sin QR}{QR}\right]\right\}. \quad (4b)$$

We have neglected any damping of the fluctuations. In reality, in particular in liquids, damping must be expected; it gives finite widths to the peaks at $\omega = \pm\omega_0$.

Equations (4) show that with the considered transition, $S_{inc.}(\vec{Q},\omega)$ depends on Q not only by the Debye-Waller factor of the thermal clouds at the two sites but also by an additional dependence similar to a diffraction pattern. The dependence indeed represents a diffraction, in spite of the

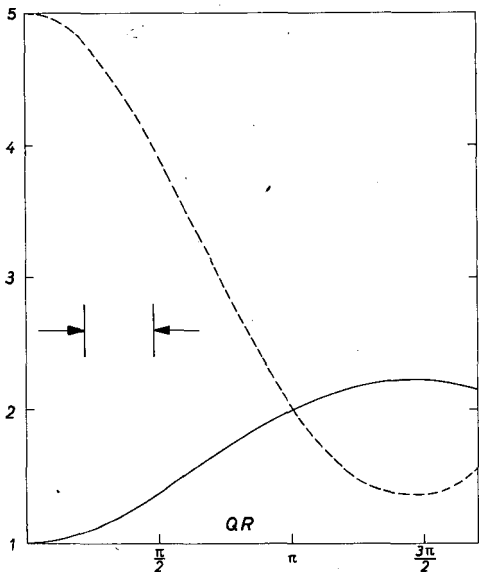

Fig. 8

Values of the functions [2 -(sin QR/QR)] (solid curve) and [2 + 3(sin QR/QR)] (dashed curve) The arrows indicate the region covered with the present experiment. (R = 0.78 Å)

proton scattering being incoherent, owing to the distribution of one proton on two lattice sites.

Figure 8 shows the functions [2 + 3(sinQR/QR)] (dashed curve) and [2 -(sinQR/QR)] (solid curve); the arrows indicate the region covered with the present experiments (R = 0.78 Å). Unfortunately it will be difficult to test the predicted Q-dependence for $QR \gtrsim 3\pi/2$, at which point the ratio of the intensity of the two inelastic peaks to the intensity of the elastic peak should go through a maximum. In particular with the filtered detector method the required large Q-values are unattainable. An increase of the intensity ratio with increasing Q is observed (Fig. 3) in agreement with Eq. (4) for the covered Q-region.[2] Such an increase of discrete energy transfers close to the elastic peak also has been observed by LARSSON et al. [2] in water.

The experimental results thus agree with the above phenomenological description of tunnel transitions at hydrogen bonding sites, at least for the liquid HF-H_2O solutions. The agreement may be considered as a further indication that this motion is the one actually observed.[3] The tunnel frequency would then be of the order of 2×10^{11} s^{-1}. As it decreases exponentially with the particle mass the disappearance of the effect in D_2O is understandable. (See Table I for the exact measured values of ν_0.)

TABLE I

FREQUENCIES OF OBSERVED ENERGY TRANSFERS

	ν_0 (10^{11} s^{-1})
H_2O-5% HF (liquid)	1.8 ± 0.1
H_2O-10% HF (liquid)	2.0 ± 0.1
H_2O-25% HF (liquid)	1.8 ± 0.15
H_2O-10% HF (solid)	1.0 ± 0.2 2.0 ± 0.1
H_2O-5% NH_4F (solid)	1.6 ± 0.3

[2] We do not, with the present experimental data, compare absolute values of the intensity ratios for two reasons. In the first place this would require a knowledge of the entire frequency distributions, and damping, as well as possible multiple transitions, would have to be taken into account. Secondly for the acid solutions exact values of R are not known.

[3] In an earlier paper [6] a different phenomenological description has been proposed, based on the assumption that within a certain time interval the self-correlation obeys a wave equation. Experimental observations with liquid HF aqueous solutions partly seemed to confirm this description, but there remained some disagreement, in particular with respect to the Q-dependence of $S_{inc.}$. Moreover, it seems doubtful whether by the considered tunnel transitions protons may actually propagate, as suggested by a wave equation, to an extent observable in neutron measurements.

The simple description, of course, cannot explain the appearance of more than one frequency, as observed in the solid HF solution and perhaps in water. For the HF solution it may be that within a rigid lattice one has, due to the distribution of OH_3 ions, a distribution of two or even more distances R and correspondingly of different valence frequencies. For other reasons the same may be true for the structure of water. But it is also possible, of course, that the second frequency has an entirely different origin, not related to the process considered here.

ACKNOWLEDGEMENTS

The author is indebted to Dr. H. Hahn for many helpful discussions and to Messrs. F. Fredel and R. Lechner for assistance with the experiments.

REFERENCES

[1] HUGHES, D., PALEVSKY, H., KLEY, W. and TUNKELO, E., Phys Rev. Lett. 3 (1959) 91.
[2] LARSSON, K., HOLMRYD, S. and OTNES, K., Inelastic Scattering of Neutrons in Solids and Liquids, IAEA, Vienna (1961) 329-41.
[3] STILLER, H. and DANNER, H., Inelastic Scattering of Neutrons in Solids and Liquids, IAEA, Vienna (1961) 363-73.
[4] BAJOREK, A., GOLIKOV, V., ZUKOWSKA, J., SHAPIRO, F., SZKATULA, A. and JANIK, J., Inelastic Scattering of Neutrons in Solids and Liquids I IAEA, Vienna (1963) 383-88.
[5] STILLER, H. and HAUTECLER, S., Z. Phys. 166 (1962) 393.
[6] STILLER, H., Physica 30 (1964) 93.
[7] YIP, S. and OSBORN, R., Phys. Rev. 130 (1963) 1860.
[8] BERNAL, J. and FOWLER, R., J. Chem. Phys. 1 (1933) 515.
[9] PAULING, L., J. Amer. chem. Soc. 57 (1935) 2680.
[10] WOLLAN, E., DAVIDSON, W. and SHULL, C., Phys. Rev. 75 (1949) 1348; PETERSON, S. and LEVY, H, Acta cryst. 10 (1957) 70.
[11] HAAS, C. and HORNIG, D., J. Chem. Phys. 32 (1960) 1763.
[12] CONWAY, B., BOCKRIS, J. and LINTON, H., J. Chem. Phys. 24 (1956) 834.

DISCUSSION

I.V.V. RAGHAVACHARYULU: Since proton tunnelling may have an important role to play in life processes (in the DNA molecule), as suggested by P.O. Löwdin of the quantum chemistry group at Uppsala, can you say conclusively that it exists in hydrogen bonds? And if it does, is there any proposal for studying molecules of real biological importance?

H. HAHN: I don't think we can definitely conclude that the peaks Dr. Stiller saw are due to proton tunnelling, as he only has a few points on their angle dependence. All we can say is that his experiments do not contradict such a proposition. As for the DNA tunnelling, Dr. Stiller and his group are planning to do some neutron work on this and related problems in molecular biology.

LIQUID HELIUM DISPERSION CURVE AT LARGE MOMENTUM

A. D. B. WOODS
CHALK RIVER NUCLEAR LABORATORIES, CHALK RIVER, ONTARIO, CANADA

(Presented by G. Dolling)

Abstract — Résumé — Аннотация — Resumen

LIQUID HELIUM DISPERSION CURVE AT LARGE MOMENTUM. Previous neutron inelastic scattering measurements of the energy (ϵ) versus momentum (p) dispersion curve for the elementary excitations in liquid helium II extended as far as $p/\hbar = 2.68$ Å^{-1}. For this value of momentum there was a strong suggestion that $d\epsilon/dp \to 0$ with a limiting value of $\epsilon = 2\Delta$, where Δ is the excitation energy at the minimum (the so-called "roton" minimum) of the dispersion curve. Such behaviour had been predicted by Pitaevskii who showed that a possible limiting form for the dispersion curve was $\epsilon(p) \to 2\Delta - \alpha \exp[-a/(p_c - p)]$ where α, a, and p_c are undetermined parameters. The parameter p_c, the value of p at which the dispersion curve terminates, must be less than $2p_0$, where p_0 is the value of p for which $\epsilon = \Delta$, i.e. at the roton minimum. At the same time the intensities of the one-quantum neutron groups tend to zero as $(2\Delta - \epsilon)\ln^2[a/(2\Delta - \epsilon)]$.

A new series of experiments performed with the rotating crystal spectrometer at Chalk River has covered the momentum range 1.8 Å$^{-1} < p/\hbar < 4$ Å^{-1}. Qualitatively the experimental results agree with the predicted behaviour; the dispersion curve levels off and has a limiting energy of approximately 2Δ, and the intensities of the one-quantum neutron groups rapidly approach zero at large p, the intensity at $p/\hbar = 3.35$ Å^{-1} being ~1% of the intensity at $p/\hbar = 1.91$ Å^{-1}. A quantitative comparison between theory and experiment is more difficult. The theoretical expressions contain three arbitrary parameters, in addition to 2Δ, in such a way that it is difficult to determine them uniquely. There is a strong suggestion, however, that the maximum observed excitation energy ($\epsilon_{max} = (17.9 \pm 0.6)$°K) does exceed $2\Delta(\Delta = (8.65 \pm 0.04)$°K) but only by an amount which is at the limit of experimental error. The intensity measurements are not sufficiently accurate for detailed comparison with theory.

COURBE DE DISPERSION DE L'HÉLIUM LIQUIDE POUR LES GRANDES VALEURS DU TRANSFERT DE LA QUANTITÉ DE MOUVEMENT. Les mesures antérieures par diffusion inélastique des neutrons de la courbe de dispersion énergie (ϵ) en fonction de quantité de mouvement (p) pour les excitations élémentaires dans l'hélium liquide II avaient été poussées jusqu'à $p/\hbar = 2,68$ Å^{-1}. Pour cette valeur de la quantité de mouvement, il y avait tout lieu de penser que $d\epsilon/dp$ tend vers 0, avec une valeur limite de $\epsilon = 2\Delta$, Δ étant l'énergie d'excitation au minimum de la courbe de dispersion (appelé minimum « roton »). Ce comportement avait été prévu par Pitaevskii, qui a montré qu'une forme limite de la courbe de dispersion pouvait être $\epsilon(p) \to 2\Delta - \alpha \exp[-a/(p_c - p)]$, où α, a et p_c sont des paramètres indéterminés. Le paramètre p_c, valeur de p pour laquelle il y a coupure de la courbe de dispersion, doit être inférieur à $2\,p_0$, p_0 étant la valeur de p pour laquelle $\epsilon = \Delta$, c'est-à-dire au minimum « roton ». Simultanément, les intensités des groupes de neutrons monoquantiques tendent vers zéro comme $(2\Delta - \epsilon)\ln^2[a/(2\Delta - \epsilon)]$.

Une nouvelle série d'expériences à l'aide du spectromètre à cristal rotatif de Chalk River a porté sur les valeurs de la quantité de mouvement telles que $1,8$ Å$^{-1} < p/\hbar < 4$ Å^{-1}. Les résultats expérimentaux concordent qualitativement avec le comportement prévu; la courbe de dispersion accuse un plateau, l'énergie limite est d'environ 2Δ et les intensités des groupes de neutrons monoquantiques tendent rapidement vers zéro pour une valeur élevée de p, l'intensité pour $p/\hbar = 3,35$ Å^{-1} étant sensiblement égale à 1% de l'intensité pour $p/\hbar = 1,91$ Å^{-1}. Il est plus difficile de faire une comparaison quantitative entre les valeurs théoriques et les résultats expérimentaux. Les expressions théoriques contiennent trois paramètres arbitraires en plus de 2Δ, de sorte qu'il est difficile de les déterminer séparément. Il est toutefois probable que l'énergie d'excitation maximum observée ($\epsilon_{max} = 17,9 \pm 0,6$°K) est supérieure à $2\Delta(\Delta = 8,65 \pm 0,04$°K), mais seulement d'une valeur voisine de la limite des erreurs d'expérience. Les mesures de l'intensité ne sont pas suffisamment précises pour permettre une comparaison détaillée avec les valeurs théoriques.

КРИВАЯ ДИСПЕРСИИ ЖИДКОГО ГЕЛИЯ ПРИ БОЛЬШОМ ИМПУЛЬСЕ. Предыдущие измерения кривой дисперсии в диаграмме энергии (ϵ) – импульс (p) при неупругом рассеянии нейтронов для элементарных возбуждений в жидком гелии II были распространены на диапазон $p/\hbar = 2{,}68\ \text{Å}^{-1}$. При таком значении импульса существуют явные признаки того, что $d\epsilon/dp \to 0$ при предельном значении $\epsilon = 2\Delta$, где Δ – энергия возбуждения в минимуме кривой дисперсии (так называемый минимум "ротона"). Такое поведение было предсказано Питаевским, который показал, что возможная предельная форма для кривой дисперсии имеет вид $\epsilon(p) \to 2\Delta - \alpha \exp\left[-a/(p_c - p)\right]$, где α, a и p_c – неопределенные параметры. Параметр p_c, т.е. такое значение p, при котором затухает кривая дисперсия, должен быть менее $2\,p_0$, где p_0 – величина p, для которой $\epsilon = \Delta$, т.е. при минимуме ротона. В то же самое время интенсивности одноквантовых групп нейтронов стремятся к нулю при $(2\Delta - \epsilon)\ln^2[a/(2\Delta - \epsilon)]$.

Новая серия экспериментов, выполненных с помощью спектрометра с вращающимся кристаллом в Чок-Ривер, охватывает диапазон импульсов $1{,}8\ \text{Å}^{-1} < p/\hbar < 4\ \text{Å}^{-1}$. В качественном отношении экспериментальные результаты согласуются с предсказанным поведением; кривая дисперсии выпрямляется и имеет предельную энергию приблизительно в 2Δ, а интенсивности одноквантовых групп нейтронов быстро приближаются к нулю при большом p, при этом величина интенсивности при $p/\hbar = 3{,}35\ \text{Å}^{-1}$ составляет приблизительно 1% от величины интенсивности при $p/\hbar = 1{,}91\ \text{Å}^{-1}$. Труднее провести количественное сравнение между теорией и экспериментом. В теоретических выражениях имеются три произвольных параметра, кроме 2Δ, так что трудно определить их однозначно. Однако существуют явные признаки того, что максимальная наблюдаемая энергия возбуждения ($\epsilon_{max} = (17{,}9 \pm 0{,}6)°\text{K}$) все же превышает 2Δ ($\Delta = (8{,}65 \pm 0{,}04)°\text{K}$), но только на величину, которая не выходит за пределы экспериментальной ошибки. Результаты измерения интенсивности недостаточно точны, чтобы производить подробное сравнение с теорией.

CURVA DE DISPERSION DEL HELIO LIQUIDO PARA ELEVADOS VALORES DE TRANSFERENCIA DEL IMPULSO. Las anteriores determinaciones -basadas en la dispersión inelástica de neutrones- de la curva de dispersión que representa la energía (ϵ) en función del impulso (p), en el caso de excitaciones elementales del helio líquido II alcanzaban hasta $p/\hbar = 2{,}68\ \text{Å}^{-1}$. Para este valor del impulso, había fuertes indicios de que $d\epsilon/dp \to 0$ con un valor límite $\epsilon = 2\Delta$, siendo Δ la energía de excitación en el mínimo (el denominado mínimo «rotón») de la curva de dispersión. Tal comportamiento había sido vaticinado por Pitaevskii, quien demostró que la curva de dispersión adoptaba posiblemente la forma límite $\epsilon(p) \to 2\Delta - \alpha \exp\left[-a/(p_c - p)\right]$, en la que α, a, y p_c son parámetros indeterminados. El parámetro p_c, o sea, el valor de p para el que termina la curva de dispersión, debe ser inferior a $2p_0$, siendo p_0 el valor de p para el que $\epsilon = \Delta$, esto es, el valor correspondiente al mínimo rotón. Al mismo tiempo, la intensidad de los grupos neutrónicos monocuánticos tiende a cero, lo mismo que $(2\Delta - \epsilon)\ln^2[a/(2\Delta - \epsilon)]$.

En una nueva serie de experimentos ejecutados con el espectrómetro de cristal giratorio de Chalk River, se ha estudiado el intervalo de impulsos $1{,}8\ \text{Å}^{-1} < p/\hbar < 4\ \text{Å}^{-1}$. Cualitativamente los resultados experimentales concuerdan con el comportamiento previsto; la curva de dispersión se aplana y presenta una energía límite del orden de 2Δ, y la intensidad de los grupos neutrónicos monocuánticos tiende rápidamente a cero para valores elevados de p, siendo la intensidad para $p/\hbar = 3{,}35\ \text{Å}^{-1} \sim 1\%$ de la correspondiente a $p/\hbar = 1{,}91\ \text{Å}^{-1}$. La comparación cuantitativa entre los datos teóricos y los resultados experimentales ofrece mayores dificultades. En las expresiones teóricas figuran tres parámetros arbitrarios, además de 2Δ, por lo que resulta difícil determinar su valor de manera unívoca. No obstante, hay fuertes indicios de que la energía de excitación máxima observada ($\epsilon_{max} = 17{,}9 \pm 0{,}6°\text{K}$) es, en efecto, superior a 2Δ ($\Delta = 8{,}65 \pm 0{,}04°\text{K}$), pero sólo en una cantidad cuya magnitud es del mismo orden que el límite de error experimental. La exactitud de las mediciones de intensidad no es suficiente para poder proceder a una comparación minuciosa con la teoría.

1. INTRODUCTION

The extraordinary properties of liquid helium in its superfluid phase (i.e. below 2.17°K) can be largely explained in terms of the hypothesis of LANDAU [1], namely that there exists in this phase of liquid helium a well-defined dispersion relation between the energy (ϵ) and momentum (p) of ex-

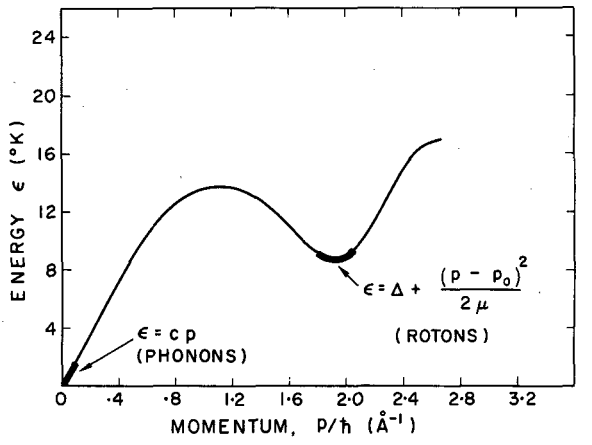

Fig. 1

The dispersion curve for excitations in liquid helium II showing the "phonon" and "roton" regions

citations above the ground state of the liquid. This curve is shown in Fig. 1. Thermodynamically, the only regions of interest at low temperatures ($T \sim 1°K$) are those near $p = 0$ and $p/\hbar \approx 1.9$ Å^{-1} (at the minimum), since these are the only states which are significantly populated. The form of the curve near zero momentum is given by $\epsilon = cp$, where c is the velocity of sound; the excitations in this region have generally been called phonons and are analogous to long wavelength phonons in a solid. Near the minimum the curve has the form $\epsilon = \Delta + (p - p_0)^2/2\mu$ where Δ is the energy gap above the ground state. The excitations in this region have been given the name of rotons and, although the implications of this name are probably not correct, it is convenient to speak in terms of the "roton minimum".

Application of the techniques of inelastic scattering of thermal neutrons to the study of this dispersion relation for the elementary excitations in liquid helium has led to very precise values for the parameters of this curve. In the experiments, the neutrons are scattered from the liquid helium specimen with the production of one or more quanta of excitation energy. Because of the requirement that both energy and momentum must be conserved in the scattering process, the one-quantum process shows up in the wavelength distribution of scattered neutrons as a sharp peak broadened only by imperfect instrumental resolution. Conservation of neutron energy gives directly the energy; conservation of momentum, the wave number of the excitation produced in the scattering process, according to the equations

$$E_0 - E' = \epsilon \tag{1}$$

$$k_0^2 + k'^2 - 2k_0 k' \cos\phi = (p/\hbar)^2 . \tag{2}$$

In these equations E_0 and E' are the energies and k_0 and k' the wave numbers of the incident and scattered neutrons, respectively, and ϕ is the angle through which the neutrons are scattered by the specimen.

The use of inelastic neutron scattering for the study of the $\epsilon(p)$ dispersion curve was suggested by COHEN and FEYNMAN [2]; experiments carried out in several laboratories [3-8] have demonstrated directly the existence of the dispersion curve and the detailed nature of its shape. In particular, some of the experiments [8] showed that at large momenta ($p/\hbar > 2.4$ Å^{-1}) the curve bends over indicating either the existence of a second maximum or a tendency to level off. PITAEVSKII [9] predicted that the dispersion curve would terminate in one of several ways. One of these has a limiting value for ϵ given by

$$\epsilon = 2\Delta - \alpha \exp[-a/(p_c - p)], \tag{3}$$

where α and a are constants and $p_c < 2p_0$. In addition he predicted that the intensities of the one-quantum neutron groups would decrease according to the formula

$$I \sim (2\Delta - \epsilon)\ln^2[a/(2\Delta - \epsilon)] \tag{4}$$

while the width of this group would not increase. For trivial experimental reasons previous experiments were confined to values of $p/\hbar \leqslant 2.68$ Å^{-1} [8] and the behaviour of the curve at large p was not determined. Accordingly a new set of experiments, specifically designed to examine this region of the dispersion curve, has been carried out under different experimental conditions. In particular, a shorter incident neutron wavelength was used which permitted the experiment to be carried out for values of $p/\hbar$ up to 4 Å^{-1}.

2. THE EXPERIMENT

The experiment was carried out using the rotating crystal spectrometer [10] at the NRU reactor, Chalk River. A schematic diagram of the spectrometer is shown in Fig. 2. Neutrons from the reactor pass through a liquid nitrogen cooled quartz filter and impinge on the rotating crystal. (The rotating collimator which makes possible order elimination and reduces background was added in the latter stages of these experiments.) Bursts of monoenergetic neutrons (whose energies are determined by the Bragg law) are scattered through the angle $2\theta_m$ and impinge on the specimen. At the specimen the neutrons are scattered through the (variable) angle ϕ and the energies of the scattered neutrons are determined by their time-of-flight from the specimen to the BF_3 detectors at a distance 3.3 m.

The specimen was a cylindrical sample of liquid helium with a diameter of 5 cm. The specimen temperature was (1.6 ± 0.1)°K.

One series of experiments was carried out over a range of ϕ from 47° to 140°. The incident neutron wavelength was 2.77 Å and was determined from the time-of-flight of the incident neutrons over known distances. A second series of experiments used an incident wavelength of 2.48 Å and a range of ϕ from 17° to 110°.

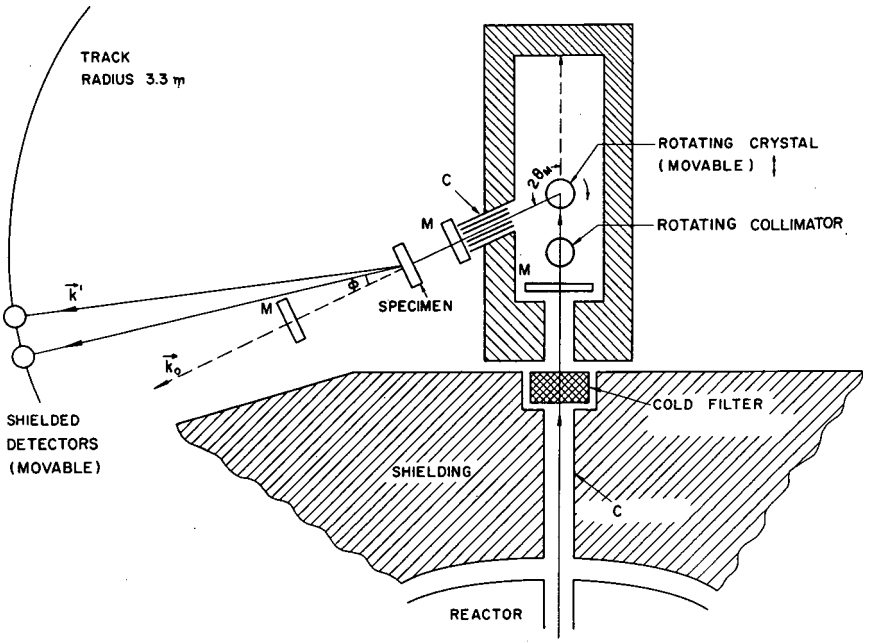

Fig. 2

Schematic diagram of the rotating crystal spectrometer
This is as described in Ref. [10] except for the rotating collimator
for order elimination and the two fission counters (designated M)
in the diffracted beam which are used for determination of the incident wavelength.

Figure 3 shows the distributions of the scattered neutrons for several different angles of scattering for each series of measurements. For values of $p/\hbar$ near the roton minimum most of the scattered intensity is in the one-quantum peak. As $p/\hbar$ increases the intensity of the one-quantum peak decreases while the intensity observed for higher energy changes increases. In particular, for the distribution at 110° using 2.48-Å incident neutrons it is not certain that a peak is observable. A definite change in the slope of the distribution is apparent at $\epsilon \approx 28°K$ and this may indicate a peak at $\epsilon \approx 24°K$. Figure 4 shows the intensity of the one-quantum peak as a function of scattering angle for the series with $\lambda_0 = 2.77$ Å. At $p/\hbar = 3.35$ Å^{-1} the integrated intensity of the one-quantum neutron group is $\sim 1\%$ of that at $p/\hbar = 2.0$ Å^{-1}.

Figure 5 shows the $\epsilon(p)$ dispersion curve derived from these measurements and compares the results with those previously obtained [8]. In the region of overlap the two sets of results are in excellent agreement with one another. The curve has a plateau at $\epsilon = 17.9°K$ for $2.7 \leq p/\hbar < 3.5$ Å^{-1} and shows a definite tendency to rise for larger values of $p/\hbar$. The results are tabulated in Table I.

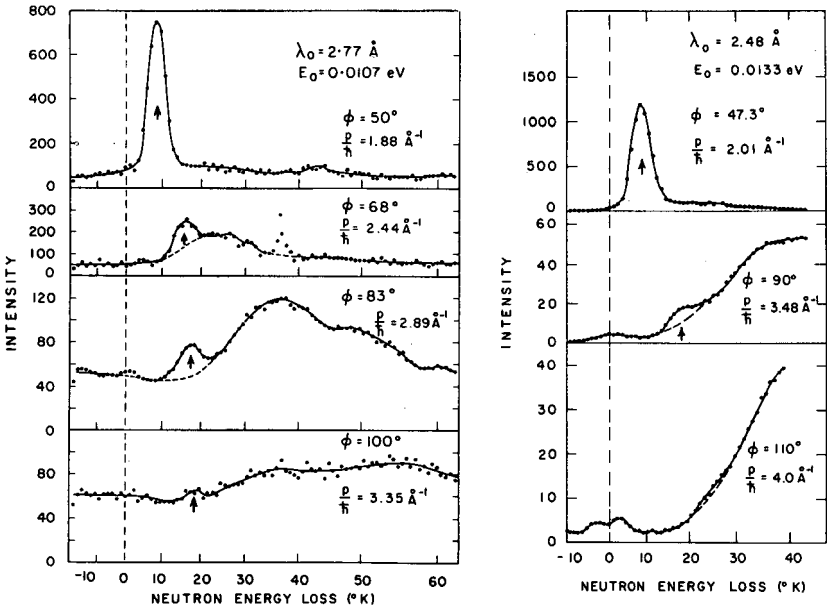

Fig. 3

Distributions of neutrons scattered from liquid helium at 1. 6°K
for several angles of scattering and for two different incident energies
The intensity scales are consistent only for each incident energy separately
and cannot be intercompared for different incident energies.

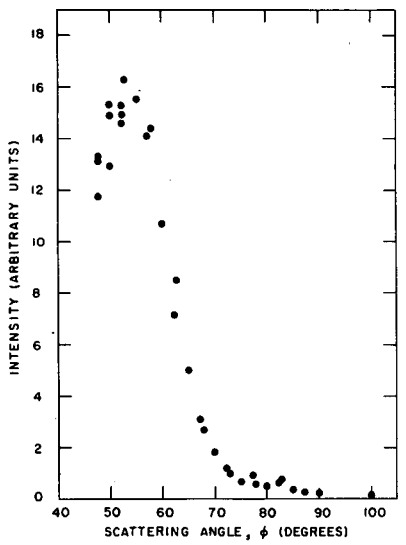

Fig. 4

The observed integrated intensity of the one-quantum peak as a function of scattering angle
$\lambda_0 = 2.77$ Å; T = 1. 6°K

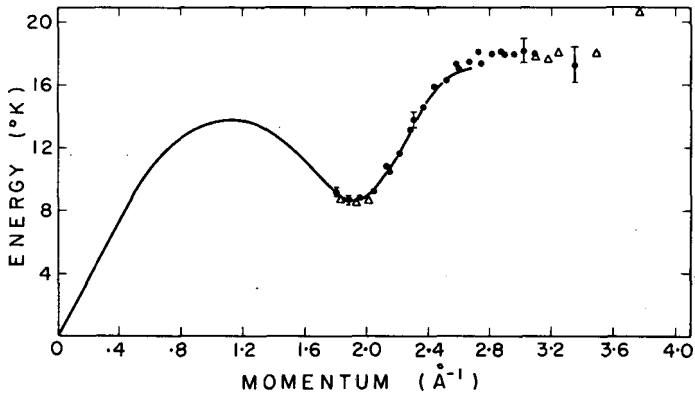

Fig. 5

The experimental results of the present investigation compared with the dispersion curve of HENSHAW and WOODS [8]

—— Henshaw and Woods

● Present results $\lambda_0 = 2.77$ Å

△ Present results $\lambda_0 = 2.48$ Å

TABLE I

ENERGIES AND MOMENTA OF EXCITATIONS IN LIQUID HELIUM AT 1.6°K

$p/\hbar$ (Å^{-1})	ϵ (°K)	$p/\hbar$ (Å^{-1})	ϵ (°K)
1.80	9.19 ± 0.3	2.59	17.1 ± 0.8
1.88	8.68 ± 0.3	2.66	17.5 ± 0.8
1.96	8.92 ± 0.3	2.72	18.1 ± 0.9
1.97	8.74 ± 0.4	2.74	17.4 ± 0.8
2.05	9.22 ± 0.4	2.81	18.0 ± 0.8
2.13	10.8 ± 0.4	2.87	18.2 ± 0.8
2.15	10.5 ± 0.5	2.89	18.0 ± 0.8
2.21	11.6 ± 0.5	2.95	18.0 ± 0.8
2.28	13.1 ± 0.5	3.01	18.2 ± 0.8
2.30	13.8 ± 0.5	3.09	17.8 ± 0.6
2.37	14.6 ± 0.5	3.17	17.6 ± 0.8
2.43	15.9 ± 0.6	3.24	18.1 ± 0.8
2.44	16.0 ± 0.7	3.35	17.3 ± 1.1
2.51	16.3 ± 0.7	3.48	18.0 ± 0.8
2.58	17.4 ± 0.9	3.76	20.6 ± 1.0

3. DISCUSSION

The observed behaviour for the dispersion curve at large momentum is in essential agreement with the theoretical predictions [9]. Some aspects of $\epsilon(p)$ in this region have also been discussed by other authors [11, 12]. It is difficult to obtain a meaningful fit to Eq. (3) because of the large number of parameters involved and the uncertainty over the range of p for which the equation is valid. The observation of the plateau with an energy of the order of 2Δ is a triumph for the theory although there is a definite suspicion that the limiting value for ϵ (17.9 ± 0.6°K) is significantly greater than 2Δ (17.3°K). It is difficult to ascertain if the width of the neutron group is larger than the resolution function of the spectrometer, but there is no reason to believe that it is. The intensities of the neutron groups approximately follow Eq. (4) if 2Δ is taken as 17.9°K, but again the number of parameters combined with the uncertainties in the experimental results make detailed comparison between theory and experiment difficult.

For $p/\hbar > 3.5$ Å^{-1} the energies corresponding to the peak positions show an increase which may indicate that the dispersion curve rises again. At these values of $p/\hbar$ such a dispersion curve may represent stable excitations [11].

The observed intensity at energies greater than that corresponding to single excitations on the dispersion curve probably represents scattering processes involving more than one excitation. Such scattering is present even for excitations near the roton minimum and is quite apparent in the distribution shown in Fig. 3 for $\phi = 50°$, $\lambda_0 = 2.48$ Å. This behaviour had been observed at large $p/\hbar$ in previous time-of-flight experiments [6] but was not as noticeable in the crystal spectrometer experiments [8]. The structure in the higher energy region of these distributions has not yet been studied in detail but at some angles contains several broad maxima and, at $\phi = 83°$, for example, (Fig. 3) extends to an energy of ~ 60°K $\approx 7\Delta$. Thus intermediate states must involve more than two excitations.

4. CONCLUSIONS

The dispersion curve for excitations in liquid helium has been shown to extend at least to values of $p/\hbar = 3.5$ Å^{-1} and possibly beyond. In the region $2.7 < p/\hbar < 3.5$ Å^{-1}, the curve has a plateau with $\epsilon = (17.9 \pm 0.6)$°K, in qualitative but not exact agreement with the predictions of PITAEVSKII [9]. For $p/\hbar > 3.5$ Å^{-1}, the curve, if it still represents a meaningful concept, shows an increase in energy. No increase in width in the one-quantum neutron groups was observed. The behaviour of the intensity of the one-quantum group is also in qualitative agreement with the theoretical prediction. These results indicate that details of the theory may need refining but the essential ideas are correct. In addition, more experimental information is needed for a complete understanding of the dispersion curve in the high momentum region.

ACKNOWLEDGEMENTS

The author would like to thank Dr. R. A. Cowley for very useful discussions. Messrs. A. L. Bell, E. A. Glaser, R. Rea and J. H. Thompson gave valuable assistance during the course of the measurements.

REFERENCES

[1] LANDAU, L., J. Phys. (USSR) 5 (1941) 71-90.
[2] COHEN, M. and FEYNMAN, R. P., Phys. Rev. 107 (1957) 13-24.
[3] PALEVSKY, H., OTNES, K., LARSSON, K.-E., PAULI, R. and STEDMAN, R., Phys. Rev. 108 (1957) 1346-47.
[4] PALEVSKY, H., OTNES, K. and LARSSON, K.-E., Phys. Rev. 112 (1959) 11-18.
[5] YARNELL, J. L., ARNOLD, G. P., BENDT, P. J. and KERR, E. C., Phys. Rev. Lett. 1 (1958) 9-11.
[6] YARNELL, J. L., ARNOLD, G. P., BENDT, P. J. and KERR, E. C., Phys. Rev. 113 (1959) 1379-86.
[7] HENSHAW, D. G., Phys. Rev. Lett. 1 (1958) 127-29.
[8] HENSHAW, D. G. and WOODS, A. D. B., Phys. Rev. 121 (1961) 1266-74.
[9] PITAEVSKII, L. P., JETP 36 (1959) 1168-78. Translation: Soviet Phys. JETP 9 (1959) 830-37.
[10] BROCKHOUSE, B. N., in Inelastic Scattering of Neutrons in Solids and Liquids, IAEA, Vienna (1961) 113-57.
[11] JACKSON, H. W. and FEENBERG, E., Rev. mod. Phys. 34 (1962) 686-93.
[12] MILLER, A., PINES, D. and NOZIERES, P., Phys. Rev. 127 (1962) 1452-64.

DISCUSSION

G. VENKATARAMAN: What type of rotating collimator was used in the experiment and how was it phased with respect to the rotating crystal?

G. DOLLING: The collimator is a simple Fermi-type chopper, about 6 cm in diameter, rotating about a vertical axis and having vertical Cd slits. It is phased with respect to the rotating crystal by means of synchronous motors.

РАССЕЯНИЕ ХОЛОДНЫХ НЕЙТРОНОВ НА ВОДЕ И НЕКОТОРЫХ ОРГАНИЧЕСКИХ ВЕЩЕСТВАХ

В.В. ГОЛИКОВ, И. ЖУКОВСКАЯ, Ф.Л. ШАПИРО,
А. ШКАТУЛА и Е. ЯНИК
ОБЪЕДИНЕННЫЙ ИНСТИТУТ ЯДЕРНЫХ ИССЛЕДОВАНИЙ, ДУБНА
СССР

Abstract — Résumé — Аннотация — Resumen

. SLOW NEUTRON SCATTERING IN WATER AND SOME ORGANIC SUBSTANCES. Results are given for measurements of quasi-elastic and inelastic scattering spectra of cold neutrons in water, ethylene glycol ($C_2H_6O_2$), benzene, acetic acid, naphthalene and dioxane. Measurements were carried out on an assembly in the pulsed IBR reactor using the time-of-flight method with flight lengths of 17 m and, in some experiments, of 45 m. The scattering angle was 75°.

Measurements in water were made over the temperature range -3 to +80°C. Data are given and discussed for expansion of the beryllium boundary. No expansion was observed for ice; the upper limit of possible expansion at -3° is $\Gamma < 10^{-5}$ eV. On transition from ice to water (+1°C), the form of the neutron scattering spectrum undergoes a noticeable change, and the frequency spectra of ice and water are accordingly quite different; in this respect, the results of these investigations differ from those of Larsson and Dahlborg for a 30° scattering angle.

Scattering in ethylene glycol was studied in the temperature range from -17 to +150°C. In the temperature region below 60°C the diffusion coefficient calculated from expansion of the beryllium boundary is considerably greater than that calculated from the viscosity, using the Stokes-Einstein formula; the latter coefficient coincides with the measurement method of spin echo. This effect, noted earlier by Larsson and Dahlborg during measurements with glycerine, is discussed from the theoretical point of view.

Measurements with the other substances were also performed over a wide temperature range including the melting point, and the authors discuss the characteristic features of quasi-elastic and inelastic scattering in these substances.

DIFFUSION DES NEUTRONS FROIDS DANS L'EAU ET DANS CERTAINES SUBSTANCES ORGANIQUES. Les auteurs exposent les résultats de mesure des spectres de diffusion quasi élastique et inélastique des neutrons froids dans l'eau, l'éthylène-glycol ($C_2H_6O_2$), le benzol, l'acide acétique, la naphtaline et le dioxane. Les mesures ont été faites, dans un dispositif rattaché au réacteur à impulsions IBR, par la méthode du temps de vol; la longueur du parcours était de 17 m ou, pour certaines expériences, de 45 m. L'angle de dispersion était de 75°.

Les mesures dans l'eau ont été faites à des températures comprises entre -3 et +80°C. Les auteurs indiquent et discutent des données sur l'élargissement de la limite relative au béryllium. Pour la glace, on n'a observé aucun élargissement; la limite supérieure de l'élargissement possible à -3°C est $\Gamma < 10^{-5}$ eV. Lors du passage de la glace à l'eau (+1°C), le spectre des neutrons diffusés change visiblement de forme et les spectres de fréquence de la glace et de l'eau accusent des différences correspondantes; à cet égard, les résultats obtenus par les auteurs se distinguent de ceux auxquels Larsson et Dahlborg sont parvenus pour un angle de dispersion de 30°.

La diffusion dans l'éthylène-glycol a été étudiée pour des températures comprises entre -17 et +150°C. A la température de 60°C ou au-dessous, le coefficient de diffusion, calculé sur la base de l'élargissement de la limite relative au béryllium, est sensiblement plus grand que le coefficient déduit de la viscosité par la formule de Stokes-Einstein, lequel coïncide avec celui qui a été calculé par la méthode de l'écho de spin. Les auteurs examinent cet effet, qui avait été observé antérieurement par Larsson et Dahlborg lors de mesures faites sur la glycérine, du point de vue des théories.

Les mesures relatives à d'autres substances ont été faites également pour une gamme étendue de températures, englobant le point de fusion. Les auteurs étudient les particularités caractéristiques de la diffusion quasi élastique et inélastique dans ces substances.

РАССЕЯНИЕ ХОЛОДНЫХ НЕЙТРОНОВ НА ВОДЕ И НЕКОТОРЫХ ОРГАНИЧЕСКИХ ВЕЩЕСТВАХ. Приводятся результаты измерений спектров квазиупругого и неупругого рассеяния холодных нейтронов в воде, этиленгликоле ($C_2H_6O_2$), бензоле, уксусной кислоте, нафталине и диоксане. Измерения проводились на установке при импульсном реакторе ИБР методом времени пролета с пролетным расстоянием 17 м и в отдельных опытах 45 м. Угол рассеяния составлял 75°.

Измерения с водой проводились в интервале температур от -3 до 80°С. Приводятся и обсуждаются данные об уширении бериллиевой границы. Для льда уширения не наблюдалось; верхняя граница возможного уширения при -3°С составляет $\Gamma < 10^{-5}$ эв. При переходе ото льда к воде (+1°С) форма спектра рассеянных нейтронов заметно изменяется, соответственно отличаются и спектры частот льда и воды; в этом отношении результаты данной работы отличаются от результатов Ларсона и Дальборга для угла рассеяния 30°.

Рассеяние в этиленгликоле изучалось в области температур -17° +150°С. В области температур 60°С и ниже коэффициент диффузии, рассчитанный по уширению бериллиевого края, значительно больше, чем рассчитанный из вязкости по формуле Стокса-Эйнштейна; последний совпадает с измеренным методом спинового эха. Этот эффект, отмеченный ранее Ларсоном и Дальборгом в измерениях с глицерином, обсуждается с точки зрения теории.

Измерения с остальными веществами также проводились в широкой области температур, включавшей температуру плавления. Обсуждаются характерные особенности квазиупругого и неупругого рассеяния в этих веществах.

DISPERSIÓN DE LOS NEUTRONES FRÍOS EN EL AGUA Y EN CIERTAS SUSTANCIAS ORGÁNICAS. Los autores presentan los resultados de las mediciones de los espectros de dispersión cuasielástica e inelástica de los neutrones fríos en agua, etilenglicol ($C_2H_6O_2$), benceno, ácido acético, naftalina y dioxano. Realizaron las determinaciones en una instalación del reactor pulsado IBR, por el método del tiempo de vuelo, siendo la trayectoria de 17 m y, en algunos casos, de 45 m. El ángulo de dispersión era de 75°.

Las mediciones en el agua se efectuaron en un intervalo de temperaturas comprendido entre -3° y +80°C. En la memoria se presentan y examinan los datos sobre el ensanchamiento de la base del espectro correspondiente al berilio. Para el hielo no se observó ensanchamiento alguno; el límite superior del ensanchamiento posible a -3°C es $\Gamma < 10^{-5}$ eV. En la transición del hielo al agua (+1°C), la forma del espectro de los neutrones dispersos cambia de manera marcada, y los espectros de las frecuencias para el hielo y el agua experimentan modificaciones de intensidad correspondiente; a este respecto, los resultados alcanzados son diferentes de los obtenidos por Larsson y Dahlborg para un ángulo de dispersión de 30°.

Los autores investigaron la dispersión en etilenglicol a temperaturas comprendidas entre -17° y +150°C. A 60° y temperaturas inferiores, el coeficiente de difusión, calculado según el ensanchamiento de la base del espectro correspondiente al berilio, es mucho mayor que el deducido de la viscosidad por la fórmula de Stokes-Einstein; este último coeficiente coincide con el calculado por el método de la resonancia del spin. Este efecto, que había sido observado anteriormente por Larsson y Dahlborg en las mediciones efectuadas en glicerina, es examinado por los autores desde el punto de vista teórico.

Efectuaron también mediciones con otras sustancias en un amplio intervalo de temperaturas, en especial en el punto de fusión. Estudiaron las características de la dispersión cuasielástica e inelástica en estas sustancias.

I. ВВЕДЕНИЕ

В последние годы выполнено большое число работ, посвященных изучению динамики молекул в различных жидкостях с помощью рассеяния холодных нейтронов [1–3].

Наибольшее число публикаций посвящено спектрам рассеяния холодных нейтронов в воде [4–8]. Интерес к воде стимулировался, в частности, результатами работ [4,5]. В этих работах, во-первых, проявились пики, соответствующие дискретным передачам очень малых порций энергии порядка 10^{-3} эв; во-вторых, наблюдаемый нейтронами коэффициент самодиффузии молекул воды в воде D был найден удивительно малым – $D < 0{,}1\ D_0$, где D_0 – коэффициент самодиффузии, измеренный классическими методами,

такими, например, как ядерный парамагнитный резонанс. В других работах [7, 8] однако, эти эффекты не наблюдались.

Для выяснения положения нами было предпринято изучение квазиупругого рассеяния нейтронов в воде с разрешающей способностью лучшей, чем использованная в предыдущих работах. Улучшение разрешения стало возможным благодаря использованию в качестве источника нейтронов импульсного быстрого реактора (ИБРа) ОИЯИ [9,10]. Измерения проводились с водой комнатной температуры. Было найдено [11], что пики, соответствующие малым дискретным передачам энергии, если и существуют, то интенсивность их очень мала — не более нескольких процентов от общей интенсивности рассеяния при данном времени пролета. Было показано, что уширение нейтронной линии при рассеянии определенно существует; если игнорировать возможное наличие малых передач энергии и считать подложку под квазиупругим пиком примерно постоянной, то наблюдаемый коэффициент диффузии равен $D = 0{,}5\ D_0$.

Представляло определенный интерес проведение подобных измерений на других водородосодержащих жидкостях, отличающихся друг от друга характером межмолекулярного взаимодействия. В настоящей работе излагаются и обсуждаются дальнейшие результаты, полученные для воды, и данные для некоторых других жидкостей, как образующих межмолекулярные водородные связи (этиленгликоль, уксусная кислота), так и не образующих подобные связи (бензол, нафталин, диоксан). Некоторое усовершенствование установки позволило распространить измерения на область больших передач энергии (неупругое рассеяние) и проводить их при различных температурах, в том числе и ниже точки плавления.

II. ОПИСАНИЕ ЭКСПЕРИМЕНТАЛЬНОГО МЕТОДА

Использованная экспериментальная установка показана на рис.1 и кратко описана в работе [12]. Быстрые нейтроны из реактора попадают на замедлитель, установленный вблизи активной зоны. Вплотную за замедлителем помещен блок бериллия длиной 32 см, являющийся фильтром холодных нейтронов. Бериллий и замедлитель охлаждаются до температуры жидкого азота. Фильтрованный пучок холодных нейтронов со средней энергией $\approx 0{,}0035$ эв и резкой границей при 0,0052 эв падает на исследуемый образец, расположенный на расстоянии ≈ 25 см от бериллия. Между бериллием и образцом находится кадмиевая заслонка, служащая для перекрывания пучка холодных нейтронов перед образцом с целью измерения фона, регистрируемого детектором.

Энергия нейтронов, рассеянных на образце на угол 75°, измеряется по времени пролета расстояния "образец-детектор" в большинстве экспериментов при помощи 1024-канального временного анализатора с шириной канала 32 мксек. В данной работе в основном использовалась пролетная база ≈ 17 м; в отдельных опытах ≈ 45 м. В качестве детектора использовался сцинтилляционный детектор площадью 2000 $см^2$ [13].

Схема контейнера, в который заключалась изучаемая жидкость, приведена на рис.2. Корпус контейнера изготовлен из толстого листа кадмия, в котором имеется углубление, глубина которого определяет толщину образца. Для уменьшения многократного рассеяния толщины образцов варь-

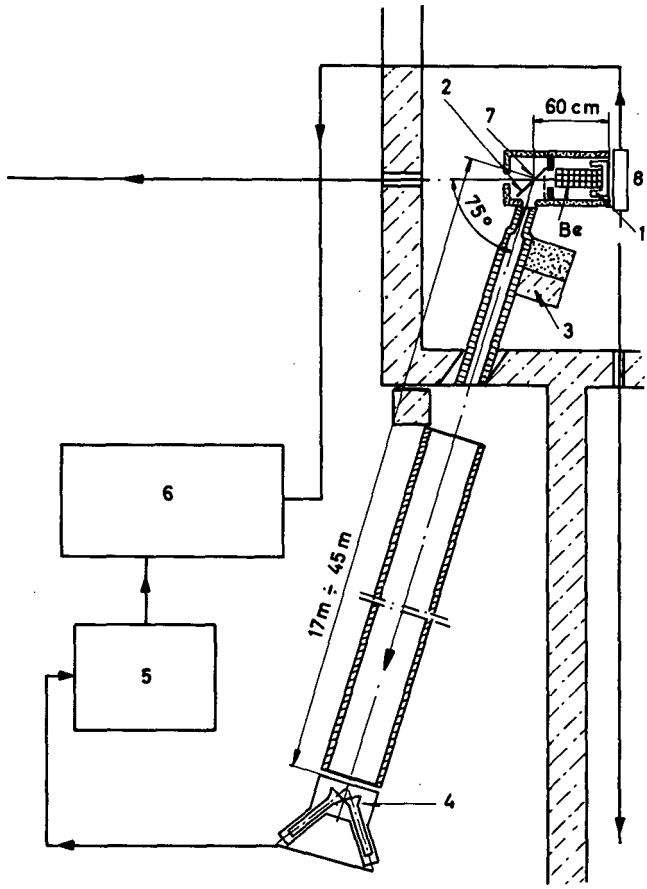

Рис.1

Схема установки при импульсном реакторе для измерений с холодными нейтронами:

1 – контейнер; 2 – образец; 3 – замедлитель и защита; 4 – сцинтилляционный детектор; 5 – дискриминатор; 6 – многоканальный анализатор; 7 – кадмиевая заслонка; 8 – парафиновый замедлитель.

ировались в пределах 0,2 – 0,7 мм; в большинстве опытов пропускание образца составляло не менее 85%. Со стороны пучка нейтронов жидкость закрывалась алюминиевой фольгой толщиной ≈ 100 микрон. Рабочая площадь образца составляла ≈ 10×15 см^2. К задней стенке кадмиевого корпуса контейнера прикреплялась система охлаждения и нагрева образца. Для нагрева образца использовалась электрическая спираль, не показанная на рис.2.

Охлаждение образца осуществлялось пропусканием потока холодного азота, поступающего из криостата с замедлителем и бериллием. Боковые и задняя поверхности контейнера покрыты тепловой изоляцией. Во избежание конденсации влаги на образце при его охлаждении ниже 0°С контей-

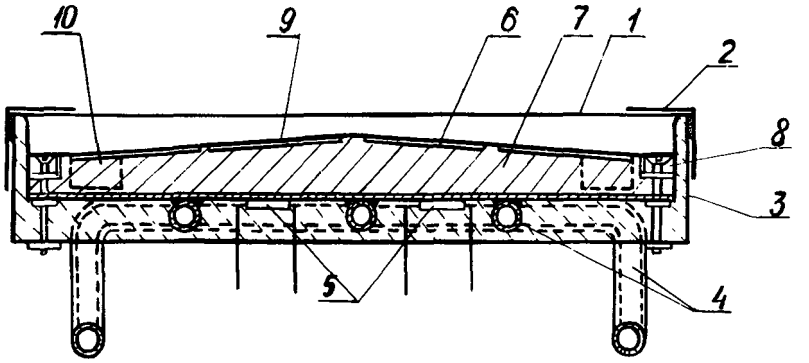

Рис.2

Схема контейнера для образца:
1 – алюминиевый кожух; 2 – кадмиевый экран;
3 – тепловая изоляция; 4 – система охлаждения образца;
5 – термосопротивления; 6 – исследуемый образец;
7 – кадмиевый корпус контейнера; 8 – вакуумное уплотнение образца;
9 – алюминиевая фольга; 10 – запасной резервуар.

нер закрыт герметичным алюминиевым кожухом толщиной ≈ 100 микрон. Регулировка поступающего для охлаждения образца потока холодного азота и регулировка нагрева образца производились автоматически, так что температура образца поддерживалась во время измерений постоянной в пределах ± 0,5°C. Пределы измерения температуры образцов составляли -20°C +200°C.

На платформе, на которой находился исследуемый образец, мог устанавливаться и второй образец (обычно ванадий). Дистанционно можно было попеременно вводить в пучок холодных нейтронов один из образцов. Периодические измерения рассеяния на ванадий использовались для контроля стабильности электронной аппаратуры и для определения спектра нейтронов, падающих на образец.

III. ЭКСПЕРИМЕНТАЛЬНЫЕ РЕЗУЛЬТАТЫ

Результаты измерений после вычитания фона с учетом теплового загрязнения пучка холодных нейтронов приводились к постоянной эффективности детектора и исправлялись на пропускание 6-миллиметрового слоя алюминия, находившегося на пути рассеянного пучка, и на ослабление пучка в воздухе (на пролетной базе участок длиной 5 м не вакуумирован). Суммарная поправка на указанные эффекты представлена на рис.3. Пик на кривой при энергии ≈ 5,1 мэв обусловлен дифракционным максимумом сечения рассеяния алюминия при этой энергии. Поправка построена на основании измерений пропускания тех самых алюминиевых листов, которые использовались в эксперименте. Это существенно, так как из-за наличия текстуры величина провала в кривой пропускания различна для разных образцов алюминия.

Некоторые из полученных таким образом нейтронных спектров приведены на рис.4–9. В измерениях использовались образцы из дважды дис-

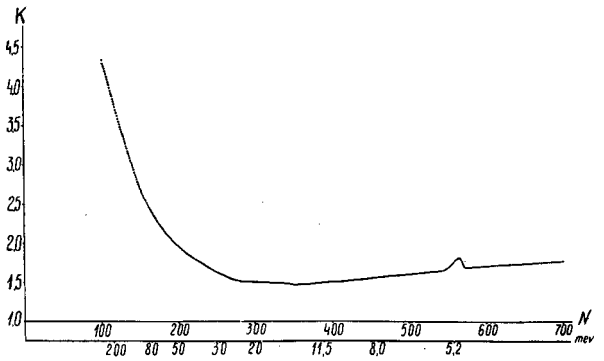

Рис.3

Кривая исправления экспериментальных данных, учитывающая эффективность детектора, пропускание алюминия и воздуха в зависимости от энергии рассеянных нейтронов и времени пролета, выраженного в номерах канала временного анализатора.

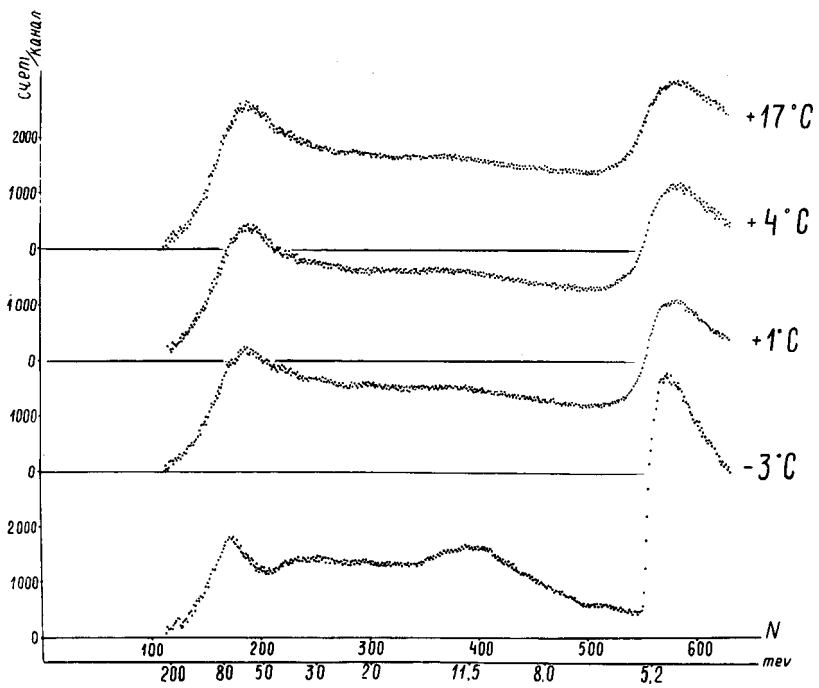

Рис.4

Спектры нейтронов, рассеянных слоем воды толщиной 0,2 мм. Расстояние от образца до детектора – 17 м. Ширина канала временного анализатора – 32 мксек.

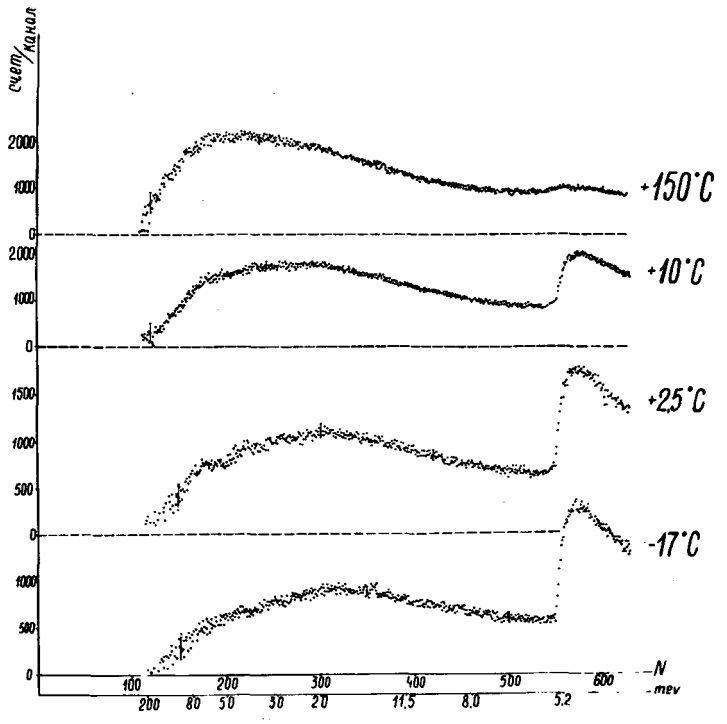

Рис.5

Спектры нейтронов, рассеянных слоем этиленгликоля толщиной 0,4 мм (температура образца -17°C и +2,5°C)и толщиной 0,7 мм (температура образца +10°C и +150°C). Расстояние от образца до детектора -17 м. Ширина канала временного анализатора — 32 мксек.

тиллированной воды, а для других жидкостей — марки "химический чистый" с дополнительным обезвоживанием; однако количественного анализа состава образцов не проводилось.

IV. КВАЗИУПРУГОЕ РАССЕЯНИЕ

В модели непрерывной диффузии молекул жидкости пик квазиупругого рассеяния моноэнергетических нейтронов имеет лоренцеву форму с полушириной [14]

$$\Gamma = 2\hbar\kappa^2 D, \qquad (1)$$

где $\hbar\vec{\kappa}$ — изменение импульса при рассеянии, D — коэффициент самодиффузии. В модели прыжковой диффузии [15] квазиупругий пик также обладает лоренцевой формой при условии, что время прыжка τ_1 много меньше

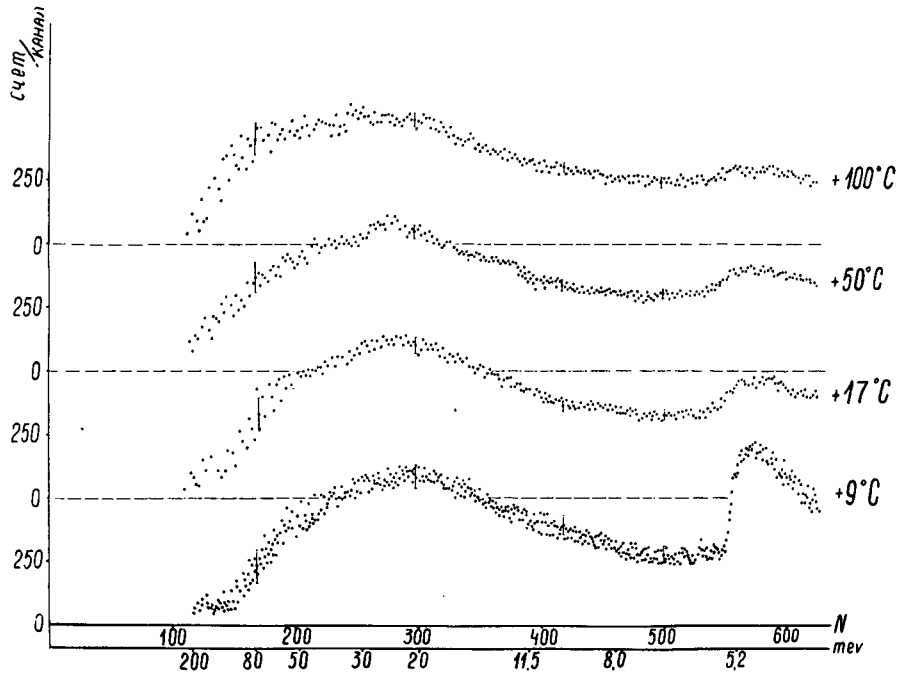

Рис.6

Спектры нейтронов, рассеянных слоем уксусной кислоты толщиной 0,25 мм. Расстояние от образца до детектора – 17 м. Ширина канала временного анализатора – 32 мксек.

времени колебательного движения τ_0. В этом случае, если средний квадрат смещения за время τ_1 много больше среднего квадрата отклонения молекулы от положения равновесия,

$$\Gamma = \frac{2h}{r_0}\left(1 - \frac{e^{-2W}}{1 + \kappa^2 D r_0}\right), \qquad (2)$$

где e^{-2W} -Дебай-Валеровский фактор.

При ступенчатой форме падающего нейтронного спектра [$F(E) = 0$ для $E > E_0$, $F(E)\,dE \approx EdE$ для $E \leq E_0$], квазиупругое рассеяние приводит к размытию границы спектра. При лоренцевой форме линии уширение границы связано с полушириной Γ соотношением [11]

$$\Gamma = \frac{8E_0}{\pi} \frac{1}{t_0/\Delta t + 5}, \qquad (3)$$

где t_0 – время пролета, соответствующее энергии E_0 бериллиевой границы, Δt – полуширина границы в шкале времени пролета (рис.10). С учетом аппаратурного разрешения Δt вычислялось по формуле

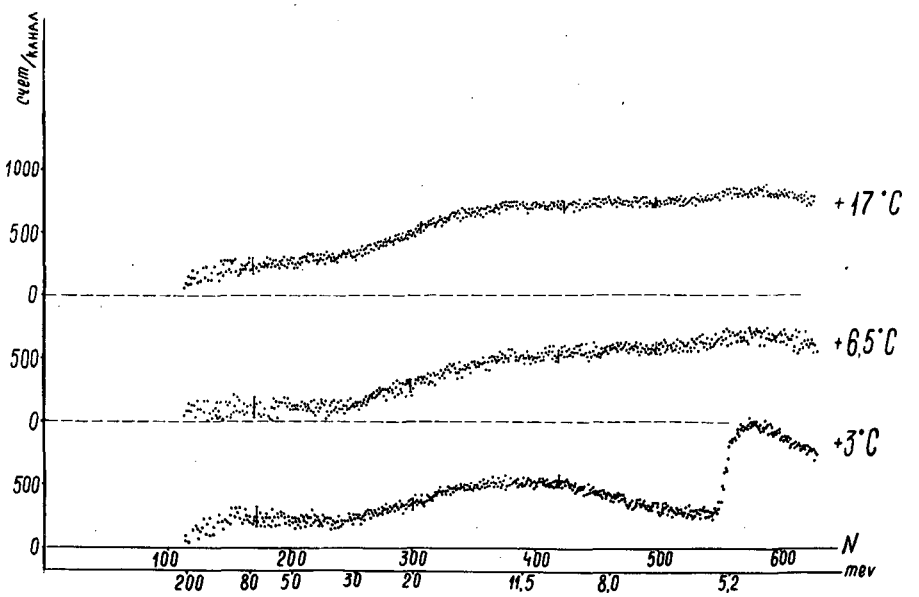

Рис.7

Спектры нейтронов, рассеянных слоем бензола толщиной 0,4 мм. Расстояние образца до детектора – 17 м. Ширина канала временного анализатора – 32 мксек.

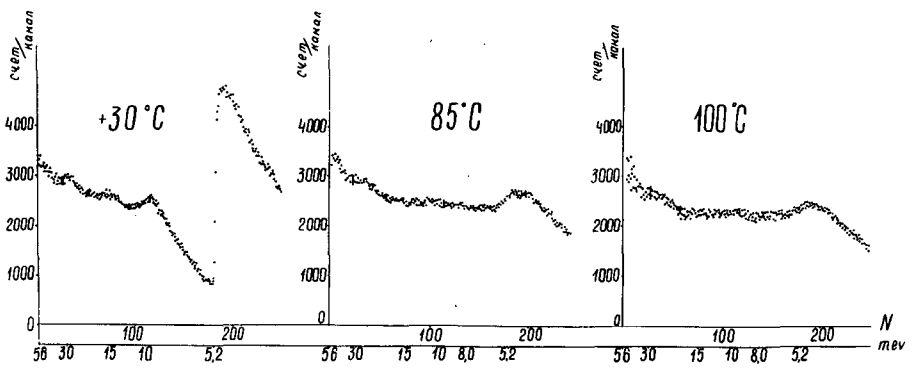

Рис.8

Низкоэнергетические части спектров нейтронов, рассеянных слоем нафталина толщиной 0,70 мм. Расстояние от образца до детектора – 17 м. Ширина канала временного анализатора – 64 мксек.

$$\Delta t = \sqrt{(\Delta t_{\text{жидк}})^2 - (\Delta t_{\text{ванад}})^2}\ . \qquad (4)$$

Здесь $\Delta t_{\text{жидк}}$, $\Delta t_{\text{ванад}}$ – полуширина для жидкости и ванадия соответственно.

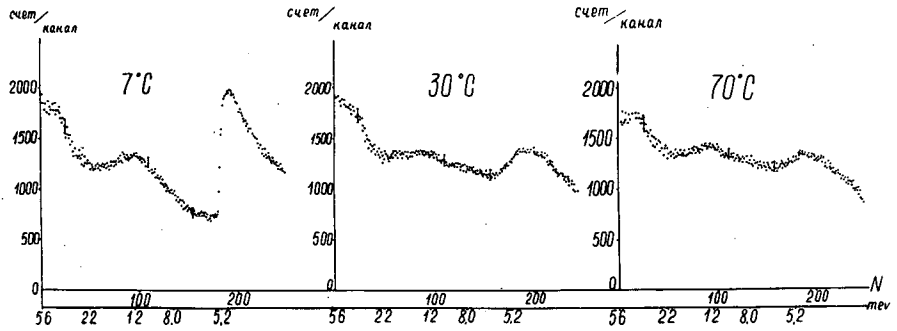

Рис.9

Низкоэнергетические части спектров нейтронов, рассеянных слоем диоксана толщиной 0,25 мм. Расстояние от образца до детектора—17 м. Ширина канала временного анализатора—64 мксек.

При определении величины уширения $\Delta t_{жидк}$ встает трудная проблема отделения квазиупругого пика от подложки, обусловленной неупругим рассеянием. Поскольку подложка слабо меняется с энергией, мы принимали ее в области бериллиевой границы постоянной, как показано на рис.10 (кри-

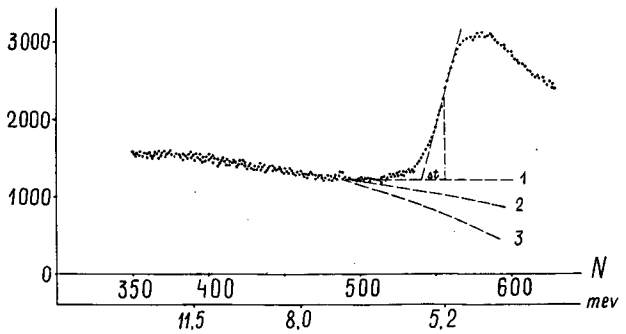

Рис.10

Определение величины уширения квазиупругого пика и различные методы вычитания подложки неупругого рассеяния.

вая 1). Другие способы плавной экстраполяции подложки от руки, указанные на рис.10 (кривые 2—3), приводили к изменению $\Delta t_{жидк}$ не более чем на 15 и 25% соответственно. Полученные таким образом значения $\Gamma \equiv \Delta E$ для изученных жидкостей при нескольких температурах приведены на рис.11—14 и в таблицах 1—2.

На рис. 11—14 пунктиром нанесены значения Γ, рассчитанные по формуле непрерывной диффузии (1) на основе значений D, измеренных неней-тронными методами или, если таких измерений нет, рассчитанных по формуле Стокса-Эйнштейна из значений вязкости η. Как известно [16,17], формула Стокса-Эйнштейна

$$D = \frac{kT}{4\pi r\eta}, \quad 2r = \left(\frac{V}{N}\right)^{\frac{1}{3}} \tag{5}$$

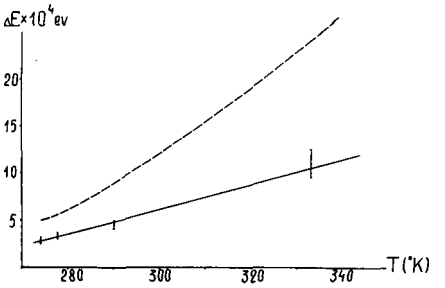

Рис.11

Температурная зависимость полуширины квазиупругого пика для воды. Сплошная кривая – экспериментальные данные; пунктирная – рассчитана по формуле непрерывной диффузии на основе значений D из работы [34].

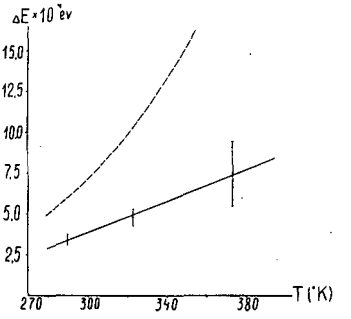

Рис.12

Температурная зависимость полуширины квазиупругого пика для уксусной кислоты. Сплошная кривая – экспериментальные данные: пунктирная – рассчитана по формуле непрерывной диффузии на основе значений D из формулы Стокса-Эйнштейна.

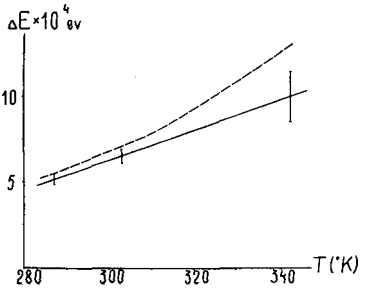

Рис.13

Температурная зависимость полуширины квазиупругого пика для диоксана. Сплошная кривая – экспериментальные данные; пунктирная – рассчитана по формуле непрерывной диффузии на основе значений D из формулы Стокса-Эйнштейна.

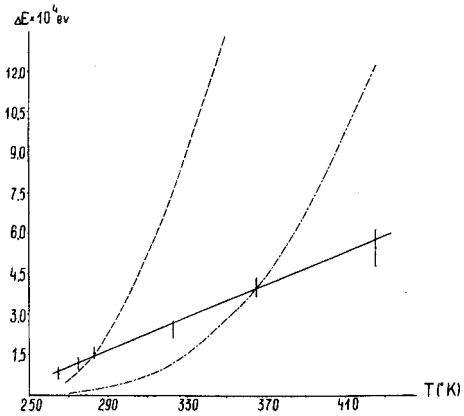

Рис.14

Температурная зависимость полуширины квазиупругого пика для этиленгликоля. Сплошная кривая – экспериментальные данные; пунктирная – данные, рассчитанные по формуле непрерывной диффузии на основе значений D из формулы Стокса-Эйнштейна (нижняя кривая) и формулы Эйринга (верхняя кривая).

(V – молярный объем, N – число Авогадро) оправдывается с точностью 10–20% для целого ряда жидкостей.

Рассмотрение рис.11–13 и таблиц 1–2 показывает, что измеренные значения Γ меньше рассчитанных, причем разница особенно велика для жидкостей, в которых существуют межмолекулярные водородные связи (H_2O, уксусная кислота, этиленгликоль при высоких температурах, рис.14). Уменьшение Γ по сравнению со значением, даваемым (1), можно объяснить прыжковым механизмом диффузии. Напрашивается вывод, что прыжковая диффузия более сильно проявляется в жидкостях с водородной связью.

Подставляя в (2) измеренное значение Γ и измеренное или вычисленное из (5) значение D, можно определить далее параметр τ_0 – среднее время между прыжками; при этом результат не слишком сильно зависит от

Таблица 1

ТЕМПЕРАТУРНАЯ ЗАВИСИМОСТЬ ПОЛУШИРИНЫ КВАЗИУПРУГОГО ПИКА ДЛЯ БЕНЗОЛА

T^0K	$\Delta E_{расч} \cdot 10^4$ эв	$\Delta E_{эксп} \cdot 10^4$ эв
280	8,5	6,6 ± 2,5
290	10,5	8,0 ± 2,5

$\Delta E_{эксп}$ – экспериментальные данные
$\Delta E_{расч}$ – рассчитанные значения по формуле непрерывной диффузии на основе величины D из формулы Стокса-Эйнштейна.

Из-за слабой выраженности квазиупругого пика не делалось попытки определить уширение при более высоких температурах

Таблица 2

ТЕМПЕРАТУРНАЯ ЗАВИСИМОСТЬ ПОЛУШИРИНЫ КВАЗИУПРУГОГО ПИКА ДЛЯ НАФТАЛИНА

T^0 K	$\Delta E_{расч} \cdot 10^4$ эв	$\Delta E_{эксп} \cdot 10^4$ эв
358	9,0	7,0 ± 2,0
373	12,0	9,0 ± 2,5

$\Delta E_{эксп}$ – экспериментальные данные
$\Delta E_{расч}$ – рассчитанные значения по формуле непрерывной диффузии на основе величины D из формулы Стокса-Эйнштейна.

фактора Дебая-Валера. В таблице 3 приведены значения τ_0, рассчитанные в крайних предположениях W=O и W=∞. Для жидкостей с водородной связью τ_0 составляет несколько единиц 10^{-12} сек. Для жидкостей, не образующих водородных связей, такой же расчет дает в несколько раз меньшие значения τ_0, однако использование формулы (2) в этом случае не очень правомерно, так как нет уверенности в справедливости условия $\tau_1 \ll \tau_0$.

Таблица 3

ЗНАЧЕНИЯ τ_0, РАССЧИТАННЫЕ В КРАЙНИХ ПРЕДПОЛОЖЕНИЯХ W=O и W=∞

Жидкость	T^0 K	$\tau_0 \cdot 10^{12}$ сек(W=0)	$\tau_0 \cdot 10^{12}$сек(W=∞)	$\tau_0 \cdot 10^{12}$сек($2W=0{,}142\kappa^2$)
Вода	274	1,5	4,2	3
	277	1,25	3,5	2,5
	290	1,1	2,6	1,9
	333	0,54	1,1	0,8
Уксусная кислота	290	1,3	3,5	
	323	1,2	2,5	
	373	1,0	1,6	
Диоксан	287		2,3	
	303	0,2	1,8	
	343		1,2	
Нафталин	358		1,7	
	373	0,2	1,3	
Бензол	280		1,8	
	290	0,2	1,5	

Значения τ_0 для различных жидкостей в зависимости от температуры, определенные при предположениях w=O и w=∞ (в случае воды приводятся также данные при использовании значения 2w из работы [6]). $2w = 0{,}142\,\kappa^2$.

V. КВАЗИУПРУГОЕ РАССЕЯНИЕ В ВЯЗКИХ ЖИДКОСТЯХ

Особого обсуждения заслуживают результаты, полученные для этиленгликоля (рис.14), вязкость которого в изученном интервале температур быстро возрастает с понижением температуры ($\eta = 1$; 2,4; 6,7; 3,5; 70 спз соответственно при $T = 150$; 90; 50; 10; 0°C [18].

На рис.14 пунктирная кривая дает полуширины квазиупругого пика, рассчитанные по модели непрерывной диффузии, формула (1), для значений коэффициента самодиффузии этиленгликоля, полученных по формуле Стокса-Эйнштейна (5) из экспериментальных значений вязкости. Как видно, при низких температурах (больших вязкостях) экспериментальные полуширины $\Gamma_{нейтр}$ оказываются больше рассчитанных на основании значений вязкости $\Gamma_{вязк}$. (При $T = 275$°K значение $\Gamma_{нейтр}$ превышает значение $\Gamma_{вязк}$ в 10 раз.). Использование для расчета $\Gamma_{вязк}$ формулы прыжковой модели диффузии еще более увеличит эту разницу.

Аналогичное расхождение было отмечено ранее Ларсоном и Дальборгом [19] при изучении рассеяния холодных нейтронов в глицерине и олеиновой кислоте и Саундерсоном и Рейни [20] в опытах со спиртами, причем в последнем случае отличие $\Gamma_{нейтр}$ от $\Gamma_{вязк}$ было не очень значительным.

Изложенные факты побуждают прежде всего рассмотреть вопрос о применимости формулы Стокса-Эйнштейна $D\eta = const/r$ в области больших вязкостей. Для некоторых металлов, для которых значения D и η известны как для жидкого, так и для твердого состояний [18,21], произведение $D\eta$ при переходе от жидкости к твердому телу возрастает на 6–8 порядков. Поскольку увеличение τ привело бы к обратному эффекту, это означает, что механизм одного из процессов, вероятно, вязкости, в твердых телах иной, чем в жидкостях. Можно было подозревать, что отклонения от формулы Стокса-Эйнштейна в очень вязких средах начинают проявляться еще задолго до полного затвердения. Эти опасения, по-видимому, отвергаются результатами А.И. Сибилева и Ю.И. Неронова, которыми были выполнены измерения коэффициента самодиффузии для этиленгликоля при температурах 10,17 и 25°C методом спинового эха. В пределах точности опыта (10–15%) полученные предварительные данные очень хорошо согласуются с рассчитанными из вязкости по формуле (5). Это согласие можно рассматривать также как указание на то, что размер диффундирующих частиц (переносящих протоны) не сильно отличается от размера молекулы этиленгликоля; естественно думать, что отдельные молекулы этиленгликоля и являются диффундирующими частицами.

Таким образом, приходится признать, что существует реальное различие между величинами коэффициентов диффузии в вязких средах, которые проявляются при рассеянии нейтронов и при других методах наблюдения, таких, как протонный магнитный резонанс.

При рассеянии нейтронов с передачей импульса $\hbar\vec{\kappa}$, характер рассеяния определяется движением рассеивающего центра в области с линейным размером порядка $1/\kappa \approx 10^{-8}$ см. Большая величина коэффициента диффузии, "наблюдаемого" нейтроном, указывает, что миграция рассеивающего центра на расстояния $\approx 10^{-8}$ см (т.е. за малое время порядка $t = 1/\kappa^2 D \approx 10^{-11}$ сек) идет с большей скоростью, чем на расстояния $\gg 10^{-8}$ см ($t \gg 10^{-11}$ сек). Эти соображения можно иллюстрировать следующей моделью (не претенду-

ющей на точность). Рассмотрим функцию автокорелляции в виде гауссиана

$$G_s(r, t) = [2\pi y(t)]^{-3/2} \exp\left\{-\frac{r^2}{2y(t)}\right\} \tag{6}$$

и положим

$$\begin{aligned} y(t) &= 2D, |t| && |t| \le t_0, \\ y(t) &= 2D, t_0 + 2D|t| && |t| \ge t_0, \end{aligned} \tag{7}$$

где $D_1 \gg D$.

Подставляя (6) и (7) в выражение для закона рассеяния

$$S(\vec{\kappa}, \omega) = \frac{1}{2\pi}\int e^{-i(\vec{\kappa}\vec{r} + \omega t)} \cdot G_s(\vec{r}, t)\, d\vec{r}\, dt, \tag{8}$$

получаем для двух предельных случаев форму линии рассеяния:

$$\kappa^2 D t_0 \gg 1, \qquad S \approx \frac{1}{\omega^2 + (\kappa^2 D_1)^2}; \tag{9}$$

$$\kappa^2 D t_0 \ll 1, \qquad S \approx \frac{1}{\omega^2 + (\kappa^2 D)^2}. \tag{10}$$

Отсюда видно, что при большом переданном импульсе $\kappa^2 \gg 1/Dt_0$ ширина линии соответствует большому начальному коэффициенту диффузии D_1. Напротив, при $\kappa_2 \ll 1/Dt_0$ ширина линии определяется малым асимптотическим коэффициентом диффузии D. Относительно высокую подвижность рассеивающего центра при малых временах наблюдения можно объяснить существованием движений с ограниченной амплитудой смещения протона, на которых не сказывается макроскопическая вязкость среды.

Такими движениями могут являться переходы молекулы между несколькими возможными положениями внутри одной квазикристаллической ячейки, диффузионные вращения и колебания молекулы или цепочки молекул и т.п.

Наряду с этими движениями существуют другие, такие, как, например, перескоки из одной квазикристаллической ячейки на вакантное место в соседней ячейке, обуславливающие асимптотическую диффузию на большие расстояния. Переходам первого типа (малые смещения) должен соответствовать меньший барьер, а значит, более медленная температурная зависимость коэффициента диффузии, чем для асимптотической диффузии, что как раз и соответствует экспериментальным данным. Ларсон [3] рассматривает эти переходы как вращения молекулы или ее частей, которые становятся возможными в результате ломки водородной связи. Указание на определяющую роль водородной связи усматривается в том, что темпе-

ратурная зависимость видимого нейтронами коэффициента диффузии глицерина соответствует энергии активации 3 ккал/моль, равной энергии разрыва одной водородной связи.

Для дальнейшего прояснения ситуации желательно провести измерения квазиупругого рассеяния в вязких жидкостях в области переданных импульсов, заметно меньших достигнутого до настоящего времени предела $\kappa^2 = 0{,}7 A^{-2}$ [3,19].

В заключение отметим, что в отличие от результата работы [3] для твердого глицерина мы не наблюдали уширения линии в этиленгликоле при температуре -17°, т.е. ниже точки замерзания -15°С, точнее, из наших данных следует $\Gamma < 2 \cdot 10^{-5}$ эв. Аналогичная оценка была получена для льда при -3 °С из измерений с пролетным расстоянием 45 м: $\Gamma < 1 \cdot 10^{-5}$ эв.

VI. НЕУПРУГОЕ РАССЕЯНИЕ

А) Вода

В самых общих чертах полученные картины спектров неупругорассеянных нейтронов согласуются с другими данными [4,6]. Кривая для льда четко показывает наличие в спектре неупругого рассеяния трех максимумов при энергиях нейтронов ≈ 70 мэв, 24 мэв и 12 мэв. При переходе через точку плавления спектр несколько видоизменяется; происходит общее уширение максимумов, картина сглаживается; высокоэнергетический максимум резко смещается в сторону меньших энергий (≈ 60 мэв), низкоэнергетический — в сторону больших энергий. Одновременно понижается интенсивность квазиупругого пика (что указывает на уменьшение дебаевского фактора в воде) и увеличивается интенсивность неупругого рассеяния. Это согласуется с измерениями полного сечения при переходе от льда к воде [33], так как скачкообразное уменьшение сечения квазиупругого рассеяния компенсируется скачкообразным увеличением сечения неупругого рассеяния.

Высокочастотный максимум, обнаруженный ранее оптическими методами, наиболее часто интерпретируется как заторможенное вращение молекул воды в поле, созданном ее соседями. Максимум при $E \approx 24$ мэв относят обычно к трансляционным колебаниям молекул, соединенных водородной связью O—H...O [22]. Однозначного истолкования низкоэнергетического максимума в настоящее время не существует [23,24]. Из-за сходства спектров рассеяния от льда и воды вблизи точки плавления Ларсон [25] для описания рассеяния нейтронов в жидкости ввел некоторый спектр частот (подобно существующему для твердого тела). В целях единообразия представления данных и возможности сравнения полученных результатов мы также рассчитали спектр частот $f(\omega)$ в однофононном приближении:

$$f(\omega) \approx I(E) \frac{k}{k_0} \cdot \frac{\omega}{\kappa^2} \left(e^{h\omega/kT} - 1\right),$$

где $I(E)$ — измеренный энергетический спектр рассеянных нейтронов; k_0, k — начальный и конечный волновые векторы нейтрона; $\vec{\kappa} \approx \vec{k} - \vec{k}_0$; $h\omega \approx E - E_0$; T — температура образца.

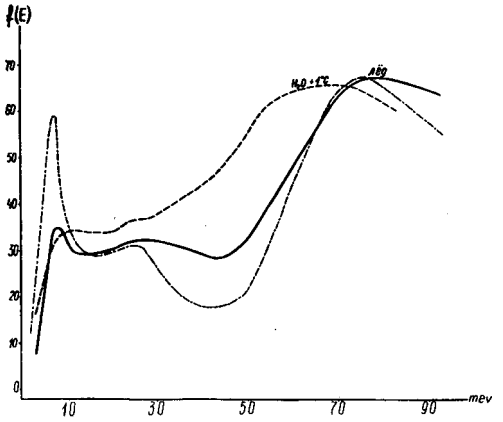

Рис.15

Спектры частот для случая льда и воды при температуре +1°С.
Пунктирная кривая — спектр частот, взятый из работы [25].

На рис.15 представлены вычисленные по указанной формуле спектры частот для льда и воды при температуре +1°С. В области больших передач энергии спектр частот для воды по сравнению со спектром частот для льда смещен в сторону меньших энергий, что согласуется со скачкообразным увеличением теплоемкости при переходе от льда к воде. На этом же рисунке представлен также спектр частот, взятый из [25], рассчитанный из измерений рассеяния холодных нейтронов на угол 30°. Наши данные отличаются от результатов Ларсона [25], показывающих полное совпадение спектров частот для льда и воды вблизи точки плавления.

Расхождение результатов в области малых передач энергии, возможно, связано с многофононными процессами, роль которых в данной энергетической области в наших измерениях (угол рассеяния 75°) больше, чем в работе [25].

Б) Этиленгликоль и уксусная кислота

Картины неупругого рассеяния холодных нейтронов в этиленгликоле и уксусной кислоте очень близки друг к другу. В твердых этиленгликоле и уксусной кислоте наблюдается в области неупругорассеянных нейтронов один очень широкий максимум при энергии 20 мэв. В общих чертах при переходе через точку плавления спектр рассеянных нейтронов изменяется очень слабо. С дальнейшим ростом температуры интенсивность этого пика увеличивается, а его максимум смещается в сторону больших энергий. (В случае этиленгликоля смещение максимума с повышением температуры в сторону больших энергий более заметно, чем в случае уксусной кислоты).

Подобные широкие максимумы в данной энергетической области ранее наблюдались у различных веществ с водородной связью как методами инфракрасного поглощения и комбинационного рассеяния [22], так и нейтронными методами [20]. Эти широкие полосы обычно относят к трансляционным колебаниям молекул, соединенных межмолекулярной водородной связью O—H...O.

Интересно заметить, что в случае этиленгликоля положение максимума этой широкой полосы в зависимости от температуры примерно совпадает с максимумом спектра нейтронов, рассеянных на одноатомном газе с массой атома, равной массе протона.

В) Бензол

При переходе через точку плавления пик, соответствующий квазиупругому рассеянию падающей нейтронной линии, проявляется в спектре жидкого бензола очень слабо. При увеличении температуры происходит дальнейшее сглаживание спектра в районе квазиупругого рассеяния. Это указывает на малое значение эффективной "дебаевской температуры" жидкого бензола. Одновременно при переходе от твердого бензола к жидкому резко возрастает интенсивность рассеянных нейтронов в низкоэнергетической части спектра, что также подтверждает идею о сильном уменьшении "дебаевской температуры" при плавлении. Высказанное в [26] предположение, что одной из причин размытия пика упругого рассеяния в жидком бензоле является наличие сильного диффузионного движения, опровергается данными [27], где экспериментально был определен коэффициент самодиффузии. При температуре 20°C $D = 2{,}14 \cdot 10^{-5}$ см^2/сек, т.е. примерно совпадает с величиной коэффициента самодиффузии для воды, характеризующейся значительным квазиупругим пиком.

Картины спектров рассеянных нейтронов в данной работе и работе [26], где проводились измерения рассеяния на жидком бензоле при комнатной температуре, близки друг к другу. Слабое изменение неупругой части рассеяния с температурой (особенно при больших передачах энергии) указывает на то, что в основном эта часть спектра обусловлена внутримолекулярными движениями протонов, что находится в согласии с измерениями инфракрасного поглощения [28]. Однако в отличие от [26] мы не наблюдали с достаточной надежностью в высокоэнергетической части спектра уровней, проявляющихся в оптическом спектре бензола. Вероятно, это связано с несколько худшей, чем в работе [26], разрешающей способностью нашей установки в данной области энергий.

Г) Нафталин

Как в нафталине, так и в диоксане, с достаточной статистической точностью была измерена только низкочастотная часть спектра, которая и приводится на рис.8–9. В твердом нафталине при 30°C в низкочастотной части спектра наблюдаются максимумы при энергиях нейтронов 9,5; 15,6; 29,6 и 52,7 мэв, хорошо совпадающие с данными, полученными методами инфракрасного поглощения и комбинационного рассеяния [22, 29, 30]. При переходе через точку плавления низкоэнергетические максимумы размываются и исчезают, что вполне согласуется с интерпретацией их происхождения как межмолекулярных колебаний кристаллической решетки [22]. Картина неупругого рассеяния на жидком нафталине очень близка к картине рассеяния нейтронов на другом представителе ароматических углеводородов – на жидком бензоле. При плавлении пик, соответствующий квазиупругому рассеянию, начинает проявляться в спектре слабо; резко возрас-

тает интенсивность рассеянных нейтронов в низкоэнергетической части спектра. При увеличении температуры происходит дальнейшее сглаживание спектра. Все эти факты дают указание на малое значение эффективной "дебаевской температуры" жидкого нафталина.

Д) Диоксан

В спектре неупругорассеянных нейтронов как в твердом, так и жидком диоксане наблюдаются два максимума при энергии нейтронов 45 и 12,5 мэв. Положение первого максимума довольно хорошо согласуется с результатами оптических измерений [31], второй максимум ранее не был обнаружен. С другой стороны, мы не наблюдали части линий, которые проявились в оптических спектрах [32].

Авторы благодарят Г.А. Вареника, В.Б. Дучица, Б.И. Киселева и Ф.А. Рябову за большую помощь при проведении измерений и их обработке во время выполнения данной работы.

ЛИТЕРАТУРА

[1] Сб. "Inelastic Scattering of Neutrons in Solids and Liquids." Proc. Vienna, 1961.
[2] Сб. "Inelastic Scattering of Neutrons in Solids and Liquids." Proc. Vol. I and Vol. II, Vienna, 1963.
[3] LARSSON K.E., DAHLBORG U. Physica, 30, 8 (1964) 1561.
[4] HUGHES D.J., PALEVSKY H., KLEY W., TUNKELO E. Phys.Rev., 119 (1960) 872.
[5] STILLER H.H., DANNER H.R. Inelastic Scattering of Neutrons in Solids and Liquids. Proc., Vienna, 363,
[6] LARSSON K.E., HOLMRYD S., OTNES K. Там же, стр. 329.
[7] BROCKHOUSE B.N. Там же, стр.113.
[8] CRIBIER D., JACROT B. Там же, стр.347.
[9] БЛОХИН Г.Е. и др. "Атомная энергия", 10 (1961) 437.
[10] БУНИН Б.Н. и др. Доклад №324 на III Международной конференции по мирному использованию атомной энергии. Женева, 1964 (в печати).
[11] БАЙОРЕК А., ГОЛИКОВ В.В., ЖУКОВСКАЯ И., ШАПИРО Ф.Л., ШКАТУЛА А., ЯНИК Е. Сб."Inelastic Scattering of Neutrons in Solids and Liquids." Proc. Vienna, 1963, 383
[12] ГОЛИКОВ В.В., ШАПИРО Ф.Л., ШКАТУЛА А., ЯНИК Е. Там же, стр.119.
[13] ГОЛИКОВ В.В., ШИМЧАК Г.Ф., ШКАТУЛА А. ПТЭ, N° 2,59 (1963).
[14] VINEYARD G.H. Phys.Rev., 110 (1958) 999.
[15] SINGWI K.S., SJOLANDER A. Phys.Rev., 119 (1960) 863.
[16] PIN CHANG J.C.M.Li, J.Chem. Phys., 23 (1955) 518.
[17] LANGHLIN E.Mc., Trans. Faraday Soc., v.55 (1959) 29.
[18] Справочник химика. ГХИ, М–Л, 1962.
[19] LARSSON K.E. Сб. "Inelastic Scattering of Neutrons in Solids and Liquids." Proc., Vol.I, Vienna, (1963).
[20] SAUNDERSON D.H., RAINEY V.S. Там же, стр.413.
[21] ГАЙСИНСКИЙ М.Н. Ядерная химия и ее приложения. Ил, М., 1961.
[22] ВОЛЬКЕНШТЕЙН М.В. Строение и физические свойства молекул. Изд.АН СССР, 1955.
[23] PIMENTEL G., McCLELLAN A. The Hydrogen Bond. N.Y., 1960.
[24] ГУРИКОВ Ю.В. Ж. структурной химии, 4, 6 (1963) 824.
[25] LARSSON K.E., DAHLBORG U. J.Nucl.Energy, 16 (1962) 81.
[26] ЗЕМЛЯНОВ М.Г.,ЧЕРНОПЛЕКОВ Н.А. Сб."Inelastic Scattering of Neutrons in Solids and Liquids". Proc. Vol.I, Vienna, 297, (1963).
[27] GRAUPNER K., WINTER E.J. Chem.Soc.(1954) 1145.
[28] БРОУДЕ В.Л. УФН, XXIV, (1961) 577.

[29] ГРОСС Е.Ф., КОРШУНОВ А.В., СЕЛЬКИН В.А. ЖЭТФ, 20 (1950) 292.
[30] MITCHELL N., NELSON D.C. J. Chem. Phys., 39 (1963) 1364.
[31] FAUCONNIER C., HARRAND M. Ann de Phys., 1 (1956) 59.
[32] MALHERBE F.E., BERNSTEIN H.J. J. Am. Chem. Soc., 74 (1953) 4408.
[33] HEINLOTH K., SPRINGER T. Сб. "Inelastic Scattering of Neutrons in Solids and Liquids, Proc. Vienna, (1961) 323.
[34] SIMPSON J.H., CARR H.Y., Phys. Rev., 111 (1958) 1201.

DISCUSSION

See discussion following the paper "Применение метода времени пролета к нейтронно-дифракционным исследованиям" И. Сосновска, Е. Сосновски, С.В. Киселев и Р.П. Озеров of these Proceedings (vol. II) (SM-58/66).

РАССЕЯНИЕ ХОЛОДНЫХ НЕЙТРОНОВ ПОЛИФЕНИЛАМИ

М.Г. ЗЕМЛЯНОВ, Н.А. ЧЕРНОПЛЕКОВ и Ю.Л. ШИТИКОВ
ИНСТИТУТ АТОМНОЙ ЭНЕРГИИ им. И.В.КУРЧАТОВА, МОСКВА
СССР

Abstract — Résumé — Аннотация — Resumen

COLD NEUTRON SCATTERING BY POLYPHENYLS. The time-of-flight method was used for spectrometric measurements of the inelastic scattering of slow neutrons in samples of benzene, diphenyl and mono-isopropyldiphenyl at ambient temperature and in samples of diphenyl at various temperatures from ambient to 362°K.

The experimentally measured scattering cross-sections are compared with the calculations carried out on models both of monatomic heavy gas with various effective mass values and monatomic gas where allowance is made for the internal vibrational degrees of freedom.

The data on the cold neutron inelastic scattering cross-section were used in a computer to restore the distribution functions for the square of displacement of hydrogen atoms from positions of equilibrium when there is vibration in the crystal lattice. The nature of the change in the distribution function of the square of displacement as the crystal passes through the melting point is studied by reference to the temperature-dependence of the scattering cross-section. The restored displacement distribution functions for benzene and solid diphenyl are compared with the results of optical investigations.

DIFFUSION DES NEUTRONS FROIDS PAR LES POLYPHÉNYLES. A l'aide d'un spectromètre à temps de vol, on a mesuré la diffusion inélastique des neutrons froids dans des échantillons de benzol, de diphényle et de mono-isopropyl-diphényle à la température ambiante, ainsi que dans un échantillon de diphényle à différentes températures allant de la température ambiante à 362°K.

Les sections efficaces de diffusion mesurées par voie expérimentale sont comparées aux résultats des calculs effectués, d'une part, sur un modèle de gaz lourd monoatomique avec diverses valeurs de masse effective et, d'autre part, sur un modèle de gaz polyatomique en tenant compte des degrés de liberté des oscillations intérieures.

En se fondant sur les données relatives à la section efficace de diffusion inélastique des neutrons froids, on a établi, à l'aide d'un ordinateur électronique, les fonctions de distribution du carré des écarts des atomes d'hydrogène par rapport à leur position d'équilibre, du fait d'oscillations dans le réseau du cristal. La relation de dépendance entre la section efficace de diffusion et la température a permis d'étudier la nature des modifications que subit cette fonction de distribution lorsque le cristal passe par le point de fusion. Les fonctions de distribution pour le benzol et le diphényle solide sont comparées aux résultats fournis par des études optiques.

РАССЕЯНИЕ ХОЛОДНЫХ НЕЙТРОНОВ ПОЛИФЕНИЛАМИ. На спектрометре по времени пролета проведены измерения неупругого рассеяния холодных нейтронов на образцах бензола, дифенила и моноизопропилдифенила при комнатной температуре, а также на образце дифенила при различных температурах в интервале от комнатной до 362°К.

Экспериментально измеренные сечения рассеяния сравниваются с результатами расчетов, проведенных как в модели одноатомного тяжелого газа с различными значениями эффективной массы, так и в модели многоатомного газа с учетом внутренних колебательных степеней свободы.

Из данных по сечению неупругого рассеяния холодных нейтронов с помощью электронной счетной машины восстановлены функции распределения квадрата смещений атомов водорода из положений равновесия при колебаниях в решетке кристалла. По температурной зависимости сечения рассеяния исследован характер изменения функции распределения квадрата смещения при переходе кристалла через точку плавления. Восстановленные функции распределения смещений для бензола и твердого дифенила сравниваются с результатами оптических исследований.

DISPERSIÓN DE NEUTRONES FRÍOS EN POLIFENILOS. Con ayuda de un espectrómetro de tiempo de vuelo, se midió la dispersión inelástica de los neutrones fríos en muestras de benceno, difenilo y monoisopropildifenilo a temperatura ambiente, así como en una muestra de difenilo a temperaturas comprendidas entre la ambiente y 362°K.

Las secciones eficaces de dispersión medidas por vía experimental se comparan con los resultados de los cálculos efectuados con un modelo de gas monoatómico pesado, en el que se atribuyen distintos valores a la masa efectiva, y con un modelo de gas poliatómico, teniendo en cuenta los grados de libertad interna de las oscilaciones.

A partir de los datos relativos a la sección eficaz de dispersión inelástica de los neutrones fríos, se determinaron, con ayuda de una calculadora electrónica, las funciones de distribución del desplazamiento cuadrático de los átomos de hidrógeno con respecto a su posición de equilibrio cuando la red cristalina experimenta vibraciones. La relación de dependencia entre la sección eficaz de dispersión y la temperatura permitió estudiar el carácter de las modificaciones que sufre esa función de distribución cuando el cristal pasa por el punto de fusión. Las funciones de distribución correspondientes al benceno y al difenilo sólido se comparan con los resultados obtenidos por métodos ópticos.

ВВЕДЕНИЕ

Ряд физических свойств полифенилов (повышенная радиационная и термическая стойкость, высокая температура кипения и т.д.) выгодно отличают их от других органических веществ, и это обусловливает большой интерес, проявляемый к этому классу соединений в реакторостроении. Естественно, что интерес существует и к изучению динамики атомов и молекул в полифенилах методами нейтронной физики, не говоря уже о том, что эти исследования представляют и самостоятельный научный интерес.

В случае твердых полифенилов, хотя имеет место преимущественно некогерентное рассеяние, вследствие очень сложной структуры не представляется возможным проведение строгого решения обратной задачи восстановления спектра колебаний по спектру неупруго рассеянных нейтронов [1]. Задача восстановления может быть решена только в определенных модельных предположениях. В случае жидких полифенилов, как и вообще для веществ в жидком состоянии, задача восстановления спектра возбуждений еще более осложняется.

В работе исследовано неупругое рассеяние холодных нейтронов на жидком бензоле и жидком моноизопропилдифениле, а также на дифениле в интервале температур от 290 до 362°К. Предварительные результаты исследования неупругого рассеяния холодных нейтронов жидким бензолом и твердым дифенилом при $T = 290°$ К публиковались ранее [2]. Эти измерения были повторены на более тонких образцах, чтобы уменьшить вклад многократного рассеяния, и с несколько лучшим разрешением в области малых энергий.

ПРОВЕДЕНИЕ И РЕЗУЛЬТАТЫ ЭКСПЕРИМЕНТА

Экспериментальное определение спектра неупругого рассеяния холодных нейтронов было выполнено на реакторе ИРТ-1000 Института атомной энергии им. И.В.Курчатова [3]. Монохроматизация падающих нейтронов осуществлялась поликристаллическим бериллиевым фильтром, а энергетический анализ рассеянных нейтронов проводился по времени пролета с помощью механического прерывателя и многоканального временного анали-

затора. Для повышения разрешения в области малых изменений энергий механический прерыватель располагался перед рассеивателем, что позволяло уменьшить влияние размытия первичной спектральной линии.

На рис.1 и рис.2 приведены кривые зависимости полного энергетического разрешения, представляющего собой свертку первичной спектралной линии и функции разрешения нейтронного спектрометра, от изменения энергии нейтрона в процессе рассеяния. Отдельно указано влияние размытия первичной спектральной линии и разрешения нейтронного спектрометра. Из сравнения кривых рис.1 и рис.2 видно, что для исследования низкоэнергетических переходов ($\epsilon \leq 20$ мэв) предпочтительным, в отношении разрешения, является расположение механического прерывателя перед рассеивателем.

Образцы исследуемого вещества заключались в специальную алюминиевую кассету с толщиной стенок ~0,1 мм. Однородность толщины слоя обеспечивалась с помощью фиксирующих центрального и кольцевого выступов. Изменение толщины слоя достигалось с помощью алюминиевых вытеснителей, вводимых в зазор между двумя алюминиевыми диафрагмами. Нагревательные элементы располагались по внешнему периметру кассеты. Контроль температуры образца обеспечивался с помощью термопар, вводимых непосредственно в слой исследуемого вещества. С целью уменьшения градиента температуры в радиальном направлении образца вся кассета окружалась алюминиевым экраном с толщиной стенки 0,03 мм.

Полученные спектры с учетом всех методических поправок, за исключением энергетического разрешения установки, представлены графически на рис.3—8. На рисунках указаны статистическая и энергетическая погрешности исходных экспериментальных данных. Там же для сравнения приводится спектр нейтронов, упруго рассеянных на металлическом ванадии с учетом его деформации за счет конечной толщины пластины. Спектры нормированы на одно и то же значение интенсивности рассеянных нейтронов в максимуме упругого рассеяния.

При рассмотрении данных по бензолу (рис.3) обращает на себя внимание то обстоятельство, что для жидкого бензола в этом случае более отчетливо, чем это наблюдалось ранее [2], проявляется максимум, соответствующих упругому рассеянию холодных нейтронов. Кроме того, интенсивность квзиупруго рассеянных нейтронов значительно превышает интенсивность неупруго рассеянных нейтронов. Такое изменение обусловлено, в основном, практическим исключением влияния процессов многократного рассеяния. Из сравнения формы спектра на бензоле в области упругого рассеяния с формой первичной спектральной линии видно, что спектральная линия значительно уширяется. Причем уширение происходит как за счет процессов, связанных с поглощением квантов возбуждения, так и с их рождением. Такое значительное уширение, очевидно, объясняется тем, что в жидком бензоле в области малых энергий имеется большая плотность уровней, связанных как с квазифононным спектром, так и с вращательными состояниями молекул, а также с наличием сильного диффузионного движения. Ширина линии на полувысоте в несколько раз превышает ширину исходной спектральной линии. Однако, несмотря на это, не представляется возможным корректно оценить величину коэффициента диффузии из величины уширения пика квазиупругого рассеяния из-за высокой плотности низкоэнергетических состояний.

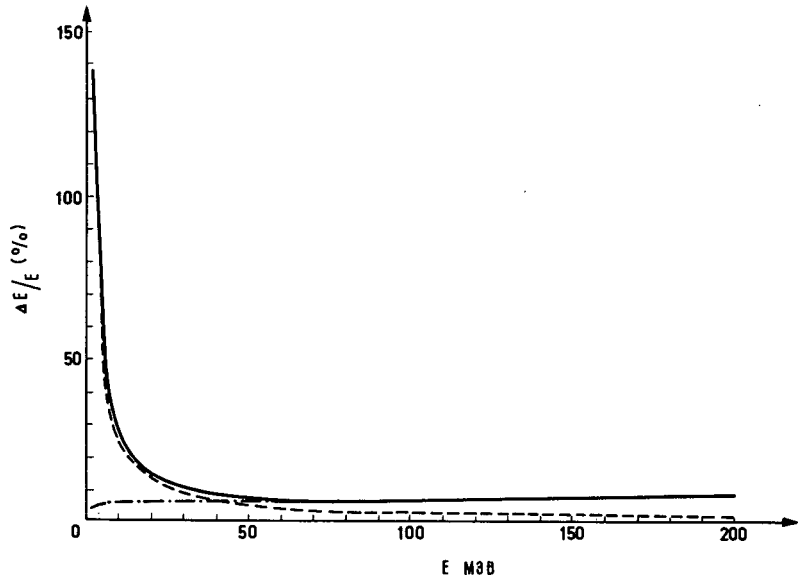

Рис.1

Полное разрешение в случае расположения механического прерывателя после рассеивателя:

——— полное разрешение
- - - падающая линия
—·—·— спектрометр

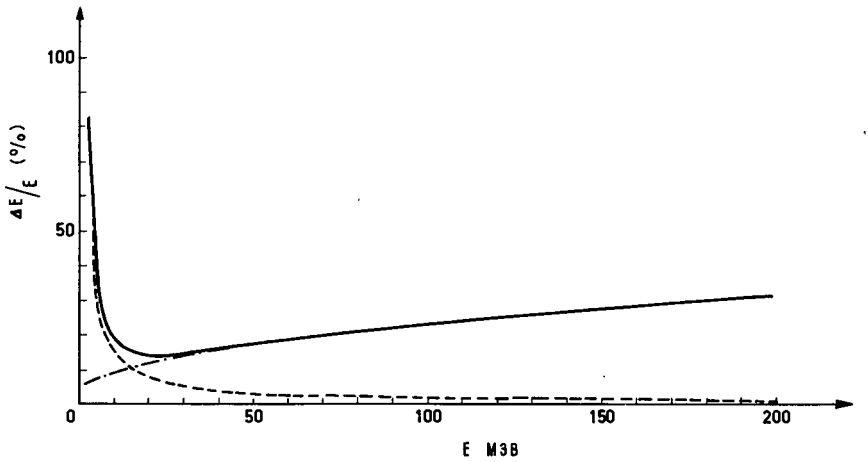

Рис.2

Полное разрешение в случае расположения механического прерывателя перед рассеивателем:

- - - падающая линия
—·—·— спектрометр
——— полное разрешение

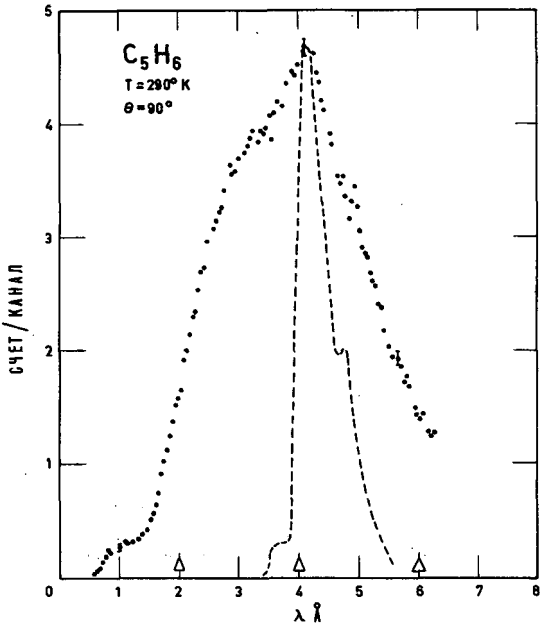

Рис.3

Спектр нейтронов, рассеянных на C_6H_6:

● ● ● бензол - - - ванадий

В спектре неупруго рассеянных нейтронов проявляются два излома, один при $\lambda = 2{,}8$ Å и второй при $\lambda = 1{,}2$ Å, что находится в полном согласии с уже опубликованными результатами [2].

На рис.4 приведены данные для дифенила в твердом состоянии, полученные при двух температурах $T = 290°$ K и $T = 340°$ K (на 1,5° K ниже точки плавления). Спектры нормированы на одну и ту же интенсивность падающих нейтронов.

В противоположность результатам по жидкому бензолу в спектре дифенила резко выражена область квазиупругого рассеяния нейтронов ($\lambda = 3{,}58$ Å и $\lambda = 3{,}95$ Å). Из сравнения с данными по рассеянию на ванадии видно, что наклон переднего фронта основного максимума упругого рассеяния при $\lambda = 3{,}95$ Å определяется только разрешением нейтронного спектрометра установки. Отсюда следует, что при температуре образца $T = 290°$ K, которая на ~50° K ниже температуры плавления дифенила, диффузионное движение в дифениле практически отсутствует. Кроме того, отношение ординат максимумов упругого рассеяния (при $\lambda = 3{,}58$ Å и $\lambda = 3{,}95$ Å) не существенно отличается от отношения ординат в первичной линии. Таким образом, можно сделать вывод, что плотность уровней в твердом дифениле в области малых энергий $\sim 10^{-3}$ эв незначительна. Повышение температуры дифенила в твердой фазе приводит, в основном, к количественному изменению спектра неупруго рассеянных нейтронов. Кроме того, с ростом температуры происходит слияние квазиупругой и неупругой частей спектра. Но вплоть до температур, которые на несколько градусов ниже точки плавления, в спектре рассеянных нейтронов сохраняется квазиупругий пик.

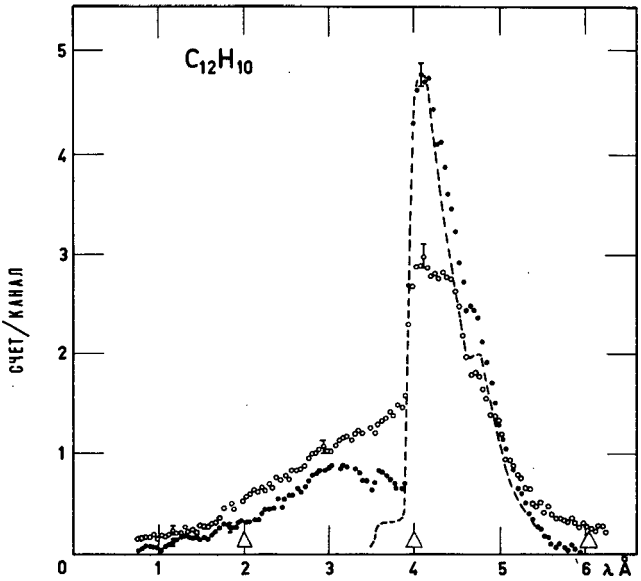

Рис.4

Спектр нейтронов, рассеянных на $C_{12}H_{10}$ в твердой фазе при T = 290° K и T = 340° K:

o o o 290° K • • • 340° K - - - ванадий

На рис.5 приведены данные по спектру рассеянных нейтронов на дифениле ниже и выше его точки плавления. Из сравнения кривых отчетливо видно, как существенно изменяется спектр при переходе образца через точку плавления. Изменение температуры всего на 3° C приводит к деформации спектра в целом, и особенно его низкоэнергетической части. Высокоэнергетическая часть спектра, которая определяется внутримолекулярными колебаниями, практически не меняется при переходе дифенила через точку плавления.

На рис.6 приведены данные, полученные для жидкого дифенила при трех различных температурах (343° K, 348° K и 362° K). Данные нормированы на один и тот же поток падающих нейтронов. Как и на рис.5, высокоэнергетическая часть спектра в пределах погрешности результатов эксперимента совпадает для трех указанных температур. Наибольшему изменению подвергается область квазиупругого рассеяния и низкоэнергетическая часть спектра неупругого рассеяния.

На рис.7 представлены отдельно результаты, полученные на жидком дифениле при T = 362° K, где для сравнения также приведены результаты для твердого дифенила при T = 290° K.

Данные нормированы на один и тот же поток падающих нейтронов. Из сравнения этих спектров видно, что в спектре для дифенила при T = 362° K квазиупругая часть непосредственно смыкается с частью спектра, отвечающей неупругому рассеянию нейтронов. Что же касается неупругой части спектра, то в ней не обнаруживается дополнительных особенностей, хотя при T = 362° K она идет значительно выше, чем при T = 290° K.

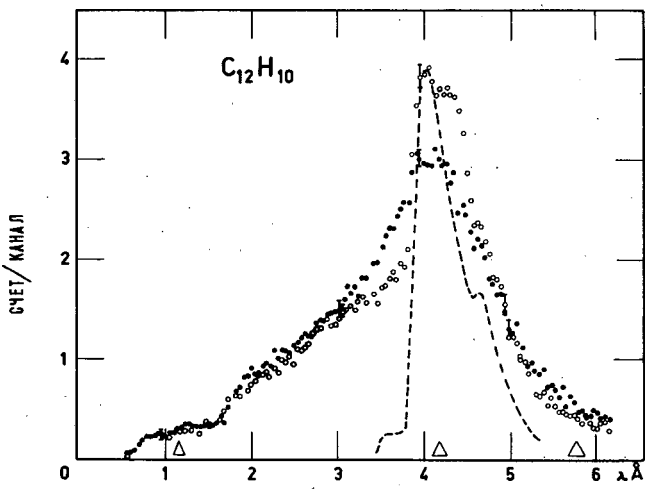

Рис. 5

Спектр нейтронов, рассеянных на $C_{12}H_{10}$ при T = 340° K и T = 343° K:

o o o 340° K ● ● ● 343° K - - - ванадий

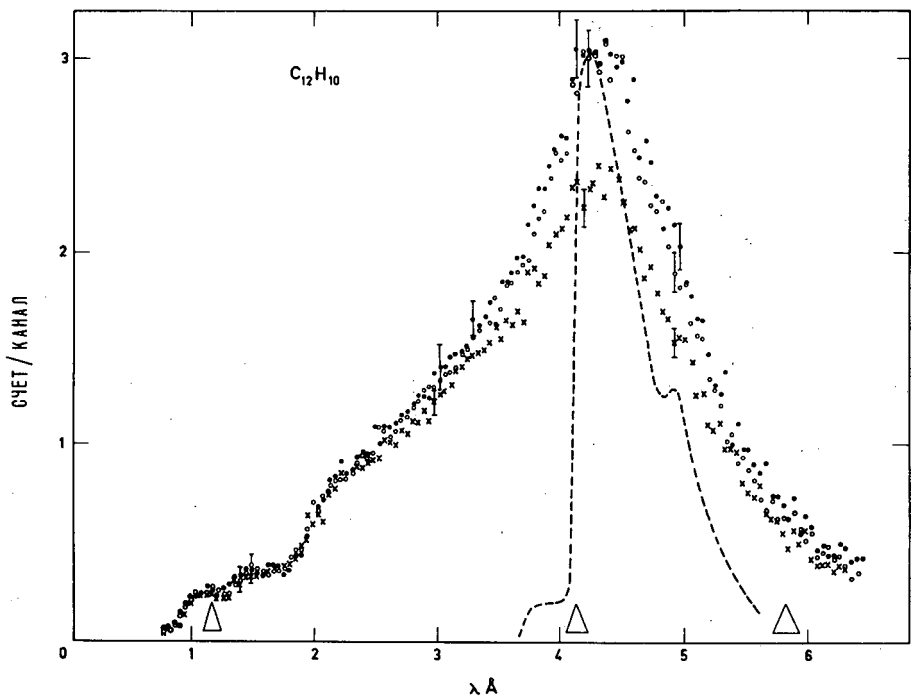

Рис. 6

Спектр нейтронов, рассеянных на $C_{12}H_{10}$ в жидкой фазе при T = 343° K, T = 348° K и T = 362° K:

● ● ● 343° K o o o 348° K

× × × 362° K - - - ванадий

Результаты для моноизопропилдифенила представлены на рис.8. В спектре моноизопропилдифенила отчетливо проявляется квазиупругая часть, которая непрерывно переходит в область неупругого рассеяния. Наблюдается сильное размытие первичной линии падающих нейтронов за счет процессов рассеяния, сопровождающихся рождением квантов возбуждения. Эта часть спектра аналогична спектру, полученному для жидкого бензола. Что касается части спектра, лежащей слева от первичной линии, то она очень существенно отличается как от результатов для жидкого бензола, так и для твердого дифенила при $T = 290°$ К. Она качественно аналогична неупругой части спектра для твердого дифенила в состоянии предплавления ($T = 340°$ К).

Полученные данные для моноизопропилдифенила позволяют сделать вывод, что в моноизопропилдифениле при $T = 290°$ К наблюдается некоторая квазикристалличность и что процессы диффузии по сравнению с жидким бензолом значительно подавлены. Подавление процессов диффузии в значительной степени объясняется более тяжелой массой молекулы моноизопропилдифенила по сравнению с бензолом.

ОБСУЖДЕНИЕ РЕЗУЛЬТАТОВ

Сечение неупругого рассеяния нейтронов в рассматриваемых водородсодержащих веществах, находящихся в твердом состоянии, записывается в следующем виде [4]:

$$\frac{d^2\sigma}{d\Omega\, d\epsilon} = \frac{K}{8\pi K_0}\,\frac{\kappa^2}{\epsilon}\,\frac{g(\epsilon)}{e^{\epsilon/KT}-1}\sum_j A_j \frac{\sigma_j}{M_j} e^{-2W_j}\,[\overline{C_j(\epsilon)}]^2,$$

где A_j – концентрация,
σ_j – сечение некогерентного рассеяния,
M_j – масса,
e^{-2W_j} – фактор Дебая-Валлера и
$|\overline{C(\epsilon)}|^2$ – квадрат вектора поляризации, соответственно, j-го сорта ядер.

Из приведенного соотношения видно, что единственно корректно, т.е. без привлечения модели, восстанавливаемой величиной из экспериментально измеренного дважды дифференциального сечения, является некая функция $\theta(\epsilon)$, где

$$\theta(\epsilon) = \frac{d^2\sigma}{d\Omega\, d\epsilon}\,\frac{8\pi K_0}{K}\,\frac{\epsilon}{\kappa^2}\,(e^{\epsilon/KT}-1).$$

В свою очередь функция $\theta(\epsilon)$ выражается через динамические характеристики вещества следующим образом:

$$\theta(\epsilon) = g(\epsilon)\sum_j A_j \frac{\sigma_j}{M_j}\, e^{-2W_j}\, |\overline{C_j(\epsilon)}|^2,$$

т.е. $\theta(\epsilon)$ представляет собой функцию распределения квадрата смещений

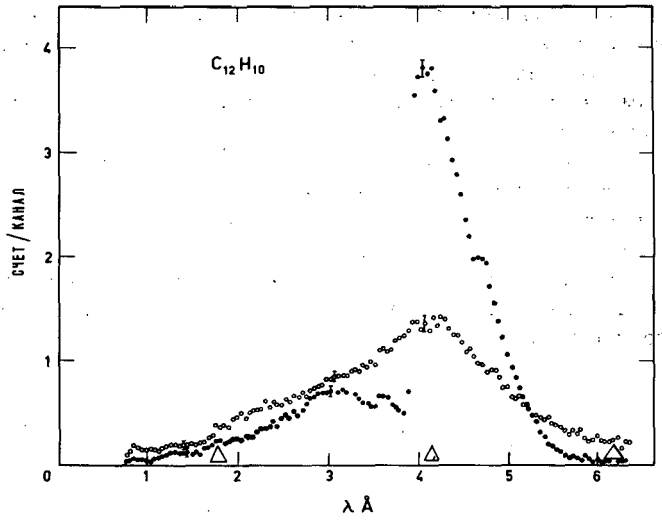

Рис. 7

Спектр нейтронов, рассеянных на $C_{12}H_{10}$ в твердой (T = 290° K) и жидкой (T = 362° K) фазах:

● ● ● 290° K o o o 362° K

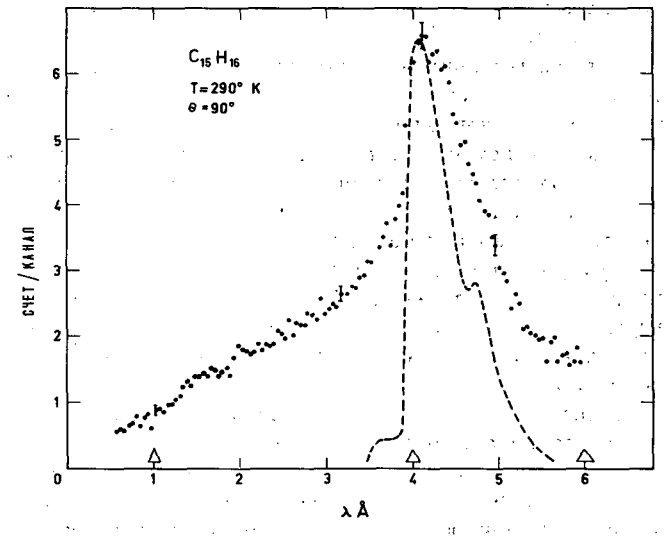

Рис. 8

Спектр нейтронов, рассеянных на $C_{15}H_{16}$:

● ● ● моноизопропилдифенил
- - - ванадий

атомов из положения равновесия при колебаниях в решетке кристалла. Для получения из экспериментально определенной $\theta(\epsilon)$ функции распределения $g(\epsilon)$ необходимо проведение расчетов энергетической зависимости векторов поляризации в модельных предположениях и фактора Дебая-Валлера, как

это было выполнено, например, в случае LiH и LiD [5]. Однако следует отметить два обстоятельства: 1) получаемое непосредственно из эксперимента распределение квадрата смещений $\theta(\epsilon)$ для оптической части спектра, в которой преимущественно колеблется водород и где $|\overline{C_H(\epsilon)}|^2 \approx 1$ качественно передает особенности спектра возбуждений и 2) более того, в этом случае распределение $\theta(\epsilon)$ может рассматриваться как динамическая характеристика вещества при изучении процессов рассеяния с участием фононной ветви возбуждения, так, например, при рассеянии на фононах нейтронов, фононов, электронов, магнонов и т.д.

Функция распределения квадрата смещений связана с обычно принятой характеристикой динамики рассеивателя — "законом рассеяния" $S(\alpha, \beta)$ — следующим соотношением:

$$\theta(\epsilon) = \frac{2K_B\beta}{\kappa^2} \cdot \mathrm{Sh}\,\beta/2 \cdot S(\alpha, \beta) .$$

Восстановление $\theta(\epsilon)$ из экспериментально измеренного сечения является строгим только для твердого состояния вещества. В случае жидкого состояния вещества такое восстановление $\theta(\epsilon)$ применимо только в квазикристаллическом приближении.

Результаты восстановления $\theta(\epsilon)$ из экспериментальных данных с учетом функции разрешения [5] для рассматриваемых водородсодержащих веществ приведены на рис.9, 10 и 11.

В нижней части на всех рисунках стрелками указаны данные, полученные из независимых оптических исследований по измерению Раман-спектров и инфракрасных спектров поглощения [6], [7], [8], [9]. Пунктирной линией на рисунках указана статистическая погрешность исходных экспериментальных данных. Хотя полного соответствия в энергетическом положении особенностей функции $\theta(\epsilon)$ с положением линий, полученных в оптических исследованиях во всем интервале частот и не следует ожидать [5], однако, из сравнения $\theta(\epsilon)$ и результатов оптических исследований можно сделать некоторые выводы. В случае бензола (рис.9) в $\theta(\epsilon)$ отчетливо проявляются три максимума. Два из них при $\epsilon = 50$ мэв и $\epsilon = 100$ мэв были установлены в ранее опубликованных результатах исследования бензола с помощью неупругого рассеяния нейтронов [2], [10]. Если максимум при $\epsilon = 100$ мэв был непосредственно установлен и в оптических исследованиях, то максимум при $\epsilon = 50$ мэв оптически не наблюдался.

Представляет интерес сравнить результаты для низкочастотных колебаний бензола, полученные по деполяризации линий комбинационного рассеяния, с результатами нейтронных исследований. В оптических измерениях в этой области частот четко проявляются три группы линий: 1) $\epsilon =$ 4,3 мэв; 2) $\epsilon = 7{,}8$ мэв и $\epsilon = 8{,}55$ мэв и 3) $\epsilon = 13$ мэв. Линии 4,3 и 8,55 мэв отвечают крутильным колебаниям молекулы бензола как целого вокруг оси шестого порядка, линии 7,8 и 13 мэв — колебаниям молекулы бензола как целого вокруг двух осей, расположенных в полоскости самой молекулы. Аналогично оптическим данным в $\theta(\epsilon)$ проявляется резкий максимум, соответствующий второй группе линий, и два более слабых максимума слева и справа от основного, соответствующих двум другим линиям. В области

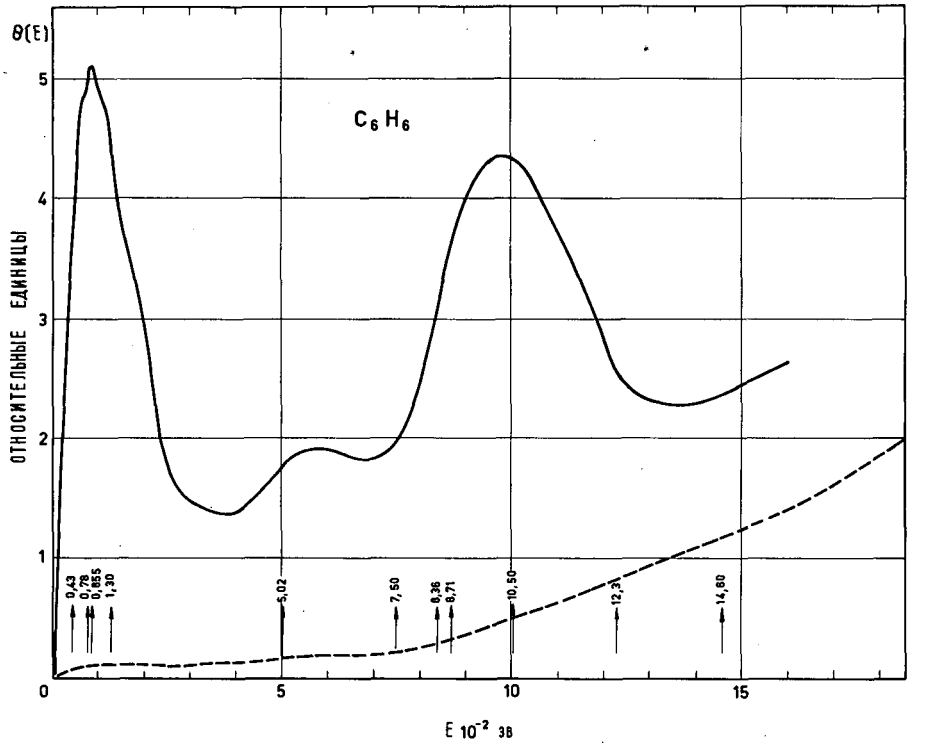

Рис.9

Функция распределения смещений $\theta(\epsilon)$ для C_6H_6.

больших передач энергии наблюдается рост $\theta(\epsilon)$ с энергией. Такое поведение $\theta(\epsilon)$, вероятно, объясняется существенным вкладом двухфононных процессов. Характерным для $\theta(\epsilon)$ является то, что в нем отсутствуют энергетические щели, которые четко устанавливаются в оптических исследованиях. Такое отличие связано с тем, что оптически активными являются только колебания с разностью фаз, равной 0 или π, а для нейтронов это условие не существенно.

На рис.10 представлены данные по $\theta(\epsilon)$, полученные для дифенила при различных температурах (290° К, 340° К, 343° К и 362° К). Все значения $\theta(\epsilon)$ нормированы на одно и то же значение падающего потока. Энергетическая зависимость $\theta(\epsilon)$ в случае дифенила получается более сложной, чем в случае жидкого бензола. Изменение температуры практически не приводит к качественному изменению $\theta(\epsilon)$. Повышение температуры для данного фазового состояния приводит к смещению энергетического положения особенностей в стороны меньших частот. Причем это наблюдается как для низкоэнергетической, так и для высокоэнергетической части $\theta(\epsilon)$. Меньшей деформации подвергается низкоэнергетическая часть $\theta(\epsilon)$. В области малых энергий при фазовом переходе наблюдается некоторое размытие пика при E = 5 мэв, а остальные особенности резко смещаются в сторону больших энергий. Ширина этих особенностей при повышении температуры и при переходе из твердого в жидкое состояние практически не изменяется. Наи-

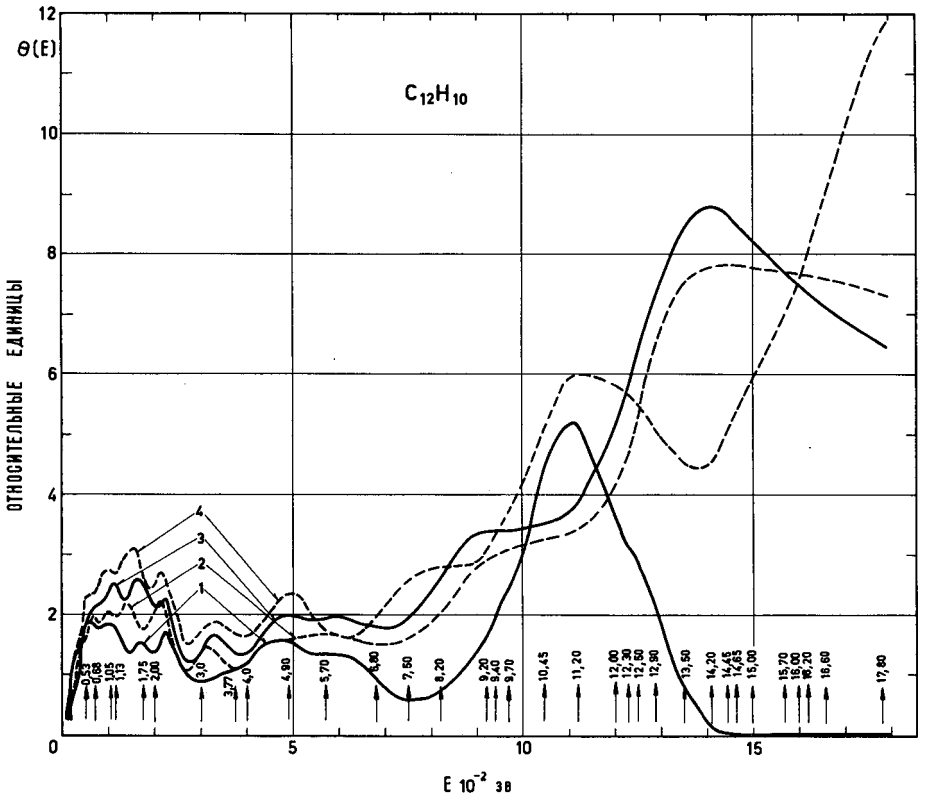

Рис.10

Функция распределения смещений $\theta(\epsilon)$ для $C_{12}H_{10}$:

1 —— 290° K 3 —— 343° K
2 - - - 340° K 4 - - - 362° K

более существенному изменению подвергается область высокоэнергетических переходов. В этой области наблюдается не только смещение особенностей, но и их существенное размытие. С повышением температуры наблюдается также значительное возрастание $\theta(\epsilon)$ в области больших передач энергии, что, вероятно, как и в случае бензола, объясняется влиянием двухфононных и двухкратных процессов. В области малых передач энергии наблюдается удовлетворительное согласие в положении линий, полученных в оптических исследованиях с положением особенностей в $\theta(\epsilon)$. Кроме того, в этой области частот в спектре неупруго рассеянных нейтронов при $\epsilon \approx$ 3,5 мэв наблюдается слабый максимум, который ранее не наблюдался в оптических исследованиях [7]. Указанный максимум, вероятно, отвечает колебаниям всей молекулы дифенила как целого вокруг оси, перпендикулярной плоскости молекулы. Эти колебания являются оптически неактивными. Поскольку им отвечает вращение вокруг оси с наибольшим моментом инерции, то эти колебания должны быть смещены в область более низких частот. Что касается области больших передач энергии, то здесь не наблюдается такого удовлетворительного согласия с данными оптических исследований.

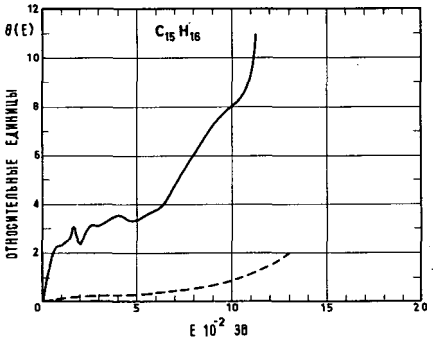

Рис.11

Функция распределения смещений $\theta(\epsilon)$ для $C_{15}H_{16}$:

Восстановленое значение $\theta(\epsilon)$ для моноизопропилдифенила приведено на рис.11. Сравнение с оптическими данными не проводится, поскольку для моноизопропилдифенила такие данные нам не известны. В низкоэнергетической части $\theta(\epsilon)$ проявляются два максимума $E = 8$ мэв и $E = 16$ мэв. В области энергий 20—50 мэв проявляются два слабых, размытых максимума, которые непрерывно переходят в область больших передач энергии. В интервале энергий > 100 мэв наблюдается резкий подъем в значении $\theta(\epsilon)$.

Общий характер $\theta(\epsilon)$ для $C_{15}H_{16}$ существенно отличается от $\theta(\epsilon)$ для жидкого бензола и $\theta(\epsilon)$ для дифенила в твердом и жидком состояниях. Из сравнения $\theta(\epsilon)$ для C_6H_6, $C_{12}H_{10}$ и $C_{15}H_{16}$ можно сказать: 1) увеличение массы молекулы полифенилов приводит к существенному уменьшению плотности квадратов смещений, отвечающих малым изменениям энергии, 2) все $\theta(\epsilon)$ имеют непрерывное распределение в отличие от дискретных линий или полос, как это следует из независимых оптических измерений и 3) наилучшими замедляющими свойствами обладает бензол, вследствие высокой плотности квадрата смещений в области малых энергий.

Представляется целесообразным провести сравнение полученных в данной работе результатов по измеренным дважды дифференциальным сечениям рассеяния нейтронов полифенилами с расчетами, проведенными в различных модельных предположениях. В первую очередь этот интерес вызван тем, что экспериментальная техника сегодняшнего дня практически не позволяет исследовать все поле значений изменений энергии и импульса в процессе рассеяния нейтрона. В то же время интересы реакторостроения требуют именно такого подробного знания сечения и особенно в области больших значений ϵ и κ. Поэтому естественным в этом отношении представляется путь использования модельных расчетов, сравнения их с экспериментально полученными данными и экстраполяции или интерполяции расчетных сечений для представляющих интерес значений ϵ и κ. Наиболее полно такие модельные расчеты дважды дифференциального сечения выполнены для бензола в работе [11]. Расчеты проведены в предположении многоатомного газа с учетом внутримолекулярных колебаний. В этом случае пренебрегается взаимодействием между молекулами, интерференцией колебаний и вращений и используется гармоническое приближение для внутримолекулярных колебаний, т.е. в выбранной для бензола модели, вра-

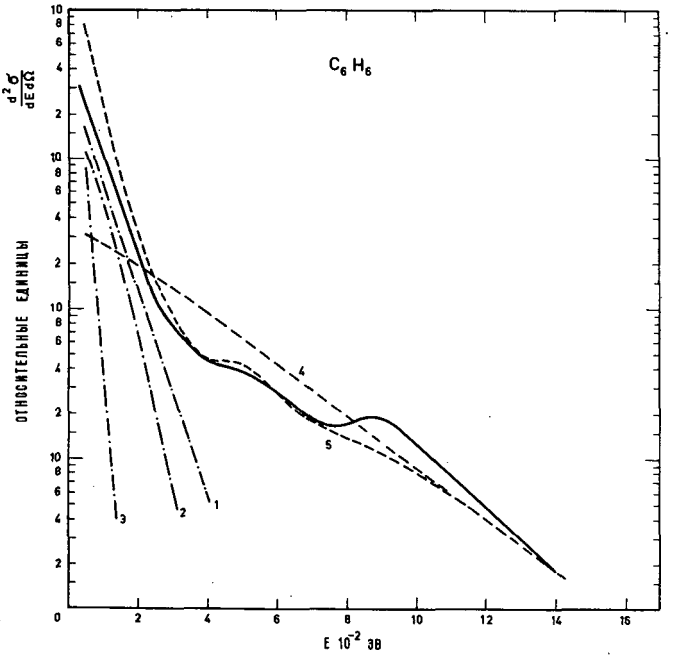

Рис.12

Энергетическая зависимость измеренного и расчетного $d\sigma/d\Omega d\epsilon$ для C_6H_6:

—— эксперимент
4 - - - M* = 1
1 — · — M* = 19,03
2 — · — M* = 21,3
3 — · — M* = 78
5 - - - M* = 21,3 (с увеличением колебаний)

щение и трансляция учитываются в приближении свободного газа, а внутримолекулярные колебания обрабатываются в приближении кубического кристалла с одним атомом в элементарной ячейке.

На рис.12 проведено сравнение экспериментально измеренного сечения неупругого рассеяния с расчетными в различных модельных предположениях для C_6H_6. При этом, поскольку в данном эксперименте не определялось абсолютное значение сечения, то сравниваются их энергетические зависимости. Расчетное сечение для бензола в модели протонного газа и определенное экспериментально нормировались на одно и то же значение в области больших передач энергии, где расчетное сечение наименее чувствительно к виду выбранной модели. Что касается сечений для тяжелого одноатомного газа, то эти сечения нормировались относительно сечения рассеяния на протонном газе. Аналогичная нормировка сечений проводилась и в случае других полифенилов.

Как видно из рис.12, расчетное сечение с учетом внутримолекулярных колебаний качественно повторяет характер энергетической зависимости измеренного экспериментально сечения в области средних передач энергий. Причем особенность в энергетическом ходе расчетного сечения в области

первого уровня внутримолекулярных колебаний бензола ($\sim 5 \cdot 10^{-2}$ эв) оказывается более отчетливо выраженной, чем в экспериментальном сечении. Такое различие объясняется, очевидно, тем, что в модельном расчете не учитываются более низколежащие уровни, соответствующие межмолекулярным колебаниям. Значительное расхождение между расчетными и экспериментальными сечениями наблюдается в области малых и больших передач энергий. В расчетном сечении совсем не проявляется максимум при $E = 100$ мэв, который отчетливо виден в экспериментальном сечении. В области малых энергий расчетное сечение идет значительно выше экспериментального, и это расхождение увеличивается с уменьшением энергии. Такое поведение расчетного сечения является, вероятно, следствием того, что в использованной модели трансляционные и вращательные движения в молекуле бензола обрабатывались в приближении свободного газа. Как уже упоминалось, на рис.12 для сравнения приведены также результаты расчетов для модели одноатомного газа с различным значением эффективной массы. Значение $M^* = 15{,}03$ отвечает учету трансляционных степеней свободы молекулы бензола, а $M^* = 21{,}3$ отвечает значению, полученному в масс-тензорном приближении. Из сравнения расчетных кривых (1,2,3,4 рис.12) с экспериментальными данными видно, что ни для одного из указанных значений эффективной массы не получается удовлетворительного согласия с экспериментом во всем рассматриваемом интервале энергий. Расчеты для рассеяния на протонном газе качественно передают относительный ход сечения в области больших передач энергии, но неудовлетворительно описывают ход сечения в области малых передач энергии. В случае рассеяния на тяжелом газе относительный ход расчетного сечения лучше передается в области малых энергий. Отсюда следует, что энергетическая зависимость расчетного сечения в случае одноатомного газа не может быть даже качественно описана моделью с постоянным значением эффективной массы. Однако подбором значений масс, зависящих от передаваемой энергии нейтроном в процессе рассеяния, вероятно, возможно описать качественно энергетическую зависимость сечения в согласии с экспериментальными результатами. Необходимо отметить, что аналогичная модель одноатомного газа с переменной по энергии нейтрона массой была ранее предложена для описания рассеяния на воде [12].

В случае дифенила специальных модельных расчетов с учетом внутримолекулярных или межмолекулярных степеней свободы не проводилось. Однако представляется оправданным проведение сравнения экспериментальных результатов для дифенила с указанными расчетами для молекулы бензола, поскольку учитываемые в этих расчетах степени свободы бензольного кольца являются характерными и для дифенила. Результаты сравнения расчетных данных с результатами измерений для твердого дифенила ($T = 290°$ K) приведены на рис.13. Модельные расчеты сечения для бензола приближенно передают относительный ход сечения дифенила, но, как и в случае бензола, наблюдается существенное различие к области малых и больших передач энергии и, кроме того, расчетное сечение не передает многих особенностей, проявляющихся в экспериментально полученном сечении. Что касается расчетного сечения в модели одноатомного тяжелого газа, то здесь различие еще более существенно, чем в случае бензола. Необходимо отметить, что в случае измерения интегральных характеристик

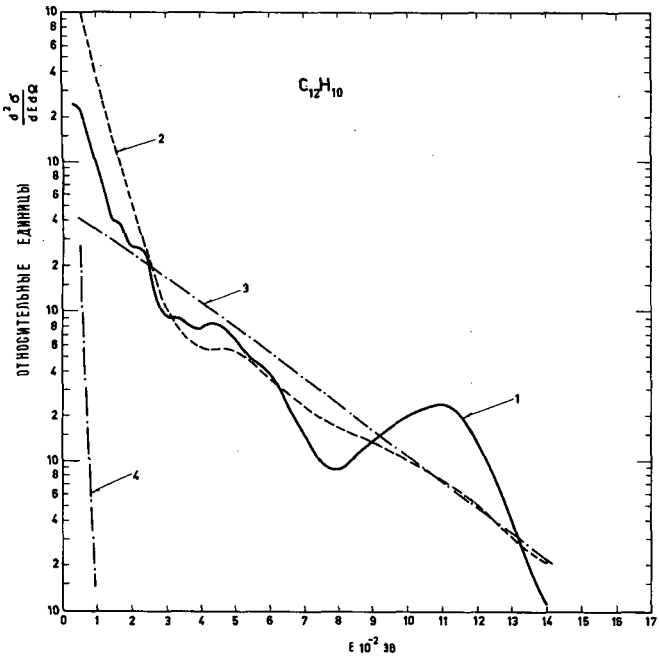

Рис.13

Энергетическая зависимость измеренного и расчетного $d\sigma/d\Omega d\epsilon$ для $C_{12}H_{10}$:

1 —— эксперимент
2 - - - $M^* = 21{,}3$ (с учетом колебаний)
3 —·— $M^* = 1$
4 —··— $M^* = 154$

взаимодействия нейтронов с дифенилом [15] наблюдается удовлетворительное согласие экспериментальных данных с результатами расчетов в модели тяжелого одноатомного газа.

На рис.14 приведено сравнение экспериментальных сечений для дифенила ($T = 290°$ K), полученных авторами [13], [14]. Из кривых рис.14 видно, что результаты для дифенила и "Даутерм А" довольно удовлетворительно согласуются с результатами, полученными по рассеянию холодных нейтронов. Что касается результатов для сечений "Сантовакса R" [14] (смесь дифенила, орто-терфенила, мета-терфенила и пара-терфенила), то они идут несколько выше, особенно в области малых изменений энергий.

Данные по сечению рассеяния на моноизпропилдифениле приведены на рис.15. Сравнение экспериментальных данных для моноизопропилдифенила с модельными расчетами для бензола является оправданным на том же основании, что и в случае дифенила. Обращает на себя внимание относительно более плавный ход экспериментального сечения для $C_{15}H_{16}$. Расчетные сечения для протонного газа и молекулы бензола, нормированные на экспериментальное значение сечения для моноизопропилдифенила в области больших энергий, идут выше экспериментальных. Такой относительный ход, вероятно, объясняется существенным вкладом многофононных процессов в той области, где производилась взаимная нормировка данных.

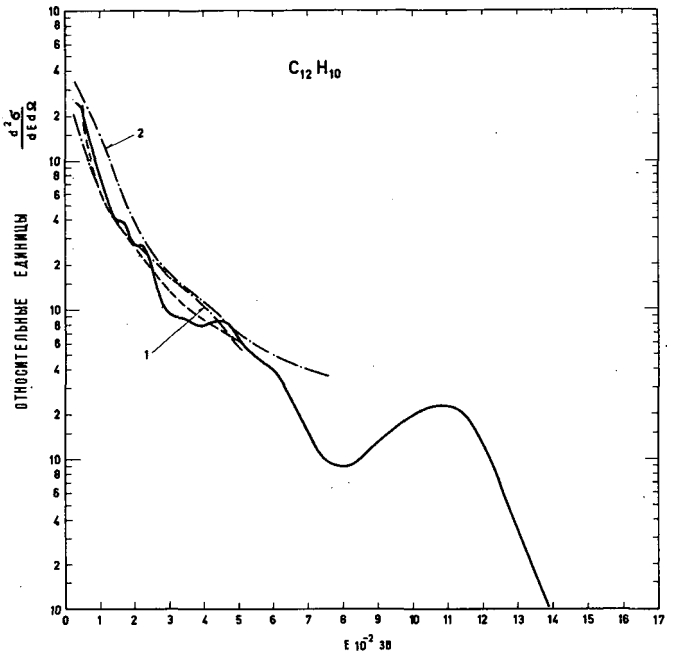

Рис.14

Энергетическая зависимость $d\sigma/d\Omega d\epsilon$ для $C_{12}H_{10}$, "Даутерм А" и "Сантовакса R":

—— эксперимент
- - - [13]
1 —·— [13]
2 —·— [14]

В экспериментальном сечении для моноизопропилдифенила не проявляется уровень при 50 мэв, который отвечает первому колебательному состоянию молекулы бензола.

Из сравнения экспериментальных данных по сечениям, а также по функциям $\theta(\epsilon)$ для бензола, дифенила и моноизопропилдифенила видно, что увеличение массы молекулы за счет добавления бензольного кольца или изопропиловой группы приводит к существенному изменению динамики молекулы.

ВЫВОДЫ

В работе исследовалось неупругое рассеяние холодных нейтронов некоторыми представителями класса колифенилов—жидким бензолом, твердым и жидким дифенилом и жидким моноизопропилдифенилом. Экспериментально полученное сечение для бензола удовлетворительно согласуется с результатами расчетов, выполненных с учетом внутримолекулярных колебаний. Однако результаты этих расчетов не находятся в согласии с экспериментальными данными для дифенила и моноизопропилдифенила. Энергетическая зависимость полученных сечений для всех трех полифенилов не может быть описана моделью одноатомного тяжелого газа с постоянным

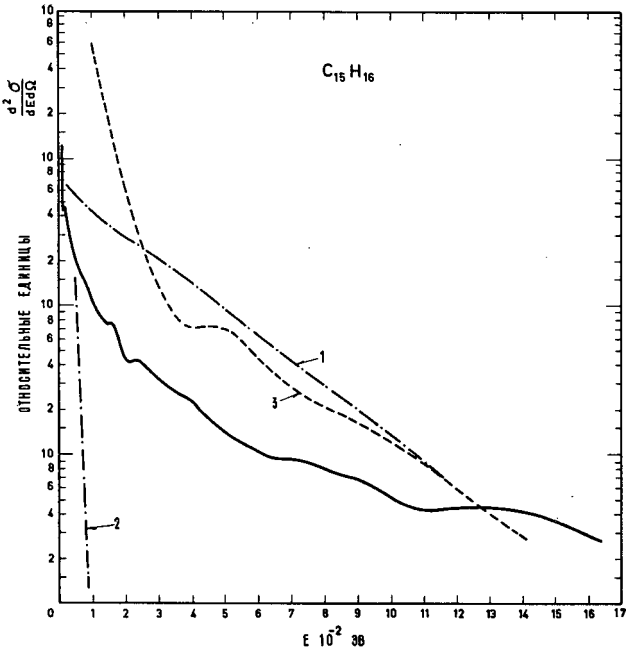

Рис. 15

Энергетическая зависимость измеренного и расчетного $d\sigma/d\Omega d\epsilon$ для $C_{15}H_{16}$:

—— эксперимент
1 — — $M^* = 1$
2 — — $M^* = 196$
3 - - - $M^* = 21{,}3$ (с учетом колебаний)

значением эффективной массы. Введение эффективной массы, зависящей от энергии нейтрона, вероятно, позволит получить качественное согласие результатов расчета и эксперимента. Для удовлетворительного описания экспериментального сечения необходим более корректный учет влияния других степеней свободы, связанных как с внутримолекулярным, так и с межмолекулярным движениями.

Без привлечения каких-либо модельных представлений из экспериментальных данных восстановлена функция распределения плотности квадрата смещения $\theta(\epsilon)$. Особенности в $\theta(\epsilon)$ для бензола и дифенила в основном согласуются с положением линий или полос, полученных независимо от оптических исследований. Кроме того, в случае жидкого бензола в $\theta(\epsilon)$ проявляется максимум при $\epsilon = 50$ мэв, который непосредственно в оптических измерениях ранее не наблюдался и который отвечает основному колебательному состоянию молекулы бензола. Для дифенила в $\theta(\epsilon)$ проявляется слабый максимум в области низких частот при $\epsilon = 3{,}5$ мэв, который также ранее не наблюдался в оптических исследованиях. Эта особенность, вероятно, связана с колебаниями всей молекулы дифенила как целого вокруг оси, перпендикулярной плоскости молекулы. Повышение температуры дифенила, а также переход через точку плавления не сопровождается

качественными изменениями в энергетической зависимости $\theta(\epsilon)$. Однако при повышении температуры наблюдается смещение энергетического положения особенностей $\theta(\epsilon)$ в сторону меньших частот.

Распределение плотности квадрата смещений для всех полифенилов имеет непрерывный вид в отличие от результатов оптических исследований, где спектр носит дискретный характер с образованием энергетических щелей между линиями спектра.

Переход от простейших полифенилов, каким является бензол, к более сложным сопровождается существенным изменением их динамики. Плотность смещений, отвечающих малым изменениям энергии, уменьшается с ростом веса молекулы. В случае моноизопропилдифенила в области больших энергий наблюдается значительный рост плотности смещений по сравнению с бензолом и дифенилом. Такой рост, вероятно, объясняется включением дополнительных степеней свободы изопропиловой группы.

В заключение выражаем благодарность Певзнеру М.И. и Бровману Е.Г. за участи в обсуждении полученных результатов, Головину А.Е., Игнашеву А.С., Федорову В.Г. и Середе Ю.В. за помощь в проведении измерений и обработке данных.

ЛИТЕРАТУРА

[1] КАГАН Ю., ЖЭТФ, 42, 5 (1962).
[2] ЗЕМЛЯНОВ М.Г., ЧЕРНОПЛЕКОВ Н.А., "Атомная энергия". 14, 3 (1963).
[3] ЗЕМЛЯНОВ М.Г., ЧЕРНОПЛЕКОВ Н.А., ПТЭ №5 (1962).
[4] ЧЕРНОПЛЕКОВ Н.А., ЗЕМЛЯНОВ М.Г., БРОВМАН Е.Г., ЧИЧЕРИН А.Г., ФТТ, 5, 1 (1963).
[5] ЗЕМЛЯНОВ М.Г., БРОВМАН Е.Г., ЧЕРНОПЛЕКОВ Н.А., ШИТИКОВ Ю.Л., Исследование динамики гидрида и дейтерида лития по неупругому рассеянию холодных нейтронов. (Доклад на симпозиум по неупругому рассеянию холодных нейтронов в твердых телах и жидкостях. Тромбей, декабрь 1964 г.). См. в этом томе.
[6] MAIR R.D., HORNIG D.F., J. Chem. Phys., 17, 1236 (1949).
[7] FRUHLING A., Annales de Physique 6, 401 (1951).
[8] БРОУДЕ В.Л., УФН, LXXIV, 4 (1961).
[9] STEELE D., LIPPINCOTT E.R., J. Mol. Spectr., 6, 238 (1961).
[10] MYERS V.W., COTTER M.J., PALEVSKY H., Bull. Amer. Phys. Soc., 6, 3 (1961).
[11] BOFFI V.C., MOLINARI V.G., PARKS D.E., Inelast. Scat. of Neutrons in Solids and Liquids. Proc. v.1, IAEA, Vienna, 1963.
[12] ДРОЗДОВ М.И., ЗАРЕЦКИИ Д.Ф., КУДРИН Л.П., СИДЕЛЬНИКОВ Т.Х., Доклад (15/P/2033) на 2-й Женевской конференции, 1958 г.
[13] GLASER W., Inelast. Scat. of Netrons in Solids and Liquids. Proc., v.1, IAEA, Vienna, 1963.
[14] BRUGER R.M., Phys. Rev., 126, 29 (1962).
[15] ЮРОВА Л.Н., СТЕПАНОВ С.Б., ОКОРОКОВ В.В., КУДРЯШОВ Е.И., "Атомная энергия" 12, 4 (1962).

DISCUSSION

H. BOUTIN: Your measurements on benzene were taken in the neighbourhood of room temperature and you did not make any correction for multiphonon processes. Under these conditions it seems of doubtful value to attempt any comparison of the frequency distribution with optical results.

M.G. ZEMLYANOV: The value of any comparison of neutron experiments with optical results is questionable, but I do not think this is very

important in carrying out neutron scattering experiments. Actually, as has been shown in the case of lithium hydride, the main deformation of phonon spectra is introduced not by multiphonon processes, which are more or less simple functions, but by the energy dependence of the polarization vector. The calculation of two-phonon processes is more difficult. One may calculate such processes most easily by using the Debye model, but this hardly seems justified in our case. We are at present developing an iterative method for calculating multiphonon processes, without introducing any model concepts and using only experimental data.

MOLECULAR DYNAMICS

MOLECULAR DYNAMICS INVESTIGATED BY NEUTRON SCATTERING

J. A. JANIK
INSTITUTE FOR NUCLEAR PHYSICS, CRACOW, POLAND

Abstract — Résumé — Аннотация — Resumen

MOLECULAR DYNAMICS INVESTIGATED BY NEUTRON SCATTERING. A short review of the present state of the problem of applicability of the Krieger-Nelkin theory as well as of the Griffing theory to gases is made. Then, on the basis of experiments with liquid methane, the applicability of the mass-tensor concept to molecules in condensed states is criticized. Strong arguments against the application of the Krieger-Nelkin theory to condensed states are: a shift of neutron energy distribution after scattering towards higher energies and the lack of dependence of the inelastic part on the scattering angle.

Further sections deal with the rotational dynamics of ammonium groups in ammonium compounds. Most of the experimental material is discussed in connection with ammonium halides on the basis of experiments by different authors. For some substances a freedom of rotation of NH_4 groups was obtained from neutron measurements, whereas for some others the rotation goes over into torsional vibration. In this case, frequencies of torsional vibrations obtained by various authors from neutron experiments were compared with those obtained from infrared spectroscopy and specific heat measurements.

The barrier-to-rotation evaluation from total neutron cross-section measurements is also discussed.

Further a comparison is made of the rotational dynamics of NH_4 groups in NH_4ClO_4 and H_3O groups in H_3OClO_4 on the basis of neutron inelastic scattering experiments. A free rotation of the NH_4 group in ammonium perchlorate was obtained even at temperatures as low as liquid nitrogen temperature. For H_3OClO_4 a torsional vibration of the H_3O group with a frequency of 497 cm^{-1} was obtained. So in spite of the identity of the crystal lattices of NH_4ClO_4 and H_3OClO_4 the dynamics of the NH_4 and H_3O groups are different. The results are compared with those known from Raman spectroscopy and nuclear magnetic resonance.

Finally, a number of other substances is discussed from the point of view of molecular dynamics.

ÉTUDE DE LA DYNAMIQUE MOLÉCULAIRE AU MOYEN DE LA DIFFUSION DES NEUTRONS. L'auteur fait le point de l'état actuel des connaissances touchant le problème de l'applicabilité des théories de Krieger-Nelkin et de Griffing dans le cas des gaz. Ensuite, sur la base d'expériences faites avec du méthane liquide, il examine d'une manière critique l'applicabilité du concept du tenseur de masse à des molécules dans l'état condensé. Les arguments les plus puissants qui militent contre l'application de la théorie de Krieger-Nelkin aux états condensés sont: a) un déplacement dans la distribution des neutrons en énergie, après diffusion, vers les grandes énergies; b) l'absence d'une relation de dépendance entre la fraction inélastique et l'angle de diffusion.

D'autres parties du mémoire traitent de la dynamique de rotation des groupes ammonium dans les composés d'ammonium. L'auteur discute la plupart des données d'expérience relatives aux halogénures d'ammonium en se fondant sur les expériences de différents auteurs. Par des mesures de neutrons, il a obtenu une liberté de rotation des groupes NH_4 pour certaines substances, tandis que pour d'autres la rotation évolue en vibration de torsion. Dans le dernier cas, il a comparé les fréquences des vibrations de torsion obtenues par divers auteurs au cours d'expériences sur les neutrons avec celles qui résultent de la spectroscopie infrarouge et des mesures de la chaleur spécifique.

L'auteur discute également l'obstacle qui s'oppose à l'évaluation de la rotation à l'aide de mesures des sections efficaces totales pour les neutrons.

En outre, il compare la dynamique de rotation des groupes NH_4 dans NH_4ClO_4 et des groupes H_3O dans H_3OClO_4, en se fondant sur des expériences de diffusion inélastique des neutrons. Il a obtenu une rotation libre du groupe NH_4 dans le perchlorate d'ammonium, même à des températures ne dépassant pas celle de l'azote liquide. Pour H_3OClO_4 il a obtenu une vibration de torsion du groupe H_3O avec une fréquence de 497 cm^{-1}. Il s'ensuit que, malgré l'identité des réseaux cristallins de NH_4ClO_4 et H_3OClO_4, la dynamique des groupes NH_4 et H_3O est différente. L'auteur compare ces résultats avec ceux qui ont été obtenus par spectroscopie de Raman et résonance magnétique nucléaire.

Enfin, il discute plusieurs autres substances du point de vue de la dynamique moléculaire.

ИССЛЕДОВАНИЕ МОЛЕКУЛЯРНОЙ ДИНАМИКИ С ПОМОЩЬЮ РАССЕЯНИЯ НЕЙТРОНОВ. Кратко рассматривается положение с вопросом о применимости теории Кригера-Нелькина и теории Гриффинга в отношении газов. Затем на основании экспериментов с жидким метаном критически рассматривается вопрос о применимости концепции тензора массы в отношении молекул в конденсированном состоянии. Убедительными доводами против применения теории Кригера-Нелькина в отношении конденсированных состояний являются: сдвиг распределения энергии нейтронов после рассеяния в сторону более высоких энергий и отсутствие зависимости неупругой части от угла рассеяния.

Следующие разделы посвящены ротационной динамике аммониевых групп в соединениях аммония. Большая часть экспериментального материала рассматривается в связи с галоидами аммония, исходя из результатов экспериментов различных авторов. Для некоторых веществ свобода вращения групп NH_4 получена на основании измерения нейтронов, тогда как для некоторых других это вращение переходит в крутильное колебание. В этом случае частоты крутильных колебаний, полученные различными авторами в результате измерения нейтронов, сравнивались с частотами, полученными с помощью инфракрасной спектроскопии и измерений удельной теплоемкости.

Рассматривается также вопрос о пределе возможности оценки вращения на основании результатов измерения общих нейтронных сечений.

Кроме того производится сравнение вращательной динамики групп NH_4 в NH_4ClO_4 и групп H_3O в H_3OClO_4 на основе результатов экспериментов по неупругому рассеянию нейтронов. Свободное вращение группы NH_4 в хлорнокислом аммонии было получено даже при таких низких температурах, как температура жидкого азота. Для H_3OClO_4 было обнаружено крутильное колебание группы H_3O с частотой 497 $см^{-1}$. Таким образом, несмотря на идентичность кристаллических решеток NH_4ClO_4 и H_3OClO_4, динамика групп NH_4 и H_3O является различной. Эти результаты сравниваются с результатами, полученными с помощью спектроскопии Рамана и ядерного магнитного резонанса.

И, наконец, ряд других веществ рассматривается с точки зрения молекулярной динамики.

ESTUDIO DE LA DINÁMICA MOLECULAR POR DISPERSIÓN NEUTRÓNICA. Se examina brevemente en qué medida la teoría de Krieger-Nelkin y la de Griffing son aplicables a los gases. A continuación, y sobre la base de experimentos realizados con metano líquido, se hace un estudio crítico de la posibilidad de aplicar el concepto de tensor másico a las moléculas en estado condensado. Los principales argumentos en contra de la aplicación de la teoría de Krieger y Nelkin a los estados condensados son: el desplazamiento hacia energías más elevadas de la distribución de las energías neutrónicas a raíz de la dispersión y la independencia de la parte inelástica con respecto al ángulo de dispersión.

Se estudia también la dinámica de rotación de los grupos amonio en compuestos amónicos. Se examina gran parte de los datos experimentales obtenidos por diferentes autores sobre los haluros de amonio. Para algunas sustancias, las mediciones efectuadas mediante dispersión neutrónica indican la libertad de rotación del grupo NH_4, mientras que para otras, la rotación se transforma en una vibración torsional. En este caso, las frecuencias de las vibraciones torsionales que diferentes autores han obtenido por dispersión neutrónica se comparan con las determinadas por espectroscopia infrarroja y medición del calor específico.

Se estudia también el cálculo basado en la medición de la sección eficaz neutrónica total de la barrera que se opone a la rotación.

Asimismo, se compara la dinámica de rotación de los grupos NH_4 en el NH_4ClO_4 y de los grupos H_3O en el H_3OClO_4 sobre la base de experimentos de dispersión inelástica de neutrones. Los resultados obtenidos indican que la rotación del grupo NH_4 en el perclorato amónico es libre, incluso a temperaturas tan bajas como la del nitrógeno líquido. En lo que respecta al H_3OClO_4, se ha observado una vibración torsional del grupo H_3O con una frecuencia de 497 cm^{-1}. Por tanto, a pesar de la identidad de las redes cristalinas del NH_4ClO_4 y del H_3OClO_4, la dinámica de los grupos NH_4 es diferente de la de los grupos H_3O. Los resultados se comparan con los obtenidos por espectroscopia Raman y resonancia magnética nuclear.

Por último, se estudia una serie de sustancias desde el punto de vista de su dinámica molecular.

1. INTRODUCTION

There is a long history in the development of the problem of neutron scattering by molecules. It begins with a paper by FERMI [1] which gives

the scattering cross-section formula for protons treated as isotropic harmonic oscillators. Then follow the SACHS and TELLER [2] theory of neutron scattering by molecules considered as rigid classical rotators; the ZEMACH and GLAUBER [3] formalism which led to the KRIEGER and NELKIN [4] cross-section formula for neutron scattering by molecules, in which molecular vibrations are quantum-mechanically treated, though translation and rotation are taken into account in a classical way; theories of neutron scattering in the subthermal and intermediate energy region (VOLKIN [5], RAHMAN [45] and GRIFFING [6]) which take into consideration the quantum structure of rotational degrees of freedom; and finally theories of neutron scattering by some special molecules. (Diatomic molecules have been considered by BRIMBERG [7] and LØVSETH [8] and symmetric ones by MESSIAH [9]).

In the present paper the situation in the sub-thermal and intermediate energy region is discussed; a comparison between the results of classical and quantum-mechanical treatment of rotations is made in section 2. In section 3 we discuss some open theoretical problems involved in the process of neutron scattering by molecules (or molecular groups) in condensed states. Three further sections report the results of various experiments on neutron scattering by simple molecular crystals, i.e. results obtained for ammonium compounds by the differential neutron cross-section technique which may be compared with those obtained by infrared spectroscopy and the thermodynamic method (see section 4), and also those given by the total cross-section technique which may be compared to the nuclear magnetic resonance (NMR) (see section 5). Section 6 presents a comparison between the two isomorphic crystals NH_4ClO_4 and $H_3O\,ClO_4$ from the point of view of the rotational dynamics of the ammonium and hydronium groups. Sections 7 to 9 are devoted to a description of neutron scattering results for liquid and solid methane; ice, water and water of crystallization; and for HF, KHF_2, KH_2F_3, NaH_2F_3, KH_2PO_4, K_2HPO_4 and K_3PO_4. Section 10 assembles information concerning the dynamics of CH_3 groups in various compounds and section 11 gives a short review concerning other substances investigated by the neutron scattering technique.

2. NEUTRON SCATTERING BY MOLECULAR GASES

As mentioned in the introduction we shall limit ourselves to neutrons of the intermediate and sub-thermal energy region. In this region it is interesting to compare the results given by the Krieger-Nelkin theory, which is based on the mass tensor concept (i.e. treats rotations of molecules classically), with those given by the Griffing theory, which is based on a quantum-mechanical treatment of rotations.

First we should note that in the thermal energy region and for not too low temperatures the Krieger-Nelkin theory is well confirmed by experiment and it is true for both the total (H_2 and CH_4 [10, 47], C_2H_4 and NH_3 [11],

H_2O [48]) and the differential (CH_4 and propane [12, 49]) cross-section formulas.[1] This situation for methane gas is presented in Figs. 1 and 2.

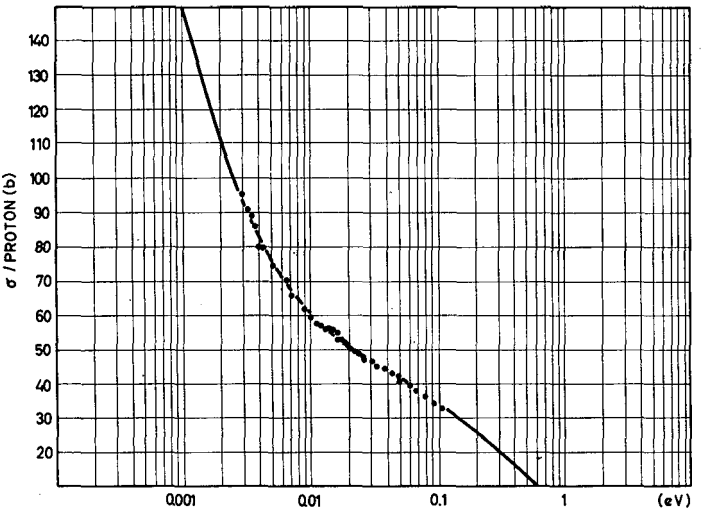

Fig. 1

Total neutron scattering cross-section of protons in CH_4 gas versus neutron energy
Experimental points of MELKONIAN [10]; curve from Krieger-Nelkin theory.

For lower neutron energies and especially for low scattering angles a deviation from the Krieger-Nelkin theory appears, as shown for methane gas in Fig. 3. Figure 4 shows to what extent the Griffing theory is better for a description of the scattering process at lower energies. One can see that the Griffing theory not only gives a much narrower quasi-elastic peak than the Krieger-Nelkin one but also gives another small peak corresponding to some neutron energy gain. In the case of the Griffing theory this peak comes from transitions between rotational levels. (It must however be noted that it does not correspond to a single transition between rotational levels but is a result of a "collective contribution" of several transitions gathered around this energy.) It is worthwhile to observe that the experimental points give evidence of such an inelastic peak caused by the quantum nature of molecular rotation. As was already stressed, a quantitative comparison between the two theories and the experimental points was made, as described above, for methane gas at room temperature, and for neutrons of 0.0252 eV energy; the scattering angle was 16.3° [6].

Another experiment was made for ammonia gas, with neutrons of 0.005 eV energy (WEBB [13]). Figure 5 shows the cross-section as a function of the energy of scattered neutrons for one of the investigated angles, 20°. A quasi-elastic peak is observed which decreases in intensity for higher scat-

[1] Recently YOUNG and KOPPEL [50] gave a theory for H_2 in which the spin dependence, rotations and vibrations are treated exactly. The theory agrees well with the experimental total cross-section results for para-hydrogen and ortho-hydrogen gas at 20.4°K obtained by SQUIRES and STEWART [51].

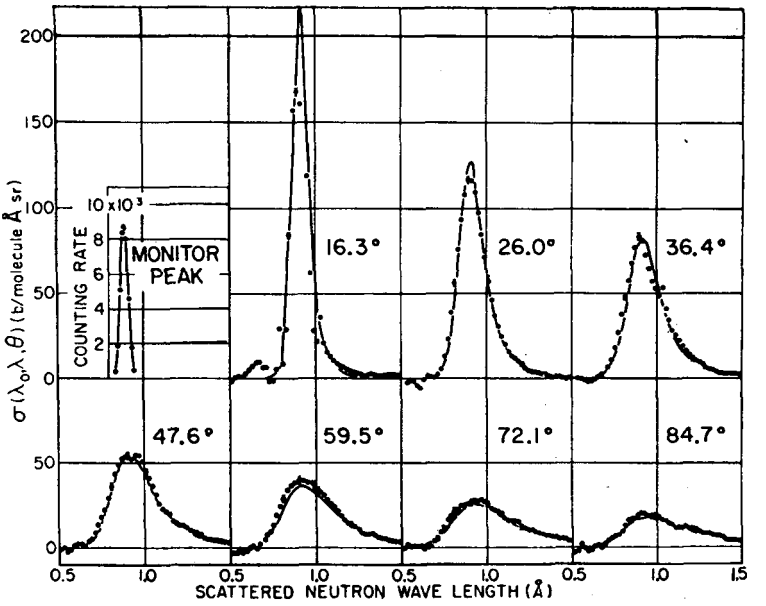

Fig. 2

The differential cross-section for neutron scattering in CH_4 gas
Incident neutron energy 0.103 eV; $\lambda_0 = 0.893$ Å;
curves from Krieger-Nelkin theory; experimental points of RANDOLPH et al. [12].

tering angles and completely disappears at 75° and 90°. Also an energy-gain peak at about 0.01 eV was obtained, which appears with unchanged intensity at all angles. Figure 5(b) shows a comparison of our calculation using the Krieger-Nelkin theory with those of CZERLUNCZAKIEWICZ and KOWALSKA [14] which were based on the Griffing theory. It is evident from this comparison that the inelastic peak is caused by a similar "collective contribution" of rotational levels of the NH_3 molecule, as already discussed in connection with the Griffing calculations for methane.

The situation described above demonstrates clearly that there is a possibility of investigation of the rotational properties of molecules by using neutrons and that this investigation should be made by using cold neutrons rather than those of intermediate or thermal energies.

It should be noted that from a practical point of view it is very important to know in which calculations it is justified to use the very simple Krieger-Nelkin theory and when, on the other hand, the much more complicated and tedious calculations based on the Griffing theory should be applied. An analysis of this problem has been made by KOSALY and SOLT [15] who gave the following results for a molecule consisting of atoms having a mass M: the Sachs and Teller mass-tensor approximation may be used only for special values of the temperature of a gas T, rotational constant B, and the $\kappa^2/2M$ value, i.e. for $T \gg B$ and $\kappa^2/2M \gg B$. One may then say that the Sachs and Teller mass-tensor approximation is a typical large-recoil, high-temperature one.

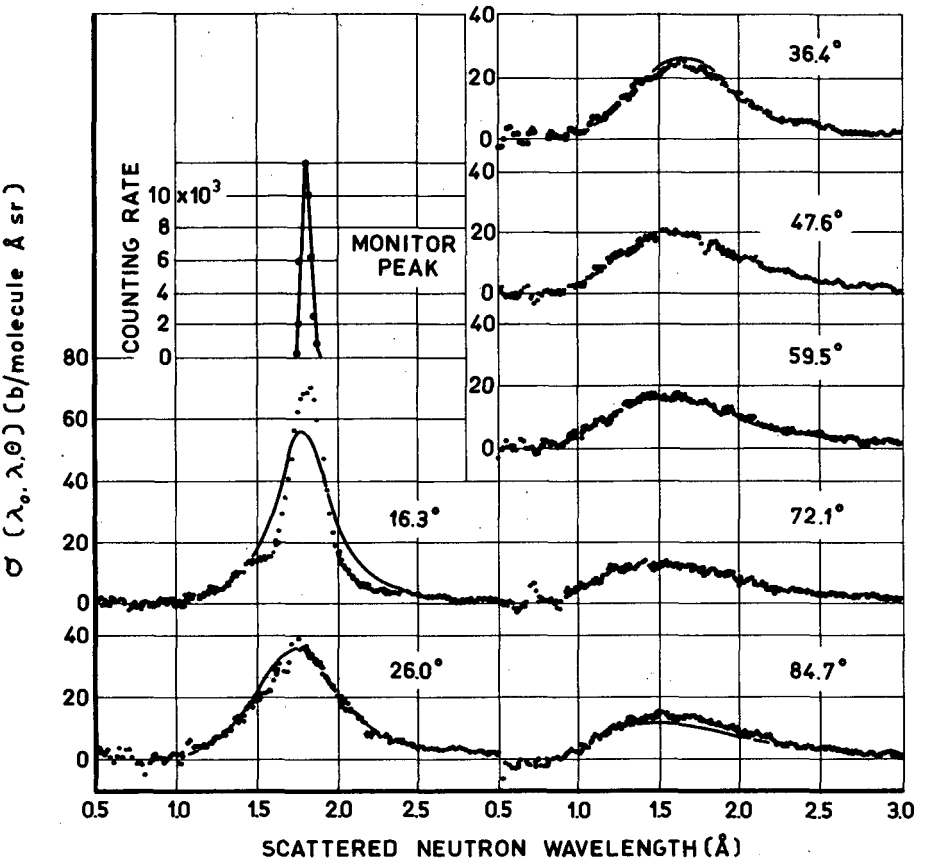

Fig. 3

The differential cross-section for neutron scattering in CH_4 gas
Incident neutron energy 0.0252 eV; $\lambda_0 = 1.803$ Å;
curves from Krieger-Nelkin theory; experimental points of RANDOLPH et al. [12].

If one now passes to the Krieger-Nelkin approximation one may check that it gives results close to the mass-tensor approximation only for small κ-values or for very high temperatures. The condition of small κ-values conflicts with the mass-tensor validity condition $\kappa^2/2M \gg B$. In practice one may conclude, according to KOSALY and SOLT [66], that the Krieger-Nelkin approximation may only be applied for the "intermediate case", $B \ll \kappa^2/2M \ll T$, which usually is quite a large region.

3. PROBLEMS IN CONNECTION WITH NEUTRON SCATTERING BY MOLECULES IN CONDENSED STATES

In all existing theories on neutron scattering by molecules a lack of intermolecular interactions was assumed, which permitted the application

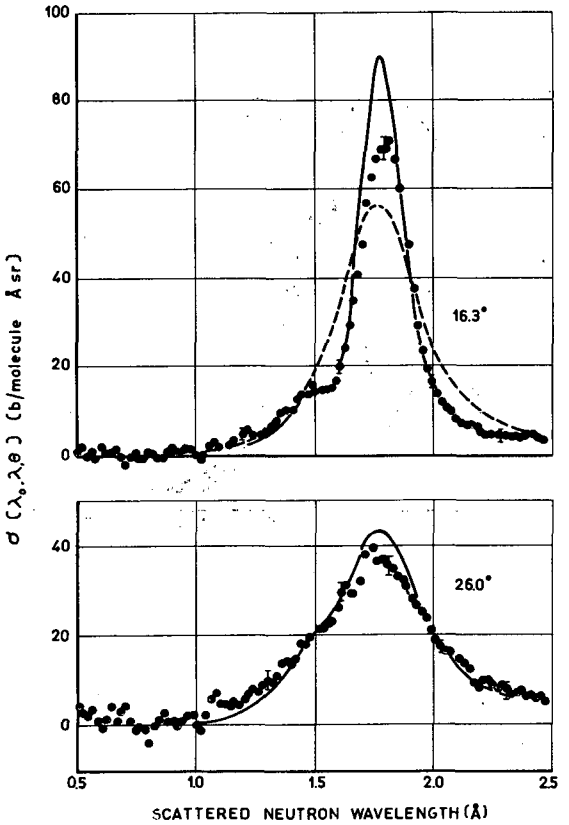

Fig. 4

A comparison of the Krieger-Nelkin theory and that of Griffing with the experiment for CH_4 gas [6]
$E_0 = 0.0252$ eV; $\lambda_0 = 1.803$ Å

of these theories to gases[2]. In some cases, however, as, for instance, for unassociated molecular liquids or even some molecular crystals, in which the molecular rotation is believed to be free or only slightly hindered, it is difficult to see any objection to the application of these theories. And, in fact, it was experimentally proved by ROGALSKA [16] and also WHITTEMORE [17] that the total cross-section for neutron scattering by liquid methane versus neutron energy is very well explained by the Krieger-Nelkin formula (Fig. 6). This agreement was even used as proof that the molecular rotation in liquid methane is free.

The situation is unfortunately not so simple if one passes from total to differential scattering cross-sections. In Fig. 7 the results for liquid methane obtained by JANIK et al. [19] at Brookhaven National Laboratory are compared with the Krieger-Nelkin theory. Incident neutrons were beryllium-

[2] It should be mentioned that the Fermi theory [1] led to entirely different applications, i.e. to crystalline hydrides of metals [18].

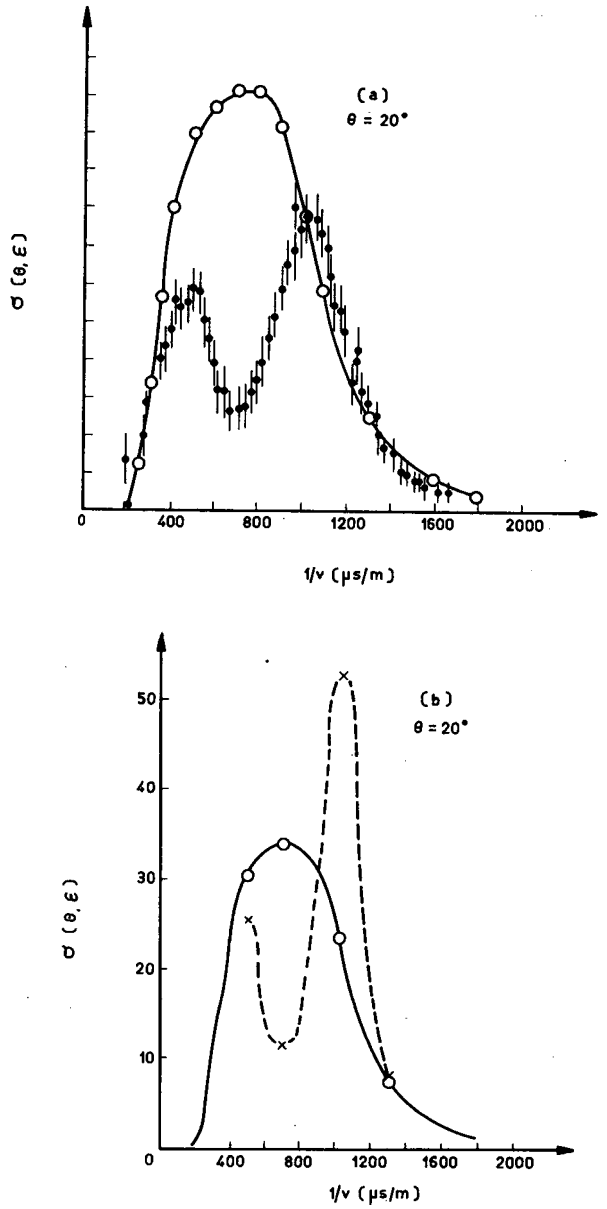

Fig. 5

A comparison of the Krieger-Nelkin theory and that of Griffing with the experiment [13] for NH_3 gas [14]

—— Krieger-Nelkin theory

– – – Griffing theory

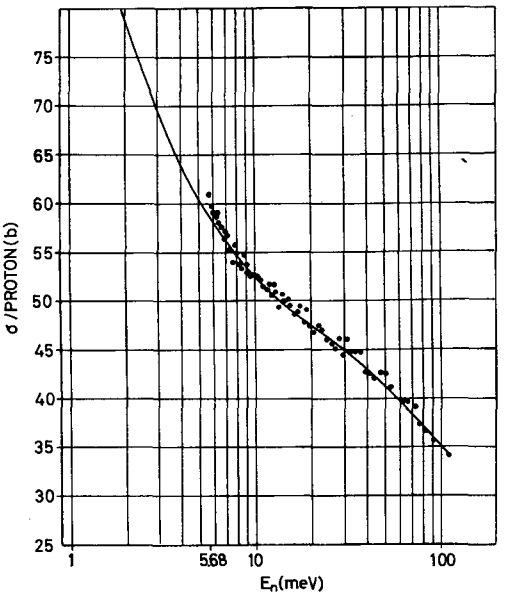

Fig. 6

A comparison of the measured total neutron scattering cross-section for liquid methane with the Krieger-Nelkin theory [16].

filtered and the scattering angle was 90°. It is true that some objections could be made to any expectation of agreement between the theoretical and experimental scattered neutron distribution, in view of the low-energy value of incident neutrons. The neutrons scattered by methane gas, however, (see Fig. 8) give a much smaller deviation from the Krieger-Nelkin theory, as was proved by OTNES [20]. A high value of the scattering angle (90°) also justifies a comparison with the Krieger-Nelkin theory in spite of low neutron energies. It can, however, be seen from Fig. 7. that there is no agreement with this theory, as the experimental scattered neutron distribution is significantly shifted towards higher energies. (It should be made clear that the theoretical curve was calculated for the effective mass value for the CH_4 molecule equal to 4 M, which corresponds to freely rotating molecules with translational motion completely hindered.) If one tries to fit the experimental points of Fig. 7 by Krieger-Nelkin-like distribution, one must have an effective mass value of 2.1 M for 90° scattering angle.) It is difficult to understand why the condensed state caused not an increase but a decrease of the effective mass.

An even stronger argument against the possibility of applying the Krieger-Nelkin theory to condensed methane may be deduced from Fig. 9, which shows the results for three angles of scattering obtained by JANIK et al. [19]. After normalization of these results to the same height of inelastic parts, one may see their lack of dependence on the scattering angle, this being in violent disagreement with the Krieger-Nelkin theory.

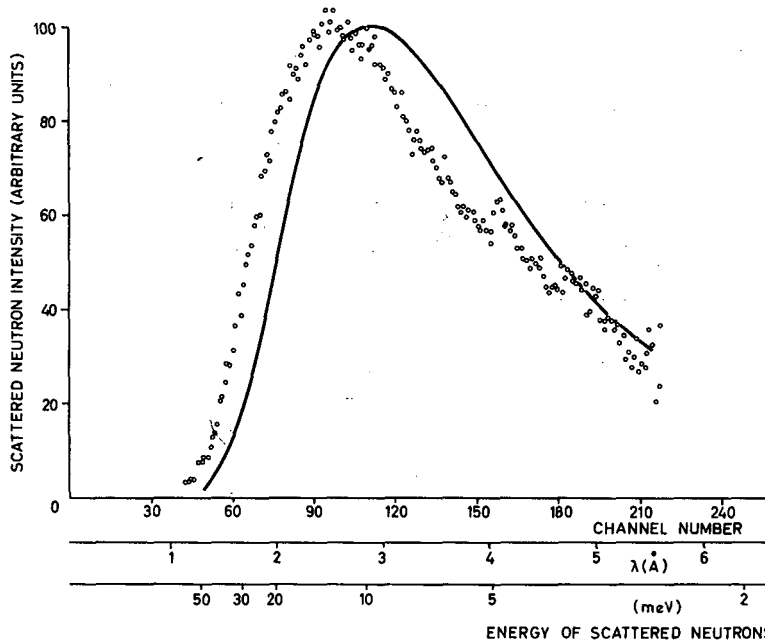

Fig. 7

A comparison of the measured scattered neutron distribution for liquid methane with the Krieger-Nelkin theory [19]
Incident neutrons were beryllium filtered.
$\Theta = 90°$ and $T = -173°C$

Thus it is evident that the ordinary Krieger–Nelkin theory cannot be applied to the differential cross-section evaluation in condensed states, even if the molecules are freely rotating as is obviously the case for liquid methane. It is believed that the Sachs and Teller mass-tensor concept cannot be maintained in condensed systems[3].

4. AMMONIUM COMPOUNDS (TORSIONAL FREQUENCY EVALUATION)

In spite of the lack of a satisfactory theory of neutron scattering by molecular liquids and crystals, neutrons have been used by various authors as a tool for investigating the rotational dynamics of molecules. This application may be treated as being complementary to the infrared or Raman spectroscopy and also to heat capacity measurements, from which information concerning either the rotational freedom or, in the case of hindered rotation, the torsional frequency value may be deduced.

[3] It should be noted here that WHITTEMORE and DANNER [85] have measured the energy distribution of primarily monoenergetic neutrons (0.065 eV) scattered at an angle of 90° by liquid para-hydrogen and liquid ortho-para-hydrogen. The distribution agreed fairly well with that given by a theory of SARMA [86], which takes the quantum rotational states into consideration. From the agreement one may deduce the fact of a free rotation of hydrogen molecules.

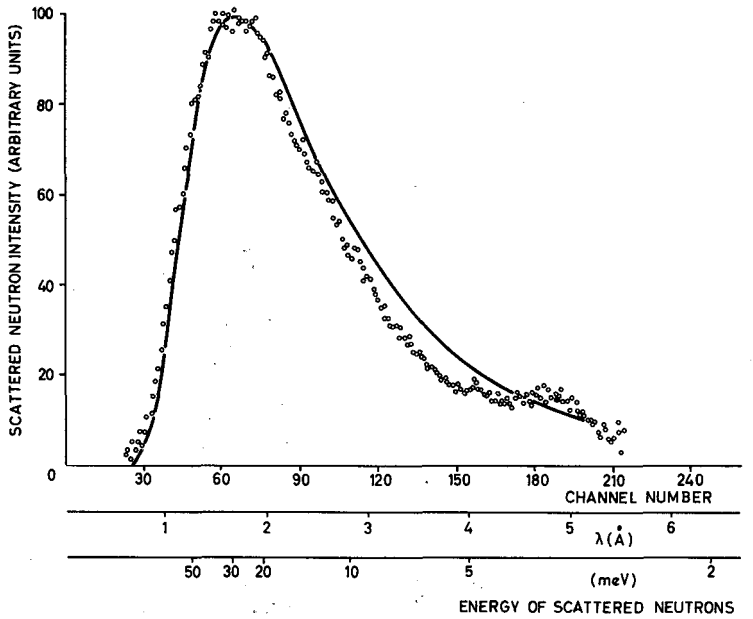

Fig. 8.

A comparison of the measured scattered neutron distribution for gaseous methane with the Krieger-Nelkin theory [20].
Incident neutrons were beryllium-filtered.
$\Theta = 90°$; room temperature

In discussing this problem we first present the situation for ammonium halides, which has been studied by various authors.

Neutrons were applied to ammonium halides both in the normal and inverted beryllium technique [21–26, 52] and in a wide temperature region, covering a number of phase transition points. As some of these points were interpreted as a transition from hindered to free rotation of the NH_4 ion it was interesting to look at the difference of neutron spectra. In fact, at higher temperatures, corresponding to phase I ($T > 185°C$ for NH_4Cl, $T > 134°C$ for NH_4Br, $T > -16°C$ for NH_4I), one obtains a broad distribution of scattered neutrons without any appearance of sharp peaks, this situation appearing to be typical for freely rotating NH_4 ions (Figs. 10 and 11). At lower temperatures, on the other hand, one obtains sharp peaks, some of which may be interpreted as being caused by torsional vibration (Figs. 11, 12, 13). If the peaks are sufficiently narrow one may calculate from their energy that of an excited level of the NH_4 ion (or the corresponding frequency in cm^{-1}). Table I shows the results obtained in this way for torsional vibrations in ammonium halides at room temperature. There is only a slight change of frequency of torsional vibrations when the temperature is lowered.

With regard to peaks other than those caused by torsional vibration it is very often difficult to give any adequate interpretation. In the case of NH_4Cl WOODS et al. [22] give the following one: The peak at 0.023 eV is

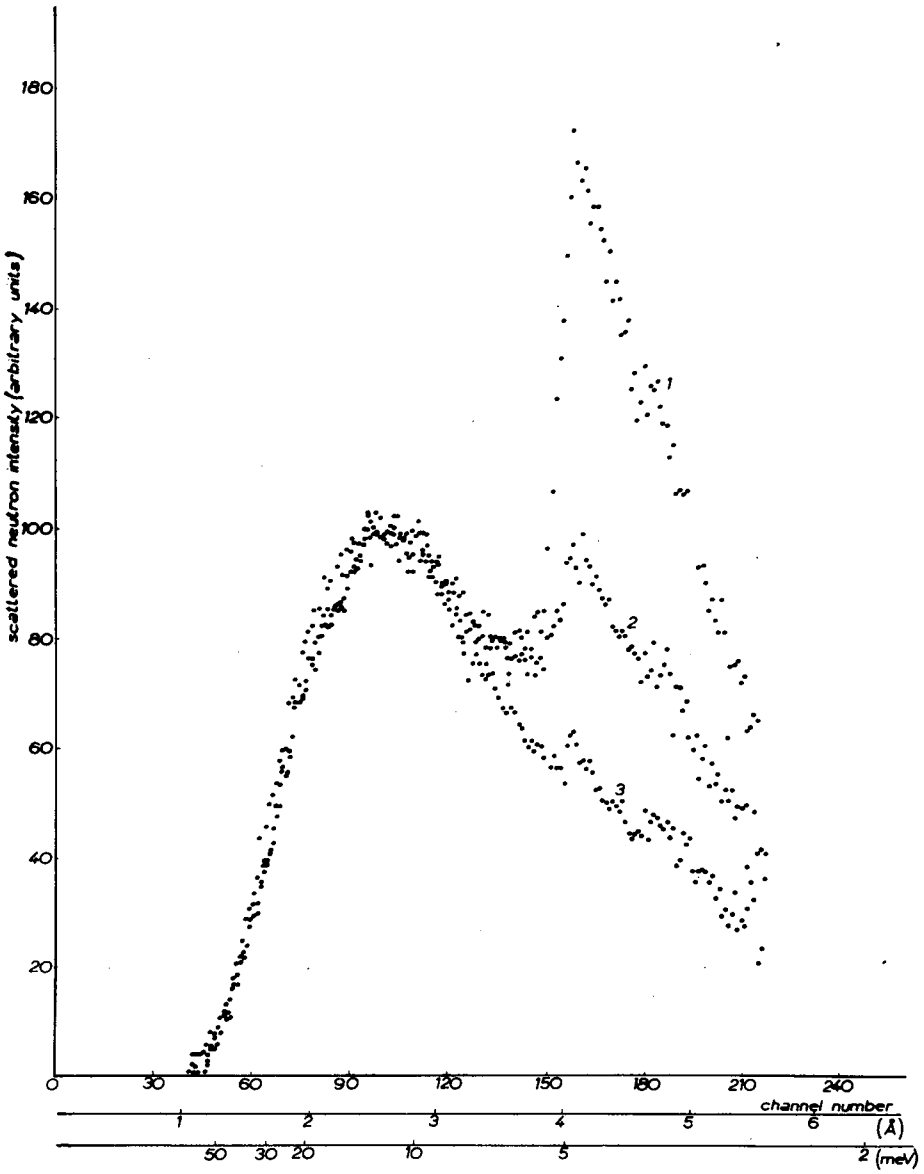

Fig. 9

Scattered neutron distributions for liquid methane measured at various scattering angles
Normal beryllium filter method; T = -173°C
1. Θ=35° 2. Θ=60° 3. Θ=90°

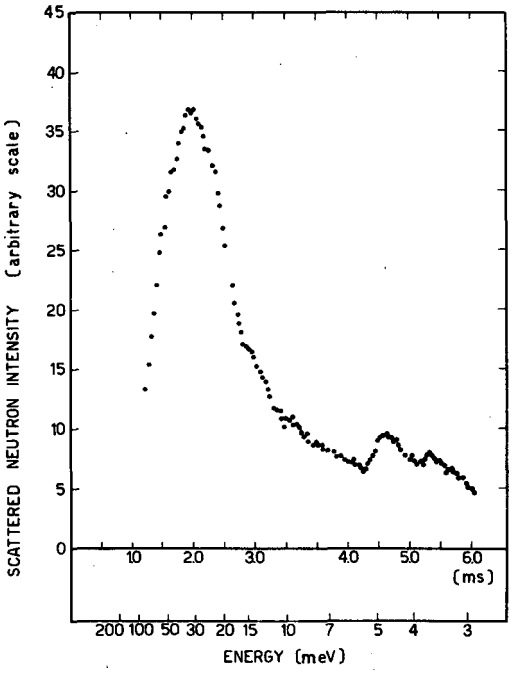

Fig. 10

Neutron spectrum after scattering by NH_4I
Scattering angle 90°; room temperature; normal beryllium filter method [25].

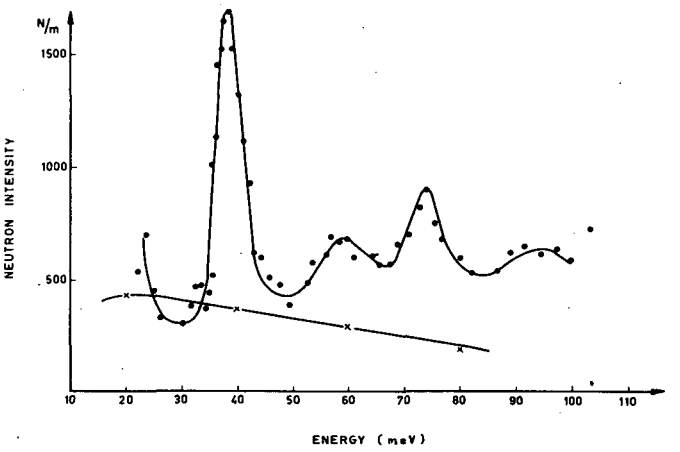

Fig. 11

Neutron spectrum after scattering by NH_4I
Scattering angle 90°; temperatures below and above the transition point; inverted beryllium filter method [23].

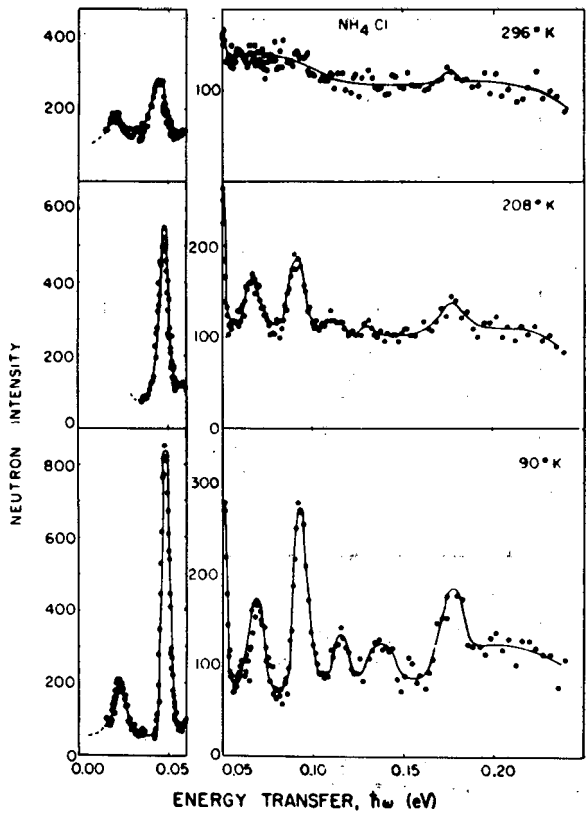

Fig. 12

Scattered neutron distribution for NH_4Cl
Scattering angle 90°; inverted beryllium filter [22].

probably connected with the optical vibration of the NH_4 radical against the Cl atom; the peak at 0.049 eV corresponds to the hindered rotation of the NH_4 ion and it is this peak which was included in Table I. Further peaks at 0.070, 0.094, 0.116, 0.138 and 0.178 eV are probably combination bands of 0.023-and 0.049-eV peaks. The peak at 0.178 eV is possibly the bending mode of the NH_4 group. It should be mentioned also that the peak at 0.025 eV obtained by PALEVSKY [21] for NH_4Br was similarly interpreted by him as a vibration of the NH_4 ion in the Br lattice.

On the basis of these results neutrons may be classified as a very good tool for obtaining information of molecular energy levels in solids in the frequency region of several hundreds of cm^{-1}. One must not forget, however, that these frequencies in ammonium halides, and also in other ammonium salts, have also been measured by using other methods, such as infrared and Raman spectroscopy and the thermodynamic method. Table II presents for comparison the torsional frequencies for ammonium halides obtained by neutrons, infrared spectroscopy and the specific heat measurements. The agreement is very good.

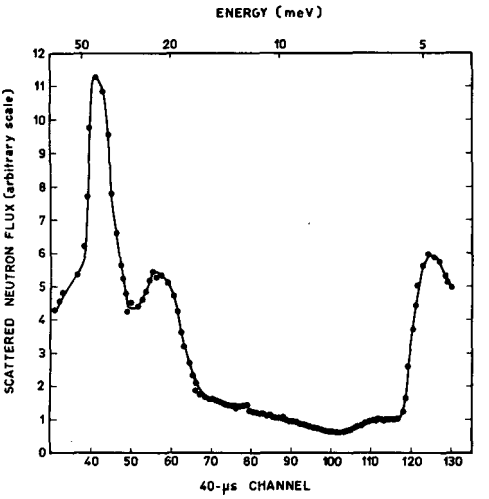

Fig. 13

Scattered neutron distribution for NH_4Br
Scattering angle 90°; room temperature (20°C); normal beryllium filter method [21].

TABLE I

NEUTRON ENERGY CHANGES AND TORSIONAL FREQUENCIES FOR AMMONIUM HALIDES AT ROOM TEMPERATURE

Substance	Energy change (meV)	Torsional frequency (cm^{-1})
NH_4F	69.2 [23]	555 [23]
NH_4Cl	43.4 [24]	350 [24]
	44.3 [23]	355 [23]
	48.5 [22]	388 [22]
NH_4Br	40.2 [24]	324 [24]
	39.3 [23]	315 [23]
		307 [21]
NH_4I	Broad distribution [23,25]	Free rotation

It should also be mentioned that from the classical neutron diffraction studies made for ammonium halides by LEVY and PETERSON [87, 88] it has already been concluded that the most probable motion of the NH_4 ion in high-temperature phase (phase I) is free rotation. Thus, if one takes all kinds of measurements, i.e. neutron diffraction, neutron inelastic scattering, Raman and infrared spectroscopy, thermodynamics and NMR, into account one obtains the following situation concerning the order and dynamics

TABLE II

A COMPARISON OF TORSIONAL FREQUENCIES OBTAINED BY DIFFERENT METHODS

Substance	Torsional frequency from neutron measurements (cm^{-1})	Torsional frequency from infrared spectra (cm^{-1})	Torsional frequency from specific heat (cm^{-1})
NH_4F	555 [23]	523 [29]	520 [27][a]
NH_4Cl	350 [24]	359 [30]	390 [27][a]
	355 [23]		
	388 [22]		
NH_4Br	324 [24]	311 [30]	335 [28][a]
	315 [23]		
	307 [21]		
NH_4I	Free rotation [23, 25]		

[a] These data correspond to a much lower temperature ~100°K.

of the NH_4 ion in ammonium halides. In the low temperature phase the NH_4 ion is ordered and performs torsional vibrations; at intermediate temperatures the NH_4 ion is disordered but this fact does not strongly affect torsional vibrations; the high temperature phase corresponds to a free rotation of the NH_4 ion.

When discussing ammonium halides, one interesting result must be remembered, i.e. the anharmonicity effect of torsional oscillations in NH_4Cl reported by VENKATARAMAN et al. [26]. By applying a neutron energy analyser with a much better resolution than an ordinary beryllium filter the authors observed near the main torsional vibration peak, 351 cm^{-1}, a second peak, 307 cm^{-1} (Fig. 14). These authors interpret the main peak as being caused by the transition from the ground to the first excited torsional state, whereas the satellite is believed to be caused by a transition from the first to the second excited level. The satellite peak does not appear at temperatures as low as 135°K, which supports the interpretation given above.

As already mentioned, neutrons scattered by NH_4I at temperatures lower than the phase transition point at -16°C show a sharp peak caused by torsional vibration. As was proved, however, by DOBRZYNSKI and MIKKE [46], in solid solutions of NH_4I in KI, where the NH_4 ions are well separated, one obtains a broad distribution of scattered neutrons without any evidence of sharp torsional vibration peaks, even at temperatures much lower than -16°C.

A detailed study of ammonium halides has recently been made by BAJOREK et al. [33] at the pulsed reactor of the Joint Institute for Nuclear Research at Dubna. Other ammonium compounds were studied, using neutrons, by BRAJOVIC et al. [31] at Brookhaven National Laboratory and also by JANIK et al. [19, 32] and BAJOREK et al. [33] at the pulsed reactor of the Joint Institute for Nuclear Research at Dubna.

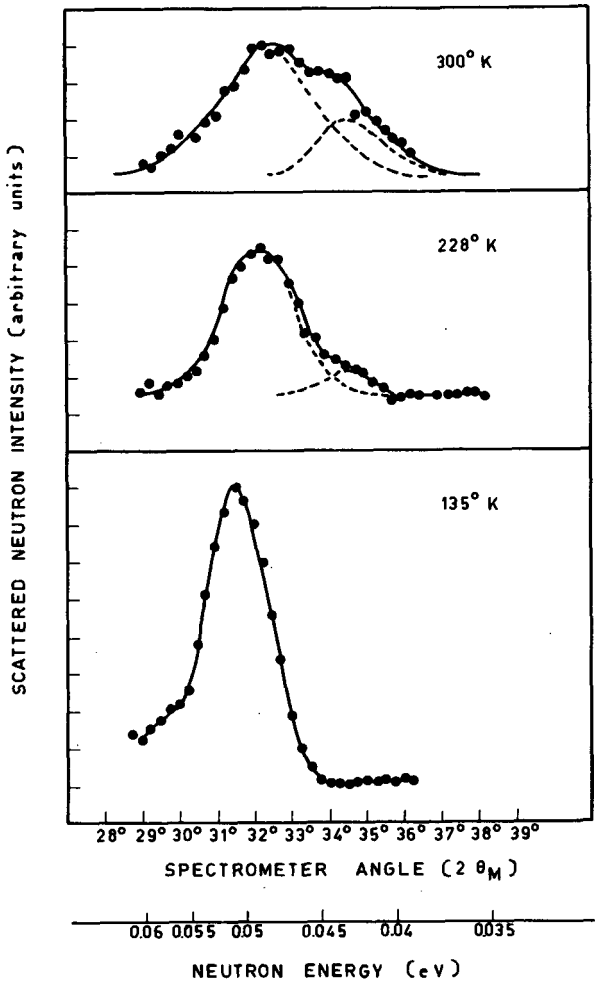

Fig. 14

Scattered neutron distribution for NH_4Cl
Scattering angle 90°; room temperature; improved resolution [26].

BRAJOVIC et al. [31] obtained for NH_4PF_6, $(NH_4)_2S_2O_8$, $NH_4K_xI_{1+x}$ and NH_4SO_3F, at room temperatures, broad distributions of scattered neutrons from which either a free rotation of the NH_4 ion or only a slight hindrance may be deduced. None of those compounds shows any appearance of the torsional vibration peak at room temperature (see Fig. 15). The authors attempt to check in the following way rotational freedom or hindrance in these compounds; if it is possible to fit the points by a Krieger-Nelkin-like curve with an adjusted rotational mass (taken as a parameter) it means that the rotation is free. If not, one must conclude a hindrance of rotation, as the authors have done, for instance, for NH_4SO_3F, the results of which are presented in Fig. 15. In view, however, of the criticism of the application

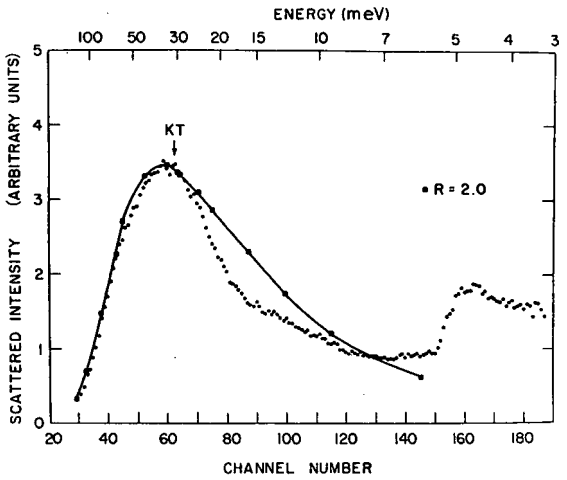

Fig. 15

Scattered neutron distribution for NH_4SO_3F
Scattering angle 90°; room temperature (24°C); normal beryllium filter method [31]

of the Krieger-Nelkin formalism to the condensed states and also in view of the fact that the rotational mass cannot be considered as a variable parameter, this treatment of data does not seem to be convincing.

Studies of ammonium compounds (NH_4NO_3, NH_4CNS, $(NH_4)_2SO_4$, $(NH_4)_2CO_3$), made by BAJOREK et al. at Dubna are discussed in Ref. [33]. The results of JANIK et al. [19, 32] obtained for NH_4ClO_4, partly at Brookhaven and partly at Dubna, are discussed in section 6 of this paper.

5. AMMONIUM COMPOUNDS (BARRIER HEIGHT ESTIMATION)

An approach, other than by scattered neutron measurements, to investigations of the rotational dynamics of NH_4 ions in ammonium compounds has been proposed by RUSH et al. [34-36]. It is based on total cross-section measurements for long wavelength neutrons (4 - 10 Å). The total cross-section versus neutron wavelength appears to be a straight line in this region and its slope seems to be directly related to the barrier-to-rotation height. Figure 16 shows that for ammonium halides there exists indeed a correlation; for instance, the slope for NH_4F is much lower than that for NH_4I, and it is well known that hindered rotation is the highest for fluoride and very low for iodide.

A method which has been used up to now for barrier determination in molecular solids is based on the NMR technique. In fact, for some ammonium salts, barriers are already known from NMR. Following the idea of RUSH et al. [35], one may then draw a calibration curve for the neutron barrier determination method by taking the cross-section slopes measured and the barriers from NMR measurements. Such a calibration curve was presented by RUSH et al. [35] and is shown in Fig. 17.

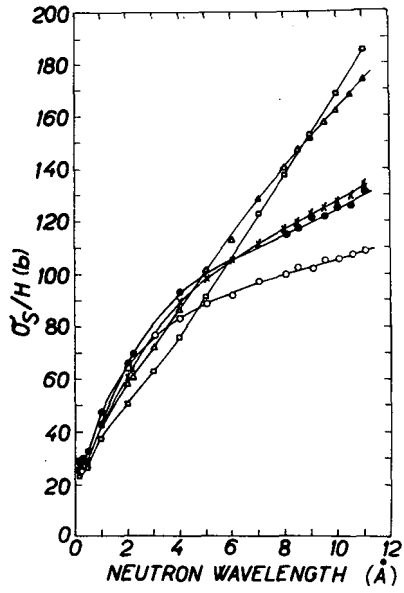

Fig. 16

Total neutron scattering cross-section versus neutron wavelength for ammonium halides [34]

△ NH_4I (11.2 b/Å)
□ NH_3 (15.5 b/Å)
● NH_4Cl ((4.8 b/Å)
× NH_4Br (5.7 b/Å)
○ NH_4F (2.8 b/Å)

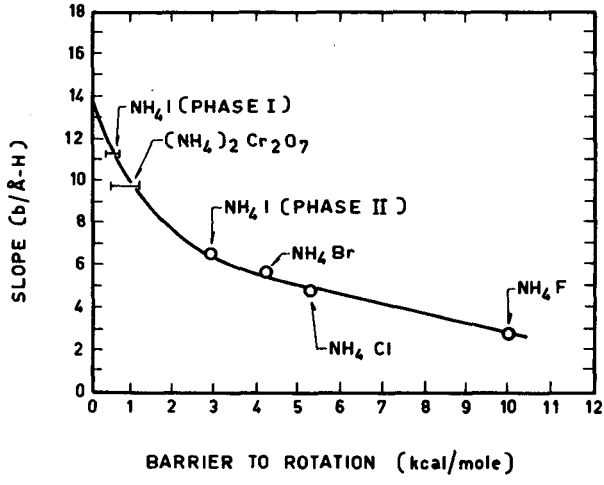

Fig. 17

Cross-section slope versus barrier-to-rotation height [35]

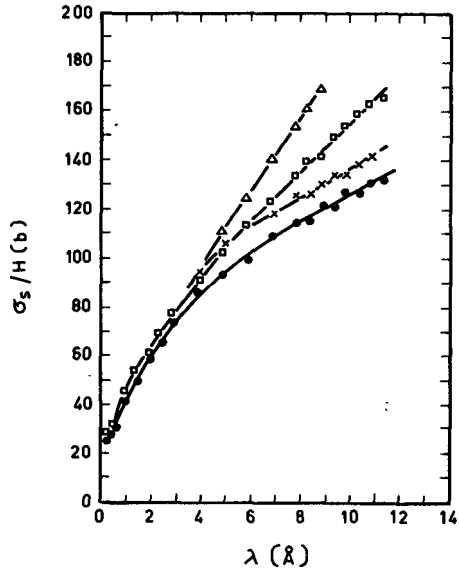

Fig. 18

Total neutron scattering cross-section versus neutron wavelength for ammonium compounds [35]

△ NH_4ClO_4 (~13 b/Å)
□ $(NH_4)_2Cr_2O_7$ (9.7 b/Å)
× NH_4CNS (5.8 b/Å)
● $(NH_4)_2CrO_4$ (5.5 b/Å)

Using this curve, and the measured slope values (Fig. 18), the authors were in a position to evaluate the unknown barriers for $(NH_4)2CrO_4$ and NH_4CNS for 4 kcal/mole and the barrier for NH_4ClO_4 for only 0.1-0.2 kcal/mole. This last barrier value is discussed in section 6.

6. COMPARISON BETWEEN THE ROTATIONAL DYNAMICS OF AMMONIUM AND HYDRONIUM GROUPS IN NH_4ClO_4 AND H_3OClO_4.

It has been proved by the X-ray technique [37, 38] that NH_4ClO_4 and H_3OClO_4 not only belong to the same orthorhombic crystallographic system but also possesss practically identical lattices of ClO_4 ions. It is therefore interesting to compare the dynamic properties of the NH_4 and H_3O groups in these crystals.

In our group three types of neutron experiments have been applied in the study of these properties. The first type, performed by JANIK et al.[19] at the Brookhaven National Laboratory utilized the beryllium filter arrangement in a normal geometry; in the second type, performed by JANIK et al. [32] at the Joint Institute for Nuclear Research at Dubna, the inverted beryllium filter in conjunction with the pulsed reactor was used; in the third type (JANIK [39]), the total neutron scattering cross-section was measured by using a slow chopper at the EWA reactor at Swierk, Poland.

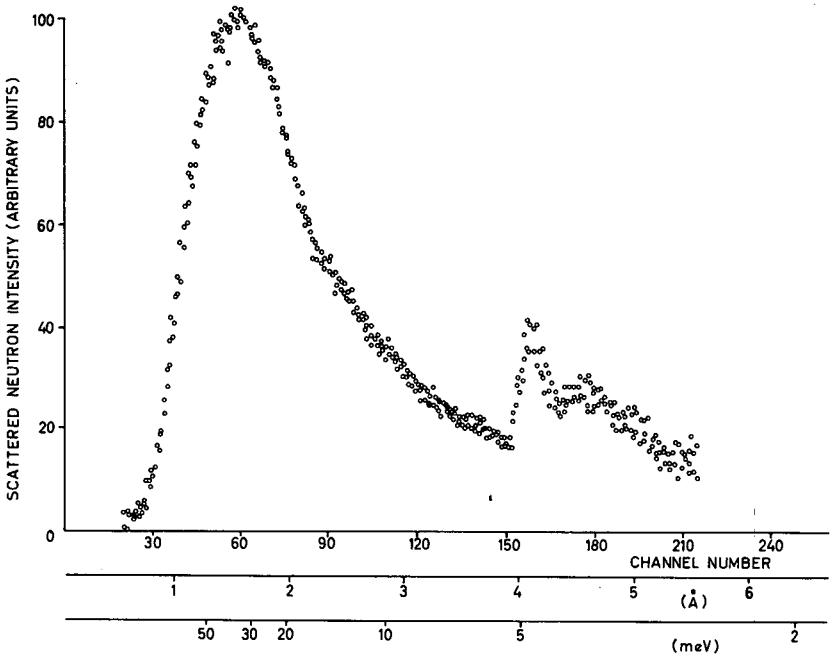

Fig. 19

Scattered neutron distribution for NH_4ClO_4
Scattering angle 90°; room temperature; normal beryllium filter method [19].

Results obtained for NH_4ClO_4 and H_3OClO_4 at room temperature at Brookhaven are presented in Figs. 19 and 20. Figures 21 and 22 show results for NH_4ClO_4 at various temperatures, between the liquid nitrogen and room temperature, and for H_3OClO_4, at room temperature, obtained at Dubna. Figure 23 presents the total neutron scattering cross-section for H_3OClO_4 versus neutron wavelength measured at Swierk.

From the lack of any sharp peak in the neutron spectra obtained for the whole temperature region for NH_4ClO_4 one may conclude that no torsional vibration levels exist and therefore the hypothesis of free rotation of NH_4 ions in this compound is strongly confirmed. This result agrees with the interpretation of data obtained by RICHARDS and SCHAEFER [40] by the NMR method, from which a low (less than 1 kcal/mole) barrier to rotation of the NH_4 ion has been concluded. (It should, however, be mentioned that IBERS' [41] NMR data were interpreted by the authors as leading to the barrier value of ~2 kcal/mole.) WADDINGTON's [42] infrared data for NH_4ClO_4 also suggest free rotation of the ammonium ion. Moreover the value of the slope of total neutron scattering obtained by RUSH et al. [35] versus neutron wavelength dependence, which amounts to 13 b/Å for the room temperature NH_4ClO_4, leads to a barrier value of 0.1 - 0.2 kcal/mole, i.e. a practically free rotation.

The neutron spectra obtained for the room temperature H_3OClO_4 show a sharp peak which is believed to be caused by the torsional vibration of the

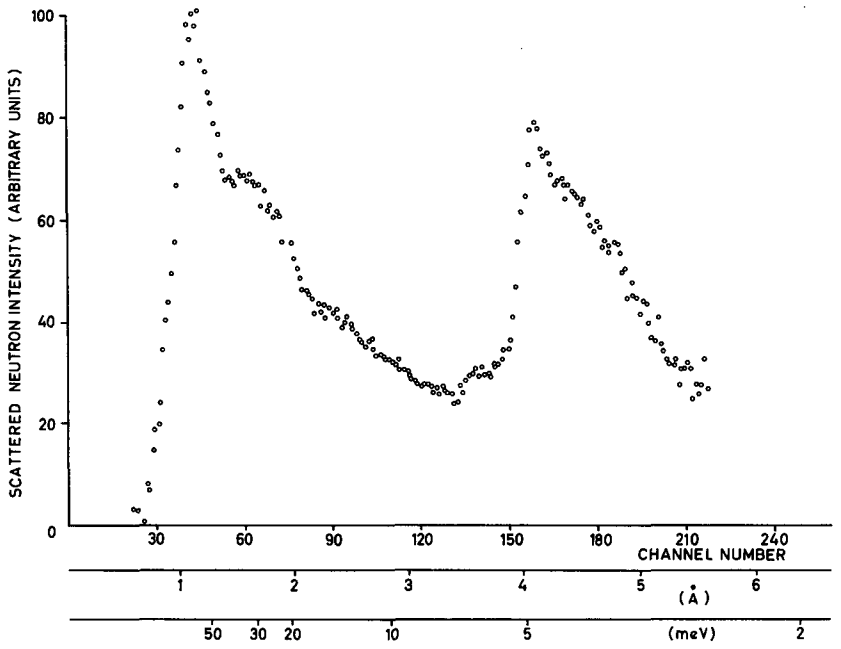

Fig. 20

Scattered neutron distribution for H_3OClO_4
Scattering angle 90°; room temperature; normal beryllium filter method [19].

H_3O ion. In the neutron spectrum of Fig. 20 this peak corresponds to an energy gain of 0.056 eV, and in the spectrum of Fig. 22 to an energy loss of 0.054 eV, so that there is an agreement within the limits of experimental errors. On the basis of data obtained at Dubna (Fig. 22) an attempt has been made to present the results in a form independent of the neutron scattering dynamics, but dependent only on the molecular dynamics of the substance. This was done by a transformation of data from a $d^2\sigma/d\Omega dE$ form to the form $p_H(\epsilon)e^{-2W}$, where p_H is the frequency distribution of hydrogen atoms, $\epsilon=\hbar\omega$ corresponds to the neutron energy loss, and e^{-2W} is the Debye-Waller factor. This function obtained for H_3OClO_4 (presented in Fig. 24) shows a maximum at $\epsilon = 0.062$ eV which, according to our interpretation, should correspond to $\hbar\omega_L$ (ω_L being torsional frequency); this gives for ω_L 497 cm^{-1}.

It is worthwhile to note that the Raman frequency, 995 cm^{-1}, obtained for H_3OClO_4 by TAYLOR and VIDALE [43] was interpreted by them as ω_L. If, however, it is not ω_L but $2\omega_L$, one obtains for ω_L 497 cm^{-1}, which is in very good agreement with our results.

With regard to the suggestion of a free rotation of an H_3O group in H_3OClO_4 made by KAKIUCHI et al. [44] on the basis of the NMR measurements, it should be pointed out that from a narrow line one cannot simply conclude a rotational freedom but only a re-orientational frequency greater than ~50 kc/s. This re-orientation does not exclude the existence of torsional vibrations.

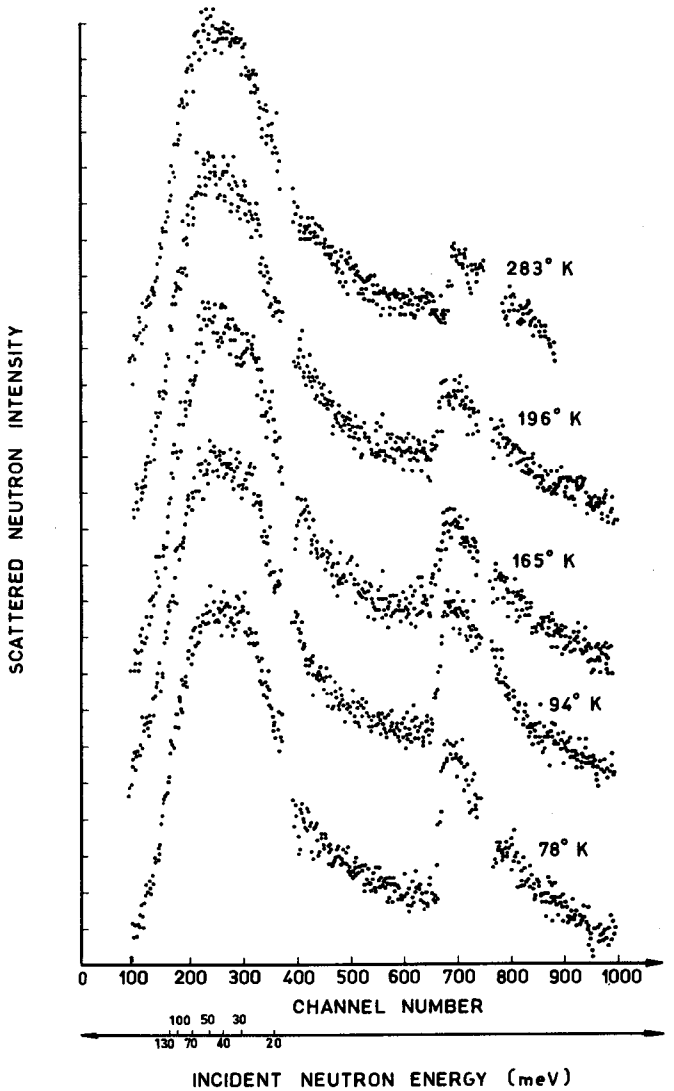

Fig. 21

Scattered neutron distribution for NH_4ClO_4 at various temperatures
Scattering angle 90°; inverted beryllium filter method [32]

Also the relatively low value of the total cross-section slope for H_3OClO_4 [39] (8 b/Å as compared with 13 b/Å for NH_4ClO_4 (Fig. 18)) as seen from Fig. 23, leads to the conclusion that the rotation of H_3O groups is hindered. If one applies the RUSH et al. [35] calibration curve (Fig. 17) to this value, one obtains for the barrier to rotation 1.8 kcal/mole.

The final conclusion, which may be made on the basis of the experiments described above, is that in spite of the identity of the ClO_4^- lattices

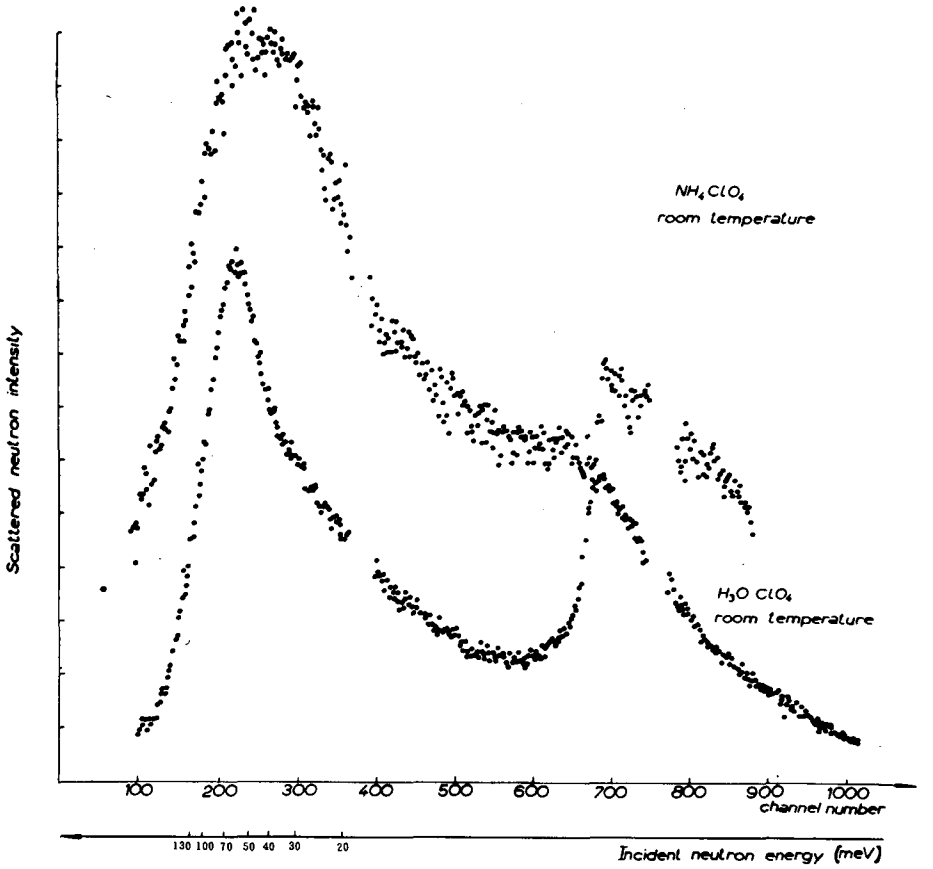

Fig. 22

Scattered neutron distribution for H_3OClO_4 and for NH_4ClO_4 at room temperature
Scattering angle 90°; inverted beryllium filter method [32]

for NH_4ClO_4 and H_3OClO_4, the molecular dynamics of ammonium and hydronium ions are entirely different. The NH_4 ion performs a free rotation even at the liquid nitrogen temperature whereas the H_3O ion performs torsional vibration with a frequency of ~497 cm^{-1} in a hindering potential of 1.8 kcal/mole.

7. LIQUID AND SOLID METHANE

The rotational dynamics of CH_4 molecules in liquid methane were first studied by the neutron scattering method by ROGALSKA [16] and WHITTEMORE [17] independently. As already mentioned in section 3, from an agreement between the experimental total neutron scattering cross-section versus

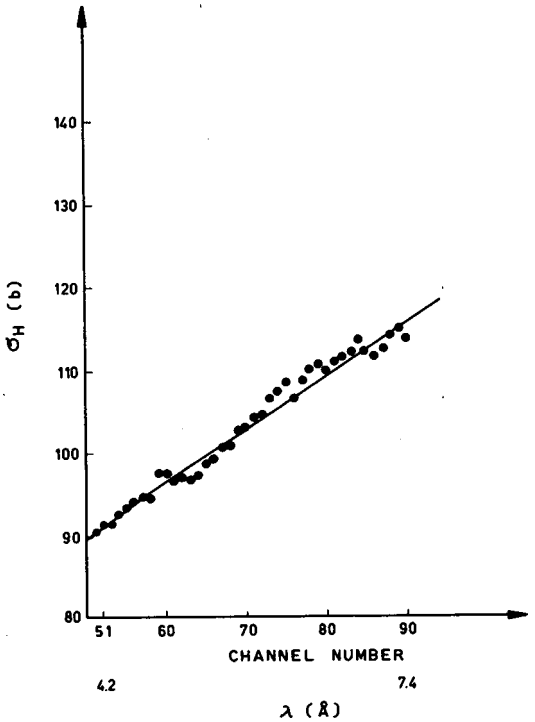

Fig. 23

Total neutron scattering cross-section versus neutron wavelength for H_3OClO_4 (8 b/Å) [39].

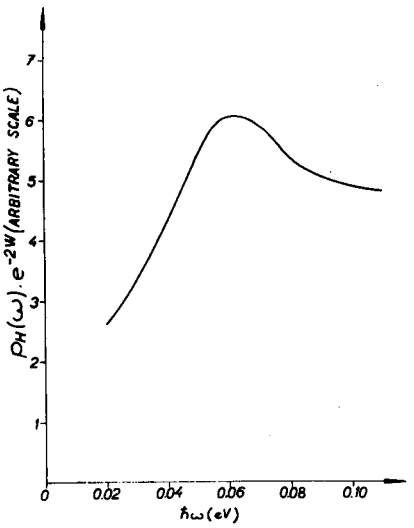

Fig. 24

$p_H(\epsilon)\, e^{-2W}$ function for H_3OClO_4 [32]

the neutron energy curve and the Krieger-Nelkin theory, a conclusion was drawn that the CH_4 molecules rotate freely in the liquid state[4].

Total cross-section measurements were then extended by ROGALSKA [55] to the long wavelength region (4.2 - 7.4 Å) and a comparison between the cross-section slopes for liquid CH_4 (105°K) and for solid CH_4 (80°K) was made. From the practical identity of these slopes (7.9 b/Å-H and 7.0 b/Å - H, respectively) a free or almost free rotation in solid methane at 80°K was concluded. Similar measurements were also made by VAN DINGENEN and NEVE de MEVERGNIES [58] but the interpretation is not based directly on the molecular motion.

A detailed study of liquid and solid methane was made by HAUTECLER and STILLER [59, 60] and DANNER and STILLER [61] by applying the inverted beryllium filter technique. Experiments gave information relating to four temperatures: 102°K (liquid), 84°K (solid), 18°K and 6.5°K. A rotational hindrance or freedom was concluded from the steps which were observed in the scattered neutron spectrum, as shown in Fig. 25. For liquid CH_4 at 102°K the steps are distinct and may be attributed to the separate rotational levels of the molecules; it may be postulated that the molecules are freely rotating, in agreement with what was obtained by Rogalska and Whittemore. The situation at 84°K is somewhat confusing and perhaps the safest statement would be to say that there is considerable hindrance of rotation which, however, is not yet degenerated to torsional oscillations. At lower temperatures, on the other hand, it may be concluded that torsional motions exist and cover the frequency ranges 5.8-8.5 meV and 10.2-15 meV.

It should be pointed out that the investigations mentioned above should be treated as complementary to those investigations made other than by neutron methods. Among these methods are the NMR experiments in solid CH_4 described by TOMITA [62]. In discussing the results the author concludes that at temperatures below 20°K there is a torsional oscillation. Above 65°K the rotation is free or slightly hindered and does not degenerate to a torsional motion.

These results agree with those obtained by SAVITSKY and HORNIG [73] using the infrared spectra. According to their interpretation there exists a rather high barrier to rotation of the CH_4 molecules in crystalline phase below 40°K.

8. ICE, WATER AND WATER OF CRYSTALLIZATION

In this section the molecular motions of H_2O molecules are only briefly discussed (see Ref. [89] for the survey on liquids). Problems concerning molecular diffusion are also not discussed here.

As in the case for liquid methane (as also for liquid NH_3 and H_2S) some information concerning molecular rotation in water has already been drawn from the total scattering cross-section by NELKIN [63], who was able to

[4] It should be mentioned here that similar measurements were also made for liquid ammonia [56] and liquid hydrogen sulphide [57], which were compared to those made for gases. From the practical identity between gas and liquid a free rotation in liquid H_2S was concluded, whereas a large difference for liquid NH_3 led to the conclusion of a rotational hindrance.

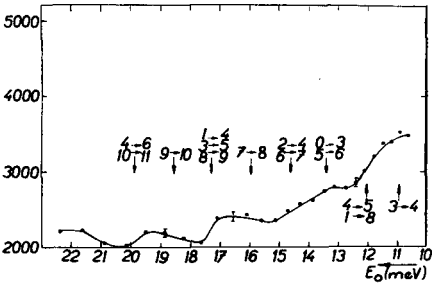

Fig. 25

Scattered neutron distribution for liquid CH_4 at 102 °K
Scattering angle 90°; inverted beryllium filter method; numbers denote the calculated rotational transitions [59].

explain the cross-section versus energy curve, assuming a torsional vibration of H_2O molecules with a frequency of 0.06 eV.

Neutron differential scattering cross-sections were measured by a number of authors [22, 64, 65, 67, -70] and some of the results are conflicting, though there is no doubt that there exists in the neutron spectrum a broad band around 0.05-0.08 eV, one corresponding to an energy change of 0.0066 eV and one around $\Delta E = 0.025$ eV. These bands appear in ice as well as in water near the freezing point. Figure 26(a) presents as an example the neutron spectra scattered from H_2O at two temperatures and Fig. 26(b) the hydrogen frequency distribution functions for solid and liquid H_2O, obtained by LARSSON and DAHLBORG [70].

Some recent measurements for ice and water made by a group working at the pulsed reactor at Dubna [71] do not agree with the statement of Larsson and Dahlborg that the frequency spectra of water and ice nearly coincide. A more detailed report on this is presented in Ref. [71].

As far as an interpretation of the bands obtained in the inelastically scattered neutron spectrum is concerned, it should be said that a generally accepted explanation of the band 0.05-0.08 eV is based on hindered rotation of water molecules. The 0.0066-eV peak may be caused by vibrations of the whole molecule around its gravity centre. The peak about 0.025 eV may perhaps be ascribed to a vibration of the OH group as a whole towards the other O atom.

It should also be mentioned that the positions of the three bands nearly coincide with those formerly obtained by the Raman technique [72].

Water of crystallization was studied by inelastic neutron scattering by BOUTIN et al. [74] for natrolite ($Na_2Al_2Si_3O_{10} \cdot 2H_2O$). Figure 27 shows the spectra of beryllium-filtered neutrons inelastically scattered at 293 and 493°K. As compared with the water or ice spectra, they show a large number of well-resolved peaks. The peak around 245 meV is interpreted as being caused by the fundamental deformation frequency of the H_2O molecule, ν_2. The peak at 18 meV is probably associated with a translational motion of two oxygens in the hydrogen bond along the O-O line. The two peaks at 60 and 78 meV suggest that torsional oscillations similar to those in water or ice exist also in water of crystallization.

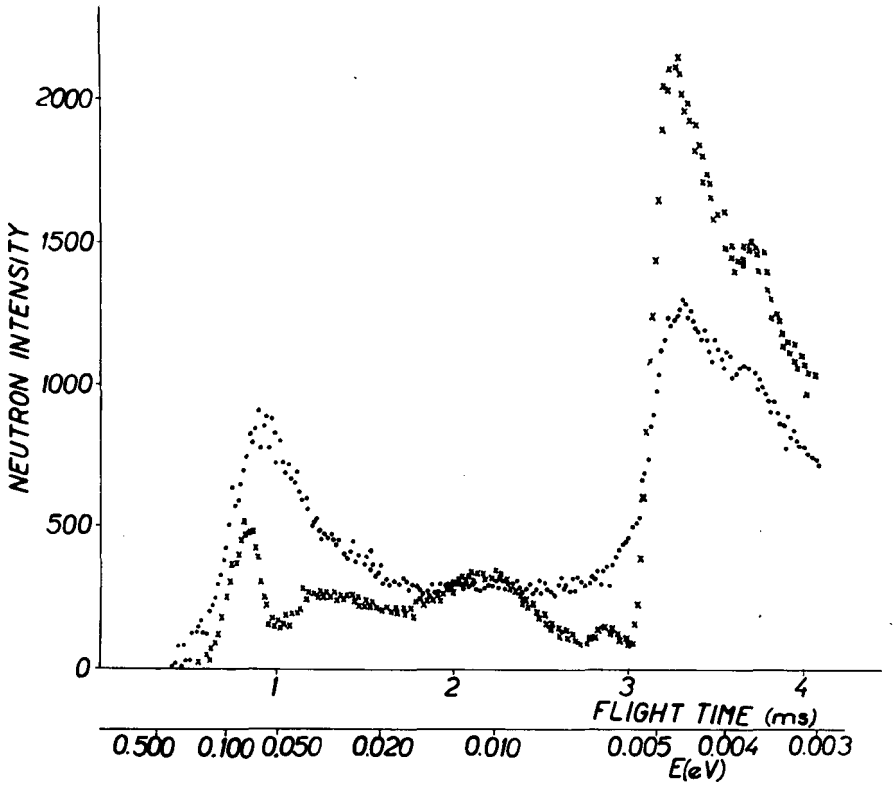

Fig. 26(a)

Scattered neutron distribution for water

Temperatures: × 275°K
• 365°K

Scattering angle: 90°

Normal beryllium-filter method

It should be pointed out that a detailed study of neutron spectra obtained by scattering from water of crystallization in $BaCl_2 \cdot 2H_2O$, $SrCl_2 \cdot 2H_2O$, $CaSO_4 \cdot H_2O$, $CuSO_4 \cdot 5H_2O$ and some others has recently been made by BAJOREK et al. [33].

9. HF, KHF_2, KH_2F_3, NaH_2F_3, KH_2PO_4, K_2HPO_4, AND K_3PO_4

Molecular motions in HF, KHF_2, KH_2F_3 and NaH_2F_3 were investigated by the neutron scattering method by BOUTIN et al. [75]. The results were interpreted by taking into account a similarity of situations of FHF units in solid HF as well as in crystals containing H_2F_3 and HF_2 ions. In this interpretation the known infrared and Raman spectra of KHF_2 were used [76, 77]. Lines occurring in these spectra are: one at 1200 cm^{-1}, interpreted as the ν_2 fundamental of the HF_2 ion; one at about 600 cm^{-1}, explained as a result

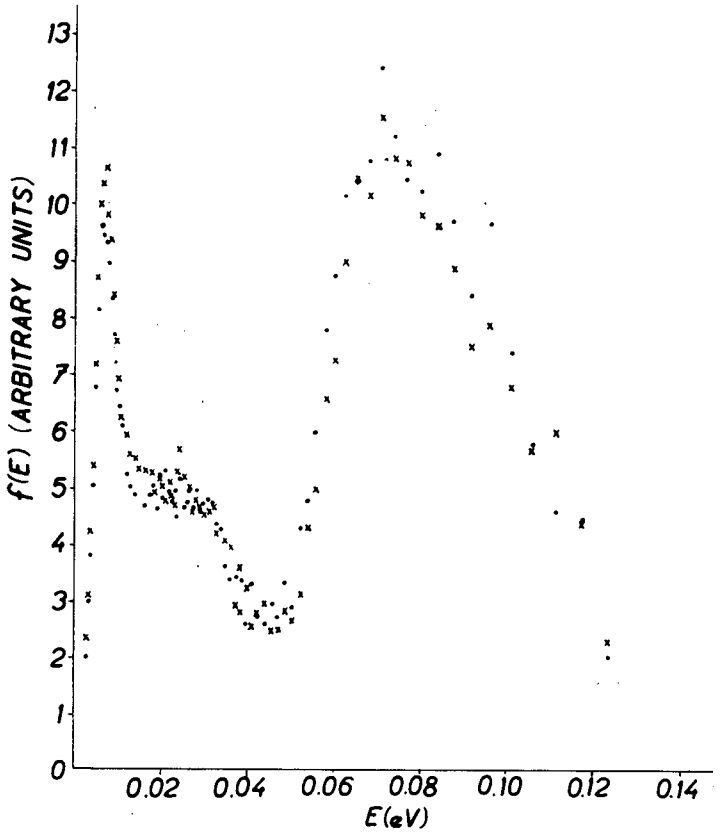

Fig. 26(b)

Hydrogen frequency distribution function for water [69]

Temperatures: x = 270°K (solid H_2O)
• = 275°K (liquid H_2O)

of a symmetric fundamental vibration in which the two F atoms move along the molecular axis in opposite directions whereas the H atom remains at rest; and the lines at 136, 100, and 90 cm^{-1}, attributed to vibrational motion of the HF_2 ion and to the motion of the K ion.

The neutron spectrum for polycrystalline KHF_2 is presented in Fig. 28. The three peaks indicated by arrows correspond to the energy-change wave numbers 1176, 600, and 104 cm^{-1}, which are in very good agreement with what was obtained by spectroscopy methods. It must be pointed out that the peak at 104 cm^{-1} should be attributed to vibrational motion and the two remaining peaks which were seen in the Raman spectra (136 and 90 cm^{-1}) are not seen by neutrons because of the small scattering cross-sections of K-nuclei.

As the neutron spectra for HF, NaH_2F_3 and KH_2F_3 show a similar general shape and as the FHF units exist in all of them it is natural to interpret peaks at 535 cm^{-1} for solid HF and at 896 cm^{-1} for solid NaH_2F_3 and

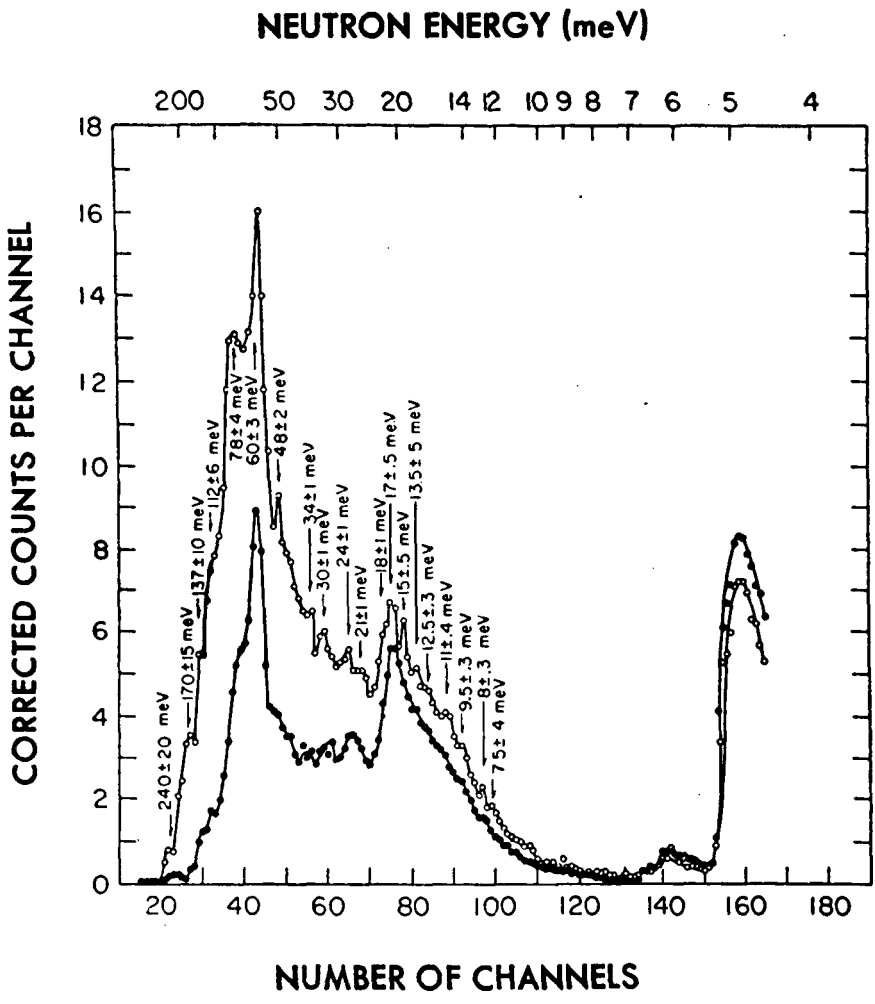

Fig. 27

Scattered neutron distribution for $Na_2Al_2Si_3O_{10} \cdot 2H_2O$
Temperatures 293 (●) and 493°K (o);
Scattering angle 90°; normal beryllium filter method [74].

KH_2F_3, similarly as that at 1176 cm^{-1} for KHF_2. The same may be said of the peaks at 260 cm^{-1} (HF), 364 cm^{-1} (KH_2F_3), 390 cm^{-1} (NaH_2F_3) and 600 cm^{-1} (KHF_2). Also the vibrational peak appears in NaH_2F_3 and KH_2F_3 at 117 cm^{-1}. In HF, NaH_2F_3, and KH_2F_3 there exist also peaks at about 50-65 cm^{-1} for which, however, it is difficult at present to give any definite interpretation.

K_3PO_4, K_2HPO_4, and KH_2PO_4 were studied by the neutron scattering method by PELAH et al. [78], a more detailed study of KH_2PO_4 being made than that by PALEVSKY et al. [79]. A band centred around a transition

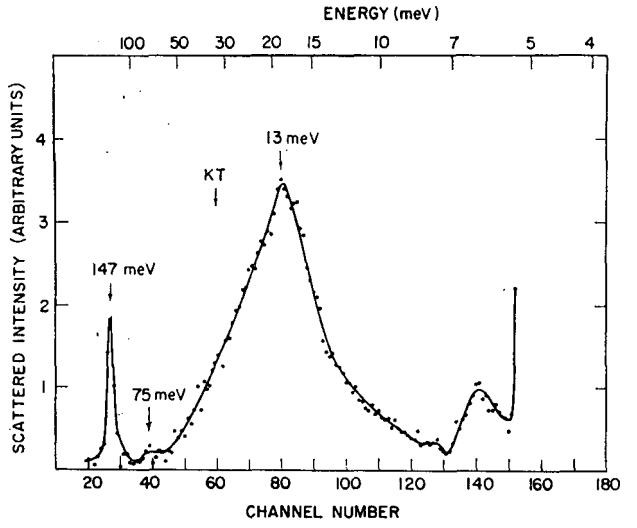

Fig. 28

Scattered neutron distribution for KHF_2
Room temperature (25°C); scattering angle 90°; normal beryllium-filter method [75]

energy of 0.028 eV (220 cm^{-1}) was attributed to hydrogen motion correlated with the O–O stretching.

10. DYNAMICS OF CH_3 GROUPS IN SOME ORGANIC COMPOUNDS

The rotational freedom of methyl groups was investigated by RUSH et al. [36] in a way similar to that for ammonium compounds, by measuring the slopes of the curves for the hydrogen scattering cross-section versus neutron wavelength. The substances investigated were o-, p- and m-xylene, mesitylene and toluene, and the slopes obtained were 9.46, 11.68, 11.01, 11.71 and 11.02 b/Å-H, respectively. One may say in general that the slope for the hydrogen atom in the methyl groups of o-xylene is 9.5 b/Å, compared with 11.4 b/Å for the other methylbenzenes. Applying the calibration curve of Fig. 17, which should be valid also for CH_3 groups, one may estimate a barrier of approximately 1 kcal/mole for o-xylene but a much smaller one (0.1–0.4 kcal/mole) for the other methylbenzenes. These values may be compared with those which were obtained by the thermodynamic method [80], namely 1.85 kcal/mole for o-xylene, 0.19 kcal/mole for mesitylene, 0.3 and 0.35 kcal/mole for m- and p-xylene, respectively, and 0.171 kcal/mole for toluene.

The differential neutron scattering cross-sections were measured by RUSH and TAYLOR [81] for polycrystalline hexamethyl benzene at 92, 104, 120, 166, and 295°K. At lower temperatures (< 110°K) an energy gain peak at 137 cm^{-1} was observed and attributed to torsional vibrations of the methyl groups. With increasing temperature the peak is shifted to ~119 cm^{-1} and at 166° and 295° disappears altogether.

Another study of molecular motion of CH_3 groups was made by JANIK et al. [19] at Brookhaven for di-methoxyazoxybenzene. By comparing and subtracting, after a proper normalization, the two spectra (one for di-methoxyazoxybenzene and the other for azoxybenzene (Fig. 29) at four tem-

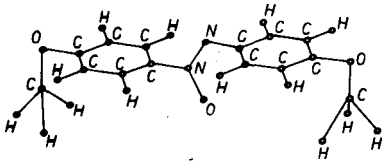

dimethoxyazoxybenzene

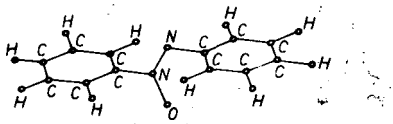

azoxybenzene

Fig. 29

The molecular structure of di-methoxyazoxybenzene and azoxybenzene.

peratures −75, 24, 125, and 145°C), the spectra which might have been attributed to the CH_3 groups were obtained. In the solid di-methoxyazoxybenzene they show two peaks corresponding to $\Delta E = 29$ and 19 meV. It is believed that the 29-meV peak arises from a hindered rotation around the threefold symmetry axis of the CH_3 groups and the 19-meV one from a hindered rotation of the whole CH_3 group around the $O-C_{arom}$ -axis. At higher temperatures the peaks disappear and one obtains broad spectra.

11. OTHER SUBSTANCES

Among other compounds whose molecular dynamics were investigated by the neutron scattering method one should mention benzene [82, 83], biphenyl [83, 84], glycerol, oleic acid and pentane [70], methyl-, ethyl-, and amylalcohol [54], and globular compounds [53]. In benzene two peaks are obtained at neutron energies of approximately 50 and 90 meV. They are consistent with Raman spectra observations. In biphenyl one obtains a number of lines which may be attributed to vibrational and internal modes.

It is possible that the broad band around 73 meV for glycerol comes from a hindered rotational motion similar to that existing in water. It is also possible that the CH_2 rocking motion is also involved in this band. In alcohols a broad band of energy transfers from 0-50 meV may arise from free and hindered rotation of alcohol molecules. A quasi-free rotation was also postulated for molecules of globular compounds at higher temperatures, since there the inelastic peaks disappear and the elastic peak broadens.

REFERENCES

[1] FERMI, E., Ric. sci. 7 (1936) 13.
[2] SACHS, R.G. and TELLER, E., Phys. Rev. 60 (1941) 18.
[3] ZEMACH, A.C. and GLAUBER, R.J., Phys. Rev. 101 (1956) 118,129.
[4] KRIEGER, T.J. and NELKIN, M.S., Phys. Rev. 106 (1957) 290.
[5] VOLKIN, H.C., Phys. Rev. 113 (1959) 866; Phys. Rev. 117 (1960) 1029.
[6] GRIFFING, G.W., Phys. Rev. 124 (1961) 1489.
[7] BRIMBERG, S., Thesis, Stockholm (1956)
[8] LØVSETH, J., Phys. norv. (1962)
[9] MESSIAH, A.M.L., Phys. Rev. 84 (1951) 204.
[10] MELKONIAN, E., Phys. Rev. 76 (1949) 1750.
[11] JANIK, J.A., JANIK, J., MANIAWSKI, F., RZANY, H., SZKATULA, A., SCIESINSKI, J. and WANIC, A., Inelastic Scattering of Neutrons in Solids and Liquids, IAEA, Vienna (1961) 297-303.
[12] RANDOLPH, P.G., BRUGGER, R.M., STRONG, K.A. and SCHMUNK, R.E., Phys. Rev. 124 (1961) 460.
[13] WEBB, F.J., Inelastic Scattering of Neutrons in Solids and Liquids I IAEA, Vienna (1963) 457-67.
[14] CZERLUNCZAKIEWICZ, B. and KOWALSKA, A., Acta phys. polon. 25 (1964) 141.
[15] KOSALY, G. and SOLT, G., Phys. Lett. 6 (1963) 51.
[16] ROGALSKA, Z., Physica 29 (1963) 491.
[17] WHITTEMORE, W.L., Nucl. Sci. Engng (1963).
[18] WHITTEMORE, W.L. and McREYNOLDS, A.W., Phys. Rev. 113 (1959) 806.
[19] JANIK, J.A., JANIK, J.M., MELLOR, J. and PALEVSKY, H., BNL Rpt. 7876 (1964); J. Phys. Chem. Solids 25 (1964) 1091.
[20] OTNES, K., Private communication.
[21] PALEVSKY, H., J. phys. Soc. Japan 17 Suppl. B-II (1962) 367.
[22] WOODS, A.D.B., BROCKHOUSE, B.N., SAKAMOTO, M. and SINCLAIR, R.N., Inelastic Scattering of Neutrons in Solids and Liquids, IAEA, Vienna (1961) 487-98.
[23] MIKKE, K. and KROH, A., Inelastic Scattering of Neutrons in Solids and Liquids II IAEA, Vienna (1963) 237-50.
[24] VENKATARAMAN, G., USHA, K., IYENGAR, P.K., VIJAYARAGHAVAN, P.R. and ROY, A.P., Inelastic Scattering of Neutrons in Solids and Liquids II IAEA, Vienna (1963) 253-62.
[25] PALEVSKY, H., Inelastic Scattering of Neutrons in Solids and Liquids II IAEA, Vienna (1963) 251.
[26] VENKATARAMAN, G., USHA DENIZ, K., IYENGAR, P.K., VIJAYARAGHAVAN, P.R. and ROY, A.P., Solid State Comm. 2 (1964) 17.
[27] STEPHENSON, C.C., WULFF, C.A. and LUNDELL, O.R., J. chem. Phys. 40 (1964) 967.
[28] COLE, A.G., Thesis, Mass. Inst. Technology (1952).
[29] PLUMB, R.C. and HORNIG, D.F., J. chem. Phys. 23 (1955) 947.
[30] WAGNER, E.L. and HORNIG, D.F., J. chem. Phys. 18 (1950) 296,305.
[31] BRAJOVIC, V., BOUTIN, H., SAFFORD, G.J. and PALEVSKY, H., J. Phys. Chem. Solids 24 (1963) 617.
[32] JANIK, J.M., JANIK, J.A., BAJOREK, A. and PARLINSKI, K., to be published in Phys. Stat. sol.
[33] BAJOREK, A., PARLINSKI, K. and MACHECHINA, T., these Proceedings II.
[34] RUSH, J.J., TAYLOR, T.J. and HAVENS, W.W., Phys. Rev. Lett. 5 (1960) 507.
[35] RUSH, J.J., TAYLOR, T.J. and HAVENS, W.W., J. chem. Phys. 35 (1961) 2265.
[36] RUSH, J.J., TAYLOR, T.J. and HAVENS, W.W., J. chem. Phys. 37 (1962) 234.
[37] VOLMER, M., Ann. Chem. 440 (1924) 200.
[38] LEE, F.S. and CARPENTER, G.B., J. phys. Chem. 63 (1959) 279.
[39] JANIK, J.M., to be published in Acta phys. polon.
[40] RICHARDS, R.E. and SCHAEFER, T., Trans. Faraday Soc. 57 (1961) 210.
[41] IBERS, J.A., J. chem. Phys. 32 (1960) 1448.
[42] WADDINGTON, T.C., J. chem. Soc. (1958) 4340.
[43] TAYLOR, R.C. and VIDALE, G.L., J. Amer. chem. Soc. 78 (1956) 5999.
[44] KAKIUCHI, Y., SHONO, H. and KOMATSU, H., J. chem. Phys. 29 (1951) 1069.
[45] RAHMAN, A., J. nucl. Energy A13 (1961) 128.
[46] DOBRZYNSKI, L. and MIKKE, K., "Studies of ammonium ion motions in solid solutions", these Proceedings II.

[47] JANIK, J.A. and KOWALSKA, A., Inst. Nucl. Phys., Rpt. 255 Cracow (1963).
[48] HOFMEYR, Ch., private communication.
[49] STRONG, K.A., MARSHALL, G.D., BRUGGER, R.M. and RANDOLPH, P.D., Phys. Rev. 125 (1962) 933.
[50] YOUNG, J.A. and KOPPEL, J.U., Phys. Rev. 135A (1964) 603.
[51] SQUIRES, G.L. and STEWART, A.T., Proc. roy. Soc. (London) A230 (1955) 19.
[52] PALEVSKY, H., MYERS, V.W. and BRAJOVIC, V.M., Bull. Amer. phys. Soc. 6 (1961) 261.
[53] BECKA, L.N., J. chem. Phys. 38 (1963) 1685.
[54] SAUNDERSON, D.H. and RAINEY, V.S., Inelastic Scattering of Neutrons in Solids and Liquids I IAEA, Vienna (1963) 413-22.
[55] ROGALSKA, Z., to be published in Acta phys. polon.
[56] JANIK, J.A., RZANY, H. and SCIESINSKI, Physica 29 (1963) 485.
[57] RZANY, H. and SCIESINSKI, J., Physica 29 (1963) 488.
[58] VAN DINGENEN, W. and NEVE de MEVERGNIES, M., Physica 30 (1964) 237.
[59] HAUTECLER, S. and STILLER, H., Inelastic Scattering of Neutrons in Solids and Liquids I IAEA, Vienna (1963) 423-33.
[60] STILLER, H. and HAUTECLER, S., Inelastic Scattering of Neutrons in Solids and Liquids II IAEA, Vienna (1963) 281-93
[61] DANNER, H. and STILLER, H., Phys. Stat. sol. 5 (1964) 511.
[62] TOMITA, K., Phys. Rev. 89 (1953) 429.
[63] NELKIN, M., Phys. Rev. 119 (1960) 741.
[64] BROCKHOUSE, B.N., Nuovo Cim. 9 Suppl. 1 (1958) 45.
[65] HUGHES, D.J., PALEVSKY, H., KLEY, W. and TUNKELO, E., Phys. Rev. Lett. 3 (1959) 91.
[66] KOSALY, G. and SOLT, G., private communication.
[67] EGELSTAFF, P.A., HAYWOOD, B.C. and THORSON, I.M., Inelastic Scattering of Neutrons in Solids and Liquids I IAEA, Vienna (1963) 343-56.
[68] KOTTWITZ, D.A. and LEONARD, B.R. Jr., Inelastic Scattering of Neutrons in Solids and Liquids I IAEA, Vienna (1963) 359-71.
[69] LARSSON, K. and DAHLBORG, U., Inelastic Scattering of Neutrons in Solids and Liquids I IAEA, Vienna (1963) 317-40.
[70] LARSSON, K. and DAHLBORG, U., Physica 30 (1964) 1561.
[71] GOLIKOV, V.V., ZHUKOVSKA, J., SHAPIRO, F.L., SHKATULA, A. and JANIK, J., these Proceedings II.
[72] MAGAT, M., Ann. Phys. 6 (1936) 108.
[73] SAVITSKY, G. and HORNIG, D., J. chem. Phys. 36 (1962) 2634.
[74] BOUTIN, H., SAFFORD, G.J. and DANNER, H.R., J. chem. Phys. 39 (1963) 488.
[75] BOUTIN, H., SAFFORD, G.J. and BRAJOVIC, V., J. chem. Phys. 39 (1963) 3135.
[76] KETELAAR, J.A.A., Recuil trav. chim. Pays-Bas 60 (1941) 523.
[77] COUTURE, L. and MATHIEU, J.P., C.R. Acad. Sci. (Paris) 228 (1949) 555; C.R. Acad. Sci. (Paris) 228 (1950) 1054.
[78] PELAH, I., LEFKOVITZ, I., KLEY, W. and TUNKELO, E., Phys. Rev. Lett. 2 (1959) 94.
[79] PALEVSKY, H., OTNES, K. and WAKUTA, Y., Inelastic Scattering of Neutrons in Solids and Liquids II IAEA, Vienna (1963) 273-78.
[80] WULFF, C.A., J. chem. Phys. 39 (1963) 1227.
[81] RUSH, J.J. and TAYLOR, T.I., Bull. Amer. phys. Soc. 9 (1964) 413.
[82] MYERS, V.W., COTTER, M.J. and PALEVSKY, H., Bull Amer. phys. Soc. 6 (1961) 262.
[83] ZEMLJANOV, M.G. and TCHERNOPLEKOV, N.A., Inelastic Scattering of Neutrons in Solids and Liquids I IAEA, Vienna (1963) 297-305.
[84] KREBS, K., SANDRONI, S. and ZERBI, G., J. chem. Phys. 40 (1964) 3502.
[85] WHITTEMORE, W.L. and DANNER, H.R., Inelastic Scattering of Neutrons in Solids and Liquids I IAEA, Vienna (1963) 273-83.
[86] SARMA, G., Inelastic Scattering of Neutrons in Solids and Liquids, IAEA, Vienna (1961) 397-408.
[87] LEVY, H.A., and PETERSON, S.W., Phys. Rev. 83 (1951) 1270; Phys. Rev. 86 (1952) 766.
[88] LEVY, H.A. and PETERSON, S.W., J. Amer. chem. Soc. 75 (1953) 1536.
[89] LARSSON, K., "Liquid dynamics", these Proceedings II.

DISCUSSION

J.J. RUSH: I have two comments. First, I should like to point out that since the infrared method extracts the torsional frequencies of the ammonium ions from combination bands, the identification and interpretation of such combinations become more difficult for complex ammonium salts with broad, and possibly split, torsional bands. In these cases, therefore, the neutron method is more advantageous.

My second point concerns free rotation in NH_4ClO_4. It has been shown by X-ray diffraction, and by the neutron diffraction work of Smith and Levy, that the ammonium ions in this compound are surrounded by a sphere of many, almost symmetrically distributed, oxygen atoms. This structure seems to explain the very low resultant barrier to rotation, which allows the ammonium ions to reorient quite easily between many equilibrium positions.

K.-E. LARSSON: I noticed that many of the neutron scattering pictures you presented showed elastically or quasi-elastically scattered peaks. Have you investigated whether there is any broadening of these peaks?

J.A. JANIK: No, I have a feeling that some broadening exists in cases when NH_4 groups are quasi-freely rotating, but this has not been studied as yet.

G. CAGLIOTI: I should like to make a comment concerning the molecular energy levels in condensed systems, as studied by coherent inelastic neutron scattering. An experiment was recently done in our laboratory to ascertain whether the vibrational mode of the diatomic molecule Br_2 preserves its individuality within liquid bromine at room temperature. Some reasonable experimental evidence was found for the existence of an energy level within the liquid corresponding to the vibrational mode of the diatomic oscillation in the gaseous phase. The experimental data were treated by a theoretical approach similar to the one independently presented by Dr. Singwi*.

H. HAHN: In connection with Professor Janik's talk, I feel I should point out that one has to be careful in attributing any "broad distribution" to free rotations. It might equally well be the frequency distribution due to a band of waves of torsional oscillations in the crystal whose critical points are washed out by anharmonic effects.

J.A. JANIK: Yes, I agree. I hope it was clear from my talk that we do not have any "detector" of the rotational freedom, and the broad distribution of neutrons might therefore equally well be explained by a band of oscillations.

H. BOUTIN: When you presented the Chalk River data on NH_4Cl, you attributed four of the observed peaks to combination bands. It seems to me that combination bands should never be observed in the neutron spectra if the data are taken properly, because combination bands arise from multiple scattering or multiphonon effects, which one always tries to eliminate by using thin samples or taking the measurements at sufficiently low temperature.

J.A. JANIK: There is of course always the problem of interpreting the peaks observed. It would be desirable to have a theory which would tell

---

* See SINGWI, K.S. and FELDMANN, G. "Coherent scattering of slow neutrons by liquid sodium". these Proceeding II.

See ANTONINI, M., ASCARELLI, P. and CAGLIOTI, G., Phys. Rev. 136 (1964) 1280.

us which peak is which. I would add that in our own measurements we always had thin samples.

N.A. NARASIMHAM: I have a few comments to make regarding the identification of vibrational and rotational modes as observed from neutron scattering experiments:

(i) Any molecular rotations observed from neutron scattering by methane in condensed states (both liquid and solid) should be related to rotational transitions of the free molecules and these can be calculated from the known data of the vibration-rotation spectrum of methane;

(ii) It is interesting to note that the inelastic scattering of neutrons by ammonium halides gives directly the low frequency torsional mode which is obtained only as a combination band in the infrared spectrum. Several other peaks observed in the case of NH_4Cl are interpreted as combination bands; in these cases, one would like to know the anharmonic effects normally associated with such combination bands and how they compare with the infrared data. Perhaps I may mention here that experiments carried on in Trombay on ammonium halides give a large anharmonicity for the hot band of 1-2 transition of the torsional mode. More accurate measurements would make possible a correct understanding of the situation;

(iii) For identification of the Raman line appearing at 995 cm^{-1} as twice the frequency of 497 cm^{-1} obtained from neutron spectra and not as ω_2, one has to be sure that the vibrational assignments have been correctly made.

LATTICE VIBRATIONS IN MOLECULAR CRYSTALS AND NEUTRON SCATTERING

H. HAHN
KERNFORSCHUNGSANLAGE JÜLICH,
FEDERAL REPUBLIC OF GERMANY

Abstract — Résumé — Аннотация — Resumen

LATTICE VIBRATIONS IN MOLECULAR CRYSTALS AND NEUTRON SCATTERING. As an introduction, a description of the vibrations of a lattice of quasi-rigid molecules in terms of molecular translations and rotations is given in the harmonic approximation valid for small amplitudes.

The neutron incoherent one-phonon scattering cross-section is investigated for the case in which there is little or no mixture between rotational and translational vibrations. This is true either if the coupling parameters between the rotations and the translations are small or if the mass involved in rotation about the molecule's centre of gravity is small compared to the total molecular mass, i. e. if the mass is concentrated in the middle of the molecule as for example, solid methane.

Simple results are obtained only for the case of cubic lattice symmetry and of circular symmetry of the librational parts of the thermal clouds of the atoms. In this case, as with incoherent scattering from simple cubic lattices, the energy distribution of the scattered neutrons gives (after division by some known function of temperature and frequency) directly the frequency distribution function of the molecular crystal. However, the spectra of the centre of mass and rotational vibrations enter the cross-section with different scale factors.

The coherent one-phonon cross-section is also given and examined as to how, from the variations in intensity along the scattering surfaces and from their shape, one can infer the character (rotational, translational, degree of mixing) of the vibrations contributing to them.

ÉTUDE SUR LES VIBRATIONS DE RÉSEAUX ET LA DIFFUSION DES NEUTRONS DANS LES CRISTAUX MOLÉCULAIRES. Dans l'introduction de son mémoire, l'auteur décrit, avec l'approximation harmonique valable pour de petites amplitudes, les vibrations d'un réseau de molécules quasi rigides exprimées en translations et en rotations de molécules.

L'auteur étudie la section efficace de diffusion neutronique incohérente à un phonon lorsque les vibrations de translation se mêlent peu à peu ou pas du tout. Tel est le cas si les paramètres de couplage des rotations et des translations sont peu importants ou si la masse entraînée par rotation autour du centre de gravité de la molécule est faible par rapport à la masse totale de la molécule - c'est-à-dire si cette masse est concentrée au milieu de la molécule. Exemple: méthane solide.

On n'obtient de résultats simples qu'en cas de symétrie de réseau cubique et de symétrie circulaire des parties en libration des nuages thermiques des atomes. En pareil cas, comme dans celui de la diffusion incohérente par des réseaux cubiques simples, la distribution en énergie des neutrons diffusés fournit directement - après division par une fonction connue de température et de fréquence - la fonction de distribution de fréquence du cristal moléculaire. Toutefois, les spectres des vibrations du centre de masse et des vibrations de rotation interviennent selon des rapports différents dans la section efficace.

L'auteur donne également la section efficace de diffusion cohérente à un phonon et étudie comment, à partir des variations de l'intensité le long des surfaces de diffusion, et de leur forme, on peut obtenir par déduction des indications sur le caractère (rotation, translation, degré de mélange) des vibrations qui contribuent à produire ces variations.

ОТНОСИТЕЛЬНО КОЛЕБАНИЙ РЕШЕТКИ В МОЛЕКУЛЯРНЫХ КРИСТАЛЛАХ И РАССЕЯНИЯ НЕЙТРОНОВ. В качестве введения приводится описание колебаний решетки квазижестких молекул с точки зрения молекулярных смещений и вращений в гармоническом приближении, справедливом для небольших амплитуд.

Сечение некогерентного однофононного рассеяния нейтронов изучается для случая, в котором отмечается незначительное смешение между колебаниями вращения и смещения или же когда такого смешения не происходит. Это имеет место в том случае, если параметры связи между вращениями и смещениями незначительны или если масса, связанная с враще-

нием вокруг центра тяжести молекулы, мала по сравнению с общей массой молекулы (т.е. если масса концентрируется в середине молекулы, например – твердый метан).

Простые результаты получаются только для кубической симметрии решетки и круговой симметрии равновесных частей тепловых облаков атомов. В этом случае, как при некогерентном рассеянии на простых кубических решетках, из распределения энергии рассеянных нейтронов непосредственно выводится функция распределения частоты молекулярного кристалла (после деления на некоторую известную функцию температуры и частоты). Однако спектры центра массы и колебания вращения фигурируют в поперечном сечении с различными коэффициентами перерасчета.

Когерентное однофононное сечение также приводится и рассматривается с точки зрения того, каким образом на основании изменений в интенсивности вдоль поверхностей рассеяния и их формы можно определить характер (вращение, смещение, степень смещения) колебаний, влияющих на них.

VIBRACIONES RETICULARES EN CRISTALES MOLECULARES Y DISPERSIÓN NEUTRONICA. Como introducción, el autor describe las vibraciones (traslación y rotación moleculares) de un reticulado de moléculas cuasirrígidas, en la aproximación armónica válida para amplitudes pequeñas.

El autor investiga la sección eficaz de dispersión monofonónica incoherente de los neutrones cuando las vibraciones de rotación y de traslación se mezclan en grado reducido o nulo; este caso se da cuando los parámetros de acoplamiento entre las rotaciones y las traslaciones son pequeños, o cuando la masa que gira en torno al centro de gravedad de la molécula es reducida en comparación con la masa total de la molécula, esto es, cuando la masa está concentrada en el centro de la molécula como sucede, por ejemplo, en el metano sólido.

Sólo se obtienen resultados simples para el caso de reticulados en que las partes vibratorias de las nubes térmicas de los átomos presentan una simetría cúbica o circular. Entonces, lo mismo que en la dispersión incoherente en reticulados cúbicos de carácter simple, la distribución energética de los neutrones dispersos da directamente (después de dividirla por una cierta función conocida de la temperatura y la frecuencia) la función de distribución de frecuencias del cristal molecular. Sin embargo, el espectro de las vibraciones rotatorias y del centro másico intervienen en la fórmula de la sección eficaz con factores de escala diferente.

El autor indica también la sección eficaz de dispersión monofonónica coherente y la analiza para evaluar de qué manera, a partir de las variaciones de la intensidad a lo largo de las superficies dispersantes, y de su forma, se puede deducir el carácter (rotatorio, de traslación, grado de mezcla) de las vibraciones contribuyentes.

1. INTRODUCTION

The molecules forming a "molecular crystal" are held together by forces (mainly "Van der Waals" forces) that are weak compared to the chemical forces which bind the atoms within each molecule.

At sufficiently low temperatures, and if only processes involving small energy transfers (e.g. slow neutron scattering) are considered, the internal vibrations of the molecules will not, in general, be excited. It then seems natural to describe the thermal motions of such a crystal entirely in terms of translational (centre-of-mass) and rotational oscillations of quasi-rigid molecules around their equilibrium positions.[1] We shall here assume that this is possible and that the vibrations may all be looked upon as harmonic[1]. For simplicity, we shall only consider crystals with one molecule per lattice cell.

We define first

$\vec{X}^{\vec{m}}$ Equal to $A\vec{m}$ with integral $\vec{m} = (m_1, m_2, m_3)$ and $A = ((A_{ij})) = ((a_j^{(i)}))$, the matrix of the three elementary lattice translation vectors $\vec{a}^{(i)}$.

[1] This picture of a molecular crystal and its validity have been discussed at some length in Ref. [1].

$S_i^{\vec{m}}$ Shift of the centre of gravity of a molecule whose equilibrium position was $\vec{X}^{\vec{m}} = A\vec{m}$, in one of the directions i (i = 1, 2, 3) of the molecule's principal axes of inertia in the equilibrium configuration.

$\omega_i^{\vec{m}}$ (Small) angle of rotation of molecule m around the i-axis.

M Mass of a molecule.

θ_i Moments of inertia of a molecule with respect to its principal axes.

$\phi^{\vec{m}\vec{n}}_{s\,s\;i\,j}$ Force constants coupling the centre-of-mass translations of molecule $\vec{m}$ to the translations of molecule $\vec{n}$.

$\phi^{\vec{m}\vec{n}}_{s\,\omega\;i\,j}$ Force constants coupling the centre-of-mass translations of $\vec{m}$ to the rotations of $\vec{n}$.

$\phi^{\vec{m}\vec{n}}_{\omega\,\omega\;i\,j}$ Force constants coupling the rotations of $\vec{m}$ to the rotations of $\vec{n}$.

Since the force constants are second derivatives of the potential energy of the crystal, they must obey the symmetry relations

$$\begin{aligned}
&\text{(a)} && \phi^{\vec{m}\vec{n}}_{s\,s\;i\,j} = \phi^{\vec{n}\vec{m}}_{s\,s\;j\,i} \\
&\text{(b)} && \phi^{\vec{m}\vec{n}}_{s\,\omega\;i\,j} = \phi^{\vec{n}\vec{m}}_{\omega\,s\;j\,i} \qquad (1) \\
&\text{(c)} && \phi^{\vec{m}\vec{n}}_{\omega\,\omega\;i\,j} = \phi^{\vec{n}\vec{m}}_{\omega\,\omega\;j\,i}\,.
\end{aligned}$$

Also, because of the periodicity of the lattice,

$$\phi^{\vec{m}\,\vec{n}}_{\ldots\;\ldots\;i\;j} = \phi^{\vec{m}-\vec{n}\,0}_{\ldots\;\ldots\;i\;j}\,. \qquad (2)$$

The equations of motion then become

$$M\ddot{\vec{S}}_i^{\vec{m}} = -\sum_{\vec{n},j} \phi_{i\,j}^{\vec{m}\vec{n}}{}_{s\,s} \cdot \vec{S}_j^{\vec{n}} - \sum_{\vec{n},j} \phi_{i\,j}^{\vec{m}\vec{n}}{}_{s\,\omega} \cdot \vec{\omega}_j^{\vec{n}}$$

$$\theta_i \ddot{\vec{\omega}}_i^{\vec{m}} = -\sum_{\vec{n},j} \phi_{i\,j}^{\vec{m}\vec{n}}{}_{\omega\,s} \cdot \vec{S}_j^{\vec{n}} - \sum_{\vec{n},j} \phi_{i\,j}^{\vec{m}\vec{n}}{}_{\omega\,\omega} \cdot \vec{\omega}_j^{\vec{n}} \,. \tag{3}$$

The crystal energy becomes

$$H = E_{kin} + \Phi = \frac{M}{2} \sum_{\vec{m},i} (\dot{\vec{S}}_i^{\vec{m}})^2 + \frac{1}{2} \sum_{\vec{m},i} \theta_i (\dot{\vec{\omega}}_i^{\vec{m}})^2 + \frac{1}{2} \sum_{\vec{m}\vec{n}\;i\,j} \phi_{i\,j}^{\vec{m}\vec{n}}{}_{s\,s} \vec{S}_i^{\vec{m}} \vec{S}_j^{\vec{n}}$$

$$+ \frac{1}{2} \sum_{\vec{m}\vec{n}} \phi_{i\,j}^{\vec{m}\vec{n}}{}_{\omega\,\omega} \vec{\omega}_i^{\vec{m}} \vec{\omega}_j^{\vec{n}} + \sum_{\vec{m}\vec{n}} \phi_{i\,j}^{\vec{m}\vec{n}}{}_{s\,\omega} \vec{S}_i^{\vec{m}} \vec{\omega}_j^{\vec{n}} \,. \tag{4}$$

With the invariance of the crystal potential energy Φ against all mere translations ($\vec{S}^{\vec{m}}$ = any vector $\vec{a}$ that is independent of $\vec{m}$; $\omega_i^{\vec{m}} \equiv 0$) one easily observes from Eqs. (2) and (4) that the force constants must satisfy

$$\sum_{\vec{n}} \phi_{i\,j}^{\vec{m}\vec{n}}{}_{s\,s} = 0, \qquad \sum_{\vec{n}} \phi_{i\,j}^{\vec{m}\vec{n}}{}_{\omega\,s} = 0. \tag{5}$$

Φ must also be invariant under any infinitesimal rotation of the whole crystal, $\vec{S}^{\vec{m}} = [d\vec{\Omega} \times \vec{X}^{\vec{m}}]$; $\vec{\omega}^{\vec{m}}$ then gives

$$\sum_{\vec{n}} \left(\phi_{i\,j}^{\vec{m}\vec{n}}{}_{s\,s} X_k^{\vec{n}} - \phi_{i\,k}^{\vec{m}\vec{n}}{}_{s\,s} X_j^{\vec{n}} \right) = 0$$

$$\sum_{\vec{n}} \left(\phi_{i\,j}^{\vec{m}\vec{n}}{}_{\omega\,s} X_k^{\vec{n}} - \phi_{i\,k}^{\vec{m}\vec{n}}{}_{\omega\,s} X_j^{\vec{n}} \right) = \sum_{\vec{n},\ell} \phi_{i\,\ell}^{\vec{m}\vec{n}}{}_{\omega\,\omega} \epsilon_{jk\ell} \tag{6}$$

where $\epsilon_{jk\ell}$ is the totally anti-symmetric tensor with $\epsilon_{123} = 1$. Equation (6) shows that setting all $\phi_{s\omega} = 0$, strictly speaking, violates the condition of rotational invariance, since the right-hand side in Eq. (6) will in general not vanish.

2. THE INCOHERENT SCATTERING LAW AND THE FREQUENCY DISTRIBUTION

For the harmonic vibrations considered here, a one-quantum scattering law can be defined in the usual manner by

$$\frac{1}{N} S^{(1)}_{inc}(\vec{Q}, \nu) = \int dt\, e^{-i\nu t} X^{(1)}_{inc}(\vec{Q}, t) \tag{7}$$

$$X^{(1)}_{inc}(\vec{Q}, t) = \sum_{\mu} \sigma_{\mu} \exp\left[-\sum_{ij} Q_i Q_j \langle \overset{\vec{0}}{s}_{i\mu}(0) \overset{\vec{0}}{s}_{j\mu}(0) \rangle_T \right]$$

$$\times \sum_{ij} Q_i Q_j \langle \overset{\vec{0}}{s}_{i\mu}(0) \overset{\vec{0}}{s}_{j\mu}(t) \rangle_T ,$$

where

N = the number of molecules in the crystal,

$\hbar\vec{Q}$ = the momentum transfer,

$\hbar\nu$ = the energy transfer,

t = the time variable,

$\langle\ \rangle_T$ = the thermal average,

$\overset{\vec{0}}{s}_{\mu}$ = the displacement of atom μ of the molecule whose equilibrium site is $\vec{m} = (0, 0, 0)$, and

σ_{μ} = its incoherent neutron-scattering cross-section.

If $\vec{a}_{\mu}$ is the equilibrium distance of atom μ from the centre of gravity of its molecule, then

$$\vec{s}^{\vec{m}}_{\mu} = \vec{S}^{\vec{m}} + [\vec{\omega}^{\vec{m}} \times \vec{a}_{\mu}] = \vec{S}^{\vec{m}} + \vec{W}^{\vec{m}}_{\mu} . \tag{8}$$

Let us assume in this section that translation-rotation coupling is small, so that we can neglect its influence. Inserting Eq. (8) into Eq. (7), we then find that all averages containing mixed products of S and W vanish.

$$X^{(1)}_{inc} = \exp\left(-\sum_{ij} Q_i Q_j \langle \overset{\vec{0}}{S}_i(0) \overset{\vec{0}}{S}_j(0) \rangle_T \right) \sum_{\mu} \sigma_{\mu} \exp\left(-\sum_{ij} Q_i Q_j \langle \overset{\vec{0}}{W}_{i\mu}(0) \overset{\vec{0}}{W}_{j\mu}(0) \rangle_T \right)$$

$$\times \sum_{ij} Q_i Q_j \left\{ \langle \overset{\vec{0}}{S}_i(0) \overset{\vec{0}}{S}_j(t) \rangle_T + \langle \overset{\vec{0}}{W}_{i\mu}(0) \overset{\vec{0}}{W}_{j\mu}(t) \rangle_T \right\} . \tag{9}$$

We know that in Bravais crystals cubic symmetry is necessary to allow us to extract the distribution of eigenfrequencies $g(\nu)$ of the crystal from the incoherent one-phonon scattering law. We want to try to find conditions under which this can be done with molecular crystals. In addition to our assumption of vanishing S-ω coupling, let us assume the crystal to possess cubic symmetry. Then,

$$\sum_{ij} Q_i Q_j \langle S_i^{\vec{0}}(0) S_j^{\vec{0}}(0) \rangle = \frac{1}{3} Q^2 \langle \{\vec{S}^{\vec{0}}(0)\}^2 \rangle = 2W_s , \tag{10a}$$

$$\sum_{ij} Q_i Q_j \langle S_i^{\vec{0}}(0) S_j^{\vec{0}}(t) \rangle = \frac{1}{3} Q^2 \sum_i \langle S_i^{\vec{0}}(0) S_j^{\vec{0}}(t) \rangle . \tag{10b}$$

We note that the normal modes of the lattice are plane waves of either pure centre-of-mass vibrations or pure librations. Let us call $\sigma_\alpha(\vec{q})$ and $\sigma_\alpha^+(\vec{q})$ the annihilation and creation operators respectively for the former, the "phonons"; and $\sigma_\beta(\vec{q})$ and $\sigma_\beta^+(\vec{q})$ the corresponding operators for the waves of torsional oscillations of the molecules, the "torsons". The corresponding frequencies are $\nu_\alpha(\vec{q})$ and $\nu_\beta(\vec{q})$ respectively. $\vec{e}(\vec{q}, \alpha)$ and $\vec{\Omega}(\vec{q}, \beta)$ are unit vectors in the direction of the polarization of the phonons and in the direction of the axis of rotation of the torsons, respectively. $\alpha = 1, 2, 3$ and $\beta = 4, 5, 6$ are polarization indices. Then we have

$$\vec{S}^{\vec{m}} = \left(\frac{\hbar}{2MN}\right)^{\frac{1}{2}} \sum_{\alpha, \vec{q}} \frac{\vec{e}(\vec{q}, \alpha)}{\nu_\alpha^{1/2}(\vec{q})} \left\{ \sigma_\alpha(\vec{q}) \exp\left(i [\vec{q}\vec{X}^{\vec{m}} - \nu_\alpha(\vec{q}) t] \right) + \sigma_\alpha^+(\vec{q}) \exp\left(- i [\vec{q}\vec{X}^{\vec{m}} - \nu_\alpha(\vec{q}) t] \right) \right\} . \tag{11a}$$

$$\vec{W}_\mu^{\vec{m}} = \left(\frac{\hbar}{2\theta N}\right)^{\frac{1}{2}} \sum_{\beta, \vec{q}} \frac{1}{\sqrt{\nu_\beta(\vec{q})}} \vec{\xi}_\mu \left\{ \sigma_\beta(\vec{q}) \exp\left(i [\vec{q}\vec{X}^{\vec{m}} - \nu_\beta(\vec{q}) t] \right) + \sigma_\beta^+(\vec{q}) \exp\left(- i [\vec{q}\vec{X}^{\vec{m}} - \nu_\beta(\vec{q}) t] \right) \right\} , \tag{11b}$$

where $\vec{\xi}_\mu = [\vec{\Omega}(\vec{q}, \beta) \times \vec{a}_\mu]$. The factors have been chosen so that

$$H = \sum_{\vec{q}} \sum_{\nu=1}^{6} \hbar \nu_\nu(\vec{q}) \left(\sigma^+ \sigma + \frac{1}{2} \right) .$$

As is well known from the Bravais crystal, we obtain

$$\langle \{\vec{S}^{\vec{0}}(0)\}^2 \rangle = \frac{1}{MN} \sum_{\alpha,\vec{q}} \frac{\epsilon(\nu, T)}{[\nu_\alpha(\vec{q})]^2}$$

$$\sum_i \langle S_i^{\vec{0}}(0) S_i^{\vec{0}}(t) \rangle = \frac{\hbar}{2MN} \sum_{\alpha,\vec{q}} \left\{ \frac{\langle n+1 \rangle}{\nu_\alpha(\vec{q})} e^{i\nu t} + \frac{\langle n \rangle}{\nu_\alpha(\vec{q})} e^{-i\nu t} \right\} \tag{12}$$

where $\langle n \rangle = [\exp(\hbar\nu/k_B T) - 1]^{-1}$ and $\epsilon(\nu, T) = \frac{\hbar\nu}{2}(2\langle n \rangle + 1)$, from which the polarization vectors $\vec{e}$ have dropped out by having been squared.

However, we may not use Eq. (10) for the rotational parts, as the "clouds" of the rotational displacements $\vec{W}_\mu^{\vec{m}}$ can never have cubic symmetry; each of them is flattened out on a sphere of radius $|a_\mu|$. To eliminate the polarization vector $\vec{\Omega}$ (namely $\vec{\xi}$), we shall have to make further assumptions.

Firstly, we consider a polycrystal with randomly oriented crystallites, so that we may average over the orientation of $\vec{Q}$ and the crystallites relative to each other.

Secondly, we assume that the rotational clouds of different atoms of the same molecule can be brought to coincide by some symmetry operation of the lattice. This implies, of course, that the atoms which participate in the rotation are all alike. In this case, the orientational averages over terms with different μ in Eq. (9) are all equal. We may then do the averaging on just one of them (see Fig. 1).

We further assume that the rotational clouds are circularly symmetric. This means that $\vec{a}_\mu$ must point in a direction of at least three-fold symmetry, i.e. the molecule must have at least tetrahedral symmetry. The direction of $\vec{a}_\mu$ is introduced as our new z-axis. Then, only

$$\langle W_x(0) W_x(0) \rangle = \langle W_y(0) W_y(0) \rangle = \gamma(0)$$

and

$$\langle W_x(0) W_x(t) \rangle = \langle W_y(0) W_y(t) \rangle = \gamma(t)$$

are different from zero, so that

$$\gamma(0) = \frac{1}{2} \langle \{\vec{W}(0)\}^2 \rangle,$$

$$\gamma(t) = \frac{1}{2} \sum_{i=1}^{3} \langle W_i(0) W_i(t) \rangle. \tag{13}$$

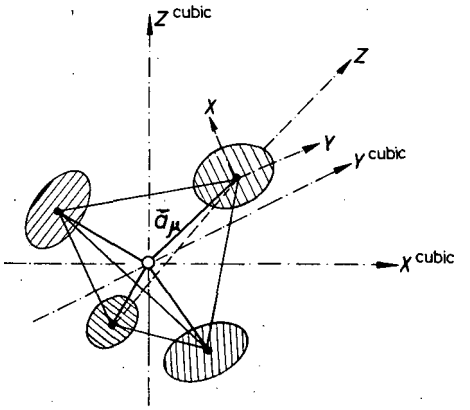

Fig. 1

A polycrystal with randomly-oriented-rotating crystallites

To average over the orientations of $\vec{Q}$ relative to this crystal-bound co-ordinate system, we express $\vec{Q}$ in polar co-ordinates with z as polar axis. We obtain

$$\overline{\exp\left(-\sum_{ij} Q_i Q_j \langle W_i(0) W_j(0)\rangle\right) \sum_{ij} Q_i Q_j \langle W_i(0) W_j(t)\rangle}$$

$$= \frac{Q^2\gamma(t)}{2} \int_{-1}^{+1} d\cos\vartheta \, \sin^2\vartheta \, \exp(-Q^2\gamma(0)\sin^2\vartheta)$$

$$= Q^2\gamma(t) \exp(-Q^2\gamma(0)) f_W(Q, \gamma(0))$$

and

$$\overline{\exp\left(-\sum_{ij} Q_i Q_j \langle W_i(0) W_j(0)\rangle\right)}$$

$$= \frac{1}{2} \int_{-1}^{+1} \exp(-Q^2\gamma(0) \sin^2\vartheta) \, d\cos\vartheta$$

$$= \exp(-Q^2\gamma(0)) f_S(Q, \gamma(0)),$$

where

$$f_W(Q, \gamma(0)) = -\frac{i}{\theta\gamma^{1/2}(0)} F(iQ\gamma^{1/2}(0)) - \frac{\partial}{\partial\beta}\left[-\frac{i}{\beta^{1/2}} F(i\beta^{1/2})\right]_{\beta = Q^2\gamma(0)}$$

$$f_S(Q, \gamma(0)) = -\frac{iF(iQ\gamma^{1/2}(0))}{Q\gamma^{1/2}(0)}$$

$F(x)$ = the Gauss error function.

With this, Eqs. (9) and (11) give, together with Eq. (13):[2]

$$\overline{X_{inc}(\vec{Q}, t)} = \frac{\hbar Q^2}{2N} \exp[-(2W_s + Q^2\gamma(0))]\left\{\sum_{\vec{q},\alpha} \frac{1}{\nu_\alpha(\vec{q})} \frac{f_S(Q, \gamma(0))}{3M}\right.$$

$$\times[\langle n_\alpha + 1\rangle e^{-i\nu_\alpha t} + \langle n_\alpha\rangle e^{-i\nu_\alpha t}] \sum_\mu \sigma_\mu$$

$$\left. + \sum_{\vec{q},\beta} \frac{1}{\nu_\beta(\vec{q})} \frac{f_W(Q, \gamma(0))}{2\theta} [\langle n_\beta + 1\rangle e^{-i\nu_\beta t} + \langle n_\beta\rangle e^{-i\nu_\beta t}] \sum_\mu \sigma_\mu |\vec{\xi}_\mu|^2 \right\}. \quad (14)$$

Because $\theta = \sum_\mu m |\vec{\xi}_\mu|^2$, with m denoting the mass of one of the atoms participating in the libration, $\sum_\mu |\vec{\xi}_\mu|^2$ cancels out of Eq. (14). Performing the Fourier transform of Eq. (7) and replacing the summation over $\vec{q}$ by an integration over $d\nu$ with frequency distributions $g_S(\nu)$ and $g_W(\nu)$, we finally obtain:

For <u>emission</u> of a quantum by the neutron:

$$\overline{S_{inc}^{em}(\vec{Q}, \nu)} = \frac{\hbar Q^2}{2\nu} e^{-2W}[-\exp(-\hbar\omega/k_B T) + 1]^{-1} \sigma_\mu \left\{ Z_r \frac{f_S(Q, \langle W^2(0)\rangle)}{3M} g_S(\nu) \right.$$

$$\left. + \frac{f_W(Q, \langle W^2(0)\rangle)}{2m} g_W(\nu) \right\}, \quad (15a)$$

where Z_r is the number of atoms participating in rotation.

---

[2] Here, we have made the simplifying, but not really necessary, assumption that the atoms participating in the rotation do all the scattering (i.e. $\sigma_{central} = 0$). A non-vanishing $\sigma_{central}$ would only introduce an additional term into Eq. (14) of the form known from the Bravais crystal, not containing <u>any</u> rotational motion, not even in the Debye-Waller factor.

For absorption:

$$\overline{S_{inc}^{abs}(\vec{Q},\nu)} = \frac{\hbar Q^2}{2\nu} e^{-2W} [\exp(\hbar\omega/k_B T) - 1]^{-1} \sigma_\mu \left\{ Z_r \frac{f_S}{3M} g_S(\nu) + \frac{f_W}{2m} g_W(\nu) \right\}. \quad (15b)$$

where in the case of W being small ($e^{-2W} \approx 1$, $f_S \approx 1$, $f_W \approx 1$) we find that the rotational part of the spectrum enters the scattering law with an enhancement factor of $3M/2mZ_r$. In the case of methane, this ratio is as big as six.

To recapitulate, the assumptions underlying Eq. (15) are: [2]

(a) Small amplitudes of internal vibrations (rigid molecules),
(b) Harmonic librations and vibrations
(c) No coupling between the two,
(d) One-quantum transitions dominate,
(e) The crystal is cubic, all atoms involved in librations are alike, and the molecule has at least tetrahedral symmetry,
(f) One has to average with equal weight over all directions of $\vec{Q}$.

3. COHERENT ONE-QUANTUM SCATTERING

The coherent one-quantum scattering law is given by the Fourier transform of

$$X_{coh}^{(1)}(\vec{Q},t) = \sum_{\vec{m}} e^{i\vec{Q}\vec{X}^{\vec{m}}} \times \sum_{\mu\mu'} \underbrace{a_\mu a_{\mu'} \exp[i\vec{Q}(\vec{a}_\mu - \vec{a}_{\mu'})] \exp\left(-\frac{1}{2}\langle\{\vec{Q}\cdot\vec{S}_\mu^{\vec{0}}(0)\}^2\rangle - \frac{1}{2}\langle\{\vec{Q}\cdot\vec{S}_{\mu'}^{\vec{m}}(0)\}^2\rangle\right)}_{F_{\mu\mu'}}$$

$$\times \langle\{\vec{Q}\cdot\vec{S}_\mu^{\vec{0}}(0)\}\{\vec{Q}\cdot\vec{S}_{\mu'}^{\vec{m}}(t)\}\rangle. \quad (16)$$

$S_{i\mu}^{\vec{m}}$ decomposes into plane waves [3]

$$S_{i\mu}^{\vec{m}} = \sum_{\vec{q}} \sum_{\alpha=1}^{6} \underbrace{\left\{ \xi_{\alpha\vec{q}} \sqrt{\frac{\hbar}{2MN\nu_\alpha}} e_i(\vec{q},\alpha) + \eta_{\alpha\vec{q}} \sqrt{\frac{\hbar}{2N\nu_\alpha}} [\vec{\Omega}_\alpha'(\vec{q}) \times \vec{a}_\mu] \right\}}_{\kappa_{i\mu}} \times \left\{ \sigma_\alpha(\vec{q}) \exp\left(i[\vec{q}\vec{X}^{\vec{m}} - \nu_\alpha(\vec{q})t]\right) + \sigma_\alpha^+(\vec{q}) \exp\left(-i[\vec{q}\vec{X}^{\vec{m}} - \nu_\alpha(\vec{q})t]\right) \right\} \quad (17)$$

[3] In Eq. (17) $\Omega_i' = \Omega_i/\sqrt{\Theta_i}$, if $(\xi e_1, \xi e_2, \xi e_3; \eta\Omega_1, \eta\Omega_2, \eta\Omega_3)$ is the normalized eigenvector α of the 6×6 frequency matrix of the crystal for the wave vector $\vec{q}$. In general, the axis of libration for the mode $(\vec{q},\alpha)$ is $\vec{\Omega}'$ and not $\vec{\Omega}$.

where $(\xi^2+\eta^2 = 1)$. In general, these plane waves partly rotate, partly translate the molecules.

By inserting Eq. (17) in Eq. (16) and carrying out the Fourier transform with respect to t, we obtain

$$S^{\{\text{em}\}}_{\{\text{abs}\}\text{coh}}(\vec{Q}, \nu) \sim \sum_{\mu\mu'} F_{\mu\mu'}(\vec{Q}) \sum_{\alpha=1}^{6} \sum_{ij} Q_i Q_j \kappa_{\mu i} \kappa_{\mu' j} \left\{ \begin{matrix} \langle n_\alpha \rangle + 1 \\ \langle n_\alpha \rangle \end{matrix} \right\} \delta\{\nu \pm \nu_\alpha(\vec{Q})\} . \tag{18}$$

The δ-function provides for the sharp scattering surfaces, of which, in the most general case, there are six; the thermal factors with the $\langle n_\alpha \rangle$'s are not new, either. We shall not enlarge on the molecular structure factors $a_\mu a_{\mu'} \exp(i\vec{Q}(\vec{a}_\mu - \vec{a}_{\mu'}))$ and the Debye-Waller factor; they can in principle be determined from coherent elastic scattering experiments. It seems difficult to say anything general about the nature of the vibrations concerned and the strength of the S-ω coupling from the dispersion curves alone that one gets from the scattering surfaces.

A few special cases have been investigated in Ref. [3].

We shall here confine ourselves to a few general remarks on the factor

$$\{\vec{Q}\vec{\kappa}_\mu\}\{\vec{Q}\cdot\vec{\kappa}_{\mu'}\}, \tag{19}$$

which appears to depend rather characteristically on the nature of the vibration observed.

(a) For pure translations ($\xi = 1$) nothing new is found when compared to Bravais crystals. $\vec{\kappa}_\mu$ is independent of μ, and we can, as usual, say that $\{\vec{Q}\vec{e}\}^2$ is zero when $\vec{e} \perp \vec{Q}$. This shows as a leak in the scattering surface.

(b) For pure rotations ($\eta = 1$) we find

$$\sum_{ij} Q_i Q_j \frac{\hbar}{2N\nu_\alpha} [\vec{\Omega}'_\alpha(\vec{q}) \times \vec{a}_\mu]_i \, [\vec{\Omega}'_\alpha(\vec{q}) \times \vec{a}_{\mu'}]_j .$$

It is impossible to excite a torson that librates around $\vec{Q}$. (See also Eq. (16)). One also sees that the geometry of the molecule plays an important role. As an extreme instance, it is impossible to make a dumbbell molecule librate by a $\vec{Q}$ parallel to its axis.

With a knowledge of the structure, one may also, for each special case, discuss the intensity variations along the scattering curves for the case when rotations and translations are mixed. This calculation is planned for solid CD_4 whose structure is expected to be determined experimentally.

REFERENCES

[1] HAHN, H. and BIEM, W., Phys. Stat. sol. 3 (1963) 1911.

[2] LEIBFRIED, G., in Handbuch der Physik 7 (1) Springer, Berlin (1955) 104 ff.

[3] BIEM, W., Phys. Stat. sol. 3 (1963) 1927.

LATTICE DYNAMICS OF SOLID METHANE

B. DORNER AND H. STILLER
KERNFORSCHUNGSANLAGE JÜLICH, FEDERAL REPUBLIC OF GERMANY
AND
CENTRE D'ÉTUDES DE L'ÉNERGIE NUCLÉAIRE, MOL, BELGIUM

Abstract — Résumé — Аннотация — Resumen

LATTICE DYNAMICS OF SOLID METHANE. Solid methane seems a comparatively simple example of a molecular crystal. Yet the internal dynamics of the system are not understood. Specific heat measurements have revealed a phase transformation at 20.4°K; recently, a second phase change has been found at 8°K. Both transitions are of the second kind. X-ray investigations have indicated that the first transition does not affect the fcc lattice positions of the carbon atoms.

The energy distribution of scattered slow neutrons has been measured for all three phases. Results for the α-phase ($T > 20.4°K$) and the β-phase ($20.4°K > T > 8°K$) were reported at the IAEA Symposium in Chalk River. With the present measurements the investigation is extended into the γ-phase ($T < 8°K$). As before, the experiments are carried out with the filtered detector technique.

Frequency distributions, derived from the assembly of experimental results, are compared to theoretical predictions, which are based on a model proposed by James and Keenan for the orientational structure. The comparison confirms the model for the γ-phase. The observed maximum frequency of acoustic vibrations, $\hbar\omega_D \simeq 4$ meV, corresponds well to what one would expect for the assumed octopole-octopole interactions. In addition, two optical bands are observed.

The ratio of their mean frequencies is found to be 1.25, which under the assumption of harmonic librations corresponds exactly to the value calculated from the proposed orientational structure. Again for octopole-octopole interaction the absolute values of these frequencies indicate $q = 0.16$ e for the effective proton charge. Thermodynamic considerations, applied by James and Keenan to CD_4, give $q = 0.13$ e.

The experimental results contradict, however, the orientational structure proposed for the β-phase. For the α-phase the theory predicts the absence of long-range orientational order. The neutron investigations show that yet the rotational motions are not entirely unhindered, but a quantitative interpretation of the spectrum observed in this phase has not been attempted.

DYNAMIQUE DES RÉSEAUX DU MÉTHANE SOLIDE. Le méthane à l'état solide semble être un exemple relativement simple de cristal à structure moléculaire. Toutefois, on ne comprend pas bien la dynamique interne du système. Des mesures de la chaleur spécifique ont mis en évidence une transformation de phase à 20,4°K et on a récemment constaté l'existence d'une deuxième transformation de phase à 8°K. Dans l'un et l'autre cas, il s'agit de transitions du second degré. Des examens aux rayons X ont permis de constater que la première transition n'a pas d'effet sur les positions des atomes de carbone dans le réseau cubique à faces centrées.

Les auteurs ont mesuré pour les trois phases la distribution en énergie des neutrons lents diffusés. Les résultats concernant la phase α ($T > 20,4°K$) et la phase β ($20,4°K > T > 8°K$) ont été présentés lors du Colloque organisé par l'AIEA à Chalk River. Les mesures décrites dans le présent mémoire étendent les recherches à la phase γ ($T < 8°K$). Comme auparavant, les recherches sont exécutées à l'aide d'un détecteur à filtre.

Les auteurs comparent les répartitions de fréquence, établies à partir de l'ensemble des résultats expérimentaux, à des prévisions théoriques fondées sur un modèle de structure d'orientation proposé par James et Keenan. La comparaison confirme le modèle pour la phase γ. La fréquence maximum observée des vibrations acoustiques, $\hbar\omega_D \simeq 4$ meV, correspond bien à ce que l'on pouvait attendre des interactions octopol-octopol présumées. On observe en outre deux bandes optiques.

On constate que le rapport de leurs fréquences moyennes est de 1,25 ce qui, en supposant l'existence de librations harmoniques, correspond exactement à la valeur calculée à partir de la structure d'orientation proposée. Pour l'interaction octopol-octopol, les valeurs absolues de ces fréquences donnent $q = 0,16$ e pour la charge efficace des protons. Les considérations thermodynamiques appliquées par James et Keenan au cas du CD_4 donnent $q = 0,13$ e.

Pour la phase β, en revanche, les résultats obtenus expérimentalement sont en contradiction avec la structure d'orientation proposée. Pour la phase α, la théorie prévoit l'absence d'un ordre d'orientation à longue distance. Il ressort des recherches à l'aide de neutrons que les mouvements de rotation ne sont cependant pas entièrement libres, mais les auteurs n'ont pas cherché à interpréter quantitativement le spectre observé dans cette phase.

ДИНАМИКА РЕШЕТКИ ТВЕРДОГО МЕТАНА. Твердый метан является, по-видимому, сравнительно простым примером молекулярного кристалла. Внутренняя динамика системы все же еще не изучена. Измерения удельной теплоемкости показали, что фазовый переход происходит при 20,4°K; недавно было обнаружено второе изменение фазы при 8°K. Оба перехода относятся ко второму виду. Исследования с помощью рентгеновских лучей показали, что первый переход не затрагивает положений атомов углерода в кубической решетке.

Для всех трех фаз измерялось распределение энергии рассеянных медленных нейтронов. О результатах для α-фазы ($T > 20{,}4°K$) и β-фазы ($20{,}4°K > T > 8°K$) сообщалось на симпозиуме МАГАТЭ в Чок Ривер. Настоящие измерения являются расширением исследований на γ-фазу ($T < 8°K$). Как и прежде, эксперименты проводятся методом фильтрующих детекторов.

Распределения частот, полученных на основании совокупности экспериментальных результатов, сравниваются с теоретическими предсказаниями, которые основываются на модели, предложенной Джеймсом и Кинаном для ориентированной структуры. Сравнение подтверждает правильность модели для γ-фазы. Наблюдаемая максимальная частота акустических колебаний $\hbar\omega_D \simeq 4$ мэв полностью соответствует тому, что следовало ожидать для предполагаемых взаимодействий октуполь-октуполь. Кроме того, наблюдаются две оптические полосы частот.

Обнаружено, что отношение их средних частот составляет 1,25, что, если предположить гармоническое равновесие, точно соответствует величине, вычисленной, исходя из предполагаемой ориентированной структуры. В случае взаимодействия октуполь-октуполь абсолютные величины этих частот показывают, что $q = 0{,}16$ э для эффективного протонного заряда. Термодинамический подход, примененный Джеймсом и Кинаном для CD_4, дает $q = 0{,}13$ э.

Экспериментальные результаты противоречат, однако, ориентированной структуре, предложенной для β-фазы. Для α-фазы теория предсказывает отсутствие дальнего ориентированного порядка. Исследования нейтронов показывают, что вращательные движения не проходят совершенно без помех, но попыток количественной интерпретации наблюдаемого в этой фазе спектра не предпринималось.

DINAMICA DE LA RED CRISTALINA DEL METANO SOLIDO. El metano sólido parece constituir un ejemplo relativamente sencillo de cristal molecular. Sin embargo, se desconoce la dinámica interna del sistema. Las mediciones del calor específico han puesto de relieve una transición de fase a 20,4°K; recientemente, se ha observado una segunda transición a 8°K. Ambas son de segundo orden. Las investigaciones efectuadas han revelado que la primera transición no afecta a las posiciones de los átomos de carbono en la red cúbica centrada en las caras.

Se ha medido, para las tres fases, la distribución de energía de los neutrones lentos dispersos. Los resultados correspondientes a la fase α ($T > 20{,}4°K$) y a la fase β ($20{,}4° > T > 8°K$) se dieron a conocer en el simposio reunido por el OIEA en Chalk River. Con las actuales mediciones, la investigación se extiende a la fase γ ($T < 8°K$). Como en los casos anteriores, los experimentos se han realizado aplicando la técnica del detector filtrado.

Las distribuciones de frecuencia, deducidas del conjunto de resultados experimentales, se comparan con las previsiones teóricas, que se basan en un modelo propuesto por James y Keenan para la estructura de orientación. La comparación confirma que el modelo para la fase γ es correcto. La frecuencia máxima observada de las vibraciones acústicas, $\hbar\omega_D \simeq 4$ meV, concuerda satisfactoriamente con el valor que cabe esperar de las interacciones octopolo-octopolo supuestas. Además, se observan dos bandas ópticas.

Se ha comprobado que la razón de sus frecuencias medias es de 1,25, lo que, dando por supuesto que las vibraciones son armónicas, corresponde exactamente al valor calculado partiendo de la estructura de orientación propuesta. Asimismo, en lo que respecta a la interacción octopolo-octopolo, los valores absolutos de estas frecuencias indican que para la carga protónica efectiva $q = 0{,}16$ e. De las consideraciones termodinámicas aplicadas por James y Keenan al CD_4, se deduce que $q = 0{,}13$ e.

Sin embargo, los resultados experimentales están en contradicción con la estructura de orientación propuesta para la fase β. *En cuanto a la fase α, la teoría prevé la ausencia de un orden de orientación* de largo alcance. Las investigaciones realizadas con neutrones muestran que los movimientos de rotación no están

enteramente libres de restricciones, pero aún no se ha intentado interpretar cuantitativamente el espectro observado en esta fase.

Solid methane exhibits phase transformations at 20.4 and at 8°K. The energy distribution of scattered neutrons is measured at 2.7°K (phase III) and at 6.5°K, where the sample is in a transition state between phases II and III. Frequency distributions $g(\omega)$ unnormalized with respect to the molecular mass and moment of inertia, are derived from the experimental results and compared to frequency distributions derived from earlier results obtained at 84°K (phase I) and at 18°K (phase II). The $g(\omega)$ at 84, 18 and 2.7°K all exhibit three distinct frequency bands. The spectra in the three phases are quite similar to each other; they are compared to what is expected from the theory of James and Keenan. The experimental results obtained at 6.5°K yield a frequency distribution surprisingly different from the others.

INTRODUCTION

Because of the high symmetry of the molecule solid methane can be considered as the simplest case of a molecular crystal. All three principal moments of inertia are equal. Owing to the absence of electrical 2^n-pole moments of order $n<3$ the intermolecular forces can be expected to be small compared to the internal binding forces, so that any influence of the internal molecular vibrations on the motions of the entire molecule certainly can be neglected. Methane, therefore, appeared to be the best sample for the beginning of studies on the lattice dynamics of molecular crystals (see [1-3]). It has two disadvantages: (i) owing to the comparatively small moment of inertia of the molecule and to the large lattice constant, hindered rotational motions can hardly be expected to be harmonic, except perhaps at very low temperature, (ii) of the crystal structure only the arrangement of the carbon atoms is known, and this also only down to 13.8°K [4]. In the vicinty of 20.4°K the structure determination, moreover, has not been unambiguous; there appeared additional diffuse lines in the X-ray diffraction patterns, which seemed to depend on the thermal history of the samples and could not be interpreted[1].

Solid methane exhibits two phase transformations of the second kind, at 20.4°K [5] and at 8°K [6]. A rather long series of neutron scattering experiments has been carried out to determine the frequency distributions in the three phases. Results for phase I ($90.8°K > T > 20.4°K$) and phase II ($20.4°K > T > 8°K$) have been reported earlier [7]. With the present experiments the investigation was extended to $T < 8°K$ (6.5 and 2.7°K).

EXPERIMENTAL RESULTS

The measurements were performed with the beryllium-filtered detector method, first [8] with the sample at $(6.5 \pm 1)°K$ using a two-axis spectro-

[1] For a determination of the complete structure, including the proton positions, neutron diffraction measurements on solid CD_4 are in progress.

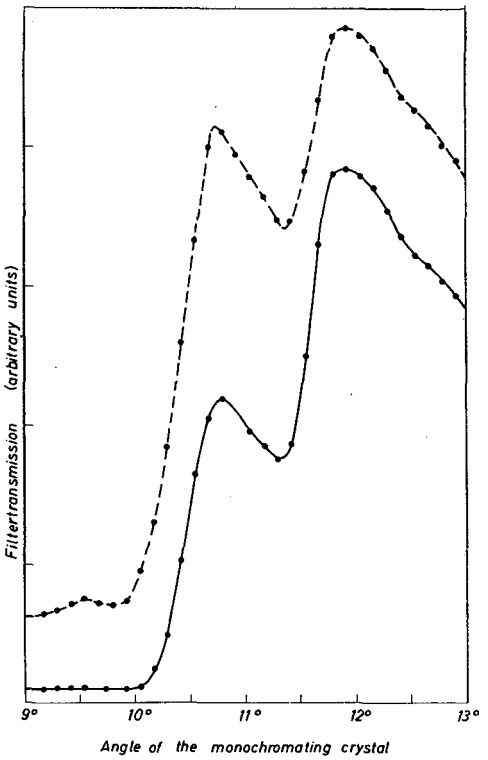

Fig. 1

Transmissions of two Be filters

---- 7-cm Be
—— 10-cm Be

meter at the reactor BR 1, then with the sample at (2.7±0.1)°K using a triple-axis spectrometer at the reactor BR 2. The filtered detector method was chosen also for the second measurements in order to facilitate a comparison of the data with those obtained earlier at higher temperatures. For the second measurements, however, the filter could be made somewhat longer (10 instead of 7 cm); this improved the transmission function. Figure 1 shows the transmissions of the two filters.

With the filtered detector technique the number of neutrons counted is [9]

$$N(E_0, \vec{Q}) \sim \int_{-\infty}^{\infty} R(E_0 - \epsilon)d\epsilon \int_0^{E_f} T(E')S(\vec{Q}, \epsilon - E')dE'$$

E_0 is the energy of the neutrons incident on the sample, E' the energy of the scattered neutrons, $\hbar\omega = \epsilon - E'$, E_f the filter cut-off energy, $\hbar\vec{Q}$ the momentum transfer, $R(E_0 - \epsilon)$ the resolution function of the apparatus, $T(E')$ the filter transmission function and $S(\vec{Q}, \epsilon - E')$ the scattering function. With

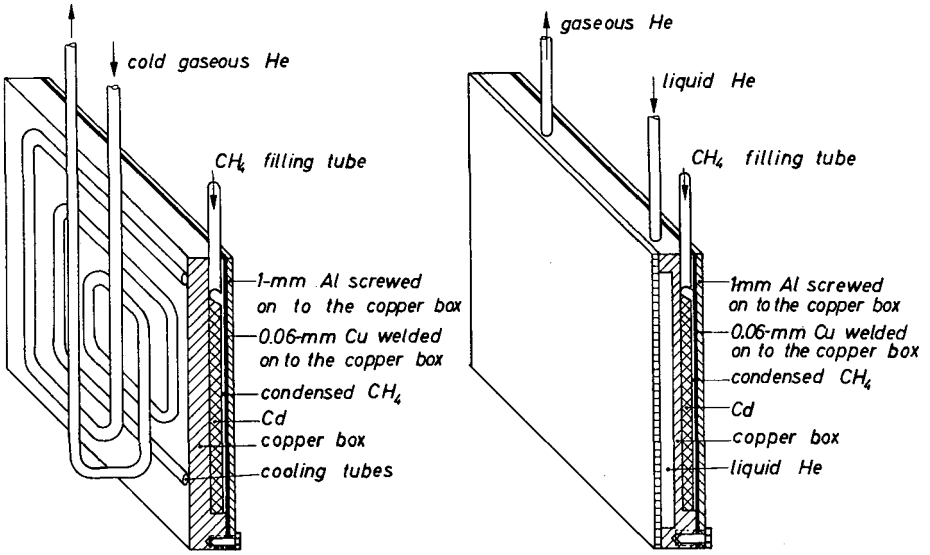

Fig. 2

Schematic drawing of sample containers

methane the neutrons are scattered predominantly by the protons, so that effectively $S = S_{inc}$. From the transmission curves of Fig. 1 one obtains for $E_0 = E_f = 5.20$ meV a full width at half maximum of $R(E_0 - \epsilon)$ of $(1.4 \pm 0.2) \times 10^{-4}$ eV for the first measurements (T = 6.5°K) and of $(2.2 \pm 0.2) \times 10^{-4}$ eV for the second measurements (T = 2.7°K).

Figure 2 gives a schematic drawing of the sample containers. In each case gaseous methane was condensed into a layer of 0.4-mm thickness, contained in a copper frame between a sheet of cadmium and a thin Cu foil (0.06-mm thick), which was welded onto the frame. An aluminium plate of 1-mm thickness was then screwed over the Cu foil. For the measurements at a sample temperature of 6.5°K cold gaseous helium was pumped through a spiral of Cu tubes attached to the rear of the Cu box. For the measurements at 2.7°K these tubes were replaced by a copper container which was filled with liquid helium. The temperature of 2.7°K was reached by lowering the pressure over the helium to between 100 and 140 Torr. The samples were placed in reflection. The measurements were carried out at scattering angles of 45° and 60° with the sample at 6.5°K and at 75° and 90° for 2.7°K.

At the BR 1 reactor for which the flux fluctuations were less than 0.2% the data were taken at constant times; at the BR 2 reactor they were taken for constant rates of a monitor counter placed into the unmonochromized beam. In both cases the data had to be normalized by the reactor spectrum to constant incident flux. Figure 3 shows the spectra at the two beam ports as measured with Thermica monochromizing crystals. The dashed curves represent Maxwellian distributions fitted to the low wavelength part of the measured spectra. The deviations of the measured curves from Maxwellian

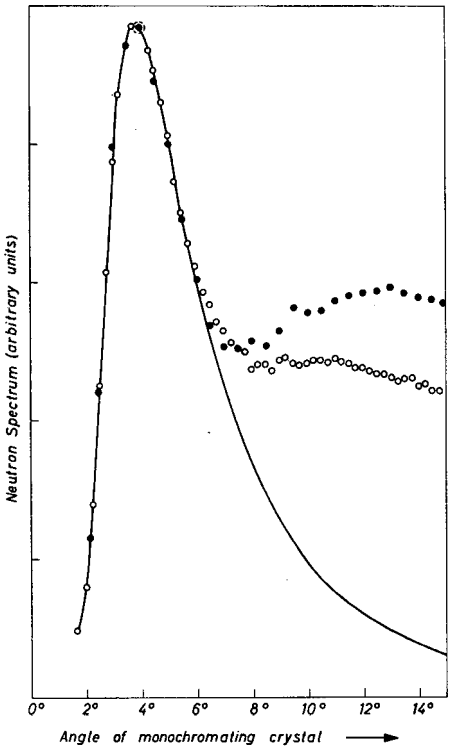

Fig. 3

(001) reflections of a Thermica single crystal at the BR 1 and BR 2 reactors
The curves are fitted to each other at their maximum values.
Absolute intensities could not be compared because of different vertical divergences of the beams

—— Calculated Maxwell spectrum
○ Spectrum BR 1
● Spectrum BR 2
◌ Fitting point

distributions are due to third and fifth order reflections from the monochromator. As has been shown already [8], within the energy region covered in the experiment the higher order contamination of the beam incident on the sample is of no importance, because the resolution width increases with increasing E_0 such that third and fifth order neutrons can contribute only a continuous background to the observed inelastic scattering.

Figure 4 shows the results of measurements at the scattering angles of 75° for a sample temperature of 2.7°K. Owing to the presence of a second filter edge, at 6.35 meV, the increases labelled 1a and 1b represent the same effect, one relative to E_{f1} and one relative to E_{f2}. The increases at larger E_0 appear only once, because for $E_0 > 11$ meV the experimental resolution no longer separates the two edges.

Figure 5 shows earlier results obtained at a sample temperature of 6.5°K [8]. The observed scattering function exhibits much more structure. The increases

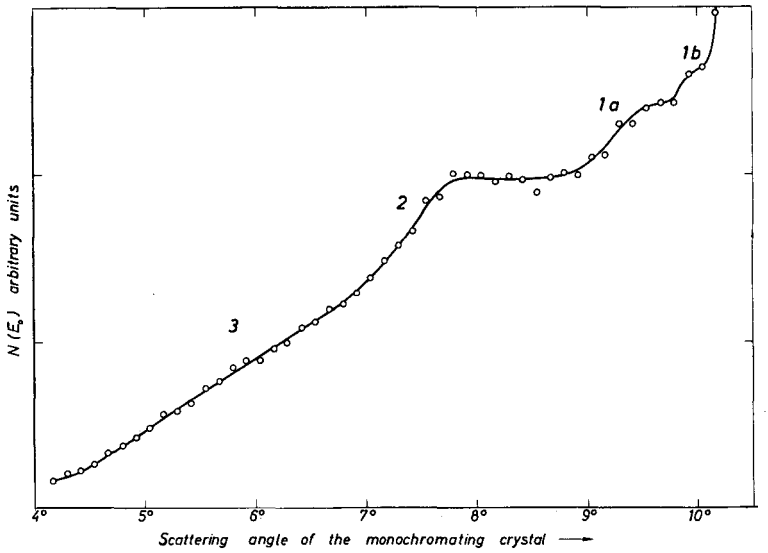

Fig. 4

Experimental results for sample temperature of 2.7°K

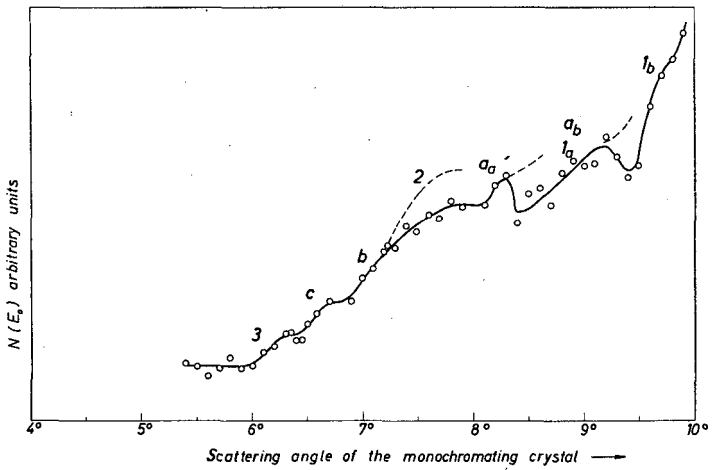

Fig. 5

Experimental results for sample temperature of 6.5°K

labelled 1a and 1b, 2a and 2b, again pair-wise, represent the same effects. The dashed curve sections indicate what curve the points would follow, if each increase would not cease to contribute to $N(E_0)$ as $E_0 - \hbar\omega$ approaches zero.

The data given in Figs. 4 and 5 are normalized to constant incident flux and corrected for background, measured with the empty containers. In critical regions, between $\theta = 5.9°$ and $\theta = 6.9°$ of Fig. 5, the curve through the

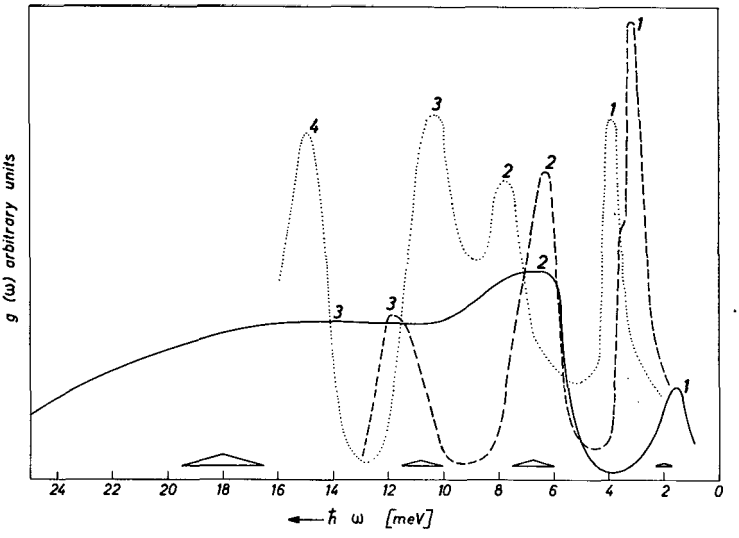

Fig. 6

Frequency spectra for phases I, II and III

.... 84°K, Phase I
---- 18°K, Phase II
—— 2.7°K, Phase III
Resolution of the apparatus

experimental points was checked by means of a χ^2 test [10], which showed that by increasing the number of measurements only 5% of the experimental points would have had larger deviations from the curve than the present data.

DISCUSSION

The earlier results have been compared [7, 8] to the theory of JAMES and KEENAN [11]. Under the assumption of octopole-octopole interactions between the molecules this theory applies classical self-consistent field calculations [12] to the problem of the phase transformations and orientational structures of CD_4; it predicts for phase I the absence of long range orientational order, for phase II a structure, in which one out of five molecules can rotate freely, and for phase III ($T < 22.2$°K in CD_4, $T < 8$°K in CH_4) a uniform orientation, which gives a tetragonal lattice symmetry. It has been shown that for the last structure two bands of librational frequencies are to be expected and that the ratio of the centres of gravity of these two bands should be 1.26.

Figure 6 represents frequency spectra of CH_4 at 84°K (phase I), 18°K (phase II) and 2.7°K (phase III)[2], calculated from the assembly of experimental data by eliminating those increases of $N(E_0)$ which as a consequence

[2] To facilitate the discussion the spectra are given on a linear energy scale, although not normalized to constant ΔE_0

of the two filter cut-offs appeared twice in one measurement, by differentiating with respect to E_0 and by multiplying with (see [13]).

$$\kappa(E_0) = \frac{k_0}{k_f} \frac{E_0 - E_f}{(\vec{k}_0 - \vec{k}_f)^2} \left(1 - \exp\left[-\frac{E_0 - E_f}{k_B T}\right]\right).$$

The $g(\omega)$ thus derived, of course, will represent true frequency distributions only if (i) there are no multi-quantum transitions, (ii) all motions are harmonic, (iii) the arrangement of the molecular centres of mass is indeed cubic, as indicated down to 13.8°K by X-ray diffraction and also assumed in the James-Keenan model, (iv) the orientational structure is cubic or tetragonal, and (v) the clouds of librational amplitudes are nearly circular. Whether the first condition is fulfilled can be tested by the Q-dependence of the observed spectra. It was found to hold for all present measurements. The other four conditions can be expected to be fulfilled at least for the phase III structure ($T < 8$°K) as proposed by James and Keenan. There are, however, two further difficulties:

(a) As a priori nothing can be said about which frequencies are to be assigned to rotations and which to translations, it is impossible to normalize the observed $g(\omega)$ unambiguously with respect to the molecular mass and moments of inertia,

(b) The behaviour of the molecular spin states (see [9, 14]) is unknown. Therefore, even for phase III the $g(\omega)$ shown in Fig. 6 certainly do not represent characteristic density distribution of the modes over energy as far as relative intensities are concerned; only the positions of the peaks can be discussed.

The most striking feature of the distributions shown in Fig. 6 is their similarity. The narrow peak 1 and the broader peaks 2 and 3 appear in all three phases. With decreasing temperature peak 1 is shifted to lower, peak 3 to higher frequencies. Peak 2, in the middle, goes first (with the I → II transition) to lower frequencies; by the II → III transition it is extended to higher frequencies with the low-frequency region unaltered (see also Fig. 7).

The appearance of three distinct frequency bands indicates that there are in all phases at least one or two optical dispersion branches. The fact that, at the lowest temperature, both peaks 2 and 3 appear largely broadened, suggests for phase III the existence of at least two optical branches, because a large dispersion, which yet does not extend to zero, can be expected for optical branches only. For phase III the broad fall-off of peak 3 to high frequencies indicates that for the higher optical branch the frequencies decrease with increasing wave vector $\vec{q}$. Some possible explanations for the detailed observed temperature dependence of the peak positions are discussed in Appendix A.

Two bands of librational frequencies are expected in the phase III orientational structure as proposed by James and Keenan. However, the ratio of the centres of gravity of the observed bands certainly is larger than 1.26. The observed similarity of the spectra for the three phases seems to disagree with the prediction of large differences in the orientational structures and degrees of rotational hindrance between the three phases. Free rota-

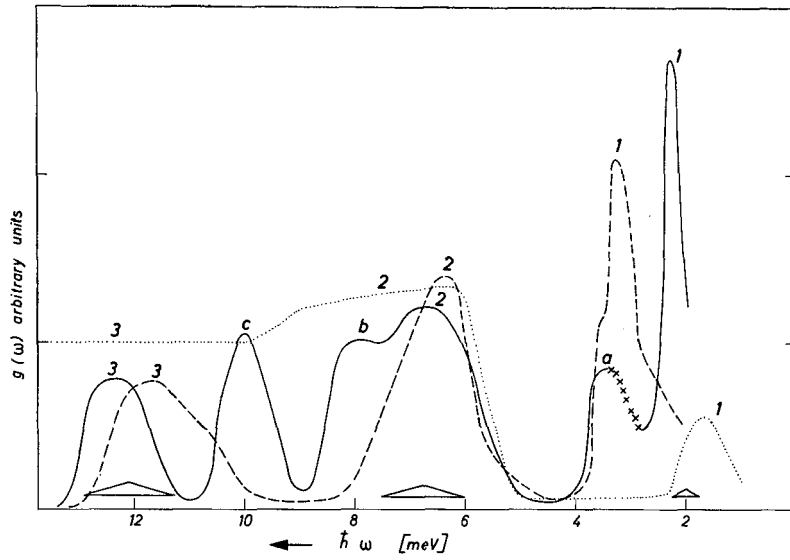

Fig. 7

Frequency spectrum at 6.5°K (between phases II and III)
For comparison the spectra observed at 18°K (phase II)
and at 2.7°K (phase III) are also shown.

---- 18°K, Phase II
—— 6.5°K
.... 2.7°K, Phase III
Resolution of the apparatus

tions, as predicted for phase II, are not seen. The only observed peak possibly representing such a transition is the one labelled 4, found in phase I. Even if it represented free rotations this would not be of much significance, as it appears at high incident energies. With sufficiently high energies one may, of course, always excite free rotations.

Figure 7 represents the $g(\omega)$ calculated from the experimental data taken at 6.5°K. At this temperature the sample supposedly is in a transition state between phases II and III [6]. Surprisingly in this state the frequency distribution is different: three additional peaks appear (a, b and c). We note in passing: the ratio of the frequencies at two of these new peaks, namely b and c, is 1.26. The absolute values of the two frequencies give (see Appendix B), under the assumption of octopole-octopole interaction, for the effective proton charge 0.16 e; the thermodynamic considerations of James and Keenan for CD_4 gave 0.13 e.

At present the considerations of James and Keenan appear to be the only theory which makes explicit predictions about the structure and the dynamics of solid methane. Other theories [15] so far have been concerned with the low temperature phase only. For this phase two models have been proposed for the structure on the basis of symmetry considerations and calculations of zero-point entropies. For one of these models only one band of librational frequencies can be expected. The other model is rather com-

plicated, with four molecules per unit cell; its dynamical consequences have not yet been analysed.

ACKNOWLEDGEMENTS

The authors wish to thank Dr. H. Hahn, Dr. T. Springer and Dr. R. Stockmeyer for helpful discussions and Mr. F. Fredel for continuous assistance with the experiments. The generous hospitality and support, which were offered to us at the laboratories of the Centre d'études de l'énergie nucléaire are gratefully acknowledged. We wish to express our special gratitude to Dr. M. Nève de Mévergnies.

APPENDIX A

For phase III, in which the librational motions are most likely to be harmonic, the appearance of three frequency bands, as discussed above, suggests dispersion relations of either one of the forms shown in Fig. 8.

For a crystal of quasi-rigid molecules with comparatively weak interaction and of high crystal symmetry, as here presumed, one may expect that qualitatively, at least for the vibrations and longitudinal librations, the essential features of the dispersion relations might be revealed by a simple model: a linear chain of two-atomic molecules. For such a chain, discussed in detail by HAHN and BIEM [1], the two dispersion branches are:

$$\{\omega_{\frac{1}{2}}(q)\}^2 = \frac{B}{2M}\left\{(1-\cos aq)+\frac{\gamma}{\vartheta}(1+\beta\cos aq)\right.$$

$$\left.\pm\sqrt{\left[(1-\cos aq)-\frac{\gamma}{\vartheta}(1+\beta\cos aq)\right]^2+\frac{16\delta^2}{\vartheta}\sin^2 aq}\right\}$$

Here B is a force constant, a is the lattice constant, M is the molecular mass. β is a parameter, which describes the coupling of rotational motions, i.e. the relative differences between forces acting on one atom from different atoms of neighbouring molecules; for instance, in the very simplest model shown in Fig. 9, $\beta = (f - f')/(f + f')$. An increase of β with decreasing temperature means that of the forces from different neighbours the strongest one increases more rapidly than the others. γ is a parameter, which takes into account the directions, in which different neighbouring atoms act, i.e. γ is determined by the lattice symmetry. ϑ is the relative amount of the molecular mass taking part in rotational motions; for CH_4

$$\vartheta = \frac{4m_H}{M_{CH_4}} = 0.25$$

δ finally describes the coupling of rotational and translational motions. For $q \to 0$ and $q \to \pi/a$ each dispersion branch is either purely rotational or purely translational.

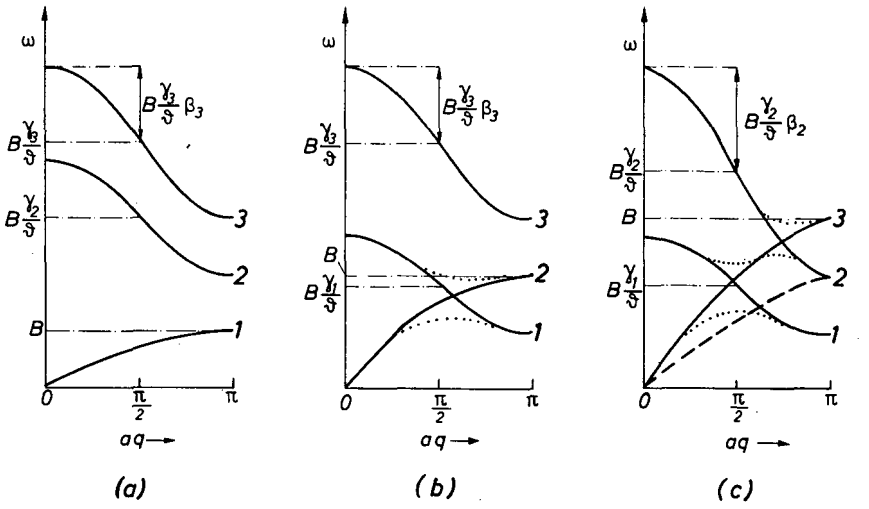

Fig. 8

Three simple dispersion relations consistent with the spectrum observed at 2.7°K (phase III)
The numbers at the horizontal parts for $q \to \pi/a$ indicate the peaks as labelled in Figs. 6 and 7.
The parameters given at the ω-axis correspond to those of the dispersion equation for a linear chain.
The parameter β is shown for the upper optical band only.
The dashed lines in (c) represent a possible second (transversal) acoustical branch.
In case (a) both optical branches are pure rotations.
In the other two cases the branches may split as indicated by the pointed lines.
In those regions each branch may be a mixture of translational and rotational motions [1].

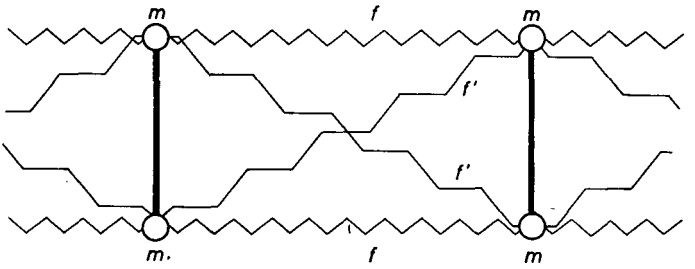

Fig. 9

Simplest case of a linear chain of two-atomic molecules with nearest-neighbour interaction only and equilibrium orientations perpendicular to the line connecting the centres of gravity.

By comparison with the above model some further speculations with respect to the dispersions proposed in Fig. 8 are possible. The similarity of the spectra suggests that the general dispersion behaviour and the number of branches are not altered by the phase transformations. In this case for model (a) the decrease of the peak 1 frequencies with decreasing temperature would mean a decrease of the general force constant B. The increase

of the peak 3 frequencies would then mean an increase of γ_3^* by the transition I → II and II → III; the slight shift of peak 2 and the broadening of peaks 2 and 3 in phase III would require increases of γ_2, β_2 and β_3 by the transformation II → III.

For model (b) the decrease of the peak 2 frequencies in phase II would mean a decrease of B by I → II, the shift of peak 1 to lower frequencies and the broadening of peak 2 in phase III would require γ_1 to be lowered and β_1 to be increased by II → III, the continuous increase of peak 3 and its broadening could be explained by γ_3 being increased by II → III and I → II and β_3 being increased by II → III. For both models a decrease of B with decreasing temperature must be assumed.

It is only with model (c) that B can be assumed to increase with decreasing temperature, as one would expect. The continuous increase of B is the reason for the continuous increase of the peak 3 frequencies. The other temperature dependencies then can be explained by

(1) A decrease of γ_1 and γ_2 at the transition I → II (peaks 1 and 2 shift to lower frequencies),
(2) A decrease of γ_1 (peak 1 shifts to lower frequencies) and an increase of β_2 (the broad fall-off to high frequencies) and possibly an increase of γ_2 by the transition II → III.

Model (c) thus suggests that the transition I → II primarily affects the orientational structure (γ), not necessarily the degree of hindrance of rotational motions. In contrast, such changes (β) may be involved in the transition II → III.

APPENDIX B

It has been shown [7, 16] that under the assumption of small librational amplitudes the potential holding the molecules in the phase III orientation, as proposed by James and Keenan, can be written

$$V = A\left(-1 + \frac{5}{4}\alpha_x^2 + \frac{5}{4}\alpha_y^2 + 2\alpha_z^2\right), \tag{1}$$

where α_x, α_y, α_z are components of the angular displacement relative to the cubic axes and [10]

$$A = \sqrt{\frac{27}{64}}\left(\frac{351}{4}\frac{I_3^2}{r^7} - \frac{3}{2}k_B T\right)$$

$$I_3 = 4\sqrt{\frac{5}{9}}\, d^3q$$

* We designate by an index 1, 2, 3 the parameters related to peaks 1, 2 and 3, respectively.

is the octopole moment, if d is the C-H distance within one molecule and q the effective proton charge. From Eq. (1) it follows that

$$\omega_z = \sqrt{\frac{4A}{\theta}} \qquad \text{and} \qquad \omega_x = \omega_y = \sqrt{\frac{5A}{2\theta}}$$

where θ is the moment of inertia. As ω_z and $\omega_x = \omega_y$ are measured, q can be calculated.

REFERENCES

[1] HAHN, H. and BIEM, W., Phys. Stat. sol 3 (1963) 1911.
[2] BIEM, W., Phys. Stat. sol. 3 (1963) 1927.
[3] HAHN, H., "Lattice vibrations in molecular crystals and neutron scattering", these Proceedings II.
[4] SHALLAMACH, A., Proc. roy. Soc. A171 (1939) 569.
[5] CLUSIUS, K., Z. phys. Chem. B3 (1929) 41.
[6] COLWELL, J., GILL, E. and MORRISON, J., J. Chem. Phys. 36 (1962) 2223.
[7] STILLER, H. and HAUTECLER, S., Inelastic Scattering of Neutrons in Solids and Liquids II IAEA, Vienna (1963) 281-93.
[8] DORNER, B. and STILLER, H., Phys. Stat. sol. 5 (1964) 511.
[9] STILLER, H. and HAUTECLER, S., Z. Physik 166 (1962) 393.
[10] EVANS, R., The Atomic Nucleus, McGraw Hill, N.Y. (1955) 774.
[11] JAMES, H. and KEENAN, T., J. Chem. Phys. 31 (1959) 12.
[12] KRIEGER, T. and JAMES, H., J. Chem. Phys. 22 (1956) 796.
[13] SJÖLANDER, A., Ark. Fys. 14 (1958) 315.
[14] COLWELL, J., GILL, E. and MORRISON, J., J. Chem. Phys. 39 (1963) 635.
[15] NAGAMIYA, T., Progr. theor. Phys. 6 (1951) 702.
[16] HAHN, H. and STOCKMEYER, R., unpublished.

THE NATURE OF HYDROGEN MOTION IN ZrH DETERMINED FROM AN EXPERIMENTAL NEUTRON STUDY OF LARGE, BOUND ENERGY LEVELS *

W. L. WHITTEMORE
GENERAL ATOMIC DIVISION OF GENERAL DYNAMICS CORPORATION,
SAN DIEGO, CALIF.,
UNITED STATES OF AMERICA

Abstract — Résumé — Аннотация — Resumen

THE NATURE OF HYDROGEN MOTION IN ZrH DETERMINED FROM AN EXPERIMENTAL NEUTRON STUDY OF LARGE, BOUND ENERGY LEVELS. The General Atomic neutron velocity selector has been used to select monoenergetic neutrons with energy ranging up to about 1.0 eV for a study of the motion and binding of hydrogen in zirconium hydride. Differential scattering measurements have been made for a variety of incident energies and at laboratory angles of 30°, 60°, 90° and 120°. The resolution of the incident energy was of the order of 6% for the highest energies used and was better for the lower energies. If the motion of the hydrogen atoms is harmonic, even though not isotropic, the differential angular quasi-elastic scattering depends in a simple manner on the momentum transfer. The experimental measurements lead to verification of the harmonic motion for $ZrH_{0.5}$ and $ZrH_{2.0}$ and indicate that the shape of the potential well is nearly quadratic at least for the ground state. With the higher incident energies, simultaneous excitation of bound harmonic levels has been observed up to the fourth level. Roughly equal spacing for these excited levels is observed as is necessary but not sufficient for a harmonic potential. A sensitive test of the shape of the potential well for the higher bound levels is provided by the present experimental study of the angular dependence of the scattering which leads to excitation of the higher levels. These various studies have led to the conclusion that the potential well is still nearly quadratic for the first excited level but deviates therefrom for the higher bound levels. The variations of the level widths are small for large changes in temperature and angle.

NATURE DES MOUVEMENTS DE L'HYDROGÈNE DANS ZrH DÉTERMINÉE A PARTIR D'UNE ÉTUDE EXPÉRIMENTALE, AVEC DES NEUTRONS, DES HAUTS NIVEAUX D'ÉNERGIE LIÉS. L'auteur a utilisé le sélecteur de vitesse des neutrons de la «General Atomic» pour sélectionner des neutrons monoénergétiques d'une énergie atteignant 1,0 eV environ afin d'étudier le mouvement et les liaisons de l'hydrogène dans l'hydrure de zirconium. Il a procédé à des mesures de la diffusion différentielle pour diverses énergies incidentes et des angles de 30°, 60°, 90° et 120°. La résolution de l'énergie incidente était de l'ordre de 6% pour les plus fortes énergies; elle était meilleure pour les faibles énergies. Si le mouvement des atomes d'hydrogène est harmonique, sans être isotrope, la diffusion angulaire différentielle quasi élastique dépend simplement du transfert de la quantité de mouvement. Les mesures expérimentales permettent de vérifier les mouvements harmoniques pour $ZrH_{0.5}$ et $ZrH_{2.0}$ et indiquent que la forme du puits de potentiel est presque quadratique, pour l'état fondamental tout au moins. Avec de plus fortes énergies incidentes, une excitation simultanée des niveaux harmoniques liés a été observée jusqu'au quatrième niveau. Ces niveaux excités sont à peu près régulièrement espacés, condition nécessaire mais non suffisante de la formation d'un potentiel harmonique. L'étude expérimentale, ici décrite, des variations, en fonction de l'angle, de la diffusion qui provoque l'excitation des niveaux supérieurs, fournit des indications précises sur la forme du puits de potentiel. Il ressort de ces différentes études que le puits de potentiel demeure presque quadratique pour le premier niveau excité mais qu'il s'écarte de cette forme pour les niveaux liés supérieurs. Les variations des largeurs du niveau sont petites pour de grands écarts de température et d'angle.

ПРИРОДА ДВИЖЕНИЯ ВОДОРОДА В ZrH, ОПРЕДЕЛЯЕМАЯ В РЕЗУЛЬТАТЕ ЭКСПЕРИМЕНТАЛЬНОГО ИССЛЕДОВАНИЯ С ПОМОЩЬЮ НЕЙТРОНОВ КРУПНЫХ УРОВНЕЙ ЭНЕРГИИ СВЯЗИ. В отделе атомной энергии нейтронный селектор скоростей использовался для селекции моноэнергетических нейтронов с энергией приблизительно до 1,0 эв с целью

* Work supported by the United States Atomic Energy Commission under Contract AT(04-3)-167.

изучения движения и связи водорода в гидриде циркония. Измерения дифференциального рассеяния проводились для целой совокупности значений энергии бомбардировки и при лабораторных углах 30, 60, 90 и 120°. Разрешающая способность энергии бомбардировки составляла величину порядка 6% для самых больших энергий. Если движение атомов водорода гармоничное, даже если оно неизотропичное, то дифференциальное угловое квазиупругое рассеяние зависит простым образом от передачи импульса. В результате проведения экспериментальных измерений проверяется гармоничное движение для $ZrH_{0,5}$ и $ZrH_{2,0}$ и указывается, что форма потенциальной ямы является почти квадратичной по крайней мере для основного состояния. При более высоких значениях энергии бомбардировки одновременное возбуждение гармонических связанных уровней наблюдалось вплоть до четвертого уровня. Приблизительно равное расстояние между этими уровнями возбуждения считается необходимым, однако недостаточным для гармонического потенциала. Чувствительное испытание формы потенциальной ямы для более высоких связанных уровней обеспечивается в результате проведения нынешних экспериментальных исследований угловой зависимости рассеяния, которое приводит к возбуждению более высоких уровней. В результате проведения таких различных исследований сделан вывод, что потенциальная яма все-таки является почти квадратичной для первого уровня возбуждения, однако она отклоняется при более высоких связанных уровнях. Удельные изменения размеров ширины уровней малы для больших изменений температуры и угла.

NATURALEZA DEL MOVIMIENTO DEL HIDROGENO EN EL ZrH DETERMINADA POR ESTUDIO NEUTRONICO DE NIVELES SUPERIORES ENLAZADOS. Se ha utilizado el selector de velocidades neutrónicas de la General Atomic para obtener neutrones monoenergéticos hasta de 1,0 eV, aproximadamente, con el fin de estudiar el movimiento y enlace del hidrógeno en el hidruro de circonio. Se ha efectuado mediciones por dispersión diferencial para varias energías de incidencia y ángulos de 30°, 60°, 90° y 120°. La resolución fue del orden del 6% para las energías inferiores. Admitiendo que el movimiento de los átomos de hidrógeno sea armónico, aunque no isotrópico, la dispersión diferencial angular cuasielástica ha de depender, según una relación sencilla, de la transferencia del impulso. Las mediciones experimentales tienden a confirmar el movimiento armónico en el caso del $ZrH_{0,5}$ y del $ZrH_{2,0}$, e indican que la forma del pozo de potencial es aproximadamente cuadrática, al menos para el estado fundamental. Para energías incidentes más elevadas, se han observado excitaciones simultáneas de los niveles armónicos enlazados, que se extienden hasta el cuarto nivel. En general, se observa un espaciamiento regular de estos niveles excitados, como es necesario, pero no suficiente, para un potencial armónico. El presente estudio experimental de la influencia del ángulo en la dispersión causante de la excitación de los niveles superiores, permite comprobar con precisión la forma del pozo de potencial correspondiente a los niveles superiores enlazados. De dicho estudio se desprende que el pozo de potencial sigue siendo aproximadamente cuadrático en el caso del primer nivel excitado, pero se aparta de dicha forma en el caso de los niveles superiores enlazados. Las variaciones de la anchura de los niveles resultan pequeñas cuando los cambios de temperatura y de ángulo son grandes.

1. INTRODUCTION

The full range of studies of neutrons interacting with ZrH can be carried out only when high-energy incident neutrons are available because of the effect of the Boltzmann population factor in populating mainly the lowest lying level at room temperature. The present neutron velocity selector in use at General Atomic with the electron linear accelerator provides monoenergetic neutrons with energies up to ~1.0 eV. These monoenergetic beams have now been used to study additional characteristics of the binding of hydrogen in ZrH. Since the harmonic frequency in ZrH is of the order of 0,14 eV, these neutrons can be used to study directly the characteristics of the higher bound levels in ZrH using energy-loss techniques.

2. EXPERIMENTAL RESULTS

Scattering patterns have been obtained for a variety of incident neutron energies and scattering angles by utilizing the General Atomic neutron velocity selector to provide monoenergetic incident neutrons. The experimental conditions were set up to optimize conditions for examining characteristics of the first or second harmonic level in ZrH.

The selection of optimum conditions for studying the first or second scattering level in ZrH ($h\nu \simeq 0.14$ eV) requires attention to multiple scattering effects. It has been shown experimentally [1] that for neutron energies greater than about 0.09 eV, the cross-section of hydrogen bound in ZrH is roughly constant in the range of 20 to 25 b. For neutron energies below 0.09 eV, the cross-section rises rapidly to much higher values. This fact alone creates a considerable problem in the selection of sample thickness. If an experiment is designed to minimize multiple scattering, this consideration is particularly important. For instance, if incident neutron energies of the order of 0.240 eV are selected and allowed to scatter on a relatively thin (transmission of 0.9) sample of ZrH, the neutron that has excited the first harmonic level will emerge from the scattering sample with an energy centred around 0.10 eV. The cross-section for such a neutron upon leaving the scattering sample is no larger than for the incident neutrons. On the other hand, if an incident energy of about 0.20 eV is selected for the incident monoenergetic beam and the same inelastic neutron interaction is studied, the outgoing neutron will have an energy centred around 0.06 eV. The multiple scattering effects for such an outgoing neutron are considerably larger than in the former case. If an even smaller incident energy is selected, a situation rapidly develops in which the outgoing neutron has practically no chance of emerging from the ZrH sample without undergoing further scattering. For the second bound level in ZrH, incident neutron energies of the order of 0.39 eV are selected. The outgoing neutron in these cases also has an energy of the order of 0.10 eV and thereby suffers the same small multiple scattering.

Typical time-of-flight results of the neutron scattering by the first bound level in ZrH are shown in Fig. 1. Observations were made at scattering angles of $\theta = 30°$ and 90° in a specimen having a chemical formula $ZrH_{0.5}$. The first measurements in this series were made with a metallic specimen having a thickness of 0.080 in. This gave a transmission of 0.9 for high-energy neutrons where the cross-section is of the order of 25 b. All later measurements in the present series were made with finely powdered $ZrH_{2.0}$. The thickness of this specimen was held quite closely to 0.020 in, also giving a transmission of the order of 0.9 for high-energy neutrons. The observed width of the harmonic level appears to be exactly the same for the hydrogen in these two different concentrations. The incident energy in this particular case is 0.239 eV. In Fig. 2 one finds similar scattering patterns for $ZrH_{2.0}$ where incident neutron energies of the order of 0.39 eV were selected. Here one sees clear evidence for excitation of the first and second harmonic levels. These data in both Figs. 1 and 2 are particularly useful for studying several aspects of the binding of hydrogen in ZrH. In Fig. 3, for purposes of comparison, we have shown the scattering patterns observed at three scattering

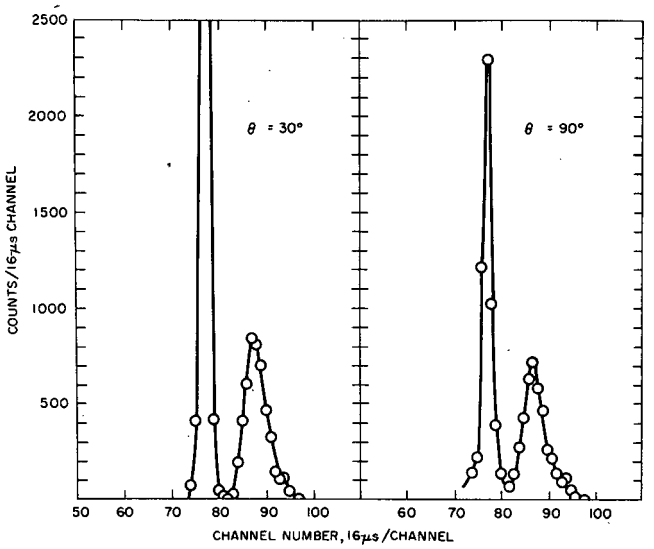

Fig. 1

Time-of-flight scattering data for $ZrH_{0.5}$ for 300°K at θ = 30° and 90°, with E_0 = 0.239 eV (background has been subtracted)

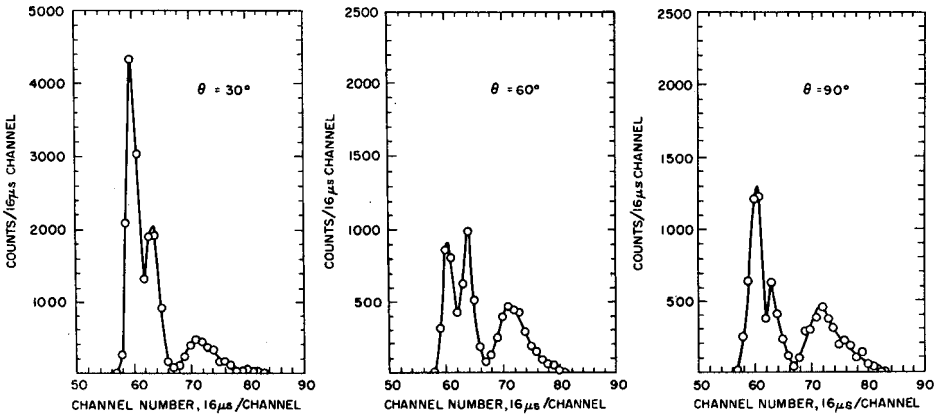

Fig. 2

Time-of-flight scattering data for $ZrH_{2.0}$ for 300°K at θ = 30°, 60° and 90°, with E_0 = 0.386 eV (background has been subtracted)

angles for a monoenergetic incident neutron beam having an energy too low to excite the first hydrogen oscillator level.

The spacing of the bound levels in ZrH has been investigated experimentally with incident monoenergetic neutrons having energy up to 0.660 eV; typical results are shown in Figs. 2 and 3. For all cases studied, including the highest in which the fourth bound level has been identified, the level spacing is uniform and equal to ~ 0.14 eV, to within the accuracy of the experimental determination.

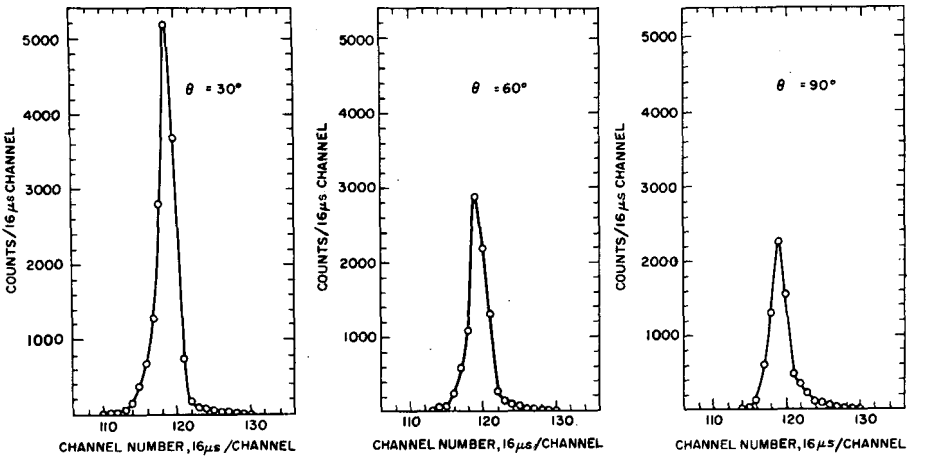

Fig. 3

Time-of-flight scattering data for $ZrH_{2.0}$ with background subtracted for 300°K at $\theta = 30°$, 60° and 90°. Incident neutron energy (E_0 = 0.10 eV) was selected to be too low to excite the first vibrational level of hydrogen; note that the wings of the quasi-elastic scattering are considerably broader than for the data taken with higher E_0 (as in Figs. 1 and 2).

3. VARIATION IN LEVEL WIDTH

Some study has been made of the width of the excited hydrogen levels as a function of scattering angle and scatterer temperature. Typical experimental results on the level width are shown in Fig. 4. The width of the first level in $ZrH_{2.0}$ corrected for resolution is 0.018 eV and the corrected width of the second level is $\sim$ 0.022 eV. From additional experiments [2] we have also determined that in lowering the scatterer temperature from 300 to 90°K, the widths of the energy levels determined from the scattered neutrons decreased very little – of the order of $\leq$ 1.25 for their ratio. Experimentally, one observes that the level width of $ZrH_{2.0}$ at 90°K shows no angular dependence and increases $\lesssim$ 10% at T = 300°K between 30° and 90°. The earlier measurements by WOODS et al. [2] at only one scattering angle using the beryllium detector method are quite consistent with the present observations that the width of the first level does not change significantly for sample temperatures in the range of 90-300°K.

4. SOME CONSIDERATIONS OF THE NATURE OF HYDROGEN BINDING IN ZIRCONIUM HYDRIDE

The quasi-elastic scattering (where the incident and outgoing energies are nearly the same) provides a test of the shape of the potential well that binds the hydrogen atom. If the potential well gives truly harmonic motion, even if not isotropic, then the differential angular scattering of this elastic scattering $(d^2\sigma/dEd\Omega)_{el}$, is given as follows:

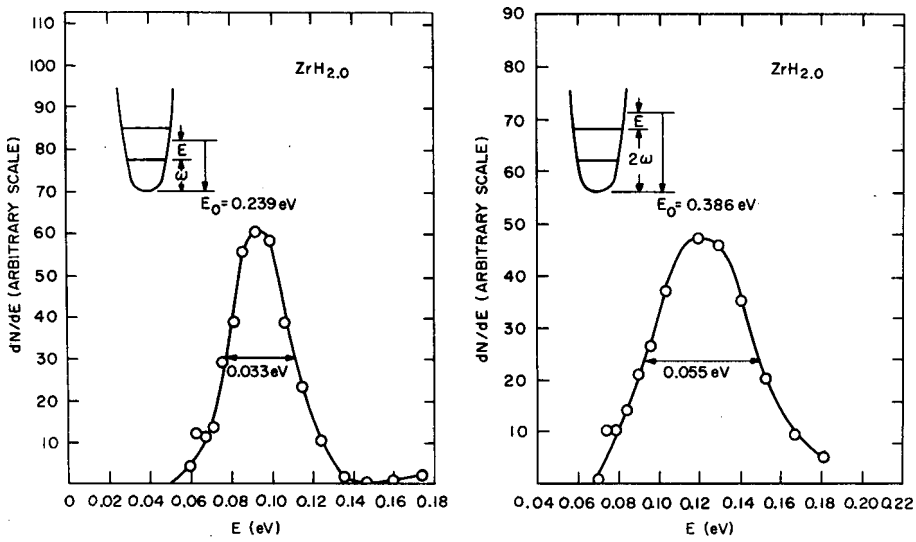

Fig. 4

Distribution in final energy for scattering from the first and second bound levels of H in ZrH Two values of E_0 were chosen, 0.239 eV and 0.386 eV; the indicated width at half maximum included instrumental resolution as well as the inherent line width of the first and second bound levels.

$$\left(\frac{d^2\sigma}{dE d\Omega}\right)_{el} = \frac{\sigma_b}{4\pi} [\exp(-\kappa^2\alpha/2)]\, \delta(E_0 - E)\ldots, \qquad (1)$$

where

σ_b = bound cross-section of the hydrogen atom;

E_0 = initial energy;

E = final energy;

κ^2 = $E_0 + E - 2(E_0 E)^{\frac{1}{2}} \cos\theta$, where θ is the scattering angle; and

α = $(2\bar{n}+1)/\omega_0$, where $\bar{n} = [\exp(\omega_0/T) - 1]^{-1}$, ω_0 is the energy of the oscillator level in eV, and T is the sample temperature in eV.

For quasi-elastic scattering, one gets, after integration over all final energy states,

$$\left(\frac{d\sigma}{d\Omega}\right)_{el} = \frac{\sigma_b}{4\pi} \exp[-4E_0\alpha \sin^2(\theta/2)] \ldots. \qquad (2)$$

From Eq. (2), one sees that a plot on semilogarithm paper of the scattered elastic intensity as a function of $[4E_0 \sin^2(\theta/2)]$ should give a slope of $\alpha \simeq (-1/h\nu)$. Figures 5(a) and (b) show a substantial amount of data for incident energies of about 0.097, 0.239, 0.335, and 0.386 eV. In these data one must deduct the elastic scattering by the zirconium lattice. This is done

by the crude expedient of assuming isotropic scattering for the zirconium atoms. This assumption is reasonable for the larger energies but may be poor for an energy as low as 0.1 eV. The resulting data, however, do indeed fit the expected curve with this correction. Figure 5 (a) for $ZrH_{0.5}$ gives data specifically designed to test the harmonic oscillator hypothesis and indicates clearly that all data fit a straight line of slope $\sim(-1/h\nu)$, as expected for a harmonic potential. The data of Fig. 5 (b) were not taken specifically for the problem at hand and may have had some systematic error in the numerous determinations which can account for the deviation from the straight line of some of the well-determined values. These data are generally consistent with a straight line of slope $\sim(-1/h\nu)$. We conclude that for both $ZrH_{0.5}$ and $ZrH_{2.0}$, the hydrogen in its ground state is bound in a potential well associated with harmonic motion.

Since the quasi-elastic scattering of neutrons by zirconium hydride indicates harmonic motion of the bound hydrogen, one can reasonably compare the observed inelastic scattering with that predicted for a harmonic oscillator. By making this comparison, one can investigate in what manner the hydrogen in zirconium hydride may deviate from a harmonic system of excited states. Making use of a phonon expansion, one can write the differential cross-section for excitation of the bound hydrogen for the first and second harmonic levels, respectively, as follows:

$$\frac{d^2\sigma_1}{dEd\Omega} = \frac{\sigma_b}{4\pi}\left(\frac{E}{E_0}\right)^{\frac{1}{2}} \exp\left(\frac{-\kappa^2\alpha}{2}\right) \exp\left(\frac{\omega_0}{2T}\right) I_1\left[\frac{\kappa^2}{2\omega_0 \sinh(\omega_0/2T)}\right]\delta\left[(E_0 - E) - \omega_0\right] \quad (3)$$

$$\frac{d^2\sigma_2}{dEd\Omega} = \frac{\sigma_b}{4\pi}\left(\frac{E}{E_0}\right)^{\frac{1}{2}} \exp\left(\frac{-\kappa^2\alpha}{2}\right) \exp\left(\frac{\omega_0}{2T}\right) I_2\left[\frac{\kappa^2}{2\omega_0 \sinh(\omega_0/2T)}\right]\delta\left[(E_0 - E) - \omega_0\right]. \quad (4)$$

Here, the bound cross-section σ_b equals 80 b; E, E_0, κ^2, α, ω_0, and T are as previously defined; and

$$I_1(x) = \frac{x}{2} + \frac{1}{2}\left(\frac{x}{2}\right)^3 + \ldots,$$

$$I_2(x) = \frac{1}{2}\frac{x^2}{2!} + \frac{1}{4}\frac{x^4}{4!} + \ldots .$$

If one integrates Eqs. (3) and (4) over all final energy states, theory and experiment can be compared without regard to instrumental resolution since the total inelastic cross-section for a single level is being compared. In Figs. 6 and 7 one finds the predictions from Eqs. (3) and (4) compared with the inelastic neutron scattering experiments.

In Fig. 6, data for $ZrH_{0.5}$ and $ZrH_{2.0}$ are compared with the theoretical curve for $E_0 = 0.239$ eV. The data for two different concentrations of hydrogen differ somewhat beyond the statistics. The data for $\theta \geq 90°$ is not believed to be influenced significantly by multiple scattering because the main effect of multiple scattering is to broaden the inelastic peaks by quasi-

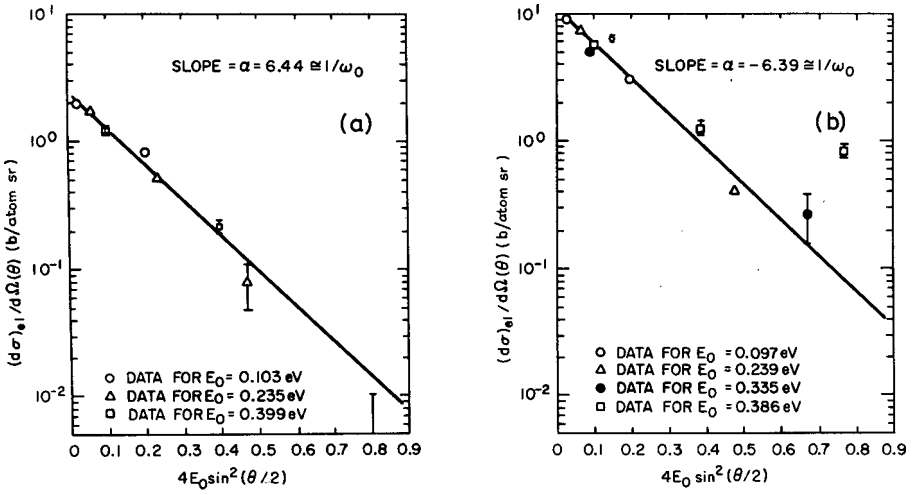

Fig. 5

Dependence of elastic scattering on $4E_0 \sin^2(\theta/2)$, the momentum transfer for (a) $ZrH_{0.5}$ and (b) $ZrH_{2.0}$
The data are consistent with a straight line and hence indicate harmonic motion of the hydrogen atoms

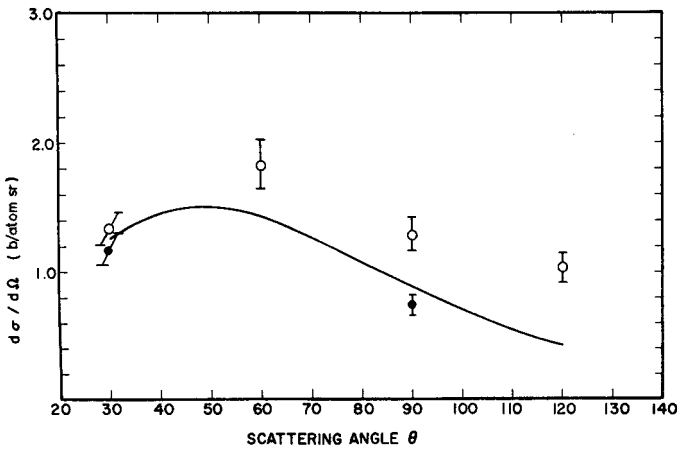

Fig. 6

Theoretical and experimental partial differential scattering $d\sigma_1/d\Omega$ for the first excited level in ZrH.

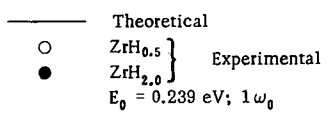

elastic scattering and not to increase the number of neutrons in the peaks. There is therefore some evidence that the angular distribution is flatter than predicted, particularly for $\theta > 90°$. Nevertheless, both sets of data can be

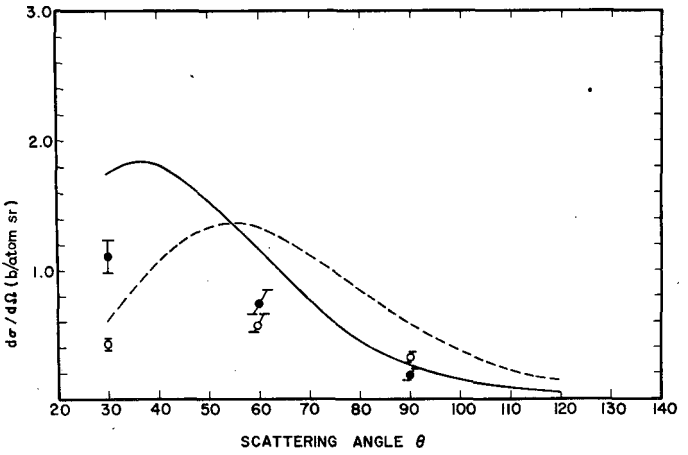

Fig. 7

Theoretical and experimental partial differential scattering by the first and second excited level in $ZrH_{2.0}$

considered to be in not too bad agreement with the very simplified theoretical treatment. In Fig. 7, data for $ZrH_{2.0}$ are compared with theory for the first and second excited level. The predictions differ from experiment in separate manners for the two levels. For the first level, the experimental angular data differ noticeably in magnitude from theory but exhibit the same angular dependence. For the second level, the experimental angular distribution is noticeably flatter than predicted, although the absolute cross-sections at 30° and 90° agree approximately with predictions.

On the basis of the sensitive tests provided by the angular dependence of the inelastic scattering, one must conclude from the data in Figs. 6 and 7 that the simple harmonic oscillator model is not entirely sufficient to explain the observed results for the excitation of the higher bound levels. The simple model, however, gives a reasonable fit of the data for lower incident neutron energies that can excite only the first bound level.

5. CONCLUSIONS

Although the relative lack of dependence of the level widths on the angle of neutron scattering and on the specimen temperature is not explained in detail, the experimental material on zirconium hydride described in this paper is consistent in most details with the assumption that the hydrogen atom executes nearly harmonic motion with some deviations for the higher excited states. These conclusions appear to apply over a quite wide range of hydrogen concentrations ($ZrH_{0.5}$ to $ZrH_{2.0}$). Specifically,

(a) The motion of the hydrogen atom in its ground state is consistent with binding in a harmonic potential well;

(b) The scattering of neutrons with only enough energy to excite the first level also agrees reasonably well with that predicted for a harmonic oscillator; and

(c) The scattering of higher-energy neutrons able to excite the second level does not agree well in magnitude or angular dependence with predictions based on simple harmonic motion of the bound hydrogen atom.

The spacings of the energy levels are not a sensitive function of deviations from a harmonic potential. Consequently, the observation of approximately constant energy spacings up to the fourth level is consistent with the above description of the hydrogen binding.

ACKNOWLEDGEMENTS

The author wishes to acknowledge profitable discussions with Dr. M. S. Nelkin and Dr. D. E. Parks. Appreciation is also expressed for the assistance of the operating staff of the General Atomic electron linear accelerator.

REFERENCES

[1] WHITTEMORE, W. L. and McREYNOLDS, A. W.; Phys. Rev. 113 (1961) 806.

[2] WHITTEMORE, W. L., Neutron interactions in zirconium hydride, General Atomic Rpt. GA-4490 (Rev.) (1964).

[3] WOODS, A. D., BROCKHOUSE, B. W., SAKAMOTO, M. and SINCLAIR, R. N., in Inelastic Scattering of Neutrons in Solids and Liquids, IAEA, Vienna (1961) 487-98.

DISCUSSION

R. J. ELLIOTT: The anharmonic effects seen on higher levels of H oscillating in a potential well can be observed more clearly on ionic crystals containing a little H by optical techniques. In the case of H in CaF_2, Hayes has seen up to the third harmonic and splittings caused by the tetrahedral site symmetry.

W. WHITTEMORE: In a metal lattice such as Z and H we must use other techniques than optical ones, and neutrons give a first approach – though admittedly the accuracy is poorer.

P. EGELSTAFF: In connection with Dr. Elliott's question, I should like to suggest that the infrared and neutron data should be compared only after making a correction for the fact that in the infrared data one measures frequencies at zero wavelength, whereas in the neutron data work one measures an average for all wave vectors.

May I also ask Dr. Whittemore to explain the relative size of the peaks at 60° in his Fig. 2.

W. WHITTEMORE: The counter bank at 60° was smaller than at 30° and 90°; therefore, the data of Fig. 2 are not directly comparable but are fewer.

ИССЛЕДОВАНИЕ НЕУПРУГОГО РАССЕЯНИЯ МЕДЛЕННЫХ НЕЙТРОНОВ НА ГИДРИДЕ ЦИРКОНИЯ

В.Г. ЛИФОРОВ, М.Н. НИКОЛАЕВ, В.З. НОЗИК, В.А. ПАРФЕНОВ
В.А. СЕМЕНОВ и В.Ф. ТУРЧИН
СССР

Abstract — Résumé — Аннотация — Resumen

STUDY OF INELASTIC SCATTERING OF SLOW NEUTRONS IN ZIRCONIUM HYDRIDE. The paper sets out the results of measurements of the doubly differential scattering cross-section for slow neutrons in zirconium hydride at 490 and 20°C. The experimental results are compared with those obtained from theory.

ÉTUDE DE LA DIFFUSION INÉLASTIQUE DES NEUTRONS LENTS DANS L'HYDRURE DE ZIRCONIUM. Le mémoire donne les résultats de mesures de la section efficace, à double différentielle, de dispersion des neutrons lents dans l'hydrure de zirconium à 490 et à 20°C; les résultats expérimentaux sont comparés aux données théoriques.

ИССЛЕДОВАНИЕ НЕУПРУГОГО РАССЕЯНИЯ МЕДЛЕННЫХ НЕЙТРОНОВ НА ГИДРИДЕ ЦИРКОНИЯ. В данной работе приведены результаты измерения дважды дифференциального сечения рассеяния медленных нейтронов на гидриде циркония при 490 и 20°С. Проведено сравнение экспериментальных результатов с теоритическими.

ESTUDIO DE LA DISPERSIÓN INELÁSTICA DE LOS NEUTRONES LENTOS EN EL HIDRURO DE CIRCONIO. En la presente memoria se presentan los resultados de mediciones de la sección eficaz de diferencial doble correspondiente a la dispersión de los neutrones lentos en el hidruro de circonio a temperaturas comprendidas entre 490° y 20°C. Los resultados experimentales se comparan con los datos teóricos.

Описанные в настоящем докладе измерения проведены на двойном спектрометре медленных нейтронов [1]. Сфазированный с ИБР' ом [2] механический прерыватель находится на пролетном расстоянии $L' = 10$ м от реактора. Специальная система автофазировки обеспечивает стабильность фазы с точностью 0,2°. Диаметр ротора прерывателя — 200 мм. Материал — гетинакс. Максимальная скорость вращения ротора — 2000 об/мин. При этом ширина нейтронного импульса прерывателя составляет 75 мксек. Расчетная ширина импульса тепловых нейтронов ИБР' а — 135 мксек. Быстрые нейтроны, вылетающие из активной зоны ИБР' а, замедляются в водяной кассете, которая размещается вплотную к активной зоне и имеет размеры $400 \times 400 \times 40$ мм. Вторая пролетная база равна 6,3 м. При этом полное разрешение спектрометра при скорости вращения 2000 об/мин составляет 22,5 мксек/м в области упругого рассеяния. Интенсивность монохроматических нейтронов на образце составляет $5 \cdot 10^4$ н/сек при $E = 25$ мэв.

В настоящее время ведутся работы по модернизации спектрометра. В новом варианте измерения будут вестись одновременно под 11 углами. Будут увеличены пролетные базы и разрешение спектрометра составит 12 — 15 мксек/м. Интенсивность монохроматических нейтронов на образце достигает $5 \cdot 10^5$ н/сек. Предполагается также значительно повысить эффективность регистрирующего устройства.

Работу на модернизированном варианте спектрометра предполагается начать во второй половине 1965 года.

Измерение спектров нейтронов, рассеянных на гидриде циркония под углом $\theta = 80°$ к падающему пучку, производилось при температурах 490°С и 20°С. Гидрид циркония $ZrH_{1,46}$ в виде порошка засыпался в алюминиевый контейнер толщиной 1,9 мм. Нагревательный элемент был отделен от контейнера слоем кадмия.

Контейнер с гидридом циркония не был герметизирован, так что имелась возможность утечки водорода из образца при измерениях с высокой температурой. Однако, анализ экспериментальных результатов по сериям позволяет утверждать, что утечка водорода была мала.

Измерения проведены для нейтронов с начальной энергией 0,02 эв. Полное разрешение спектрометра в области упругого рассеяния составляло 45 мксек/м. Разрешение по второй пролетной базе – 18 мксек/м. Ширина канала анализатора 32 мксек. На рис.1 и 2 показаны аппаратурные

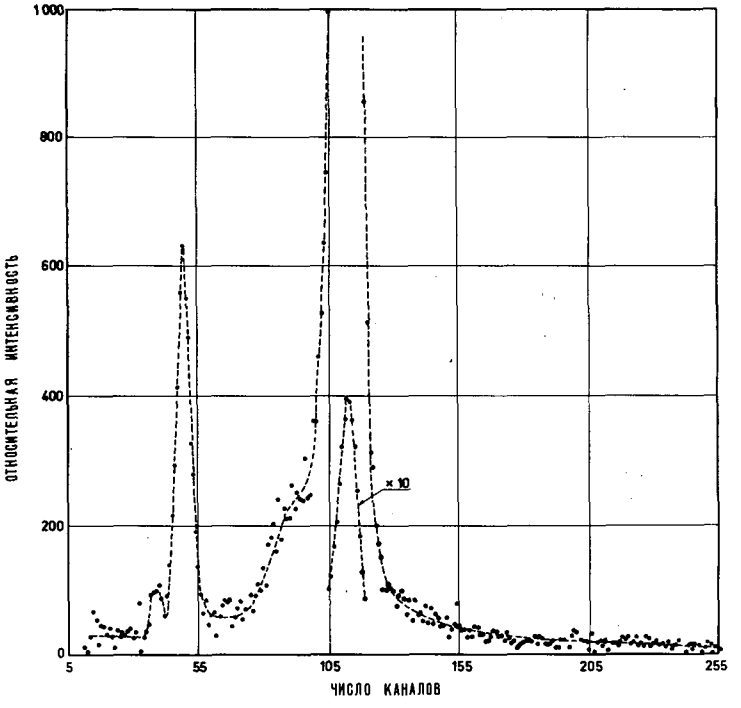

Рис. 1

Аппаратурный спектр рассеянных $ZrH_{1,46}$ нейтронов при температуре 490°С.

спектры нейтронов, рассеянных на $ZrH_{1,46}$ при температурах 490°С и 20°С соответственно. На рис.1 экспериментальные точки соответствуют чистому эффекту, а на рис.2 – эффекту с фоном. Экспериментальный фон изображен на этом же рисунке сплошной линией.

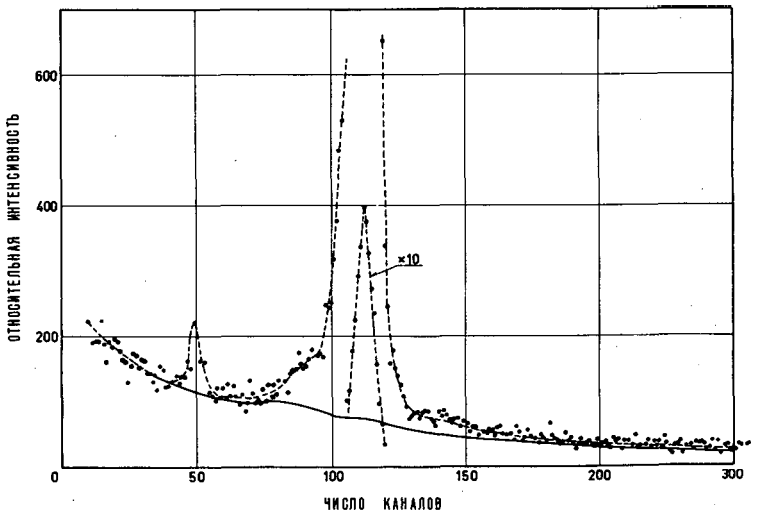

Рис. 2

Аппаратурный спектр рассеянных $ZrH_{1,46}$ нейтронов при температуре 20°С.

Наблюдаемое сечение рассчитано по формуле

$$\sigma_{\text{наб}}(E_0, E, \theta) = \frac{I(E_0, E, \theta)\beta(E)}{A\Delta\Omega N\ell} \text{ барн/эв. стер,}$$

где $I(E_0, E, \theta)$ – аппаратурный спектр в энергетической шкале;
$\beta(E)$ – поправка на поглощение и рассеяние нейтронов в нейтронопроводе и на эффективность борных счетчиков;
$\Delta\Omega$ – телесный угол детектора;
N – число атомов водорода в 1 см^3 образца;
ℓ – толщина образца;
A – аппаратурная постоянная.

Для определения A были проведены дополнительно аналогичные измерения с ванадием.

Сечения рассеяния при температурах 490°С и 20°С показаны на рис.3 и 4 соответственно.

Эксперимент при температуре 20°С характеризуется значительной статистической погрешностью, поэтому его сопоставление с сечением при 490°С может носить только качественный характер.

СРАВНЕНИЕ С ТЕОРИЕЙ

Вычисление сечений с помощью непосредственного интегрирования по времени является весьма удобным для проверки теоретических предсказаний экспериментом. Как известно, в некогерентном приближении и

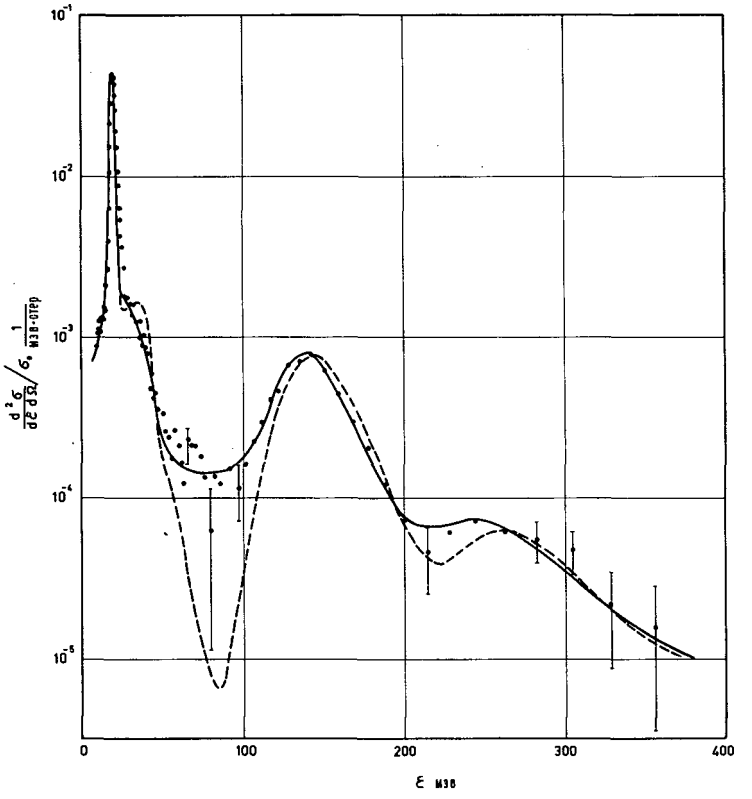

Рис. 3

Дифференциальное сечение рассеяния нейтронов $ZrH_{1,46}$ при температуре 490°С.

с учетом гауссовского вида пространственно-временной корреляционной функции

$$G_s(\bar{r}, t) = [2\pi\Gamma(t)]^{-\frac{3}{2}} \exp\left\{-\frac{r^2}{2\Gamma(t)}\right\}$$

дважды дифференциальное сечение рассеяния имеет вид:

$$\frac{d^2\sigma}{dE\,d\Omega} = \frac{\sigma_0}{4\pi} \cdot \left(1+\frac{1}{\mu}\right)^2 \cdot \left(\frac{E}{E_0}\right)^{\frac{1}{2}} \cdot e^{\epsilon/2T} \cdot \tilde{S}(q,\epsilon),$$

$$\tilde{S}(q,\epsilon) = \frac{1}{2\pi}\int_{-\infty}^{\infty} e^{-q\gamma(t)} \cdot e^{-i\epsilon t}\,dt, \qquad (1)$$

где $\epsilon = E_0 - E$,

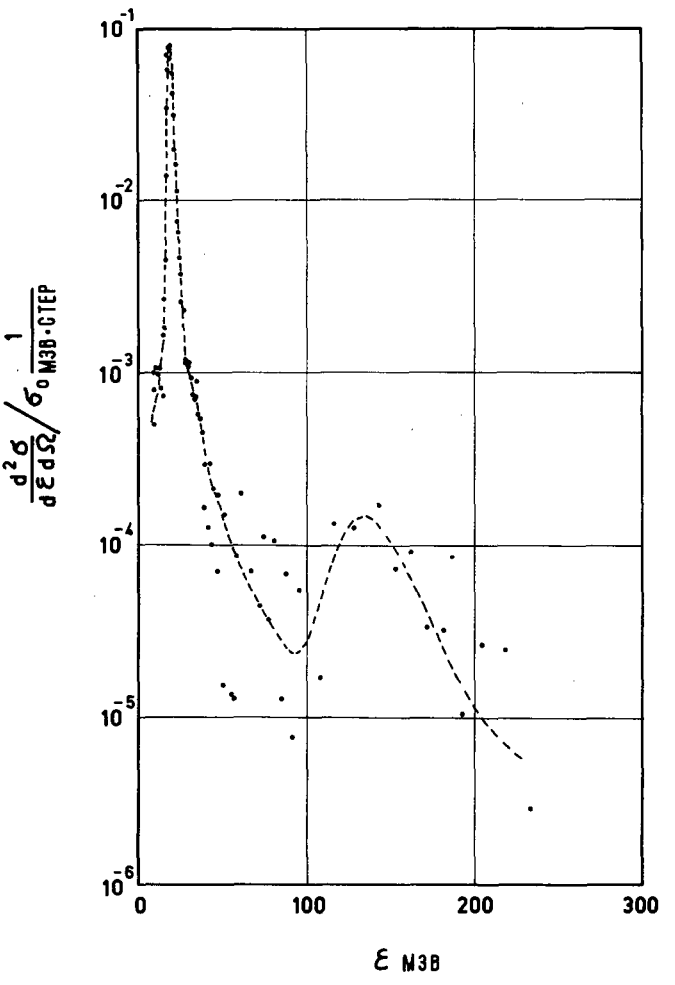

Рис. 4

Дифференциальное сечение рассеяния нейтронов $ZrH_{1,46}$ при температуре 20°С.

$$q = \frac{h^2(K - K_0)^2}{2M} = \frac{1}{\mu}(E + E_0 - 2\sqrt{E_0 E}\cos\theta),$$

$$\gamma(t) = \frac{2M}{h^2}\Gamma(t).$$

Для вычисления сечений интегрированием по времени в (1) заменим $\tilde{S}(q, \epsilon)$ на

$$\tilde{S}'(q, \epsilon) = \frac{1}{2\pi}\int_{-\infty}^{\infty} e^{-q\gamma(t)} \cdot e^{-\frac{\delta^2 t^2}{2}} \cdot e^{-i\epsilon t} dt. \qquad (2)$$

По известному свойству преобразований Фурье $\tilde{S}'(q, \epsilon)$ является сверткой $\tilde{S}(q, \epsilon)$ с Фурье-образом функции $\exp\left\{-\frac{\delta^2 t^2}{2}\right\}$:

$$\tilde{S}'(q, \epsilon) = \int \tilde{S}(q, \epsilon') \cdot \varphi(\epsilon - \epsilon') d\epsilon' , \qquad (3)$$

где $\varphi(\epsilon - \epsilon') = \frac{1}{\sqrt{2\pi\delta^2}} e^{-\frac{(\epsilon - \epsilon')^2}{2\delta^2}}$

Таким образом, введение функции $\tilde{S}'(q, \epsilon)$, во-первых, упрощает ее вычисление, т.к. интеграл выражения $\tilde{S}'(q, \epsilon)$, благодаря фактору $\exp\{-\delta^2 t^2/2\}$, сходится гораздо лучше, чем интеграл в $\tilde{S}$ и, во-вторых, при вычислении сечения теперь автоматически может быть учтено разрешение прибора. Последнее легко понять, если вспомнить, что $\varphi(\epsilon)$ — в (3) имеет гауссовский вид, а свертка и есть операция усреднения истинного сечения по разрешению прибора, которое обычно с хорошей точностью может быть представлено гауссианом.

На этом принципе был разработан алгоритм, который реализован в виде программ ПРАССИВ [3]. Программы ПРАССИВ вычисляют $\sigma(E_0 \to E, \theta)$, нулевой и первый угловые и энергетические моменты и другие интегральные характеристики сечений как для кристаллического вещества (когда коэффициент самодиффузии равен нулю никаких модельных приближений для вычисления $\gamma(t)$ не делается), так и для жидкости с использованием модели, предложенной Турчиным В.Ф. [4].

Для вычисления дважды дифференциального сечения рассеяния на гидриде циркония в первом приближении исходные данные по спектру нормальных колебаний кристалла ZrH брались из модельных представлений с известными из литературы параметрами. Акустическая часть спектра представляет собой дебаевское распределение с температурой 20 мэв, а оптическая часть — треугольник: $\hbar\omega = 130$ мэв и полушириной 25 мэв. Веса оптической и акустической частей относятся как массы атомов Zr и H. Функция разрешения представляется в виде гауссиана с полушириной

$$\Delta E = \sqrt{\alpha^2 + (\beta E_0^{\frac{3}{2}})^2 + (\gamma E^{\frac{1}{2}})^2}$$

Коэффициенты α, β, γ находятся из сравнения с экспериментальной кривой разрешения. Таким образом, рассчитанное сечение можно непосредственно сравнить с наблюдаемым. Из рис.3 видно, что уже в первом приближении (пунктирная кривая) имеется качественное согласие с экспериментом. Исключение составляет область между оптическим и акустическим переходами. Последнее, прежде всего, свидетельствует о том, что нет резкого обрыва в акустической части при дебаевской температуре. Кроме того, можно думать, что реальный спектр нормальных колебаний отличен от нуля между оптической и акустической частями.

После двукратного внесения поправок в спектр нормальных колебаний получено хорошее согласие расчетного сечения с экспериментальным. Окончательный вид спектра колебаний гидрида циркония показан на рис.5. Пунк-

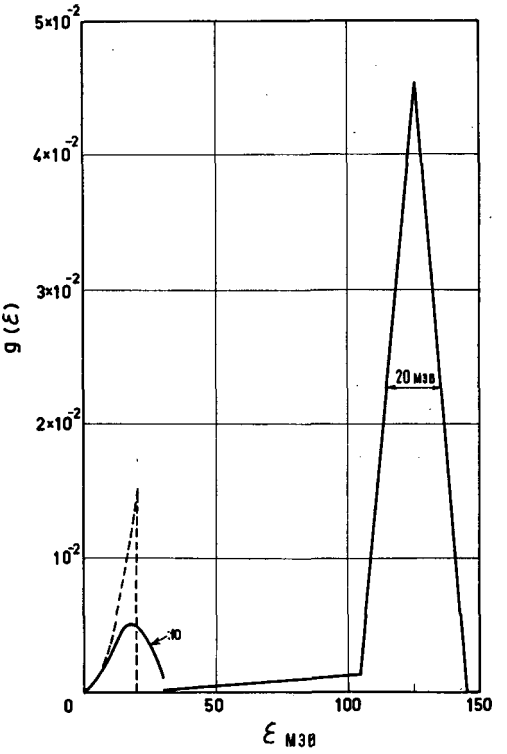

Рис. 5

Спектр колебаний гидрида циркония

тиром нанесен дебаевский спектр (для наглядности акустическая часть увеличена в 10 раз). Следует отметить, что полученное в данной работе значение оптического кванта равное 125 мэв несколько меньше известного из литературы. Ширина оптического уровня также меньше и составляет 20 мэв

Несмотря на хорошее согласие теоретического и экспериментального сечений нет уверенности в том, что спектр нормальных колебаний $g(\epsilon)$ в области между оптикой и акустикой выбран правильно.

Действительно, добиться согласия с экспериментальной кривой (а в этой области из-за плохой статистики оно весьма неоднозначно) можно как за счет однофононного рассеяния с непрерывным спектром колебаний, так и за счет многофононных процессов, путем деформации акустической части. Наиболее ценной проверкой правильности восстановленного фононного спектра явилось бы сравнение сечения измеренного под другим углом рассеяния с расчетом, использующим восстановленный спектр колебаний.

Небольшое разногласие на правом склоне упругого пика может быть объяснено следующим образом: форма упругого сечения в теоретической кривой имеет вид гауссиана с полушириной 3,5 мэв. Экспериментальная функция разрешения (а упругий пик и представляет собой реальную функцию разрешения), в основном совпадая с гауссианом, отличается от него на "крыльях", что и имеет место в данном случае.

ЗАКЛЮЧЕНИЕ

Полученные предварительные результаты говорят о том, что даже из приведенных грубых измерений удается получить ценную информацию о динамике атомов вещества. В настоящее время измерения на ZrH проводятся более тщательно и с повышенной точностью. Представляют значительный интерес измерения параметров оптического уровня.

В заключение авторы благодарят А.И. Лейпунского и Ф.Л. Шапиро за внимание к работе.

ЛИТЕРАТУРА

[1] БОНДАРЕНКО И.И. и др. Inelastic scattering of neutrons in solids and liquids. Proc. Vol. 1 Vienna 1963p. 127.

[2] БЛОХИН Г.Е. и др. Импульсный реактор на быстрых нейтронах. "Атомная энергия", 10 (1961) 437.

[3] ТУРЧИН В.Ф. "Атомная энергия" (в печати).

[4] ТУРЧИН В.Ф. Медленные нейтроны. М., 1963.

INDICATION OF PROTON TUNNELLING IN KH_2PO_4 BY COMPARING NEUTRON INELASTIC SCATTERING AND INFRARED MEASUREMENTS

I. PELAH, E. WIENER AND J. IMRY
ISRAEL ATOMIC ENERGY COMMISSION, SOREQ RESEARCH ESTABLISHMENT, YAVNE, ISRAEL

Abstract — Résumé — Аннотация — Resumen

INDICATION OF PROTON TUNNELLING IN KH_2PO_4 BY COMPARING NEUTRON INELASTIC SCATTERING AND INFRARED MEASUREMENTS. Proton motions will show up predominantly in the spectra of neutron inelastic scattering because of its high cross-section. Infrared absorption on the other hand will indicate only the modes allowed by selection rules. Therefore the motions of the proton and their characteristics can sometimes be determined by comparing the results of the two techniques. The spectra of KH_2PO_4 in the region 200 to 700 cm^{-1} are similar in both methods; one observes two rather sharp lines at 540 and 410 cm^{-1} that are $PO_4^{\equiv}$ characteristic modes. On the other hand, one gets in KH_2PO_4 two peaks in infrared absorption; a sharp one at 540 cm^{-1} and a very broad one from 450 to 250 cm^{-1}. In the neutron inelastic scattering spectra, one observes just one broad peak extended from 600 to 250 cm^{-1}. These results lead to the conclusion that the proton is involved also in modes of vibrations that are not characteristic to $PO_4^{\equiv}$ group and that these low proton frequency modes are prohibited by infrared selection rules. Low proton modes of this type can be explained as being caused by proton motion in a slightly asymmetric double minima potential. The vibrational ground level of the proton is then split into two closely lying levels with a separation of about 400 cm^{-1}. The wave functions of the lower level are concentrated in the deeper well while those of the higher one are concentrated in the upper well. Infrared selection rules predict low intensity to this mode in infrared absorption but it will show up clearly in neutron inelastic scattering. The assumption of proton tunnelling in KH_2PO_4 type crystals, that is strongly supported by the results of this work, leads to an explanation of phase transition on these interesting materials, namely the ferroelectric Curie point and melting point.

EFFETS «TUNNEL» DES PROTONS DANS KH_2PO_4 OBSERVÉS PAR COMPARAISON ENTRE LES MESURES DE LA DIFFUSION INÉLASTIQUE DES NEUTRONS ET DE L'ABSORPTION INFRAROUGE. Les mouvements des protons apparaissent surtout dans les spectres de la diffusion inélastique des neutrons, en raison de leur forte section efficace. En revanche, l'absorption infrarouge ne met en évidence que les modes permis par les lois de sélection. Il est donc parfois possible d'établir les mouvements du proton et leurs caractéristiques en comparant les résultats obtenus à l'aide de ces deux méthodes. Les spectres de K_2HPO_4 dans la région comprise entre 200 et 700 cm^{-1} sont semblables avec l'une et l'autre méthodes; on observe à 540 et 410 cm^{-1} deux raies assez nettes qui sont les modes caractéristiques de $PO_4^{\equiv}$. D'autre part, on observe dans KH_2PO_4 deux pics d'absorption infrarouge, un pic aigu à 540 cm^{-1}, et un pic étalé de 450 à 250 cm^{-1}. Dans les spectres de la diffusion inélastique des neutrons, on n'observe qu'un seul pic très étalé qui s'étend de 600 à 250 cm^{-1}. Ces résultats amènent à conclure que le proton entre également en jeu dans des modes de vibrations qui ne sont pas caractéristiques du groupe $PO_4^{\equiv}$ et que ces modes à basse fréquence sont écartés par les lois de sélection infrarouge. On peut attribuer les modes protoniques à basse fréquence de cette nature aux mouvements des protons dans un potentiel à deux minima légèrement asymétriques. Le niveau bas des vibrations des protons se dédouble alors en deux niveaux rapprochés, séparés d'environ 400 cm^{-1}. Les fonctions d'onde du niveau bas sont concentrées dans le puits inférieur, tandis que celles du niveau plus élevé sont concentrées dans le puits supérieur. Les règles de sélection infrarouge prévoient que ce mode aura une faible intensité dans l'absorption infrarouge, mais il apparaît nettement dans la diffusion inélastique des neutrons. L'hypothèse de l'existence d'un effet «tunnel» dans les cristaux du type KH_2PO_4, qui est très bien corroborée par les résultats de ces travaux, fournit une explication de la transition de phase pour ces cristaux intéressants, à savoir le point de Curie et le point de fusion ferroélectriques.

ИНДИКАЦИЯ ТУННЕЛЬНОГО ЭФФЕКТА ПРОТОНА В KH_2PO_4 ПУТЕМ СРАВНЕНИЯ РЕЗУЛЬТАТОВ ИЗМЕРЕНИЙ НЕУПРУГОГО РАССЕЯНИЯ НЕЙТРОНОВ И ИНФРАКРАСНЫХ

ИЗМЕРЕНИЙ. Движения протона будут заметно выделяться в спектрах неупругого рассеяния нейтронов благодаря его большому поперечному сечению. С другой стороны, инфракрасное поглощение указывает лишь на колебания, подпадающие под правила отбора. Поэтому движения протонов и их характеристики можно иногда определить, сравнивая результаты этих двух методов. Спектры KH_2PO_4 в пределах от 200 до 700 $см^{-1}$ являются аналогичными при обоих методах: наблюдаются две довольно острые линии при 540 и 410 $см^{-1}$, что является характеристической формой колебания $PO_4^{\equiv}$. С другой стороны, при инфракрасном поглощении получаются два пика в KH_2PO_4: острый пик при 540 $см^{-1}$ и очень широкий в пределах от 450 до 250 $см^{-1}$. В спектрах неупругого рассеяния нейтронов можно наблюдать только один широкий пик в пределах от 600 до 250 $см^{-1}$. Эти результаты приводят к заключению, что протон связан также с формами колебаний, которые не являются характерными для группы $PO_4^{\equiv}$, и что эти колебания низкой частоты не подпадают под правила инфракрасного отбора. Протонные колебания этого типа могут быть объяснены движением протона в несколько асимметричном потенциале с двумя минимумами. Основной колебательный уровень протона расщепляется затем на два близко расположенных уровня с разделением около 400 $см^{-1}$. Волновые функции более низкого уровня сосредоточены в более глубокой яме, в то время как волновые функции более высокого уровня сосредоточены в верхней яме. Правила инфракрасного отбора предсказывают низкую интенсивность для этой формы колебаний при инфракрасном поглощении, но она четко выделяется при неупругом рассеянии нейтронов. Предположение, что протон имеет туннельный эффект в кристаллах типа KH_2PO_4, что определенно подтверждается результатами данной работы, позволяет объяснить фазовое превращение в этих интересных материалах, а именно, ферроэлектрическую точку кюри и точку плавления.

OBSERVACIÓN DE UN EFECTO TÚNEL PARA LOS PROTONES EN EL KH_2PO_4 POR COMPARACIÓN DE LA DISPERSIÓN INELÁSTICA DE NEUTRONES Y LAS MEDICIONES EN LA ZONA INFRARROJA. Los movimientos protónicos predominan en los espectros de dispersión inelástica de neutrones debido a la elevada sección eficaz de éstos. Pro otra parte, la absorción en la zona infrarroja indica solamente los modos permitidos por las reglas de selección. La comparación de los resultados obtenidos por ambas técnicas permite algunas veces determinar los movimientos de los protones y sus características. Los espectros del KH_2PO_4 en la región de 200 a 700 cm^{-1} obtenidos por ambos métodos son similares; se observan dos rayas bastante nítidas a 540 y 410 cm^{-1} que corresponden a modos característicos del grupo $PO_4^{\equiv}$. Por otra parte, el KH_2PO_4 origina dos máximos de absorción en el infrarrojo; uno nítido a 540 cm^{-1} y otro muy ancho entre 450 y 250 cm^{-1}. En el espectro de dispersión inelástica de neutrones se observa solamente un máximo muy ancho que se extiende desde 600 hasta 250 cm^{-1}. Dichos resultados sugieren que el protón interviene también en modos vibratorios que no son característicos del grupo $PO_4^{\equiv}$ y que estos modos de frecuencia protónica más baja son prohibidos de conformidad con las reglas de selección en el infrarrojo. Dichos modos inferiores pueden explicarse como consecuencia de los movimientos de los protones en un potencial de doble mínimo, ligeramente asimétrico. En estas condiciones, el nivel vibratorio fundamental del protón se desdobla en otros dos niveles próximos, con una separación de unos 400 cm^{-1}. Las funciones ondulatorias del nivel inferior se concentran en el pozo más profundo, mientras que las del superior se concentran en el pozo más alto. Las reglas de selección en el infrarrojo indican que la intensidad de este modo en la absorción infrarroja será reducida, pero que aparecerá claramente en la dispersión inelástica de neutrones. Los resultados obtenidos por los autores confirman la existencia de un efecto túnel para los protones en los cristales del tipo del KH_2PO_4, lo que explicaría las transiciones de fase (punto de Curie ferroeléctrico y punto de fusión) en estos interesantes materiales.

1. INTRODUCTION

In KH_2PO_4 type crystals it is known that the motion of the protons is responsible for the ferroelectric transition. This is seen for example from the large shift in the Curie point upon deuteration. Moreover, the hydrogen bond, being the weakest bond in the crystal, is probably also responsible for the low melting point of these crystals (e.g. 253°C for KH_2PO_4 as against 1340°C for K_3PO_4). The neutron diffraction data of PEASE and BACON [1] on KH_2PO_4 show a symmetrically elongated proton distribution along the axis of the hydrogen bond, above the Curie temperature, and a more con-

centrated distribution below it. There are several ways of explaining their results above the Curie point; the proton might be located asymmetrically near one of the oxygens, although it is statistically disordered in the crystal sites, or the proton may actually be near both oxygens as a result of one of several possible anharmonic motions. Further information about the motions of the protons can be gained by studying the spectral consequences of these hypotheses, using the various techniques of spectroscopy. Three main techniques were used to attack this problem, namely infrared absorption, Raman scattering and neutron inelastic scattering spectra. The main advantages of the neutron inelastic scattering method are high sensitivity to proton vibrations because of the large proton scattering cross-section and the fact that the selection rules are different from those existing in infrared and Raman spectra. However it lacks the good resolution one finds in the latter methods. By comparing the results obtained by the different techniques in measuring the same phenomenon more insight can sometimes be gained into the problem. In the case of KH_2PO_4 crystals we show that a comparison of the different spectra helps us to establish the existence of very broad low energy hydrogen modes that appear pronouncedly only in neutron inelastic scattering data. The existence of these low proton modes supports the picture that in the non-ferroelectric phase, on the average, there exists a slightly asymmetrical double minimum potential well where the protons tunnel quantum-mechanically. Such a picture of the motion of the protons has been used to explain the phase transitions in KH_2PO_4, namely the ferroelectric Curie point and the melting point.

2. INFRARED AND NEUTRON INELASTIC SCATTERING SPECTRA OF KH_2PO_4

The infrared spectrum of KH_2PO_4 has been measured down to 500 cm^{-1} by MURPHY and WEINER [2] (scattering) and BLINC and HADZI [3] (absorption). The latter authors explained their results above the Curie temperature by assuming a split hydrogen level at 2400 cm^{-1} and 2800 cm^{-1} due to proton tunnelling in a symmetric double minimum potential well. On the other hand, infrared measurements by the same authors [3]; by LAZAROV and ZAITZEV [4] and in our laboratory [5] have failed to show any narrowing of this double splitting below the Curie point, as should be expected theoretically from proton tunnelling. Exploiting the advantages of the neutron inelastic technique for studying proton motions, PELAH et al. [6] measured the time-of-flight spectra of inelastically scattered neutrons in three polycrystalline phosphates KH_2PO_4, K_2HPO_4 and K_3PO_4 at room temperature. Comparing the results, they came to the conclusion that a wide hydrogen vibration band exists near 400 cm^{-1} in the non-ferroelectric KH_2PO_4; however they were unable to explain the two peaks occurring in K_2HPO_4 in the same region. Using the same method PALEVSKY et al. [7] and WAKUTA [8] compared the spectra of KH_2PO_4 above and below the Curie temperature and reported no change in the low frequency modes of KH_2PO_4 when the Curie point is crossed. However this result is inconclusive since the levels above thermal ones are not populated in the cold sample and therefore no transitions could be observed in energy gain experiments.

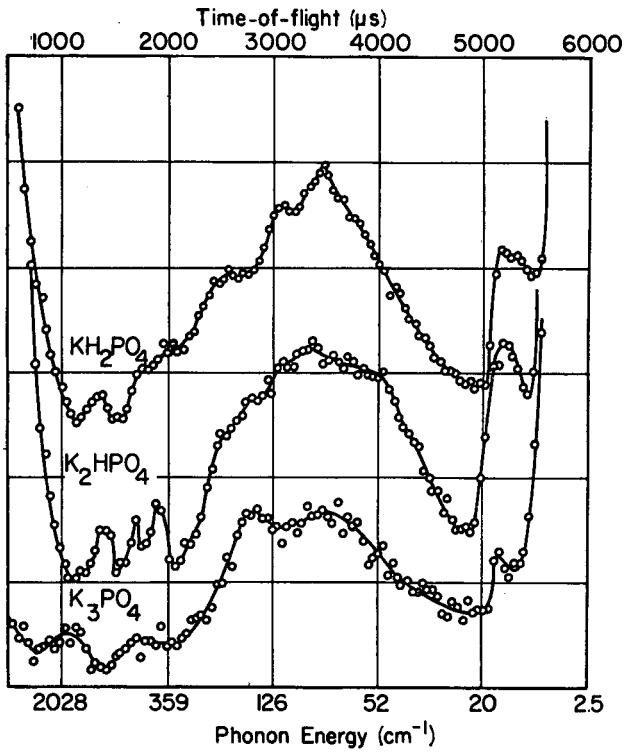

Fig. 1

Neutron time-of-flight spectra of K_3PO_4, K_2HPO_4 and KH_2PO_4 at room temperature

Comparing the results of KH_2PO_4 and KD_2PO_4 they also suggested a band of frequencies near 180 cm^{-1} associated with hydrogen vibrations; this was interpreted as confirmation of REID's theory [9]. However coherent effects are probably important in KD_2PO_4 and one cannot rely solely on intensity considerations. Convinced of the importance of this problem, KREBS and PELAH [10] repeated their first experiment on the phosphates K_3PO_4, K_2HPO_4 and KH_2PO_4, using the time-of-flight facility in Ispra (see Fig. 1). The same three phosphates were also measured by the authors of this article with a 521 Perkin Elmer far-range infrared spectrometer, and the results for the wave-number range 2000 cm^{-1} to 250 cm^{-1} are given in Fig. 2. We also scanned KH_2PO_4 above and below the Curie temperature [5] and found that a major change occurs in the wide peak extending from 250 cm^{-1} to 450 cm^{-1}, which becomes two narrow peaks at 350 cm^{-1} and 420 cm^{-1}, below the Curie point.

3. DISCUSSION

The spectra of K_2HPO_4 obtained by neutron inelastic scattering and infrared absorption in the region 250 cm^{-1} to 700 cm^{-1} are very similar;

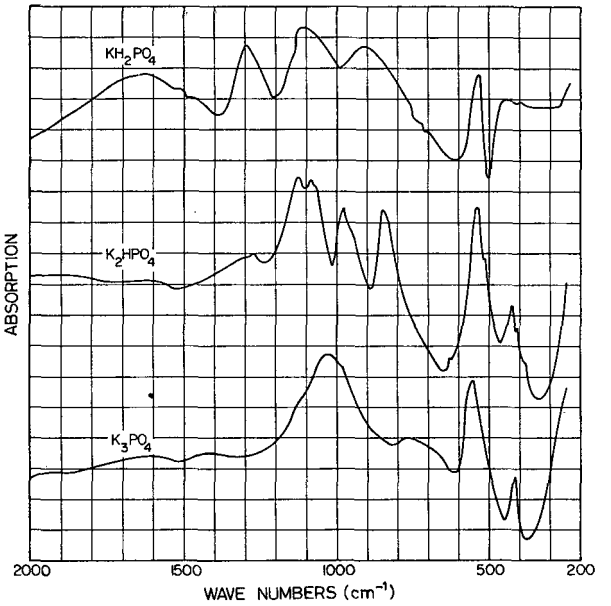

Fig. 2

Infrared spectra of K_3PO_4, K_2HPO_4 and KH_2PO_4 for the wave numbers 2000 cm^{-1} to 250 cm^{-1} at room temperature

one observes two rather sharp peaks at 540 cm^{-1} and 420 cm^{-1}. Theoretical considerations [11] allow us to assume that these modes are characteristic PO_4 modes υ_4 = 540 cm^{-1} and υ_2 = 420 cm^{-1}. (See also the recent work of THOMPSON [12].) Turning now to K_3PO_4 we find the same peaks in the infrared spectrum, but they are quite absent in neutron inelastic scattering data. As the difference between K_3PO_4 and K_2HPO_4 is that the hydrogen is replaced by potassium, we assumed that the peaks in the neutron inelastic scattering spectra of K_2HPO_4 appear predominantly because of the hydrogen which is strongly coupled to the characteristic vibrations of PO_4. In the infrared spectra of KH_2PO_4 we get two peaks: a sharp one at 540 cm^{-1} and a broad one from 450 cm^{-1} to 250 cm^{-1}. On the other hand in neutron inelastic scattering spectra one observes just one broad peak extending from 600 cm^{-1} to 250 cm^{-1}. As resolution is good enough to separate the peaks in this region, these results show that the protons are also involved in low energy modes that are not PO_4 characteristic; these modes extend from 600 cm^{-1} to 250 cm^{-1} and appear predominantly in neutron inelastic scattering but not in infrared absorption. Extremely broad and low energy proton transitions of this type can be accounted for by assuming the existence of an average slightly asymmetric double minimum potential well along the O-H ... O bond, where the proton tunnels quantum-mechanically (see Fig. 3). The vibrational ground level of the proton is split into two close levels with a separation of about 400 cm^{-1}. The wave function of the lower level (symmetric) is concentrated in the lower well, while that of the higher one (asymmetric) is concentrated in the upper well. It seems that the small overlap

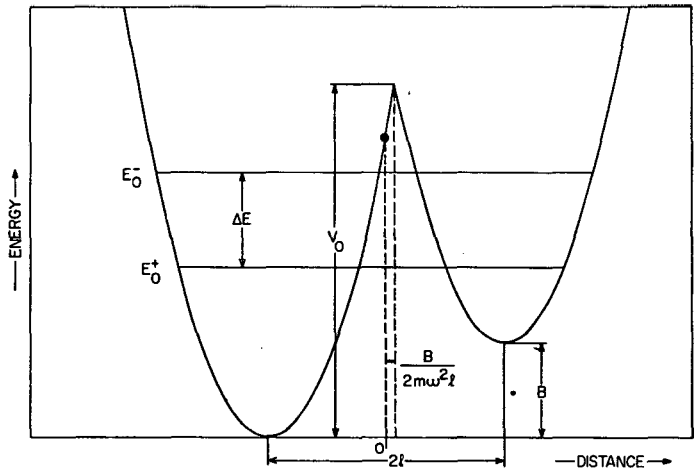

Fig. 3

Double minimum asymmetric potential well

2ℓ - distance between the minima
$B > 0$ - asymmetry parameter
V_0 - height of barrier
X - relevant co-ordinate, such as the position of the proton along O-H... O bond
ω - frequency of each oscillator

in wave functions excludes transitions between the levels in infrared absorption and Raman scattering, but allows them in neutron inelastic scattering. CHAPELLE's [13] and NARAGAHAN's [14] results for the Raman spectra of KH_2PO_4 show the same sharp peaks at 540 cm^{-1} and 420 cm^{-1}, and an additional peak at 360 cm^{-1} not allowed by infrared selection rules; however the broad proton peak is absent. Returning now to the model of the asymmetric double minimum potential for the proton, the positions of the lower and upper wells are assumed to alternate as a result of the dynamics of the crystal. Because of this averaging process, which is however slow relative to the proton motion, there is complete symmetry between the oxygens on a long time scale. The alternation of the wells along the bond is supported by the nuclear magnetic resonance measurements of SCHMIDT and UEHLING [15]. Further studies [16, 17] on a slightly asymmetrical double minimum potential well for the protons, predict stronger binding for the higher level (E_0^-), which causes a negative temperature coefficient for the O-O distance in the non-ferroelectric phase. This non-ferroelectric temperature region of the KH_2PO_4 crystal is bounded by two end points, namely the Curie ferroelectric point and the melting point, where the structure becomes unstable and regenerative processes occur. Below the Curie point the proton potential well becomes extremely asymmetric and the proton sticks to one oxygen in an orderly manner, causing ferroelectricity.

REFERENCES

[1] PEASE, R. S. and BACON, G. E., Proc. roy. Soc. A236 (1955) 359.
[2] MURPHY, G.M. and WEINER, G., J. chem. Phys. 22 (1954) 1322.
[3] BLINC, R. and HADZI, D., Mol. Phys. 1 (1958) 391.
[4] LAZAROV, A.N. and ZAITZEV, A.S., Soviet Phys. – sol. State 2 (1960) 2688.
[5] WIENER, E. and PELAH, I., Infrared indication of low frequency hydrogen modes in KH_2PO_4, to be published.
[6] PELAH, I., LEFKOVITZ, I., KLEY, W. and TUNKELLO, E., Phys. Rev. Lett. 2 (1959) 94.
[7] PALEVSKY, H., OTNES, K. and WAKUTA, Y., Inelastic Scattering of Neutrons in Solids and Liquids II IAEA, Vienna (1963) 273-78.
[8] WAKUTA, Y., J. phys. Soc. Japan 18 (1963) 672.
[9] REID, C., J. chem. Phys. 30 (1959) 182.
[10] KREBS, K. and PELAH, I., Euratom (Ispra) internal report 424 (March 1963).
[11] HERZBERG, G., Infrared and Raman Spectra, D. Van Nostrand Co. Inc. N.Y. (1945) 167.
[12] THOMPSON, W.K., J. chem. Soc. (Jan. 1964) 371.
[13] CHAPELLE, J., J. chem. Phys. 49 (1949) 30.
[14] NARAGAHAN, P.S., Proc. Ind. Acad. Sci. A33 (1951) 240.
[15] SCHMIDT, V.H. and UEHLING, E.A., Phys. Rev. 126 2 (1962) 447.
[16] IMRY, J. and PELAH, I., Proton tunneling negative thermal expansion and phase transitions in H-bonded systems, to be published.
[17] IMRY, J. and PELAH, I., Israel AEC Rpt. IA-861 (1963), to be published.

DISCUSSION

V.M. PADMANABHAN: From single-crystal neutron diffraction studies at lower temperature Bacon has shown that the hydrogen position becomes ordered, and that it changes when the direction of an applied electric field is reversed. Will this positional variation cause any change in your spectrum ?

I. PELAH: Most of the spectra shown are at room temperature in the non-ferroelectric phase. In the case of the infrared spectra below the Curie point, one does not expect a change on reversal of the field.

K.P. SINHA: You said that the ferroelectric Curie point and the melting point are related. This relation would depend on certain modes of vibration involving protons. Is it possible to pin down the specific mode of vibration which is responsible for the phase transition?

I. PELAH: The tunnelling theory of the short hydrogen bond predicts that the minima in free energy with respect to O-O distance disappear at both points. Also, negative thermal expansion of O-O distance follows. Thus, one might expect a lowering of frequencies towards both points for motions of the oxygen in the direction of the hydrogen bond.

H. HAHN: If one attributes the measured difference betwen Dr. Stiller's two tunnelling peaks in water to an asymmetric double-well potential, I think one could perhaps theoretically relate the negative expansion coefficient in water – or at least the temperature where the minimum volume occurs – to the variation of this peak separation with distance.

STUDY OF LOW-FREQUENCY MOTIONS IN SEVERAL FERROELECTRIC SALTS BY THE INELASTIC SCATTERING OF COLD NEUTRONS*

J. J. RUSH
NATIONAL BUREAU OF STANDARDS, WASHINGTON, D. C.
AND
ARGONNE NATIONAL LABORATORY, ARGONNE, ILL.
AND
T. I. TAYLOR
COLUMBIA UNIVERSITY, NEW YORK, N. Y.
UNITED STATES OF AMERICA

Abstract — Résumé — Аннотация — Resumen

STUDY OF LOW-FREQUENCY MOTIONS IN SEVERAL FERROELECTRIC SALTS BY THE INELASTIC SCATTERING OF COLD NEUTRONS. Energy-gain spectra for the inelastic scattering of cold neutrons by ferroelectric $K_4Fe(CN)_6 \cdot 3H_2O$, NH_4HSO_4, $(NH_4)_2SO_4$ and $(NH_4)_2BeF_4$ have been measured above and below their Curie points, using the Argonne cold-neutron facility.

For $K_4Fe(CN)_6 \cdot 3H_2O$ ($T_C = 249°K$) scattered spectra were obtained at 121, 175 and 296°K. The results were quite similar in both the high temperature and ferroelectric phases. A broad band centred at an energy gain 435 ± 40 cm^{-1} (54 ± 5 meV) is observed at all three temperatures and assigned to the librations of the water molecules. A second broad peak around 165 cm^{-1} is possibly due to the translational motions of the water molecules in the lattice.

The room-temperature spectra for NH_4HSO_4 (T_C at 154 and 270°K) and $(NH_4)_2SO_4$ ($T_C = 224°K$) show broad bands peaked at about 260 cm^{-1} and 300 cm^{-1}, respectively, which are primarily due to the torsional motions of the ammonium ions. The NH_4HSO_4 spectrum at 177°K shows an indication of splitting, with little shift in the centre of the band. At 125°K the spectrum is clearly split, with peaks at 290 ± 25 and 190 ± 16 cm^{-1}. The $(NH_4)_2SO_4$ results at 172°K also exhibit a split band, with peaks centred at 335 ± 25 and 200 ± 16 cm^{-1}. In both cases the higher-energy peaks are assigned to torsional vibrations. The $(NH_4)_2BeF_4$ spectra also show broad "torsional" bands with several indicated maxima in the 175-290 cm^{-1} range. No great differences were observed in the spectra above and below the ferroelectric transitions for any of the ammonium salts.

The results for all of the compounds studied indicate that the ferroelectric transitions are not related to any large change in the average rotational freedom of the ammonium ions and water molecules. In addition the measurements show that the average barriers to reorientation are relatively small ($V_0 \lesssim 4$ kcal/mole) in every case. These conclusions do not preclude changes in the ordering of the protons at the transitions. The results are compared with total cross-section data and with data obtained by other techniques.

ÉTUDE DES MOUVEMENTS DE BASSE FRÉQUENCE DANS PLUSIEURS SELS FERROÉLECTRIQUES AU MOYEN DE LA DIFFUSION INÉLASTIQUE DES NEUTRONS FROIDS. Les auteurs ont mesuré, au moyen de la source de neutrons froids du Centre d'Argonne, les spectres de gain d'énergie dans la diffusion inélastique des neutrons froids par les sels ferroélectriques $K_4Fe(CN)_6 \cdot 3H_2O$, NH_4HSO_4, $(NH_4)_2SO_4$ et $(NH_4)_2BeF_4$, au-dessus et au-dessous de leur point de Curie.

Pour $K_4Fe(CN)_6 \cdot 3H_2O$ ($T_C = 249°K$), ils ont obtenu des spectres dispersés à 121, 175 et 296°K. Les résultats étaient presque identiques aux trois températures. Une large bande dont le centre est situé au niveau d'un gain d'énergie correspondant à 435 ± 40 cm^{-1} (54 ± 5 meV) est observée aux trois températures et attribuée aux vibrations des molécules d'eau. Un deuxième pic étalé, voisin de 165 cm^{-1}, est peut-être dû aux mouvements de translation des molécules d'eau dans le réseau.

A la température ambiante, les spectres de NH_4HSO_4 (T_C à 154 et 270°K) et $(NH_4)_2SO_4$ ($T_C = 224°K$) présentent de larges bandes dont les pics se situent, respectivement, à environ 260 et 300 cm^{-1} et que l'on attribue

* Work supported by the United States Atomic Energy Commission.

aux oscillations de torsion des ions ammonium. Le spectre de NH_4HSO_4 semble se partager à 177°K, le déplacement du centre de la bande étant très faible. A 125°K, le spectre est nettement partagé, avec des pics à 290 ± 25 cm^{-1} et 190 ± 16 cm^{-1}. Les résultats pour $(NH_4)_2SO_4$ à 172°K révèlent également une bande partagée dont les pics se situent à 335 ± 25 cm^{-1} et 200 ± 16 cm^{-1}. Dans les deux cas, les pics pour l'énergie la plus élevée sont attribués aux oscillations de torsion. Les spectres de $(NH_4)_2BeF_4$ ($T_C = 176$°K) font eux aussi apparaître de larges bandes de torsion avec plusieurs maxima entre 175 et 290 cm^{-1}. Les auteurs n'ont observé d'écarts sensibles dans les spectres au-dessus et au-dessous des transitions ferroélectriques pour aucun des sels d'ammonium.

Les résultats relatifs à tous les composés étudiés montrent que les transitions ferroélectriques ne sont liées à aucune modification sensible de la liberté de rotation moyenne des ions ammonium et des molécules d'eau. En outre, les mesures montrent que les barrières moyennes à une réorientation sont relativement faibles ($V_0 \lesssim 4$ kcal/mole) dans chaque cas. Ces conclusions n'excluent pas des modifications dans l'ordonnancement des protons aux transitions. Les auteurs comparent ces résultats aux données relatives à la section efficace totale et aux données obtenues par d'autres méthodes.

ИЗУЧЕНИЕ НИЗКОЧАСТОТНЫХ ДВИЖЕНИЙ В НЕКОТОРЫХ ФЕРРОЭЛЕКТРИЧЕСКИХ СОЛЯХ С ПОМОЩЬЮ НЕУПРУГОГО РАССЕЯНИЯ ХОЛОДНЫХ НЕЙТРОНОВ. Спектры приращения энергии при неупругом рассеянии холодных нейтронов на ферроэлектрических $K_4Fe(CN)_6 \cdot 3H_2O$, NH_4HSO_4, $(NH_4)_2SO_4$ и $(NH_4)_2BeF_4$ были измерены выше и ниже их точек Кюри на Аргонской установке для получения холодных нейтронов.

Для $K_4Fe(CN)_6 \cdot 3H_2O$ ($T_c = 249$° K) спектры рассеяния снимались при 121, 175 и 296° K. Результаты были совершенно одинаковыми как для высокой температуры, так и для ферроэлектрических фаз. Широкая полоса вокруг точки приращения энергии, соответствующей 435 ± 40 см$^{-1}$ (0,054 ± 0,005 эв), наблюдалась при всех трех температурах, она объясняется колебаниями молекул воды. Второй широкий пик вокруг точки 165 см$^{-1}$ объясняется, возможно, поступательными движениями молекул воды в решетке.

В снятых при комнатной температуре спектрах для NH_4HSO_4 ($T_c = 154$ и 270° K) и $(NH_4)_2SO_4$ ($T_c = 224$° K) видны широкие полосы с пиками вокруг точек 260 и 300 см$^{-1}$ соответственно, которые объясняются, главным образом, крутильными колебаниями ионов аммония. В спектре для NH_4HSO_4 при 177° K имеются признаки расщепления с небольшим смещением в центре полосы. При 125° K спектр явно расщепляется и имеет два пика в точках 290 ± 25 и 190 ± 16 см$^{-1}$. Результаты по $(NH_4)_2SO_4$ при 172° K также показывают расщепление полосы с пиками около точек 335 ± 25 и 200 ± 16 см$^{-1}$. В обоих случаях пики для более высоких энергий объясняются крутильными колебаниями. В спектрах $(NH_4)_2BeF_4$ ($T_c = 176$° K) также видны широкие "крутильные" полосы с несколькими показательными максимумами в диапазоне 175–290 см$^{-1}$.

Ни для одной соли аммония не обнаружено большой разницы в спектрах выше и ниже точек ферроэлектрических переходов.

Результаты, полученные по всем исследованным соединениям, показывают, что ферроэлектрические переходы не связаны с каким-либо большим изменением средней свободы вращения ионов аммония и молекул воды. Кроме того, измерения показывают, что средние барьеры для переориентации относительно невелики в каждом случае ($V_0 \lesssim 4$ ккал/моль). Эти выводы не исключают возможности изменения порядка протонов при переходах. Результаты сравниваются с данными по полному сечению и данными, полученными другими методами.

ESTUDIO DE LOS MOVIMIENTOS DE BAJA FRECUENCIA EN VARIAS SALES FERROELECTRICAS POR DISPERSIÓN INELÁSTICA DE NEUTRONES FRÍOS. Los espectros de ganancia de energía correspondientes a la dispersión inelástica de neutrones fríos en las sales ferroeléctricas $K_4Fe(CN)_6 \cdot 3H_2O$, NH_4HSO_4, $(NH_4)_2SO_4$ y $(NH_4)_2BeF_4$, se han medido por encima y por debajo de los respectivos puntos de Curie, utilizando el generador de neutrones fríos de Argonne.

En lo que respecta al $K_4Fe(CN)_6 \cdot 3H_2O$ ($T_C = 249$° K), se determinaron los espectros de dispersión a 121, 175 y 296° K. Los resultados obtenidos fueron muy parecidos tanto en las fases a elevada temperatura como en las ferroeléctricas. A dichas temperaturas se observa una ancha banda centrada en una ganancia de energía de 435 ± 40 cm^{-1} (54 ± 5 meV), que se atribuye a las oscilaciones de las moléculas de agua. Un segundo pico ancho que aparece en las proximidades de 165 cm^{-1} se debe posiblemente a los movimientos de traslación de las moléculas de agua en la red.

Los espectros, obtenidos a la temperatura ambiente, del NH_4HSO_4 (T_C a 154 y 270° K) y del $(NH_4)_2SO_4$ ($T_C = 224$° K) presentan bandas anchas con picos en las proximidades de 260 cm^{-1} y de 300 cm^{-1}, respectivamente, que se deben sobre todo a los movimientos de torsión de los iones amonio. A 177° K el espectro del NH_4HSO_4

muestra indicios de desdoblamiento, con escaso desplazamiento en el centro de la banda. A 125°K el espectro aparece claramente desdoblado, con picos en 290 ± 25 y 190 ± 16 cm^{-1}. Los resultados obtenidos para el $(NH_4)_2SO_4$ a 172°K presentan también un desdoblamiento de banda, con picos centrados en 335 ± 25 y 200 ± 16 cm^{-1}. En ambos casos los picos de elevada energía se atribuyen a vibraciones torsionales. Los espectros del $(NH_4)_2BeF_4$ (T_C = 176°K) presentan también anchas bandas «torsionales» con varios máximos, que se indican, en la memoria, en el intervalo 175-290 cm^{-1}. En ninguna de las sales amónicas se han observado grandes diferencias entre los espectros obtenidos por encima y por debajo de la transición ferroeléctrica.

Los resultados obtenidos con todos los compuestos estudiados indican que la transición ferroeléctrica no guarda relación con alteraciones significativas de la libertad media de rotación de los iones amonio y de las moléculas de agua. Además, las mediciones muestran que las barreras medias que se oponen a la reorientación son relativamente bajas (V_0 < 4 kcal/mole) en todos los casos. Estas conclusiones no excluyen cambios en la ordenación de los protones en los puntos de transición. Los resultados se comparan con los datos relativos a la sección eficaz total, así como con datos obtenidos por otros procedimientos.

I. INTRODUCTION

Within the past decade a number of "soft" hydrogen-bonded ferroelectrics have been discovered and their dielectric, thermal and structural properties investigated [1, 2]. In many cases, however, the nature of the ferroelectricity and the mechanism of the ferroelectric transitions are not clearly understood. Among the compounds studied considerably in recent years are the ammonium salts $(NH_4)_2SO_4$, NH_4HSO_4 and $(NH_4)_2BeF_4$, and potassium ferrocyanide trihydrate, $K_4Fe(CN)_6 \cdot 3H_2O$ (hereinafter designated as KFCT), all of which possess ferroelectric phases below room temperature. The Curie points determined for these crystals are as follows: $(NH_4)_2SO_4$ - 224°K [3]; NH_4HSO_4 - 270 and 154°K [4]; $(NH_4)_2BeF_4$ - 176°K [5]; KFCT - 249°K [6]. The ferroelectric phase transitions in $(NH_4)_2SO_4$ and the lower-temperature transition in NH_4HSO_4 are of first order, while those in $(NH_4)_2BeF_4$ and KFCT, and the higher temperature transition in NH_4HSO_4 are apparently of second order. NH_4HSO_4 is ferroelectric only in the temperature range between its two Curie points, as shown by the sharp drop of the spontaneous polarization to zero at the low transition temperature [4]. The stable crystal modifications of the ammonium salts are all either orthorhombic or pseudo-orthorhombic [1, 2], while the ferroelectric and nonpolar phases of KFCT have quite similar monoclinic structures [7]. In every case the transition to the ferroelectric phase involves only small changes in the basic unit cell and heavy-atom positions in the crystal.

In such hydrogen-bonded crystals the orientation and dynamics of the protons and their possible role in the ferroelectric transitions is of considerable interest. Recently, the reorientations of the ammonium ions in the above ammonium salts have been investigated by the PMR (proton magnetic resonance) second-moment method [8-10]. The results of these measurements showed little or no correlation between the magnetic resonance line-width and second-moment transitions and the ferroelectric phase changes. From this it was assumed that the ferroelectric transitions are not related to changes in the rotational freedom of the ammonium ions [10]. MILLER et al. [11], however, have pointed out that such measurements are insensitive to changes in the frequency of reorientation if the reorientation rate is greater than $\sim 10^5$ c/s in both phases. These authors have measured spin-lattice relaxation times as a function of temperature

and have concluded from their results that a change in the barrier to reorientation of the ammonium ions accompanies transitions in each of these salts. Similarly, it has been suggested from proton magnetic resonance [7, 12, 13] and infrared [13] studies on KFCT that the onset of the ferroelectric phase is associated with a decrease in the reorientation frequency of the water molecules.

In the present experiment, the low-frequency motions of the ammonium ions and water molecules in these compounds have been investigated above and below the ferroelectric transitions by the inelastic scattering of cold neutrons. The neutron method is particularly appropriate for such a study, due to the large, incoherent proton scattering cross-section and to the lack of selection rules. Since most of the scattering in these solids is from the protons, the inelastic scattering will primarily reflect the rotational and vibrational motions of the hydrogenous groups.

II. EXPERIMENTAL PROCEDURE

The inelastic scattering results reported here were obtained using the cold-neutron facility at the CP-5 research reactor at Argonne National Laboratory. The ANL facility utilizes a beryllium-filtered beam of neutrons with a sharp cut-off at 3.95 Å (5.2 meV) and a mean energy of about 3.4 meV. The external apparatus consists of a single, disc-type chopper to provide periodic bursts of cold neutrons, a sample holder, and a bank of 14 enriched BF_3 detectors (1-in diameter, 12-in long, 160-cm pressure). Scattered-neutron spectra are measured by the conventional time-of-flight technique, using an RIDL 400 channel analyser. In our experimental arrangement, however, the samples are positioned after the chopper, so that a small correction for the time-of-flight of the neutron beam from chopper to sample had to be applied to the data. A 1-cm by 10-cm cadmium slit is placed in front of the chopper to define the neutron beam striking the sample. For the measurements on KFCT, $(NH_4)_2SO_4$ and NH_4HSO_4 the detectors were positioned 3.65 m from the samples at an angle of 90°. For $(NH_4)_2BeF_4$ the flight path was 3.10 m and the scattering angle 60°. In every case, corrections for background, air scattering in the flight path, and counter efficiency were applied to the observed counts.

The thin, reagent-grade polycrystalline samples were backed with cadmium and contained in aluminium holders, milled-out to the appropriate sample depth. The ammonium-salt samples varied in thickness from 0.4 to 0.7 mm, while the KFCT was about 1.7 mm thick. The samples were covered by 0.35-mm aluminium windows and were masked with cadmium to prevent scattering from the sample holder.

To obtain scattered spectra at low temperatures the samples were placed in an aluminium cryostat. Liquid nitrogen was used as the coolant and a heating block was connected to the sample holder to provide temperatures above 80°K. Temperatures were measured with a copper-constantan thermocouple attached to the face of the sample holder.

III. RESULTS AND DISCUSSION

The scattered-neutron spectra for KFCT and the ammonium salts are shown in Figs. 1-4 on a time-of-flight scale. The arbitrary neutron intensity scales for the several temperatures in the individual figures are not normalized with respect to one another. The width per channel in these spectra is 37.5 μs, except for the $(NH_4)_2\,BeF_4$ measurements, in which a 25-μs channel width was used. The energy gains corresponding to the various peaks in the scattered intensity are obtained by subtracting the mean energy of the incident neutrons ($\bar{E}_n \simeq 3.4$ meV) from the scattered-neutron energy. These energy peaks are indicated in the figures in units of meV and cm^{-1}, along with the estimated uncertainties in the peak positions on the time-of-flight scale, due primarily to systematic errors and to the difficulties in ascertaining the centre of non-symmetric and over-lapping peaks.

$K_4Fe(CN)_6 \cdot 3H_2O$

The results for KFCT above and below the Curie temperature (249°K) are shown in Fig. 1. The room-temperature spectrum exhibits an intense band centred at an energy gain corresponding to 435 ± 40 cm^{-1} (54 ± 5 meV), as well as indications of two broad peaks at about 165 and 110 cm^{-1}. The elastic scattering of the incident spectrum around the beryllium cut-off is

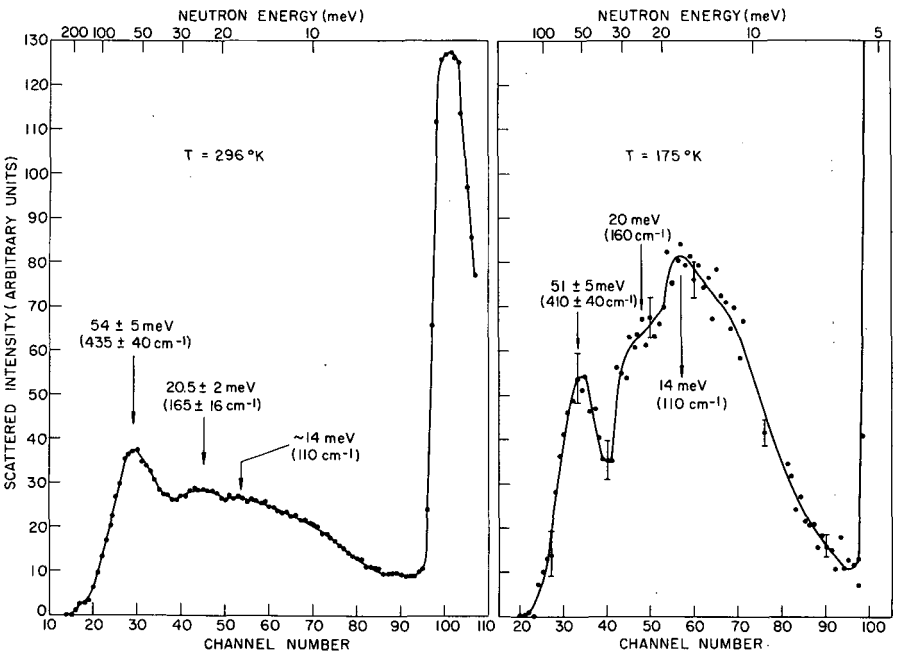

Fig. 1

Time-of-flight distributions of neutrons scattered at an angle of 90° by polycrystalline $K_4Fe(CN)_6 \cdot 3H_2O$ at 296 and 175°K
Also shown are the energy transfers at the maximum intensities of the broad inelastic peaks.

also shown in the upper channels. In the spectrum at 175°K, the same peaks are observed with different relative intensities, due primarily to differences in the relative population of states at the lower temperature. A third spectrum, measured at 121°K, not shown in Fig. 1, also exhibits broad peaks centred about 400 and 100 cm^{-1}.

The high-energy band in the KFCT spectra is assigned to the librations of the water molecules. A number of high-intensity peaks in the 400-800 cm^{-1} range have recently been observed and similarly assigned in cold-neutron measurements on a number of crystal hydrates [14, 15]. There are twelve water molecules per unit cell in the monoclinic KFCT structure, with two different crystal environments in the non-polar phase and more than two in the ferroelectric phase [7]. Although the orientations of the water molecules are somewhat in doubt, it has been deduced from the X-ray studies [7] that four molecules possess a relatively short (2.8 Å) O-H ... N hydrogen bond, while the others have rather large O-O and O-N distances. Thus the broadness of the "torsional" peak, which persists in the low-temperature phase, is to be expected, since it represents energy gains from all the water molecules in their excited librational states, or, alternatively, a series of overlapping maxima.

The significant point, however, is that these results indicate little or no change in the rotational motions of the water molecules at the ferroelectric transition. This conclusion is in disagreement with the predictions from NMR (nuclear magnetic resonance) results [7, 12, 13] of a decrease in the reorientation rate of the water molecules with the onset of the ferroelectric phase. In addition, infrared spectra have also been measured [13] which show no peaks in the spectra at 298°K that could be attributed to water librations, but indicate a peak near 540 cm^{-1} at 77°K, which the author assigns to a librational mode. This was taken as additional evidence for a significant increase in the average barrier to rotation of the water molecules in the ferroelectric phase, again in sharp contrast to our neutron results. It should be pointed out, however, that water librations in complex, weakly-bound hydrates are many times difficult, if not impossible, to observe by IR techniques [16], so that the disagreement is probably not significant. Moreover, recent total cross-section measurements on KFCT at long neutron wavelengths [17] show no sudden change in the cross-section and its variation with wavelength in passing through the ferroelectric transition. This again indicates little change in the motions of the water molecules. Deuteron magnetic resonance measurements in progress at this Laboratory [18] have also yielded results consistent with the neutron data. Thus it appears certain that the rearrangements of the protons at the onset of the ferroelectric phase do not involve an increase in the average barriers hindering the reorientations of the water molecules.

It is also interesting to note that the other two broad maxima in the KFCT spectra are essentially the same in both phases. The peak indicated at about 165 cm^{-1} may be due to the "optical" translations of the water molecules in the lattice. Such modes have previously been observed in the same frequency region in infrared [19] and neutron [14, 15] experiments. The broad band peaking around 110 cm^{-1} is probably due to the acoustical lattice vibrations. It might also be expected that oscillations and translations of the CN groups also lie in the region below 200 cm^{-1}.

The comparatively low frequency at the centre of the torsional band in KFCT indicates a rather low average barrier to reorientation of the water molecules in both phases. In fact the peak energy of 435 cm^{-1} is somewhat smaller than that observed in the neutron spectra for liquid water (480 cm^{-1}) [20], indicating greater freedom of rotation in KFCT. Such a conclusion is supported by the fact that the total cross-section slope at long wavelengths is greater at room temperature in KFCT (7 b/Å-H) than in water (6 b/Å-H) [17]. Relatively low activation energies for water molecule reorientation in KFCT are also suggested from the NMR results [7, 13].

$(NH_4)_2SO_4$ and NH_4HSO_4

The scattered-neutron spectra for $(NH_4)_2SO_4$ (T_c = 224°K) and NH_4HSO_4 (T_c at 270 and 154°K) are shown in Figs. 2 and 3. The results at room temperature exhibit inelastic bands peaked at energy transfers of about

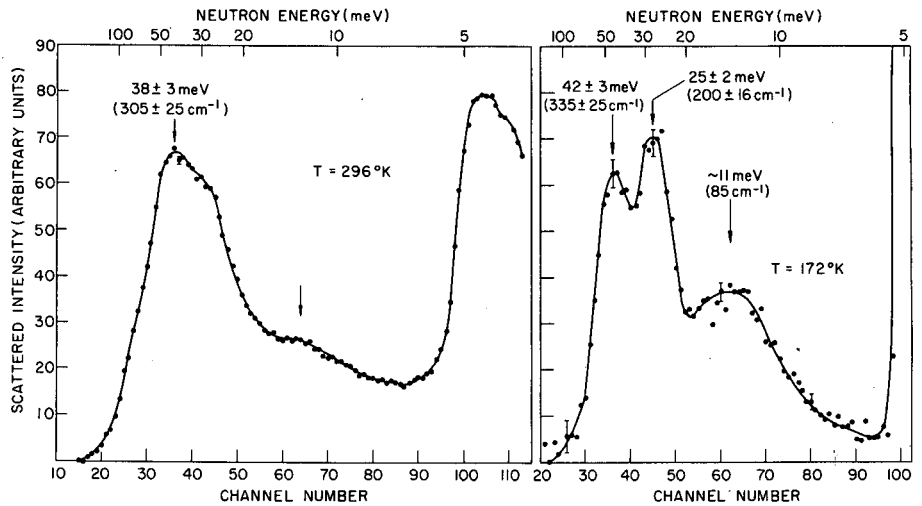

Fig. 2

Time-of-flight distributions of neutrons scattered at θ = 90° by $(NH_4)_2SO_4$ at 296 and 172°K.

300 cm^{-1} (38 meV) for $(NH_4)_2SO_4$ and 260 cm^{-1} (32 meV) for NH_4HSO_4, which are primarily due to the torsional motions of the ammonium ions. The width of the peaks in both cases indicates that the torsional branches in the vibrational spectra are quite broad. Moreover the indication of a shoulder on the low-energy side of the $(NH_4)_2SO_4$ peak suggests the overlapping of separate bands. Such complex spectra are to be anticipated, since the orthorhombic and pseudo-orthorhombic structures in $(NH_4)_2SO_4$ and NH_4HSO_4 possess four and eight molecules respectively per unit cell, with varying distances between the NH_4 ions and the oxygen atoms of the sulphate groups. In $(NH_4)_2SO_4$, for example, X-ray data indicate two sets of four NH_4 ions, with one type having considerably shorter N-H...O bonds than the other [8, 10]. In spite of the complex spectra, however, the position of the tor-

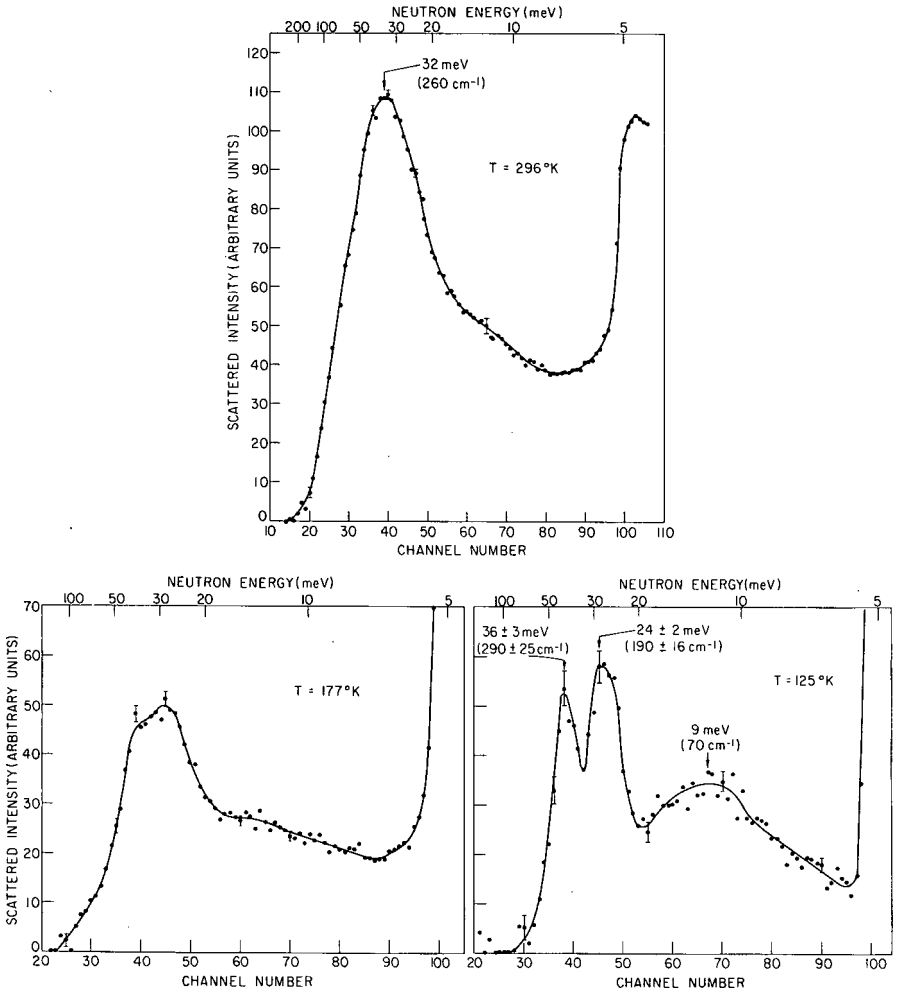

Fig. 3

Time-of-flight spectra of neutrons scattered at $\theta = 90°$ by NH_4HSO_4 at 296, 177 and 125°K

sional peaks do suggest that the rotational freedom of the NH_4 ions is greater in NH_4HSO_4 than in $(NH_4)SO_4$. This conclusion is supported by the fact that the total cross-section slope at long wavelengths appears slightly higher for NH_4HSO_4 than for $(NH_4)_2SO_4$ (~ 8 b/Å-H) [21].

The $(NH_4)_2SO_4$ spectrum at 172°K is clearly split, with two overlapping peaks at 335 and 200 cm^{-1}, and a third broad band centred at about 85 cm^{-1}. The two higher-energy peaks can possibly be attributed to two branches in the torsional vibration spectrum. Such an assignment is quite consistent with the structural data discussed above, as well as with NMR line-width measurements [8-10], which are interpreted to indicate the presence of both "frozen-in" and rapidly reorientating NH_4 ions at low temperatures. It would also be plausible, however, to assign the 200 cm^{-1} peak and the shoulder

in the room-temperature spectrum to the "optical" translations of the NH_4 ions. Peaks in the 150-200 cm^{-1} range have been observed by inelastic scattering measurements on the ammonium halides and other ammonium salts [22-24] and attributed to such translational modes.

Thus only the maximum at 335 cm^{-1} can be assigned with certainty to torsional vibrations. The fact that this torsional peak is shifted very little from the position of the maximum in the room-temperature band, however, strongly indicates that the rotational freedom of the NH_4 ions undergoes little change with the onset of the ferroelectric phase. This conclusion is in sharp disagreement with calculations from spin-lattice relaxation measurements [11] of an increase in the barrier to NH_4 ion reorientation from 2 ± 1 kcal/mole (1 kcal/mole = 350 cm^{-1}) in the high-temperature phase to 6 ± 1 kcal/mole in the ferroelectric phase.

The NH_4HSO_4 spectrum in the ferroelectric phase at 177°K (Fig. 3) exhibits a broad inelastic band similar to that at room temperature, with a slight indication of splitting. The centre of the band at 177°K is also shifted to slightly lower energy, probably due to the relative depletion of excited states on the high-energy side of the band. These results again indicate little change in the motions of the NH_4 ions in passing from the non-polar (centrosymmetric) phase to the ferroelectric phase. At 125°K, below the second Curie point, the NH_4HSO_4 spectrum shows a distinct splitting in the "torsional" band quite similar to that in $(NH_4)_2SO_4$, with peaks at about 290 and 190 cm^{-1}. Again, as for $(NH_4)_2SO_4$, the higher-energy peak is assigned to torsional vibrations, while the second peak is attributed either to a second torsional branch or to the optical NH_4 ion translations. The broad low-energy peak at around 70 cm^{-1}, and the similar peak at about 85 cm^{-1} in the $(NH_4)_2SO_4$ spectrum are considered primarily due to acoustical lattice vibrations.

The distinct torsional peak at 290 cm^{-1} might indicate a small increase in the average rotational barriers of the NH_4 ions in the polar (but non-ferroelectric) phase below 154°K. A slight increase in the barrier to reorientation at the lower transition from 2.0 ± 0.5 to 2.9 ± 0.4 kcal/mole has been suggested from the NMR results [11].

$(NH_4)_2BeF_4$

The neutron spectra for $(NH_4)_2BeF_4$ at 300, 200 and 150°K are shown in Fig. 4. The results above the ferroelectric transition (T_c = 176°K), like those of the other ammonium salts, exhibit a broad inelastic band, with maxima indicated at about 290, 225, and 175 cm^{-1}. As is expected the relative intensity at the high-energy side of the band is somewhat reduced at 200°K, with a slight shift of the highest-energy "peak" to about 275 cm^{-1}. In the ferroelectric phase, at 150°K, the spectrum is again quite similar, with an indication of split maxima in the same energy region and a further reduction of intensity at high energies.

Again the interpretation of the $(NH_4)_2BeF_4$ spectra, with its several broad maxima, is somewhat difficult. The highest-energy peak is almost definitely due to the torsional motions of the NH_4 ions. It would seem plausible to assign the maximum at about 225 cm^{-1} to a second torsional branch and the shoulder around 175 cm^{-1} to optical translations. The broad peak

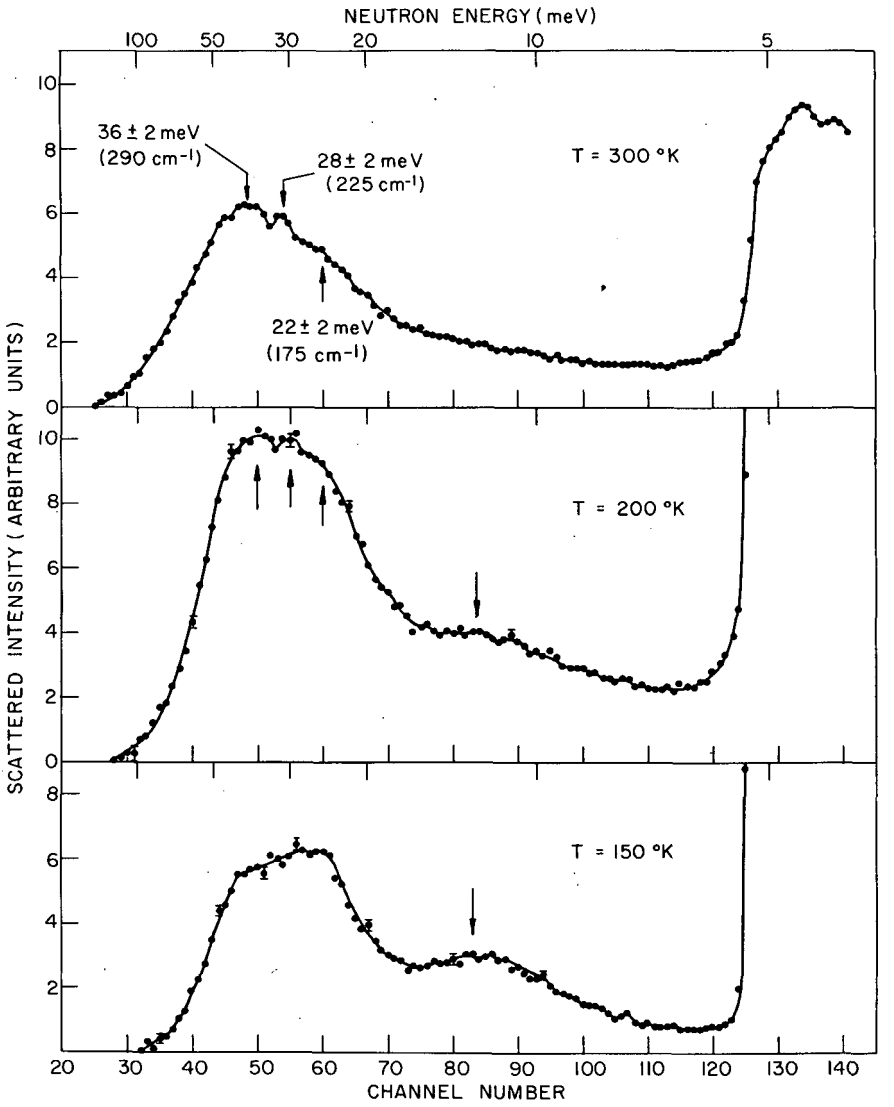

Fig. 4

Time-of-flight spectra of neutrons scattered at $\theta = 60°$ by $(NH_4)_2BeF_4$ at 300, 200 and 150°K.

observed at lower energies (~ 70 cm^{-1}) in the low-temperature spectra is again attributed primarily to acoustic lattice vibrations. The fact that the width of the torsional bands for $(NH_4)_2BeF_4$, as well as for the other salts, extends to rather high energies is probably explained not only by the natural width of the torsional branches, but by the population of excited levels above the first.

The diffuse spectra and low-energy peaks for $(NH_4)_2BeF_4$ indicate a relatively low average barrier to rotation for the NH_4 ions, with little change

at the ferroelectric transition. This is again in disagreement with calculations from NMR relaxation-time measurements [11], which suggest a large increase in the potential barrier to reorientation from 1.5 ± 0.7 to 6 ± 1 kcal/mole at the onset of the ferroelectric phase. The absence of a PMR second-moment transition in the temperature region down to 90°K [9], however, is a further indication of a low barrier in both phases.

IV. CONCLUSIONS

The results discussed in section III provide good evidence that the onset of the ferroelectric phases in the compounds studied is not correlated with a "freezing-in" of the NH_4 ions or water molecules, as suggested from some of the NMR studies. Indeed there appears to be little change in the rotational freedom of the hydrogenous groups at any of the phase transitions. This does not, of course, preclude some changes in the ordering of the protons.

The broad torsional peaks at about 435 cm^{-1} in KFCT and from 200-335 cm^{-1} in the ammonium salts indicate relatively low barriers to reorientation in every case. Due to the rather complex crystal structures, as well as to uncertainties in the analysis of the neutron spectra, it is difficult to make accurate barrier determinations. Assuming barriers close to four-fold for the ammonium ions [25], however, the $(NH_4)_2SO_4$ results and its total cross-section slope of about 8 b/Å-H indicate an average barrier near 3 kcal/mole [26]. Since the average torsional frequencies for NH_4HSO_4 and $(NH_4)_2\,BeF_4$ are less than that for $(NH_4)_2SO_4$ but greater than 200 cm^{-1}, their rotational barriers are estimated to be in the 2-3 kcal range. The activation energies for water-molecule reorientation in KFCT are also rather low, as discussed in section III.

The role of the NH_4 ions and water molecules in the ferroelectric transitions is obviously still in doubt. The ferroelectric properties may involve a change in the equilibrium orientations of the weak hydrogen bonds or some distortion of the ionic groups [9]. It is clear that a precise determination of the positions and orientations of the protons in the various phases is necessary. Such a study on KFCT is in progress at ANL by both deuteron-resonance [18] and neutron-diffraction [27] techniques. Moreover we are attempting to further elucidate the bands in the neutron spectra for all the compounds by a study of deuterated samples.

ACKNOWLEDGEMENTS

The authors are extremely grateful to D.W. Connor and O.C. Simpson of the Solid State Science Division at Argonne National Laboratory for their support and encouragement during the course of this research. We would also like to thank G. Ostrowski, T. Erickson, R. Kleb and R. Stefiuk for their technical assistance, and C. Thaper for his help in processing the data. Useful discussions with D. O'Reilly, T. Tsang and R.S. Carter are also gratefully acknowledged.

REFERENCES

[1] JONA, F. and SHIRANE, G., Ferroelectric Crystals, Pergamon Press, Oxford (1962) 318-73.
[2] DEVONSHIRE, A.F., in Reports on Progress in Physics 27 Physical Society of London (1964) 1-22.
[3] MATTHIAS, B.T. and REMEIKA, J.P., Phys. Rev. 103 (1956) 262.
[4] PEPINSKY, R., VEDAM, K., HOSHINO, S. and OKAYA, Y., Phys. Rev. 111 (1958) 1508.
[5] PEPINSKY, R. and JONA, F., Phys. Rev. 105 (1957) 344.
[6] WAKU, S., HIRUBAYASHI, H., TOYODA, H., IWASAKI, H. and KIRIYAMA, R., J. phys. Soc. Japan 14 (1959) 973.
[7] KIRIYAMA, R., KIRIYAMA, H., WADA, T., NIIZEKI, N. and HIRABAYASHI, H., J. phys. Soc. Japan 19 (1964) 540.
[8] RICHARDS, R.E. and SCHAEFER, T., Trans. Faraday Soc. 57 (1961) 210.
[9] BLINC, R. and LEVSTEK, I., Phys. Chem. Solids 12 (1960) 295.
[10] BURNS, G., Phys. Rev. 123 (1961) 64.
[11] MILLER, S.R., BLINC, R., BRENMAN, M. and WAUGH, J.S., Phys. Rev. 126 (1962) 528.
[12] LUNDIN, A.G., MIKHAILOV, G.M. and GABUDA, S.P., Dokl. Akad. Nauk SSSR 136 (1961) 864.
[13] BLINC, R., BRENMAN, M. and WAUGH, J.S., J. chem. Phys. 35 (1961) 1770.
[14] BOUTIN, H., SAFFORD, G.J. and DANNER, H.R., J. chem. Phys. 40 (1964) 2670.
[15] RUSH, J.J., to be published.
[16] FERRARO, J. and WALKER, A., J. chem. Phys., to be published.
[17] LEUNG, P., private communication.
[18] TSANG, T., McCORMICK, G.K., O'REILLY, D.E. and SCHACHER, G.E., Bull. Amer. phys. Soc. 9 (1964) 503.
[19] PIMENTEL, G.C. and McCLELLAN, A.L., The Hydrogen Bond, W.H. Freeman and Co., San Francisco (1960).
[20] HUGHES, D.J., PALEVSKY, H., KLEY, W. and TUNKELO, E., Phys. Rev. 119 (1960) 872.
[21] RUSH, J.J. and BOUTIN, H., unpublished data.
[22] PALEVSKY, H., J. phys. Soc. Japan 17, Suppl. B-II (1962) 367.
[23] MIKKE, K. and KROH, A., Inelastic Scattering of Neutrons in Solids and Liquids II IAEA, Vienna (1963) 237-50.
[24] RUSH, J.J., Bull. Amer. phys. Soc. 9 (1964) 623.
[25] GUTOWSKY, H.S., PAKE, G.E. and BERSOHN, R., J. chem. Phys. 22 (1954) 643.
[26] RUSH, J.J., TAYLOR, T.I. and HAVENS, W.W., Jr., J., chem. Phys. 37 (1962) 234.
[27] MUELLER, M. and TAYLOR, J., private communication.

DISCUSSION

J.A. JANIK: Don't you think that the ordinary Be technique is unsuitable for low-temperature measurements owing to a lack of population of excited states?

J.J. RUSH: I would agree that, for vibration involving energy transfers much greater than kT, an energy-loss measurement is in general desirable. However, the finite range of incident neutron energies in an energy-loss experiment may not permit the observation of very low frequency modes. In addition, the complex spectra resulting from the complex crystal structure in these materials might make the interpretation of such measurements quite difficult.

V.M. PADMANABHAN: Is it possible to get additional information if one uses a single crystal? For example, in ammonium sulphate, a single crystal could be mounted along the C-axis, since the polar axis happens to be along C.

J.J. RUSH: I don't think so. In such a complicated incoherently scattering crystal one might see some effect, but it would be very difficult to interpret. Perhaps an experiment with a deuterated crystal might give a more informative result.

B. DORNER: I think the number of molecules per unit cell is not important as regards the experimental arrangement but only for the interpretation of the results. The beryllium-filter technique gives a somewhat better resolution in energy than the time-of-flight method.

J.J. RUSH: Again, I would say that an energy-loss experiment is, in principle, desirable. In such complex crystals, however, exhibiting very broad torsional bands with definite indications of splitting, the observation of 0-1, 0-2 and 1-2 transitions by energy-loss would probably yield a very complicated spectrum, which would be even more difficult to interpret.

STUDY OF ELASTIC INCOHERENT SCATTERING BY AMMONIUM SALTS

G. VENKATARAMAN, K. USHA DENIZ, P. K. IYENGAR,
P. R. VIJAYARAGHAVAN AND A. P. ROY
ATOMIC ENERGY ESTABLISHMENT TROMBAY, BOMBAY, INDIA

Abstract — Résumé — Аннотация — Resumen

STUDY OF ELASTIC INCOHERENT SCATTERING BY AMMONIUM SALTS. The angular distribution of incoherent elastic scattering from several ammonium salts has been studied using a triple-axis spectrometer giving neutrons of energy 0.07 eV and having a window of 0.012 eV at the incident energy. In the case of NH_4Cl (300°K), NH_4Br (300°K) and NH_4I (220°K), the form factor was found to be Gaussian and values for $\overline{U^2}$, the mean square amplitude, were derived. In NH_4I, $(NH_4)_2SnCl_6$ and $(NH_4)_2SnBr_6$ (all at room temperature), the form factor, besides being non-Gaussian, is much sharper, indicating greater freedom of motion for the NH_4^+ ion. The latter results are compared with calculations based on the uniaxial and the free-rotation model for the ion.

ÉTUDE DE LA DIFFUSION ÉLASTIQUE INCOHÉRENTE PAR DES SELS D'AMMONIUM. Les auteurs ont étudié la distribution angulaire de la diffusion élastique incohérente dans différents sels d'ammonium, avec un spectromètre triaxial utilisant des neutrons incidents de 0,07 eV et possédant une bande d'énergie de 0,012 eV axée sur l'énergie incidente. Dans le cas de NH_4Cl (300°K), NH_4Br (300°K) et NH_4I (220°K), ils ont constaté que le facteur de forme est gaussien et ont ainsi calculé des valeurs de l'amplitude quadratique moyenne, $\overline{U^2}$. Pour NH_4I, $(NH_4)_2SnCl_6$ et $(NH_4)_2SnBr_6$ (à la température ambiante), le facteur de forme n'est pas gaussien et il est beaucoup plus prononcé, ce qui laisse supposer une plus grande liberté de mouvement de l'ion NH_4^+. Ces derniers résultats sont comparés à ceux obtenus par des calculs fondés sur un modèle d'ion à rotation sur un seul axe et à rotation libre.

ИЗУЧЕНИЕ УПРУГОГО НЕКОГЕРЕНТНОГО РАССЕЯНИЯ НА СОЛЯХ АММОНИЯ. Угловое распределение некогерентного упругого рассеяния на нескольких солях аммония было изучено с помощью трехосного спектрометра, регистрирующего нейтроны с энергией 0,07 эв и имеющего полосу пропускания в 0,012 эв в области энергии падающего потока. Было установлено, что для NH_4Cl (300° K), NH_4Br (300° K) и NH_4J (220° K) формфактор имеет гауссовский вид, и были получены значения для $\overline{U^2}$, являющиеся среднеквадратической амплитудой. Для NH_4J, $(NH_4)_2SnCl_6$ и $(NH_4)_2SnBr_6$ (все при комнатной температуре) формфактор, помимо того, что не является гауссовским, является еще более острым, что говорит о большей свободе движения иона NH_4^+. Последние результаты сравниваются с результатами расчетов, основанных на модели, предполагающей одну ось и свободное вращение для ионов.

ESTUDIO DE LA DISPERSIÓN ELÁSTICA INCOHERENTE POR SALES DE AMONIO. Se ha estudiado la distribución angular en la dispersión elástica incoherente por varias sales de amonio, utilizando un espectrómetro triaxial que proporciona neutrones de 0,07 eV de energía, y con una ventana de 0,012 eV en la energía de incidencia. En el caso del NH_4Cl (300°K), del NH_4Br (300°K) y del NH_4I (220°K), se observó que el factor de forma es gaussiano y se dedujeron los valores de $\overline{U^2}$, esto es, la amplitud cuadrática media. En el caso del NH_4I, del $(NH_4)_2SnCl_6$ y del $(NH_4)_2SnBr_6$ (a la temperatura ambiente), el factor de forma, además de no ser gaussiano, es mucho más acusado, lo que indica una mayor libertad de movimiento del ion NH_4^+. Estos últimos datos se comparan con resultados de cálculos basados en un modelo monoaxial y de rotación libre para el ion.

I. INTRODUCTION

This paper describes some investigations on the motion of the ammonium ion in several salts by the measurement of the angular distribution of

incoherent elastic scattering. These experiments were a result of the study of the dynamics of the ammonium ion by inelastic scattering techniques carried out by us earlier [1]. The angular distribution method of studying molecular motion was first used by BROCKHOUSE [2] in his experiments on water. In the present case the technique has been adapted to solids [3].

II. THEORY

The principle underlying the present experiments may be understood as follows: Consider the scattering of neutrons by a crystal which contains the molecule whose motion is to be investigated. Let us suppose that the scattering by the molecule consists predominantly of incoherent scattering by one of the constituent nuclei.

The partial differential cross-section per nucleus is given by

$$\frac{d^2\sigma_{inc}}{d\Omega d\omega} = \frac{\sigma_{inc}}{8\pi^2}\frac{k'}{k_0}\int e^{i(\vec{Q}\cdot\vec{r}-\omega t)}\, G_s(\vec{r}, t)d\vec{r}dt\ , \tag{1}$$

where $G_s(\vec{r}, t)$ is the well known Van Hove self-correlation function [4] for the nucleus in question; the other symbols have their usual meaning. Following Van Hove, we now write $G_s(\vec{r}, t)$ as

$$G_s(\vec{r}, t) = G_s^{\infty}(\vec{r}) + G_s'(\vec{r}, t)\ . \tag{2}$$

Here $G_s^{\infty}(\vec{r})$ describes the asymptotic self-correlation function and gives rise to elastic scattering while $G_s'(\vec{r}, t)$ describes the deviation from the asymptotic form and leads to inelastic scattering. It can be shown from the definition of $G_s(\vec{r}, t)$ that the asymptotic form can be written as

$$G_s^{\infty}(\vec{r}) = \int d\vec{r}'\, \rho_s(\vec{r}'-\vec{r})\rho_s(\vec{r}'), \tag{3}$$

where $\rho_s(\vec{r})$ is the density distribution in the "thermal cloud" of the nucleus concerned. Using Eqs. (2) and (3), Eq. (1) becomes

$$\frac{d^2\sigma_{inc}}{d\Omega d\omega} = \frac{\sigma_{inc}}{4\pi}\frac{k'}{k_0}\left[\delta(\omega)\left|\int e^{i\vec{Q}\cdot\vec{r}}\rho_s(\vec{r})d\vec{r}\right|^2 + \int e^{i(\vec{Q}\cdot\vec{r}-\omega t)}G_s'(\vec{r}, t)d\vec{r}dt\right]. \tag{4}$$

The angular distribution of neutrons scattered incoherently and without energy change is therefore given by

$$\left[\frac{d^2\sigma_{inc}}{d\Omega d\omega}\right]_{\omega=0} = \frac{\sigma_{inc}}{4\pi}\left[\left|\int e^{i\vec{Q}_0\cdot\vec{r}}\rho_s(\vec{r})d\vec{r}\right|^2 + \int e^{i\vec{Q}_0\cdot\vec{r}}d\vec{r}\int G_s'(\vec{r}, t)dt\right], \tag{5}$$

where $\vec{Q}_0$ is the value of the wave vector transfer $\vec{Q}$ for elastic scattering. If the molecule is well bound in the solids, the "thermal cloud" will be built up rapidly and the contribution from the second term will be small. The angular distribution will then be simply proportional to the square of the Fourier transform of the fully developed "cloud". For a polycrystal the scattering will depend only on $|\vec{Q}_0|$ and the angular distribution simplifies to

$$\left[\frac{d^2\sigma_{inc}}{d\Omega d\omega}\right]_{\omega=0} \approx \frac{\sigma_{inc}}{4\pi}\left|\int_0^\infty 4\pi r^2 \rho_s(r)\frac{\sin Q_0 r}{Q_0 r}dr\right|^2. \quad (6)$$

It is clear from Eq.(6) that the study of the incoherent elastic form factor can lead to information about the size and shape of the "thermal cloud" and thereby about molecular motion. The method works best when the following conditions are satisfied.

(1) There is only one type of ion or molecule containing the incoherently scattering nucleus.
(2) The scattering from the nucleus concerned outweighs the scattering from all other nuclei in the sample.
(3) The scattering nucleus is located far away from the centre of mass of the molecule. This makes the form factor sensitive to the rotational motions of the molecule.

The ammonium salts studied in the present experiment, namely NH_4Cl, NH_4Br, NH_4I, $(NH_4)_2SnCl$ and $(NH_4)_2SnBr$, fulfil these requirements.

III. EXPERIMENT

The form factor measurements were carried out using the triple-axis spectrometer at the Canada-India Reactor (CIR). Monochromatic neutrons of energy 0.07 eV (1.08_5 Å) selected by (111) planes of an aluminium single crystal were allowed to fall on the specimen and the scattered neutrons were selected by Bragg reflection from the (111) planes of a second aluminium crystal. The analyser was set to reflect neutrons having the same energy as the incident neutrons and had an energy resolution of 0.012 eV. The samples were packed between thin aluminium foils and held in vacuum. The thickness of the sample was adjusted to give about 10% scattering. The angular distributions were measured in steps of 0.25° in scattering angle. The contribution from the sample holder was measured separately and subtracted. Data points in the region of the various Bragg reflections from the sample were rejected and the remaining points were averaged over suitable small angular intervals. Corrections were applied for geometrical effects, but no corrections were made either for multiple scattering or the contribution from inelastic scattering within the resolution of the analyser. All measurements were performed at room temperature and in the case of NH_4I an additional run was taken at 220°K corresponding to the tetragonal phase. The scattering from vanadium was also studied as a check.

IV. RESULTS AND DISCUSSION

The results for vanadium, NH_4Cl and NH_4Br at 300°K and NH_4I at 220°K are shown in Fig. 1. All the distributions have been normalized to unity in the forward direction. The extrapolation of the observed data to zero

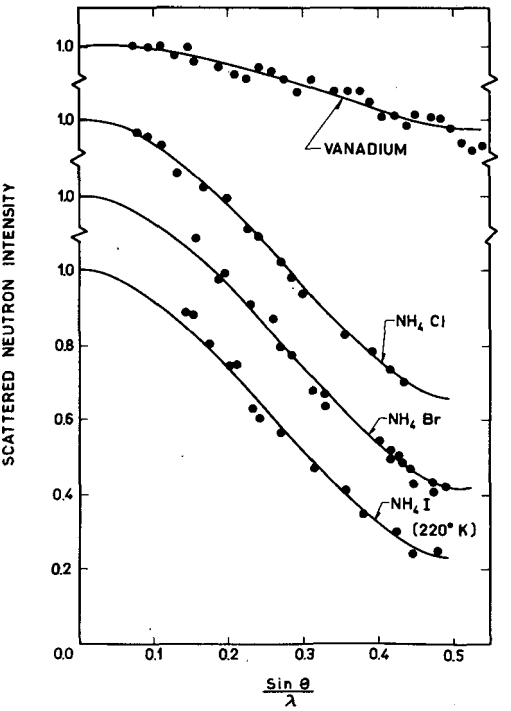

Fig. 1

Form factors for vanadium, NH_4Cl and NH_4Br at 300°K and NH_4I at 220°K plotted as a function of $\sin\theta/\lambda$, where 2θ is the scattering angle
The solid lines are Gaussians fitted to the observed data.

scattering angle presented no problem as the data could be fitted to a Gaussian. Writing the Gaussian in the familiar form $\exp-[Q_0^2 \overline{U}^2]$, the values shown in Table I were derived by least square fitting for $\overline{U}^2$, the component of mean square radius of the 'cloud' along $\vec{Q}_0$.

The value of $\overline{U}^2$ obtained from vanadium leads to a Debye temperature of (349 ± 10)°K, in fair agreement with that reported in the literature [5, 6]. The Gaussian behaviour observed in the case of NH_4Cl, NH_4Br and NH_4I clearly indicates that the proton motions in these salts can be described by a conventional Debye-Waller factor. This is not unexpected since inelastic scattering experiments [1, 7-9] show that in these substances, the rotational motions which can cause deviation from the Gaussian form, consist essentially of small amplitude torsional oscillations.

Figure 2 shows the results for NH_4I (at 300°K, NaCl phase) $(NH_4)_2SnCl_6$ and $(NH_4)_2SnBr_6$. In the case of these salts, the form factor could not be

TABLE I

MEAN SQUARE DISPLACEMENTS

Substance	Temperature (°K)	$\overline{U^2}$ (Å^2)
Vanadium	300	(0.0073 ± 0.0004)
NH_4Cl (CsCl phase, disordered)	300	(0.040 ± 0.002)
NH_4Br (CsCl phase, disordered)	300	(0.042 ± 0.004)
NH_4I (tetragonal phase, ordered)	220	(0.046 ± 0.002)

fitted to a Gaussian. Extrapolation to the forward direction was done by drawing a smooth line and is therefore likely to contain greater errors than in the previous case. The broken lines indicate typical limits that could be placed on the observed form factor. Comparison with Fig. 1 shows that the form factor is falling off more rapidly indicating that the NH_4^+ ion is relatively free in these salts. The contribution from inelastic scattering (the second term in Eq. (5)) may therefore not be negligible at large values of Q_0. The data at small Q_0, however, do not suffer from such limitations and are quite significant, for purposes of comparison, with calculations based on some model of ion motion.

Several years ago, LEVY and PETERSON [10], in connection with their diffraction experiments, considered the possibility that the NH_4^+ ion in NH_4I in the NaCl phase was performing uniaxial rotation. A calculation based on this assumption (without considering any other type of motion) is shown in Fig. 2. It is seen that the overall agreement is poor. One of the shortcomings of this model is that it predicts too much intensity at backward angles. Inclusion of other modes does not lead to any great improvement. Uniaxial rotation in the NaCl therefore seems unlikely. Free rotation of the ion can also be ruled out since this predicts a much sharper form factor than observed (see Fig. 2). This lack of agreement between experiment and both uniaxial-rotation and free-rotation models is similar to what has been observed in inelastic scattering [1, 8, 11] and spectroscopic experiments [12]. No detailed determination of the actual motions performed by the ion has been attempted. All that can be said from the present experiments is that the ammonium ion is relatively free in NH_4I in the NaCl phase, making perhaps large amplitude torsional oscillations. Similar conclusions apply to the ammonium stannous salts where specific heat measurements [13] suggest that the barrier is low enough to permit large amplitude motion of the ion. The form factor in stannous bromide is slightly sharper than in the chloride indicating a greater freedom of movement for the ion and a correspondingly lower barrier height.

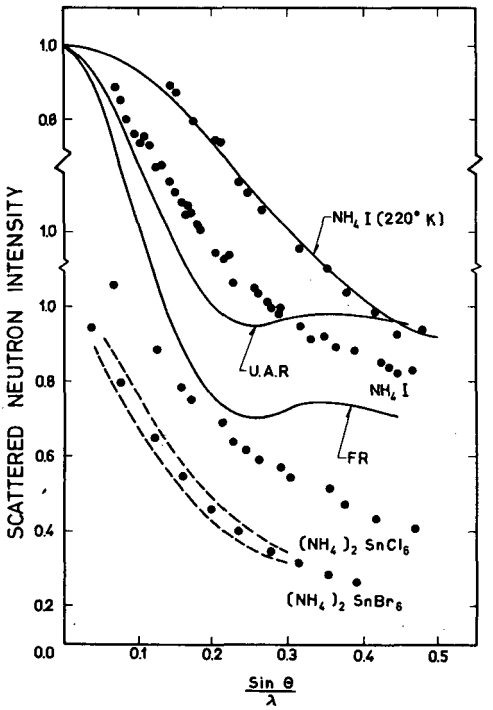

Fig. 2

Form factors for NH_4I, $(NH_4)_2SnCl_6$ and $(NH_4)_2SnBr_6$, all at room temperature
The normalization to unity at forward angles was done by extrapolation.
The broken lines show typical limits that may be placed on the
observed form factor due to errors in extrapolation.
For comparison, the form factor for NH_4I at 220°K is also given.
The solid lines marked U. A. R. and F. R. show calculations based on
uniaxial-rotation and free-rotation models, respectively.

In summary, form factor experiments can, in suitable cases, provide a useful complement to inelastic scattering experiments. Applied to single crystals they can help to show up anisotropy of thermal motion.

ACKNOWLEDGEMENTS

We would like to thank Dr. R. Chidambaram and Mr. B. A. Dasannacharya for helpful discussions.

REFERENCES

[1] VENKATARAMAN, G., USHA DENIZ, K., IYENGAR, P. K., VIJAYARAGHAVAN, P. R. and ROY, A. P., Inelastic Scattering of Neutrons in Solids and Liquids II IAEA, Vienna (1963) 253-62; Solid State Comm. 2 (1964) 17; to be published.

[2] BROCKHOUSE, B.N., Nuovo Cim. Suppl. 9 (1958) 45.
[3] CAGLIOTI, G, Acta cryst. 17 (1964) 1202.
[4] VAN HOVE, L., Phys. Rev. 95 (1954) 249.
[5] BROCKHOUSE, B.N., Canad. J. Phys. 33 (1955) 889.
[6] TURBERFIELD, K.C. and EGELSTAFF, P.A., Phys. Rev. 127 (1962) 1017.
[7] WOODS, A.D.B., BROCKHOUSE, B.N., SAKAMOTO, M. and SINCLAIR, R.N., Inelastic Scattering of Neutrons in Solids and Liquids, IAEA, Vienna (1961) 487-98.
[8] MIKKE, K. and KROH, A., Inelastic Scattering of Neutrons in Solids and Liquids II. IAEA, Vienna (1963) 237-50.
[9] PALEVSKY, H., Proc. Int. Conf. on Magnetism and Crystallography, J. phys. Soc. (Japan) 17 Suppl. BIII (1961).
[10] LFVY, H.A. and PETERSON, S.W., J. chem. Phys. 21 (1953) 366.
[11] PALEVSKY, H., Inelastic Scattering of Neutrons in Solids and Liquids II IAEA, Vienna (1963) 251.
[12] VEDDER, W. and HORNIG, D.F., J. chem. Phys. 35 (1961) 1561.
[13] MORFEE, R.G.S., STAVELLY, L.A.K., WALTERS, S.T. and WIDEY, D.L., J. Phys. Chem. Solids 13 (1960) 132.

ИССЛЕДОВАНИЕ ДИНАМИКИ МОЛЕКУЛЯРНЫХ ГРУПП NH_4^+ И H_2O В КРИСТАЛЛАХ

А. БАЙОРЕК, Т.А. МАЧЕХИНА и К. ПАРЛИНЬСКИ
ОБЪЕДИНЕННЫЙ ИНСТИТУТ ЯДЕРНЫХ ИССЛЕДОВАНИЙ, ДУБНА
СССР

Abstract — Résumé — Аннотация — Resumen

INVESTIGATION OF THE DYNAMICS OF NH_4^+ AND H_2O MOLECULAR GROUPS IN CRYSTALS. The authors give the results of thermal neutron scattering measurements in crystals containing ammonium ion (NH_4Cl, NH_4Br, NH_4I, NH_4F, NH_4NO_3, NH_4CNS, $(NH_4)_2SO_4$, $(NH_4)_2S_2O_8$, $(NH_4)_2Cr_2O_7$, $(NH_4)_2CO_3$) and water of crystallization ($BaCl_2 \cdot 2H_2O$, $SrCl_2 \cdot 6H_2O$, $CuSO_4 \cdot 5H_2O$). The investigations were made to study the influence of various crystal lattices on the dynamics of these groups and the connection between scattering processes and phase transitions.

In spite of the structural differences of the substances examined, the spectra obtained at the temperature of liquid nitrogen proved to be similar. As a rule, there are two peaks, one in the 15-20 meV energy transfer range, and the other in the 35-70 meV range, associated with the torsional vibrations of ammonium ions. The intensity of the peaks depends on the structure of the substances under examination and falls as the sample temperature rises.

It was found that there is a jump in the elastic region of the spectrum at certain phase transitions (in the cases of NH_4I, NH_4NO_3 and $(NH_4)_2SO_4$).

At increased temperatures an additional peak appears in NH_4Cl, NH_4Br and $(NH_4)_2(COO)_2$, to the lower energy side of the rotational retardation peak.

The spectra of neutrons scattered in crystals containing water of crystallization also resemble one another. Three groups of peaks are observed in the spectra, associated with optical vibrations and rotational retardation of the water molecules.

ÉTUDE DE LA DYNAMIQUE DES GROUPES MOLÉCULAIRES NH_4^+ ET H_2O DANS LES CRISTAUX. Les auteurs indiquent les résultats qu'ils ont obtenus en mesurant la diffusion des neutrons thermiques par des cristaux contenant un ion ammonium (NH_4Cl, NH_4Br, NH_4I, NH_4F, NH_4NO_3, NH_4CNS, $(NH_4)_2SO_4$, $(NH_4)_2S_2O_8$, $(NH_4)_2Cr_2O_7$, $(NH_4)_2CO_3$) et de l'eau liée ($BaCl_2 \cdot 2H_2O$, $SrCl_2 \cdot 6H_2O$, $CuSO_4 \cdot 5H_2O$). Les travaux avaient pour objet d'étudier l'influence exercée par différents réseaux cristallins sur la dynamique des groupes mentionnés, et les liens existant entre les phénomènes de diffusion et les transitions de phase.

Malgré les différences de structure des substances étudiées, on obtient à la température de l'azote liquide des spectres analogues; en règle générale, ils accusent deux pics: le premier est situé dans la région des transferts d'énergie de 15 à 20 meV; le second dans celle de 35 à 70 meV, qui est associée aux oscillations de torsion des ions ammonium. L'intensité des pics dépend de la structure des substances et diminue avec l'augmentation de la température de l'échantillon.

On a constaté que, lors de certaines transitions de phase, l'intensité de la partie élastique du spectre se modifie brusquement (dans les cas de NH_4I, NH_4NO_3, $(NH_4)_2SO_4$).

Lorsque la température de NH_4Cl, NH_4Br et $(NH_4)_2(COO)_2$ augmente, il apparaît un pic supplémentaire, déplacé dans la direction des faibles énergies par rapport aux pics de rotation différée.

Les spectres des neutrons diffusés par des cristaux contenant de l'eau liée se ressemblent également. On y observe trois groupes de pics associés aux oscillations optiques et à la rotation différée des molécules d'eau.

ИССЛЕДОВАНИЕ ДИНАМИКИ МОЛЕКУЛЯРНЫХ ГРУПП NH_4 И H_2O В КРИСТАЛЛАХ. В докладе представлены результаты измерений рассеяния тепловых нейтронов на кристаллах, содержащих аммониевый ион (NH_4Cl, NH_4Br, NH_4J, NH_4F, NH_4NO_3, NH_4CNS, $(NH_4)_2SO_4$, $(NH_4)_2S_2O_8$, $(NH_4)_2Cr_2O_7$, $(NH_4)_2CO_3$) и кристаллизационную воду ($BaCl_2 \cdot 2H_2O$; $SrCl_2 \cdot 6H_2O$; $CuSO_4 \cdot 5H_2O$). Целью исследования было изучение влияния различных кристаллических решеток на динамику указанных групп, и связи процессов рассеяния с фазовыми переходами.

Несмотря на различие структур исследуемых веществ, получаемые спектры при температуре жидкого азота оказываются похожими друг на друга: как правило, наблюдаются

два пика — первый в области передач энергии 15—20 мэв, другой в области 35—70 мэв, связанный с торсионными колебаниями аммониевых ионов. Интенсивность пиков зависит от структуры исследуемых веществ и уменьшается с увеличением температуры образца.

Обнаружено, что интенсивность упругой части спектра при некоторых фазовых переходах совершает скачок (в случаях NH_4J, NH_4NO_3, $(NH_4)_2SO_4$).

С увеличением температуры в NH_4Cl, NH_4Br, $(NH_4)_2(COO)_2$ возникает дополнительный пик, сдвинутый в сторону меньших энергий от пика заторможенного вращения.

Спектры нейтронов, рассеянных на кристаллах, содержащих кристаллизационную воду, также схожи между собой. В спектрах наблюдаются три группы пиков, связанных с оптическими колебаниями и заторможенным вращением молекул воды.

ESTUDIO DE LA DINÁMICA DE LOS GRUPOS MOLECULARES NH_4^+ Y H_2O EN CRISTALES. En la memoria se presentan los resultados de las mediciones de la dispersión de neutrones térmicos en cristales que contienen el ion amonio (NH_4Cl, NH_4Br, NH_4I, NH_4F, NH_4NO_3, NH_4CNS, $(NH_4)_2SO_4$, $(NH_4)_2S_2O_8$, $(NH_4)_2Cr_2O_7$, $(NH_4)_2CO_3$) y agua de cristalización ($BaCl_2.2H_2O$; $SrCl_2.6H_2O$, $CuSO_4.5H_2O$). La finalidad de las investigaciones era estudiar la influencia ejercida por las distintas redes cristalinas sobre la dinámica de los mencionados grupos, y la relación existente entre los procesos de dispersión y las transiciones de fase.

A pesar de la distinta estructura de las sustancias estudiadas, los espectros obtenidos a la temperatura del nitrógeno líquido son análogos; por regla general, se observan dos picos: el primero en la región de transferencia energética de 15 a 20 meV, el segundo en la región correspondiente a 35-70 meV, que está relacionado con las oscilaciones de torsión de los iones amonio. La intensidad de los picos, que depende de la estructura de las sustancias estudiadas, disminuye al aumentar la temperatura de la muestra.

Se observó que la intensidad de la parte elástica del espectro, en ciertas transiciones de fase, presenta discontinuidades (en los casos del NH_4I, NH_4NO_3 y $(NH_4)_2SO_4$).

Al aumentar la temperatura del NH_4Cl, NH_4Br, $(NH_4)_2(COO)_2$, aparece otro pico, desplazado hacia las energías más bajas con respecto a los picos de rotación restringida.

Los espectros correspondientes a los neutrones dispersos en cristales que contienen agua de cristalización también presentan analogías. Se observaron tres grupos de picos, asociados a las oscilaciones ópticas y a la rotación restringida de las moléculas de agua.

I. ВВЕДЕНИЕ

Во многих химических соединениях атомы выступают в виде определенных структурных элементов — молекулярных групп, определяющих в значительной степени физические и химические свойства этих соединений. В кристаллах, образованных такими соединениями, можно ожидать существования низкоэнергетических ротационных колебаний молекулярных групп в дополнение к низкоэнергетическим трансляционным колебаниям, имеющим место в простых кристаллах.

Исследование динамических свойств молекулярных групп представляет собой значительный интерес и проводится различными способами — оптическими методами, методами ядерного и электронного резонансов, методами рассеяния рентгеновских лучей и нейтронов.

Метод нейтронной спектроскопии особенно пригоден для исследования свойств водородосодержащих групп в соединениях, содержащих водород только в этих группах. Спектр рассеянных нейтронов в таких случаях содержит информацию о движении протонных групп в условиях окружения другими атомами или группами.

Существует целый ряд легко доступных соединений, содержащих аммониевый ион или кристаллизационную воду. Это дает возможность систематически исследовать движение этих групп в различных кристаллических структурах. В настоящей работе сообщаются данные такого исследования,

выполненного для веществ, содержащих группу NH_4^+, т.е. NH_4F; NH_4Br; NH_4Cl; NH_4J; NH_4CNS; $(NH_4)_2S_2O_8$; $(NH_4)_2SO_4$; $(NH_4)_2CO_3$; $(NH_4)_2(COO)_2$, а также $BaCl_2 \cdot 2H_2O$; $SrCl_2 \cdot 6H_2O$; $CuSO_4 \cdot 5H_2O$, содержащих кристаллизационную воду, и проводится обсуждение полученных результатов, которое является пока предварительным.

II. ТЕХНИКА ЭКСПЕРИМЕНТА

Измерения проводились на нейтронном спектрометре по времени пролета с фильтром перед детектором [1], установленном при импульсном быстром реакторе ОИЯИ в Дубне [2]. Полученный импульс замедленных нейтронов имеет ширину на половине высоты 80 мксек. Нейтроны, выходящие из замедлителя, попадают на образец, пролетая базу $L_1 = 20$ м. Под углом 90° относительно падающего пучка установлен бериллиевый фильтр, охлаждаемый до температуры жидкого азота. Профильтрованные нейтроны регистрируются сцинтилляционным счетчиком. Расстояние образец-детектор L_2 равно примерно 0,7 м.

Импульсы детектора передаются на многоканальный временной анализатор.

Средняя энергия $\overline{E'}$ рассеянных нейтронов ~3,7 мэв определяется полосой пропускания Be-фильтра. Энергию ϵ, потерянную нейтроном при рассеянии, можно определить из формулы:

$$T = \overline{\tau} + \frac{\alpha L_1}{\sqrt{\epsilon + \overline{E'}}} + \frac{\alpha L_2}{\sqrt{\overline{E'}}},$$

где T – время регистрации рассеянных нейтронов, отсчитываемое от середины вспышки быстрых нейтронов,

$\overline{\tau}$ – среднее время жизни нейтронов в замедлителе.

Исследуемые вещества в виде кристаллических порошков помещались в плоскопараллельные герметические алюминиевые формы с тонкими стенками (~0,5 мм) размером 180×200 мм^2. Толщина слоя веществ была примерно 1 мм, что соответствует пропусканию ~85%.

Измерения ниже комнатной температуры проводились в криостате с большой теплоемкостью, охлаждаемом жидким азотом. Контроль температуры образца производился с помощью термосопротивления с точностью ±2°C. Для измерений при температурах выше комнатной, образец подогревался электроплиткой.

Поток нейтронов, падающих на образец, измерялся по методу времени пролета базы L_1 замедлитель–образец с помощью тонкого борного счетчика, установленного перед образцом.

Результаты измерений представлены ниже в двух видах:

1. В виде временного спектра рассеянных нейтронов, исправленного на просчеты анализатора и фон, но не нормированного к постоянному значению потока падающих на образец нейтронов. Поправка на просчеты не превышала 20%. Фон составлял ~5% от эффекта.

2. В виде частичного спектра колебаний протонов $p_H(\omega)$, т.е. произведения обычного спектра частот кристалла $g(\omega)$ и квадрата амплитуды колебаний протонов $|\xi_H(\omega)|^2$:

$$p_H(\omega) = g(\omega)\,|\xi_H(\omega)|^2,$$

вычисленного в однофононном приближении:

$$p_H(\omega) \approx \sqrt{\frac{E_0}{E'}}\,\frac{1}{\kappa^2}\,\epsilon(1 - e^{-\frac{\epsilon}{T}})\,e^{\gamma_H \kappa^2}\,\frac{d^2\sigma^{inc}}{d\Omega\, d\lambda_0}\,\frac{1}{n(\lambda_0)}.$$

В последней формуле:

E_0, E' – энергия падающего и средняя энергия рассеянного нейтрона,

T – температура образца,

$e^{\gamma_H \kappa^2}$ – фактор Дебая-Валера (принимался равным единице),

$\frac{d^2\sigma^{inc}}{d\Omega\, d\lambda_0}$ – дифференциальное сечение рассеяния нейтронов с длиной волны λ_0,

$n(\lambda_0)$ – поток падающих на образец нейтронов на единичный интервал длины волны.

Частичный спектр частот $p_H(\omega)$ использовался для определения значений энергии и относительных интенсивностей пиков, соответствующих энергетическим уровням кристалла, не искаженных формой спектра падающего на образец пучка нейтронов.

III. РЕЗУЛЬТАТЫ ИЗМЕРЕНИЙ И ИХ ОБСУЖДЕНИЕ

A. Соединения, содержащие аммониевые группы

A-1. Галогены аммония

Простейшими соединениями, содержащими аммониевые группы, являются галогены аммония, – аммоний иодистый, бромистый и хлористый. Они выступают в разных кристаллографических фазах [3] (табл.1). В фазе I аммониевые ионы размещены на поверхности куба, созданного ионами галогенов, а в фазах II и III – в его центре. Нейтронографические исследования [4,5] указывают, что в фазе III аммониевые пирамиды размещены в кристалле вполне упорядоченно: либо параллельно друг другу (тетрагональная структура), либо антипараллельно (структура типа CsCl), тогда как в фазе II размещение их хаотическое. Таким образом, непосредственно была подтверждена гипотеза Френкеля [6], согласно которой аномалия типа λ, наблюдаемая в поведении теплоемкости в галогенах аммония при переходе между II и III фазами, связана с нарушением упорядоченности ориентации ионов NH_4^+.

Таблица 1

ТЕМПЕРАТУРЫ ФАЗОВЫХ ПЕРЕХОДОВ В ГАЛОГЕНАХ АММОНИЯ
(при атмосферном давлении)

Фазы Вещество	I → II (NaCl) (CsCl)	II → III (CsCl) (тетраг)	II → III (CsCl) (CsCl)	III (тетраг) (CsCl)
NH_2Cl	458° K	...	243° K	...
NH_4Br	411° K	235° K	...	100° K
NH_4J	254° K	227° K	...	...

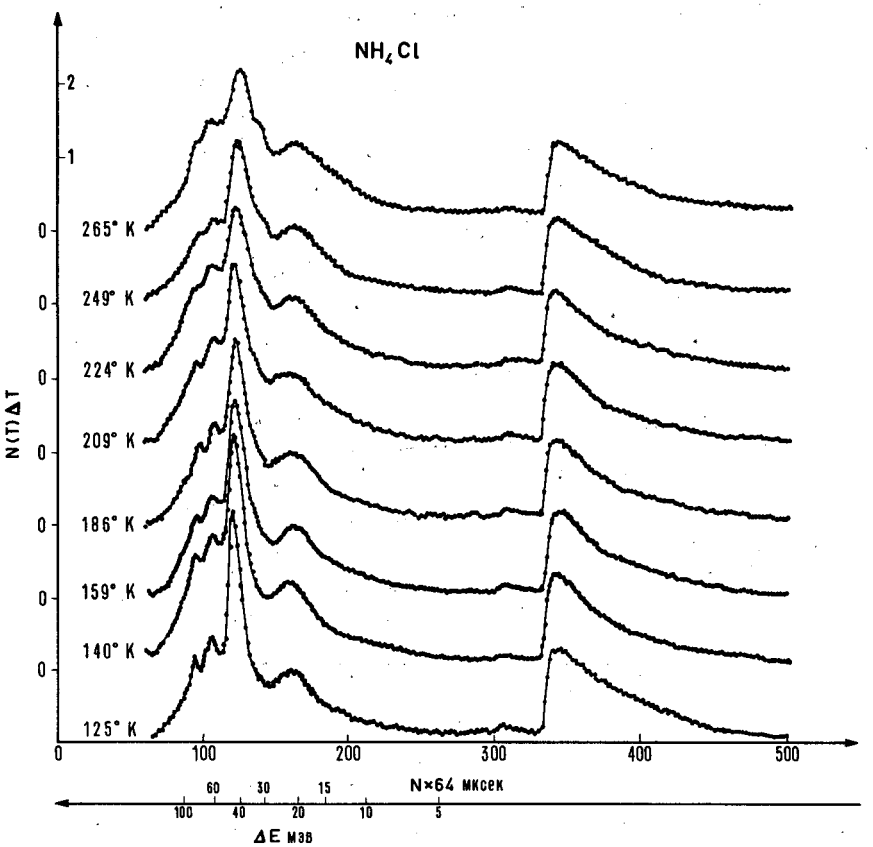

Рис.1

Спектр нейтронов, рассеянных на NH_4Cl при различных температурах образца.

Теория фазовых переходов в этих соединениях была создана Нагамией [7]. Он указал, что упорядочение ионов NH_4^+ определяется взаимодействием октупольных моментов. На основе этой теории можно вычислить высоту потенциального барьера V, зная частоту ν_T торсионных колебаний ионов.

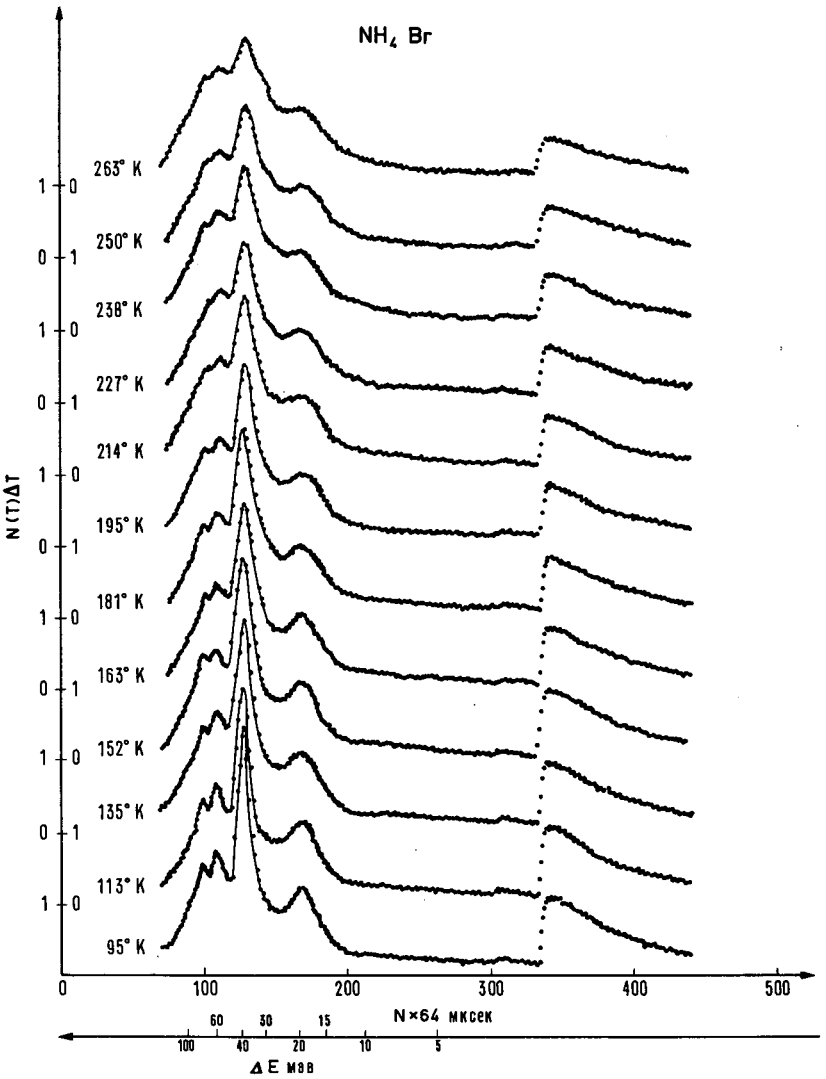

Рис.2

Спектр нейтронов, рассеянных на NH_4Br при различных температурах образца.

Частоты ν_T могут быть определены косвенным путем с помощью инфракрасной [8,9] и рамановской [10] спектроскопии, а непосредственно — методом неупругого рассеяния нейтронов [11,12,13]. Динамика аммониевых групп в галогенах исследовалась методом протонного резонанса [14—16] и путем измерения полных нейтронных сечений [17]. Все вышеприведенные методы указывают на сильно заторможенный характер вращений ионов NH_4^+ в фазах II и III и относительно свободной в фазе I.

Спектры рассеяния нейтронов на NH_4J, NH_4Cl, NH_4Br, полученные в данной работе в диапазоне температур от температуры жидкого азота до ком-

натной и представленные на рис. 1–3, подтверждают эту точку зрения. Спектры для всех соединений при низких температурах образцов очень похожи друг на друга: в каждом наблюдаются низкоэнергетические пики при энергиях $\epsilon = 22{,}2$ мэв, $\epsilon = 20$ мэв, $\epsilon = 18$ мэв соответственно для Cl, Br и J; далее при энергиях $\epsilon = 49{,}2$ мэв; 42,5 мэв; 36,5 мэв; видны узкие интенсивные пики заторможенных вращений, а также ряд пиков при больших энергиях.

Форма спектров, как и энергия пиков, довольно хорошо согласуется с данными, полученными др. авторами [11,12,13]. Форма вращательных пиков с большой точностью отражает вид кривой разрешающей способности установки, что указывает на малую истинную ширину этих линий. С увеличением температуры интенсивность вращательных пиков постепенно падает, одновременно уменьшается и интенсивность упругого рассеяния, температурный ход которого показан на рис.4.

Общий характер спектров не меняется при переходах через точки λ. При увеличении температуры форма вращательных пиков несколько меняется: со стороны меньших энергий появляются изломы, растущие с температурой; они указывают на присутствие неразрешенных дополнительных пиков с энергией, меньшей основного пика на 4–7 мэв. Это хорошо видно в спектрах для NH_4Cl и NH_4Br (рис.1–2). Эти пики можно интерпретировать как переходы между возбужденными уровнями ионов NH_4^+, колеблющихся в потенциальном поле с уже заметным ангармонизмом.

Структура NH_4J при температуре -19°C из структуры типа CsCl превращается в кубическую – типа NaCl. При этом переходе спектр рассеянных нейтронов меняется: в неупругой части исчезает пик заторможенного вращения, так что при более высоких температурах эта часть имеет вид широкого плавного распределения; интенсивность же упругой части спектра скачкообразно уменьшается (рис.4). Подобные скачкообразные изменения в полном сечении нейтронов наблюдались Ращем и др. [17]. Эти факты укзывают на значительное увеличение свободы вращения при переходе в кубическую фазу.

Спектр нейтронов, рассеянных на NH_4F (рис.5), имеет особенности, отличающие его от спектров других галогенов аммония. Особенности эти обусловлены структурой соединения NH_4F, имеющего решетку типа вюрцита и наличием сильной водородной связи N–H–F между всеми ионами NH_4^+ и ионами F.

Пики акустического и заторможенного вращения проявляются при энергиях больших по сравнению с другими галогенами аммония ($\epsilon = 31{,}5$ мэв, $\epsilon = 72$ мэв). Кроме этих пиков наблюдается низкоэнергетическая полоса с максимумом при энергии 8,5 мэв. Так как подобные полосы имеют место в нейтронных спектрах веществ с водородными связями типа H–F [18], то можно предположить, что низкоэнергетическая полоса в спектре NH_4F объясняется межмолекулярными колебаниями ионов с водородной связью.

Более слабая температурная зависимость интенсивности как пиков, так и упругой части в спектрах NH_4F указывает на большую величину барьера заторможенного вращения ионов NH_4^+ в этом соединении по сравнению с остальными галогенами аммония.

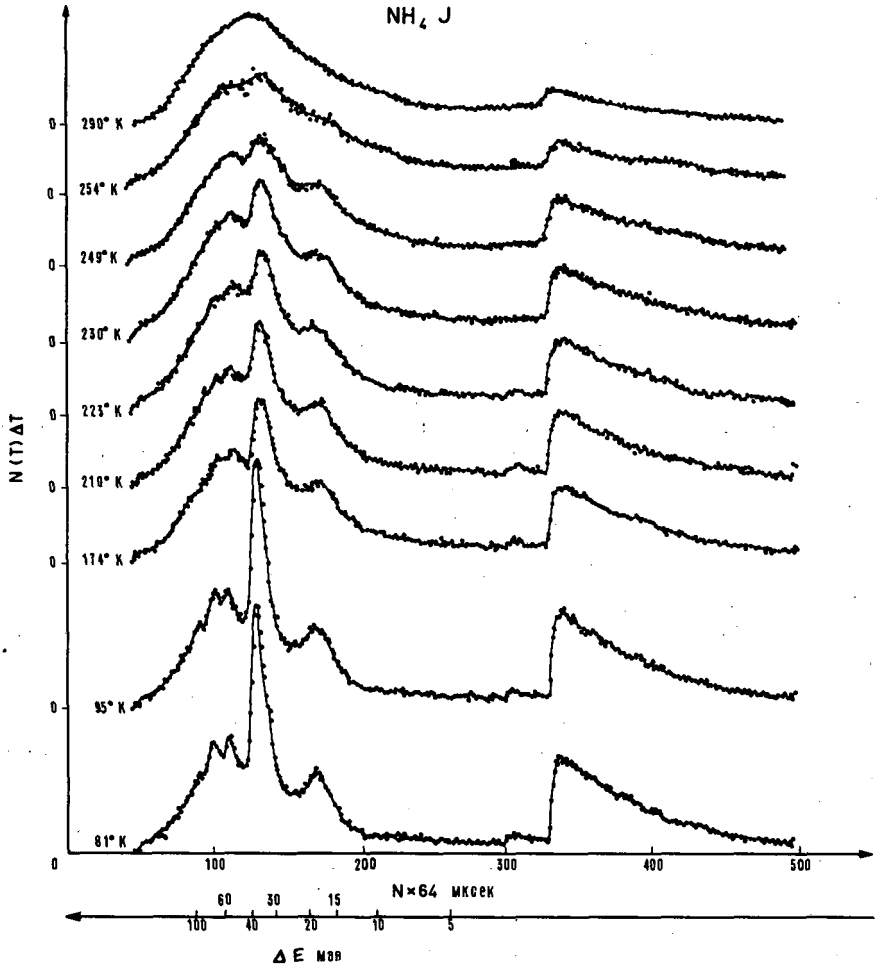

Рис.3

а) спектр нейтронов, рассеянных на NH_4J при различных температурах образца;

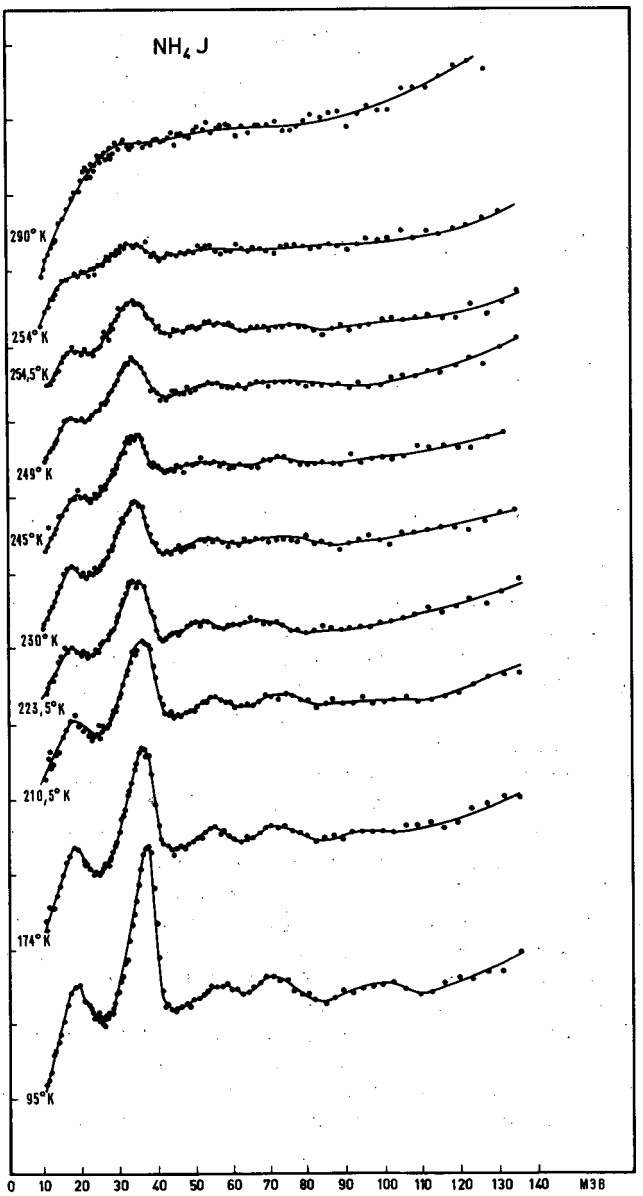

Рис.3

б) спектр частот $p_H(\omega)$ для NH_4J при различных температурах образца.

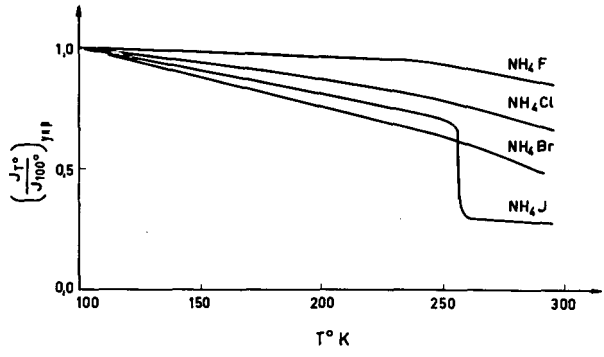

Рис.4

Зависимость интенсивности упругой части спектра от температуры образцов NH_4F, NH_4Cl, NH_4Br, NH_4J.

A-2. NH_4NO_3

Азотнокислый аммоний выступает в пяти кристаллографических конфигурациях (табл.2). Особенности типа λ выступают при температурах -160° и ~60° C [19].

Результаты рентгенографических исследований [20] указывают на свободное вращение иона NO_3 в кубической фазе и заторможенное в фазах низшей симметрии. Относительно мало изучено поведение аммониевого иона в NH_4NO_3. Предполагается [21], что переход из гексагональной фазы в тетрагональную (T = -18° C), а также λ—переход при -60° C связан с поведением именно этого иона.

Нейтронный спектр этого соединения показан на рис.6 а, в. При низких температурах кроме пика при энергии $\epsilon = 24{,}5$ мэв наблюдаются два близко расположенных оптических пика различных интенсивностей при энергиях $\epsilon = 42$ мэв и $\epsilon = 50$ мэв. Оптические пики остаются при переходе через λ-точки при -160° и -60° C и исчезают в диапазоне от -20° до 0° C, т.е. в области перехода от гексагональной фазы к тетрагональной.

Неупругая часть спектра нейтронов, рассеянных на образце в фазах с IV по I, имеет плавный вид. В температурном поведении упругой части наблюдается скачкообразное изменение интенсивности при переходах между фазами IV—III и II—I. При переходе в кубическую структуру (фаза I) создаются условия для одновременного свободного вращения обеих молекулярных групп. Об этом свидетельствует наблюдаемое скачкообразное уменьшение интенсивности упругой части спектра при переходе в фазу I (рис.7).

A-3. $(NH_4)_2SO_4$.

Сульфат аммония имеет ромбическую слоистую решетку с параметрами a = 5,94 Å, b = 10,60 Å, c = 7,70 Å. Элементарная ячейка содержит 8 аммониевых ионов, расположенных в двух неэквивалентных положениях. Расстояние между атомами кислорода и аммониевыми ионами меняется от

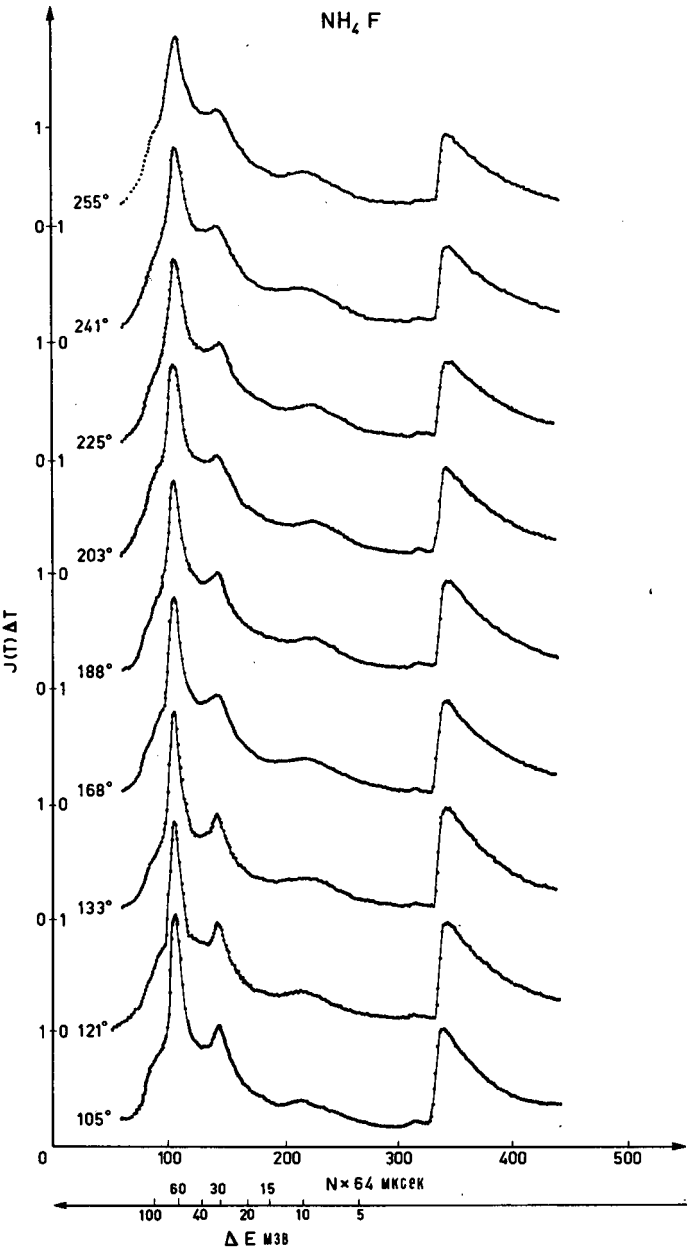

Рис.5

Спектр нейтронов, рассеянных на NH_4F при различных температурах образца (в °К).

Таблица 2

ТЕМПЕРАТУРЫ ФАЗОВЫХ ПЕРЕХОДОВ ДЛЯ NH_4NO_3

Фаза	I	II	III	IV	V
Структура	кубическая	тетра-гональная	орто-ромбическая	орто-ромбическая	гекса-гональная
Температура перехода		125,2°C	84,2°C	32,3°C	-18°C

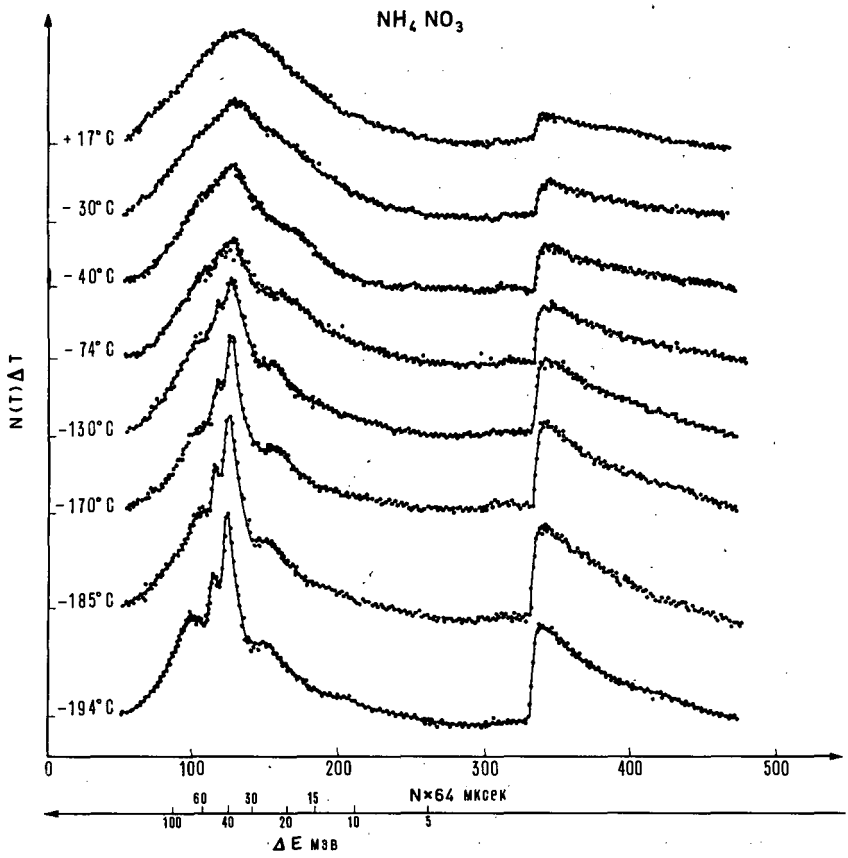

Рис.6

а) спектр нейтронов, рассеянных на NH_4NO_3 при температурах образца ниже комнатной;

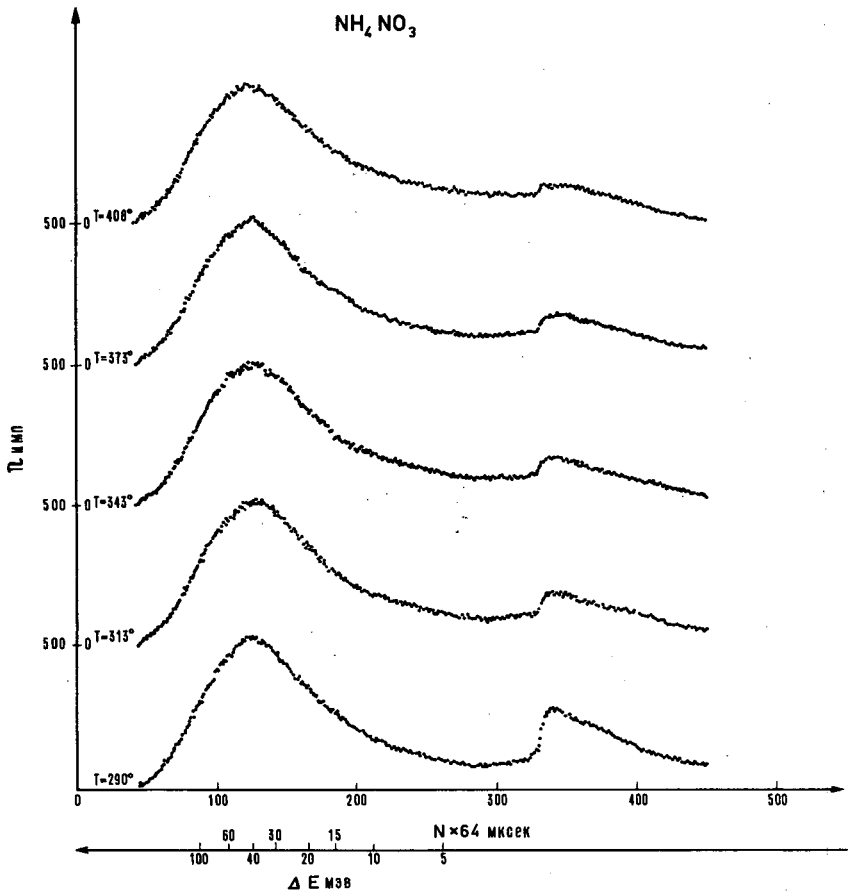

Рис. 6

б) спектр нейтронов, рассеянных на NH_4NO_3 при температурах образца выше комнатной (в °К).

2,66 Å до 3,60 Å. При температуре примерно -50° С соль становится сегнетоэлектриком, и это состояние объясняется существованием водородной связи типа N—H—O [22]. В районе этой температуры обнаружены аномальные поведения теплоемкости [23], диэлектрической проницаемости [24, 25] и инфракрасного поглощения [26].

Результаты наших исследований представлены на рис. 8. В области передач энергии $\epsilon = 50$ мэв виден широкий интенсивный пик нерегулярной формы, состоящий, по всей вероятности, из неразрешенных близко расположенных пиков. Эти пики могут возникнуть в результате неэквивалентного положения аммониевых ионов в решетке. Энергия пика мало отличается от наблюдаемой в инфракрасном спектре линии с частотой 447 $см^{-1}$ [28].

С увеличением температуры этот пик уменьшается и уширяется, постепенно сливаясь с подложкой. В районе температуры фазового перехода интенсивность упругой части спектра быстро, но не скачкообразно уменьшается.

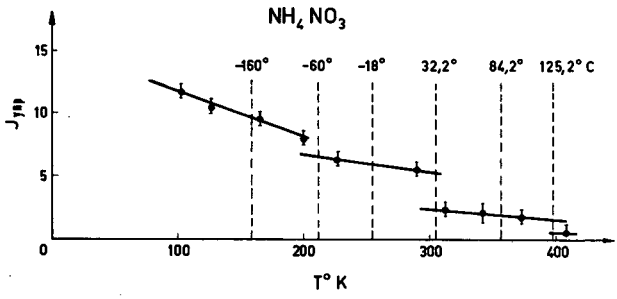

Рис.7

Зависимость интенсивности упругой части спектра нейтронов, рассеянных на NH_4NO_3, от температуры образцов.

Таблица 3

ЭНЕРГИЯ ПИКОВ (в мэв) В СПЕКТРАХ ЧАСТОТ АММОНИЕВЫХ СОЛЕЙ ПРИ ТЕМПЕРАТУРЕ ≈ 100° К

Вещество	Энергия наблюдаемых пиков, мэв				
	*				
NH_4Cl	22,2	49,2	71	96	112
NH_4Br	20	42,5	67	88	
NH_4J	18	36,5	56	69	98
NH_4F	31,5	72			
NH_4NO_3	24,5	42	50	62	78
NH_4CNS	24,5	42,5			
$(NH_4)_2SO_4$	29	49,5			
$(NH_4)_2S_2O_8$	19	35,5	52		
$(NH_4)_2Cr_2O_7$	27,5	39,5			
$(NH_4)_2CO_3$	26,5	51,5–56,5			
$(NH_4)_2(COO)_2$	26	59	83		

* пики торсионных колебаний.

A-4. NH_4CNS

Аммоний роданистый имеет моноклинную слоистую структуру с четырьмя молекулами в элементарной ячейке [29]. Вокруг каждого иона NH_4^+ расположены два атома азота, связанные с ним водордными связями N–H–F, и два атома серы с ионными связями. Данные о динамике ионов NH_4^+ в этом соединении известны из измерений полных сечений Раша и др. [17] и протонного резонанса [27, 16].

Сравнивая величину наклона линейной части зависимости полного сечения рассеяния нейтронов от их длины волны λ при комнатной температуре образца с аналогичной величиной для других аммониевых солей, Раш и др.

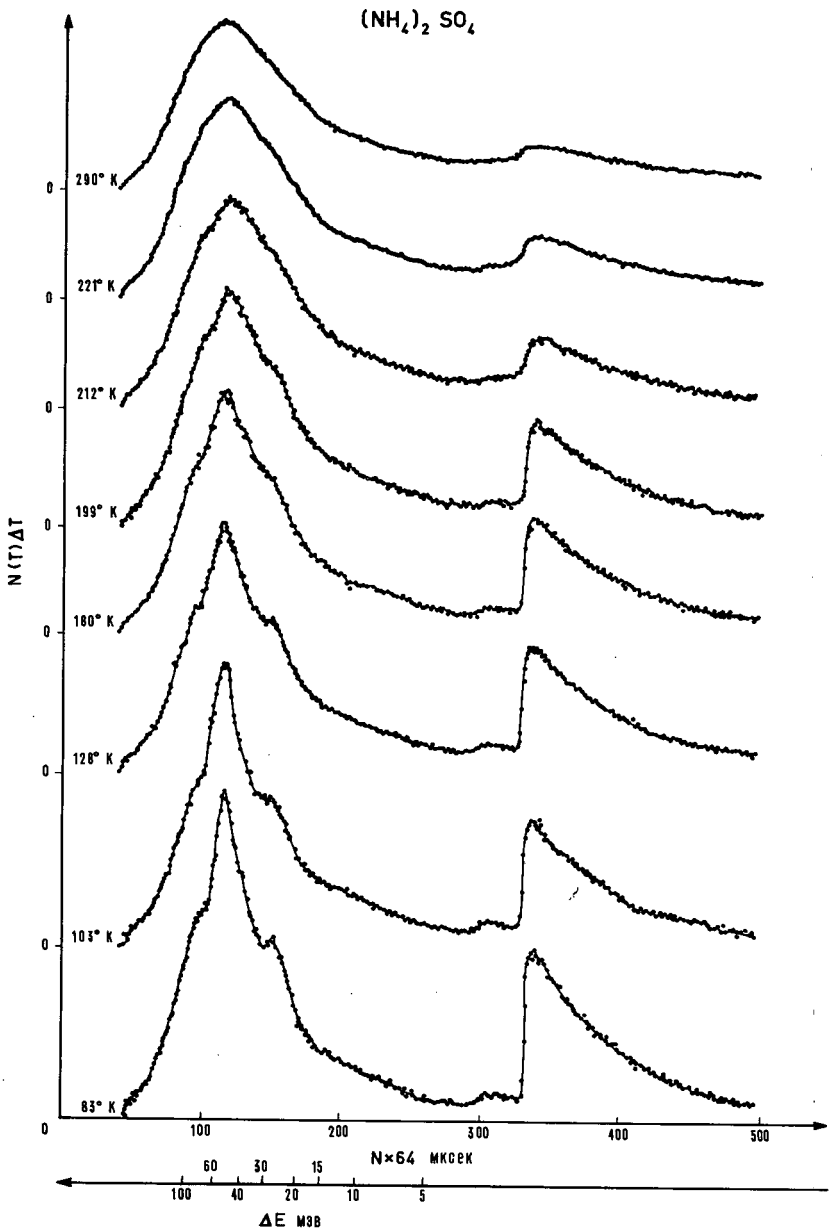

Рис. 8

Спектр нейтронов, рассеянных на $(NH_4)_2SO_4$ при различных температурах (в °K).

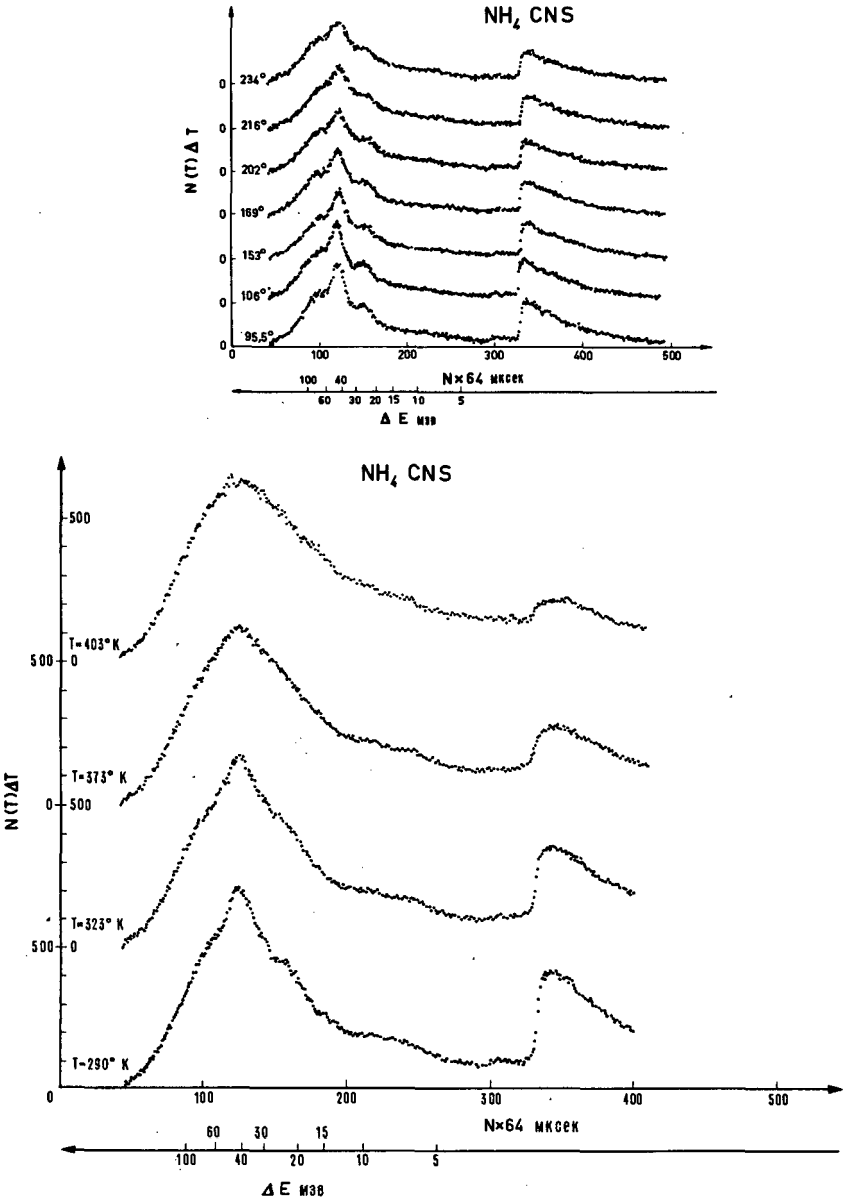

Рис.9

а) спектр нейтронов, рассеянных на NH_4CNS при температурах образца ниже комнатной (°K);
б) спектр нейтронов, рассеянных на NH_4CNS при температурах образца выше комнатной.

[17] высказали предположение, что динамическое поведение группы NH_4^+ в роданистом и бромистом аммонии должно быть похожим.

Наблюдаемая нами энергия пика торсионных колебаний иона NH_4^+ в NH_4CNS (рис.9 а, в) действительно близка к величине энергии, полученной для основного пика NH_4Br. Однако форма пика для NH_4CNS имеет несколько иной вид, а его ширина значительно больше ширины пика в NH_4Br. Это различие может быть связано либо нарушением тетраэдрической симметрии группы NH_4^+ ввиду несимметричной водородной связи, либо влиянием колебаний группы CNS^-. Интересно заметить, что метод протонного резонанса также дает для NH_4CNS и NH_4Br близкие результаты для значений ширины линии и температуры, при которой она скачкообразно меняется [16, 27].

A-5. $(NH_4)_2S_2O_8$ и $(NH_4)_2Cr_2O_7$

Кристаллографическая структура этих соединений, как и результаты, полученные методом протонного резонанса, свидетельствуют об относительно свободном вращении аммониевых групп в этих веществах. Оба вещества имеют моноклинную структуру с большими размерами элементарной ячейки (~8 Å). Геометрия решеток определяется, главным образом, размерами разветленных анионных групп, создающих ряд "ловушек", в которых помещены группы NH_4^+.

Исследования структуры $(NH_4)_2S_2O_8$ [30] указывают, что 12 атомов кислорода размещены почти симметрично на поверхности шара с радиусом ~3,18 Å вокруг каждого иона NH_4^+. Благодаря этому ионы NH_4^+ находятся в силовом поле высокой симметрии, вследствие чего их движение должно быть слабо заторможенным. Эту точку зрения подтверждают данные протонного резонанса [16, 31], указывающие на величину барьера тормозного вращения меньшую, чем 700 кал/моль. На барьер такой же величины указывают измерения полных нейтронных сечений [17].

Спектры нейтронов, неупруго рассеянных на образце, при температурах 348° К и комнатной по данным Браевича и др. [32] не имеют пиков, характерных для заторможенного вращения.

Однако в полученных нами спектрах нейтронов, рассеянных на образце при низкой температуре (рис.10), довольно четко виден пик при энергии $\epsilon = 35{,}5$ мэв. Как нам известно, частота этого пика ниже всех наблюдаемых частот в аммониевых солях. Изменения формы неупругой части спектра и интенсивности упругой, возникающие при увеличении температуры образца, указывают на происходящее увеличение свободы вращения атомов. Пик заторможенного вращения исчезает при температуре 250° К. При высоких температурах форма спектра совпадает с формой, полученной Браевичем [32].

Аналогичные результаты получены для $(NH_4)_2Cr_2O_7$ (рис.11). Пик заторможенного вращения, как и в случае $(NH_4)_2S_2O_8$, накладывается на широкую довольно интенсивную подложку. Его энергия выше чем у $(NH_4)_2S_2O_8$, и равна $\epsilon \approx 40$ мэв, что указывает на высоту барьера, ближе подходящую к оценке в 1000 кал/моль, данной Морфи [31], нежели к данным Шафера — 700 кал/моль [16]. Пик заторможенного вращения исчезает в области температуры 230° К. При более высоких температурах неупругая

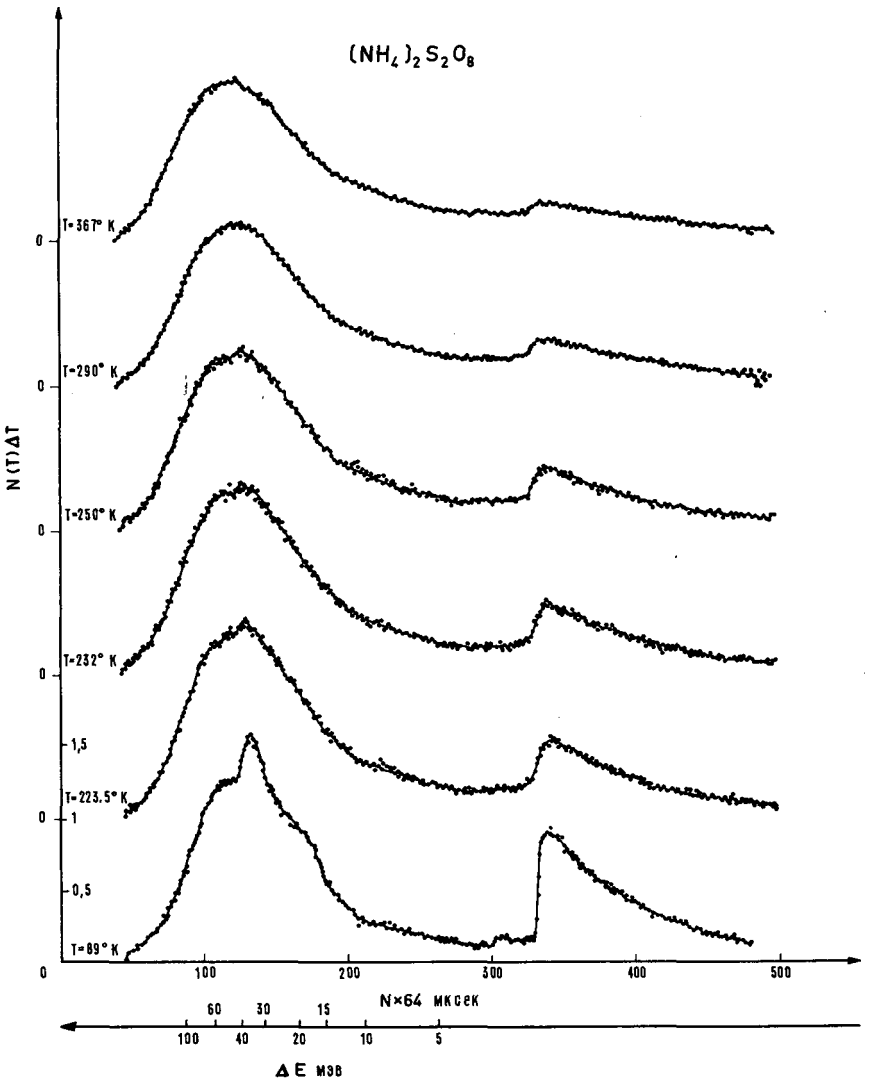

Рис.10

Спектр нейтронов, рассеянных на $(NH_4)_2S_2O_8$ при различных температурах образца.

часть спектра имеет вид широкого распределения, интенсивность же упругой части быстро падает, так что при температуре 350°С становится почти незаметной.

А-6. $(NH_4)_2CO_3$ и $(NH_4)_2(COO)_2$

В настоящее время имеется мало данных о структуре и динамике аммониевых групп в указанных соединениях.

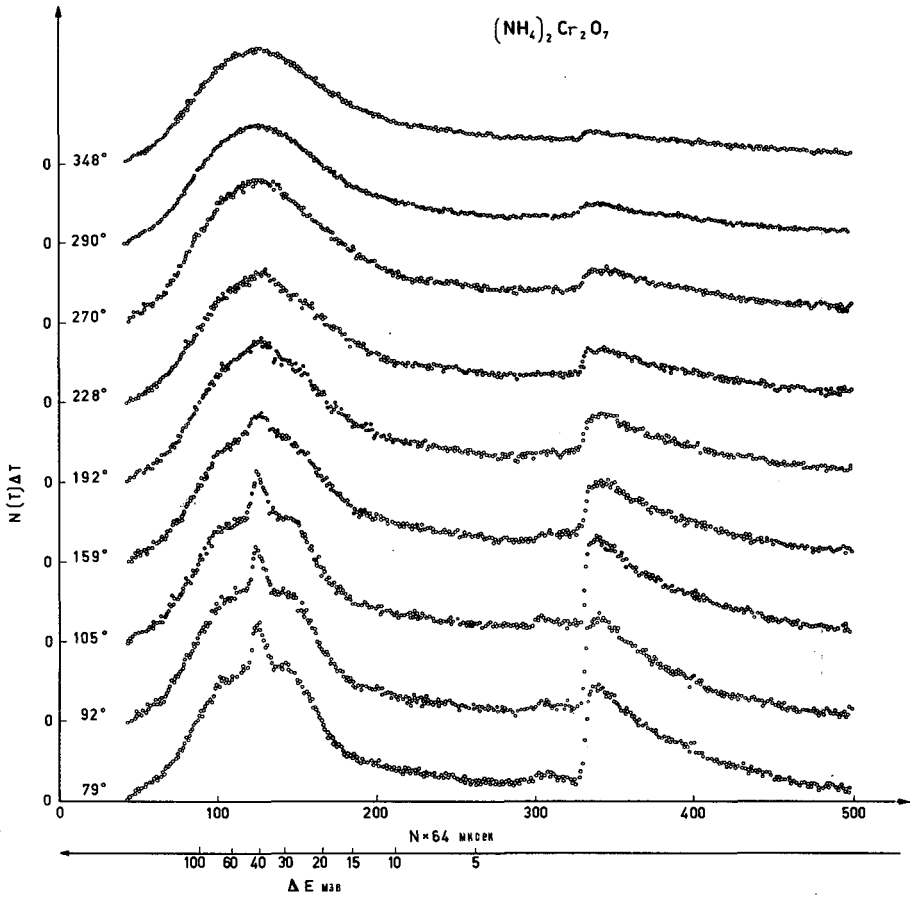

Рис.11

Спектр нейтронов, рассеянных на $(NH_4)_2Cr_2O_7$ при различных температурах образца (в °К).

Результаты наших измерений, представленные на рис.12, 13, указывают на сильно заторможенные вращения ионов NH_4^+ в этих соединениях в широком диапазоне температур. Пики заторможенных вращений выступают при высоких энергиях $\epsilon = 51{,}5-56{,}5$ мэв для $(NH_4)_2CO_3$ и $\epsilon = 59$ мэв для $(NH_4)_2(COO)_2$. Их интенсивность, как и интенсивность упругой части, мало меняется с температурой.

В спектре нейтронов, рассеянных на $(NH_4)_2(COO)_2$, с повышением температуры наблюдается асимметрия пика заторможенного вращения, как и в случаях с NH_4Cl и NH_4Br. С другой стороны, пик заторможенного вращения для $(NH_4)_2CO_3$ имеет явно выраженную тонкую структуру во всем исследуемом диапазоне температур. Относительные положения ($\Delta E = 5$ мэв) и интенсивность пиков тонкой структуры не меняются с температурой.

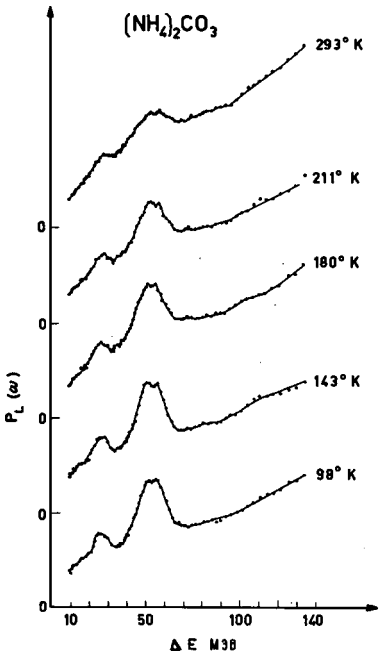

Рис.12

Спектр частот $p_H(\omega)$ для $(NH_4)_2CO_3$ при различных температурах образца.

В. Соединения, содержащие группу H_2O

Вторая исследованная нами молекулярная группа H_2O выступает в соединениях, как в связанном, так и в свободном состояниях. Динамика молекул H_2O в ее собственном окружении исследовалась разными методами, в том числе и нейтронными [33—35]. Полученные нами спектры нейтронов, неупруго рассеянных на льде и воде (рис.14), в общих чертах совпадают с ранее полученными результатами [33—35].

В спектре льда видны три характерные полосы, а именно: интенсивный пик с максимумом при $\epsilon = 78$ мэв, связанный с заторможенным вращением молекул H_2O в поле соседей; далее полоса нерегулярной формы ($\epsilon = 25—35$ мэв), определяемая оптическими ветвями трансляционных движений молекул и,наконец, широкая интенсивная полоса с максимумом при 8 мэв, т.е. в области проявления низкоэнергетических оптических и акустических колебаний решетки и водородной связи. При переходе через точку плавления упругая часть спектра скачкообразно уменьшается — появляется уширение, связанное с диффузионным движением молекул воды. В неупругой части спектра пик перемещается в сторону меньших энергий (примерно на 15 мэв) и значительно уширяется. Спектр становится более сглаженным, но все-таки содержит особенности, характерные для спектра льда, что отражает квазикристаллическую структуру воды.

Нейтронный спектр для льда дает характерную картину динамики групп H_2O в относительно сложной кристаллической сруктуре.

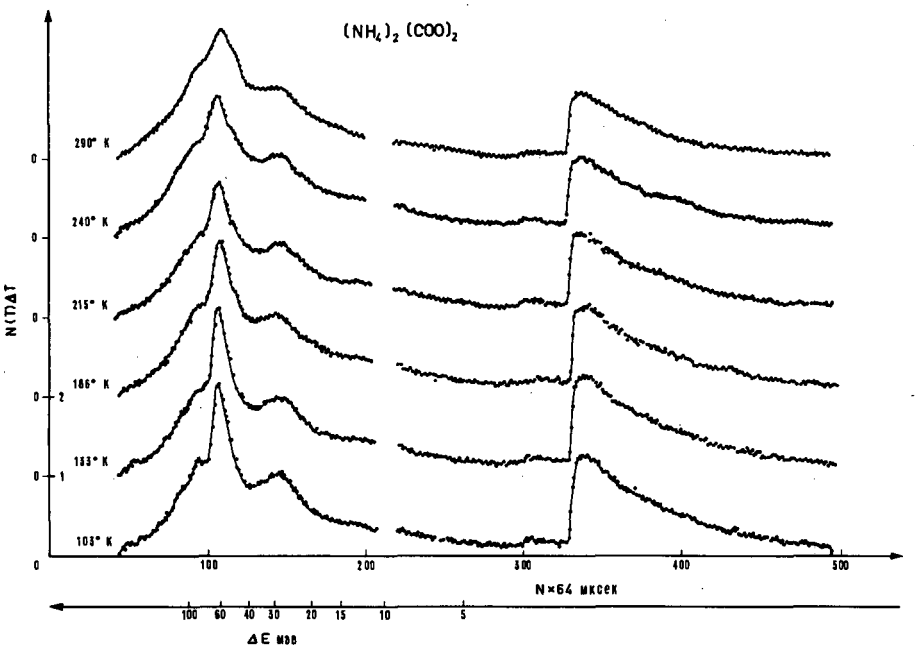

Рис.13

Спектр нейтронов, рассеянных на $(NH_4)_2(COO)_2$ при различных температурах образца.

Очевидно, подобные картины должны наблюдаться и в случае кристаллогидратов, так как внутренняя структура H_2O в них, особенно угол H—O—H, мало меняется, что следует из нейтронографических исследований [36—37]. Это обстоятельство подтверждают также спектроскопические исследования кристаллогидратов, дающие похожие, а в некоторых случаях более простые спектры, чем для льда [38, 39].

Измерения для кристаллогидратов $BaCl_2 \cdot 2H_2O$; $SrCl_2 \cdot 6H_2O$; $CuSO_4 \cdot 5H_2O$ и др. проводились аналогично исследованиям аммониевых солей в интервале температур от жидкого азота до комнатной. Ввиду того, что во всех случаях не наблюдалось температурной зависимости в спектрах рассеянных нейтронов, приводятся результаты для самой низкой температуры, мало искаженные многофононными процессами.

B-1. $BaCl_2 \cdot 2H_2O$

Кристаллы $BaCl_2 \cdot 2H_2O$ имеют моноклинную структуру с 4 молекулами в элементарной ячейке [40, 41]. В ячейках удается выделить по две группы ионов Cl и H_2O и одну группу Ba. Кристалл состоит из слоев параллельных плоскостей a c, связанных между собой сильными взаимодействиями.

Молекулы воды первой группы $(H_2O)_I$ связаны водородными связями с атомами Cl_I, а вода второй группы $(H_2O)_{II}$ — с атомами хлора своего слоя Cl_{II} и с атомами кислорода молекул воды соседнего слоя $(H_2O)_I$. Неэквивалентно размещенные молекулы воды I и II групп имеют разные частоты заторможенного вращения как вокруг осей a, так и вокруг c, на что ука-

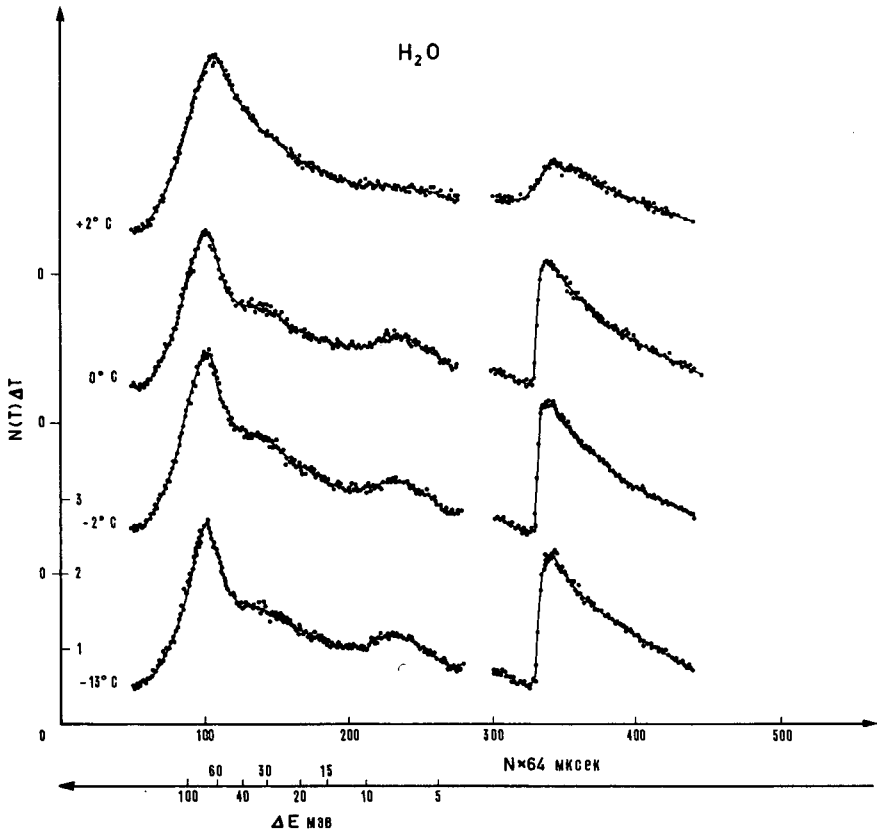

Рис.14

Спектр нейтронов, рассеянных на льду и воде.

зывает инфракрасный спектр [42]. Обе частоты вращений молекул $(H_2O)_{II}$ больше частот $(H_2O)_I$. Это положение отражается и в нейтронном спектре (рис.15), в котором область, соответствующая заторможенным вращениям, обладает четко выраженной тонкой структурой.

Пики 2 и 4 с энергиями $\epsilon = 75$ мэв и $\epsilon = 32$ мэв соответствуют вращениям $(H_2O)_I$, вокруг осей a и c, тогда как изломы 1 и 3 при $\epsilon = 85$ мэв и $\epsilon = 68$ мэв связаны с заторможенным вращением воды второй группы вокруг обеих осей. Двойной пик 5—6 с максимумами при $\epsilon = 29$ мэв и $\epsilon = 25$ мэв связан с трансляционным движением молекул воды относительно соседних ионов. Кроме этих пиков наблюдаются переходы в полосе проявления водородных связей 7,8 при $\epsilon = 11$ мэв и $\epsilon = 6$ мэв. Полученные результаты согласуются с результатами Боутина и др. [43], проведенными для комнатной температуры.

B-2. $SrCl_2 \cdot 6H_2O$

Кристаллы $SrCl_2 \cdot 6H_2O$ образуют ромбоэдрическую систему. Элементарная ячейка содержит одну молекулу. По Енсену [44] атомы составляют

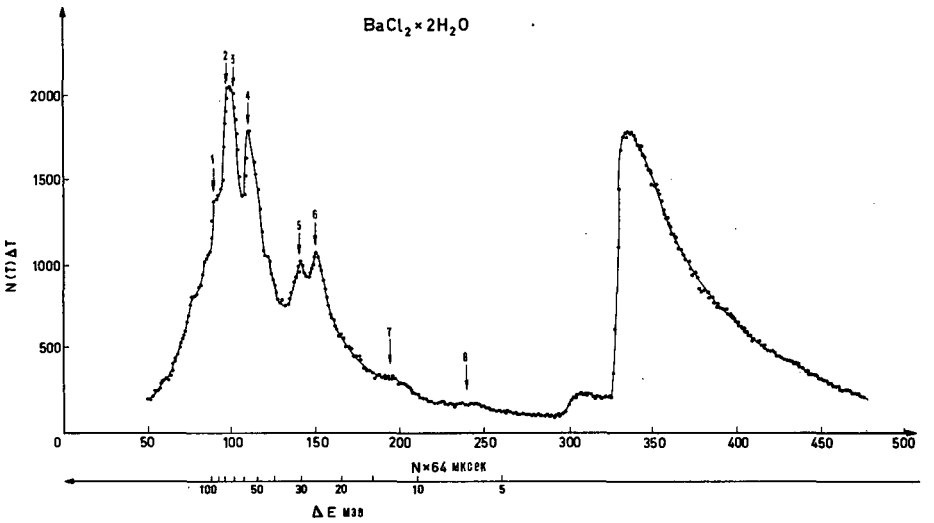

Рис.15

Спектр нейтронов, рассеянных на $BaCl_2 \cdot 2H_2O$ при температуре жидкого азота.

столб Sr—Sr—Sr—..., каждый член которого окружен 9 молекулами H_2O, выступающими в 2-х группах: "плоского" типа (3 атома кислорода O_I и ион Sr находятся в одной плоскости) и тетраэдрического типа с атомом Sr в одном из узлов. Молекулы воды обоих типов образуют водородные связи с соседними атомами хлора, расположенными на расстояниях $O_I - Cl = 3{,}17$ Å и $O_{II} - Cl = 3{,}10$ Å. Существование двух групп молекул воды приводит, как и в случае $BaCl_2 \cdot 2H_2O$, к тонкой структуре спектра рассеянных нейтронов (рис.16).

Полоса заторможенного вращения содержит как минимум 5 пиков: хорошо разрешены пик 1 при $\epsilon = 87$ мэв и четыре пика (2—5) в диапазоне энергий $\epsilon = 51 - 69$ мэв. Вторую группу пиков 7,8 видно в области энергии $\epsilon = 20 - 40$ мэв с разрешенным переходом $\epsilon = 21$ мэв (пик 8) и неразрешенную группу пиков 7 в области энергий $\epsilon = 25 - 39$ мэв. Они связаны с трансляционными вибрациями молекул $(H_2O)_{I,II}$ относительно атомов Cl. Между ними проявляется пик 6 с максимумом при $\epsilon = 37$ мэв, не наблюдаемый в случае $BaCl_2 \cdot 2H_2O$; он обусловлен, по всей вероятности, движениями молекул H_2O, связанными с вибрационными колебаниями решетки [45]. В низкоэнергетической части спектра выступает полоса 9 при $\epsilon = 15$ мэв. Энергия этой полосы совпадает с энергией линий 11,4 и 13,8 мэв спектра комбинационного рассеяния света, обнаруженными Коршуновым и др. [46] и объясняемыми авторами вращательными колебаниями октаэдров кристаллизационной воды.

В-3. $CuSO_4 \cdot 5H_2O$

Распределение молекул воды в $CuSO_4 \cdot 5H_2O$ более сложное, нежели в веществах, описанных ранее. Они образуют водородные связи как между

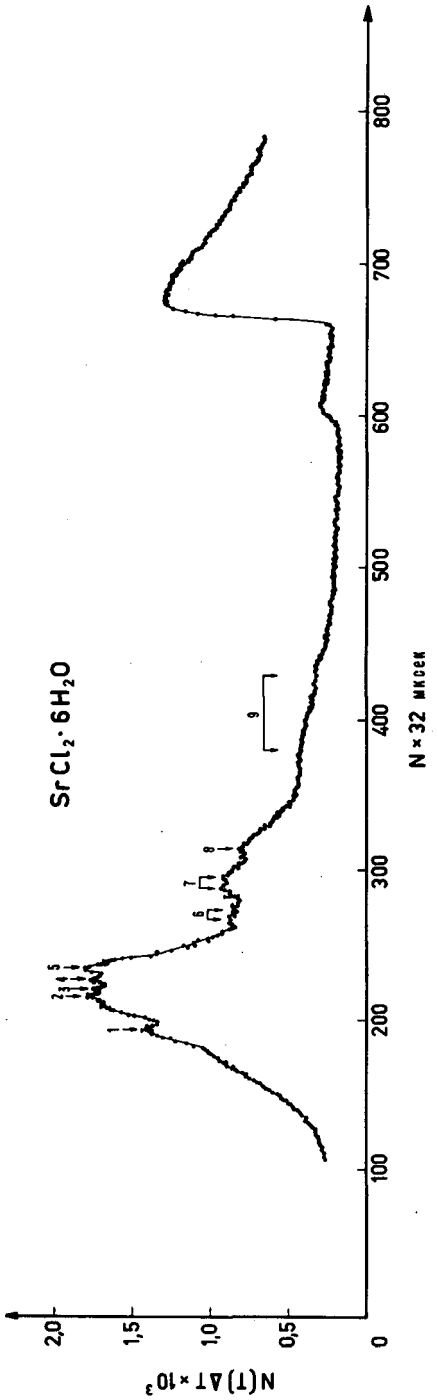

Рис.16

Спектр нейтронов, рассеянных на $SrCl_2 \cdot 6H_2O$ при температуре жидкого азота.

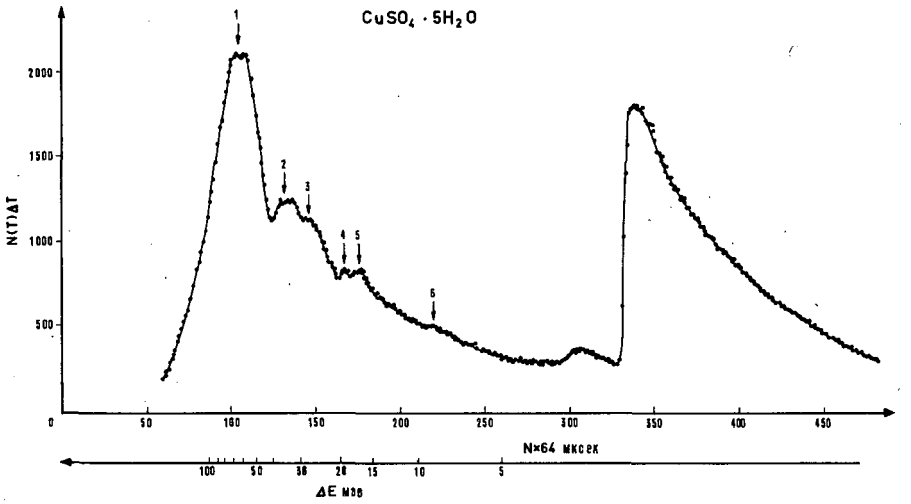

Рис.17

Спектр нейтронов, рассеянных на $CuSO_4 \cdot 5H_2O$ при температуре жидкого азота.

собой, так и с атомами кислорода иона SO_4^{2-}. Некоторые из молекул воды находятся, кроме того, в сфере координации иона Cu^{2+}. Эти обстоятельства отражаются как в инфракрасном [47], так и в нейтронном спектрах [43]. Хотя общий вид спектра нейтронов (рис.17), рассеянных на $CuSO_4 \cdot 5H_2O$, похож на спектры, полученные для $BaCl_2 \cdot 2H_2O$ и $SrCl_2 \cdot 6H_2O$, однако, в нем не удалось выделить отдельные пики. Полоса 1 пиков, связанных с заторможенными вращениями молекул H_2O, выступает в этом случае при энергиях $\epsilon = 59-80$ мэв, пики 3–5 трансляционных вибраций H_2O относительно соседей – при $\epsilon = 29$ мэв (пик 3) и $\epsilon = 20-17$ мэв (пик 4,5), а широкая полоса 2 при $\epsilon = 34-40$ мэв соответствует наблюдаемой в $SrCl_2 \cdot 6H_2O$ полосе 6 при $\epsilon = 37$ мэв. В полосе проявления водородных связей виден пик 6 с энергией $\epsilon = 8$ мэв.

ВЫВОДЫ

Несмотря на большую разницу в структурах исследуемых веществ нейтронные спектры, получаемые как для соединений с группой NH_4^+, так и для кристаллогидратов довольно схожи между собой. Во всех них при низких температурах проявляются в узкой области энергий характерные пики, связанные с торсионными колебаниями молекулярных групп. Энергия этих пиков зависит как от самой группы, так и от свойств кристаллической решетки соединения, содержащего эту группу. Энергия пиков заторможенных колебаний молекул H_2O, как правило, больше, нежели для NH_4^+.

Вид пиков чувствителен к форме потенциального поля, имеющегося в месте расположения ионов. Энергетически неэквивалентное размещение групп в кристаллической решетке, как и ангармонизм потенциалов, приводят к тонкой структуре линий, иногда не разрешаемой ввиду недостаточной разрешающей способности установки.

Результаты исследования динамики аммониевых групп показали, что характер движения ионов NH_4^+ не меняется при переходе через λ точку. Во всех случаях пики заторможенного вращения наблюдались при температурах выше и ниже температуры перехода. В области этого перехода в большинстве случаев не наблюдалось скачкообразных изменений в температурном ходе интенсивности упругой части спектра.

С другой стороны, скачкообразные изменения имели место при переходах в фазу кубической структуры из фаз более низкой симметрии.

Более подробный анализ полученных результатов ограничен современным состоянием теории динамики кристаллических решеток сложных молекулярных соединений.

Авторы выражают свою благодарность коллективу Лаборатории нейтронной физики ОИЯИ за помощь в проведении работы, Ф.Л. Шапиро и Е.А. Янику за проявленный интерес к работе и полезные обсуждения, а также Ф.А. Рябовой, В.Б. Дучицу, Г.А. Варенику, Б.И. Киселеву за техническую помощь.

ЛИТЕРАТУРА

[1] БАЙОРЕК А., МАЧЕХИНА Т.А., ПАРЛИНЬСКИ К., ШАПИРО Ф.Л., Препринт ОИЯИ Р-1899, 1964.
[2] БЛОХИН Г.Е. и др. "Атомная энергия", 10, 437 (1961).
[3] STEVENSON R., J. Chem. Phys., 34, 1757 (1961).
[4] LEVY H.A., PETERSON S.W., Phys. Rev., 83, 1270 (1951); 86, 766 (1952); J. Chem. Phys.,w21, 366 (1953); J. Am. Chem. Soc., 75, 1536 (1953).
[5] SHULL C.G., WOLLAN E.O. Solid State Phys., 3, 154 (1956).
[6] FRENKEL J., Acta Physicochimica, 3, 23 (1953).
[7] NAGAMIYA T., Proc. Phys. Math. Soc. Japan, 24, 137 (1952); Changements de Phase (Societe de chimie Physique) Paris, 1952.
[8] WAGNER F.D., HORNING D.F., J. Chem. Phys., 18, 296 (1950); 18, 305 (1950).
[9] BOVEY L.F., J. Opt. Soc. Amer., 41, 836 (1951).
[10] KRISHNAN R.S., Proc. Ind. Acad. (A) 26, 432 (1947); (A) 27, 321 (1948).
[11] MIKKE K., KROH A., Inelastic Scattering of Neutrons in Solids and Liquids, Proc. Vol.I, IAEA, Vienna 1963 p. 237
[12] VENKATARAMAN G., USHA K., IYENGAR P.K., VIJAYARASHAVAN P.R., ROY A.P., Inelastic Scattering of Neutrons in Solids and Liquids Proc. Vol.I IAEA, Vienna 1963, p. 253
[13] WOODS A.D.B., BROCKHAUSE B.N., SAKAMOTO M., SINCLAIR R.N., Inelastic Scattering of Neutrons in Solids and Liquids, Proc. IAEA Vienna 1961.
[14] GUTOWSKY H.S., PAKE G.E., BERSCHN B., J. Chem. Phys., 22, 643 (1954).
[15] COCKE A.H., DRAIN L.E., Proc. Phys. Soc. (London) A65, 894 (1952).
[16] RICHARDS R.E., SCHAEFER T.S., Trans. Faraday Soc., 57, 210 (1961).
[17] RUSH J.J., TAYLOR T.I., HAVENS W.W., Jr. Phys. Rev. Letters, 5, 507 (1960); Bull. Am. Phys. Soc., 6, 261 (1961); J. Chem. Phys., 35, 2265 (1961); J. Chem. Phys., 37, 234 (1962).
[18] BOUTIN H., SAFFORD D.J., BRAJOVIC V., J. Chem. Phys., 39, 3135 (1963).
[19] JOFFRAY. Compt. Rend., 244, 2346 (1947).
[20] SHINNAKA Y., J. Phys. Soc. Japan, 11, 393 (1956), 14, 1073 (1959), 14, 1707 (1959).
[21] MORAND J., Ann. Chim., 10, 1018 (1955).
[22] MATTHIAS B.T., REMEIKA J.P., Phys. Rev., 103, 262 (1956).
[23] CRENSHOW I.L., RETTER I., Z. Physik. Chem., B16, 143 (1932).
[24] GUILLIEN R., Compt. Rend., 208, 980 (1939).
[25] KANIYCSHI Kon-Ichi, MIYAMOTO Toshiniko, J. Chem. Phys., 22, 756 (1954).
[26] HETTNER G., SIMON F., Z. Physik. Chem., B1, 293 (1921).
[27] GUTOWSKY H.S., PAKE G.E., J. Chem. Phys., 16, 1164 (1948).
[28] HORVATH J.I., J. Chem. Phys., 16, 851 (1948).

[29] ЗВОНКОВА З.В., ЖДАНОВ Г.С., Ж. Физ. Хим., 23 (1949) 1495.
[30] XACHARIASEN W.H., MOONEY R.C.L., Z. Krist. 88, 63 (1934).
[31] MORFEE, STAVELEY, WALTERS, WIGLEY. J. Phys. Chem. Solids, 13, 132 (1960).
[32] BRAJOVIC V., BOUTIN H., SAFFORD C.J., PALEVSKY H., J. Phys. Chem. Solids, 24, 617 (1963).
[33] EISENHAUER C., PELAH I., HUGHES D.J., PALEVSKY H., Phys. Rev., 109, 1046 (1958).
[34] LARSSON K.F., DAHLBORG U.P., Inelastic Scattering of Neutrons in Solids and Liquids, IAEA, Vienna 1963.
[35] ГОЛИКОВ В.В., ЖУКОВСКАЯ И., ШАПИРО Ф.Л., ШКАТУЛА А., ЯНИК Е., Препринт ОИЯИ, Р-1903, 1964.
[36] ОЗЕРОВ Р.П., Сборник статей – Водородная связь, Москва, 1964 г.
[37] АТОЛ М., RUNDLE R.E., J. Chem. Phys., 29, 1306 (1958).
[38] LYON W., KINSEY E.L., Phys. Rev., 61, 482 (1942).
[39] DRONARD E., C.R. Acad. Sci. Fr., 240, 1700 (1955).
[40] SILVIDI A.A., McGRATH J.W., J. Chem. Phys., 32, 924 (1960).
[41] JENSEN A.T., Math. Physiske Meddelelser Ac. Copenhaque, 1945-1946, 22, 1.
[42] J. Van der ELSKEN, ROBINSON D.W., Spectrochim. Acta, 17, 1248 (1961).
[43] BOUTIN H., SAFFORD G.J., DANNER H.R., J. Chem. Phys., 40, 2648 (1964).
[44] JENSEN A.T., Math. Physiske Mleddelelser Ac. Copenhaque, 1939-1949, 12, 24.
[45] SPRINGER T., Nukleonik, 3, 110 (1961).
[46] КОРШУНОВ А.В., КОЛОВСКИЙ А.А., ПОДГАЕЦКАЯ Р.И., Оптика и спектроскопия-11. АН СССР, 1963.
[47] ЛАНДСБЕРГ П.С., БАРИШОНСКАЯ Ф.С., Сборник – Памяти С.И. Вавилова, АН СССР, 1952.

DISCUSSION

J.J. RUSH: In connection with this paper I should like to mention that I have measured total and differential scattering cross-sections for a number of these ammonium salts. I would question the assignment of the peak at 35 meV in $(NH_4)_2S_2O_8$ to the torsional frequency. Our total cross-section data at long neutron wavelengths indicates a barrier of about 1 kcal/mole for this compound at room temperature. In addition, the variation of the cross-section with temperature down to 80°K indicates no great change in the rotational freedom of the ammonium ions in this range. A 35-meV torsional frequency, on the other hand, would indicate a barrier of something like 3 kcal/mole.

V.M. PADMANABHAN: Single-crystal, neutron-diffraction studies which we carried out on $BaCl_2 \cdot 2H_2O$* showed that one of the hydrogens in the crystal has a bifurcated hydrogen bond. The fact that the crystal twins easily by pressure may be due to this, and the unusual O-H bond may also explain some of the features of the spectrum obtained in the paper just presented.

H. BOUTIN: You show the variation of the elastic peak versus temperature for NH_4I. How do you measure the height of the elastic peak?

K. PARLINSKI: The intensity of the elastic part of the spectrum was determined by subtracting the contribution of inelastic scattering from the mean count for the channel in the most elastic part of the spectrum. The magnitude of the inelastic scattering was obtained by continuing the inelastic part into the elastic part of the spectrum. The magnitude of all the jumps is greater than the error of this approximation.

* Acta Cryst. (1963) Rome Conf. Abstracts.

I. PELAH: Can you offer any explanation for the abrupt changes of elastic intensity at some temperature points?

K. PARLINSKI: In NH_4I a jump in the intensity of the elastic part of the spectrum is observed for certain temperatures at the point of transition from the phase of hindered NH_4 rotation to the phase of free rotation. In NH_4NO_3 the jump at 125.2°C (Fig. 7) is connected with the increased free rotation of the NO_3 group. Not all the jumps can be explained at present but apparently an abrupt change in intensity of the elastic part of the spectrum is found only for first-order phase transitions.

STUDIES OF AMMONIUM ION MOTIONS IN SOLID SOLUTIONS

K. MIKKE AND L. DOBRZYŃSKI
INSTITUTE OF NUCLEAR RESEARCH, SWIERK, POLAND

(Presented by B. Buras)

Abstract — Résumé — Аннотация — Resumen

STUDIES OF AMMONIUM ION MOTIONS IN SOLID SOLUTIONS. As has been shown by Mikke and Kroh in an earlier paper, pure NH_4I, studied by means of inelastic scattering of neutrons, shows in liquid nitrogen temperature a sharp peak which is connected with the hindered rotation of ammonium ions and a broad distribution at room temperature attributed at that time to free rotation. To study how these motions depend on the ammonium ion-ion interaction the energy distribution of initially monochromatic neutrons scattered inelastically at 90° from solid solutions of ammonium iodide in potassium iodide were measured by the inverted filter method. Measurements were made at room and liquid nitrogen temperature for two samples having concentrations of about 17 and 25% NH_4I in KI.

For these samples both in room and liquid nitrogen temperature no peaks were observed, which suggests that ammonium ions rotate freely in these solutions. The analysis of these results shows that the sharp peak observed at liquid nitrogen temperature for pure NH_4I is due to a strong ammonium ion-ion interaction and suggests that the broad peak occurring at room temperature for pure NH_4I is connected with torsional oscillation perpendicular to the axis of rotation of the $N\text{-}H\text{--}I^-$ in accordance with the model proposed by Vedder and Hornig.

The results are compared with Krieger-Nelkin theory. A model of simultaneously existing different types of rotation is proposed.

ÉTUDE DU MOUVEMENT DES IONS AMMONIUM DANS DES SOLUTIONS SOLIDES. Comme Mikke et Kroh l'ont montré dans un mémoire présenté antérieurement, en étudiant NH_4I pur au moyen de la diffusion inélastique des neutrons, on obtient, à la température de l'azote liquide, un pic étroit, qui est en relation avec la rotation freinée des ions ammonium et, à la température ambiante, une distribution étalée qui avait été attribuée à l'époque aux effets de la rotation libre. Pour étudier dans quelle mesure ces mouvements dépendent de l'interaction entre les ions ammonium, les auteurs ont mesuré, par la méthode du filtre inversé, les distributions en énergie de neutrons initialement monochromatiques diffusés inélastiquement à 90° dans des solutions solides d'iodure d'ammonium dans l'iodure de potassium. Les mesures ont été effectuées à la température ambiante et à la température de l'azote liquide sur deux échantillons contenant environ 17 et 25% de NH_4I dans KI.

Pour ces échantillons, on n'a pas observé de pics à la température ambiante ou à la température de l'azote liquide, ce qui semble indiquer que les ions ammonium sont en rotation libre dans ces solutions. L'analyse de ces résultats montre que le pic étroit observé à la température de l'azote liquide pour NH_4I pur est dû à une forte interaction entre les ions ammonium et donne à penser que le pic étalé apparaissant à la température ambiante pour NH_4I pur est lié à une oscillation de torsion perpendiculaire à l'axe des rotations du système $N\text{-}H\text{--}I^-$ conformément au modèle de Vedder et Hornig.

Les auteurs comparent les résultats avec la théorie de Krieger-Nelkin et proposent un modèle de différents types de rotation existant simultanément.

ВРАЩЕНИЕ ИОНОВ АММОНИЯ В ТВЕРДЫХ РАСТВОРАХ. Как показали К. Микке и А. Крох, в предыдущей работе чистый NH_4J, исследованный посредством неупругого рассеяния нейтронов, дает при температуре жидкого азота острый пик, который связан со стесненным вращением ионов аммония, и широкое распределение при комнатной температуре, которое объяснялось тогда свободным вращением. Для того чтобы изучить, каким образом эти движения зависят от взаимодействия ион-ион аммония, было измерено распределение энергий первоначально монохроматических нейтронов, неупруго рассеянных при температуре 90° на твердых растворах иодида аммония в иодиде калия. При этом применялся метод ин-

вертированного фильтра. Измерения производились при комнатной температуре и температуре жидкого азота на двух образцах, содержащих приблизительно 17 и 25 процентов NH_4J и KJ.

На этих образцах не наблюдалось пиков ни при комнатной температуре, ни при температуре жидкого азота, что дает основание полагать, что ионы аммония вращаются свободно в этих растворах. Анализ этих результатов показывает, что острый пик, наблюдаемый при температуре жидкого азота для чистого NH_4J, объясняется сильным взаимодействием ион-ион аммония и позволяет предполагать, что широкий пик, возникающий для чистого NH_4J при комнатной температуре, связан с крутильной осцилляцией, перпендикулярной к осям вращения $N-H--J^-$ в соответствии с моделью, предложенной Веддером и Хорнигом.

Результаты сравниваются с теорией Кригера-Нелькина. Предлагается модель одновременно существующих различных видов вращения.

ESTUDIO DE LOS MOVIMIENTOS DEL ION AMONIO EN SOLUCIONES SOLIDAS. Como Mikke y Kroh señalaron en una memoria anterior, el NH_4I puro estudiado por dispersión inelástica de neutrones presenta, a la temperature del nitrógeno líquido, un pico pronunciado (que se relaciona con la rotación restringida de los iones amonio), y una distribución aplanada a temperatura ambiente (que se atribuye a la rotación libre). A fin de estudiar la manera en que estos movimientos dependen de las interacciones entre iones amonio se midió, por el método del filtro invertido, la distribución energética de neutrones inicialmente monocromáticos dispersos inelásticamente a 90° en soluciones sólidas de yoduro amónico en yoduro potásico. Las mediciones se efectuaron a la temperatura ambiente y a la temperatura del nitrógeno líquido, con dos muestras cuyas concentraciones aproximadas eran de 17 y 25% de NH_4I en KI.

En estas muestras no se observó pico alguno a la temperatura ambiente ni a la del nitrógeno líquido, lo que indica que los iones amonio giran libremente en esas soluciones. El análisis de los resultados muestra que el pico pronunciado que se observa a la temperatura del nitrógeno líquido en el caso del NH_4I puro se debe a una fuerte interacción entre iones amonio, y sugiere que el pico aplanado, que aparece a la temperatura ambiente en el caso del NH_4I puro guarda relación con una oscilación de torsión perpendicular al eje de rotación del $N-H--I^-$, de conformidad con el modelo propuesto por Vedder y Hornig.

Los autores comparan los resultados con la teoría de Krieger-Nelkin y proponen un modelo de diferentes tipos de rotación coexistentes.

1. INTRODUCTION

As has been shown in recent years by several authors [1, 2, 3], ammonium iodide, NH_4I, studied by means of inelastic scattering of neutrons shows in liquid nitrogen temperature (CsCl-type structure) a sharp peak at 295 cm^{-1} and at room temperature (NaCl-type structure) a broad distribution. The sharp peak was attributed to the hindered rotation of ammonium ions with a 2-kcal/mole [3] high barrier. The broad distribution at room temperature was at that time ascribed [1] to a free or nearly free rotation. The total cross-section measurements [2, 3] have shown that in this case the barrier height is about 0.5 kcal/mole. To study how the motion of the ammonium ion depends on the ammonium ion-ion interaction, the energy distribution of initially monochromatic neutrons scattered inelastically at 90° from a solid solution of ammonium iodide in potassium iodide was measured by the inverted beryllium filter technique [4].

2. MEASUREMENTS AND RESULTS

The experimental set-up was basically the double-crystal spectrometer described earlier in [5]. The necessary modifications of that spectrometer

and some details of measurement were described in [1]. Measurements were made at room and liquid nitrogen temperatures for two samples of concentrations of about 17 and 25% NH_4I in KI.

The curves obtained (neutron intensity versus incident neutron energy) for these samples are shown in Figs. 1-4. It can be observed from the in-

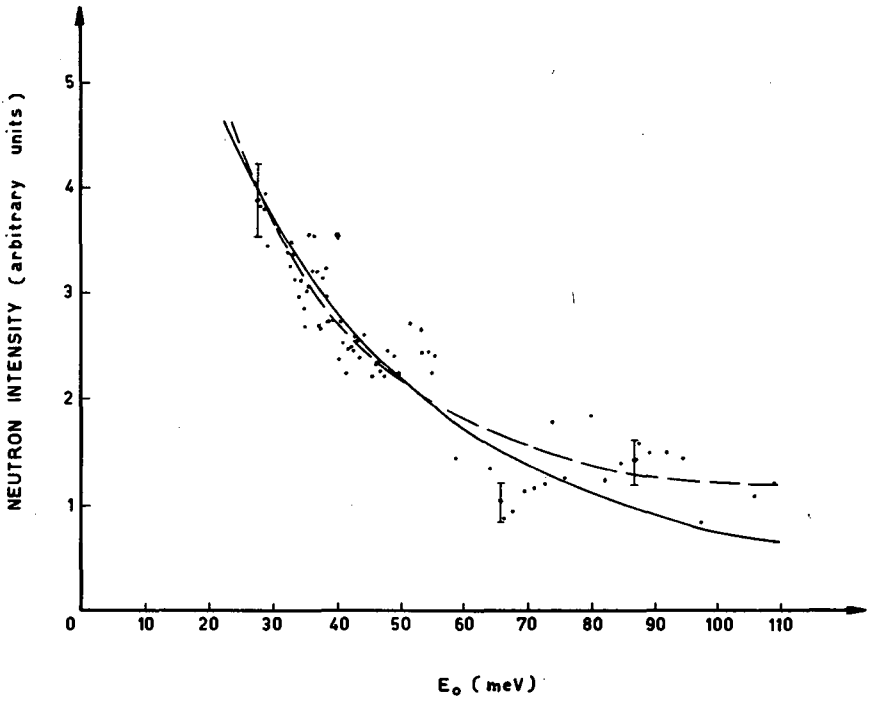

Fig. 1

Energy distribution of neutrons scattered by a solid solution of 17% concentration NH_4I in KI

Scattering angle 90°; Temperature 297°K

——— Krieger-Nelkin theory, R = 3.0

– – – – – $\left[\frac{d^2\sigma}{d\Omega dE}\text{ (one-axis rotation)} + 5.4\,\frac{d^2\sigma}{d\Omega dE}\,(R = 1)\right] \times k_0$

spection of the energy distributions obtained that their character is substantially different from those obtained for pure NH_4I as described in Ref. [1] (Figs. 5(a), (b), (c)). No maxima can be observed at liquid nitrogen temperature. In particular there is no peak corresponding to the hindered rotation, which indicates that ammonium ions rotate freely in these solutions and this, in turn, suggests that this peak in pure NH_4I is due to a strong ammonium ion-ion interaction.

The results obtained at room temperature must be analysed very carefully because of the small statistics of measurements obtained in this case. However, the broad peak occurring at room temperature for pure NH_4I vanishes in the solid solution and, as at liquid nitrogen temperature, no peak

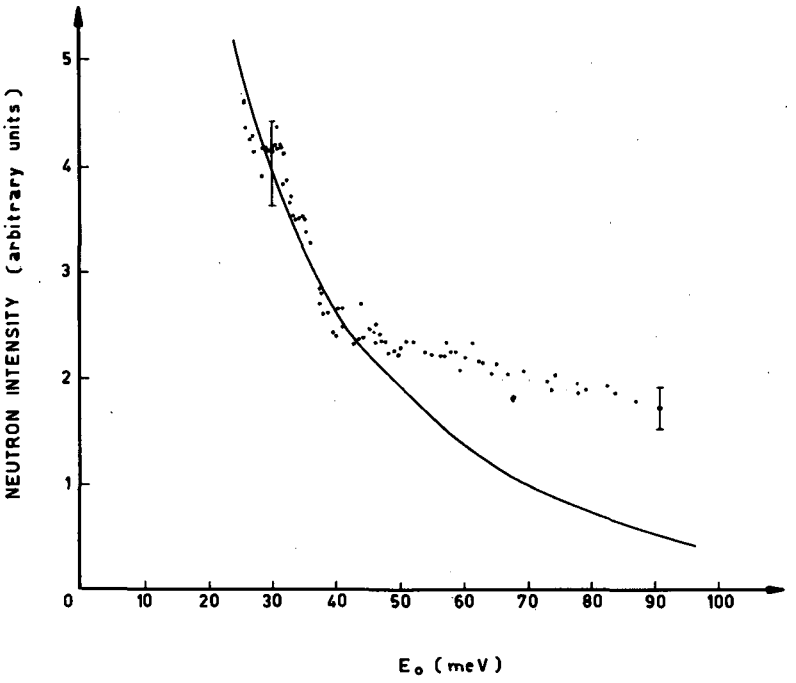

Fig. 2

Energy distribution of neutrons scattered by a solid solution of 25% concentration NH_4I in KI

Scattering angle 90°; Temperature 297°K

——— Krieger-Nelkin theory, R = 4.0

is observed. It suggests that the peak for pure NH_4I at room temperature may be connected with a torsional oscillation perpendicular to the rotation axis of N-H--I^-, in accordance with the model proposed by VEDDER and HORNIG [6]. This torsional oscillation is supposed to be connected with the ammonium ion-ion interaction and vanishes in solid solutions. The general conclusion is that the ammonium ion motion depends strongly on the ammonium ion-ion interaction, and only slightly on the "host lattice".

Because of the large distances between ammonium ions in the solutions under study, the interaction between ammonium ions can be neglected and they can be treated, with a good approximation, as gas molecules. With this model in mind the Krieger-Nelkin theory [7] is applicable and the well-known expression for the differential cross-section can be used

$$\frac{d^2\sigma}{d\Omega\, dE} = a^2 \frac{k}{k_0}\sqrt{\frac{\bar{M}}{2\pi\kappa^2 T}}\ \exp\left[-\gamma\kappa^2 - \frac{M}{2\kappa^2 T}\left(\epsilon + \frac{\kappa^2}{2\bar{M}}\right)^2\right],$$

where

a = scattering amplitude

$\vec{k}$ = wave vector of scattered neutrons

$\vec{k}_0$ = wave vector of incident neutrons

$\vec{\kappa} = \vec{k} - \vec{k}_0$, momentum transfer

$\epsilon = \frac{\hbar^2}{2m}(k^2 - k_0^2)$, energy transfer

$\gamma = \frac{1}{6}\sum_{\lambda} \frac{(C^{(\lambda)})^2}{\omega^{(\lambda)}}$, vibrational constant, where

$C^{(\lambda)}$ = amplitude of the normal mode $\omega^{(\lambda)}$

$\overline{M}$ = effective mass of the molecule.

As it can be shown, no effective mass parameter $R = \overline{M}/m$ (where m is the neutron mass) can be found which would give a good agreement with the results obtained (solid lines in Figs. 1-4). Deviations from the Krieger-Nelkin theory begin in the region of hindered rotation of ammonium ions in

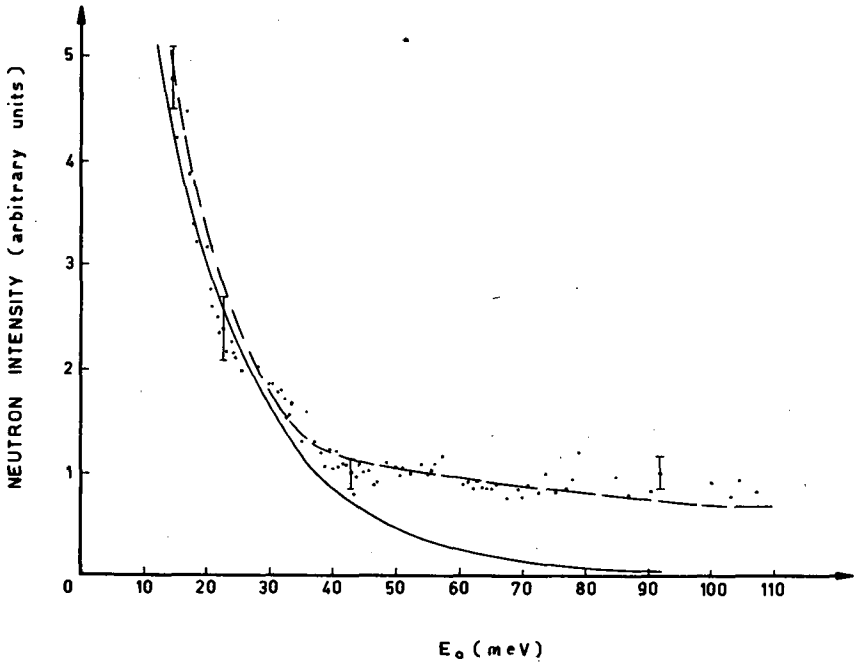

Fig. 3

Energy distribution of neutrons scattered by a solid solution of 17% concentration NH_4I in KI

Scattering angle 90°; Temperature 78°K

——— Krieger-Nelkin theory, R = 3.0

– – – – – $\left[\frac{d^2\sigma}{d\Omega dE}\text{ (one-axis rotation)} + \frac{d^2\sigma}{d\Omega dE}\text{ (R = 1)}\right] \times k_0$

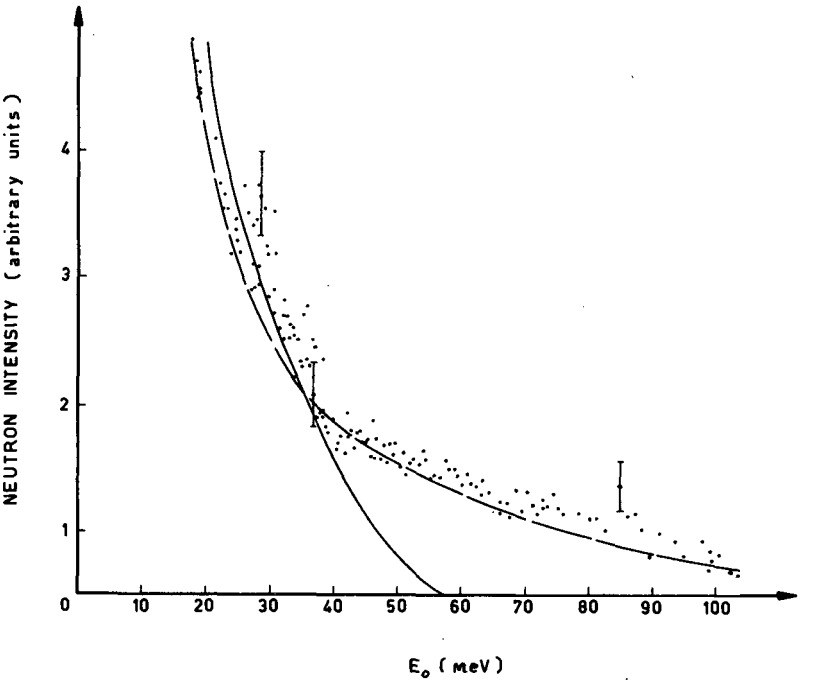

Fig. 4

Energy distribution of neutrons scattered by a solid solution of 25% concentration NH_4I in KI

Scattering angle 90°; Temperature 78°K

——— Krieger-Nelkin theory, R = 3.0

– – – – – $\left[\frac{d^2\sigma}{d\Omega dE}\text{ (one-axis rotation)} + 2.6\frac{d^2\sigma}{d\Omega dE}(R=1.5)\right] \times k_0$

pure NH_4I. Of course, these deviations may be due to the non-applicability of the Krieger-Nelkin theory to solids. Nevertheless, three possibilities should be considered:

(a) The concentration of the solutions are higher than required for a complete destruction of the hindered rotation.
(b) These deviations are due to multiple scattering of neutrons in the samples.
(c) Different types of rotation exist simultaneously in the solution.

The comparison of our results with the results obtained by PALEVSKY et al. [8] for room temperature indicates that, in the region of concentration from 5 to 25%, the distributions do not depend strongly on the concentrations. (Palevsky's result for concentration of 5% is in qualitative agreement with our results, however the energy resolution in the region of high energies is far better in our case.) This seems to exclude the first possibility.

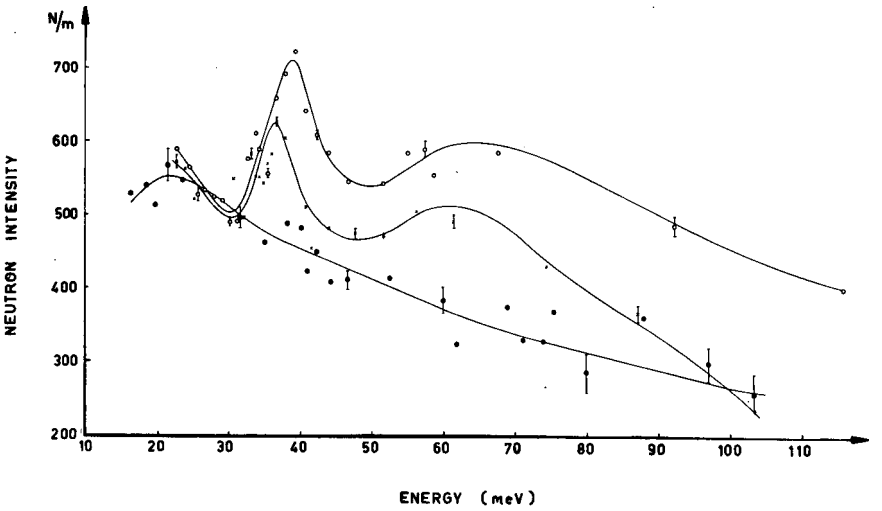

Fig. 5(a)

Energy distribution of neutrons scattered by pure ammonium iodide from a thick sample

● + 20°C
○ - 65°C
× - 20°C

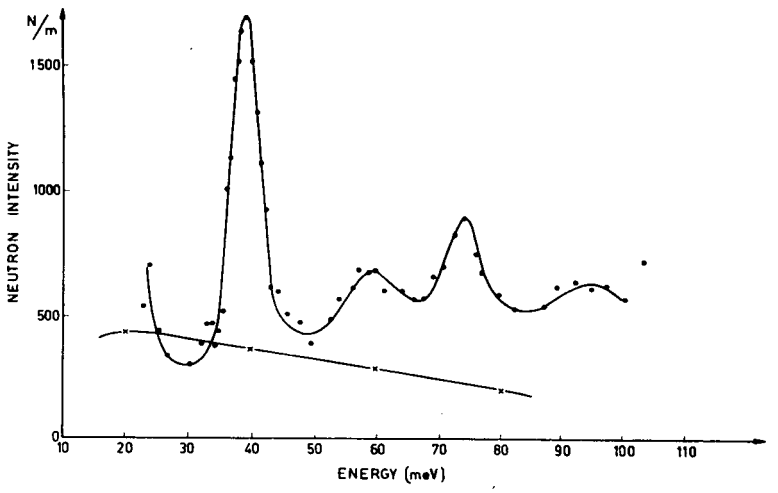

Fig. 5(b)

Energy distribution of neutrons scattered by pure ammonium iodide from a thick sample

● -150°C
× + 20°C

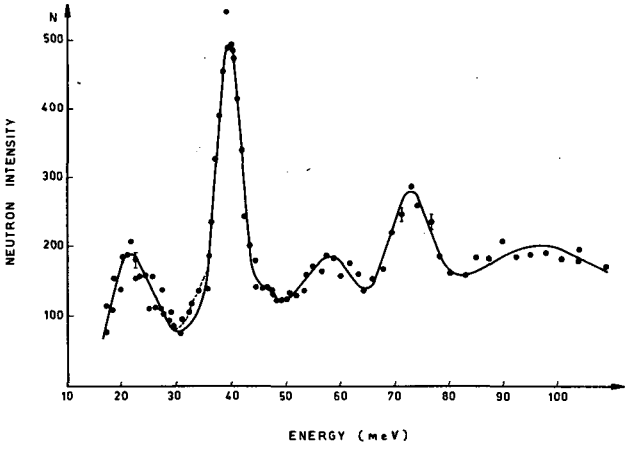

Fig. 5(c)

Energy distribution of neutrons scattered by pure ammonium iodide from a thin sample

● -150°C

The multiple scattering of neutrons seems to have a small contribution to present results as the incoherent scattering cross-sections are low, both for potassium and iodine. In addition, the thickness of measured samples was not higher than the thickness for the samples of pure NH_4I. For the latter case it was shown [1] that the contribution of multiple scattering is negligible (Figs. 5(b) and 5(c)). Considering that in the case of solid solutions the number of ammonium ions was much lower than in pure NH_4I samples we can assume that the deviations from theoretical curves are not connected with the multiple scattering.

To check the possibility of simultaneous existence of different types of rotation in the solid solutions, it was assumed that one part of ammonium ions rotates around one axis N-H--I^- and another rotates with an unknown mass parameter R. It has been demonstrated for three cases out of four which were measured that it is possible to obtain a good fit for R around 1 (dashed lines on Figs. 1-4). This may be treated as an argument in favour of the mentioned hypothesis, but no definite quantitative predictions regarding the possible modes of motion and their mutual interactions can be checked in this way.

ACKNOWLEDGEMENTS

The authors wish to express their gratitude to Professor B. Buras for the encouragement and constant interest in the work and to Messrs. R. Kula and S. Szafran for their help during the measurements.

REFERENCES

[1] MIKKE, K. and KROH, A., Inelastic Scattering of Neutrons in Solids and Liquids II IAEA, Vienna (1963) 237-50.
[2] PALEVSKY, H., Inelastic Scattering of Neutrons in Solids and Liquids II IAEA, Vienna (1963) 251.
[3] RUSH, J.J. et al., Phys. Rev. Lett. 5 (1960) 507; J. chem. Phys. 35 (1961) 2265; J. chem. Phys. 37 (1962) 234.
[4] BROCKHOUSE, B.N., Inelastic Scattering of Neutrons in Solids and Liquids, IAEA, Vienna (1961) 487.
[5] INSTITUTE OF NUCLEAR RESEARCH, Rpt. INR 46, Swierk.
[6] VEDDER, W. and HORNIG, D.F., J. chem. Phys. 35 (1961) 1560.
[7] KRIEGER, T.J. and NELKIN, M.S., Phys. Rev. 106 (1957) 290.
[8] PALEVSKY, H. et al., J. Phys. Chem. Solids 24 (1963) 617.

DISCUSSION

G. VENKATARAMAN: Your Fig.1 shows a dotted curve marked "one-axis rotation". Can you please indicate how these calculations were done?

B. BURAS: It was assumed that part of the ammonium ions rotate around one axis and others rotate with an unknown mass parameter (all in accordance with the Krieger-Nelkin theory). Personally, however, I would not attach too much attention to these calculations. With two parameters it is not difficult to fit a smooth curve.

STUDIES OF THE SOLID AND LIQUID PHASES OF HF, HCl AND HBr BY SLOW NEUTRON INELASTIC SCATTERING*

H. BOUTIN
PICATINNY ARSENAL, DOVER, N.J. AND
BROOKHAVEN NATIONAL LABORATORY, UPTON, N.Y.
AND
G.J. SAFFORD**
BROOKHAVEN NATIONAL LABORATORY, UPTON, N.Y.,
UNITED STATES OF AMERICA

Abstract — Résumé — Аннотация — Resumen

STUDIES OF THE SOLID AND LIQUID PHASES OF HF, HCl AND HBr BY SLOW-NEUTRON INELASTIC SCATTERING. The liquid and solid phases of HF, HCl and HBr were studied between 30 and 1200 cm^{-1} using the inelastic scattering of cold neutrons (0.005 eV). These measurements were made in order to examine systematically the influence of an increasing degree of electronegativity and anion size on the low frequency molecular motions in both the solid and liquid phases. HF was first studied because it was known from X-ray diffraction data to form long zigzag hydrogen bonded chains in the solid state. The spectra of neutrons inelastically scattered from the liquid and solid phases of HF emphasize the high degree of association that exists through the liquid phase due to hydrogen bonding. The data for HF were compared for purposes of interpretation with similar scattering data for HF_2^- and $H_2F_3^-$ ions which have structures similar to those units which comprise the zigzag hydrogen bonded chains in HF. The data were also compared with Raman and infrared measurements on HF_2^- ions. These comparisons allowed frequencies characteristic of a single unit to be differentiated from those characteristics of the entire chain and from the low frequency lattice modes. A line observed at 0.067 eV has been associated with the deformation frequency ν_2 of the F-H···F group in solid HF and has been correlated with similar frequencies in $H_2F_3^-$ and HF_2^- ions as a function of the F-F distance. In addition, a broad peak observed at 0.007 eV has been attributed to a rotational motion of the F-H···F unit around the F-F bond. The spectrum of liquid HF is also discussed with respect to these motions. The spectra of liquid HCl (180°K), solid HCl Phases I and III (143 and 85°K, respectively), liquid HBr (193°K) and solid HBr Phases I and II (153 and 103°K, respectively) have been compared with the above data for HF. Those spectra show an increasing complexity compared to that of HF. This can be attributed to a weaker degree of association, which is expected from the decreasing electronegativity of the anion. The systematic study of these spectra in the various phases and at various temperatures allows a distinction to be made between the low frequency motions characteristic of the lattice or of an hydrogen-bonded chain and those low frequency motions which involve nearest-neighbour interactions or short-range forces. The results of these measurements are in agreement with previous infrared data and indicate that hydrogen bonding is an influential factor in explaining the spectra of the solid phases of both HCl and HBr. These data are not in agreement, however, with theories that account for the solid phases of these compounds only in terms of simple dipole arrays or in terms of long-range interactions involving the dipole moment of one single unit interacting with an average electric field.

ÉTUDE DES PHASES SOLIDE ET LIQUIDE DE HF, HCl ET HBr PAR LA DIFFUSION INÉLASTIQUE DES NEUTRONS LENTS. Les auteurs ont étudié les phases liquide et solide de HF, HCl et HBr entre les raies d'absorption 30 et 1200 cm^{-1} en employant la méthode de la diffusion inélastique des neutrons froids (0,005 eV). Ils ont procédé à ces mesures pour examiner systématiquement l'influence qu'un accroissement du degré d'électronégativité et la dimension des anions exercent sur les mouvements moléculaires de basse fréquence dans

* This work was performed using both the Brookhaven National Laboratory Reactor and the United States AMRA Research Reactor, Watertown Arsenal, Watertown, Mass.

** Now with Union Carbide Corporation, Nuclear Division, Tuxedo, N.Y.

la phase solide et la phase liquide. L'étude a d'abord porté sur HF du fait que les données obtenues par diffraction des rayons X avaient montré que dans ce composé à l'état solide apparaissaient de longues chaînes en zigzag liées par l'hydrogène. Les spectres des neutrons inélastiquement diffusés par les phases liquide et solide de HF font ressortir le haut degré d'association qui existe dans toute la phase liquide en raison de la liaison hydrogénée. Aux fins d'interprétation, les auteurs comparent les données relatives à HF à des données analogues relatives aux ions HF_2^- et $H_2F_3^-$ dont les structures sont semblables à celle des éléments de réseau qui comportent des chaînes en zigzag liées par l'hydrogène. Ils les comparent également aux résultats des mesures faites sur les ions HF_2^- par la méthode de Raman et au moyen de l'infrarouge. Grâce à ces études comparatives, ils ont pu différencier les fréquences caractéristiques d'un seul élément de celles qui caractérisent la chaîne entière et des modes de réseaux de basse fréquence. La raie observée à 0,067 eV a été associée à la fréquence de déformation ν_2 du groupe F-H...F dans HF solide et rapportée aux fréquences semblables dans les ions $H_2F_3^-$ et HF_2^- sous la forme d'une fonction de la distance F-F. En outre, l'origine d'un large pic, observé à 0,007 eV, a été attribuée à un mouvement de rotation de l'élément F-H···F autour de la liaison F-F. Le spectre de HF à l'état liquide fait également l'objet d'une discussion du point de vue de ces mouvements. Les spectres de HCl liquide (180°K), des phases I et III de HCl solide (143 et 85°K respectivement), de HBr liquide (193°K) et des phases I et II de HBr solide (153 et 103°K respectivement) font l'objet d'une comparaison avec les données susmentionnées relatives à HF. Ces spectres accusent une complexité croissante par rapport à celui de HF. Cette particularité peut être due au moins haut degré d'association auquel on peut s'attendre étant donné la diminution de l'électronégativité de l'anion. L'étude systématique de ces spectres dans diverses phases et à diverses températures permet de faire une distinction entre les mouvements de basse fréquence qui caractérisent le réseau ou une chaîne liée par l'hydrogène et les mouvements de basse fréquence qui font intervenir des interactions entre les voisins les plus proches ou des forces de faible portée. Les résultats de ces mesures concordent avec les données obtenues auparavant avec l'absorption infrarouge et indiquent que la liaison par l'hydrogène facilite dans une grande mesure l'explication des spectres correspondant aux phases solides de HCl et de HBr. Cependant, ces données ne concordent pas avec les théories qui rendent compte des phases solides de ces composés uniquement en fonction d'arrangements dipolaires simples ou d'interactions à grande distance faisant intervenir le moment dipolaire d'un seul élément de réseau en interaction avec un champ électrique moyen.

ИЗУЧЕНИЕ ТВЕРДЫХ И ЖИДКИХ ФАЗ HF, HCl И HBr С ПОМОЩЬЮ НЕУПРУГОГО РАССЕЯНИЯ МЕДЛЕННЫХ НЕЙТРОНОВ. Жидкие и твердые фазы HF, HCl и HBr изучались между 30 и 1200 $см^{-1}$ при помощи неупругого рассеяния холодных нейтронов (0,005 эв). Эти измерения производились с целью систематического изучения влияния увеличения отрицательного электрического заряда и размеров анионов на низкочастотные молекулярные движения как в твердой, так и в жидкой фазах. HF исследовался первым, т.к. данные дифракции рентгеновских лучей показывали, что в твердом состоянии он образует длинные зигзагообразные цепи с водородной связью. Спектры нейтронов, неупруго рассеянных от жидкой и твердой фаз HF, ясно показали высокую степень ассоциации, существующую во всей жидкой фазе благодаря водородной связи. С целью интерпретации данные по HF были сопоставлены с данными аналогичного рассеяния ионов HF_2^- и $H_2F_3^-$, которые имеют структуры, аналогичные тем составным частям в HF, которые включают зигзагообразные цепи с водородной связью. Эти данные были также сопоставлены с результатами измерений с помощью инфракрасных лучей и измерений по методу Рамана на ионах HF_2^-. Эти сопоставления позволили отличить частотную характеристику отдельной составной части от частотной характеристики всей цепи и от низкочастотных колебаний решетки. Линия, наблюдавшаяся при 0,067 эв, была ассоциирована с частотой деформации ν_2 группы F—H···F в твердом HF, и была установлена ее связь с аналогичными частотами в ионах $H_2F_3^-$ и HF_2^- как фракции расстояния F—F. Кроме того, широкий пик, отмеченный при 0,007 эв, был приписан вращательному движению составной части F—H···F вокруг связи F—F. Спектр жидкого HF также будет рассматриваться с точки зрения этих движений. Спектры жидкого HCl (180° K), фаз I и III твердого HCl (143 и 85° K соответственно), жидкого HBr (193° K) и фаз I и II твердого HBr (153 и 103° K соответственно) были сопоставлены с вышеуказанными данными для HF. Эти спектры показывают еще большую сложность, чем у HF. Это может быть объяснено более слабой степенью ассоциации, которую можно ожидать в связи с уменьшением отрицательного заряда аниона. Систематическое изучение этих спектров в различных фазах и при различных температурах позволяет провести различие между характеристиками низкокачественных движений решетки или цепи с водородной связью и характеристиками тех низкочастотных движений, которые затрагивают взаимодействия ближайшего соседа или близкодействующие силы. Результаты

этих измерений согласуются с имеющимися данными, полученными с помощью инфракрасных лучей, и показывают, что водородная связь является существенным фактором объяснения спектров твердых фаз как HCl, так и HBr. Однако эти данные не согласуются с теорией, которая объясняет твердые фазы этих соединений только с точки зрения простых дипольных систем или с точки зрения дальних взаимодействий, затрагивающих дипольный момент одной отдельной составной части, взаимодействующей со средним электрическим полем.

ESTUDIO DE LAS FASES SOLIDA Y LIQUIDA DEL HF, HCl Y HBr POR DISPERSIÓN INELÁSTICA DE NEUTRONES LENTOS. Los autores han estudiado las fases líquida y sólida del HF, HCl y HBr, entre 30 y 1200 cm^{-1}, recurriendo a la dispersión inelástica de neutrones fríos (0, 005 eV). Estas mediciones se realizaron a fin de examinar sistemáticamente la influencia que ejerce el aumento del grado de electronegatividad y del tamaño de los aniones sobre los movimientos moleculares de baja frecuencia, tanto en fase sólida como líquida. Se estudió en primer lugar el HF por saberse -según datos obtenidos en experimentos de difracción realizados con rayos X- que en el estado sólido forma largas cadenas enlazadas en zigzag por el hidrógeno. El espectro de los neutrones inelásticamente dispersos en las fases líquida y sólida del HF pone de relieve el alto grado de asociación que existe en el estado sólido como consecuencia del enlace hidrógeno. Los autores han comparado, con fines de interpretación, los datos correspondientes al HF con datos análogos sobre la dispersión en el caso de los iones HF_2^- y $H_2F_3^-$, que presentan estructuras semejantes a las de las unidades que comprenden, en el HF, las cadenas enlazadas en zigzag por el hidrógeno. También compararon esos datos con los resultados de las mediciones Raman y del espectro infrarrojo en los iones HF_2^-. Estas comparaciones permitieron distinguir entre las características de frecuencia de una sola unidad, y de las características de la cadena entera y de los modos reticulares de baja frecuencia. La raya observada a 0, 067 eV ha podido asociarse a la frecuencia de deformación ν_t del grupo F-H···F en el HF sólido, y se ha correlacionado con frecuencias análogas en los iones $H_2F_3^-$ y HF_2^- como una función de la distancia F-F. Además, el máximo ensanchado que se observa a 0, 007 eV se ha atribuído a un movimiento rotatorio del grupo F-H···F alrededor del enlace F-F. Los autores tratan también del espectro del HF líquido en lo que respecta a esos movimientos. Han comparado los datos ya mencionados, relativos al HF, con los espectros del HCl líquido (180°K), de las fases sólidas I y III del HCl (143 y 85°K, respectivamente), del HBr líquido (193°K) y de las fases sólidas I y II del HBr (153 y 103°K, respectivamente). La mayor complejidad que esos espectros ofrecen en comparación con el del HF puede atribuirse a un menor grado de asociación, lo que es de esperar dada la decreciente electronegatividad del anión. El estudio sistemático de estos espectros en las diversas fases y a distintas temperaturas permite distinguir entre los movimientos de baja frecuencia, característicos de la red o de una cadena de enlaces hidrógeno, y aquellos movimientos de baja frecuencia en los que intervienen interacciones de los átomos más próximos o fuerzas de corto alcance. Los resultados de estas mediciones concuerdan con los datos acerca del espectro infrarrojo obtenidos previamente, e indican que el enlace hidrógeno constituye un importante factor para explicar los espectros del HCl y del HBr en fase sólida. No obstante, esos datos no responden a las teorías que explican las fases sólidas de esos compuestos únicamente en función de disposiciones dipolares simples o de interacciones de largo alcance en las que interviene el momento dipolar de una sola unidad en interacción con un campos eléctrico de intensidad media.

INTRODUCTION

The series of the hydrogen halides HF, HCl and HBr in their various solid and liquid phases allow a systematic study to be made of the effects of decreasing molecular association with decreasing electronegativity and of their influence on the molecular motions in the different phases of these compounds. Previous work [1] has shown that the solid phase of HF consists of "zig-zag" quasi-infinite hydrogen bonded chains which have relatively weak interactions between one another. While little information is available on the structure of the liquid phase, average molecular weight measurements as a function of temperature [2] indicate a considerable degree of association which decreases with increasing temperature. Indeed, polymeric association as high as six molecular units exists even in the gas phase.

TABLE I

PHYSICAL CHARACTERISTICS OF HF, HCl AND HBr

	HF	HCl	HBr
Melting temperatures (°K)	191.7	159	186
Transition temperatures (°K)		no phase II I <--> III	
I <----> II		98.4	115
II <----> III			90
Structural data HF (solid)[a]		Orthorhombic 4 mol/unit cell (a = 3.42 Å, b = 4.32 Å, c = 5.41 Å)	
HCl Solid phase III[b] Solid phase I		fco[c] fcc (a = 5.50 Å)	
HBr Solid phase III[b] Solid phase II Solid phase I		fco fct (c/a 1) fcc (a = 5.77 Å)	

[a] ATOJI, M. and LIPSCOMB, W.N., Acta cryst. 7 (1956) 173
[b] NATTA, G., Gazz. Chim. Ital. 63 (1933) 425
[c] fco = face-centred orthorhombic
fct = face-centred tetragonal
fcc = face-centred cubic

Studies of HCl and HBr by dielectric relaxation [3, 4] and by specific heat measurements [5] have shown a number of first- and second-order transitions between the solid phases which are summarized in Table I. PAULING [6] suggested that such transitions in HCl and HBr might result from the onset of rotation about one axis of symmetry and expansion of the crystal along that axis. Later POWLES [3] considered these transitions in terms of reorientation of dipoles through barriers determined by repulsive crystal forces. This latter explanation was in part supported by nuclear magnetic resonance (NMR) [7] and infrared studies [8] which showed that there existed no free or nearly free rotation in any of the solid phases. However, recent infrared measurements [9, 10] cast doubt on the validity of an explanation of these transitions only in terms of a pure dipole interaction. The interpretation given these measurements is that the low-temperature phases of solid HCl and HBr are composed of "zig-zag" hydrogen bonded chains similar in structure to those found in the solid phase of HF. Moreover, RANK et al. [11] have reported that the Raman spectrum of pure HCl gas shows strong evidence for dimer formation at 195°K while VIDALE and TAYLOR [12] have shown that HCl molecules in solution are held together by weak hydrogen bonds which are stable at low temperature. Thus it appears necessary to consider the influence of some dimeric and polymeric association on the molecular motions in the liquid and solid phases of HCl and of HBr.

While there exists little information on the low-frequency motions in HF, HCl and HBr, it should be noted that the "zig-zag" chains found in the low-temperature phase of these compounds are similar in structure to those of high density polyethylene for which there has been much experimental [13] and theoretical [14] work on the types of low-frequency motions that exist. While the chain configurations are similar, the hydrogen bonds on the hydrogen halides are expected to be weaker than the covalent bonds on the polyethylene chain, especially as the electronegativity of the halides decreases. This introduces the complication that appreciable chain scission may occur with increasing temperature. Measurements and calculations of the normal modes of an infinite polyethylene chain [13, 14] in the trans-configuration show a clear separation in the vibrational spectrum with optical branches lying above 700 cm^{-1} and two acoustic modes, a combination skeletal stretching and bending mode and a skeletal torsional vibration, lying below 700 cm^{-1}. In addition to lattice modes, internal rotations of chain segments are taking place which can give rise to a multitude of chain conformations. As the temperature is increased from that of the lowest solid phase, these internal rotations are expected to become less hindered. The possible occurrence of such motions must be considered in the interpretation of the data obtained in the present experiment.

The low-energy spectra of molecular motions in the solid and the liquid phases of HF, HCl and HBr have been studied by inelastic neutron scattering in the frequency region between 10 and 900 cm^{-1}. It is in this low-frequency region that torsional and translational co-operative chain vibrations are expected to occur. In previous measurements [9], frequencies of such modes were deduced from combination bands or overtone lines in the infrared spectra, while in neutron scattering measurements all possible frequencies of these modes may be observed directly as there is no requirement with regard to optically active vibrations.

The evaluations of the observed modes were studied as a function of phase and of temperature. In the case of HF, in order to distinguish between those motions characteristic of a co-operative-chain vibration and those motions characteristic of a single-chain unit, the spectra were compared with those of compounds containing the HF_2^- and $H_2F_3^-$ ions [15]. These ions have structures similar to those units which comprise the hydrogen-bonded chains in HF.

The energy of the incident neutrons (0.005 eV) in the present measurements is small compared to the thermal excitation energy (kT) of the sample and only those neutrons are observed which have gained energy in a single scattering event. Therefore, the observed peaks represent transitions between levels populated by thermal excitation. As the scattering cross-section of hydrogen is both relatively large (20 b free atom) compared to those of the other elements in these compounds and mostly incoherent, the most intense peaks in the spectra will represent motions of hydrogenous units and the scattering will, to a good approximation, be isotropic for the samples investigated.

EXPERIMENTAL APPARATUS

The present experiment utilized the cold-neutron facilities at the Brookhaven National Laboratory research reactor and at the United States AMRA Research Reactor. The neutron beam incident on the scatterer is filtered through 8 in of refrigerated beryllium. No Bragg (elastic) scattering can occur for the low-energy (0.005 eV) incident neutrons, and the neutrons which are scattered at 90° by the sample are those which have gained energy or have been elastically scattered by the sample. The energy spectrum of the scattered neutrons was determined by the chopper time-of-flight technique.

The liquid and the polycrystalline samples were contained in an aluminium sample holder which was shielded by cadmium so that neutrons could only be scattered off the samples. The effective thickness of the polycrystalline or liquid material was sufficiently small (1 mm) so that multiple scattering was negligible.

The sample was cooled by a flow of cold gas boiled off from liquid nitrogen through coils in contact with the sample holder. By regulation of the nitrogen flow, the sample could be maintained at any desired temperature within ±2° between 294 and 90°K as determined by copper-constantan thermocouples in contact with the sample. The data for HF, HCl and HBr obtained in this manner are corrected for background, chopper transmission, detector efficiency and air scattering in the flight path.

RESULTS AND DISCUSSION

The interpretation of the observed spectra must take into account:
(a) The decreasing electronegativity of the anions in going from HF to HCl to HBr,
(b) The existence of hydrogen-bonded chains in the low-temperature phases of these compounds, with weak interaction between chains,
(c) The evolution of the spectra with phase and with temperature,
(d) Infrared, Raman, NMR, and diffraction data and
(e) Neutron inelastic scattering measurements on HF_2^- and $H_2F_3^-$ ions.
The results of the present measurements for HF, HCl and HBr will now be considered in detail.

HF

The time-of-flight distributions of neutrons scattered from the liquid and solid phases of HF are shown in Fig. 1(a) through 1(c) with an energy scale appended. The sharp rise in the distributions at 0.0052 eV followed by the more gradual decrease at lower energies constitutes the elastic ($E = E_0$) scattering. The sharp peak at 0.068 eV results from the two secondary Bragg cut-offs in Be at 0.0068 and 0.0064 eV. It should be noted that in Fig. 1(c), the residual rise at 0.005 eV is due, within statistical error, to the (200) Bragg cut-off in the Al of the chopper. This absence of an elastic peak implies the presence of a dense level system such that the

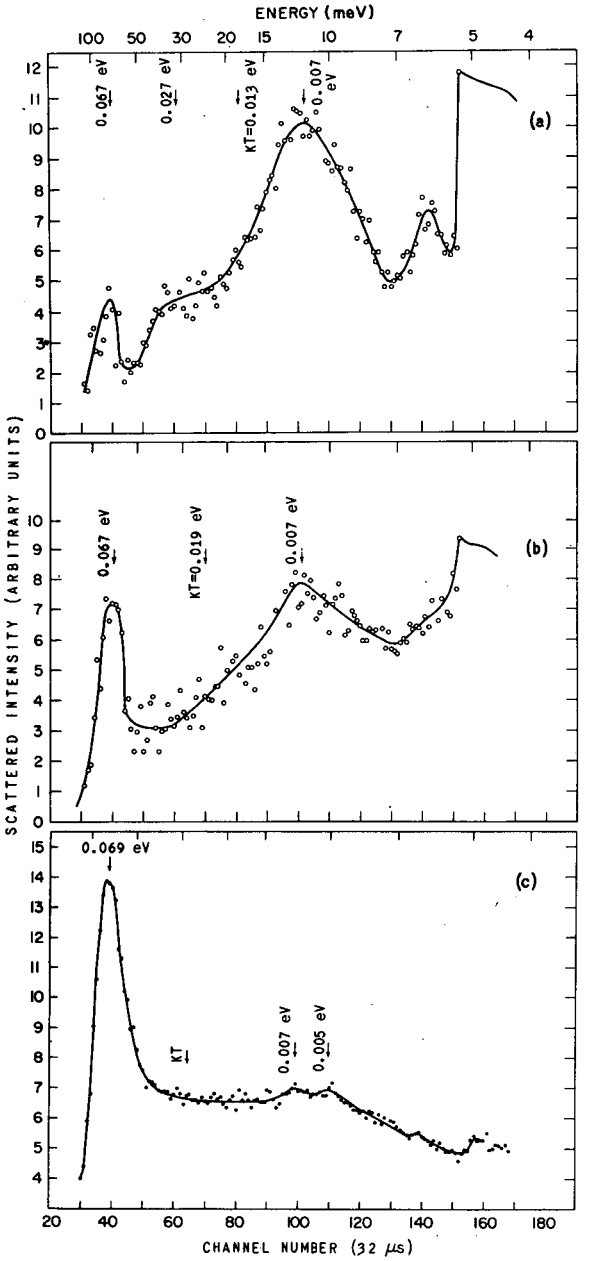

Fig. 1

The neutron time-of-flight spectra of 0.005 eV for incident neutrons scattered at a 90° angle by HF in (a) the solid phase at T = 153°K, (b) the liquid phase at T = 219°K and (c) the liquid phase at T = 280°K. The lower scale in abscissa represents times of flight (number of 32-μs channels) and the upper one is an energy scale

multiphonon-scattering cross-section is approaching the "classical limit" and is a monotonically decreasing function of the neutron energy.

In Fig. 1 it is seen that there exists a sharp peak at 0.067 eV (536 cm^{-1}) which does not alter its position significantly with temperature in the range between 153 to 280°K, or with phase. Similar peaks have been observed at 1176 cm^{-1} for the HF_2^- ion in KHF_2 and at 896 cm^{-1} for the $H_2F_3^-$ ions in both KH_2F_3 and NaH_2F_3 [15]. This vibration has also been observed in infrared measurements on KHF_2 [16] and has been attributed to a fundamental stretching ν_2 of the HF_2^- ion. This line is observed to shift to lower frequencies in going from HF_2^- to $H_2F_3^-$ to HF and as the F-F distances increase from 2.26 to 2.33 to 2.49 Å, respectively. This shift is quite pronounced but is quite similar in magnitude to those predicted by REID [17] for the low-frequency stretching vibration of the OH---O system as a function of the O-O distance. Moreover, the fact that this peak does not shift its frequency appreciably with temperature, with phase or with reduction in average molecular weight, lends further support to assigning this peak at 535 cm^{-1} in HF to a localized stretching mode involving only a single-chain segment and not to a mode involving co-operative vibration of the entire chain.

In the solid phase of HF, a shoulder is observed at 0.027 eV (116 cm^{-1}) and a broad asymmetrical peak is observed at 0.007 eV in the liquid phase. The shoulder rapidly disappears and the peak at 0.007 eV broadens with increasing temperature accompanied by a rapid decrease in the elastic peak as noted above. This behaviour is very similar to that previously observed for the temperature variation of the low-frequency co-operative deformation (ν_5) and torsional (ν_9) modes in high density polyethylene. It was noted that when the chain conformation was well defined and "frozen-in" (below the glass transition) both ν_5 and ν_9 appeared as acoustic branches with high-frequency cut-offs of 500 and 190 cm^{-1}, respectively. However, as the temperature was increased above the glass transition temperature, ν_5 quickly disappeared, while ν_9 gave way with increasing temperature to a large degree of internal rotational freedom [13].

Indeed at 428°K in the polyethylene spectrum, no elastic peak is observed, and the spectrum shape approaches that for free rotation with the exception of the optical CH_2 "rocking mode" at 720 cm^{-1} whose frequency is nearly independent of temperature. It is expected that in a manner similar to polyethylene, the HF chains in the solid should also give rise to a co-operative deformation and torsional mode but that these vibrations will be shifted to a lower frequencies than in polyethylene due to the fact that the intramolecular forces along the chain are weaker. In addition, in the solid phase of HF, it is expected that little internal rotation of chain segments will occur and that chain vibrations will occur about the equilibrium configuration. Thus, the shoulder in solid HF at 0.027 eV and the broad peak at 0.007 eV are associated with co-operative deformation and torsional modes respectively, while the peak at 0.067 eV corresponds to an optical mode involving the stretching of an F-H---F unit.

HCl, HBr

The spectra of neutrons which have gained energy in a single scattering event were measured for HCl liquid at 183°K and for solid phases I and III

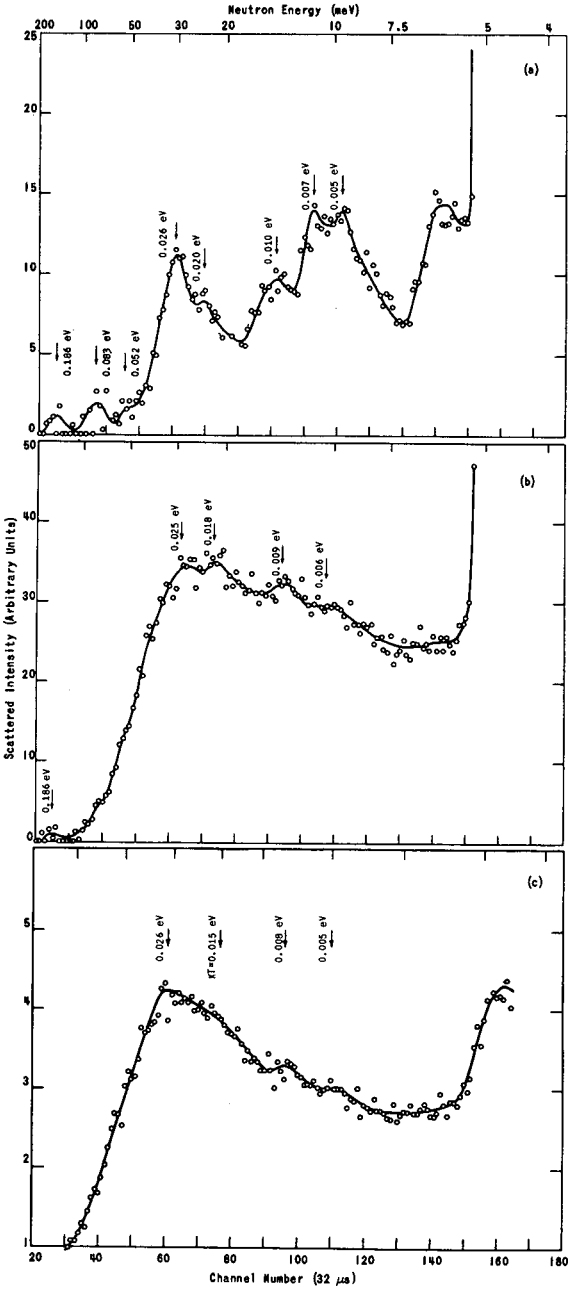

Fig. 2

The neutron time-of-flight spectra of HCl at a 90° angle for (a) the solid phase III at T = 85°K, (b) for solid phase I at T = 143°K and (c) for the liquid phase at T = 183°K

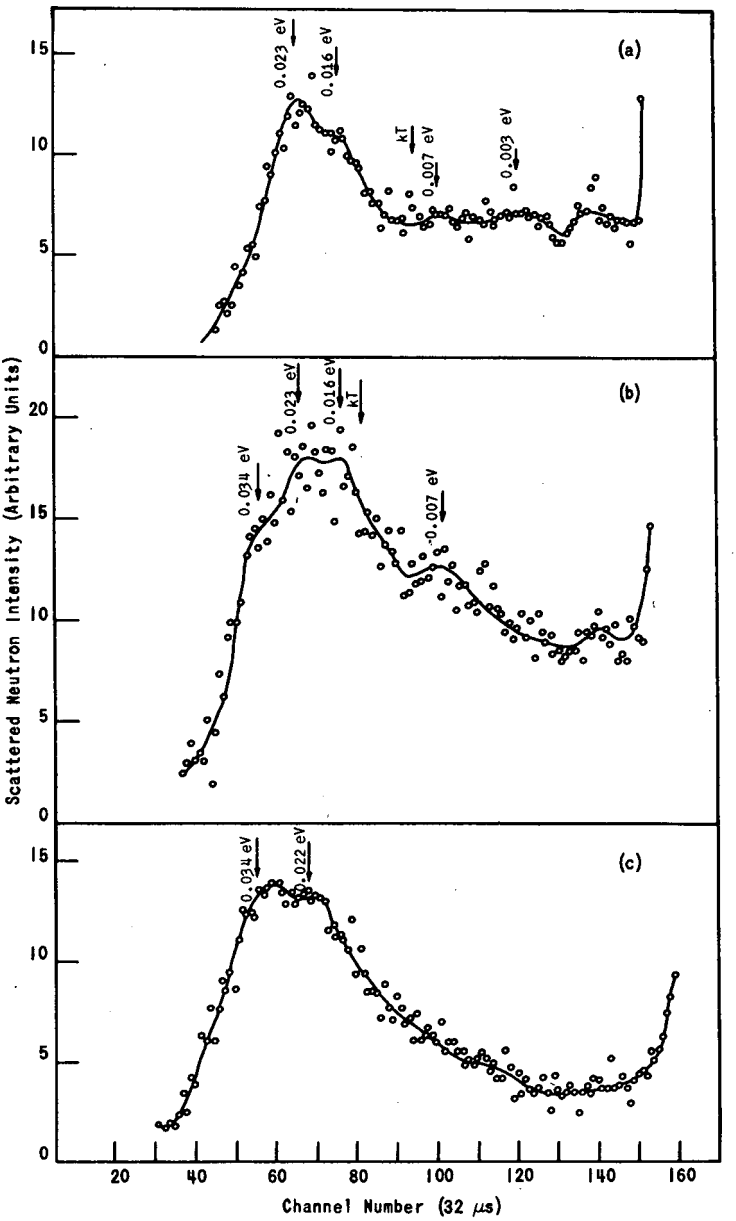

Fig. 3

The neutron time-of-flight spectra of HBr at a 90° angle for the (a) solid phase II at T = 103°K, (b) for solid phase I at T = 153°K and (c) for the liquid at T = 193°K

at 143° and 85°K, respectively, and are shown in Fig. 2 (a) (b) and (c). Spectra were also measured for HBr liquid at 193°K and for solid phases I and II at 153 and 103°K, respectively. The spectrum of solid phase III (below

TABLE II

COMPARISON OF THE FREQUENCIES OF THE LINES OBSERVED BY FAR INFRARED AND NEUTRON INELASTIC SCATTERING FOR SOLID HCl AND SOLID HBr

HCl		
Gebbie[a] (Solid Phase III, 77°K)	Hornig[b] (Solid Phase III, 77°K)	This work (Solid Phase III, 100°K)
		40
		56
86	71	80
109	109	152
217	223	208
	240	
296	266	264
496	496	416
		664
HBr		
Gebbie[a] (Solid Phase III)	Hornig[b] (Solid Phase III)	This work (Solid Phases I and II)
		24
57		
71	71	72
	109	
	132	128
200		184
218	240	
269	266	272
	400	

[a] ANDERSON, A., WALMSLEY, S.H. and GEBBIE, H.A., Phil. Mag. (Ser. 8) 7 (1952) 1243.
[b] HORNIG, D.F. and OSBERG, W.E., J. chem. Phys. 23 (1955) 662.

90°K) of HBr was not measured. These spectra are shown in Fig. 3. The energies of the various maxima obtained in the spectra of HCl and HBr and the corresponding frequencies are listed in Table II.

A peak at 0.026 eV and a shoulder at 0.019 eV in HCl phase III are observed together with lower energy peaks at 0.010, 0.007, and 0.005 eV. A shoulder at approximately 0.033 eV appears in the spectra of HCl phase I and persists in the liquid phase. It is not observed in the spectrum of HCl phase III. A similar peak is observed in the spectra of HBr at 0.031 eV. It is barely visible in HBr phase II, becoming more pronounced as the temperature increases up to the liquid phase. The peak at 0.023 eV persists in all phases. The peak at 0.019 eV is not observed in the liquid phase. The lowest energy peaks are much weaker in solid HBr than in solid HCl, and they disappear in the liquid phase of HBr.

The interpretation of neutrons scattered from HCl and HBr must take into account:

(a) Any similarity between the spectrum for solid HF and the spectrum for HCl phase III as hydrogen-bonded chains should exist in both, and internal rotation should be minimal. It may be expected that any co-operative chain vibrations will be shifted to lower frequencies in HCl phase III as the hydrogen bonding is weaker than for HF.

(b) The evolution of the maxima with increasing temperature and phase. As the intramolecular forces along a chain become progressively weaker, intermolecular forces will become more important; chain scission may occur, and internal rotation at a given temperature will become freer.

(c) The observed similarity between the spectrum of HCl phase I and the spectra of both HBr solid phases.

(d) The fact that maxima observed in the spectra of certain of the phases are broad and may be composed of unresolved lines.

In Table II the frequencies observed by neutron inelastic scattering are compared with the data of Gebbie and the frequencies observed by Hornig as combination lines of the HCl stretching fundamental. It is expected that lines caused by the torsion or stretching of an HCl molecule in the field of its neighbours might persist into phase I and the liquid phase while lines characteristic of the lattice structure of phase III would vary strongly and disappear with increasing temperature.

A comparison of the time-of-flight distributions for solid phase III and solid phase I (Fig. 2(a) and (b) shows that maxima observed in phase III at 0.027, 0.019, 0.009 and 0.006 eV also appear as weak maxima superimposed upon a broad distribution at 0.024, 0.018, 0.008 and 0.005 eV respectively, in solid phase I. In addition, the broad distribution is accompanied by a rapid decrease in the elastic peak. A similar behaviour has been observed in previous studies of polyethylene and polypropylene as the sample temperature was increased. Heating increased internal rotation and resulting chain disorder, giving rise to a broad multiphonon distribution. Indeed, at temperatures well above the melt, this distribution approached the shape expected for free rotation. However, structure similar to that observed in the spectrum of HCl phase I was observed which was due to the persistence of skeletal chain vibrations as long as the chain maintains its identity. A similar behaviour is observed for the solid phases I and II in HBr (Fig. 3(a) and (b)), but the persistence of the structure is less pronounced. Such behaviour strongly suggests that at least long segments of the hydrogen-bonded "zig-zag" chains peculiar to the lowest temperature phases of both HCl and HBr maintain their identity in the higher temperature solid phases. However, it is noted that the broad multiphonon distribution and hence the onset of internal rotation occurs at progressively lower temperatures with decreasing electronegativity. Likewise the persistence with increasing temperature of the structure, characteristic of a chain, decreases rapidly in the series HF, HCl and HBr.

The spectrum of liquid HCl (Fig. 2(c)) indicates a much lower degree of association than that observed for HF. The presence of peaks at 0.008 eV and 0.005 eV indicates that some of the vibrations characteristic of a chain as observed in the low-temperature solid phase still exist in the liquid. The

ratio of elastic to inelastic scattering is decreased relative to either of the solid phases. However, the presence of an elastic peak, together with the fact that the broad distribution peaks well above kT, indicates that the free rotational limit has not been reached. A frequency of 160 cm^{-1} (0.020 eV) was calculated by YIP and OSBORN [18] for a hindered rotation of an HCl molecule in the field of its neighbours. However, it should be pointed out that the theory of Yip and Osborn ignores any hydrogen bonding and assumes only an interaction of the dipole moment of a given molecule with an electric field representing the average influence of the nearest-neighbour molecules. They associate the energy of the peak in the neutron spectrum with $\sqrt{2V_0B}$ as predicted by the theory. While B is known, V_0 is not, and therefore was obtained from the present set of data. This correlation of experimental data with their theory is speculative, however, especially in the low-temperature phase of HCl where hydrogen bonding is important.

CONCLUSION

The present experiment has confirmed the existence of long zig-zag hydrogen-bonded chains in solid HF which persist through the liquid phase. A localized stretching frequency involving a segment of the chain has been observed at the same frequency (535 cm^{-1}) through the entire temperature range of the experiment. There is a large increase in the degree of internal rotational freedom as the temperature increases through the liquid phase. The observed peaks in the neutron spectrum of HF and their temperature behaviour have been correlated with similar features previously obtained for long chains, such as polyethylene.

In the spectra of HCl and HBr, part of the structure observed in the low-temperature phases is seen to persist into the liquid without appreciable shift in frequency. In addition, a broad multiphonon distribution is already apparent in the neutron spectrum of solid phase I and increases through the liquid phase. The first of these features suggests that hydrogen-bonded chains also exist in solid HCl and even in solid HBr, and keep some identity in the liquid phase. The second feature may be due in part to an increase in the degree of internal rotational freedom of segments along the chain together with an increased translational and rotational freedom of individual molecules in the field of their neighbours. This last effect is expected to be more pronounced in HCl and in HBr than in HF, since the influence of intermolecular forces increases as the electronegativity of the anions involved decreases. Some of the maxima observed in the present study for the solid phases of HCl and HBr compare reasonably well with the results of far infrared measurements. No attempt was made, however, to assign all the peaks to specific vibrations in view of the complexity of the structures. Such assignments must await a calculation of the low-frequency normal modes and of the lattice modes for the solid phases of HCl and HBr, similar to the calculations performed for polyethylene. The present results cast some doubt on the theories which attempt to account for the solid phases of these compounds only in terms of simple dipole models.

ACKNOWLEDGEMENT

The authors are indebted to Dr. V. Brajovic for his help and his interest in this work. They also wish to thank Dr. E.O. Salant and Dr. B.C. Frazer for useful discussions in the early stage of this work.

REFERENCES

[1] ATOJI, M. and LIPSCOMB, W.N., Acta cryst. 7 (1956) 173.
[2] International Critical Tables of Numerical Data of Physics, Chemistry, Technology VII (WASHBURN, W., Ed.), McGraw Hill Book Co., N.Y. (1930) 232.
[3] POWLES, J.G., Trans. Faraday Soc. (1952) 430; J. de Phys. Radium 13 (1952) 121.
[4] PHILLIPS, C.S.E., J. de Phys. Radium 13 (1952) 216.
[5] EUCKEN, A., Z. Elektrochem. 45 (1939) 126.
[6] PAULING, L., Phys. Rev. 36 (1930) 430.
[7] ALPERT, N.L., Phys. Rev. 75 (1949) 398.
[8] LEE, E., SUTHERLAND, G.B.B.M. and WU, C.K., Proc. roy. Soc. (London) A176 (1960) 493.
[9] HORNIG, D.F. and OSBERG, W.E., J. chem. Phys. 23 (1955) 662.
[10] HORNIG, D.F. and HIEBERT, G.L., J. chem. Phys. 27 (1957) 752.
[11] RANK, D.H., SITEARAM, P., GLICKMAN, W.A. and WIGGINS, T.A., J. chem. Phys. 39 (1963) 2673.
[12] VIDALE, G.L. and TAYLOR, R.C., J. Amer. chem. Soc. 78 (1956) 296.
[13] DANNER, H.R., SAFFORD, G.J., BOUTIN, H. and BERGER, M., J. chem. Phys. 40 (1964) 1617.
[14] TASUMI, M., SCHIMANOUCHI, T. and MIYAZAWA, T., J. mol. Spectry. 9 (1962) 261.
[15] BOUTIN, H., SAFFORD, G.J. and BRAJOVIC, V., J. chem. Phys. 39 (1963) 3135.
[16] KETELAAR, J.A.A., Recuil. trav. chim. Pays-Bas. 60 (1961) 523.
[17] REID, C., J. chem. Phys. 30 (1959) 182.
[18] YIP, S. and OSBORN, R.J., J. chem. Phys. 130 (1963) 1860.

STUDY OF THE LOW-FREQUENCY MOLECULAR MOTIONS IN POLYETHYLENE AND THE N-PARAFFINS BY SLOW NEUTRON INELASTIC SCATTERING*

H. BOUTIN, H. PRASK, S. F. TREVINO
PICATINNY ARSENAL, DOVER, N. J.,
AND
H. DANNER**
ARMY MATERIALS RESEARCH AGENCY, WATERTOWN, MASS.,
UNITED STATES OF AMERICA

Abstract — Résumé — Аннотация — Resumen

STUDY OF THE LOW-FREQUENCY MOLECULAR MOTIONS IN POLYETHYLENE AND THE N-PARAFFINS BY SLOW-NEUTRON INELASTIC SCATTERING. The time-of-flight spectra of slow neutrons inelastically scattered from samples of highly crystalline polyethylene at room temperature have been measured. A comparison has been made between the observed structure in the spectra and calculations of intra- and intermolecular motions of crystalline polyethylene. With the exception of a peak at 300 cm^{-1}, all of the structure has been accounted for in this manner. The possible origin of this peak is also discussed. The time-of-flight spectra of slow neutrons scattered from samples of solid n-butane, n-pentane, n-hexane and n-heptane were also obtained. Tentative identification of the observed frequencies on the basis of a normal mode calculation of intramolecular vibrations is made. In addition, a simple explanation for the behaviour of the melting temperature as a function of chain length is proposed.

ÉTUDE DES MOUVEMENTS MOLÉCULAIRES DE BASSE FRÉQUENCE DANS LE POLYÉTHYLÈNE ET LES PARAFFINES-N AU MOYEN DE LA DIFFUSION INÉLASTIQUE DES NEUTRONS LENTS. Les auteurs ont mesuré les spectres de temps de vol des neutrons lents diffusés de façon inélastique par des échantillons de polyéthylène fortement cristallin à la température ambiante. Ils ont comparé la structure observée dans les spectres et les calculs des mouvements intramoléculaires et intermoléculaires du polyéthylène cristallin. A l'exception d'un pic à 300 cm^{-1}, l'ensemble de la structure a pu être expliqué de cette manière. Les auteurs étudient l'origine éventuelle de ce pic. Ils ont également obtenu les spectres de temps de vol des neutrons lents diffusés par des échantillons solides de butane-n, pentane-n, hexane-n et heptane-n. Ils identifient provisoirement les fréquences observées en se fondant sur un calcul du mode normal des vibrations intramoléculaires. Enfin, ils proposent une explication simple des variations de la température de fusion en fonction de la longueur de la chaîne.

ИЗУЧЕНИЕ НИЗКОЧАСТОТНЫХ МОЛЕКУЛЯРНЫХ ДВИЖЕНИЙ В ПОЛИЭТИЛЕНЕ И N-ПАРАФИНАХ С ПОМОЩЬЮ НЕУПРУГОГО РАССЕЯНИЯ МЕДЛЕННЫХ НЕЙТРОНОВ. Были измерены по времени пролета спектры медленных нейтронов, неупруго рассеянных на образцах сильно кристаллизованного полиэтилена при комнатной температуре. Было произведено сравнение наблюдаемой структуры спектров с результатами расчетов внутримолекулярных и межмолекулярных движений кристаллического полиэтилена. Таким образом объясняется вся структура, за исключением пика 300 $см^{-1}$. Рассматривается также возможная причина этого пика. Получены также по времени пролета спектры медленных нейтронов, рассеянных на образцах твердых n-бутана, n-пентана, n-гексана и n-гептана. Произведено предварительное определение наблюдаемых частот на основе обычного расчета внутримолекулярных колебаний. Кроме этого, предлагается простое объяснение зависимости температуры плавления от длины цепи.

ESTUDIO POR DISPERSIÓN INELÁSTICA DE NEUTRONES LENTOS DE LOS MOVIMIENTOS MOLECULARES DE BAJA FRECUENCIA EN EL POLIETILENO Y LAS PARAFINAS NORMALES. Por el método de tiempo de vuelo

* This work was performed at the United States AMRA Research Reactor, Watertown, Mass.

** Guest scientist from the University of Missouri, Columbia, Mo.

se han medido los espectros de neutrones lentos inelásticamente dispersos en muestras de polietileno altamente cristalino, a la temperatura ambiente. Se han comparado la estructura observada de los espectros con los valores calculados de los movimientos intra e intermoleculares en el polietileno cristalino. De esta manera se ha logrado explicar toda la estructura, salvo un pico que aparece a 300 cm^{-1}. Se estudia también el posible origen de este pico. Asimismo, se han obtenido los espectros de tiempo de vuelo de neutrones lentos dispersos en muestra de n-butano, n-pentano, n-hexano y n-heptano sólidos. Se trata de identificar las frecuencias observadas basándose en el cálculo de las vibraciones intramoleculares según modos normales. Además, se propone una explicación sencilla de la influencia de la longitud de la cadena sobre el punto de fusión.

INTRODUCTION

Inelastic neutron scattering measurements directed toward the measurement of the low-frequency thermal vibrations in polyethylene have been reported previously [1]. Although subject to a number of simplifying assumptions, calculations of the normal modes in this simple polymer indicate that both the acoustic chain vibrations [2] and all of the intermolecular vibrations [3] lie in the frequency range investigated. The results of these calculations as well as the comparison with infrared and Raman measurements [4] are used as a guide in the interpretation of the neutron scattering results. However, the neutron spectra are not limited by selection rules, as are the optical spectra, and are, in general, more sensitive to the motions at low frequency. A knowledge of the low-frequency motions is essential to a more complete understanding of the physical properties of the solid polymer.

On the basis of present experimental evidence [5], a solid polymer may be completely amorphous or it may exhibit a very high degree of crystallinity. Whether or not a given polymer "crystallizes" depends not only on the size and complexity of the units which link together to form the chain, but also on the method of preparation and the thermal history of the sample. In polyethylene, for example, although samples prepared by slowly cooling from the melt at normal pressures show a high degree of crystallinity, they nevertheless exhibit properties which strongly suggest the presence of regions in which the material is amorphous. The existence of the glass transition interval, defining a temperature below which all internal rotations in the amorphous region are "frozen" out, seems to support the "fringed-micelle" model of polyethylene. According to this model, the individual chains pass successively through regions of order (crystalline) and regions of disorder (amorphous). Recently, however, single crystals of polyethylene in the form of thin platelets have been prepared both from solution [6] and from the melt under pressure [7]. X-ray analyses of these samples indicate that the chains are folded in an ordered lattice-like configuration and suggest that the amorphous regions are distributed around lattice defects.

An interpretation of the inelastic neutron scattering spectrum of a sample of polyethylene Marlex 6050, which is about 85% crystalline* at 100°K (below the glass transition), was suggested [1], which assumed the existence of crystalline and amorphous phases and used the results of a calculation of the normal modes of vibration of an infinite transplanar polyethylene chain [2]. It was postulated that the individual chains consisted of long trans-

* As determined by density measurements.

planar segments gauche-linked with short segments (also transplanar) 3-5 units long corresponding to crystalline and amorphous regions, respectively. This model tried to take into account the influence of the amorphous region of the sample on the normal vibrations in the crystalline regions. In particular it provided, by means of segment coupling, an explanation for the additional structure present in the neutron spectrum not predicted by the calculations. However, in this model only intramolecular motions were considered to explain the observed maxima, and intermolecular motions were neglected.

The purpose of the present paper is twofold:

(a) To examine samples of polyethylene of a higher degree of crystallinity in order to decrease the influence of the amorphous regions for comparison with previous results, and to consider a re-interpretation of the neutron spectra in the light of intermolecular motions whose frequencies have been recently calculated [3].

(b) To extend the study to the short chain n-paraffins in the solid state. These samples, which are assumed to be crystalline, afford a comparison with a calculation [8] of the normal modes using a set of force constants similar to those used for polyethylene.

EXPERIMENT

The data presented were obtained using a conventional slow neutron time-of-flight spectrometer. The spectrometer is installed at the 1-MW AMRA light-water swimming pool type reactor. In this method, beryllium-filtered neutrons which are scattered through an angle of 90° pass through a chopper rotating at 7200 rpm and are energy-analysed by measuring the flight time through a 5-m evacuated flight path. The data were corrected for background, chopper transmission and detector efficiency. The frequency distributions were deduced from the neutron time-of-flight spectra in the one-phonon approximation assuming a Debye-Waller factor equal to 1. This seems to be a reasonably good approximation for samples in the solid phase. The n-paraffins were contained in a flat aluminium holder (3 mm thick) backed with cadmium. The holder was mounted on an aluminium plate through which liquid nitrogen was circulated.

DISCUSSION

At 100°K there is an appreciable decrease in the effect of rotational isomerism in the samples and its large contribution to the scattering. In the interpretation of the spectra, one has to differentiate between the contribution of intramolecular and intermolecular vibrations which often overlap below 500 cm^{-1}. For an infinite chain, the intramolecular vibrations will be composed of acoustic and optical branches. The optical branches of normal modes occupy a relatively narrow frequency range with a higher density of states at the zone boundaries giving rise to sharp peaks in the neutron spectra. An acoustic branch should present a sharp high-frequency cut-off. This was observed in the neutron spectrum of polyethylene [1]. If the chain is of

finite length, there will be discrete frequencies which correspond to the various types of motion, e.g. CH_2 or CH_3 rocking, C-C-C bending or C-C torsion. The assignment of observed maxima was undertaken for the neutron spectra of the n-paraffins in the solid state. As for the intermolecular motions of translational nature (lattice modes), their number depends on the symmetry of and number of molecules in the unit cell. In most cases, however, lattice modes are too close in frequency and too numerous to be well resolved, and they form a broad peak in the neutron spectrum.

Polyethylene

The neutron spectrum of a sample of polyethylene Marlex 6050 examined at 100°K [1] essentially showed three maxima below 150 cm^{-1}, a sharp cut-off at 200 cm^{-1}, and two broad peaks at 300 and 500 cm^{-1}, respectively. The theory of TASUMI et al. [2]* predicts that for an infinite transplanar zig-zag chain of polyethylene two cut-off frequencies exist at 200 and 500 cm^{-1} which represent two acoustical branches of normal modes corresponding to torsion and deformation of the chain, respectively. ENOMOTO and ASAHINA [3] have recently calculated the lattice modes in polyethylene and showed that the six lattice modes all lie below 125 cm^{-1}. There are four optical and two acoustic branches. The extent of the optical (R_z, R_z', T_x', T_y') and the cut-offs of the acoustic (T_x, T_y) branches are shown in Fig. 1. There are peaks in the neutron spectrum at 40, 80, and 120 cm^{-1} which are associated with two optical branches (40 cm^{-1}, 120 cm^{-1}) and an acoustic cut-off (80 cm^{-1}) in Enomoto's calculated dispersion curves. Miyazawa in Ref. [3] has also calculated peaks near 80 and 100 cm^{-1}, due respectively to overall rotations of an entire chain about its axis and translatory vibrations of adjacent chains. A peak at 79 cm^{-1} is also seen in infrared measurements [9] and is shown to be caused by lattice vibrations. The main discrepancy between these calculations and the neutron measurements lies therefore in the existence of the broad peak around 300 cm^{-1}. It was suggested that the peak at 300 cm^{-1} arose from the existence of amorphous regions in the sample not taken into account by the theory. The spectra of single crystals of polyethylene grown from solution and of stretch-oriented Marlex 6050 samples are shown in Fig. 1 at room temperature. They are essentially similar to the spectra of Marlex 6050 taken previously. The peak at 300 cm^{-1} still exists and therefore may be due to segment coupling as originally suggested. This peak could be attributed to a difference line between ν_5 and ν_9 vibrations. If so, it would arise from multiple scattering or multiphonon effects in the sample. The neutron spectrum was not significantly altered when samples of 0.02 cm and 0.3 cm thickness were used so that this peak cannot be attributed to multiple scattering. The contribution of two phonon processes was recently estimated [10] and was shown to be negligible even at room temperature. It is therefore unlikely that the peak at 300 cm^{-1} could be attributed to a difference line. It seems to be characteristic of a polyethylene chain, although it is neither seen by infrared spectroscopy nor predicted by the theory of T.S.M. and is insensitive to the degree of crystallinity of the sample. A further test of the set of force constants used by T.S.M. for polyethylene

* Hereafter referred to as T.S.M.

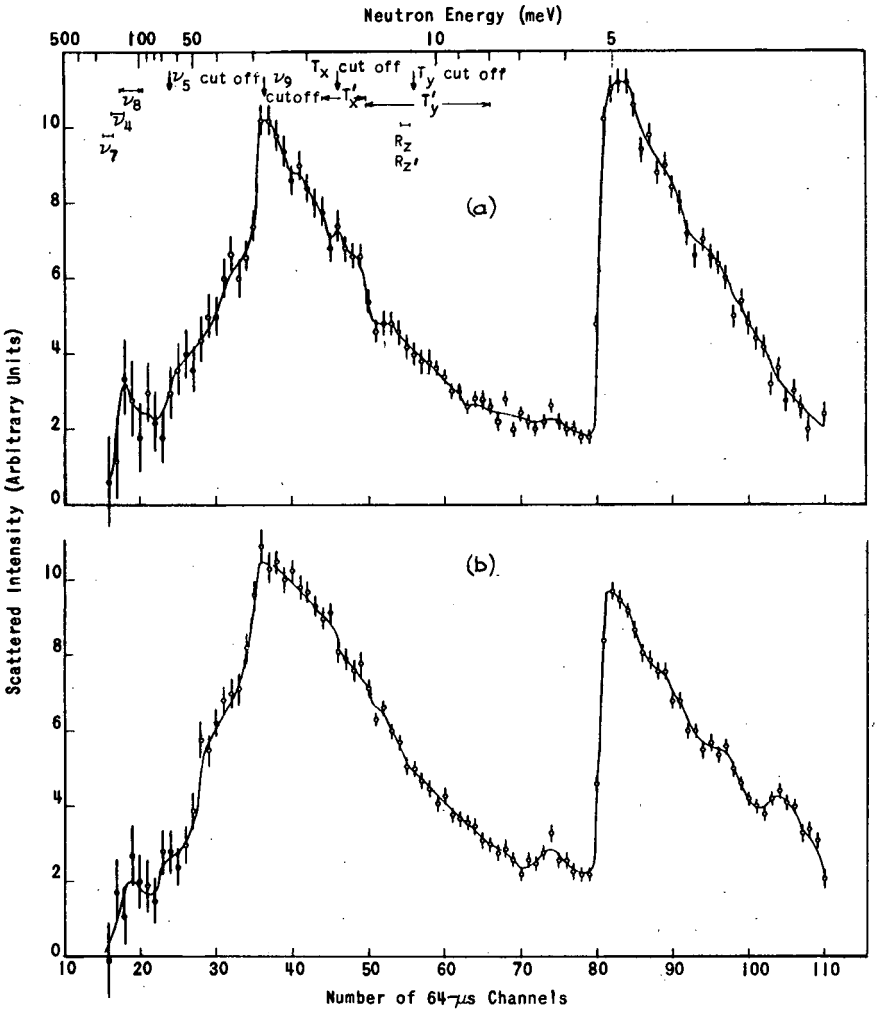

Fig. 1

Time-of-flight distribution of neutrons scattered at 298°K and at $\phi = 90°$ from
(a) a crystalline polyethylene sample, and
(b) a stretch-oriented Marlex 6050 polyethylene sample.

The arrows indicate the positions of the various cut-offs as calculated by Tasumi et al. and by Enomoto and Asahina. The horizontal bars indicate the calculated dispersion of some of the optical modes from calculations of Tasumi et al. and of the lattice modes as calculated by Enomoto and Asahina. The lower abscissa scale represents times-of-flight (number of 64-μs channels) and the upper one is an energy scale.

would be the comparison of measured and calculated frequencies of the short chain paraffins, since it has been shown that it is reasonable to assume that the force constants are transferable between polyethylene and the normal n-paraffins [8].

n-Paraffins

SCHACHTSCHNEIDER and SNYDER [8] report the infrared spectra of the normal paraffins from C_4H_{10} through $C_{19}H_{40}$ and of polyethylene. Their measurements extend down to approximately 400 cm^{-1}. An extensive normal co-ordinate calculation was performed by these authors of the vibrational frequencies of the paraffins and of the optically active frequencies of polyethylene. A thirty-five parameter valence force field was used to reproduce some 270 fundamental frequencies with an average error of 0.25%. In the low-frequency range, however, very few of the frequencies due to C-C-C angle bending and none due to C-C torsion were available. The torsion force constant was chosen so as to reproduce the infrared frequency (280 cm^{-1}) of the torsional mode of ethane. The values of the optically active frequencies of polyethylene calculated by these authors are in agreement with those of T.S.M. Transferability of force constants amongst the paraffins and polyethylene was assumed.

In the present measurements, the spectra of butane, pentane, hexane and heptane at 100°K were obtained. The samples used were chromatoquality. The spectra and corresponding frequency distributions are shown in Figs. 2, 3, 4 and 5. The calculated frequencies of Schachtschneider and Snyder are indicated on the figures as are the observed frequencies. Table I contains the observed frequencies of the present measurements, and of infrared [8] and Raman [4] measurements, and tentative assignments from the calculations of Schachtschneider and Snyder. The additional frequencies unaccounted for by the calculations must await further measurements for identification.

MATSUDA et al. [11] have recently formulated a general method for obtaining normal vibrations of short chain molecules. The method explicitly separates the contribution of the end groups from that of the structure of the original infinite molecule. Using this method, the high-frequency modes measured by Snyder and Schachtschneider of the paraffins are analysed, and the corresponding optical dispersion curves of T.S.M. are reproduced. A similar analysis of the low-frequency motions of the paraffins is difficult because of the incompleteness of the method and the uncertainty in the assignments of the frequencies observed in the present experiment.

Although no calculations or previous observations of the lattice modes of the crystalline paraffins are available, it is expected that there will be a reasonably large number of overlapping modes present. These modes would exhibit themselves as a broad unresolved peak in the spectrum of the solid paraffins. This general structure is observed at low frequencies in the spectra of the paraffins investigated in the present measurement. It should be noted that as the length of the chain increases, the lattice frequencies and the intramolecular frequencies are more intermingled.

CONCLUSION

The time-of-flight spectrum of cold neutrons scattered from samples of highly crystalline polyethylene has been measured. All of the maxima exhibited by these spectra can be accounted for by intramolecular or inter-

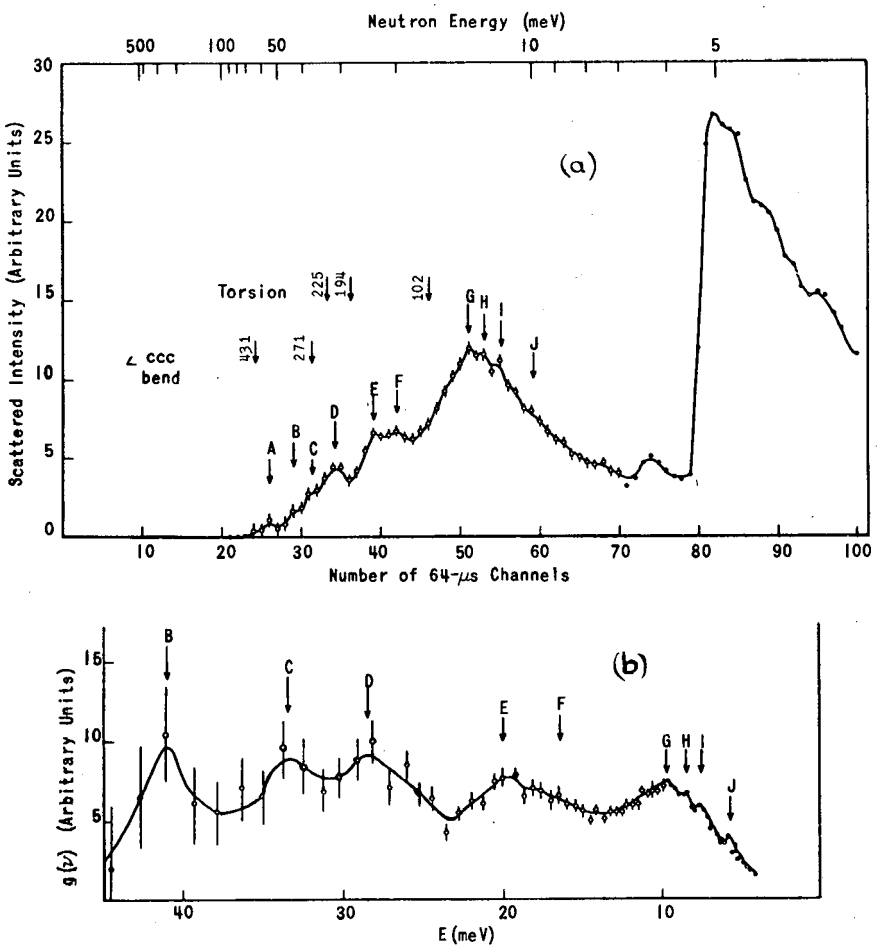

Fig. 2

(a) Time-of-flight distribution of neutrons scattered from solid butane at 100°K and at $\phi = 90°$. The arrows labelled with letters indicate the energy of the various observed frequencies. The two upper sets of arrows indicate the peaks calculated by Schachtschneider and Snyder. The numbers are expressed in cm^{-1}.
(b) The frequency distribution $g(\nu)$ derived from (a) in the one phonon approximation; $\hbar\omega$ is the phonon energy.

molecular vibrations with the exception of a peak at approximately 300 cm^{-1}. This peak seems to be insensitive to the degree of crystallinity in the sample and therefore cannot be attributed to the effects of the amorphous regions as was previously suggested. It also seems unlikely that this peak could be explained in terms of multiphonon or multiple scattering effects. However, the configuration assumed in the calculations both for intermolecular and intramolecular vibrations, namely extended transplanar zig-zag chains, is not rigorously satisfied in the present measurement. A more stringent test of the validity of these calculations would be provided by a sample of poly-

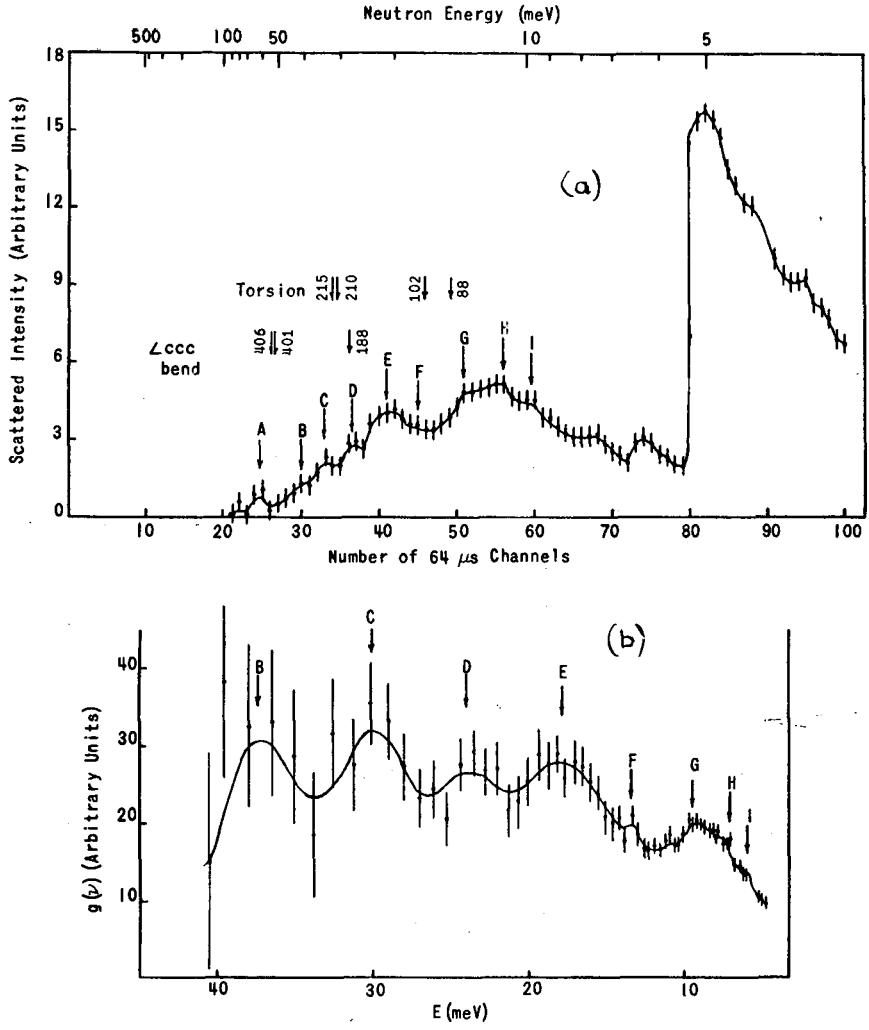

Fig. 3

(a) Time-of-flight distribution of neutrons scattered from solid pentane at 100°K and at $\phi = 90°$. The arrows labelled with letters indicate the energy of the various observed frequencies. The two upper sets of arrows indicate the peaks calculated by Schachtschneider and Snyder. The numbers are expressed in cm^{-1}.
(b) The frequency distribution $g(\nu)$ derived from (a) in the one phonon approximation; $\hbar\omega$ is the phonon energy.

ethylene grown from the melt under pressure in which it has been shown [7] that the chains are in an extended transplanar configuration.

A comparison is made between the observed frequencies obtained from the neutron spectra of the short n-paraffins and calculated frequencies. The agreement is generally good although there are a few cases in which the assignment is ambiguous. An interesting feature of the present measurements

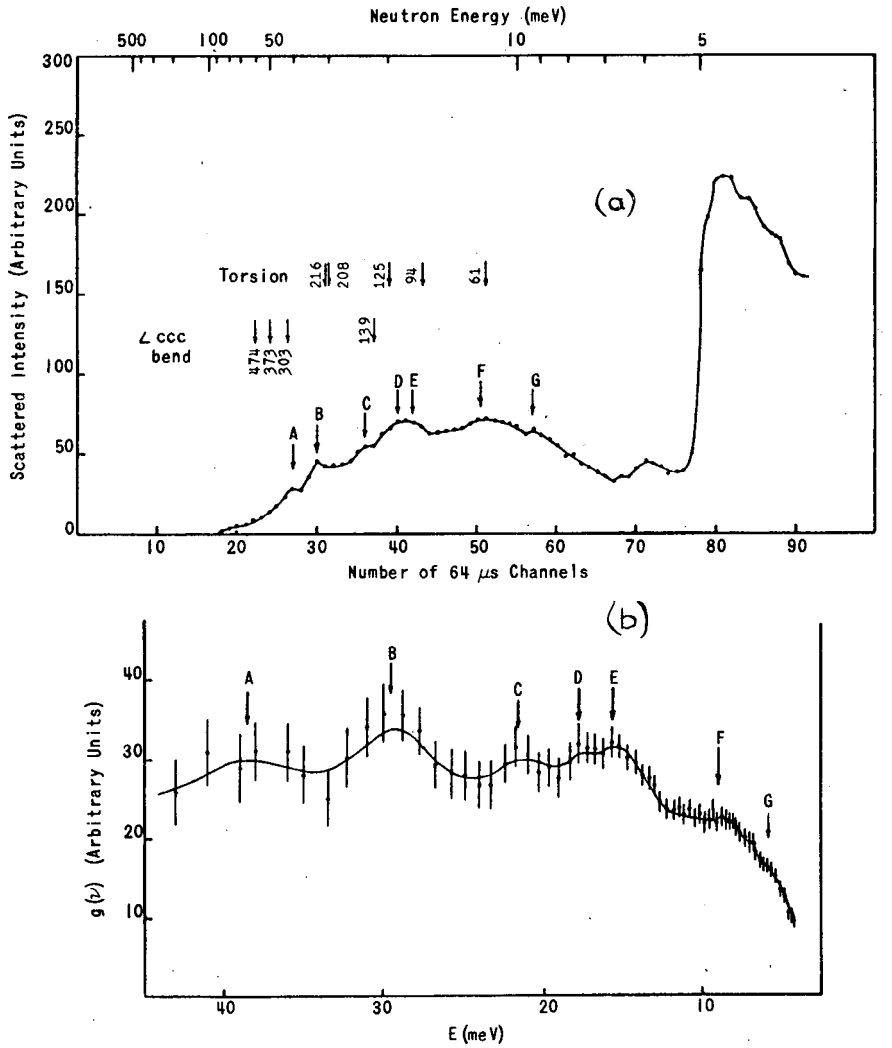

Fig. 4

(a) Time-of-flight distribution of neutrons scattered from solid hexane at 100°K and at $\varphi = 90°$. The arrows labelled with letters indicate the energy of the various observed frequencies. The two upper sets of arrows indicate the peaks calculated by Schachtschneider and Snyder. The numbers are expressed in cm^{-1}.
(b) The frequency distribution $g(\nu)$ derived from (a) in the one phonon approximation; $\hbar\omega$ is the phonon energy.

is that as the number of carbon atoms in the chain increases, the separation between the frequencies of intramolecular and intermolecular vibrations decreases. This could provide a simple explanation for the increase in the melting temperature with increasing chain length. If an intramolecular vibration can easily share its energy with the entire lattice (as would be the

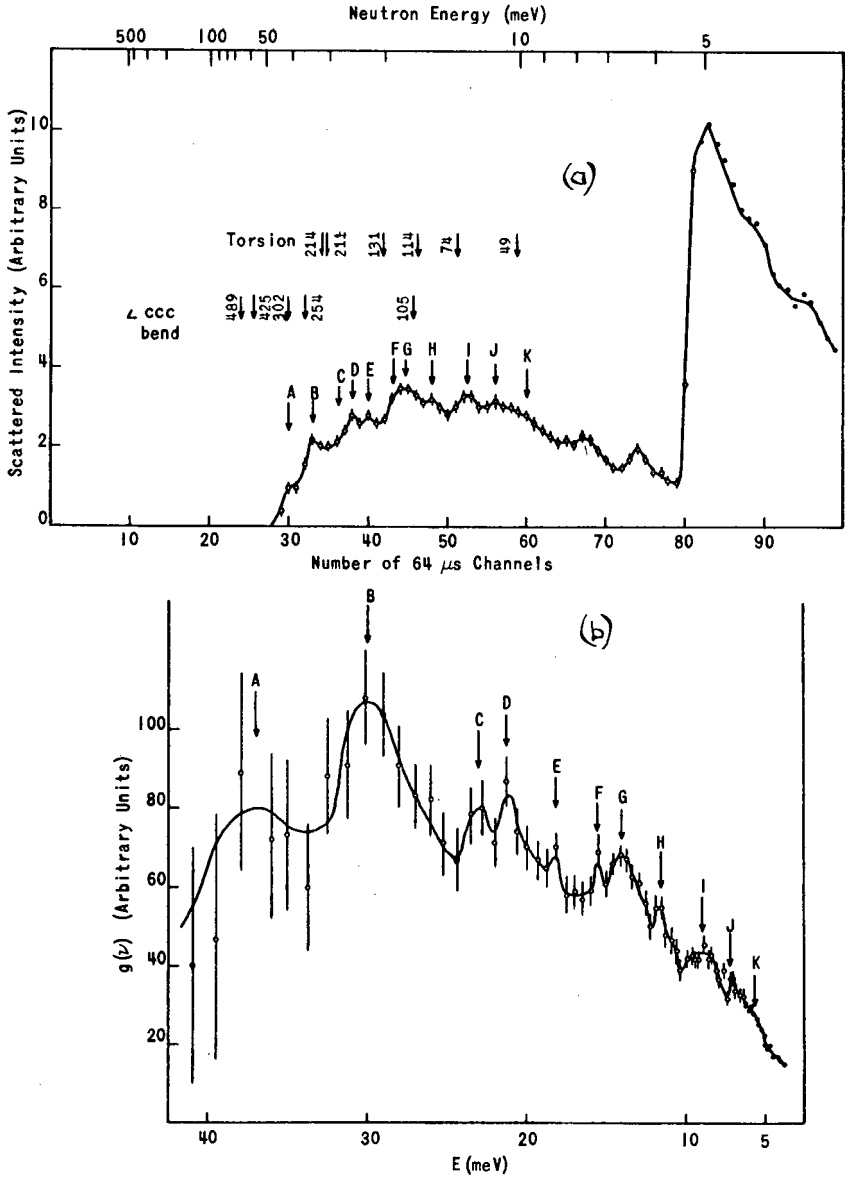

Fig. 5

(a) Time-of flight distribution of neutrons scattered from solid heptane at 100°K and at $\phi = 90°$. The arrows labelled with letters indicate the energy of the various observed frequencies. The two upper sets of arrows indicate the peaks calculated by Schachtschneider and Snyder. The numbers are expressed in cm^{-1}.

(b) The frequency distribution $g(\nu)$ derived from (a) in the one phonon approximation; $\hbar\omega$ is the phonon energy.

TABLE I

COMPARISON OF THE OBSERVED AND CALCULATED FREQUENCIES OF THE N-PARAFFINS

Sample	Observed (this work)[a] (cm^{-1})	Calculated and mode[b] (cm^{-1})	Observed (other work)[c] (cm^{-1})
BUTANE	415 s	431 bending	427(IR, S.)[b], 425 (R., S.)
	328 w		320 (R., Liq.)
	268 w	271 bending	287 (R., Liq.)
	228 s	225 torsion	259 (R., Liq.)
	160 s	194 torsion	207 (R., Liq.)
	132 w	102 torsion	
	78 s		
	68 w		
	60 s		
	45 vw		
PENTANE	471 w		467 (R., Liq.)
		401 bending	399 (IR, S.)[b], 400(R., Liq.)
		406 bending	406 (R., S.)
	298 w		333 (R., Liq.)
	240 s	210, 215 torsion	
	192 s	188 bending	
	142 s		
	110 w	102 torsion	
	75 s	88 torsion	
	56 w		
	46 w		

[a] s - strong, w - weak, vw - very weak.

[b] SCHACHTSCHNEIDER, J. H. and SNYDER, R. G., Spectrochim. Acta 19 (1963) 117.

[c] The Raman measurements are taken from: MIZUSHIMA, S., Structure of Molecules and Internal Rotations, Academic Press Inc., New York (1954).

case if there were a similar vibrational frequency for the two motions), it would be more difficult to store energy, at a given temperature, in those intramolecular motions (torsion and angle bending) which presumably are responsible for melting [12].

TABLE I (cont.)

Sample	Observed (this work)[a] (cm^{-1})	Calculated and mode [b] (cm^{-1})	Observed (other work)[c] (cm^{-1})
HEXANE	300 s	303 bending	
	236 s	216 torsion	
	172 s	208 torsion	
	141 s	139 bending	
	125 w	125 torsion	
		94 torsion	
	72 s	61 torsion	
	46 w		
HEPTANE			310(R., Liq.), 311(R., S.)
	296 w	302 bending	285(R., Liq.), 309(IR, S.)[b]
	240 s	254 bending	222 (R., Liq.)
	184 vw	214 torsion	198(R., Liq.)
	170 s	211 torsion	
	145 w	131 torsion	
	124 w	114 torsion	
	112 s	105 bending	
	92 s		
	72 s	74 torsion	
	45 w	49 torsion	

[a] s - strong, w - weak, vw - very weak.

[b] SCHACHTSCHNEIDER, J. H. and SNYDER, R. G., Spectrochim. Acta 19 (1963) 117.

[c] The Raman measurements are taken from: MIZUSHIMA, S., Structure of Molecules and Internal Rotations, Academic Press Inc., New York (1954).

ACKNOWLEDGEMENTS

The authors would like to thank Professor R.S. Stein for providing the samples of crystalline polyethylene.

REFERENCES

[1] DANNER, H. R., SAFFORD, G. J., BOUTIN, H. and BERGER, M., J. chem. Phys. 40 (1964) 1417.
KING, J. S. and DONOVAN, J. L., Bull. Amer. phys. Soc. 9 (1964) 623.
ZEMLYANOV, M. G. and CHERNOPLEKOV, N. A., Inelastic Scattering of Neutrons in Solids and Liquids I IAEA, Vienna (1963) 297-305.

[2] TASUMI, M., SCHIMANOUCHI, T. and MIYAZAWA, T., J. mol. Spectry. 9 (1962) 261.
LIN, T.P. and KOENIG, J.L., J. mol. Spectry. 9 (1962) 228.
[3] ENOMOTO, S. and ASAHINA, N., J. polymer Sci. 2 (1964) 3523.
MIYAZAWA, T. and KITAGAWA, T., Polymer Lett. 2 (1964) 395.
[4] KRIMM, S, LIANG, C.T. and SUTHERLAND, G.B.B.M., J. chem. Phys. 25 (1956) 549.
MIZUSHIMA, S., Structure of Molecules and Internal Rotations, Academic Press Inc., N.Y. (1954).
[5] GEIL, P.H., Polymer Single Crystals, Interscience, N.Y. (1963).
[6] KELLER, A., J. polymer Sci. 17 (1955) 291; 351.
[7] WUNDERLICH, B. and ARAKAWA, T., J. polymer Sci. 2 (1964) 3697.
[8] SCHACHTSCHNEIDER, J.H. and SNYDER, R.G., Spectrochim. Acta 19 (1963) 117.
[9] BERTI, J.E. and WHALLEY, E., J. chem. Phys. 41 (1964) 575.
[10] SUMMERFIELD, G.C. and ERICKSON, J.D., Bull. Amer. phys. Soc. 9 (1964) 623.
[11] MATSUDA, H., OKADA, K., TAKASE, T. and YAMAMOTO, T., J. chem. Phys. 41 (1964) 1527.
[12] BUNN, C.W., J. polymer Sci. 16 (1955) 323.

DISCUSSION

M.G. ZEMLYANOV: For complicated systems like polyethylene there is no simple relationship between the measured double differential neutron-scattering cross-section and the frequency distribution function, as there is in the case of monatomic crystals with cubic symmetry. The relationship is complicated by the unknown energy dependence of the polarization vectors. It does not seem entirely correct, therefore, to make a comparison between results obtained directly from the experimental cross-section and those obtained from calculations.

S.F. TREVINO*: The expression used in the present work relating the double differential cross-section and the frequency-distribution function is that of Kothari and Singwi**. The expression was derived for cubic symmetry and its use in the present work constitutes an approximation. Thus, the exact shape of the frequency distribution is not known with sufficient accuracy to allow meaningful calculation of, for example, specific heat. On the other hand, we feel that the observed structure is reliable and information concerning the characteristic energies of the vibrations of the sample can be extracted.

* The following answer to Mr. M.G. ZEMLYANOV'S question was submitted by mail by Mr. S.F. TREVINO on behalf of Mr. H. BOUTIN.

** KOTHARI, L.S. and SINGWI, K.S., Solid State Phys. 8 (1959) 109.

INELASTIC SCATTERING OF NEUTRONS IN ETHYLENE

D. BALLY, S. TODIREANU AND V. TARINĂ
INSTITUTE OF ATOMIC PHYSICS, BUCHAREST, ROMANIA

(Presented by J. Janik)

Abstract — Résumé — Аннотация — Resumen

INELASTIC SCATTERING OF NEUTRONS IN ETHYLENE. A study was made of the inelastic scattering of neutrons in ethylene using a triple-axis spectrometer. The resolution of the spectrometer in the incident neutron energy range explored, expressed by the ratio $\Delta E/E$, where ΔE is the total half-height width of the curve describing the energy distribution of the neutrons diffused by vanadium, was below 0.12. The incident neutron energy was varied over the range 22 -72 meV, and the diffusion angle between 5° and 90°.

At the upper limit of the energy range studied, good agreement is observed between the experimental data and the theoretical curve of Krieger and Nelkin. For lower incident neutron energy values, the curve representing the experimental data has a shape similar to that observed by Randolph et al. for methane; the half-height width of the experimental curve is less than the theoretical width calculated by the Krieger-Nelkin formula. This discrepancy between experimental and theoretical data is probably due to the discrete structure of the molecular rotation levels, and shows that in this case use of the formula proposed by Griffing is called for.

Measurements carried out on methane gave partial differential cross-section values which were in agreement with those of Randolph et al., and which, in the region of maximum, are different from those calculated by Griffing. It is probable that stricter treatment of the contribution from the resolving power of the apparatus would improve the degree of agreement between the theoretical and experimental data.

Curves S(d) were drawn for different values of the parameter β, and for low values of β satisfactory agreement with the theoretical curves under the Krieger-Nelkin formula was obtained.

DIFFUSION INÉLASTIQUE DES NEUTRONS DANS L'ÉTHYLÈNE. On a étudié la diffusion inélastique des neutrons dans l'éthylène en utilisant un spectromètre à trois axes. La résolution du spectromètre dans le domaine énergétique exploré des neutrons incidents, exprimé par le rapport $\Delta E/E$, où ΔE est la largeur totale à mi-hauteur de la courbe qui décrit la distribution énergétique des neutrons diffusés par le vanadium, a été inférieure à 0,12. On a varié l'énergie des neutrons incidents dans l'intervalle 22-72 meV, et l'angle de diffusion entre 5° et 90°.

Pour la limite supérieure de l'intervalle énergétique étudié, on observe une bonne concordance entre les données expérimentales et la courbe théorique de Krieger et Nelkin. Pour des valeurs plus petites de l'énergie des neutrons incidents, la courbe qui décrit les données expérimentales a une inflexion analogue à celle observée par Randolph et al. pour le méthane; la largeur à mi-hauteur de la courbe expérimentale est inférieure à la largeur théorique calculée selon le formalisme Krieger-Nelkin. Cette non-concordance entre les données expérimentales et théoriques est probablement due à la structure discrète des niveaux moléculaires de rotation; elle indique que, dans ce cas, il est convenable d'employer le formalisme proposé par Griffing.

Les mesures effectuées sur le méthane ont conduit pour la section efficace différentielle partielle à des valeurs qui concordent avec celles de Randolph et al. et qui, dans la région du maximum, sont différentes de celles calculées par Griffing. Il est probable que le traitement plus correct de la contribution de la résolution de l'appareil améliorerait la concordance entre les données théoriques et expérimentales.

On a représenté les courbes S(d) pour de différentes valeurs du paramètre β en obtenant pour des faibles valeurs de β une correspondance satisfaisante avec les courbes théoriques selon le formalisme Krieger et Nelkin.

НЕУПРУГОЕ РАССЕЯНИЕ НЕЙТРОНОВ В ЭТИЛЕНЕ. Изучение неупругого рассеяния нейтронов в этилене проводилось с помощью трехосевого спектрометра. Разрешающая способность спектрометра в изучаемой энергетической области бомбардирующих нейтронов, выраженной отношением $\Delta E/E$, где ΔE – общая ширина к полувысоте кривой, которая дает представление об энергетическом распределении рассеиваемых ванадием нейтронов, состав-

ляет менее 0,12. Энергия бомбардирующих нейтронов изменялась в пределах от 22 до 72 мэв, а угол рассеяния – между 5 и 90°.

В отношении верхнего предела изучаемого энергетического интервала наблюдалось хорошее совпадение экспериментальных данных с теоретической кривой Кригера и Нелькина. Что касается более мелких значений энергии бомбардирующих нейтронов, то дающая представление об экспериментальных данных кривая имеет наклон, аналогичный тому, который отмечался Рандольфом и др. в отношении метана; ширина к полувысоте экспериментальной кривой ниже теоретической ширины, рассчитанной по формуле Кригера-Нелькина. Это несовпадение экспериментальных и теоретических данных обусловлено, вероятно, дискретной структурой ротационных молекулярных уровней; оно указывает, что в данном случае следует применять предложенную Гриффином формулу.

В отношении парциального дифференциального эффективного сечения проведенные с метаном измерения привели к значениям, которые соответствуют значениям Рандольфа и др. и которые в районе максимума отличаются от значений, рассчитанных Гриффином. Возможно, что более точная обработка данных относительно разрешающей способности прибора улучшила бы соответствие между теоретическими и экспериментальными данными.

Представлены кривые S(d) для различных значений бета-параметра; при этом для малых значений бета было достигнуто удовлетворительное соответствие с теоретическими кривыми, выведенными по формуле Кригера и Нелькина.

DISPERSIÓN INELÁSTICA DE NEUTRONES EN EL ETILENO. Los autores han estudiado la dispersión inelástica de neutrones en el etileno empleando un espectrómetro triaxial. El poder de resolución de ese instrumento se expresa por el cociente $\Delta E/E$, donde ΔE es el ancho total a la semialtura de la curva que describe la distribución energética de los neutrones dispersos por el vanadio, y en el intervalo de energía estudiado es inferior a 0,12. La energía de los neutrones incidentes se hizo variar entre 22 y 72 meV, y el ángulo de dispersión, entre 5° y 90°.

Para las energías más altas se observa que los resultados experimentales concuerdan satisfactoriamente con la curva teórica de Krieger y Nelkin. La curva que describe los datos experimentales en el caso de neutrones incidentes de menor energía presenta una inflexión análoga a la observada por Randolph y colaboradores al estudiar el metano; el ancho a la semialtura de la curva experimental es inferior al valor calculado teóricamente según el formalismo de Krieger-Nelkin. Esta discrepancia se debe probablemente a la estructura discreta de los niveles moleculares de rotación, e indica que, en este caso, es preferible el formalismo propuesto por Griffing.

Las mediciones efectuadas con metano dieron para la sección eficaz diferencial parcial valores que concuerdan con los de Randolph y colaboradores, pero que, en la región del máximo, difieren de los calculados por Griffing. Es probable que si se tuviera en cuenta más correctamente la contribución del poder de resolución del aparato, los datos teóricos concordarían mejor con los experimentales.

Se han representado las curvas S(d) para diferentes valores del parámetro β. Cuando los valores de β son reducidos, concuerdan satisfactoriamente con las curvas teóricas obtenidas con arreglo al formalismo de Krieger y Nelkin.

1. INTRODUCTION

The study of inelastic scattering of slow neutrons in methane has shown that there is only a limited possibility to treat the spectrum of molecular rotations as a continuous spectrum [1]. It has been established that for scattering angles smaller than 30° and for energies of the incident neutrons under 25 meV the theoretical curves computed according to the approximation method suggested by KRIEGER and NELKIN [2] do not describe the experimental results satisfactorily.

A good agreement with experimental results has been obtained by GRIFFING [3]; he applied the formalism of ZEMACH and GLAUBER [4] and considered the discrete structure of the molecular rotation spectrum.

By applying the method suggested by Griffing, CZERLUNCZAKIEWICZ and KOWALSKA [5] have computed the partial differential cross-section for

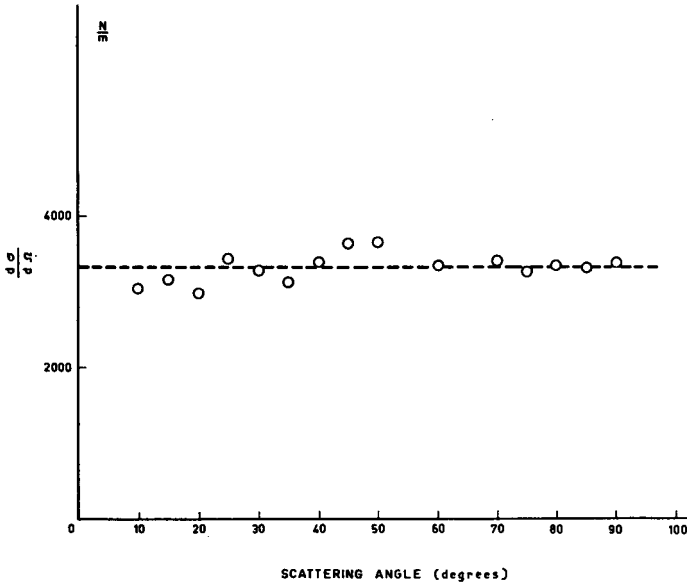

Fig. 1

Angular distribution of scattered neutrons by the vanadium sample

E_0 = 0.0250 eV.

ammonia and obtained a good agreement with experimental data given by WEBB [6].

The purpose of the present work is the study of the inelastic scattering of neutrons by ethylene, to establish the limits within which the computational methods proposed by GRIFFING [3] and KRIEGER and NELKIN [2] may be applied to the description of the experimental results.

2. EXPERIMENTAL METHOD

The measurements were made with a triple-axis neutron spectrometer. Lead monocrystals with the (111) plane normal to the crystal face were used both for the monochromator and the analyser. The width of the mosaic spread was about 15 min of arc. A battery of $B^{10}F_3$ counters was used as detector. The resolving power of the spectrometer was determined for every value of the incident neutrons' energy; this was achieved by measuring the spectrum of neutrons scattered by a vanadium target. In order to check if the multiple scattering in the vanadium sample may be neglected, the angular distribution of scattered neutrons was measured. The angular distribution for incident neutrons of 25 meV is shown in Fig. 1. The spectrum of neutrons scattered by vanadium for the same energy of incident neutrons and a scattering angle of 16.3° is shown in Fig. 2. The resolving power of the spectrometer is $\Delta E/E = 0.12$ where ΔE is the full width at half maximum

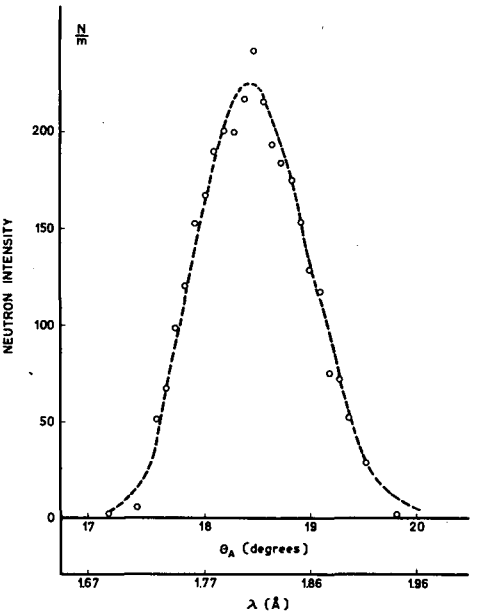

Fig. 2

Spectrum of neutrons scattered by the vanadium sample

E_0 = 0.0250 eV;
φ = 16.3°;
λ = 1.81 Å.

of the curve represented in Fig. 2. The transmission of the gas target was over 75%.

The differential partial cross-section measurements were effected for energies of incident neutrons between 22 and 72 meV and for scattering angles between 5° and 90°. The procedure described in [7] has been applied to express the experimental results in barn per molecule-Å-steradian. The relations given by HOLM [8] were used for reflectivity corrections. The second order reflection for 1.81-Å wavelength was estimated to be not higher than 14%.

The errors indicated in the graphs, which do not exceed 4%, are the statistical errors only. They do not include errors caused by higher order contaminations and by leaving out multiple scattering.

3. RESULTS

Measurements carried out on ethylene for incident neutrons of 71.4 meV gave the results shown in Fig. 3. The comparison with the theoretical curves, computed according to Krieger-Nelkin relations, has been effected by normalizing the experimental results over the computed values. As for methane, with sufficiently high energies of incident neutrons, a good agreement was obtained between the theory and the experimental results. The

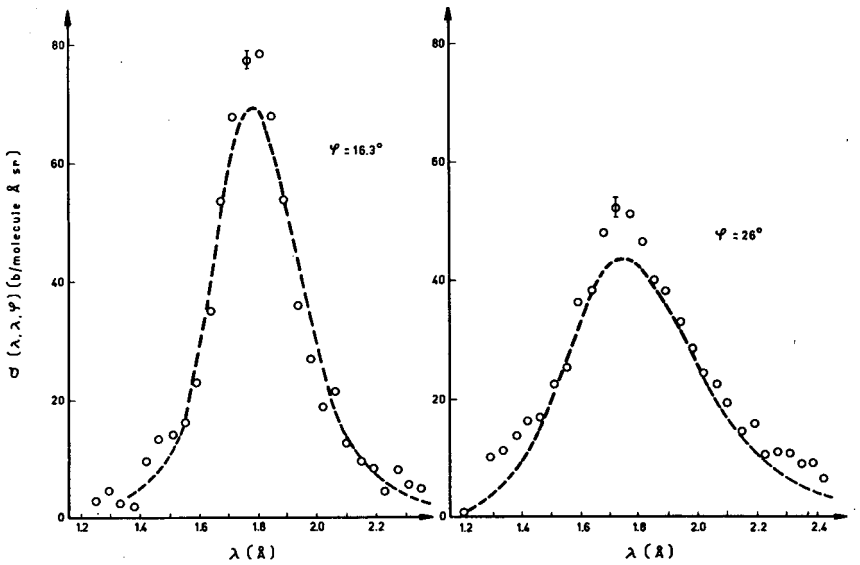

Fig. 3

The ethylene partial differential cross-section in relative units

E_0 = 0.0250 eV;
λ = 1.81 Å;
--- = Krieger-Nelkin

higher width of the experimental curve obtained for a scattering angle of 10° may be ascribed to the resolving power of the spectrometer.

For lower values of the energy of incident neutrons and for scattering angles less than 30°, the experimental data and the theoretical curves computed according to the Krieger-Nelkin relations are no longer in agreement.

Figure 4 shows the values of the partial differential cross-section, expressed in absolute units, obtained with incident neutrons of 25 meV and two values of scattering angle. In the main peak region the measured values are higher than the computed ones, while the width of the experimental curve is smaller than that of the theoretical curve computed by using the Krieger-Nelkin approximation. The disagreement between the experimental results and the Krieger-Nelkin theory for incident neutrons of low energy is probably determined by the contribution of the discrete structure of the rotational energy. In this case it is to be expected that the experimental results were correctly described by the curves calculated according to the method proposed by Griffing.

Figure 5 gives the differential partial cross-section of methane for the same energy of incident neutrons. The results obtained are in agreement with the values given by RANDOLPH et al. [1]. In our measurements we observed too that the peak of the experimental curve is substantially lower than that predicted by Griffing. This disagreement between theoretical and experimental results may be ascribed to the finite resolution of the spectrometer and an estimation of its contribution should be of interest.

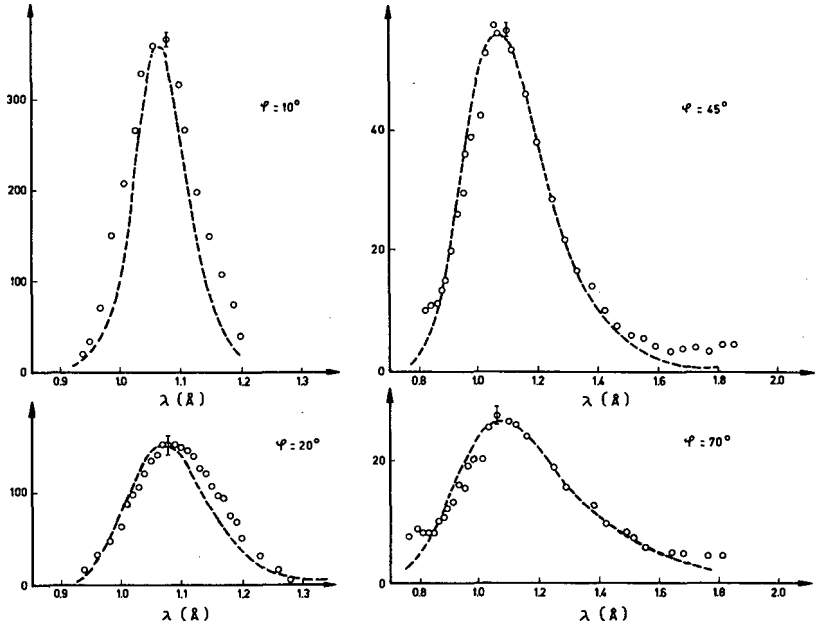

Fig. 4

The ethylene partial differential cross-section corresponding to an energy of incident neutrons of 0.025 eV

E = 0.0714 eV;
λ = 1.07 Å;
---- = Krieger-Nelkin

The scattering law for ethylene is given in Fig. 6. The experimental data for the function $S(\alpha)$ corresponding to four values of the parameter β are compared with the theoretical curves computed using the Krieger-Nelkin formula. The parameters α and β have the well-known significance given in [9].

The agreement between experimental and theoretical data calculated in the Krieger-Nelkin approximation is satisfactory for $\beta = 0$ and $\beta = 0.18$ only. For higher values of β where the statistical errors are great, the spread of the experimental points [1] is great, as in the case for methane.

The spread of experimental points obtained for different values of E_0, for $\beta = 0$, may be ascribed to the fact that no account has been taken of multiple scattering and high order reflections.

It is interesting to express the scattering law as a function of parameters $x^2 = |\vec{k}^2 - \vec{k}_0^2|^2$ and $\epsilon = E - E_0$ where x = momentum transfer and ϵ = energy transfer, and to compare the experimental points for $S(k^2, \epsilon)$ and $\beta = 0$ with the theoretical curve calculated by the method proposed by Griffing. Evidence of coherence effects might be obtained by applying the above method.

The experimental results for ethylene were compared with the Krieger-Nelkin formula only, due to the practical difficulties of calculation.

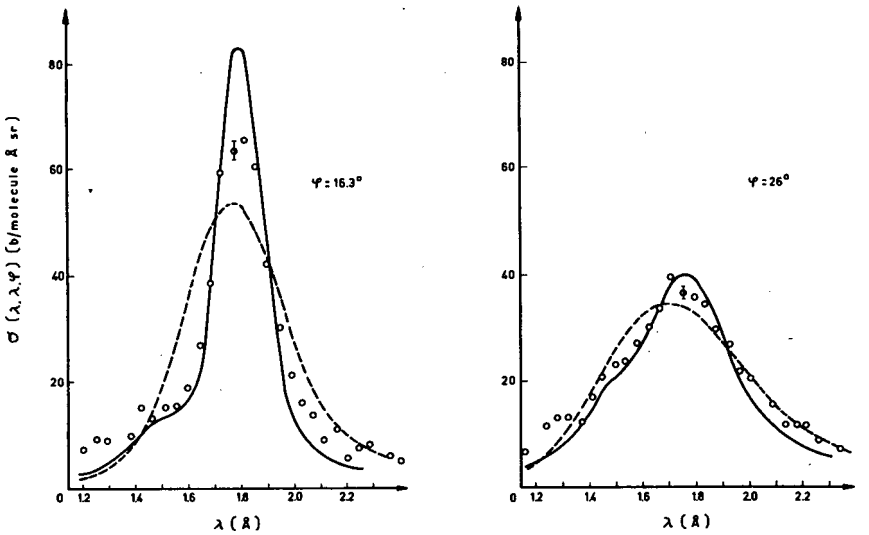

Fig. 5

The methane partial differential cross-section corresponding to an energy of incident neutrons of 0.025 eV
The solid line curve represents the curve computed by Griffing and the dashed curve represents the curve computed according to the Krieger-Nelkin formula.

$\lambda = 1.81$ Å.

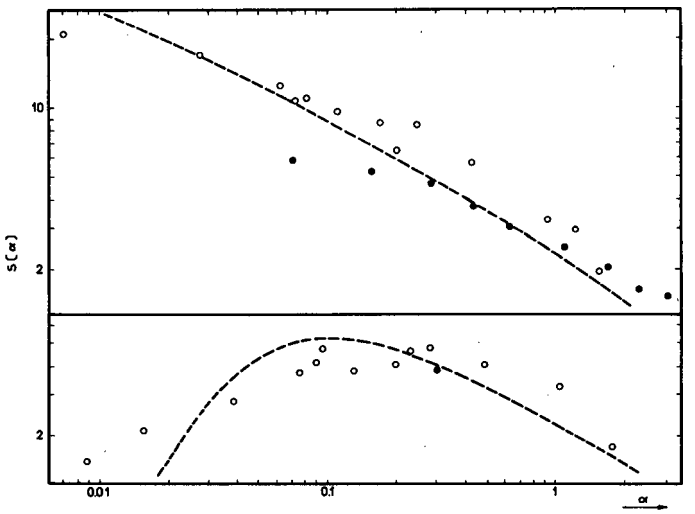

Fig. 6(a)

Values of the function S(α) for ethylene corresponding to β = 0 (upper) and β = 0.18 (lower)
The dashed curve was computed according to the Krieger-Nelkin formula.

○ E = 0.0229 eV.
● E = 0.0587 eV.

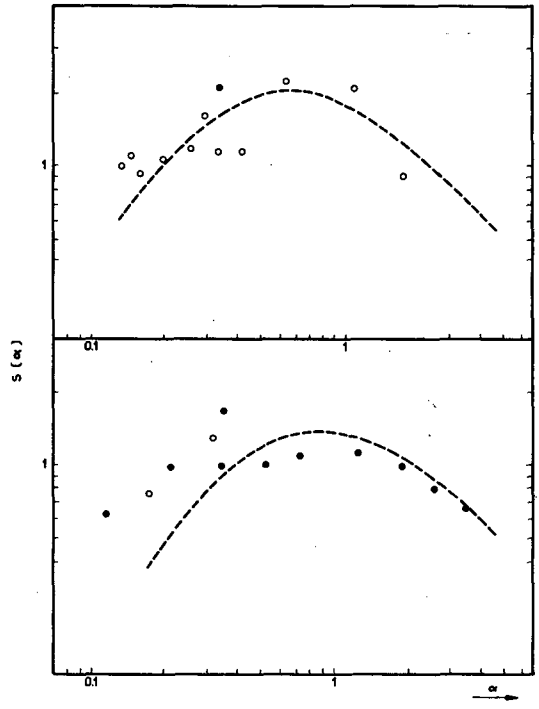

Fig. 6(b)

Values of the function S(α) for ethylene corresponding to β = 0.481 (upper) and β = 0.615 (lower) The dashed curve is computed according to the Krieger-Nelkin formula.

ACKNOWLEDGEMENTS

The authors would like to thank Dr. Griffing for supplying them with the computed values for methane and V. Trepădus for assistance in measurements and calculations.

REFERENCES

[1] RANDOLPH, P. D., BRUGGER, R. M., STRONG, K. A. and SCHMUNK, R. E., Phys. Rev. 124 (1961) 460.
[2] KRIEGER, T. J. and NELKIN, M. S., Phys. Rev. 106 (1957) 290.
[3] GRIFFING, G. W., Phys. Rev. 124 (1961) 1489; Phys. Rev. 127 (1962) 1179; Inelastic Scattering of Neutrons in Solids and Liquids I IAEA, Vienna (1963) 435-50.
[4] ZEMACH, A. C. and GLAUBER, R. J., Phys. Rev. 101 (1956) 118.
[5] CZERLUNCZAKIEWICZ, B. and KOWALSKA, A., Acta phys. polon. 25 (1964) 14.
[6] WEBB, F. J., Inelastic Scattering of Neutrons in Solids and Liquids I IAEA, Vienna (1963) 457-67.
[7] BALLY, D., Rev. Roum. Phys. 9 (1964) 507.
[8] HOLM, M. W., I. D. O. 16115/1955.
[9] EGELSTAFF, P. A., COCKING, S. J., ROYSTON, R. and THORSON, I., Inelastic Scattering of Neutrons in Solids and Liquids, IAEA Vienna (1961) 309-20.

DISCUSSION

G. KOSÁLY: Looking at the curves presented in various papers, one sees a definite disagreement between the Griffing theory and experimental results. The same disagreement can be seen in the case of NH_3 between the measurements of Webb and the calculations done by Kowalska. Have you any idea of the reasons for this?

J. JANIK: There is indeed disagreement in all these cases, but I am afraid I can offer no explanation for it.

ИССЛЕДОВАНИЯ ДИНАМИКИ ГИДРИДА И ДЕЙТЕРИДА ЛИТИЯ ПО НЕУПРУГОМУ РАССЕЯНИЮ ХОЛОДНЫХ НЕЙТРОНОВ

М.Г. ЗЕМЛЯНОВ, Е.Г. БРОВМАН, Н.А. ЧЕРНОПЛЕКОВ
и Ю.Л. ШИТИКОВ
ИНСТИТУТ АТОМНОЙ ЭНЕРГИИ им. И.В. КУРЧАТОВА, МОСКВА
СССР

Abstract — Résumé — Аннотация — Resumen

STUDY OF THE DYNAMICS OF LITHIUM HYDRIDE AND DEUTERIDE IN THE INELASTIC SCATTERING OF COLD NEUTRONS. The paper sets out the results of experimental investigations on the inelastic scattering of cold neutrons in polycrystalline samples of Li^7H and Li^7D. The measurements are carried out by the time-of-flight method, using a beryllium filter and mechanical chopper.

In processing the data, allowance is made for the instrumental resolution and the statistical accuracy of the experimental data.

A detailed theory is described for LiH and LiD crystals in models of stable ions. Calculations are made of frequency distribution functions and the energy dependence of the polarization vectors, and the Debye-Waller factor is found. The authors discuss the peculiar behaviour of the neutron inelastic scattering cross-section resulting from the presence of two atoms in the elementary nucleus. The phonon spectra for lithium hydride and deuteride are established using the values computed from the experimental results. The paper includes a comparison of the experimental and theoretical results.

ÉTUDE DE LA DYNAMIQUE DE L'HYDRURE ET DU DEUTÉRURE DE LITHIUM AU MOYEN DE LA DIFFUSION INÉLASTIQUE DES NEUTRONS FROIDS. Les auteurs donnent les résultats d'une étude expérimentale sur la diffusion inélastique des neutrons froids dans des échantillons polycristallins de ^7LiH et ^7LiD. Les mesures ont été effectuées par la méthode du temps de vol, avec utilisation d'un filtre de béryllium et d'un sélecteur mécanique.

Les résultats obtenus ont fait l'objet d'un traitement mathématique qui tient compte du pouvoir de résolution de l'appareil et de l'exactitude statistique des données expérimentales.

Les auteurs décrivent la théorie des cristaux LiH et LiD dans un modèle d'ions durs. On a calculé la fonction de distribution des fréquences et la relation entre l'énergie et les vecteurs de polarisation; on a ensuite déterminé le facteur de Debye-Waller. On examine le comportement spécifique de la section efficace de diffusion inélastique des neutrons, dû à la présence de deux atomes dans la cellule élémentaire. En tenant compte des données fournies par les calculs et des résultats de l'expérience, on a établi les spectres phononiques de l'hydrure et du deutérure de lithium. Les résultats expérimentaux sont comparés aux données théoriques.

ИССЛЕДОВАНИЯ ДИНАМИКИ ГИДРИДА И ДЕЙТЕРИДА ЛИТИЯ ПО НЕУПРУГОМУ РАССЕЯНИЮ ХОЛОДНЫХ НЕЙТРОНОВ. В работе сообщаются результаты экспериментального исследования неупругого рассеяния холодных нейтронов на поликристаллических образцах Li^7H и Li^7D. Измерения выполнены по методу времени пролета с использованием фильтра и механического прерывателя.

Проведена математическая обработка полученных результатов с учетом аппаратурного разрешения и статистической точности экспериментальных данных.

Дана подробная теория кристаллов LiH и LiD в модели жестких ионов. Проведены расчеты функции распределения частот, энергетического хода векторов поляризации и найден фактор Дебая-Валлера. Обсуждается своеобразное поведение сечения неупругого рассеяния нейтронов, обусловленное наличием двух атомов в элементарной ячейке. С учетом расчетных данных по результатам эксперимента восстановлены фононные спектры гидрида и дейтерида лития. Проводится сравнение экспериментальных и теоретических результатов.

ESTUDIO DE LA DINÁMICA DEL HIDRURO Y DEL DEUTERURO DE LITIO POR DISPERSIÓN INELÁSTICA DE NEUTRONES FRÍOS. En la memoria se presentan los resultados de un estudio experimental de la dispersión

inelástica de neutrones frfos en muestras policristalinas de ^{7}LiH y ^{7}LiD. Las mediciones se efectuaron por el método del tiempo de vuelo utilizando un filtro de berilio y un selector mecánico.

En el tratamiento matemático de los datos obtenidos se tuvo en cuenta el poder de resolución del aparato y la precisión estadística de los datos experimentales.

En la memoria se expone en detalle la teoría de los cristales de LiH y LiD en un modelo de iones rígidos. Se calculó la función de distribución de las frecuencias, y la relación existente entre la energía y los vectores de polarización; seguidamente se determinó el factor de Debye-Waller. Se examina el comportamiento característico de la sección eficaz de dispersión inelástica de los neutrones, condicionada por la presencia de dos átomos en la celda elemental. Tomando en consideración los datos calculados y los resultados experimentales, se establecieron los espectros fonónicos del hidruro y del deuteruro de litio. Los resultados experimentales se comparan con los datos teóricos.

I. ВВЕДЕНИЕ

Среди водородсодержащих веществ, широко исследуемых в последнее время с помощью неупругого рассеяния нейтронов, значительное место занимают гидриды металлов. Интерес к исследованию динамики гидридов металлов обусловлен двумя причинами:

а) все возрастающим практическим применением гидридов металлов в различных областях техники, в частности в реакторостроении, где они используются как материалы для замедлителей и защиты;

б) своеобразием динамики двухкомпонентных решеток гидридов, состоящих из атомов с большой разницей масс. Один из компонентов гидридов — водород имеет большую амплитуду некогерентного рассеяния, что позволяет использовать неупругое некогерентное рассеяние нейтронов для исследования динамики гидридов. Однако прямое определение фононного спектра, в противоположность одноатомным некогерентно рассеивающим кристаллам кубической симметрии, в этом случае невозможно. Как было показано в [1, 2], спектр колебаний, определяемый по рассеянию нейтронов, оказывается искаженным неизвестной энергетической зависимостью векторов поляризации колебаний.

Поэтому в опубликованных к настоящему времени результатах измерений неупругого рассеяния нейтронов на гидридах ряда металлов [3—7] практически исследована только область оптических колебаний водорода в решетке гидрида. При этом ни в одной из работ количественного определения фононного спектра решетки в целом не проведено.

В работе сообщаются результаты исследований с помощью неупругого рассеяния холодных нейтронов динамики гидрида и дейтерида Li^{7}. Указанные соединения являются простейшими как по своей кристаллической структуре — это кубические кристаллы с решеткой типа NaCl, так и по характеру упорядочения — это гидриды замещения. Кроме того, в случае $Li^{7}H$ имеет место наименьшая возможная разница масс между металлом и водородом. Следует отметить, что существующая принципиальная возможность выделения фононного спектра двухкомпонентной системы путем комбинирования результатов измерений неупругого рассеяния на решетках с различным изотопическим составом [1] в случае гидрида и дейтерида лития не может быть реализована, так как при замене H на D меняются не только сечения рассеяния, но и сама динамика решетки.

Поэтому в данной работе сделана попытка получить из данных по неупругому рассеянию холодных нейтронов на LiH и LiD количественную информацию о фононных спектрах указанных соединений, предварительно определив энергетическую зависимость векторов поляризации с помощью расчета в определенных модельных представлениях. Как показывают результаты работы, такой путь оказывается плодотворным в случае гидрида и дейтерида лития, и из нейтронного эксперимента восстанавливаются спектры колебаний, т.е. необходимая и достаточная информация для термодинамического описания фононной ветви возбуждения кристалла.

II. ОПИСАНИЕ ЭКСПЕРИМЕНТА И ОБРАБОТКИ ЭКСПЕРИМЕНТАЛЬНЫХ ДАННЫХ

Поскольку естественная смесь изотопов лития содержит 7,5% изотопа Li^6, сильно поглощающего нейтроны, то для измерений использовались образцы гидрида и дейтерида Li, полученные на основе смеси изотопов, обогащенной Li^7 до 99,9%. Из-за высокой гигроскопичности образцы заключались в герметичные алюминиевые кассеты. Площадь образцов составляла около 100 $см^2$, толщина стенок кассеты ~0,1 см.

Исследование неупругого рассеяния нейтронов на LiH и LiD проводилось на нейтронном спектрометре по времени пролета, причем механический прерыватель располагался после образца [8]. Энергетический анализ нейтронов, рассеянных под углом 90° к падающему пучку, проводился в интервале энергий от 4 до 160 мэв. Разрешение нейтронного спектрометра по времени пролета в указанном интервале энергий было приблизительно постоянным и равным $\Delta E/E \simeq 5\%$, а полное энергетическое разрешение установки с учетом конечной ширины спектральной линии холодных нейтронов менялось от ~30% в области малых энергий до 6% на границе исследованного интервала. Пропускание образцов для средней энергии холодных нейтронов 3,6 мэв составляло соответственно 0,68 для Li^7H и 0,77 для Li^7D. Полное время измерений было около 800 часов.

Экспериментальные данные по спектрам неупруго рассеянных нейтронов на Li^7H и Li^7D приведены на рис.1. В них введены поправки на отклонение эффективности детектора нейтронов от закона $1/v$, на поглощение нейтронов в воздухе на пролетном пути между образцом и детектором, на деформацию спектра падающих и рассеянных нейтронов за счет поглощения в материале образца, а также вычтен фон быстрых нейтронов. Для сравнения на этом рисунке приведены данные по фону, обусловленному рассеянием холодных нейтронов на материале самой кассеты. Указанные данные получены в независимых измерениях. Поправки на многократные и многофононные процессы не учтены. Как видно из рис.1, области упругого и неупругого рассеяния нейтронов отчетливо разделяются.

Последним этапом обработки экспериментальных данных является учет влияния полной функции разрешения, представляющей собой свертку функции разрешения спектрометра по времени пролета и первичной линии холодных нейтронов. Этот учет проводился следующим образом. Приближенное ре-

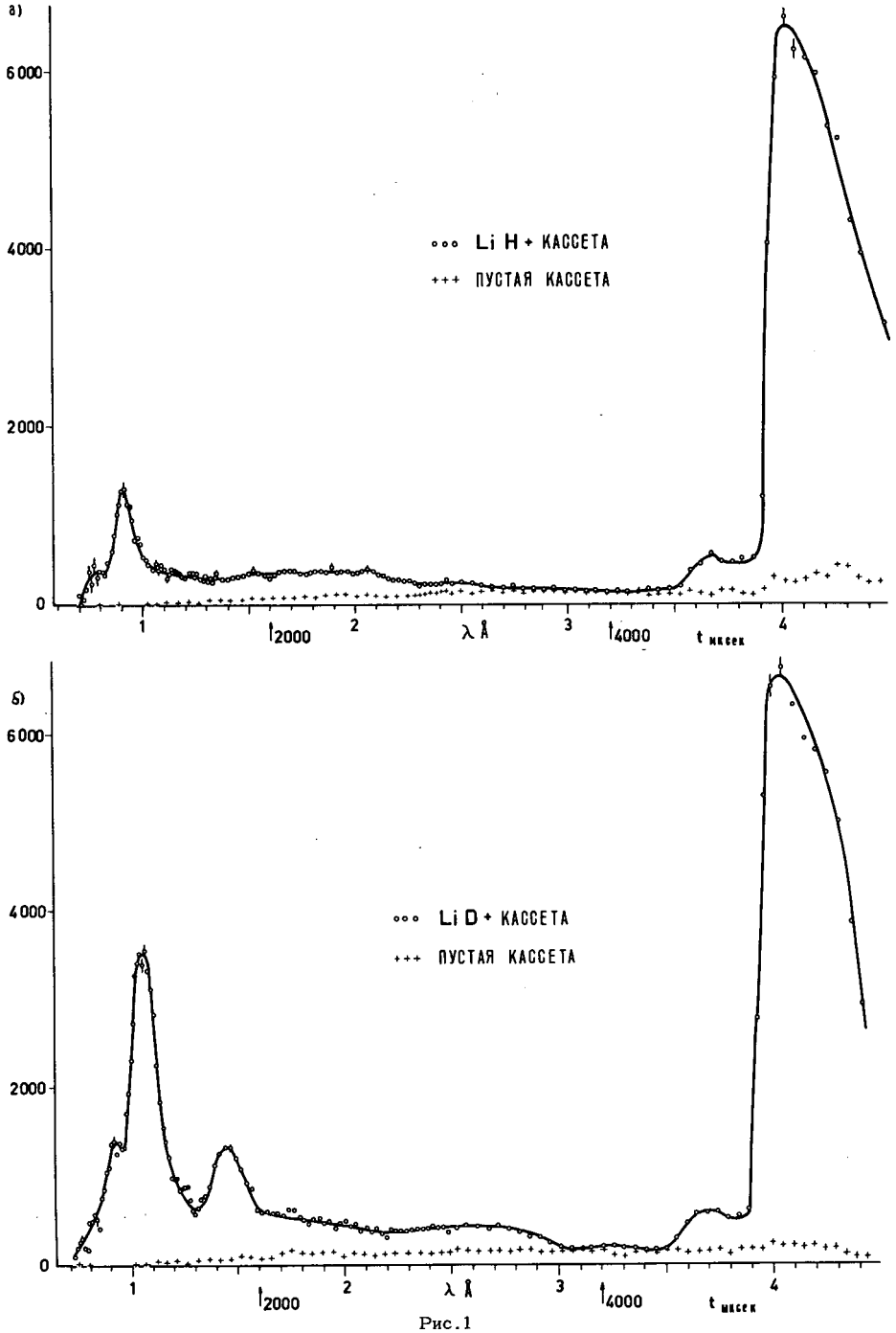

Рис.1

а) Спектр нейтронов, рассеянных на Li^7H.
б) Спектр нейтронов, рассеянных на Li^7D.

шение интегрального уравнения, описывающего результаты эксперимента,

$$\int K(E,E')\sigma(E)dE = \tilde{\sigma}(E_n),$$

где $K(E,E')$ – полная функция разрешения, $\sigma(E)$ – искомая энергетическая зависимость сечения неупругого рассеяния и $\tilde{\sigma}(E_n)$ – экспериментальные значения сечения, искалось по методу, предложенному А.Г. Чичериным. Решение конструировалось из функций разрешения. Из-за перекрытия функции разрешения не образуют ортогональной системы, однако, использование их для построения решения эквивалентно разложению с положительными коэффициентами и поэтому не приводит к появлению отрицательных значений $\sigma(E)$, которые не имеют физического смысла. Алгоритм решения имел вид:

$$\sigma_{\alpha+1}(E) = \sigma_\alpha(E)\frac{\dfrac{\tilde{\sigma}(E_n)}{\sum_n \gamma_n \sigma_\alpha(E_n)} K(E,E_n)}{\sum_n \gamma_n K(E,E_n)}, \qquad (1)$$

где

$$\tilde{\sigma}_\alpha(E_n) = \int K(E,E_n)\sigma_\alpha(E)dE \qquad (2)$$

и γ_n – статистический вес экспериментальных точек. При $\alpha \simeq 8$ получается приближение $\sigma_\alpha(E)$, которое согласно (2) дает $\tilde{\sigma}_\alpha(E)$, совпадающее в пределах статистической точности с экспериментальными значениями $\tilde{\sigma}(E_n)$. Энергетическая зависимость сечения неупругого рассеяния холодных нейтронов на LiH и LiD, восстановленная с учетом функции разрешения, представлена на рис.2. Пунктирными линиями на графиках рис.2 указана статистическая точность исходных экспериментальных результатов. Сплошной линией в нижней части рис.2 приведена зависимость сечения двухфононных процессов от передаваемой энергии. Учет функции разрешения, как и следовало ожидать, приводит к обострению экспериментально наблюдаемых особенностей сечения. Вся обработка данных по неупругому рассеянию нейтронов на LiH и LiD была проведена с помощью электронной счетной машины.

Представляет интерес провести сравнение полученных в данной работе экспериментальных результатов с опубликованными ранее. В работе Вудса и др. [5] сообщены результаты исследования по методу бериллиевого детектора неупругого рассеяния нейтронов на LiH. Исследование проводилось в интервале энергий от 60 до 170 мэв. На рис.3 приведено сравнение этих данных с данными по холодным нейтронам, причем сравниваются между собой величины, не зависящие от метода измерений. В случае холодных нейтронов эта величина определяется как

$$\theta(\epsilon) = \frac{d^2\sigma}{d\Omega\, d\epsilon}\sqrt{\frac{E_0}{E}}\frac{\epsilon}{E+E_0}\left(e^{\epsilon/KT}-1\right),$$

а в случае тепловых (нейтроны при рассеянии теряют энергию) как

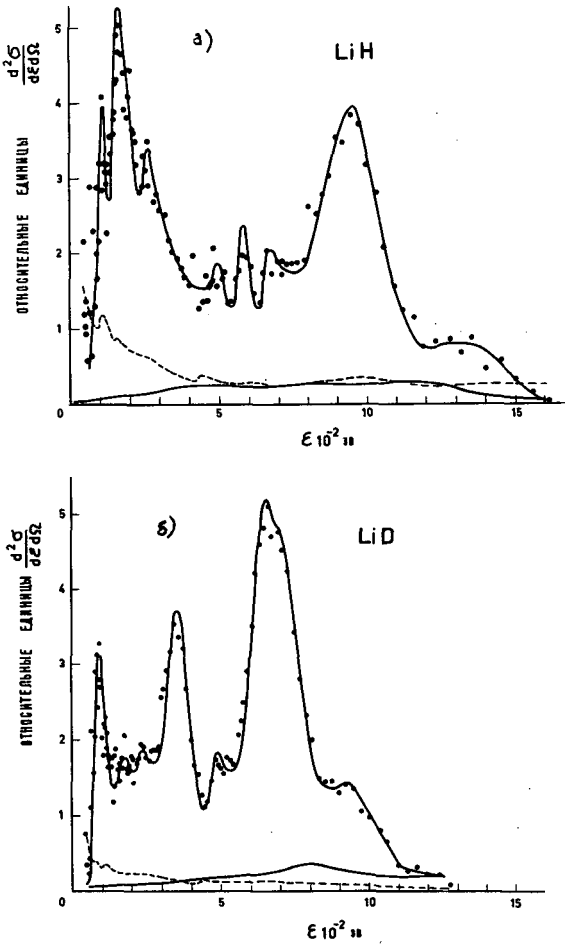

Рис.2

а) Энергетическая зависимость $d^2\sigma/d\epsilon\, d\Omega$ для Li^7H с учетом влияния разрешения.
б) Энергетическая зависимость $d^2\sigma/d\epsilon\, d\Omega$ для Li^7D с учетом влияния разрешения.

$$\theta(\epsilon) = \frac{d^2\sigma}{d\Omega\, d\epsilon} \sqrt{\frac{E_0}{E}} \frac{\epsilon}{E+E_0}(1 - e^{-\epsilon/KT}),$$

где E_0 и E, соответственно, энергия падающих и рассеянных нейтронов, а $\epsilon = E - E_0$. Для сравнения результаты отнормированы на одно значение в максимуме низкоэнергетического пика. Энергетическое положение обоих пиков, связанных с оптическими колебаниями в решетке LiH, совпадает с хорошей точностью. Что же касается относительного хода $\theta(\epsilon)$, полученного в методе прямого и обратного фильтров, то он несколько различается.

Такое различие объясняется, вероятно, тем, что в работе [5] не учитывалась деформация спектра падающих и рассеянных нейтронов за счет конечной толщины образца (пропускание для LiH в [5] было ~0,6).

III. ТЕОРЕТИЧЕСКАЯ ЧАСТЬ

В случае одноатомных систем, некогерентно рассеивающих нейтроны, измеряемое на эксперименте дважды дифференциальное сечение пропорционально функции распределения частот $g(\omega)$ и, вследствие этого, представляется возможным проведение строгого решения обратной задачи без привлечения каких-либо модельных предположений.

В случае же двухатомных систем, подобных LiH и LiD, наблюдаемое экспериментально сечение оказывается пропорциональным фононному спектру и функции, зависящей от комбинации векторов поляризации.

Если учесть кубическую симметрию кристаллов типа NaCl, то дважды дифференциальное сечение некогерентного рассеяния нейтронов с поглощением фонона запишется в следующем виде:

$$\frac{d^2\sigma}{d\Omega\, d\epsilon} \sim \frac{K}{K_0}\frac{\kappa^2}{\epsilon}\frac{1}{e^{\epsilon/KT}-1}\sum_{\alpha}\int d^3f\left[\frac{\sigma_1}{M_1}|\bar{e}_1(\bar{f},\alpha)|^2 e^{-2W_1} + \frac{\sigma_2}{M_2}|\bar{e}_2(\bar{f},\alpha)|^2 e^{-2W_2}\right]\delta(\hbar\omega_\alpha(\bar{f})-\epsilon), \tag{3}$$

где M_1, M_2, σ_1 и σ_2 – массы и сечения некогерентного рассеяния составляющих решетку ионов; K_0 и K – начальный и конечный импульс нейтрона; ϵ, κ – соответственно, изменение энергии и импульса нейтрона при рассеянии; α – номер ветви колебательного спектра; f – волновый вектор фонона; $\bar{e}_j(\bar{f},\alpha)$ – вектор поляризации; W_j – фактор Дебая-Валлера, который для кубического кристалла принимает вид:

$$2W_j = \frac{\kappa^2}{M_j}\cdot\frac{1}{3}\sum_{\bar{f},\alpha}\frac{|\bar{e}_j(\bar{f},\alpha)|^2}{\omega_\alpha(\bar{f})}\left[\frac{1}{e^{\frac{\hbar\omega}{KT}}-1}+\frac{1}{2}\right]. \tag{4}$$

Как видно из (3) и (4), для получения функции распределения частот из дважды дифференциального сечения рассеяния необходимо знание энергетической зависимости векторов поляризации и фактора Дебая-Валлера, который в свою очередь зависит также от векторов поляризации. Таким образом, задача восстановления $g(\omega)$ сводится к определению векторов поляризации во всем фазовом пространстве.

Вектора поляризации могут быть определены экспериментально из измерений когерентного однофононного рассеяния [10]. Однако эти эксперименты очень трудоемкие, поскольку они связаны не только с определением энергетического положения максимумов когерентного рассеяния нейтронов, но и с определением абсолютной интенсивности этих максимумов.

Альтернативный этому подход состоит в определении векторов поляризации в модельных предположениях с использованием уравнений Борна-Кармана. Как показали нейтронные исследования ряда ионных кристаллов,

расчеты на основании уравнений Борна-Кармана удовлетворительно описывают результаты экспериментов. Поэтому такой подход представляется вполне оправданным. При решении уравнений Борна-Кармана может быть найдена не только энергетическая зависимость векторов поляризации, но и функция распределения частот $g(\omega)$ и полученное значение $g(\omega)$ сравнено с экспериментально определенным.

Для проведения расчетов была выбрана простейшая модель колебаний ионных кристаллов — модель точечных и недеформируемых ионов. Эта модель была впервые использована Келлерманом [11]. Если сравнить кривые дисперсии для ионных кристаллов, полученные экспериментально из когерентного рассеяния нейтронов [12], с расчетными по модели Келлермана, то оказывается, что принятая модель удовлетворительно описывает акустические и поперечные оптические ветви колебаний и дает завышенные значения частот для продольных оптических ветвей.

Следуя Келлерману [11], запишем систему уравнений Борна-Кармана в виде:

$$M_k \ddot{U}^{\ell}_{k\alpha} - \sum_{k'} \sum_{\ell'} \sum_{\alpha'} (\Phi^{\ell-\ell'}_{kk'})_{\alpha\alpha'} U^{\ell}_{k'\alpha'} = 0 . \qquad (5)$$

Здесь k — номер атома в элементарной ячейке;

ℓ — координата узла решетки;

α — индекс декартовой координаты ($\alpha = 1, 2, 3$);

$\ddot{U}^{\ell}_{k\alpha}$ — смещение из положения равновесия соответствующего иона;

$(\Phi^{\ell-\ell'}_{kk'})$ — обычная матрица силовых постоянных.

Вектор положения равновесия узла решетки запишем в следующем виде

$$\bar{r}^{\ell}_k = \bar{a}^{\ell} + \bar{r}_k ,$$

где $\bar{a}^{\ell}$ — равновесное положение элементарной ячейки;

$\bar{r}_k$ — равновесное положение k-го иона в пределах элементарной ячейки.

Ищем решение системы уравнений (3) в виде плоской волны с волновым вектором f, частотой ω и вектором поляризации $\bar{e}_k(f)$

$$\bar{U}^{\ell}_k = \bar{e}^{\ell}_k(\bar{f}) \exp\{2\pi i(\bar{f}\bar{r}^{\ell}_k) - i\omega t\} . \qquad (6)$$

Подставляя решение (6) в уравнение (5), получаем систему уравнений 6-го порядка для определения векторов поляризации и частот:

$$\omega^2 M_k e^{\alpha}_k(\bar{f}) + \sum_{k\alpha'} \left[{k\,k' \atop \alpha\alpha'} \right] e^{\alpha'}_k(\bar{f}) = 0 . \qquad (7а)$$

$$\left[{k\,k' \atop \alpha\alpha'} \right] = \sum_{\alpha} (\Phi^{\ell}_{kk'})_{\alpha\alpha_1} \exp\{2\pi i(\bar{f}\bar{r}^{\ell}_{kk'})\} , \qquad (7б)$$

здесь $\bar{r}^{\ell}_{kk'} = \bar{r}^{\ell}_k - \bar{r}^{\ell}_{k'}$.

Матрица 6-го порядка (7б) носит название динамической матрицы и является Фурье обращением (на дискретном множестве) матрицы силовых постоянных. Для построения динамической матрицы необходимо найти взаимодействие между ионами решетки. Это взаимодействие обусловлено кулоновскими силами и силами отталкивания, возникающими за счет взаимного перекрытия оболочек ионов.

Соответственно:

$$\left[\begin{smallmatrix} kk' \\ \alpha\alpha' \end{smallmatrix}\right] = \left[\begin{smallmatrix} kk' \\ \alpha\alpha' \end{smallmatrix}\right]_{\text{кул}} + \left[\begin{smallmatrix} kk' \\ \alpha\alpha' \end{smallmatrix}\right]_{\text{отт}}. \tag{8}$$

Кулоновское взаимодействие определяет потенциал $\psi(\bar{r}) = e_k e_{k'}/|r|$, который и соответствует дальнодействующей, медленно спадающей с расстоянием силе.

Используя метод Эвальда, Келлерман просуммировал вклады от всех точек решетки и нашел $\left[\begin{smallmatrix} kk' \\ \alpha\alpha' \end{smallmatrix}\right]_{\text{кул}}$ для решетки типа NaCl в 48 точках 1-й зоны Бриллюэна. В полученные суммы параметры решетки входят в виде множителя e^2/v_0, где $v_0 = 2r_0^3$ – объем элементарной ячейки, а r_0 – ближайшее расстояние между ионами. Поэтому представляется разумным воспользоваться расчетами Келлермана для кулоновской части динамической матрицы с учетом r_0 для LiH.

Как уже отмечалось, ионы, лежащие на близком расстоянии друг от друга, могут взаимодействовать еще и из-за перекрытия электронных оболочек. Эти силы короткодействующие и в хорошем приближении могут считаться центральными.

Выберем соответствующий потенциал в виде

$$\psi(\bar{r})_{\text{отт}} \sim \frac{1}{r^h},$$

коэффициент при $1/r^h$ находится из условия равновесия решетки. Для этого ищем минимум потенциальной энергии, приходящейся на одну элементарную ячейку:

$$\alpha\frac{e^2}{r} + \frac{\sigma\beta}{r^h} = E(r); \tag{9}$$

здесь α – постоянная Маделунга для решетки типа NaCl. Минимум должен достигаться для $r = r_0$.

Отсюда

$$\psi(\bar{r})_{\text{отт}} = \alpha\frac{e^2}{r^h}\frac{r_0^{h-1}}{\sigma_n}. \tag{10}$$

Используя потенциал (10), найдем соответствующую часть динамической

матрицы (8). Короткодействующий потенциал дает вклад только во взаимодействие с "чужими" ионами. Учитывая (7б), легко находим:

$$\frac{v_0}{e^2}\left[\begin{matrix}1 & 2\\ x & x\end{matrix}\right]_f^{\text{отт}} = \alpha(n+1)\frac{2}{3}\cos 2\pi f_x r_0 - \frac{2\alpha}{3}\left[\cos 2\pi f_y r_0 + \cos 2\pi f_z r_0\right];$$

$$\frac{v_0}{e^2}\left[\begin{matrix}1 & 2\\ y & y\end{matrix}\right]_f^{\text{отт}} = \alpha(n+1)\frac{2}{3}\cos 2\pi f_y r_0 - \frac{2\alpha}{3}\left[\cos 2\pi f_x r_0 + \cos 2\pi f_z r_0\right]; \quad (11)$$

$$\frac{v_0}{e^2}\left[\begin{matrix}1 & 2\\ z & z\end{matrix}\right]_f^{\text{отт}} = \alpha(n+1)\frac{2}{3}\cos 2\pi f_z r_0 - \frac{2\alpha}{3}\left[\cos 2\pi f_x r_0 + \cos 2\pi f_y r_0\right].$$

Для нахождения диагональных по номерам атомов членов необходимо использовать условия инвариантности относительно смещения кристалла как целого

$$(\Phi^0_{kk'})_{\alpha\alpha'} = -\sum_{k'}\sum_{\ell}(\Phi^{\ell}_{kk'})_{\alpha\alpha'}. \quad (12)$$

Отсюда

$$\frac{v_0}{e^2}\left[\begin{matrix}1 & 1\\ x & x\end{matrix}\right]^{\text{отт}} = \frac{v_0}{e^2}\left[\begin{matrix}1 & 1\\ y & y\end{matrix}\right]^{\text{отт}} = \frac{v_0}{e^2}\left[\begin{matrix}1 & 1\\ z & z\end{matrix}\right]^{\text{отт}} = -\frac{2}{3}\alpha(n+1) + \frac{4}{3}\alpha. \quad (13)$$

Остальные элементы матрицы находятся из соотношений:

$$\left[\begin{matrix}1 & 1\\ \alpha & \beta\end{matrix}\right]^{\text{отт}} = \left[\begin{matrix}2 & 2\\ \alpha & \beta\end{matrix}\right]^{\text{отт}}; \qquad \left[\begin{matrix}1 & 2\\ \alpha & \beta\end{matrix}\right]^{\text{отт}} = \left[\begin{matrix}2 & 1\\ \alpha & \beta\end{matrix}\right]^{\text{отт}}. \quad (14)$$

Элементы матрицы с $\alpha \neq \beta$ из-за симметрии решетки обращаются в нуль.

Рассмотрим специально случай $f \to 0$. В этом пределе Келлерман использовал уравнение Пуассона и получил $\omega^2 = 0$ — для трех акустических ветвей,

$$\omega^2 = \frac{e^2}{v_0}\left(\frac{m_1 + m_2}{m_1 m_2}\right)\left[\frac{2}{3}\alpha(n-1) - \frac{4}{3}\pi\right] \quad (15)$$

— для трех оптических ветвей. Таким образом, получаются три вырожден-

ных оптических ветви. Этот результат неверен и является следствием неправильного предельного перехода.

Проведя процедуру предельного перехода более корректно, Лиддейн и Герцфельд [13] обеспечили частичное снятие вырождения и получили известное соотношение

$$\omega_{\text{прод}} = \left(\frac{\epsilon_0}{\epsilon_\infty}\right)^{\frac{1}{2}} \omega_{\text{попер}} , \tag{16}$$

где ϵ_0 и ϵ_∞, соответственно, диэлектрические постоянные в статическом и высокочастотном полях.

Однако при расчете статистических свойств системы, которые определяются интегралом по спектру возбуждения, вклад от колебаний при $f \to 0$ столь незначителен, что можно воспользоваться соотношением (15).

Модель, описанная выше, имеет один свободный параметр – величину n. Обычно n определяется из величины сжимаемости. Однако гораздо удобнее n определить из экспериментальных данных по инфракрасному спектру вещества.

Значения частот инфракрасного спектра поглощения для LiH получены в работе [9]: $\nu_{\text{попер}} = 600$ см$^{-1}$ и $\nu_{\text{прод}} = 1120$ см$^{-1}$.

Используя соотношение (15) для поперечной частоты и значение $\omega_{\text{попер}} = 11{,}3 \cdot 10^{12}$ сек$^{-1}$, получим $n = 5{,}77$. В случае LiD предполагалось, что силовые постоянные не меняются по сравнению с LiH, т.е. n остается прежним, а различие частот обусловлено различием в массах. Из (15) легко получаем

$$\frac{\omega^2_{\text{LiH}}(0)}{\omega^2_{\text{LiD}}(0)} = \frac{m_{\text{Li}} + m_{\text{H}}}{m_{\text{Li}} + m_{\text{D}}} \cdot \frac{m_{\text{D}}}{m_{\text{H}}} .$$

Для кристаллов кубической симметрии неприводимая часть зоны Бриллюэна составляет 1/48 полной фазы. Если ввести вместо волновых векторов f безразмерные фазы q согласно $f_i = q_i / 2r_0$, то эта неприводимая часть будет представлять многогранник, определяемый неравенствами:

$$\begin{gathered} 0 \le q_z \le q_y \le q_x \le 1 ; \\ q_x + q_y + q_z \le \frac{3}{2} . \end{gathered} \tag{17}$$

Для расчета выбираем стандартные точки фазового пространства, соответствующие делению

$$q_i = \frac{1}{10} P_i ; \qquad P_i = 0, 1, \ldots, 10 .$$

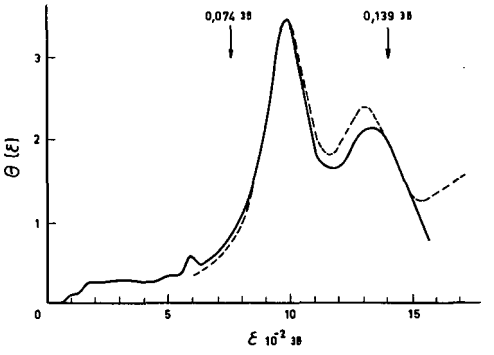

Рис.3

Сравнение экспериментальных данных для LiH.

В результате в области (17) будет находиться 48 точек. Для того, чтобы одну точку не учитывать дважды при пересчете на полную зону Бриллюэна, необходимо каждой точке сопоставить условный "вес". Так, пусть внутренней точке соответствует "вес" 48, тогда точке, лежащей на грани зоны — "вес" 24 и т.д. Сумма всех "весов" в неприводимой части зоны оказывается равной 1000.

В каждой из 48 точек $\{P_i\}$ производилась диагонализация динамической матрицы, находились собственные частоты ω и вектора поляризации $e_\kappa^\alpha(\vec{f})$. Функция распределения частот $g(\omega)$ определялась суммированием "весов" точек, попавших в определенный интервал частот $\Delta\omega$. Интервал $\Delta\omega$ выбирался таким образом, чтобы не было статистических флуктуаций из-за малой плотности точек. Затем производилось сглаживание полученных гистограмм.

Расчетные функции распределения $g(\omega)$ приведены на рис.4. На этом рисунке указаны также граничные значения низкочастотной области оптических ветвей. Характерным для обоих кристаллов является большая ширина интервала оптических частот. Это вызвано электростатическим характером взаимодействия. Интересно отметить, что поперечная оптическая частота при $f=0$ для модели Келлермана является минимальной для оптической области частот, а продольная — максимальной, так что ширина указанной области частот может быть определена из уравнения (16).

Форма спектра $g(\omega)$ в области акустических частот очень близка для обоих кристаллов, кроме того, область акустических частот занимает один и тот же интервал энергий. Однако оптическая часть спектра в LiH отделена от акустической энергетической щелью, в то время как в LiD происходит сильное перекрытие, приводящее к слиянию двух пиков в области $\sim 7\cdot10^{-2}$ эв. В области $1{,}5\cdot10^{-2}$ эв и $2\cdot10^{-2}$ эв в обоих спектрах наблюдались небольшие пики, а также наблюдалось расщепление основных максимумов акустического спектра, однако малая плотность точек в этой области не позволила установить их с необходимой достоверностью.

Для получения расчетного значения дважды дифференциального сечения необходимо определить энергетическую зависимость векторов поляризации.

Пусть $\psi(\omega)$ есть квадрат вектора поляризации, усредненный по изоэнергетической поверхности, или, в данном случае, усредненный по выбранному

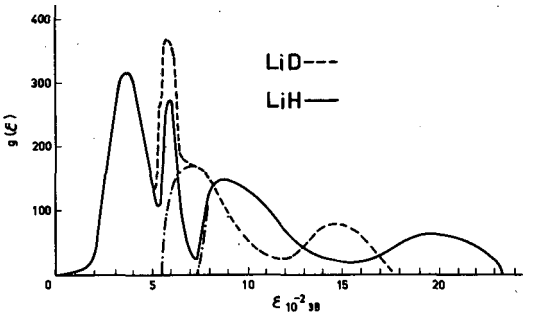

Рис.4

Расчетные $g(\epsilon)$ в модельных предположениях для Li^7H и Li^7D.

интервалу частот $\Delta\omega$. Поскольку, как оказалось, $\psi(\omega)$ гораздо более гладкая функция, чем $g(\omega)$, то при усреднении может быть использован больший интервал частот $\Delta\omega$. Окончательный вид $\psi_H(\omega)$ и $\psi_D(\omega)$ представлен на рис.5. Для обоих кристаллов $\psi_{Li}(\omega)$ находится из условий нормировки, которые в данном случае приводят к соотношениям:

$$\begin{aligned} &\psi_{Li}(\epsilon)+\psi_H(\epsilon)=1 \qquad \text{для LiH;} \\ &\psi_{Li}(\epsilon)+\psi_D(\epsilon)=1 \qquad \text{для LiD;} \end{aligned} \tag{18}$$

где $\psi(\epsilon) \equiv \psi(\omega)$.

Интересно отметить, что $\psi(\epsilon)$ для H и D имеет характерный вид с минимумом в области акустических частот и почти постоянным ходом в области

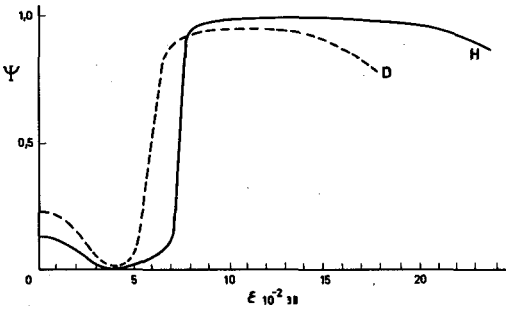

Рис.5

Энергетическая зависимость векторов поляризации $\psi(\epsilon)$ для H и D.

оптических. Переход в $\psi(\epsilon)$ от акустической к оптической области происходит в LiH несколько быстрее, чем в случае LiD из-за перекрытия в последнем оптических и акустических ветвей.

Изменение $\psi(\epsilon)$ подтверждает широко известный факт о том, что легкий атом колеблется, в основном, в оптических ветвях, а тяжелый в акустических [14]. Значения $\psi(\epsilon)$ для $f=0$ легко найти аналитически:

$$\psi_H(0) = \frac{m_H}{m_H + m_{Li}} \quad \text{и} \quad \psi_H(\omega_{\text{попер}}) = \frac{m_{Li}^2}{m_{Li}^2 + m_H^2} .$$

С учетом векторов поляризации перепишем соотношение (3) в следующем виде:

$$\frac{d^2\sigma}{d\Omega\, d\epsilon} \approx \frac{K}{K_0} \frac{\kappa^2}{\epsilon} \frac{g(\epsilon)}{e^{\epsilon/KT} - 1} \left[\psi_1(\epsilon) e^{-2W_1} + \beta \psi_2(\epsilon) e^{-2W_2} \right] . \qquad (19)$$

Здесь

$$\beta = \frac{\sigma_2 m_1}{\sigma_1 m_2} .$$

Аналогично имеем

$$2W_j = \frac{\kappa^2}{m_j} 2 \int \frac{g(\epsilon)\psi_j(\epsilon)}{\epsilon} \left[\frac{1}{e^{\epsilon/KT} - 1} + \frac{1}{2} \right] d\epsilon . \qquad (20)$$

При расчете фактора Дебая-Валлера использовалось спектральное распределение, приведенное на рис.4. Результаты расчетов приведены в верхней части рис.6.

IV. ОБСУЖДЕНИЕ РЕЗУЛЬТАТОВ

Согласно выражению (19) без привлечения модели из экспериментально определенного сечения неупругого рассеяния можно восстановить только функцию $\theta(\epsilon)$:

$$\theta(\epsilon) = g(\epsilon)[\psi_1(\epsilon) e^{-2W_1} + \beta \psi_2(\epsilon) e^{-2W_2}] ,$$

поэтому первоначальное сравнение между собой экспериментальных и расчетных данных по LiH и LiD целесообразно провести на уровне функций $\theta(\epsilon)$. Энергетический ход теоретически рассчитанных функций $\theta(\epsilon)$ для LiH и LiD приведен на рис.7, а экспериментальных — на рис.8, причем для получения $\theta(\epsilon)$ из экспериментальных данных необходимо умножить энергетическую зависимость сечения неупругого рассеяния на фактор

$$\sqrt{\frac{E}{E_0}} \frac{\epsilon}{E + E_0} \cdot (e^{\epsilon/KT} - 1) .$$

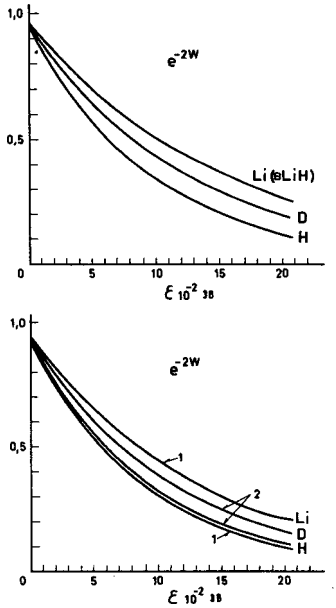

Рис.6

Энергетическая зависимость фактора Дебая-Валлера.

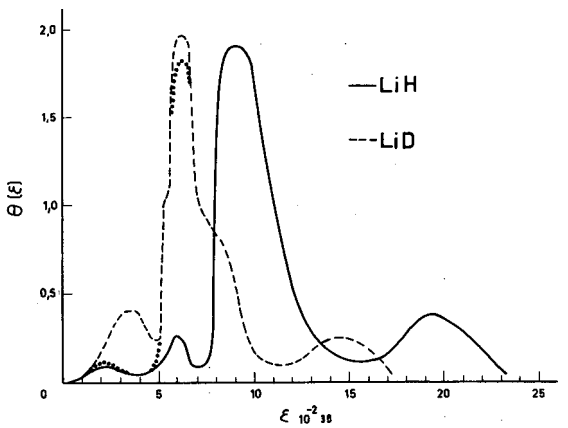

Рис.7

Расчетное значение $\theta(\epsilon)$ для Li^7H и Li^7D.

Как видно из этих рисунков, положения теоретических максимумов, соответствующих акустическим и поперечным оптическим колебаниям, и в случае LiH, и в случае LiD хорошо совпадают с найденными экспериментально. Однако максимум, отвечающий продольным оптическим колебаниям, рассчитанным в модели Келлермана, оказался смещенным в область более высоких частот. Это вполне согласуется со сделанным ранее замечанием

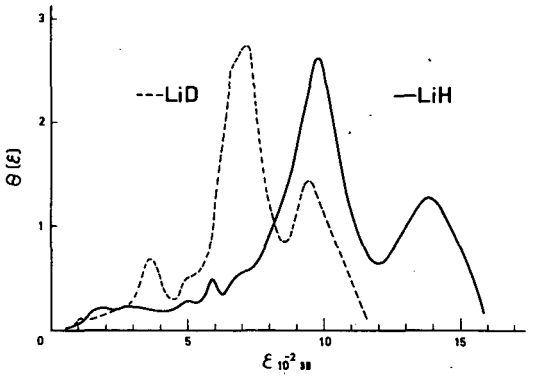

Рис.8

Экспериментальное значение $\theta(\epsilon)$ для Li^7H и Li^7D.

о том, что модель Келлермана неудовлетворительно описывает продольные оптические колебания.

На рис.7 для LiD приведены две кривые $\theta(\epsilon)$. Точками указана кривая для $\beta = 0$, что соответствует пренебрежению рассеянием на ядрах Li. Эта кривая в области малых энергий имеет вид, аналогичный виду $\theta(\epsilon)$ для LiH, где коэффициент β действительно очень близок к нулю. Сплошная кривая соответствует истинному значению β для LiD, равному 0,104 и найденному из реальных масс и сечений [15]. Разность в энергетическом ходе этих двух кривых для LiD говорит о вкладе рассеяния на Li, поэтому можно утверждать, что экспериментально наблюдаемый пик в $\theta(\epsilon)$ при $\epsilon \simeq 35$ мэв обусловлен преимущественно рассеянием на Li. Кроме того, пик при $\epsilon \simeq$ 70 мэв в $\theta(\epsilon)$ для LiD заметно асимметричен. Эта асимметрия объясняется перекрытием акустической и оптической ветвей в фононном спектре LiD, что наглядно видно на рис.4.

При использовании экспериментальных значений $\theta(\epsilon)$ (рис.8) и расчетных значений $\psi(\epsilon)$ (рис.5) были восстановлены функции распределения частот колебаний для LiH и LiD. Результаты восстановления приведены на рис.9 (а, б). Для сравнения на этих рисунках пунктирной линией приведены значения дважды дифференциальных сечений $d^2\sigma/d\epsilon\, d\Omega$. Кривые для $g(\epsilon)$ и $d^2\sigma/d\epsilon\, d\Omega$ не нормированы относительно друг друга. Весьма важным обстоятельством, обращающим на себя внимание при сравнении экспериментальных данных по сечению неупругого рассеяния нейтронов на LiH и LiD и значению функций $\theta(\epsilon)$ с восстановленными из эксперимента фононными спектрами $g(\epsilon)$, является их резкое отличие. Нагляднее всего это отличие можно проследить на примере LiH (рис.9а). Максимум в акустической части фононного спектра LiH при $\epsilon \simeq 40$ мэв настолько сильно подавлен минимумом функции $\psi(\epsilon)$ (рис.5), что практически не проявляется в экспериментальных данных ни по сечению $d^2\sigma/d\epsilon\, d\Omega$, ни по функции $\theta(\epsilon)$. Наряду с этим, в экспериментальном сечении четко проявляются три максимума: при $\epsilon = 11$ мэв, $\epsilon = 16$ мэв и $\epsilon = 26$ мэв. В восстановленном значении $g(\epsilon)$ в этой области энергий наблюдаются слабые изломы, которые вследствие своеобразной энергетической зависимости произведения $g(\epsilon)\psi(\epsilon)$ проявляются очень отчетливо в сечении $d^2\sigma/d\epsilon\, d\Omega$. Поэтому можно утверждать,

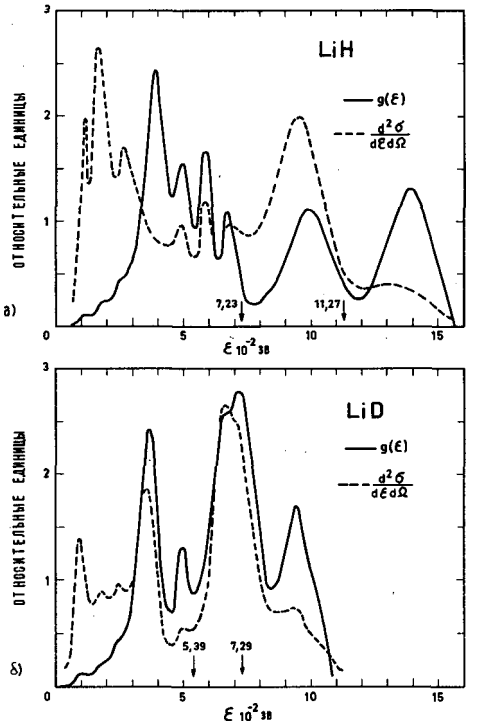

Рис.9

а) Функция распределения частот для Li^7H, восстановленная из нейтронного эксперимента.
б) Функция распределения частот для Li^7D, восстановленная из нейтронного эксперимента.

что без знания энергетической зависимости векторов поляризации нельзя прямо переносить особенности сечения неупругого рассеяния на фононный спектр исследуемого вещества, т.к. получаемую из эксперимента функцию $\theta(\epsilon)$ никак нельзя отождествлять с функцией распределения частот. В этой связи представляются неоправданными попытки такого отождествления, которые делаются в ряде работ последнего времени (например, [16]). Функция $\theta(\epsilon)$ без какого-либо ее преобразования с учетом энергетического хода функции $\psi(\epsilon)$ для многоатомной системы может быть использована только для расчета характеристик взаимодействия нейтронов с веществом, например при рассмотрении задач термолизации и др., в которые информация о фононном спектре входит в виде произведения $g(\epsilon)\sum_j \psi_j(\epsilon)$.

Интересным также является сравнение между собой теоретических и экспериментальных данных по фононным спектрам LiH и LiD. Восстановленный из эксперимента спектр в акустической части оказывается более сложным, чем это следует из расчетов по модели Келлермана. В спектре четко проявляются четыре максимума при $\epsilon \simeq 42$ мэв, $\epsilon \simeq 50$ мэв, $\epsilon \simeq 58$ мэв и $\epsilon \simeq 67$ мэв, причем два первых проявляются как функции распределения частот для LiH, так и для LiD. Совпадает не только их энергетичес-

кое положение, но и сохраняется отношение их ординат. Что касается двух других максимумов, то они проявляются только в LiH, а в LiD, вследствие частичного перекрытия акустической и оптической частей спектра, их обнаружить не удается. В области низких частот и в LiH и в LiD наблюдаются три небольших излома, энергетическое положение которых совпадает. В оптической части спектра проявляются два максимума, которые занимают довольно широкий интервал частот. Такое размытие оптической части спектра, как уже отмечалось, обусловлено ионным характером взаимодействия. Энергетическое положение поперечных оптических ветвей для LiH и LiD хорошо согласуется с расчетным, что касается продольных ветвей, то расчетные значения оказываются смещенными в область больших частот. В случае LiD оптический пик, соответствующий поперечным колебаниям, как и в расчетном спектре, оказывается асимметричным. Он значительно выше максимума акустической части спектра и оптического пика, соответствующего продольным колебаниям. Такой характер пика определяется деформацией его за счет слияния с акустической частью фононного спектра. Указанное различие между расчетными и восстановленными из эксперимента функциями $g(\epsilon)$ объясняется недостатками использованной модели, в которой не учитывается деформация иона, а также ковалентность связи, составляющая в случае LiH ~12,5%. Из сравнения экспериментальных функций распределения $g(\epsilon)$ для LiH и LiD между собой видно, что при замене в решетке гидрида водорода на дейтерий акустическая часть спектра практически не изменяется, т.е. остаются неизменными амплитуды и ширины акустических максимумов. Что же касается оптической части спектра, то замена H на D приводит к смещению максимумов, связанных с продольными и поперечными оптическими колебаниями, в сторону меньших частот, причем частоты всех оптических особенностей с хорошей точностью уменьшаются в $\sqrt{2}$ раз. Но в этом случае изменяются также ширины и амплитуды оптических максимумов, причем ширины уменьшаются, а амплитуды – увеличиваются, так что площадь (число состояний) оптической части фононного спектра остается неизменной. К подобным же результатам приводит сравнение между собой расчетных значений функций распределения и для LiH и LiD. Таким образом, в двухатомных системах, аналогичных гидриду и дейтериду лития, при изотопическом или эквивалентном изотопическому замещении легкой компоненты изменению подвергается преимущественно оптическая часть фононного спектра. Акустическая часть спектра не изменяется. Представляется целесообразным сравнить полученные данные по $g(\epsilon)$ в данной работе с результатами оптических исследований [9], [17], [18]. На рис. 9 (а, б) стрелками указаны значения граничных оптических частот, определенные в работе [17]. Для LiH результаты получены непосредственно из измерений спектра поглощения U.K.-лучей, а для LiD экспериментальные данные получены только для граничной частоты продольной оптической ветви, а граничная частота поперечной ветви была вычислена по соотношению Сцигети из измеренного значения сжимаемости. Результаты нейтронного эксперимента удовлетворительно согласуются с данными оптических измерений и для LiH и для LiD [17]. Что касается результатов других работ [9] [18], то значения граничных частот поперечной оптической ветви и для LiH и для LiD удовлетворительно согласуются с результатами этой работы, однако для продольной оптической ветви данные оптических измерений [9]

оказываются значительно завышенными. При использовании восстановленных значений функций распределения частот для LiH и LiD была вычислена энергетическая зависимость фактора Дебая-Валлера для H, D и Li. Эта зависимость приведена на рис.6. Для сравнения на этом же рисунке приведены данные (1) работы [19], полученные из нейтронно- и рентгеноструктурных измерений. Из приведенных данных следует, что результаты, полученные в данной работе, качественно согласуются с расчетами по модели Келлермана и количественно удовлетворительно согласуются с результатами работы [19]. Наблюдается резкая энергетическая зависимость фактора Дебая-Валлера, причем как для легкой составляющей, так и для лития. Такая зависимость для H и D является следствием отсутствия параметра малости m/M, который имеет место при рассеянии нейтронов на тяжелых ядрах.

В случае лития, хотя и имеется параметр малости 1/7, резкая энергетическая зависимость фактора Дебая-Валлера объясняется своеобразным поведением векторов поляризации Li, завышающих роль акустических частот. Поэтому различие в величинах фактора Дебая-Валлера для Li и для H не такое большое, как это следовало бы просто из отношения масс. Очевидно, что больший интерес представляет расчет термодинамических функций для LiH и LiD на основании фононных спектров, восстановленных из экспериментальных данных по неупругому рассеянию нейтронов. В настоящее время проводится такой расчет.

В заключение представляется необходимым отметить два обстоятельства, вытекающих из результатов данной работы и касающихся некоторых особенностей исследования динамики вещества по неупругому некогерентному рассеянию холодных нейтронов. В экспериментах с холодными нейтронами оказывается возможным исследовать с необходимой статистической точностью акустическую область фононного спектра таких решеток, как LiH, в которых акустическая область относительно подавлена функцией $\psi_H(\epsilon)$. Это наглядно видно по сечению неупругого рассеяния на LiH, приведенном на рис.2, сечения в области, отвечающей акустической и оптической частям фононного спектра, оказываются приблизительно одинаковой величины. В то же время в экспериментах с тепловыми нейтронами (метод сброса) акустическая область спектра практически не проявляется.

Второе обстоятельство связано с результатами исследования неупругого рассеяния нейтронов на дейтериде лития. Казалось бы, из-за значительной доли сечения когерентного рассеяния для D в сечении неупругого рассеяния должно наблюдаться заметное влияние когерентного неупругого рассеяния. Но оказывается, что в фононном спектре, восстановленном из экспериментальных данных, не проявляются эффекты когерентного рассеяния. Это указывает на то, что когерентное неупругое рассеяние холодных нейтронов не оказывает существенного влияния на связь между сечением неупругого рассеяния и функцией распределения частот. Для случая некогерентно рассеивающей смеси изотопов никеля и естественного никеля указанное обстоятельство отмечалось ранее [20]. Поэтому широко используемое в последнее время некогерентное приближение для обработки данных по неупругому рассеянию холодных нейтронов даже на образцах с большой примесью когерентного рассеяния [21] хотя и не имеет еще удовлетворительного теоретического обоснования, тем не менее находит практическое подтверждение.

V. ВЫВОДЫ

1. В интервале энергий от 4 до 160 мэв измерено сечение неупругого рассеяния холодных нейтронов на поликристаллических образцах Li^7H и Li^7D.

2. В модели жестких ионов с учетом эффективного заряда и данных инфракрасного спектра произведен расчет фононных спектров и энергетической зависимости векторов поляризации для решеток гидрида и дейтерида Li. На основе сравнения с экспериментальными данными показано, что модель недеформируемых ионов удовлетворительно описывает акустические и поперечные оптические ветви фононного спектра. На основании теоретических данных рассчитана энергетическая зависимость факторов Дебая-Валлера для LiH и LiD.

3. С учетом энергетической зависимости векторов поляризации из экспериментальных данных по неупругому рассеянию восстановлены функции распределения частот $g(\omega)$ для LiH и LiD. Показано, что особенности сечения неупругого рассеяния нейтронов на решетках из атомов с большой разницей масс и сечений не всегда однозначно связаны с особенностями фононного спектра.

4. Как результат теоретических расчетов и эксперимента, еще раз продемонстрировано, что тяжелый атом колеблется, главным образом, в акустических, а легкий — в оптических ветвях.

5. Показано, что при изотопическом или эквивалентном изотопическому замещении легкого атома в двухатомной решетке изменению подвергается только оптическая область фононного спектра, в то время как акустическая остается неизменной.

6. Отмечено, что в кристаллах, подобных гидриду и дейтериду лития, неупругое рассеяние холодных нейтронов позволяет надежно исследовать наряду с оптической и акустическую область фононного спектра.

7. В дополнение к случаю изотопического и естественного никеля получено еще одно подтверждение на LiD, что когерентные эффекты, во всяком случае, не искажают связь между сечением неупругого рассеяния и функцией распределения частот. Поэтому так называемое "некогерентное приближение" является удовлетворительным для целей восстановления фононного спектра из экспериментальных данных по неупругому рассеянию холодных нейтронов на поликристаллических образцах с одним атомом в элементарной ячейке.

В заключение выражаем благодарность М.И. Певзнеру и Ю.М. Кагану за участие в обсуждении полученных данных, В.П. Бочину за приготовление образцов Li^7H и Li^7D, А.Г. Чичерину за дискуссию по учету функции разрешения, Л. Касаткиной за проведение расчетов на электронно-счетной машине, А.Е. Головину, В.Г. Федорову и А.С. Игнашеву за помощь в проведении экспериментов.

ЛИТЕРАТУРА

[1] КАГАН Ю., ЖЭТФ, 42, 5 (1962).
[2] ЧЕРНОПЛЕКОВ Н.А., ЗЕМЛЯНОВ М.Г., БРОВМАН Е.Г., ЧИЧЕРИН А.Г., ФТТ, 5, 1 (1963).

[3] PELAH I., EISENHAUER C. M., HUGHES D. J., PALEVSKY H., Phys. Rev. 108 (1958) 1091.
[4] МАК-РЕЙНОЛЬДС А., НЕЛКИН М., РОЗЕНБЛЮТ М., УИТМОР У., Избранные доклады иностранных ученых, т.2, Нейтронная физика, 1959.
[5] WOODS A. D., BROCKHOUSE B. N., SAKAMOTO M., SINCLAIR R. N., "Inelast. Scat. of Neutrons in Solids and Liquids" I. A. E. A. Proc., Vienna, 1961.
[6] BERGSMA J., GOEDKOOP J. A., Physica 26 (1960) 9.
[7] SAUNDERSON D. H., COCKING S. J., "Inelast. Scat. of Neutrons in Solids and Liquids". Proc. Vol. II, I. A. E. A., Vienna, 1963.
[8] ЗЕМЛЯНОВ М.Г., ЧЕРНОПЛЕКОВ Н.А., ПТЭ №5 (1962).
[9] FILLER A. S., BURSTEIN E., Bull. Amer. Phys. Soc., 5 (1960) 198.
[10] BROCKHOUSE B. N., BECKA L. N., RAO K. R., WOODS A. D., "Inelast. Scat. of Neutrons in Solids and Liquids". Proc. Vol. II, I. A. E. A. Vienna, 1963.
[11] KELLERMAN E. W., Phil. Trans. Roy. Soc. 238A (1940) 513.
[12] WOODS A. D., "Inelast. Scat. of Neutrons in Solids and Liquids". Proc. Vol. II, I. A. E. A., Vienna (1963).
[13] LYDDANE R. H., HERZFELD K. F., Phys. Rev. 54 (1938) 846.
[14] КАГАН Ю., МАСЛОВ В.А., ЖЭТФ, 41, 10 (1961).
[15] BACON G. E., "Neutron Diffraction" 2ed., 1962.
[16] SINCLAIR R. N., "Inelast. Scat. of Neutrons in Solids and Liquids", Proc. Vol. II, I.A.E.A., Vienna, 1963.
[17] PRETZEL F. E., RUPERT G. N., MADER C. L., STORMS E. K., GRITTON G. V., RUSHING C. C., J. Phys. Chem. Solids 16 (1960) 1/2.
[18] ZIMMERMANN W. B., MONTGOMERY D. J., Phys. Rev. 120 (1960) 2.
[19] CALDER R. S., COCHRAN W., GRIFFITHS D., LOWDE R. D., J. Phys. Chem. Solids 23 (1962) 6.
[20] ЧЕРНОПЛЕКОВ Н.А., ЗЕМЛЯНОВ М.Г., ЧИЧЕРИН А.Г., ЛЯЩЕНКО Б.Г., "Inelast. Scat. of Neutrons in Solids and Liquids", Proc. Vol. II, I. A. E. A., Vienna, 1963.
[21] MOZER B., OTNES K., PALEVSKY H., BNL-7240 (1963).

EXPERIMENTAL METHODS

EXPERIMENTAL EQUIPMENT AND METHODS FOR INELASTIC NEUTRON SCATTERING MEASUREMENTS*

H. PALEVSKY
BROOKHAVEN NATIONAL LABORATORY, UPTON, N.Y.,
UNITED STATES OF AMERICA

Abstract — Résumé — Аннотация — Resumen

EXPERIMENTAL EQUIPMENT AND METHODS FOR INELASTIC NEUTRON SCATTERING MEASUREMENTS. The overall problem for obtaining improved inelastic neutron scattering data at nuclear reactors may be divided into four parts: (1) reactor design considerations; (2) spectrometer developments; (3) detector developments and (4) data handling methods.

With the HFBR about to go critical, it is worthwhile to review the progress made at Brookhaven in these four related phases of experimental technique.

(1) From an experimentalist's point of view the problem of obtaining good data is twofold. First, one wishes the highest usable counting rate and second, the lowest background. These two requirements are not independent in terms of reactor design and the optimizing of either one will have an adverse effect on the other. The HFBR was designed to provide a compromise for the overall experimental programme and allows for further optimization of each experiment.

(2) The major factor in spectrometer design is the balance of intensity versus resolution. Optimum design depends on the particular measurement contemplated. In order to accomodate a broad range of possible experiments at various energies, three spectrometers were designed and are nearing completion: (a) three-rotor time-of-flight spectrometer; (b) three-crystal spectrometer and (c) hybrid crystal-time-of-flight spectrometer.

(3) Development of detectors was undertaken with three factors in mind: (a) high neutron efficiency; (b) low gamma-ray efficiency and (c) small size. Two systems show promise: (1) scintillation detectors using Li glass and (2) He^3 proportional counters.

(4) Data handling systems have developed around small digital computers. These systems perform functions of data sorting and storage, data manipulation, and automatic adjustment of experimental conditions. Two systems have evolved, one for use with time-of-flight spectrometers, the other for use with crystal spectrometers.

The HFBR and associated equipment will be in operation during the summer of 1964. It is expected that the first measurements using the new equipment will be completed towards the end of 1964.

MATÉRIEL ET MÉTHODES POUR EXPÉRIENCES DE MESURE DE LA DIFFUSION INÉLASTIQUE DES NEUTRONS. Le problème général à résoudre si l'on veut améliorer les constantes de diffusion inélastique des neutrons dans les réacteurs nucléaires peut se diviser en quatre points: 1. considérations relatives à l'étude des réacteurs; 2. mise au point de spectromètres; 3. mise au point de détecteurs et 4. méthodes de traitement des données.

HFBR (High Flux Beam Research Reactor = réacteur de recherche à faisceaux de haut flux) étant sur le point de diverger, il est utile d'examiner les progrès réalisés à Brookhaven sur ces quatre points.

1. Du point de vue de l'expérimentateur, le problème de l'amélioration des constantes est double. Il faut, en premier lieu, obtenir le taux de comptage le plus élevé possible, et, en second lieu, réduire au minimum le bruit de fond. Ces deux caractéristiques sont interdépendantes: dans les études de réacteurs, l'optimisation de l'une produira un effet défavorable sur l'autre. HFBR a été conçu de manière à fournir une solution de compromis pour l'ensemble du programme expérimental et à se prêter à une optimisation plus poussée pour chaque expérience.

2. L'aspect principal de l'étude d'un spectromètre est le compromis à trouver entre l'intensité et le pouvoir de résolution. L'optimisation de l'appareil dépend de la mesure que l'on veut faire. Pour pouvoir

* Work supported by the United States Atomic Energy Commission.

procéder à une gamme étendue d'expériences à des énergies différentes, on a conçu les trois spectromètres ci-après dont la construction sera bientôt achevée: a) spectromètre à temps de vol à trois rotors; b) spectromètre à trois cristaux; c) spectromètre hybride à temps de vol et à cristal.

3. Dans l'étude des détecteurs, on a tenu compte des trois facteurs suivants: a) efficacité élevée pour les neutrons; b) faible efficacité pour les rayons gamma; c) petite dimension. Deux appareils semblent ouvrir des perspectives intéressantes: 1° le détecteur à scintillation utilisant du verre au lithium; 2° le compteur proportionnel à ^{3}He.

4. Les méthodes de traitement des données sont essentiellement fondées sur l'emploi d'ordinateurs. Elles permettent les opérations suivantes: tri et stockage des données; manipulation des données; ajustement automatique des conditions expérimentales. Deux méthodes ont été mises au point, dont l'une est employée avec les spectromètres à temps de vol et l'autre avec les spectromètres à cristal.

HFBR et le matériel connexe ont été mis en service en été 1964. Il était prévu que les premières mesures à l'aide du nouveau matériel seraient terminées vers la fin de 1964.

ЭКСПЕРИМЕНТАЛЬНОЕ ОБОРУДОВАНИЕ И МЕТОДЫ ИЗМЕРЕНИЯ НЕУПРУГОГО РАССЕЯНИЯ НЕЙТРОНОВ. Всю проблему получения более точных данных по неупругому рассеянию нейтронов на ядерных реакторах можно разбить на четыре части: 1) вопросы, связанные с конструкцией реактора; 2) вопросы разработки спектрометров; 3) вопросы разработки детекторов; 4) методы обработки данных.

В связи с тем, что реактор HFBR скоро достигнет критичности, имеет смысл рассмотреть, какие успехи достигнуты в Брукхейвене в этих четырех взаимосвязанных областях экспериментальной техники:

1) С точки зрения экспериментатора проблема получения точных данных двояка. С одной стороны, желательно иметь максимальную скорость счета, а с другой — минимальный фонд. Эти два требования зависят от конструкции реактора, и оптимизации одной из этих характеристик приводит к ухудшению другой. Реактор HFBR был сконструирован так, чтобы обеспечить компромиссное решение всей экспериментальной программы, он позволяет еще больше оптимизировать каждый эксперимент.

2) Основным фактором для конструкции спектрометра является баланс между интенсивностью и разрешающей способностью. Оптимальность конструкции определяется характером конкретного задуманного эксперимента. Чтобы обеспечить возможность выполнения широкого круга экспериментов при различных энергиях, сконструированы и будут в скором времени изготовлены три следующих спектрометра: а) трехроторный спектрометр по времени пролета; б) спектрометр с тремя кристаллами; и в) смешанный кристаллический спектрометр по времени пролета.

3) При разработке детекторов преследовались три цели: а) высокая эффективность по нейтронам; б) низкая эффективность по гамма-лучам; и в) небольшой размер. Перспективными представляются две системы: 1) сцинтилляционные детекторы с использованием литиевого стекла; 2) пропорциональные счетчики с He^3.

4) В основу разработки систем для обработки данных положены небольшие цифровые вычислительные машины. Эти системы производят сортировку, хранение и обработку данных, а также автоматическое регулирование условий экспериментов. Уже разработаны две системы: одна для использования с спектрометрами по времени пролета, а другая — с кристаллическими спектрометрами.

Реактор HFBR и связанное с ним оборудование были пущены в эксплуатацию летом 1964 года. Первые измерения с помощью нового оборудования были закончены в конце 1964 года.

EQUIPO Y MÉTODOS EXPERIMENTALES DE MEDICIÓN POR DISPERSIÓN INELÁSTICA DE NEUTRONES. El problema general de mejorar los datos obtenidos por dispersión inelástica de neutrones en los reactores nucleares puede dividirse en cuatro partes: 1. Consideraciones relativas al diseño de los reactores; 2. Perfeccionamiento de los espectrómetros; 3. Perfeccionamiento de los detectores, y 4. Métodos de elaboración de datos.

Hallándose el reactor HFBR (High Flux Beam Research Reactor) a punto de alcanzar la criticidad, merece la pena examinar los progresos logrados en Brookhaven en estas cuatro esferas afines de la técnica experimental:

1. Desde el punto de vista del experimentador, el problema de obtener datos satisfactorios es doble. En primer lugar, se desea aumentar al máximo la velocidad de recuento aprovechable y, en segundo, reducir al mínimo la actividad de fondo. Estos dos requisitos no son independientes en lo que respecta al diseño del reactor y, en general, sólo se podrán obtener valores óptimos de uno de los parámetros a expensas del otro.

El HFBR se ha concebido de modo que satisfaga razonablemente todas las exigencias del programa experimental, con la posibilidad de mejorar las condiciones de cada experimento particular.

2. El factor primordial en el diseño de espectrómetros es encontrar un equilibrio adecuado entre intensidad y poder de resolución. El diseño óptimo depende de las mediciones concretas que se quieran efectuar. Para poder llevar a cabo una amplia variedad de experimentos a diversas energías se han diseñado tres espectrómetros cuya construcción está a punto de terminarse: a) un espectrómetro de tiempo de vuelo de tres rotores; b) un espectrómetro de tres cristales; c) un espectrómetro mixto de cristal y tiempo de vuelo.

3. En la construcción de detectores se han tenido en cuenta tres factores: a) elevado rendimiento neutrónico; b) escaso rendimiento gamma; c) dimensiones reducidas. Presentan interés dos sistemas: 1) detectores de centelleo con vidrio litiado; 2) contadores proporcionales de ^3He.

4. Los sistemas de elaboración de datos se han desarrollado en torno a las pequeñas calculadores numéricas. Tales sistemas desempeñan funciones de selección y acumulación de datos, manipulación de los mismos y ajuste automático de las condiciones experimentales. Se han perfeccionado dos sistemas, destinados respectivamente a los espectrómetros de tiempo de vuelo y a los espectrómetros de cristal.

The Brookhaven High Flux Beam Reactor (HFBR) is scheduled to go critical in the spring of next year, and we hope to be making first measurements on the various new apparatus in early summer. I therefore thought that this would be an appropriate time to review those features of the reactor and associated equipment which we feel will allow us to be active again in the inelastic scattering field. There will be more emphasis on some phases of the work than others. This only reflects the fact that these parts were done in the Neutron Physics Group and, therefore, I have a first-hand knowledge of these phases and only a second-hand knowledge of other phases. One word about Brookhaven organization I think is appropriate. At the graphite reactor there were a very large number of beam ports, in the order of 50, and essentially every experimenter or experimental group had its own beam hole and equipment. The new reactor obtains a high flux by the virtue of a small core and reflector and so the beam ports are limited to nine. It was clear that we could not accommodate everyone in the same manner as before. Therefore it was decided that we would try to build various pieces of apparatus to give us a great flexibility in measurement capability, but that the facilities would now be shared by all the various groups.

The Brookhaven HFBR is the first reactor in the United States to be designed specifically for the needs of the experimental physicists. All previous reactors were conceived by reactor physicists who were trying to improve, in one way or another, on reactor technology. The HFBR was designed using existing technology and the effort was placed on trying to satisfy the needs of experimenters, particularly those who used neutron beams for measurements. Table I lists the design parameters; only a few will be of interest to this group. The peak thermal flux (in reflector) is 7×10^{14} n/cm^2 s, and the epicadmium flux in the core is 1.6×10^{15} n/cm^2 s. The D_2O flow rate in the core will be 17 600 gal/min at the full power of 40 MW. Figure 1 shows the flux characteristics. The solid curves are calculated in a four-energy group calculation, the dashed curve represents measurements carried out in a critical facility assembled in 1960 to check the effect of beam ports on reactivity. Note that by terminating the end of the beam hole at various distances into the reflector the quality of the flux can be altered. It was the job of each experimental group in charge of building a piece of apparatus to specify where their beam tube would be terminated. Figure 2 shows the

TABLE I

HFBR DESIGN PARAMETER LIST

Power	40 MW	
Neutron flux		
Core, total epithermal	1.6×10^{15}/cm² s	
Reflector thermal flux, max.	7×10^{14}/cm²s	
Materials		
Coolant, moderator, and reflector	D_2O	
Fuel	U^{235}-Al alloy	
Core structure, beam tubes	6061 aluminium	
Lower vessel	6061 aluminium	
Upper vessel	stainless steel	
Primary pipes & process equipment	stainless steel	
Fuel element and core		
Type	ETR, flat-plate	
Uranium concentration in meat alloy	30 wt.%	
Meat thickness	0.020 in U-Al	
Cladding thickness	0.015 in 8001 Al	
Fuel region dimensions per element	2.6×3.0×21 in	
U^{235} loading per element	260 g	
Number of fuel elements	28	
Core volume	86 l	
Total U^{235} loading	7.28 kg	
Water-to-metal volume ratio	1.23	
D/U^{235} atom ratio	169	
Al/U^{235} atom ratio	123	
Cycle time for 20% burn-up	40 d	
Temperature and void coefficients		
Core metal coefficient	-0.36×10^{-3}% k/°C	
Core water coefficient	-6.15×10^{-3}% k/°C	
Reflector water coefficient	-10.5×10^{-3}% k/°C	
Total temperature coefficient	-17.01×10^{-3}% k/°C	
Core void coefficient	-0.33×10^{-3}% k/cm³	
Excess reactivity requirements	Maximum (%)	Normal (%)
Burn-up, plus Sm and stable f.p.'s	5.0	2.8
Xenon, steady state	3.4	3.4
Temperature	0.5	0.5
Control and experiments	1.1	1.1
Total	10.0	7.8
Control rods		
Number of main rods	8	
Individual main rod, total worth	4.1% k	
8 main rods in gang, total worth	31% k	
Number of auxiliary rods	8	
Individual auxiliary rod, total worth	1.07% k	
8 auxiliary rods in gang, total worth	8% k	
Total worth of all rods	39% k	

TABLE I (*cont.*)

Core thermal design data	
Water channel thickness	0.105 in
Fuel plate thickness	0.050 in
Fuel plate length, active	21 in
Water channel width	2.231 in
Core alloy width	2.00 in
Heat transfer surface per element	11.1 ft^2
Total heat transfer surface, core	311 ft^2
Water flow data	
Water channel flow area per element	0.0326 ft^2
Total channel flow area, core	0.912 ft^2
Water velocity in channels	35 ft/s
Water flow per element	520 gal/min
Water flow, 28 elements	14,560 gal/min
Water flow in control rods, approx.	2,000 gal/min
Water flow in bypass, approx.	1,000 gal/min
Total water flow, approx.	17,600 gal/min
Total primary loop pressure drop	60 lb/in^2
Pressure drop in fuel elements	25 lb/in^2
Process system design	
Maximum operating pressure	250 lb/in^2 gauge
Maximum operating temperature	150°F
Vessel design temperature	200°F
Beam tube design temperature	400°F
Core power conditions	
Radial peak-to-average power density	2.3
Over-all peak-to-average power density	2.82
Bulk hot channel factor	1.36
Film hot channel factor	1.87
Average power density	0.465 MW/L
Maximum power density	1.31 MW/L
Core thermal analysis results	
Reactor inlet temperature	120°F
Reactor outlet temperature	133.4°F
ΔT bulk	13.4°F
Hot spot surface temperature	360°F
Operating hot spot pressure	173 lb/in^2 gauge
Saturation temperature at hot spot	376°F
Blanket gas pressure	196 lb/in^2 gauge
Average heat flux, BTU/hr ft^2	0.387×10^6
Maximum heat flux, BTU/hr ft^2	1.09×10^6
Burn-out heat flux, BTU/hr ft^2	4.4×10^6
Neutron prompt lifetime	672 μs

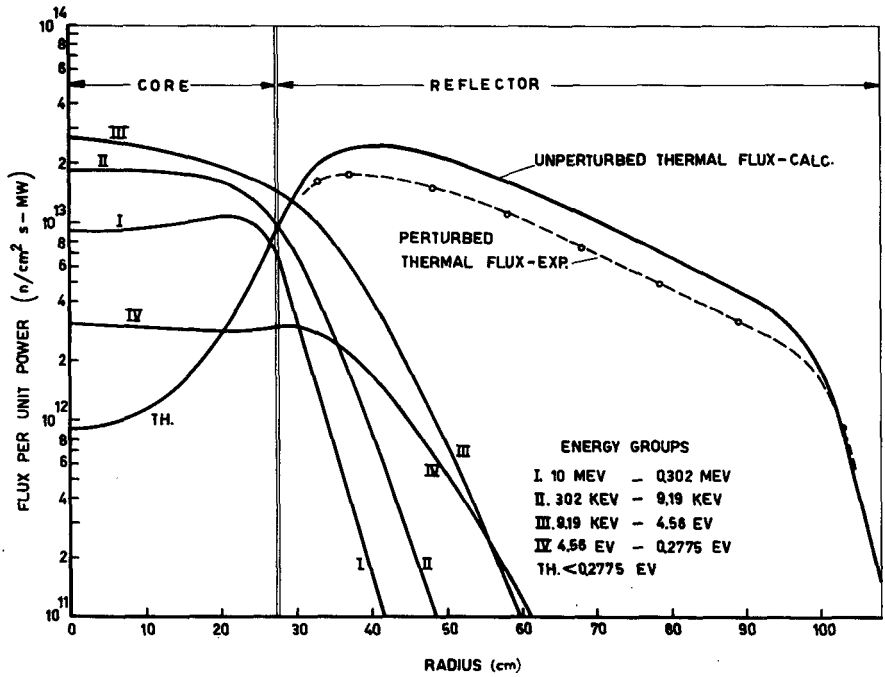

Fig. 1

HFBR flux versus radius

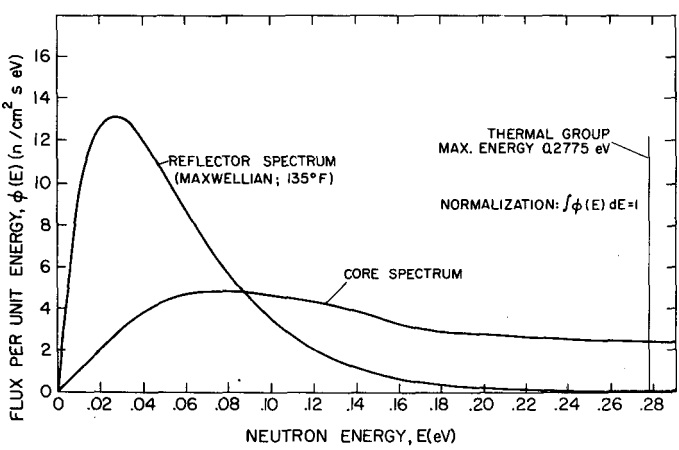

Fig. 2

Thermal neutron group spectra in core and reflector

thermal energy spectra in the core and reflector. The core is undermoderated and so the thermal flux is depressed. Those experiments requiring essentially thermal beams, such as the diffractometers, are ar-

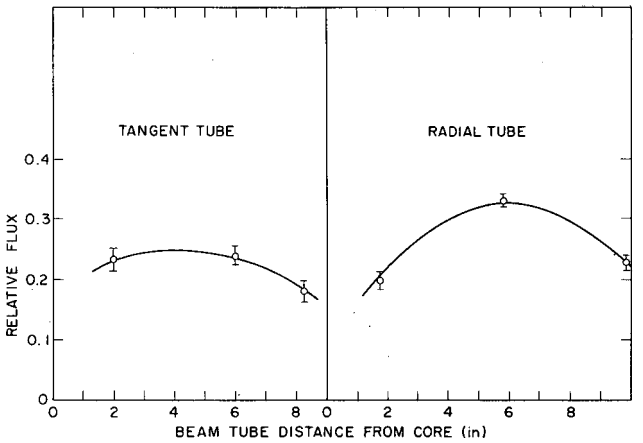

Fig. 3

Narrow angle collimated thermal neutron flux from beam tubes

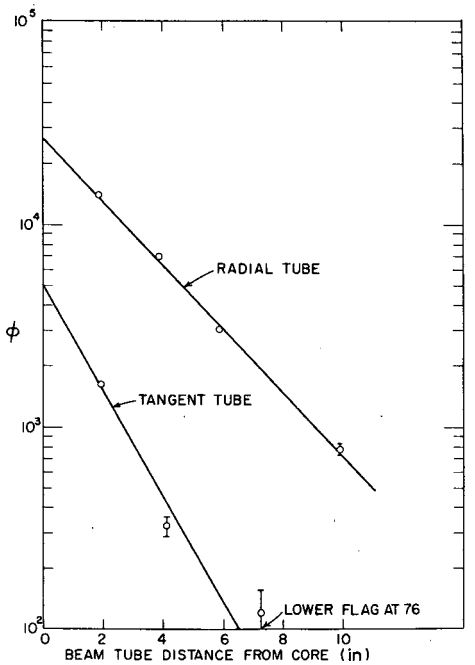

Fig. 4

Proton recoil neutron flux from beam tubes

ranged to view the reflector spectrum. Some further tests on beam tube characteristics at the critical facility proved interesting. These are shown in Fig. 3. Here we have beam tubes running radially and tangentially to the fuel assembly. Note the tangential thermal flux, which peaks at about 6 in

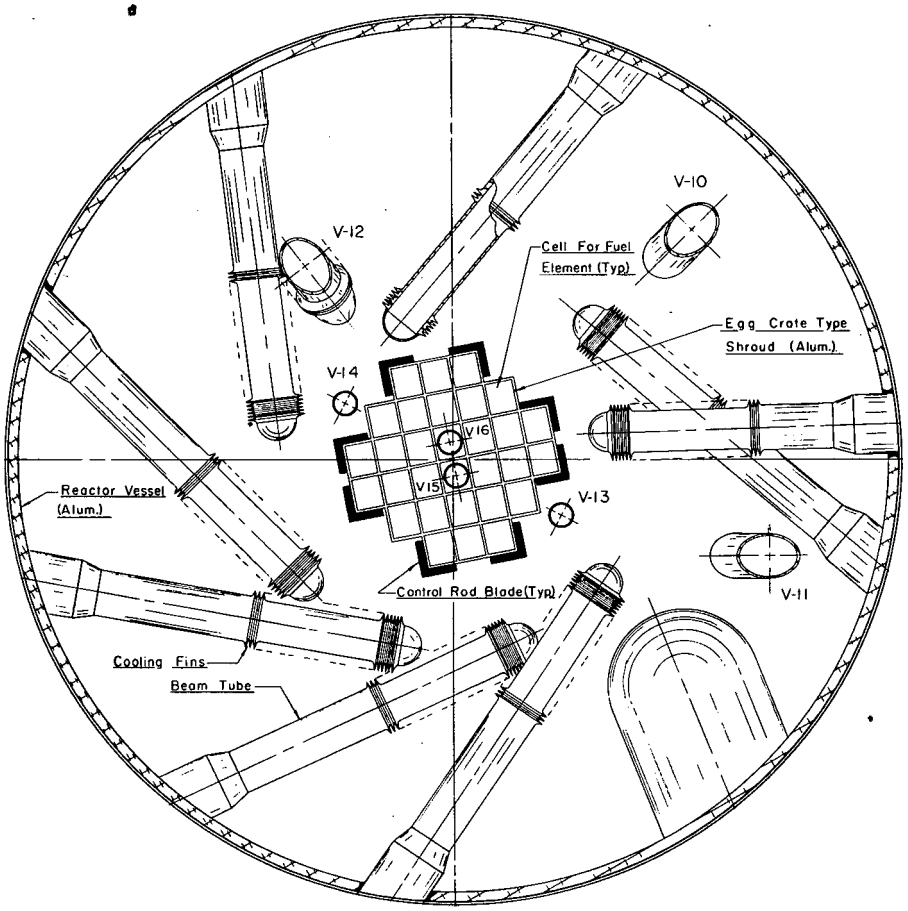

Fig. 5

Plan view of experimental beam tubes in reactor vessel

from the edge of the core, is only approximately 30% down from the radial flux. This small difference is characteristic of a D_2O moderated reactor. Now Fig. 4 shows the fast neutron flux as measured with a proton recoil counter. At 6 in from the core the fast flux is about a factor of 30 below that emerging from a radial tube. On the basis of these considerations the beam hole configuration was set as shown in Fig. 5. Note there is only one radial beam hole and that is for the fast chopper nuclear physics facility. All holes are 4 in in diameter except for the cold neutron port which is 12 in in diameter. Figure 6 shows a typical beam port in plan view; the shutter is 30 in in length, the biological shield is approximately 3 m, and the total radial distance to the centre of the core only 4 m. High density concrete is used as to allow the smallest distance between the radiating surface and the apparatus. The fact that thermal flux is peaked outside the core also makes the distance between experimental equipment and radiating source shorter for those experiments using thermal neutrons. The cold neutron beam port

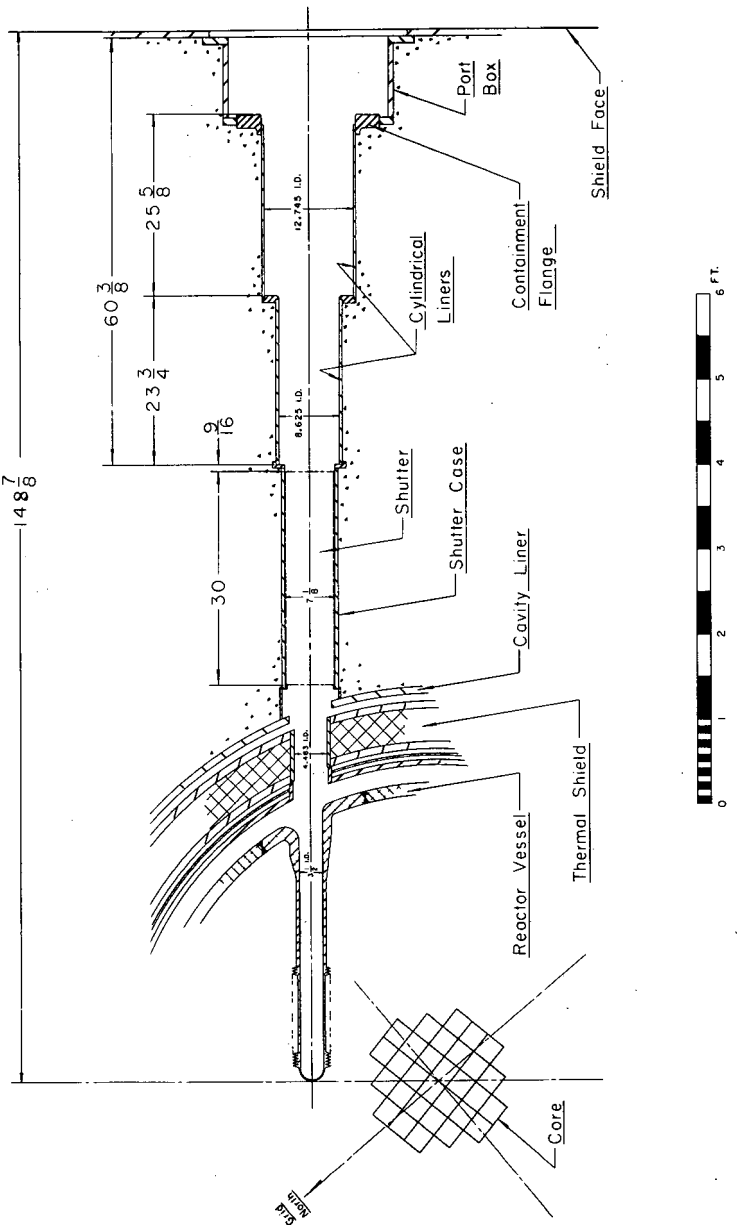

Fig. 6
Plan of HFBR (Beam tube H-3)
(All dimensions in inches)

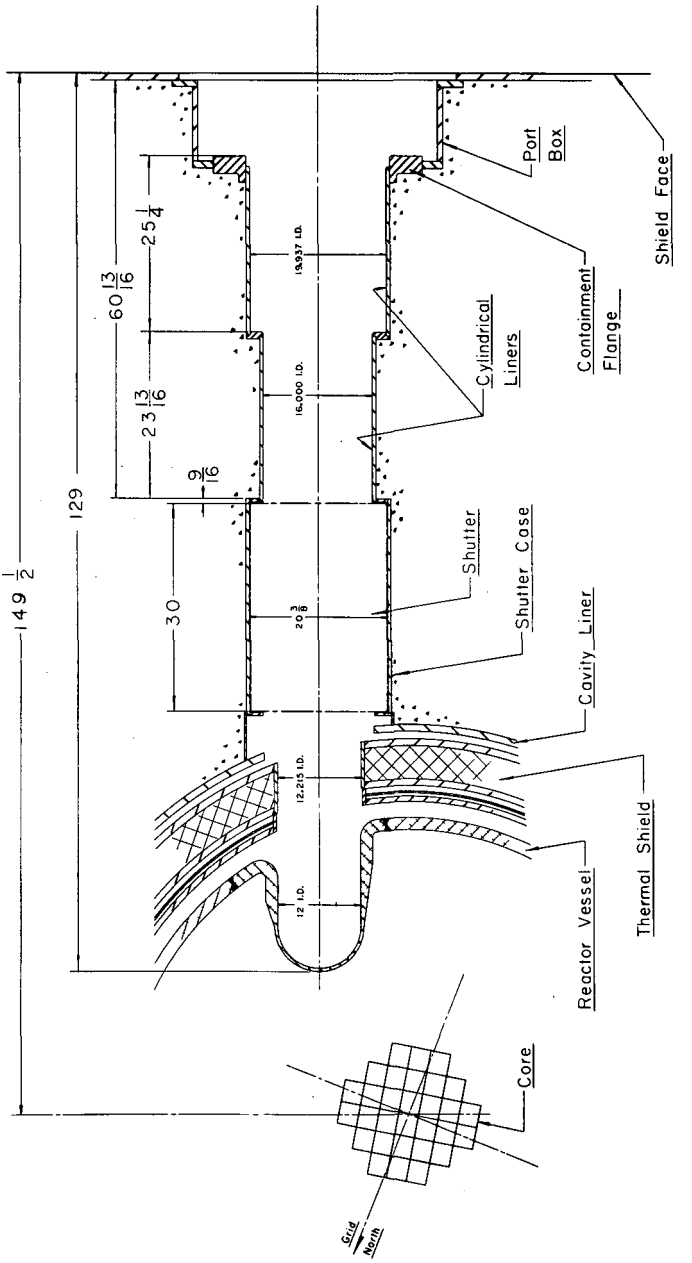

Fig. 7

Plan of HFBR (Beam tube H-9)
(All dimensions in inches)

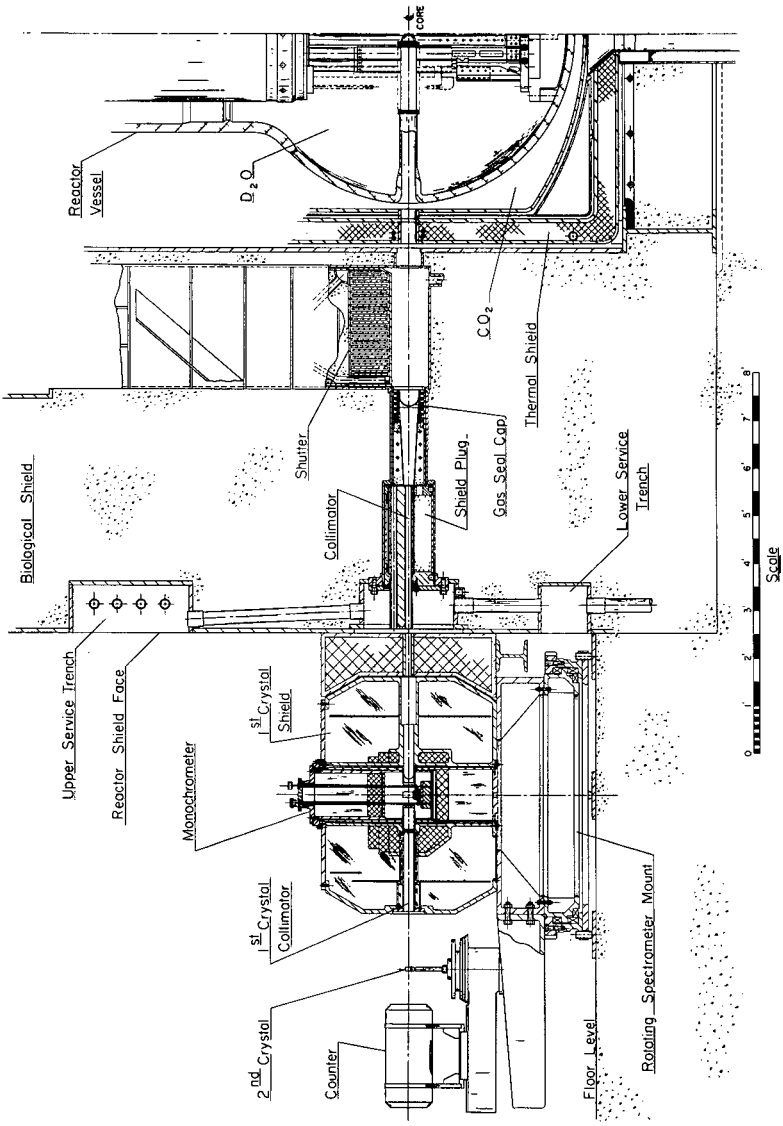

Fig. 8

Elevation of typical neutron diffraction experimental setup

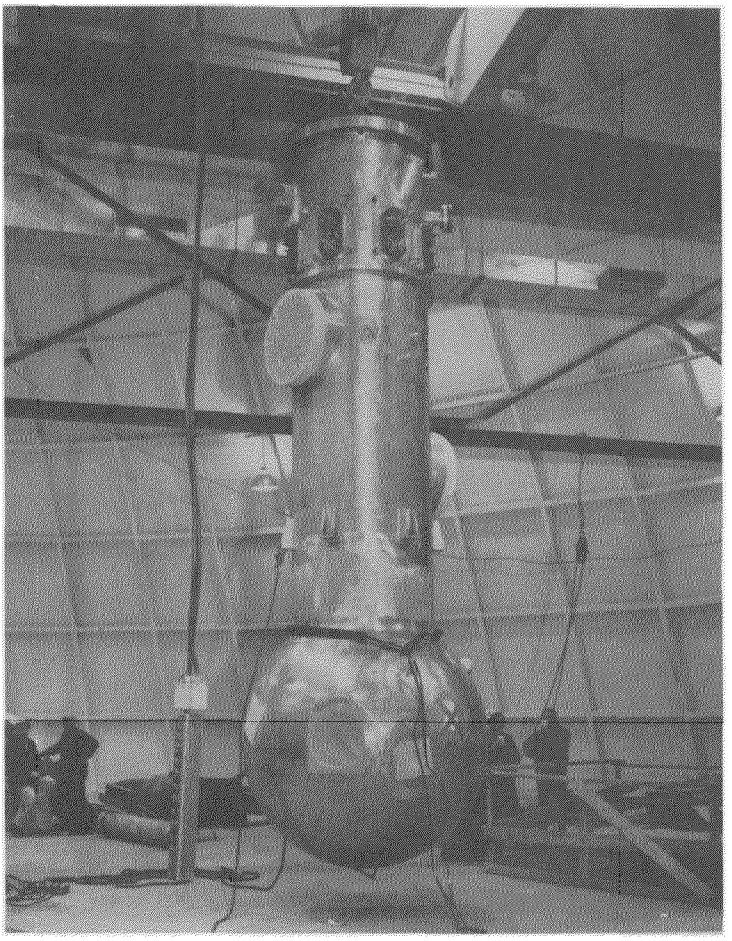

Fig. 9

Reactor vessel ready for installation
Covered holes in spherical section are beam tubes. Ports in neck are for D_2O cooling water.

is shown in Fig. 7; note the 12 in hole. Figure 8 shows the beam profile of a typical diffractometer setup. The shutter is operated from above. Figure 9 shows the reactor vessel and various holes for beam ports; the largest one is for cold neutrons. Also seen is the inlet and exit for cooling water. I will end this part of the discussion with a few figures which show the present state of the reactor. Figure 10 is what we hope will soon be a rare view, the empty reactor hull. The experimental floor extends some 25 m beyond the face of the reactor shield. The people on the floor are surveying the beam holes for alignment. Note that the shield looks very small. The reactor physicists nevertheless claim that the fast neutron flux issuing from the shield will be less than one fast neutron/cm^2/min.

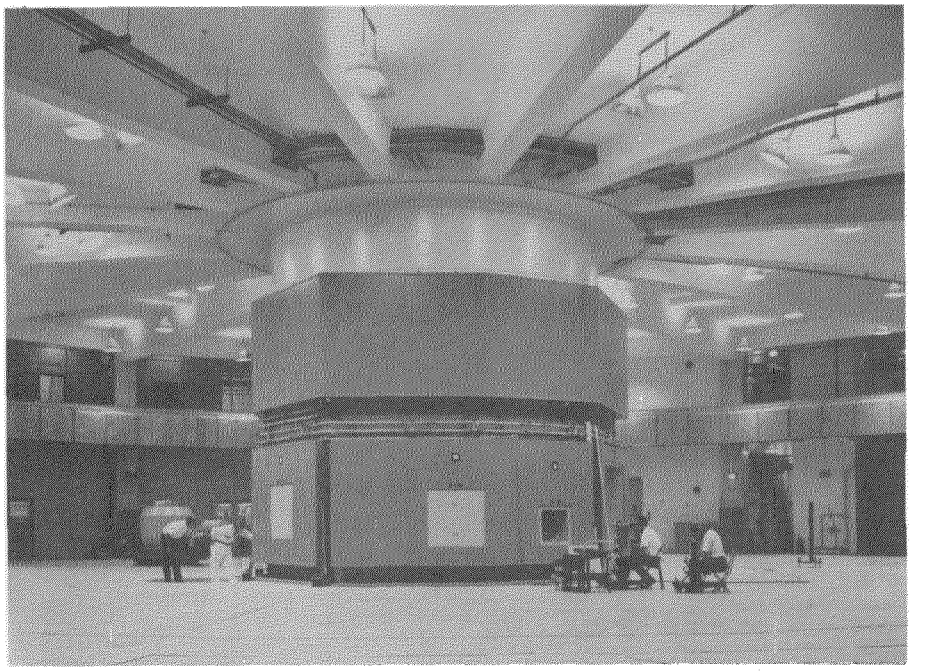

Fig. 10

View of experimental floor of HFBR
Technicians are surveying beam tube alignment before installation of experimental equipment.

Of the nine experimental beam ports available at the HFBR, seven will be used for solid state physics. For inelastic scattering work there will be three facilities available initially: a three-rotor time-of-flight spectrometer, a three-axis spectrometer, and a hybrid crystal and chopper apparatus. The three-rotor system is the one described in Ref. [1]. Shown diagrammatically in Fig. 11, the system consists of a vertically shafted chopper monochromator, plus two horizontally shafted choppers. The apparatus is designed to give maximum intensity for a given resolution. The far pair of rotors runs in such a way that the slits are moving in an opposing sense so as to produce a shorter burst. This pair will be used for energy gain experiments. For energy loss and quasi-elastic experiments, where we require better incoming wavelength resolution, it is much better as regards intensity to obtain the needed resolution by using a third rotor separated from the two, instead of making the slits of the pair smaller. Figure 12 shows a horizontally shafted rotor made from High Duty Alloys' Cd-Mg alloy, which is now undergoing creep tests; it is designed for a maximum at 15 000 rpm, 12 000 rpm corresponding to 4-Å wavelength neutrons. Figure 13 shows the present vertically shafted rotor, made of high strength aluminium and cadmium plated. Figure 14 shows the top half removed so that one can see the plastic inserts which will stop fast neutrons. A feature of this design is that when neutrons are emerging from the rotor and hitting the sample the full 10 in of plastic is in the beam. We have tested the cad-

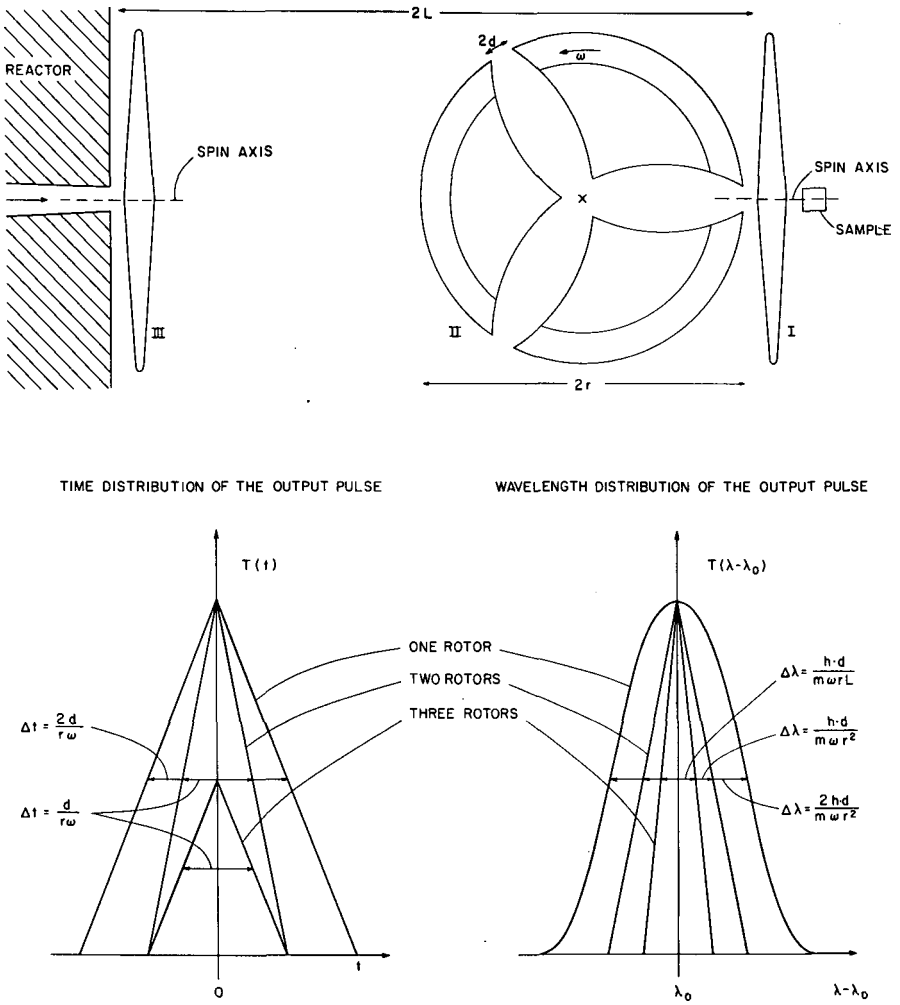

Fig. 11

Phased rotor system
Upper half shows diagrammatic view of rotor configuration. Bottom half shows calculated time and wavelength distributions of output pulses.

mium plating with model rotors and it appears to have the required adhesive strength. We are now in the process of spin testing this cadmium-plated rotor. The calculated intensities and resolution for this apparatus installed at the HFBR is as follows. For a slit size of 1.25 cm×5 cm, the two-rotor system at 4 Å will have a burst width of 12 μs with a wavelength width of 0.125 Å and the intensity issuing from the slit will be approximately 10^7 n/s. The three-rotor system will provide a factor of two reduction in the wavelength spread with a corresponding decrease of a factor of eight in intensity. One three-axis spectrometer of conventional design is now nearing com-

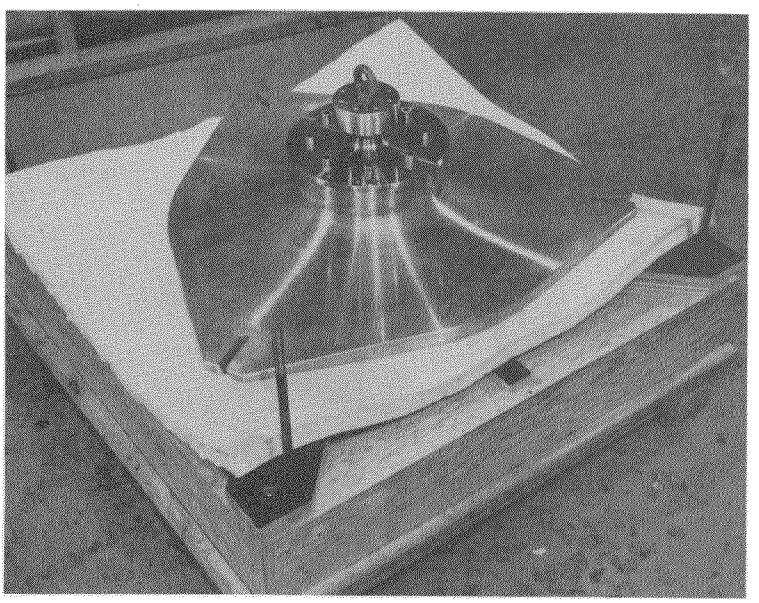

Fig. 12

Horizontally shafted rotor for slow chopper phased rotor system

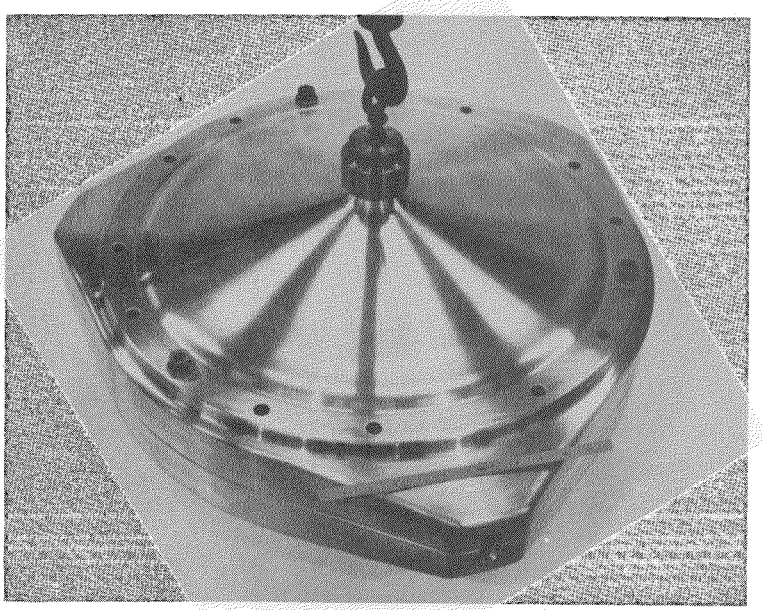

Fig. 13

Top view of vertically shafted rotor

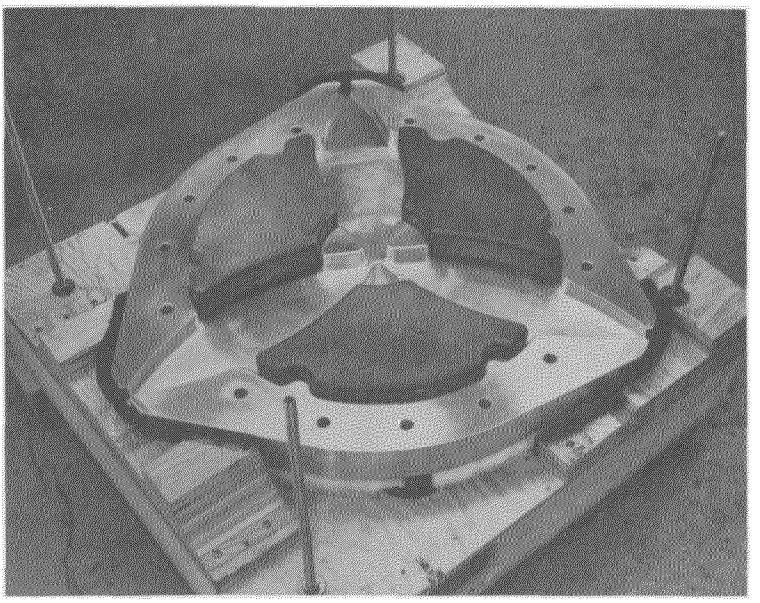

Fig. 14

Vertically shafted rotor with upper forging removed, showing phenolic neutron stopping material

pletion, and long-term plans call for possible construction of two more of these units after some experience is gained with the first one. In addition to these two instruments, it was decided that one hybrid instrument should be built that would offer the possibility of using high-incident-energy neutrons and obtaining extremely good resolution. OTNES in Ref.[1] suggested that the logical way to obtain such an instrument was to use a crystal monochromator for the incoming beam and a simple chopper as an analyser following the sample. Suppose one wishes to look at a molecular level, say at 0.5 eV (about 4000 cm^{-1}); one would then set the monochromator for an energy slightly above this using a crystal with small mosaic spread and fine collimation, say 0.1°. If the comparable collimation were required at the exit the loss in intensity would be too great. Because the scattered neutrons come off at low energy, a chopper subtending a large solid angle of the scattered beam can be used and good energy resolution still obtained. The idea is very similar to that underlying the window-filter scheme developed at Trombay by Iyengar and his co-workers.

The detector development at Brookhaven has been mainly aimed at trying to obtain efficient neutron detectors that are small in size, in particular, thin in the direction of the beam. One attempt was to use the enriched Li glass detectors. These worked fine in the laboratory but when tested in our present cold neutron facility they gave poor results because of high background. When we investigated the source of the background we found that we had a flux of 50 r of gamma rays hitting our sample, and the background was mainly coming from those gamma rays being scattered by the sample

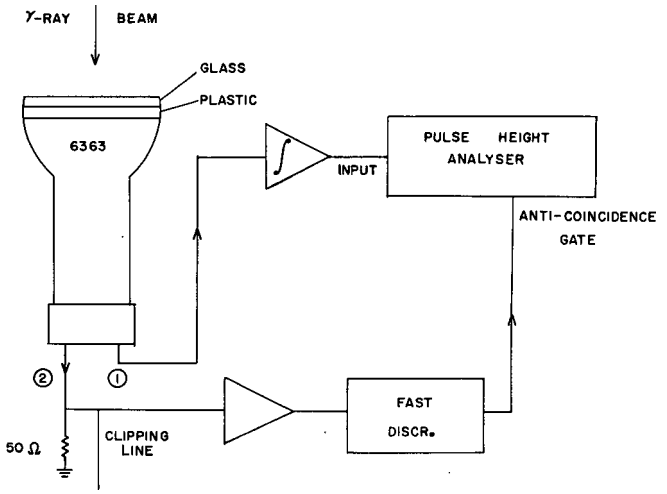

Fig. 15

Diagram of neutron scintillation counter scheme to eliminate gamma-ray background

into the detector. To reduce this effect we evolved a scheme best illustrated in Fig. 15. We placed a thin piece of plastic scintillator between the glass and photomultiplier. The rise times of the pulses of the glass and plastic are 100 and 10 ns, respectively. This difference is then utilized to reject gamma rays which are stopped in the glass and give rise to electrons which penetrate into the plastic scintillator. The pulses are clipped and put into anticoincidence with a multichannel pulse height analyser which looks at all pulses through an integrating circuit, so that good pulse height resolution is obtained. Figure 16 illustrates the basic operation of the anticoincidence action. Figure 17 shows the operation of the scheme using a ThC'' source. We see that when the anticoincidence circuit is operating, gamma-ray pulses falling in the region of the neutron peak are nearly all eliminated. When the system was tried at the reactor it was found that 80% of the gamma rays were removed and only 5% of the neutrons were lost, but there was still more background than observed with a BF_3 counter bank. A calculation showed that these came from the fact that even in a 1-mm glass scintillator some 20% of the electrons resulting from gamma-ray interactions essentially do not get out, that is, they come off perpendicular with respect to the beam. To overcome this effect we are now fabricating thin wafers of glass granules dispersed in pilot B. We have succeeded in getting fairly uniform dispersions of about 0.5 g of 30-μm granules in disks of 20 $cm^2 \times 1$ mm plastic. A parallel attempt at improved detectors was carried out with He^3. First those characteristics of the gas related to proportional counters were investigated by FRIEDES and CHRIEN [2] at Brookhaven, and on the basis of their data we designed a counter, 30 cm × 30 cm, which is shown in Fig. 18 with the cover removed. Notice the thin 6-mil wire which is strung around $\frac{1}{4}$ in insulators spaced $\frac{1}{2}$ in apart; active volume is 25 cm × 25 cm, 6 mm thick. This counter is then filled with 6 atm He^3 and 2 atm of argon. The

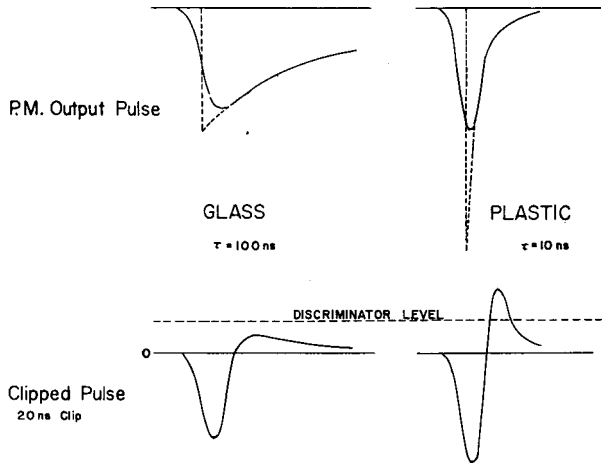

Fig. 16

Pulse shapes arising in neutron scintillation counter
Top: photomultiplier output - dashed curves
theoretical shape for infinitely fast electronics - solid lines, observed shape.
Bottom: pulses after clipping - dashed line, discriminator level for anticoincidence circuit.

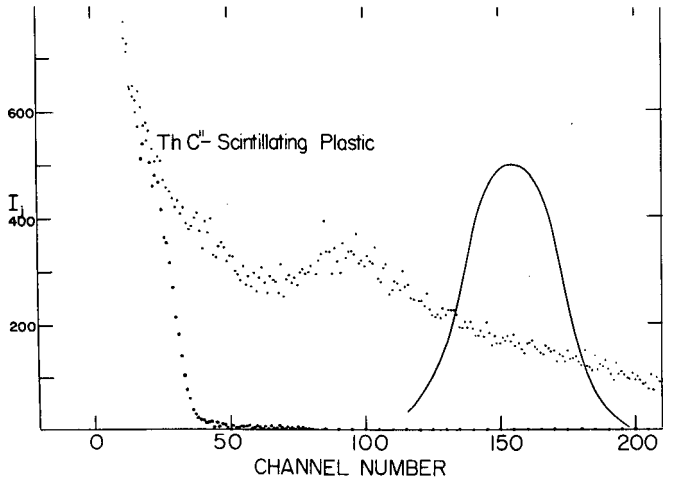

Fig. 17

Pulse height distribution of gamma-ray pulses from plastic scintillator part of neutron detector
Upper points, anticoincidence circuit off
Lower points, anticoincidence circuit on
Solid line, position of neutron peak in glass-plastic scintillator combination.

resulting neutron pulse height distribution from such a gas mixture is shown in Fig. 19. From this we see we have a perfectly satisfactory counter.

I should like to talk now about two data handling systems that are being evolved for use with reactor experiments. One will be used by our Neutron

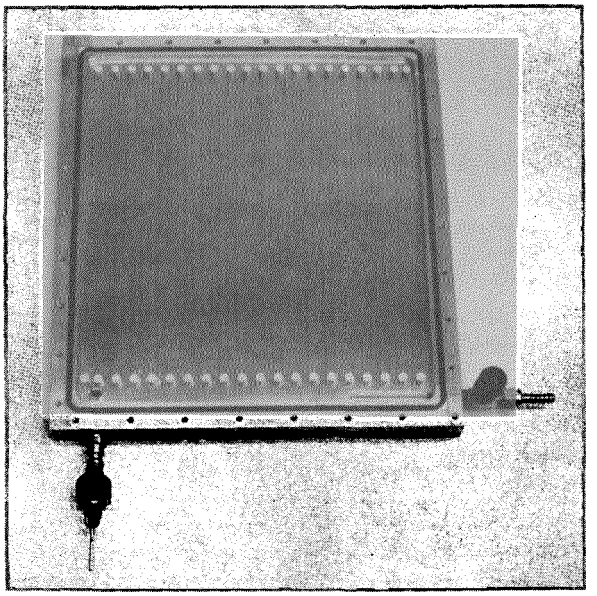

Fig. 18

He^3 neutron detector with cover removed

Fig. 19

Multichannel pulse height spectrum of neutron events in He^3 counter

Physics Group for cold neutron equipment and the fast chopper [3] – a nuclear physics experimental setup – and the other system will be used by the Solid State Physics Group for controlling seven spectrometers. Both systems are built around Scientific Data Systems' computers. The Solid State Group uses the SDS-920 and our group the SDS-910. The SDS-910 that we use has 4096 words of memory, 24 bits to a word. It has an 8-μs cycle time, and most instructions consist of two or three cycles. The most important feature

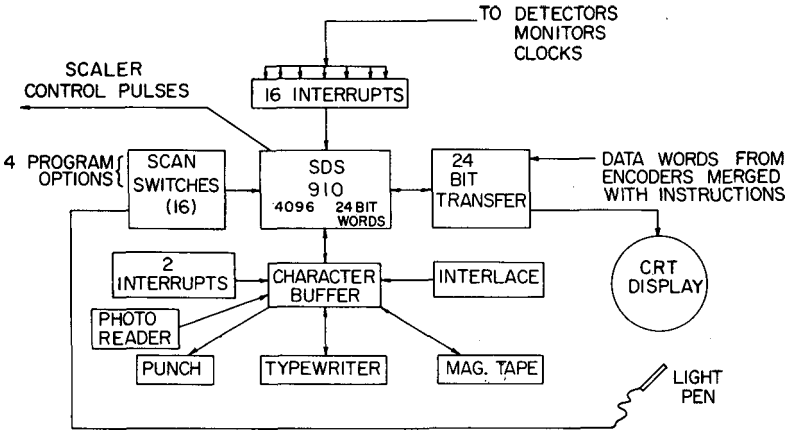

Fig. 20

Hardware organization of neutron physics data handling system

of this machine is in the interrupt system. This system allows the computer to respond to an external signal by automatically jumping to a memory location and executing an appropriate sub-routine. In our computer there are 16 such lines arranged in a priority sequence, each line capable of sending the computer into an appropriate routine. After completion of the sub-routine the computer returns to its main programme. Figure 20 illustrates the various components of the system. The machine has a photo-reader, paper tape punch, typewriter, magnetic tape unit and a light pen used for manipulation of data on the scope face. The neutron time-of-flight is measured by an oscillator analogue-to-digital converter and then is fed into the 24 bit transfer upon receipt of an interrupt signal. The computer is actually used for two separate unrelated experiments, one dealing with the inelastic scattering of cold neutrons, the other collecting neutron transmission data from the fast chopper. In addition the computer is available to the experimenter as a general purpose computational facility for data processing. This triple sharing is made possible by the interrupt feature of the computer. Figure 21 shows a view of the computer and associated equipment. The control of the computer is exercised by means of the typewriter. For the normal data handling processes we devised a set of four-letter mnemonics. The use is illustrated in Fig. 22. In this figure the response of the typewriter to four different mnemonics is illustrated. The programme is written in such a way that the "conditions" of the experiment, time, totals, monitor and rpm of the chopper, are always typed out on every command. The first two commands, FCON and SCON, specifically call for the experimental conditions only and are used as quick checks on the progress of the measurement. The third command, STYP, calls for typing out the contents of the slow chopper time-of-flight data, and the fourth command, FPUN, initiates an output of fast chopper data on punched paper tape.

The next several figures illustrate the use of the computer to perform simple numerical manipulations of the data. Figure 23 represents some raw data taken with NH_4Br at room temperature. The abscissa in this dis-

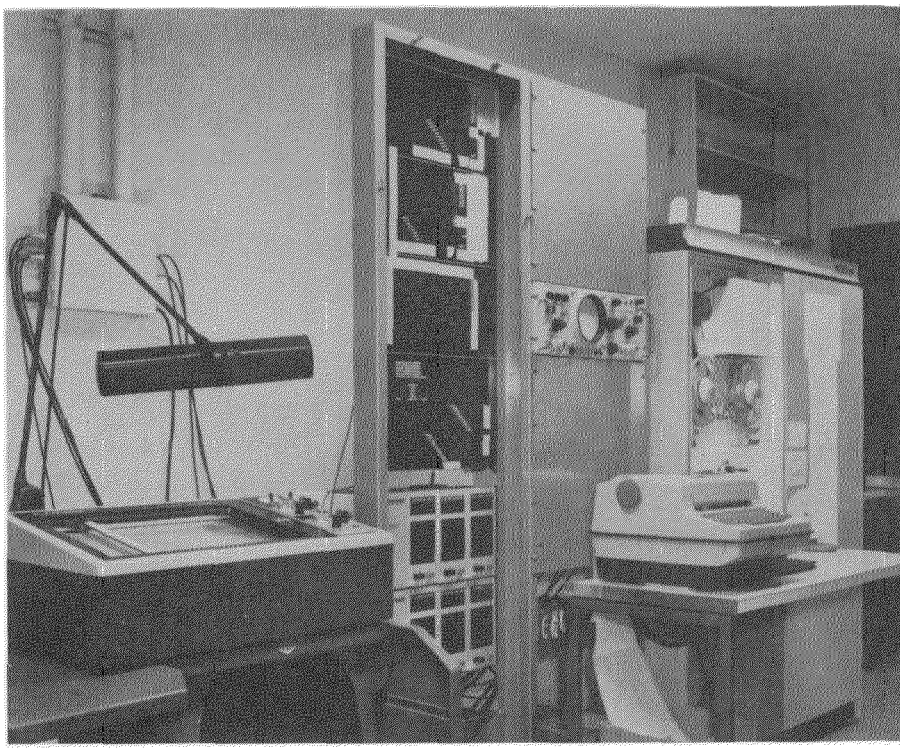

Fig. 21

Photograph of computer and associated equipment for data handling

play is the time-of-flight channel and the ordinate is the number of counts in each channel. The peak at the right (long time-of-flight or low energy) is the Be-filtered pile spectrum and the peaks at the left are the torsional oscillations and vibrations of the NH_4 group in the Br lattice, respectively. Figure 24 shows an expanded display of the data in the region of the high energy peaks. The lower straight line is a measure of the background run for a shorter time than the sample data. Figure 25 shows the background data normalized to the same number of monitor counts versus the sample data. Figure 26 shows the data with the background subtracted and total corrections applied. These are corrections for chopper transmission function, detector efficiency, air scattering and several other small corrections. Figure 27 illustrates one use of the light pen. The data shown are once again the high energy peaks in NH_4Br. The alpha numerics shown along the bottom are the first and last channel numbers displayed. By placing the light pen on the left hand dot at the left side of the oscilloscope display the display proceeds to scan the memory by increasing channel number. By placing the pen on the right hand dot the display moves towards lower channel numbers. Removing the light pen produces a stationary pattern. The dots on the right side of the display are used for scale expansion and contraction. Figure 28 illustrates the result of placing the light pen on the displaced channel corres-

```
FCON     ABS. TIME: 17560

         FAST:    TIME          TOTALS        MONITOR       RPM
SAMPLE IN         07878         00615         16179         05858
NO SAMPLE         07117         00553         14599
BACKGROUND        01358         00086


SCON     ABS. TIME: 17572

         SLOW:    TIME          TOTALS        MONITOR       RPM
                  02772         00062         02656         07031


STYP     ABS. TIME: 17578

         SLOW:    TIME          TOTALS        MONITOR       RPM
                  02776         00062         02659         07968

00091  00086  00090  00073  00080  00073  00066  00062
00076  00079  00075  00076  00068  00088  00074  00086
00090  00087  00071  00099  00064  00071  00089  00086
00069  00082  00084  00089  00084  00065  00070  00090
00081  00084  00081  00094  00089  00085  00098  00086
00084  00088  00074  00104  00106  00107  00104  00113
00121  00116  00108  00125  00084  00135  00111  00158
00165  00218  00277  00287  00331  00333  00325  00310
00319  00313  00310  00345  00399  00345  00326  00337
00304  00289  00278  00250  00222  00238  00201  00185
00180  00183  00183  00165  00168  00196  00192  00177
00187  00192  00191  00178  00161  00172  00158  00170
00149  00142  00164  00155  00174  00152  00135  00112
00134  00151  00150  00145  00153  00128  00147  00139
00127  00104  00127  00114  00121  00126  00137  00131
00138  00118  00123  00121  00106  00112  00134  00119
00122  00118  00128  00130  00140  00165  00152  00195
00170  00261  00299  00261  00257  00243  00255  00236
00220  00197  00195  00209  00210  00186  00190  00484
00927  01123  01102  01185  01213  01219  01181  01204
01072  01083  01030  00970  01000  00973  00891  00854
00772  00784  00707  00678  00661  00651  00628  00606
00530  00504  00507  00501  00545  00492  00480  00393
00452  00459  00380  00377  00323  00381  00320  00301
00297  00288  00258  00245  00269  00219  00214  00233
00183  00198  00190  00147  00158  00152  00160  00143
00150  00144  00128  00131  00127  00127  00098  00105
00113  00114  00094  00104  00102  00116  00088  00110
00104  00098  00084  00101  00083  00095  00081  00068
00084  00077  00090  00090  00067  00089  00081  00055
00088  00085  00081  00074  00075  00073  00077  00085
00074  00069  00078  00075  00077  00068  00086  00083

FPUN     ABS. TIME: 17614

         FAST:    TIME          TOTALS        MONITOR       RPM
SAMPLE IN         07889         00616         16201         05858
NO SAMPLE         07119         00553         14602
```

Fig. 22

Typewriter output of computer illustrating mnemonic instructions: FCON, SCON, STYP and FPUN

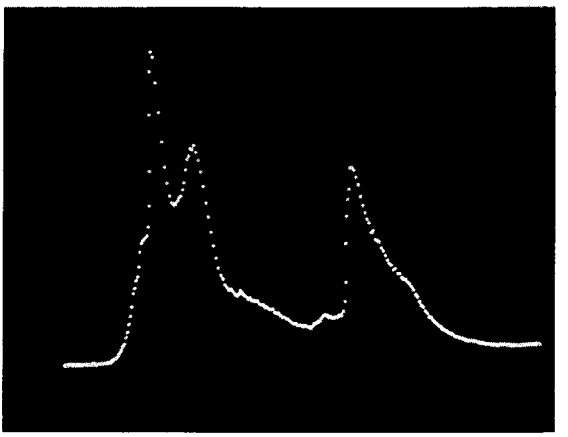

Fig. 23

Oscilloscope display of raw data taken with NH_4Br sample
Abscissa is time-of-flight; ordinate is the number of counts.

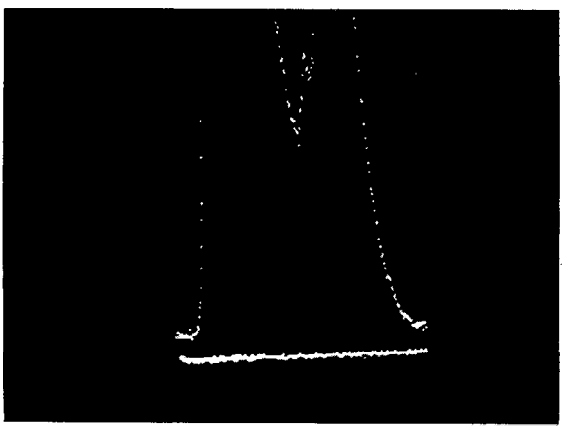

Fig. 24

Expanded display of sample and background counts

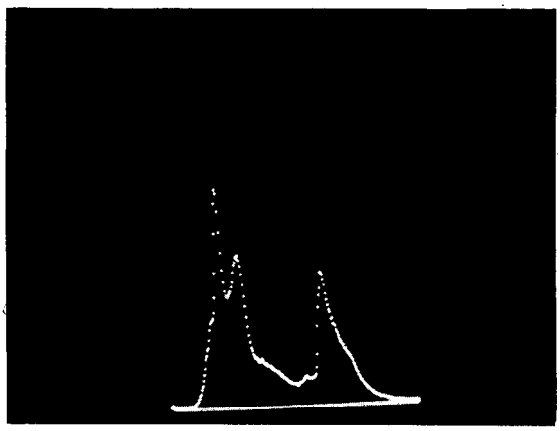

Fig. 25

Display of sample and background counts normalized to same monitor reading

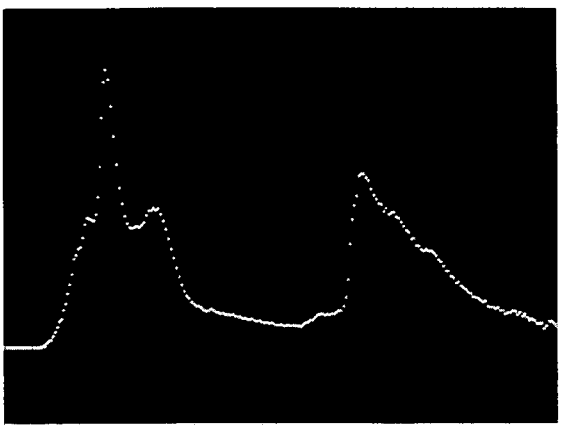

Fig. 26

Display of corrected NH_4Br data

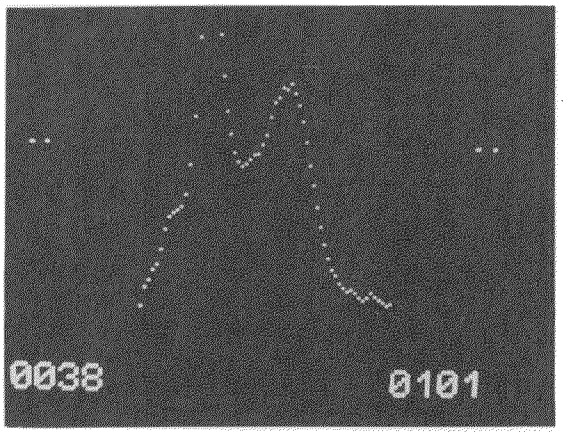

Fig. 27

Expanded display of 64 time-of-flight channels starting with channel No. 38

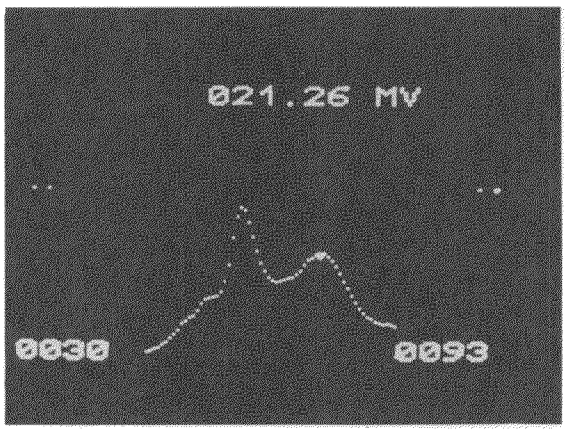

Fig. 28

Display illustrating readout of peak energy using the light pen

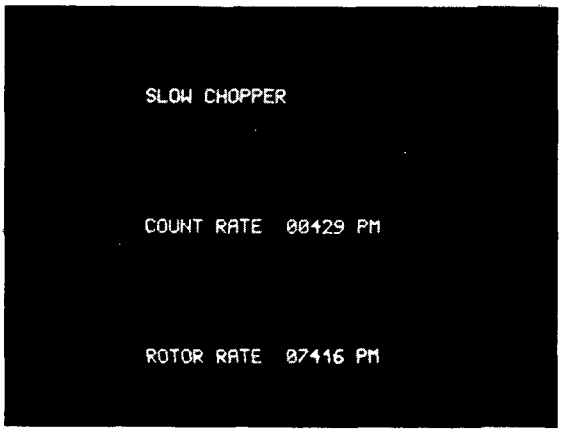

Fig. 29

Display of overall experimental conditions useful for initial setup of experiment

ponding to the peak of the Raman vibration. This results in a display of the calculated energy on the top of the oscilloscope pattern. The final figure, Fig. 29, shows a useful display for the initial setup of a run. It displays the counting rate versus the slow chopper rotor revolution rate. There are many other routines available but I believe these suffice to illustrate what can be done with a small computer as a data handling system.

REFERENCES

[1] OTNES, K. and PALEVSKY, H., Inelastic Scattering of Neutrons in Solids and Liquids I IAEA, Vienna (1963) 95-106.

[2] FRIEDES, J.L. and CHRIEN, R.E., Rev. Sci. Instrum. 35 (1964) 469-72.

[3] CHRIEN, R.E., RANKOWITZ, S. and SPINRAD, R.J., Rev. Sci. Instrum. 35 (1964) 1150-56.

DISCUSSION

W. GLÄSER: As regards the type of data acquisition system which you use, does a small computer present any advantage over a larger one, available on a time-sharing basis? Also, how far can you go with your small computer in processing the data; for example, can it be used for such problems as resolution or multiple scattering corrections?

H. PALEVSKY: It is difficult to give a clear-cut answer to your question. I think that physicists would prefer to have small computers over which they had complete control, but this is an expensive arrangement and eventually large laboratories may be compelled, for reasons of economy, to go over to time-sharing on a large central computer. For the time being, however, there is likely to be an increase in the use of small computers, first because the problem of organizing a large computer for efficient time-sharing has not yet been worked out and, second, because small computers seem at present to be getting cheaper by comparison with larger ones.

As for the second part of your question, a small computer of the type I have described can be used for simple calculations, but its memory is too small for efficient performance of any involved calculations. For example, machine analysis for obtaining Breit-Wigner parameters from transmission data is feasible with the IBM-7094, but in the case of problems taking several minutes of running time it is generally cheaper to use a large machine.

G. VENKATARAMAN: What was the reason for providing a big beam hole for your cold neutron experiments? Are you planning to introduce a cold source into this space and if so, of what type?

H. PALEVSKY: Our reason for making the hole large was, as you surmise, so that we could install a cold source later on. As yet, however, we have not decided on the exact design of the source.

G. VENKATARAMAN: Do you find any deterioration in the performance of He^3 detectors, possibly due to contamination of the gas by the gasket?

H. PALEVSKY: We have not used the counter long enough to see any contamination coming from the gasket. However, I do not expect the noble gases to cause any deterioration in the neoprene gasket that would result in impaired operation of the proportional counter.

W. GLÄSER: I should like to comment briefly on the subject of neutron detectors. We have been using commercially available, high-pressure He^3 counters (diam. 1 in) for over a year and find that they work as satisfactorily as BF_3 tubes.

K.-E. LARSSON: What is the expected time resolution $\Delta t/t$ of your new chopper system for a wavelength of 4 Å?

H. PALEVSKY: This can be quickly calculated from the fact that our expected burst time at 4 Å is approximately 10 μs. Therefore $\Delta t/t \sim 10/(3 \times 10^3) \sim 3 \times 10^{-3}$.

RECENT METHODS IN CRYSTAL SPECTROMETRY

P. K. IYENGAR
ATOMIC ENERGY ESTABLISHMENT,
TROMBAY, BOMBAY, INDIA

Abstract — Résumé — Аннотация — Resumen

RECENT METHODS IN CRYSTAL SPECTROMETRY. The principle of crystal diffraction has afforded a simple way for measuring the energy distribution of slow neutrons. A quantitative determination of the energy distribution however depends on various parameters depending on the structure of the unit cell of the crystal monochromator and geometrical arrangement of the spectrometer. The triple-axis spectrometer has been widely used for inelastic scattering work. It has a crystal monochromator and crystal analyser. The geometrical arrangement and the dispersion due to non-linear variation of angle with wavelength introduces focusing effects. This aspect is reviewed for various cases like elastic diffraction and neutron groups due to single-phonon interactions.

A polycrystalline filter combined with a detector has been used as an analyser very effectively resulting in gain in intensity in inelastic scattering measurements. One difficulty with its use with coherently scattering samples is the uncertainty in the momentum transfer. A combination of two filters with different cut-offs, and a counter to detect the back-scattered neutrons from the second filter, forming a window has recently been used in inelastic scattering work. This provides better resolution in energy and definition of momentum transfer. Some measurements on the characteristics of this type of filter will be presented. Taking advantage of the definition in wave vector of the detected neutrons, the window filter has been used successfully in determining phonon dispersion curves in crystal lattices. Because of the fact that a two-axis instrument will serve the purposes of a three-axis instrument, it results in a simplification of the apparatus. The constant-$\vec{Q}$ method has been used with this device. Typical measurements are presented.

The main drawback of the crystal spectrometry method is that only one scattering angle is used at a time. This can be overcome by using a multi-arm spectrometer. The design and use of a multi-arm spectrometer for measurements of energy distribution is illustrated. A further advantage in the study of single-crystal samples comes from the possibility of operating all the arms with the analysing spectrometers in the constant-$\vec{Q}$ mode. This would, in future, greatly increase the rate of data collection using the crystal spectrometer technique.

MÉTHODES RÉCENTES DE SPECTROMÉTRIE A CRISTAL. Le principe de la diffraction dans les cristaux fournit un moyen simple de mesurer la distribution des neutrons lents selon l'énergie. Toutefois, la détermination quantitative de cette distribution dépend de paramètres différents selon la structure de la cellule élémentaire du cristal monochromateur et la disposition géométrique du spectromètre. Le spectromètre triaxial a été beaucoup utilisé dans des travaux sur la diffusion inélastique. Il comporte un cristal monochromateur et un analyseur à cristal. La disposition géométrique et la dispersion due à la variation non linéaire de l'angle en fonction de la longueur d'onde entraînent des effets de focalisation. L'auteur examine cet aspect du problème pour divers cas, tels que la diffraction élastique et les groupes de neutrons dus à des interactions à un phonon.

L'auteur a utilisé comme analyseur un ensemble comprenant un filtre polycristallin et un détecteur, ce qui permet de réaliser un gain en intensité dans les mesures de diffusion inélastique. Une des difficultés que présente l'emploi de cet ensemble avec des échantillons à diffusion cohérente réside dans l'incertitude relative au transfert de la quantité de mouvement. On a utilisé récemment, pour l'étude de la diffusion inélastique, une combinaison de deux filtres de caractéristiques différentes, et un compteur destiné à détecter les neutrons rétrodiffusés à partir du deuxième filtre formant fenêtre. Il en résulte un meilleur pouvoir de résolution en énergie et une meilleure définition du transfert de la quantité de mouvement. L'auteur présente certaines mesures qui portent sur les caractéristiques de ce type de filtre. Tirant parti de la définition en

vecteur d'onde des neutrons décelés, l'auteur a utilisé avec succès le filtre à fenêtre pour déterminer les courbes de dispersion des phonons dans des réseaux cristallins. Un instrument biaxial remplaçant un instrument triaxial, il en résulte une simplification de l'appareillage. Avec ce dispositif, l'auteur a appliqué la méthode de $\vec{Q}$ constant. Il présente certaines mesures caractéristiques.

Le principal inconvénient de la méthode de la spectrométrie à cristal réside dans le fait que l'on n'utilise qu'un angle de diffusion à la fois. On peut le pallier un utilisant un spectromètre à bras multiples. L'auteur montre comment monter et utiliser un spectromètre à bras multiples pour les mesures de la distribution en énergie. D'autre part, l'avantage de l'étude d'échantillons monocristaux réside dans le fait qu'il est possible d'utiliser tous les bras avec les spectromètres d'analyse dans le mode de $\vec{Q}$ constant. Cela permettrait d'accélérer considérablement le rassemblement des données à l'avenir en appliquant la méthode du spectromètre à cristal.

НОВЫЕ МЕТОДЫ КРИСТАЛЛИЧЕСКОЙ СПЕКТРОМЕТРИИ. Принцип дифракции на кристалле открывает путь для простого распределения энергии медленных нейтронов. Однако на количественное определение распределения энергий влияют различные параметры, зависящие от структуры элементарной ячейки кристаллического монохроматора и геометрического расположения спектрометра. Для проведения работ по неупругому рассеянию широко применялся трехосный спектрометр. Он состоял из кристаллического монохроматора и кристаллического анализатора. Геометрическое расположение и дисперсия в результате нелинейного изменения угла с изменением длины волны приводят к эффектам фокусировки. Этот вопрос рассматривается для различных случаев, например упругой дифракции и нейтронных групп, связанных с взаимодействиями одиночного фонона.

В качестве анализатора очень эффективно использовался поликристаллический фильтр, объединенный с детектором, что приводит к увеличению интенсивности при измерении неупругого рассеяния. Единственной трудностью его применения для измерения когерентно рассеивающих образцов является неопределенность с передачей импульса. В последнее время для проведения работ по неупругому рассеянию применяется комбинация, состоящая из двух фильтров с различными порогами и одного счетчика для измерения обратного рассеяния нейтронов от второго фильтра, образующего окно. Это обеспечивает лучшую разрешающую способность по энергии и позволяет определять передачу импульса. Излагаются некоторые результаты измерений характеристик фильтров этого типа. Благодаря определению волновых векторов обнаруженных нейтронов, окошечный фильтр с успехом применялся для определения кривых дисперсии фононов в кристаллических решетках. Возможность использования двухосного прибора вместо трехосного приведет к упрощению этого спектрометра. При применении этого устройства использовался метод "постоянной $\vec{Q}$". Будут описаны типичные измерения.

Основным недостатком метода кристаллической спектрометрии является то, что одновременно используется только один угол рассеяния. Этот недостаток можно устранить путем применения многоплечевого спектрометра. Показаны конструкция и использование многоплечевого спектрометра для измерения распределения энергий. Другим преимуществом с точки зрения исследования монокристаллических образцов является возможность использования всех плечей с анализирующими спектрометрами по методу "постоянной $\vec{Q}$". В будущем это сильно увеличит скорость сбора данных с помощью метода кристаллической спектрометрии.

MÉTODOS RECIENTES DE ESPECTROMETRÍA CRISTALINA. El principio de la difracción por cristales permite evaluar de manera sencilla la distribución de energía de los neutrones lentos. Pero la determinación cuantitativa de esa distribución de energía depende de varios parámetros, que son a su vez función de la estructura de la celda unitaria del cristal monocromador y de la disposición geométrica del espectrómetro. El espectrómetro triaxial se utiliza ampliamente para trabajos de dispersión inelástica. Está provisto de un monocromador y de un analizador cristalinos. La disposición geométrica y la dispersión debida a la variación no lineal del ángulo con la longitud de onda originan efectos de focalización. Este aspecto se examina en relación con varios casos, tales como dispersión elástica y existencia de grupos de neutrones debidos a interacción de monofonones.

Se ha empleado como analizador de gran eficacia un filtro policristalino combinado con un detector, que permite ganar intensidad en las mediciones por dispersión inelástica. Una dificultad que suscita su empleo con muestras de dispersión coherente es la indeterminación de la transferencia de impulso. Recientemente se han utilizado en trabajos de dispersión inelástica dos filtros combinados, con cortes diferentes, y un contador para detectar los neutrones retrodispersos por el segundo filtro, que forma una ventana. Esto permite mejorar la resolución energética y la definición de la transferencia de impulso. Se presentan algunas mediciones

relativas a las características de este tipo de filtro. Aprovechando la definición en vector de onda de los neutrones detectados, el filtro de ventana se ha utilizado con éxito para determinar las curvas de dispersión de fonones en redes cristalinas. Como este instrumento biaxial sirve para los mismos fines que el triaxial, supone una simplificación constructiva. Se ha aplicado con tal dispositivo el método de $\vec{Q}$ constante. Se presentan resultados de mediciones típicas.

El principal inconveniente de la espectrometría mediante cristales es que sólo se utiliza un ángulo de dispersión cada vez. Puede superarse empleando un espectrómetro de varios brazos. Se describen las características y empleo de un espectrómetro de este tipo para medir la distribución de la energía. La posibilidad de hacer funcionar todos los brazos del espectrómetro según el modo de $\vec{Q}$ constante supone una ventaja adicional para el estudio de muestras monocristalinas. Este procedimiento permitiría en el futuro aumentar considerablemente la velocidad de acopio de datos cuando se emplee la técnica del espectrómetro de cristal.

DISCUSSION

B. DORNER: I wonder why you didn't see the second filter cut-off in Be at approximately 3.5 Å when you measured the transmission of your window filter.

P.K. IYENGAR: Our beryllium filter consists of beryllium plates, 1/4 in thick, interleaved with cadmium, so that multiple scattering in the filter is minimized and we correct the back-scattered neutrons from the second scattering. Hence I do not think we should see this step at 3.5 Å.

G. CAGLIOTI: What is the ratio of the luminosities associated with a given phonon, say, in magnesium, for measurements performed with a three-axis spectrometer and a window filter?

P.K. IYENGAR: The increase in intensity resulting from the use of window filters is of the order of five.

G. CAGLIOTI: What is the ratio of the luminosities of window filters using Be, BeO or Mo as anti-filters?

P.K. IYENGAR: I have no figures as the measurements were taken at different times and with different set-ups.

SLOW NEUTRON SPECTROMETERS AT THE SWEDISH REACTORS

U. DAHLBORG AND K. SKÖLD
AB ATOMENERGI, STOCKHOLM
AND
K.-E. LARSSON
ROYAL INSTITUTE OF TECHNOLOGY, STOCKHOLM, SWEDEN

Abstract — Résumé — Аннотация — Resumen

SLOW NEUTRON SPECTROMETERS AT THE SWEDISH REACTORS. At the two Swedish research reactors, R1 in Stockholm and R2 in Studsvik, there are at present possibilities to use four different neutron spectrometers for neutron inelastic scattering experiments. In Stockholm at the 600-kW heavy-water moderated reactor R1 two slow chopper time-of-flight spectrometers are in simultaneous operation. At one of these we permanently use a beryllium filter as monochromator, while at the other one either a beryllium filter or a crystal monochromator may be used. Angular distribution measurements using the combination of a crystal monochromator and time-of-flight analysis have been found to give very valuable results even though the intensity as well as the resolution is relatively poor. A mechanical velocity selector with 4.2% wavelength resolution has recently been tested. The instrument is, however, not yet used in experiments.

The time-of-flight spectrometer in Studsvik at the 30-MW light-water moderated reactor R2 uses, for monochromatizing purposes, the combined action of a beryllium filter and a chopper with a narrow transmission curve. At this spectrometer, as well as at one in Stockholm, the chopper is placed before the sample, thus offering the possibility of simultaneous recording of data at different angles of observation. At R2 a triple-axis crystal spectrometer is also in operation.

Different properties of the different instruments, such as intensities, resolutions, as well as their suitability for certain measurements, is given. Thus figures are given showing that a high intensity loss follows from a rather limited improvement in resolution. It is interesting to note in comparing R1 and R2 as neutron sources for beam tube work that one loses about a factor of ten from the hundred-times-larger neutron flux of R2 in taking out the neutrons. The reason for this loss is the narrow beam tubes and the filters necessary to reduce the fast neutron and the gamma flux. Scattering data on H_2O obtained at different instruments is briefly discussed for illustrational purposes. A comparison between the light- and heavy-water moderated reactors for beam tube work shows the distinct advantages of the heavy-water type.

SPECTROMÈTRES A NEUTRONS LENTS DES RÉACTEURS SUÉDOIS. Aux centres créés autour des deux réacteurs de recherche suédois, R1 à Stockholm et R2 à Studsvik, on a maintenant la possibilité d'utiliser quatre spectromètres différents pour les expériences de diffusion inélastique des neutrons. A Stockholm, le réacteur R1 de 600 kW, ralenti à l'eau lourde, est équipé de deux spectromètres mécaniques à neutrons lents qui fonctionnent simultanément. Avec l'un, on utilise toujours un monochromateur à filtre en Be; avec l'autre, on peut employer soit le même genre de monochromateur, soit un monochromateur à cristal. On a constaté que pour les mesures de distribution angulaire, on obtient d'excellents résultats en combinant un monochromateur à cristal et un spectromètre mécanique, même si l'intensité et le pouvoir de résolution sont relativement faibles. Récemment on a fait l'essai d'un sélecteur de vitesse mécanique ayant un pouvoir de séparation des longueurs d'onde de 4,2%. Cependant, cet instrument n'est pas encore utilisé pour les expériences.

Le spectromètre mécanique de Studsvik, avec lequel le réacteur R2 de 30 MW ralenti à l'eau légère est équipé, utilise pour la monochromatisation l'action combinée d'un monochromateur à filtre de Be et d'un hacheur à courbe de transmission étroite. Dans ce spectromètre, de même que dans celui de Stockholm, le hacheur est placé avant l'échantillon, ce qui permet l'enregistrement simultané de données pour des angles d'observation différents. Un spectromètre à cristal triaxial est aussi en service près du réacteur R2.

Les auteurs donnent certaines caractéristiques de ces instruments, notamment l'intensité, le pouvoir de résolution, et indiquent dans quelle mesure ils conviennent pour certaines opérations. Ainsi, il ressort des données numériques mentionnées qu'une amélioration assez faible du pouvoir de résolution entraîne une

perte d'intensité importante. Il est intéressant de noter qu'en comparant les réacteurs R1 et R2 en tant que sources de neutrons pour les travaux dans les canaux, on constate qu'à la sortie des neutrons, le flux cent fois supérieur de R2 subit des pertes correspondant à un facteur de dix environ. Ce phénomène s'explique par le faible diamètre des canaux et par la nécessité d'employer des filtres pour réduire les flux de neutrons rapides et de rayons gamma. A titre d'exemple, les auteurs discutent brièvement quelques données sur H_2O obtenues par diffusion à l'aide des divers instruments. Une comparaison entre réacteurs à eau légère et réacteurs à eau lourde montre que pour les travaux dans les canaux les réacteurs à eau lourde présentent des avantages certains.

СПЕКТРОМЕТРЫ МЕДЛЕННЫХ НЕЙТРОНОВ НА ШВЕДСКИХ РЕАКТОРАХ. В настоящее время на двух шведских исследовательских реакторах R1 в Стокгольме и R2 в Студсвике, имеются возможности для использования четырех различных спектрометров нейтронов в опытах по неупругому рассеянию нейтронов. В Стокгольме на тяжеловодном реакторе R1 мощностью 600 квт одновременно используются два спектрометра по времени пролета с медленно действующим прерывателем. На одном реакторе мы постоянно используем бериллиевый фильтр в качестве монохроматора, в то время как на другом реакторе можно использовать либо бериллиевый фильтр, либо кристаллический монохроматор. Обнаружено, что при измерениях углового распределения с использованием комбинированного анализа методом кристаллического монохроматора и методом времени пролета получают очень ценные результаты, несмотря даже на относительно плохую интенсивность и разрешающую способность. Недавно был испытан механический селектор скоростей с разрешающей способностью 4,2% по длине волны. Однако этот прибор пока не используется во время экспериментов.

Спектрометр по времени пролета в Студсвике на реакторе R2 мощностью 30 мгвт с водным замедлителем используется в целях монохроматизации комбинированного бериллиевого фильтра и прерывателя с узкой кривой пропускания. На этом спектрометре, а также на спектрометре в Стокгольме прерыватель ставится перед образцом, и тем самым создается возможность одновременной регистрации данных при различных углах наблюдения. На реакторе R2 также действует трехосевой кристаллический спектрометр.

Приводятся различные свойства разнообразных приборов, например интенсивность, разрешающие способности и пригодность для определенных измерений. Так, приводятся цифры, показывающие, что большая потеря интенсивности связана с довольно ограниченным улучшением разрешающей способности. Интересно, что когда сравниваются между собой реакторы R1 и R2 в качестве нейтронных источников для работы с каналом для выпуска пучка, то при работе с выводом нейтронов поток нейтронов реактора R2, являющийся в 100 раз большим, уменьшается примерно в 10 раз. Эта потеря объясняется узкими каналами для выпуска пучка и фильтрами, необходимыми для уменьшения потока быстрых нейтронов и гамма-излучения. Кратко обсуждаются в целях иллюстрации данные по рассеянию H_2O, полученные на различных приборах. В результате сравнения между собой реактора с водным замедлителем и тяжеловодного реактора с точки зрения работы каналов для выпуска пучка отчетливо можно видеть преимущество реактора тяжеловодного типа.

ESPECTROMETROS PARA NEUTRONES LENTOS EN LOS REACTORES DE SUECIA. En los dos reactores de investigación suecos, el R1 de Estocolmo y el R2 de Studsvik, se da actualmente la posibilidad de utilizar cuatro diferentes espectrómetros neutrónicos para llevar a cabo experimentos de dispersión inelástica. En el reactor R1 de Estocolmo, de 600 kW y moderado por agua pesada, funcionan simultáneamente dos espectrómetros de tiempo de vuelo con selectores de neutrones lentos. En uno de ellos se emplea permanentemente un filtro de Be en calidad de monocromador, mientras que en el otro se puede utilizar este filtro o un monocromador de cristal. Se ha comprobado que las mediciones de la distribución angular en las que se combina un monocromador de cristal y un analizador de tiempo de vuelo dan resultados muy útiles, aunque tanto la intensidad como la resolución obtenidas son relativamente bajas. Recientemente se ha ensayado un selector mecánico de velocidad con un poder de resolución de 4, 2% referido a la longitud de onda, pero el instrumento no se emplea todavía en los experimentos.

El espectrómetro de tiempo de vuelo de Studsvik, instalado en el reactor R2, de 30 MW moderado por agua ligera, emplea como monocromador el efecto combinado de un filtro de Be y un selector con una curva de transmisión estrecha. En este espectrómetro, lo mismo que en el de Estocolmo, el selector se coloca delante de la muestra para poder registrar simultáneamente datos a diferentes ángulos de observación. En el reactor R2 se encuentra también instalado un espectrómetro triaxial de cristal.

Los autores describen diversas características de los instrumentos, tales como las intensidades y los poderes de resolución alcanzados, e indican en qué medida se adaptan a ciertas determinaciones. Demues-

tran con datos numéricos que un aumento relativamente pequeño del poder de resolución ocasiona una elevada pérdida de intensidad. Cuando se comparan los reactores R1 y R2 como fuentes neutrónicas para experimentos en el orificio de haz, es interesante observar que, si bien el flujo neutrónico del reactor R2 es 100 veces mayor, el rendimiento en neutrones es unas 10 veces menor. El fenómeno se debe a la estrechez de los orificios de haz y a los filtros que son necesarios para reducir los flujos gamma y de neutrones rápidos. Como ilustración, la memoria discute brevemente datos de dispersión en H_2O obtenidos con los diversos instrumentos. La comparación demuestra que, para experimentos con el orificio de haz, el reactor de agua pesada presenta ventajas innegables.

INTRODUCTION

The main problem in neutron inelastic scattering experiments is to select a narrow energy interval out of the continuous reactor spectrum which can be used in the investigation of the interaction of neutrons with matter. The problem can be solved along different lines. Thus crystals, both single crystals and polycrystals, have been successfully used. Systems involving one or many rotors with rotating axes perpendicular to the neutron beam or parallel to the beam as well as the combination of a crystal and a rotor may be advantageous in different cases. In spectrometers involving rotors with axes perpendicular to the beam the rotor performs both a monochromatizing and an energy analysing action simultaneously while in the other systems the energy analysis is carried out either by introducing another rotor or another crystal into the system. At the two Swedish research reactors, R1 in Stockholm and R2 in Studsvik, there are at present possibilities to use four different types of spectrometers, all of them employing different ways for monochromatizing.

A. DATA FOR THE DIFFERENT SPECTROMETERS

The simplest and perhaps the most generally used method to obtain a monoenergetic neutron beam is the filter method. In Fig. 1 a vertical section of the slow chopper time-of-flight spectrometer at the 600-kW heavy-water moderated reactor R1 in Stockholm is shown [1]. The neutrons hitting the sample have passed through the 25-cm thick piece of polycrystalline beryllium which has been placed in the channel. According to the cross-section of beryllium this means that the transmitted neutron spectrum should have a sharp edge at 5.2×10^{-3} eV, the energy corresponding to the crystalline cut-off of beryllium, whereafter the intensity should approximately decay at EdE or $\lambda^{-5}\, d\lambda$, where E is the neutron energy and λ the neutron wavelength. This is, however, not the case. Due to constructional materials in the beam tube through which the neutrons must pass, the spectrum of the neutrons emerging from the reactor looks rather complex, as can be seen in Fig. 2. The determination of the energy distributions of the scattered neutrons at one selected scattering angle is performed by slow chopper time-of-flight technique. The method yields a rather high intensity. Starting out with about 6×10^{11} n/cm^2 s at the reactor tank wall one arrives at about 1.8×10^6 n/cm^2 s at the sample position. As the sample area can be as large as 5 cm by 10 cm the number of neutrons to be scattered in the sample every second is just below 10^8.

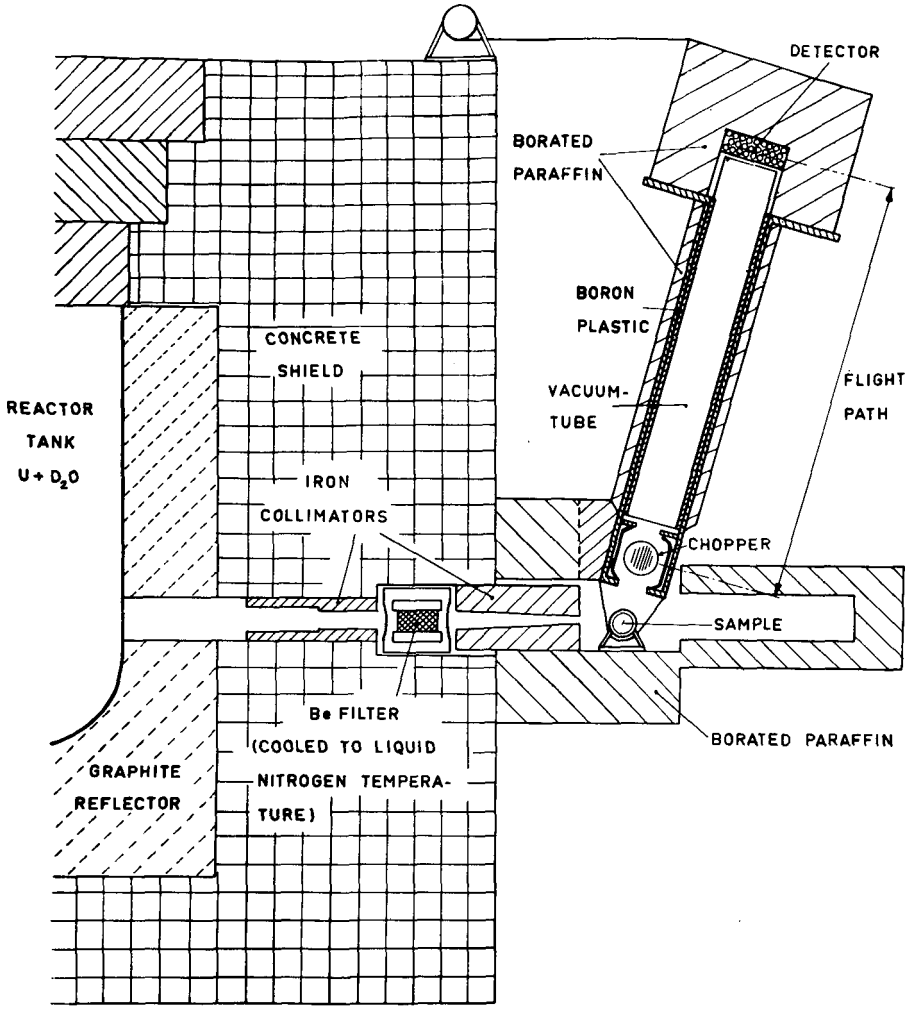

Fig. 1

Vertical section of the slow chopper time-of-flight spectrometer at R1

The time resolution at the analysing side is 1.5 - 2%, depending on the chopper speed.

In studying relatively small energy transfers the width of the beryllium filtered neutron spectrum has a considerable drawback. A large improvement is the time-of-flight spectrometer used at the 30-MW light-water moderated reactor R2 in Studsvik [2]. A horizontal section of the instrument is shown in Fig. 3. The main difference between this instrument and the one at R1 is that in the Studsvik case the chopper is placed before the sample and that its transmission curve has been made to have a narrow width. The principle of the combined action of filter and chopper is illustrated in Fig. 4 [3]. The chopper parameters have been chosen so as to give maximum trans-

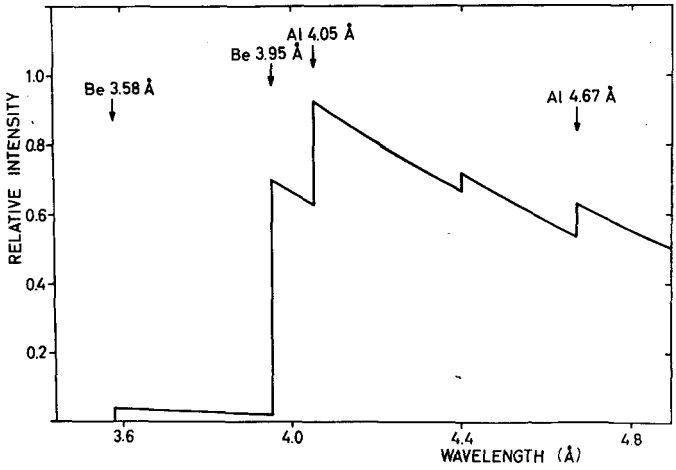

Fig. 2

Neutron spectrum as measured at the beam tube exit, showing the distortions of constructional materials on the spectrum

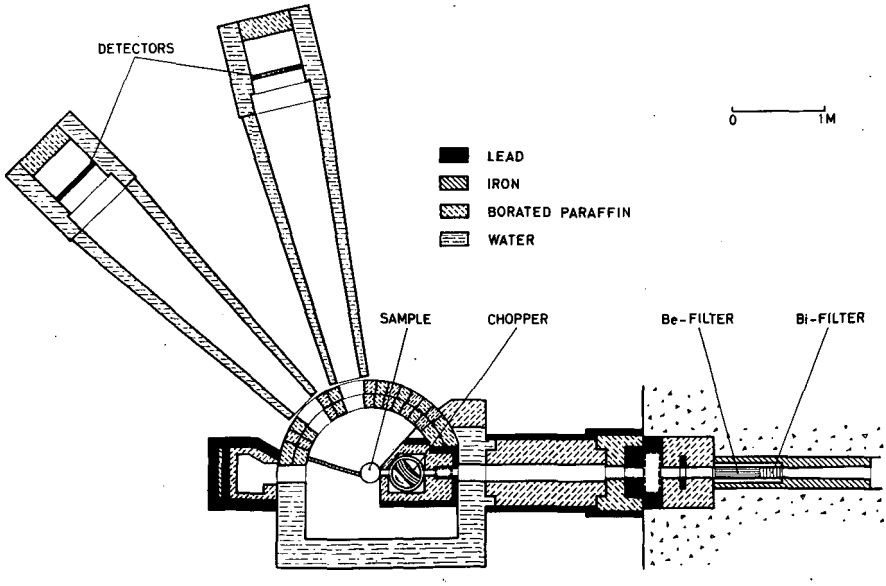

Fig. 3

Horizontal section of the time-of-flight spectrometer at R2

mission of the chopper at 4 Å at a given speed of rotation. The width of the spectrum transmitted would then be half the width of the transmission curve. A 20-cm thick bismuth filter has had to be inserted in the channel in front of the beryllium filter in order to reduce the fluxes of fast neutrons and gammas. Some measured properties of the instrument are shown in

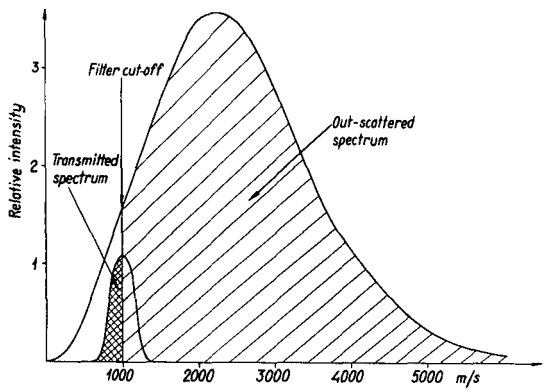

Fig. 4

Principle of the combined action of filter and chopper

Fig. 5. In general $\Delta\lambda/\lambda$ is chosen to be 7.5%. The time resolution of the analysing system is, at a chopper speed corresponding to a wavelength spread in the impinging neutron spectrum of 7.5%, as good as 1.2%.

The flux at the bottom of the channel is about 6×10^{13} n/cm^2 s and the flux at the sample position has been measured to be about 7×10^6 n/cm^2 s without the chopper in the beam. Thus starting with a 100 times higher flux at R2 one arrives at a useful flux only four times larger than the flux at R1. The reason for this small net gain is mainly due to the flux quality and the unsuitable dimensions of the beam tubes. Thus for example the distance between the reactor tank wall and the sample is 2.2 times larger at R2 than at R1. This gives a loss factor for R2 of about 5. Also the neutron emitting area seen by the sample is 1.6 times smaller at R2 due to the narrow beam tubes. The necessary bismuth filter reduces the cold neutron flux by a factor of 2. As the absolute transmission of the chopper is four times smaller compared to the one in use at R1, the equivalent fluxes at the sample position are about the same at R2 and R1. However, because the chopper is placed before the sample the recording of data is faster at R2 depending on the fact that one can use several detectors simultaneously.

Another way of obtaining a beam of monoenergetic neutrons is by the use of single crystals. At R2 a conventional three-axis crystal spectrometer is operating. In Fig. 6 a horizontal section of the spectrometer is shown. As was the case at the time-of-flight spectrometer an extra filter had to be inserted in the channel to reduce the fast neutron flux. In this case the most suitable is a quartz filter, cooled to liquid nitrogen temperature. However, it also reduces the thermal flux by about a factor of 4. A copper monochromator ((220) reflection) gives $(1\text{-}2) \times 10^5$ n/cm^2 s in the region 0.2 to 0.5 eV. The collimation is usually 0.4° horizontally and 0.9° vertically. The intensity stated is then an average value for a beam 6.5 cm by 6 cm. With this collimation and monochromator the energy resolution is 2% at 0.04 eV. From the relatively low intensity which follows from the very good resolution a recording of a single phonon peak in aluminium at

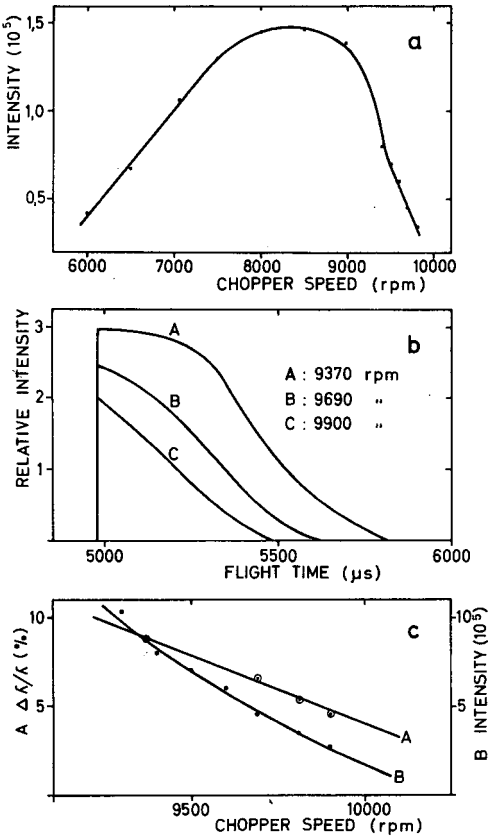

Fig. 5

Different properties of the Studsvik time-of-flight spectrometer

(a) The intensity at the sample position as a function of the chopper speed.
(b) The shape of the incident neutron spectrum at different chopper speeds.
(c) The width at half height of the incident spectrum (the scale on the left axis) and the intensity at the sample position (the scale on the right axis) as functions of the chopper speed.

liquid nitrogen temperature takes about 15 h. The natural width of the phonons are measurable with this instrument even at -196°C.

The crystal spectrometer in Stockholm yields too small intensity for single phonon measurements. Instead it is used for measurements of large line widths and of angular distributions in hydrogenous liquids. In this use there are no collimators placed in the beam tube so as to give the highest possible intensity. An aluminium monochromator ((200) reflection) with a measured reflectivity of 26% at 1.4 Å is used. The energy analysis of the scattered neutrons is made by time-of-flight technique. At 3 Å, the wavelength mostly used, the wavelength resolution is ~3%. Even if the intensity, as well as the resolution, is relatively poor the apparatus has been able to give very valuable data, complementary to those obtained at the other spec-

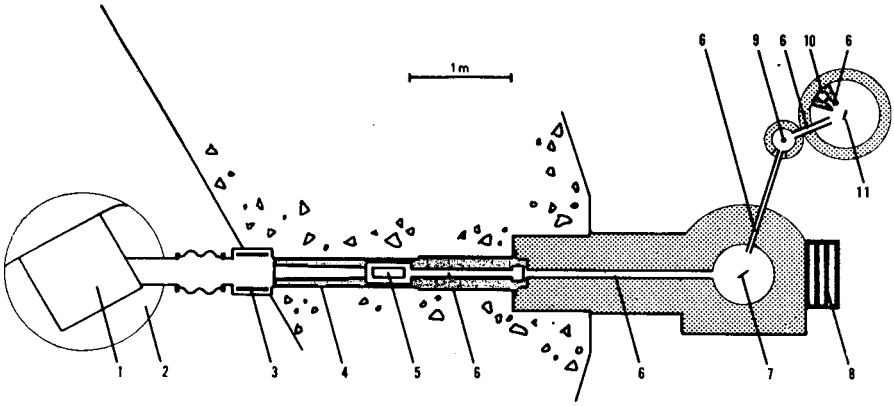

Fig. 6

Horizontal section of the three-axis crystal spectrometer at R2

1 Reactor core
2 D_2O
3 Lead shutter
4 Cast-iron plug
5 Beam filter
6 Collimator (subdividing plates not shown)
7 Monochromator crystal
8 Beam stop
9 Sample
10 Detector
11 Analyser crystal

trometer at R1. The higher order reflections are advantageous in the sense that it is possible to make measurements at several momentum transfers simultaneously. Also we have the possibility of recording data at several scattering angles simultaneously as the chopper is placed before the sample.

In Table I the resolution and the intensity at the sample position are shown for all spectrometers in operation. The utilization factor is defined as the ratio of the number of neutrons absorbed in the detector to the number of neutrons leaving the source per time interval.

The mechanical monochromator constructed in Stockholm has not yet been put into continuous operation but it has recently been tested. The monochromator consists of a rotor with helical slots. In Fig. 7 a sketch of the instrument is shown. The rotor is built up by 24 disks, each of them 1.25 cm thick. In each disk a radial slot is made with a pitch angle varying along the slot. The slot height is 7 cm and the width at half the slot height is 0.175 cm. The geometrical transmission of the rotor is 41%. The material in the rotor is a Mg-Cd alloy containing 10% Cd. As the instrument is intended for monochromatization of cold neutrons only, it has been possible to keep the length as well as the absorbing material in the rotor within practical limits. The rotor is spinning in vacuum with a highest speed of about 11 000 rpm.

TABLE I

DATA FOR THE NEUTRON SPECTROMETER AT THE REACTORS R1 AND R2

	Resolution of monochromating system $\Delta\lambda/\lambda$ (%)	Intensity at sample position (n/s)	Resolution of analysing system		Utilization factor
			dt/t (%)	dE/E (%)	
Time-of-flight spectrometer at R1	~ 25 at 4 Å	9×10^7	2		7×10^{-15}
Single-crystal slow-chopper combination at R1	3.2 at 3 Å	3×10^6	2.7		$2 \times 2 \times 10^{-16}$ (2 detectors)
Time-of-flight spectrometer of R2	7.5 at 4 Å	3×10^8 [a]	1.2		$2 \times 2 \times 10^{-17}$ (2 detectors)
Three-axis crystal spectrometer at R2		6×10^6		2 (at 0.04 eV)	$\sim 10^{-18}$

[a] Without chopper in the beam.

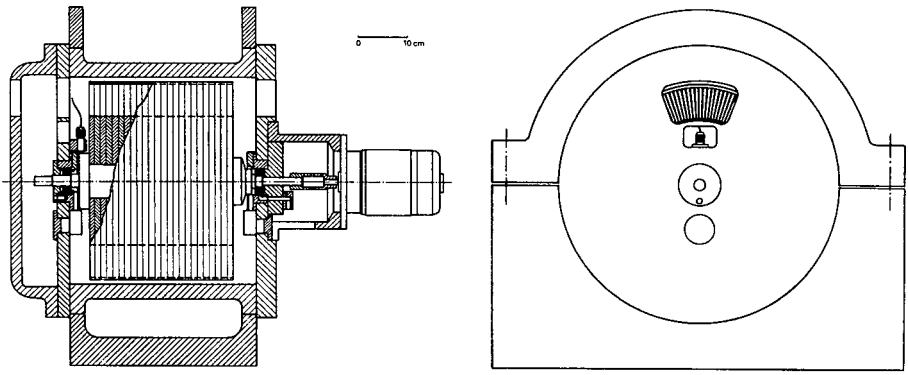

Fig. 7

Vertical section of the mechanical monochromator

The resolution of the rotor is given by

$$\frac{\Delta\lambda}{\lambda} = \frac{dv}{lu} = \frac{d}{r\Theta}, \tag{1}$$

where

d = half the slot width,

v = velocity of selected neutrons,

l = length of the rotor,

u = peripheral speed of the rotor,

r = rotor radius and

Θ = angle the rotor has turned during the passage of the neutron.

Thus $\Delta\lambda/\lambda$ is constant for the rotor. Together with an ideal collimator the resolution is calculated to 4.18%. In Fig. 8(a) an example of a transmitted neutron spectrum is shown. The width is measured to 4.15%, in excellent agreement with the calculations. The curve through the experimental points is a Gaussian with the same width and normalized to the top.

The transmitted intensity through the rotor may be written as

$$I(\lambda) = 2\phi_0 \frac{d^2h^2}{4\pi l^2} \cdot T \cdot \frac{\Delta\lambda}{\lambda} \cdot \left(\frac{\lambda_0}{\lambda}\right)^4 \exp\left[-\left(\frac{\lambda_0}{\lambda}\right)^2\right], \tag{2}$$

where

ϕ_0 = the neutron flux of the source, presumed to obey a Maxwellian density distribution law,

$\frac{d^2h^2}{4\pi l^2}$ = transmission of the ideal collimator and

T = geometrical transmission of the rotor.

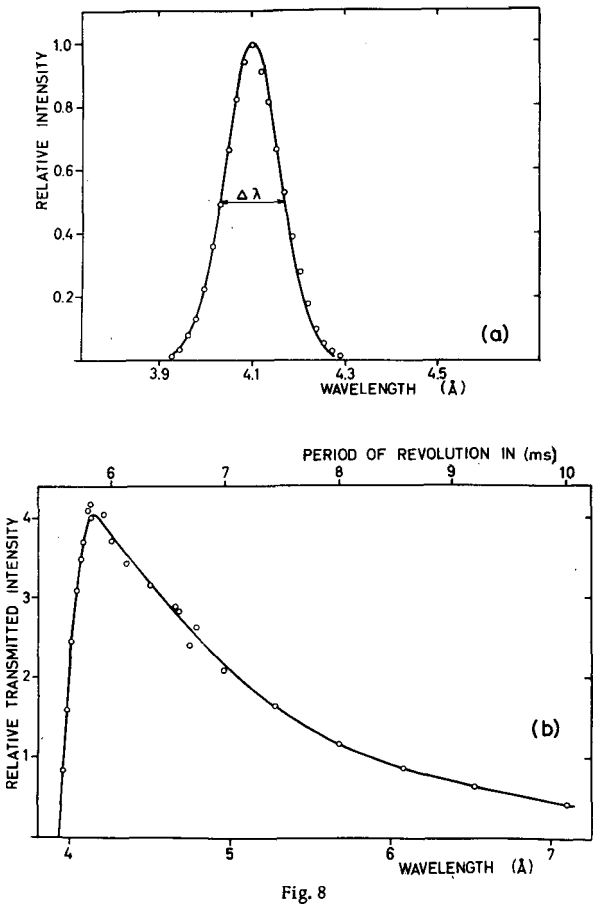

Fig. 8

Different properties of the mechanical monochromator

(a) Example of a transmitted neutron spectrum

$$\frac{\Delta\lambda}{\lambda} = \frac{0.17}{4.1} = 4.15\%$$

(b) The transmitted intensity as a function of wavelength and period of revolution.

In Fig. 8(b) the measured total transmitted intensity is plotted as a function of the neutron wavelength and of the period of revolution of the rotor. The curve follows Eq. (2) quite well. Also the absolute value of the transmission agrees within 10% of the calculated one.

B. COMPARISON OF THE DIFFERENT INSTRUMENTS AND THEIR SUITABILITY FOR CERTAIN MEASUREMENTS

The neutron spectrometers discussed above can be divided into two different groups. The instruments using neutrons with wavelengths larger than

4 Å belong to one group; those using neutrons with wavelengths smaller than 4 Å belong to the other. In the first group we include mainly spectrometers working in conjunction with a beryllium filter but also the crystal-chopper combination, while in the second we have the three-axis crystal spectrometer. The division could also have been done on the basis of experimental suitability for different measurements. The crystal spectrometer is most advantageous when used in measuring dispersion relations, phonon lifetimes and similar objects. The instruments taken together in the first group are, as the energy analysis is performed by time-of-flight technique, most suitable for spectral distribution measurements, line width and angular distribution measurements. In the following the types belonging to this group will be compared with respect to intensity and resolution.

For this purpose we assume that we have a circular neutron-emitting surface with a diameter of 30 cm. This is about the size of the cold source which will be installed at the Stockholm reactor. The distance between the surface and the sample position is taken to 400 cm. The sample area is assumed to be 5 cm by 10 cm in all cases discussed below, except those where the monochromator device will put a limit to the size. The comparison is made at 4 Å and the energy analysis of the scattered neutrons is assumed to be performed by time-of-flight technique.

The counting rate in the detector may in all cases be written as

$$I_{det} = 2\phi_0 \cdot T_c \cdot c_m \cdot R_m \left(\frac{\lambda_0}{\lambda}\right)^4 \exp\left[-\left(\frac{\lambda_0}{\lambda}\right)^2\right] \frac{d\Sigma}{d\Omega} \cdot c_a \cdot d\Omega \cdot \epsilon, \qquad (3)$$

where

ϕ_0 = neutron flux at the source, presumed to obey a Maxwellian density distribution law,

T_c = transmission of the used collimator,

c_m, c_a = characteristic numbers for the monochromating and analysing part, respectively,

$R_m = \frac{\Delta\lambda}{\lambda}$ = wavelength resolution,

$\frac{d\Sigma}{d\Omega}$ = macroscopic scattering cross-section of the sample,

$d\Omega$ = solid angle of the analysing part and

ϵ = detector efficiency

The cases where the chopper is placed before and after the sample will now be treated separately.

1. *Chopper placed after sample*

If the chopper is placed after the sample the characteristic numbers c_m and c_a are defined as shown in Table II.

TABLE II

DEFINITION OF PARAMETERS

For the spectrometer using as monochromator :	Definition of c_m and c_a
Beryllium filter only	c_m = filter transmission c_a = actual chopper transmission
Single crystal and a beryllium filter	c_m = product of the fraction of reflected neutrons within the wavelength interval $\Delta\lambda$ and the filter transmission c_a = actual chopper transmission
Mechanical velocity selector and a beryllium filter	c_m = product of the geometrical transmission of the rotor and the filter transmission c_a = actual chopper transmission

In Table III the values of the different quantities are shown, assuming the source size mentioned above. The damping factor D_f written in the fourth column is defined as

$$D_f = 2 \cdot T_c \cdot c_m \cdot R_m \cdot \left(\frac{\lambda_0}{\lambda}\right)^4 \exp\left[-\left(\frac{\lambda_0}{\lambda}\right)^2\right]. \quad (4)$$

Thus the intensity at the sample position is obtained as the product $\phi_0 D_f$. The spectrometer types have been numbered and for short these numbers will be used below.

For spectrometer I the wavelength resolution has been put equal to 25%. This figure will vary somewhat from one neutron beam facility to another due to the distortion of the ideal spectrum by Bragg scattering in constructional materials in the beam tube, such as aluminium and iron. The neutron spectrum as measured at the exit of a beam tube always shows a spectral distribution as shown in Fig. 2. In calculating the damping factor the integral form of Eq. (3) has been used. For spectrometer II a Pb single crystal is assumed to be used as monochromator. For reflection in the (111)-plane of 4-Å neutrons the Bragg angle is about 45°. Then the largest possible wavelength spread of the reflected neutrons is calculated to 7.5% or 0.30 Å at 4 Å from the size of the beam tube. In case III one has to take into account that the collimator used should be fan-shaped while the neutron-emitting surface is circular. In the actual case this implies a reduction in intensity at the sample position of about 30%. From the values of the damping factors it is obvious that the use of a beryllium filter as monochro-

TABLE III

CHARACTERISTICS OF SPECTROMETERS WITH CHOPPER AFTER SAMPLE

Spectrometer type	For a spectrometer using as monochromator :	$\Delta\lambda/\lambda$ (%)	T_c	c_m	Damping factor D_f	dt/t (%)	I_{det}, if $\phi_0 = 10^{13}$ n/cm² s (n/s)
I	Beryllium filter only	~ 25	1.8×10^{-2}	0.9	2.1×10^{-4}	1.8	190
II	Single-crystal Pb(111)-reflection	7.5	1.8×10^{-2}	0.63	4.3×10^{-5}	1.8	39
III	Mechanical monochromator and a beryllium filter	4.2	2.7×10^{-3}	0.37	2.2×10^{-6}	1.8	2.0

mator yields an intensity at the sample position about 5 times larger than for apparatus II and 100 times larger than for apparatus III. The reason for this is of course the large wavelength spread of the neutron spectrum.

In obtaining the counting rates in the detector the following values were adopted for the quantities $d\Sigma/d\Omega$, c_a, $d\Omega$ and ϵ:

$\frac{d\Sigma}{d\Omega} = 8 \times 10^{-3}$, which implies 90% transmission in the sample; thus a "thin" sample is used.

$c_a = 3.2 \times 10^{-3}$, which implies a time resolution of about 1.8% at 4 Å. The value of c_a is a product of the maximum transmission (6.4×10^{-3}) of the chopper and a relative transmission (0.5) as the chopper transmission curve does not have its maximum at 4 Å when yielding 1.8% time resolution. (Most of the neutrons are scattered elastically)

$d\Omega = 7 \times 10^{-3}$, which implies a detector area of 20 cm by 30 cm at the end of a 3-m flight path

$\epsilon = 0.5$, which is a probable average value of the wavelength efficiency of the detector.

The chopper having the resolution and transmission stated above is the one now in use at the time-of-flight spectrometers in Stockholm. In predicting the time resolution figure, 1.8%, the contributions from the detector thickness and the channel width of the time analyser have been neglected. The detector efficiencies can be kept high even if the thickness is to be kept small by use of high pressure BF_3 counters or by use of lithium glass detectors. If the source flux is taken to 10^{13} n/cm^2 s one arrives at the counting rates written in the last column of Table III. The ratio between these numbers is of course the same as for the D_f figures.

2. *Chopper placed before sample*

Table IV gives the equivalent figures if the chopper is placed before the sample. This position of the chopper has a very large advantage in that it is possible to record data at many scattering angles simultaneously. The signal-to-noise ratio is generally also larger in this case. In cases I, II and III the same chopper as above is assumed to be used, while in IV a semi-monochromating chopper with the same parameters as the one in use in Studsvik is assumed to be used. In this case the solid angle between the sample and the detector is the same as before but from the parameters of the chopper the distance between the sample and the detector has been increased to 4.6 m. The numbers c'_m given in Table IV are the product of c_m and c_a used in [1]. For spectrometer I it is obvious that the chopper, when it is placed before the sample, has a monochromating effect as the wavelength resolution is improved from 25 to 10%. The expense for this improvement is an intensity loss of 2.5. The spectrometers II and III show a slight decrease in counting rates in comparison to the figures given in Table III. The difference originates from the fact that the neutrons transmitted through

TABLE IV

CHARACTERISTICS OF SPECTROMETERS WITH CHOPPER BEFORE SAMPLE

Spectrometer type	For a spectrometer using as monochromator:	$\Delta\lambda/\lambda$ (%)	T_c	c'_m	Damping factor D_f	dt/t (%)	I_{det}, if $\phi_0 = 10^{13}$ n/cm^2 s (n/s)
I	Beryllium filter only	~10	1.8×10^{-2}	2.3×10^{-3}	2.7×10^{-7}	1.8	76
II	Single-crystal Pb(111)-reflection	7.5	1.8×10^{-2}	1.6×10^{-3}	1.1×10^{-7}	1.8	31
III	Mechanical monochromator and a beryllium filter	4.2	2.7×10^{-3}	9.5×10^{-4}	5.5×10^{-9}	0.9	1.6
IV	Semi-monochromating chopper in conjunction with a beryllium filter	7.5	1.4×10^{-2}	1.7×10^{-3}	9.1×10^{-8}	1.2	25

the chopper now are monoenergetic while, in obtaining the values shown in Table I, the effect of inelastically scattered neutrons with higher transmission through the chopper was taken into consideration. The difference is, however, to some degree arbitrary. For a spectrometer of type III there is a very large improvement in placing the chopper before the sample as the time resolution is decreased from 1.8 to 0.9%.

The figures written in the last columns of Tables III and IV show the total intensity reaching the detector. The main part of it consists of neutrons which have been scattered elastically. The fraction of inelastically scattered neutrons is impossible to predict as it depends on certain properties of the sample and of the scattering angle.

A very large drawback in using the type I spectrometer in inelastic scattering experiments is the large width of the beryllium filtered neutron spectrum. Small energy transfers can hardly be studied with this method as all details in the cross-section will be smeared out. In measuring large energy transfers, so large that the wavelength spread in the impinging neutron spectrum is negligible, the technique is suitable as it yields a high intensity. In quasi-elastic scattering experiments the method has a very wide use as the infinitely sharp beryllium cut-off can be used to define an energy of the impinging neutrons. As the intensity associated with this method is very high the time resolution dt/t may be considerably decreased. If one tolerates an intensity decrease of about 12 it is possible, by choosing another chopper and by introducing a collimator in the beam tube, to get 0.5% time resolution. Thus it is possible to measure very small broadenings of the elastic peak, much smaller than is possible with the other spectrometers of Table IV.

A very capable spectrometer when measuring small energy transfers and moderate broadenings of the elastic peak seems to be the one using a crystal monochromator. If one uses the combined action of the beryllium cut-off and the Bragg reflection in Pb it is possible to decrease $\Delta\lambda/\lambda$ to 3.75% with a loss of intensity of a factor 2. By choosing a chopper, which has the maximum of its transmission curve at 4 Å and half the absolute transmission compared to the one described above, it is possible to obtain 0.9% time resolution and 1.9% wavelength spread in the spectrum of impinging neutrons when the number of neutrons absorbed in the detector per second is about 5. For comparison it can be mentioned that the counting rate at the time-of-flight spectrometers at the Stockholm reactor is about 2 c/s.

The combination of a semi-monochromatizing chopper and a beryllium filter has about the same properties as the crystal-chopper arrangement. By speeding up the chopper it is possible, when the counting rate is about 6 c/s to get 3.75% wavelength resolution. Thus the intensity is somewhat lower with this arrangement at equal wavelength resolution. This fact is emphasized even more when trying to obtain even smaller $\Delta\lambda/\lambda$ values. The spectrometer serves, however, as a very good compromise between types I and II spectrometer in the sense that it is possible to change in a simple way the wavelength spread and thus the counting rate in the detector.

The mechanical monochromator system yields a very low intensity as compared to the other spectrometers. To be useful in scattering experiments, larger solid angles must be used. If the scattering process is cylindrically symmetric, which is true for liquids, a ring detector may be used.

REFERENCES

[1] LARSSON, K.-E., DAHLBORG, U., HOLMRYD, S., OTNES, K. and STEDMAN, R., Ark. Fys. 16 (1959) 199.
[2] HOLMRYD, S., SKÖLD, K., PILCHER, E. and LARSSON, K.-E., Nucl. Instrum. Meth. 27 (1964) 61.
[3] HOLMRYD, S., LARSSON, K.-E. and OTNES, K., Nucl. Instrum. Meth. 12 (1961) 355.

DISCUSSION

P. EGELSTAFF: For what purpose have you built the mechanical monochromator and the hybrid instrument consisting of a crystal spectrometer and a slow chopper?

K.-E. LARSSON: The monochromator is intended for work with very long wavelengths in combination with a cold moderator. The other instrument is intended to serve as a flexible tool for the selection of ingoing wavelengths. At the same time, it incorporates the advantages of time-of-flight energy analysis.

G. VENKATARAMAN: You remarked in your oral presentation that it is preferable to use thermal neutrons instead of cold neutrons for studying the angular dependence of the intensity of the quasi-elastic distribution. But don't you think that, apart from the limitation that large momentum transfers cannot be reached, cold neutrons are just as good, provided one uses a monochromatic beam instead of the entire filtered spectrum?

K.-E. LARSSON: Yes, I do.

PERFORMANCE OF A THREE-AXIS SPECTROMETER IN EXPERIMENTS OF ELASTIC DIFFRACTION OF NEUTRONS

G. CAGLIOTI
COMITATO NAZIONALE PER L'ENERGIA NUCLEARE,
CENTRO COMUNE RICERCHE EURATOM, ISPRA, VARESE,
AND
D. TOCCHETTI
ISTITUTO DI FISICA NUCLEARE, UNIVERSITY OF PAVIA,
ITALY

Abstract — Résumé — Аннотация — Resumen

PERFORMANCE OF A THREE-AXIS SPECTROMETER IN EXPERIMENTS OF ELASTIC DIFFRACTION OF NEUTRONS. The method of elastic diffraction of neutrons can be advantageously utilized both in the study of liquid dynamics and in the analysis of some interesting problems in the field of crystal physics.

In the present communication the main features of the experimental technique of elastic neutron diffraction are recalled, and its possible applications are reviewed. Furthermore, a study is presented concerning the instrumental energy resolution of a three-axis spectrometer in experiments of coherent elastic diffraction.

PERFORMANCE D'UN SPECTROMÈTRE TRIAXIAL DANS DES EXPÉRIENCES SUR LES SOLIDES AU MOYEN DE LA DIFFUSION ÉLASTIQUE DES NEUTRONS. La méthode de la diffusion élastique des neutrons peut être appliquée avec succès à l'étude de la dynamique des liquides et à l'analyse de plusieurs problèmes intéressants qui se posent en physique des cristaux.

Les auteurs rappellent les principes essentiels de la méthode expérimentale fondée sur la diffusion élastique des neutrons et indiquent ses possibilités d'application. En outre, ils étudient le pouvoir de résolution en énergie d'un spectromètre triaxial dans les expériences sur la diffusion élastique cohérente.

РАБОТА ТРЕХОСНОГО СПЕКТРОМЕТРА ПРИ ПРОВЕДЕНИИ ЭКСПЕРИМЕНТОВ ПО УПРУГОЙ ДИФРАКЦИИ НЕЙТРОНОВ. Метод упругой дифракции нейтронов может с успехом применяться для изучения как динамики жидкостей, так и некоторых интересных проблем в области физики кристаллов.

В настоящем сообщении напоминаются основные особенности экспериментального метода упругой дифракции нейтронов и рассматриваются возможные виды его применения. Кроме того, приводятся результаты исследования разрешающей способности по энергии трехосного спектрометра при проведении экспериментов по когерентной упругой дифракции.

RESULTADOS SOBRE DISPERSIÓN ELÁSTICA DE NEUTRONES OBTENIDOS CON UN ESPECTRÓMETRO TRIAXIAL. El método de la dispersión elástica de neutrones puede utilizarse provechosamente para estudiar la dinámica de los líquidos y analizar algunos interesantes problemas de física de las estructuras cristalinas.

En la memoria se recuerdan las características principales de la técnica de experimentación por dispersión elástica de neutrones y se examinan sus posibles aplicaciones. Asimismo, se hace un estudio del poder de resolución de energía de un espectrómetro triaxial en experimentos de dispersión elástica coherente.

1. INTRODUCTION

The representation in momentum space of the scattering processes of radiation in matter strongly depends, in general, on the nature of the sample under study and of the radiation probe. For instance, when X-rays are dif-

fracted with a certain amount of momentum change, the polygonal of the wave vector of the impinging and outgoing photon, and the wave vector transfer $\vec{Q}$ is always practically an isosceles triangle. In fact the energy transfer $\hbar\omega$ eventually accompanying the scattering process (~ 0.1 eV at most) is very low compared with the energy of the impinging X-ray (~ 10 keV).

This is not the case for the thermal neutron probe, due to the different energy-momentum relationship for neutron and photon. When a thermal neutron is scattered by a solid or a liquid and interacts with the thermal excitations, its original energy ($10^{-2} - 10^{-1}$eV) generally undergoes radical changes which are naturally coupled with important changes of wavelength and wave vector magnitude. As a consequence, the wave vector polygonal is sensitively dependent on the nature of the sample, i.e. on the scattering law $S(\vec{Q}, \omega)$; the polygonal reduces to an isosceles triangle in the particular case of the Bragg reflection.

These circumstances determined in recent years the development of a number of studies of the dynamical behaviour of solids and liquids by inelastic scattering of neutrons [1, 2].

More recently, it seemed interesting to investigate also the nature of the information obtainable by an analysis of only those processes which are not accompanied by an experimentally detectable neutron energy transfer (elastic diffraction). This investigation was done both for the case of solids [3] and liquids [4, 5].

It seems appropriate to recall here the main features (section 2) and the possible applications (section 3) of the method of elastic diffraction of neutrons. In section 4 a discussion is presented on the instrumental energy resolution of a three-axis crystal spectrometer utilized for this purpose in coherent scattering processes.

2. THE METHOD OF ELASTIC DIFFRACTION OF NEUTRONS

The simplest experimental arrangement suitable for elastic neutron diffraction is perhaps a three-axis spectrometer whose analysing spectrometer is prepared so as to select only the neutrons that did not suffer energy transfer as a consequence of the diffraction process. The energy selection performed by the analysing spectrometer, in most cases, prevents the diffracted neutrons from proceeding toward the counter. This is equivalent to fold the scattering law $S(\vec{Q}, \omega)$ by the instrumental energy resolution function of the spectrometer. Correspondingly the experimental information, as shaped by the instrument, is equivalent to a picture of the system which is not instantaneous (as it happens for X-ray diffraction and also, within the limits of validity of the static approximation, for conventional neutron diffraction) but is taken over a time Δt determined by the inverse of the energy resolution ΔE of the spectrometer (full width at half maximum), according to the relationship [4]

$$\Delta t \sim 8 \ln 2 \, \hbar/\Delta E . \qquad (1)$$

3. POSSIBLE APPLICATIONS OF ELASTIC NEUTRON DIFFRACTION

In our laboratory attention was focussed on the applications of the elastic neutron diffraction to some problems concerning liquid and solid systems. By this method we studied liquid bromine [4], obtaining information on the local atomic movements within the relaxed structure of the liquid during the time of observation. More recently, elastic diffraction patterns of simple solid materials have been obtained by a three-axis spectrometer, in order to study, also experimentally, the possibility of improving accuracy in the determination of the Debye-Waller factor. It was indeed found that elastic diffraction permits one to eliminate the thermal diffuse background between the Bragg reflections or to reduce it beneath them. A remarkable improvement in resolution was also achieved, together with a reduction of the effects of second order wavelength contamination in the monochromatic beam.

Similarly, this technique is found to be useful whenever one is interested in mapping the intensity of the elastically diffracted neutrons at any individual point of the reciprocal space. For instance, a study is under way on the analysis of disorder scattering in a crystal structure undergoing a phase transition [6]. This method could also be utilized for the analysis of crystal structures of alloys undergoing order-disorder transformations.

4. THE INSTRUMENTAL ENERGY RESOLUTION OF A THREE-AXIS SPECTROMETER IN EXPERIMENTS OF COHERENT ELASTIC DIFFRACTION OF NEUTRONS

To study the performance of a three-axis spectrometer in experiments of elastic diffraction of neutrons, in a recent paper [7] an extension was made of some general expressions (previously developed for a two-axis neutron diffractometer) giving the full width at half maximum of the Bragg reflections at any scattering angle and their instrumental luminosities in terms of the typical angular parameters of a crystal spectrometer (i.e. angular divergences of the Soller type collimators, mosaic spread of the crystals and wavelength dispersion parameter). Reference [7] proposes some criteria for a convenient choice of these angular parameters.

By further extension of the procedure adopted in [7], we will discuss in detail the important quantity ΔE_{coh} (see Eq. (1)), as determined by the experimental arrangement for the process of coherent Bragg reflection in a solid.* As discussed in [3], this process is elastic only at the exact reciprocal lattice point associated with the Bragg reflection. The knowledge of ΔE_{coh} could be of some interest for very accurate determinations of the temperature factor in crystal structure analysis. In more practical cases, the knowledge of ΔE_{coh} and ΔE_{inc} defines the limits of the energy resolution of a three-axis spectrometer for cases, so-to-say, intermediate between coherent Bragg reflection and incoherent scattering. In these cases (such as disorder scat-

* In Ref. [3] it was shown how to compute ΔE in terms of the typical angular parameters of a spectrometer, for the case of an incoherent scattering process in a solid. This value of ΔE_{inc} to a good approximation, can also be referred to the scattering by a liquid sample, at least beyond the first diffraction peak wherein the de GENNES [8] energy narrowing is expected to occur.

tering) this knowledge would help to eliminate or control the intensity associated with the dynamical contributions to the effect under investigation.

The starting equation for the computation of ΔE_{coh} is obtained from column (a) of Table I in Ref. [7]. The distribution function $I(\delta)$ for the Bragg angle displacements $\delta \equiv \vartheta_M - \vartheta_{M_0}$ associated with individual neutron rays susceptible of being detected by the counter set in its central position ($\rho = 0$) is:

$$I(\delta) = H \int_{-\infty}^{\infty} d\phi_1 \exp - \left[\left(\frac{\phi_1}{\alpha'_1} \right)^2 + \left(\frac{\delta - \phi_1}{\beta'_1} \right)^2 + \left(\frac{2\delta - \phi_1}{\alpha'_2} \right)^2 \right.$$

$$+ \left(\frac{(a_1 - 2)\,\delta + \phi_1}{\beta'_2} \right)^2 + \left(\frac{2(a_1 - 1)\,\delta + \phi_1}{\alpha'_3} \right)^2 + \left(\frac{[a_2 - 2(a_1 - 1)]\,\delta - \phi_1}{\beta'_3} \right)^2$$

$$\left. + \left(\frac{2(a_2 - a_1 + 1)\,\delta - \phi_1}{\alpha'_4} \right)^2 \right]. \qquad (2)$$

Here, as usual, $\alpha'_i = \alpha_i / 2(\ln 2)^{\frac{1}{2}}$ and similarly $\beta'_j = \beta_j / 2(\ln 2)^{\frac{1}{2}}$; α_i is the angular divergence of the collimators and the index i ($i = 1, 2, 3, 4$) identifies the four collimators as one proceeds from the in-pile collimator ($i = 1$) to the one located between the analysing crystal and the counter ($i = 4$). β_j ($j = 1, 2, 3$) is the crystal mosaic spread of monochromator, sample and analyser, respectively. ϕ_1 is the projection on the horizontal plane of the angle between any individual ray and the centreline of the first collimator. The wavelength dispersion parameters a_1 and a_2 are defined by the ratios $\tan\vartheta/\tan\vartheta_M$ and $\tan\vartheta_A/\tan\vartheta_M$, where ϑ_M, ϑ and ϑ_A are the Bragg angles at the monochromator, sample and analyser, respectively.

If one performs the integration in Eq. (2), one obtains for $I(\delta)$ a Gaussian function, whose full width at half maximum $W_{\frac{1}{2}}$ is of the type:

$$W_{\frac{1}{2}}^2 = N_{00} / (D_{00} - D_{10}\, a_1 + D_{20}\, a_1^2 + D_{01} a_2 + D_{02} a_2^2 - D_{11}\, a_1 a_2). \qquad (3)$$

The coefficients N_{00} and D_{lm} (l, m = 0, 1, 2) are the following:

$$N_{00} = \alpha_1^2 \beta_1^2 \alpha_2^2 \beta_2^2 (\alpha_3^2 \beta_3^2 + \alpha_3^2 \alpha_4^2 + \beta_3^2 \alpha_4^2) + \alpha_1^2 \beta_1^2 \alpha_2^2 \alpha_3^2 \beta_3^2 \alpha_4^2$$
$$+ \beta_2^2 \alpha_3^2 \beta_3^2 \alpha_4^2 (\alpha_1^2 \beta_1^2 + \alpha_1^2 \alpha_2^2 + \beta_1^2 \alpha_2^2)$$

$$D_{00} = \alpha_2^2 \beta_2^2 (\alpha_1^2 + 4\beta_1^2)(\alpha_3^2 \beta_3^2 + \alpha_3^2 \alpha_4^2 + \beta_3^2 \alpha_4^2) + \alpha_3^2 \beta_3^2 \alpha_4^2 [\alpha_2^2 \beta_2^2 + (\alpha_2^2 + \beta_2^2)(\alpha_1^2 + 4\beta_1^2)]$$

$$D_{10} = 2\alpha_2^2 (\alpha_1^2 + 2\beta_1^2)[2\beta_2^2 (\alpha_3^2 \beta_3^2 + \alpha_3^2 \alpha_4^2 + \beta_3^2 \alpha_4^2) + \alpha_3^2 \beta_3^2 \alpha_4^2]$$

$$D_{20} = (\alpha_1^2\beta_1^2 + \alpha_1^2\alpha_2^2 + \beta_1^2\alpha_2^2)[\beta_3^2\alpha_4^2(\alpha_3^2 + 4\beta_2^2) + 4\beta_2^2\alpha_3^2(\beta_3^2 + \alpha_4^2)]$$
$$+ \alpha_1^2\beta_1^2\alpha_2^2(\alpha_3^2\beta_3^2 + \alpha_3^2\alpha_4^2 + \beta_3^2\alpha_4^2)$$

$$D_{01} = 2\alpha_2^2\beta_2^2\alpha_3^2(\alpha_1^2 + 2\beta_1^2)(\alpha_4^2 + 2\beta_3^2)$$

$$D_{02} = \beta_2^2\alpha_3^2(\alpha_1^2\beta_1^2 + \alpha_1^2\alpha_2^2 + \beta_1^2\alpha_2^2)(\alpha_4^2 + 4\beta_3^2) + \alpha_1^2\beta_1^2\alpha_2^2[\beta_2^2\alpha_3^2 + (\alpha_4^2 + 4\beta_3^2)(\beta_2^2 + \alpha_3^2)]$$

$$D_{11} = 2\alpha_3^2(\alpha_4^2 + 2\beta_3^2)[2\beta_2^2(\alpha_1^2\beta_1^2 + \alpha_1^2\alpha_2^2 + \beta_1^2\alpha_2^2) + \alpha_1^2\beta_1^2\alpha_2^2].$$

$W_{\frac{1}{2}}$ exhibits a complicated dependence on α_j and β_i. In order to disentangle from $W_{\frac{1}{2}}$ its implications, we made a numerical analysis of the case of practical interest $a_2 = 1$ and $\alpha = \sqrt{2}\,\beta$, α and β being the common value attributed to the α_j's and β_i's. Once $W_{\frac{1}{2}}$ is obtained as a function of α and a_1, the energy resolution ΔE_{coh} (full width at half maximum) is given by [9],

$$\Delta E_{coh} = 4\, d_M \cos\vartheta_M (0.286)^{-1} E^{3/2} \cdot W_{\frac{1}{2}}, \tag{4}$$

where d_M is the spacing of the Bragg-reflecting crystal planes in units of 10^{-8} cm and E is the central value of the energy of the monochromatic beam in eV.

In Fig.1 we show the behaviour of $W_{\frac{1}{2}}/\alpha$ as a function of a_1 for the above described instrumental arrangement of the spectrometer. It is interesting to notice that a maximum for the instrumental broadening $W_{\frac{1}{2}}$ and ΔE_{coh} occurs at $a_1 = 1$. The peak value of the elastic Bragg reflections $I_{\rho=0} = \int_{-\infty}^{+\infty} I(\delta)\, d\delta$ behaves in a similar way, attaining a maximum at $a_1 = 1$, while the corresponding full width at half maximum $A_{\frac{1}{2}}$ has an opposite trend, reaching a minimum at the focussing position $a_1 = 1$ (see Fig.1 and the discussion of section 3.1 in Ref. [7]).

Finally, a numerical computation of ΔE_{coh} in the typical case of $\lambda = 1.25$Å, $a_1 = 1 = a_2$, $\alpha = 20'$, leads to an instrumental energy resolution

$$\Delta E_{coh} = 1.32 \text{ meV} \tag{5}$$

when the Al(111) Bragg reflection of the crystal monochromator is utilized. For the same arrangement of the spectrometer, utilized in an incoherent elastic scattering experiment, the energy resolution ΔE would turn out to be exactly twice as broad:

$$\Delta E_{inc} = 2.64 \text{ meV}. \tag{6}$$

We feel that the computing technique presented above for the case of coherent elastic scattering should also lead to a useful evaluation of the error accompanying the measurement of the energy of a phonon by a crystal

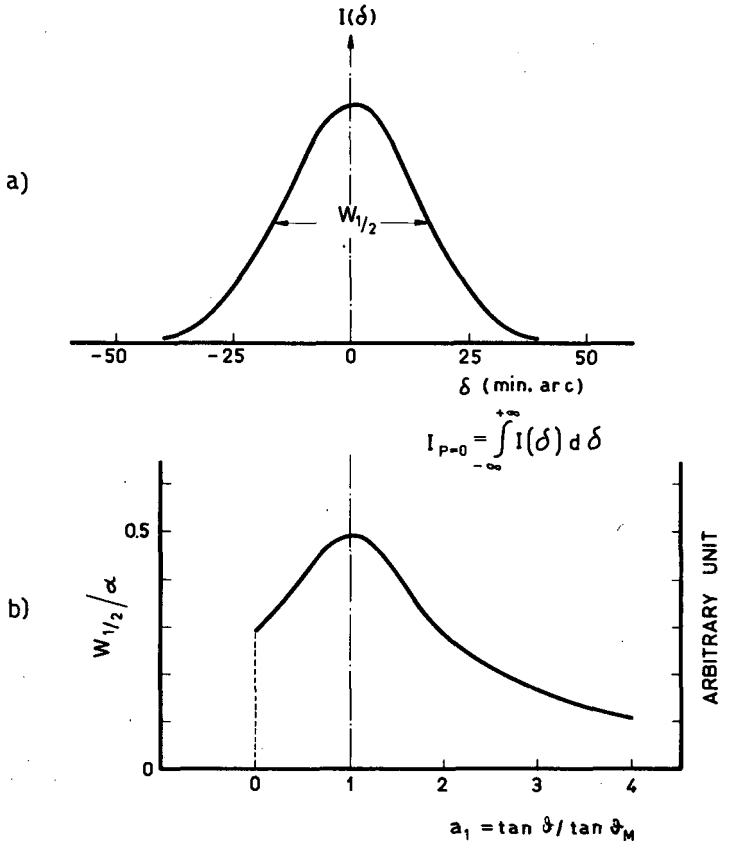

Fig. 1

(a) The physical meaning of $W_{\frac{1}{2}}$

This quantity is the full width at half-maximum of the distribution function $I(\delta)$ associated with neutrons eventually reaching the detector. Since $\delta = \vartheta_M - \vartheta_{M_0}$ is the displacement of the Bragg angle ϑ_M of any individual ray at the monochromator, as measured with respect to the central ray, $W_{\frac{1}{2}}$ is directly connected with the instrumental energy resolution of the three-axis spectrometer prepared for elastic diffraction and utilized in measurements of coherent scattering.

(b) The behaviour of $W_{\frac{1}{2}}$ as a function of the wavelength dispersion parameter

$a_1 = \tan \vartheta / \tan \vartheta_M$, in the practical case $\alpha_j = \sqrt{2}\, \beta_i$, $a_2 \equiv \tan \vartheta_A / \tan \vartheta_M = 1$; $W_{\frac{1}{2}}$ and, with it, the instrumental energy resolution ΔE_{coh} get coarser at the focussing position ($a_1 = 1$, in this instance). Evidently the

$I_{\rho=0} = \int_{-\infty}^{+\infty} I(\delta)\, d\delta$, corresponds to a situation where neutrons belonging to a wide energy range are accepted

by the instrument.

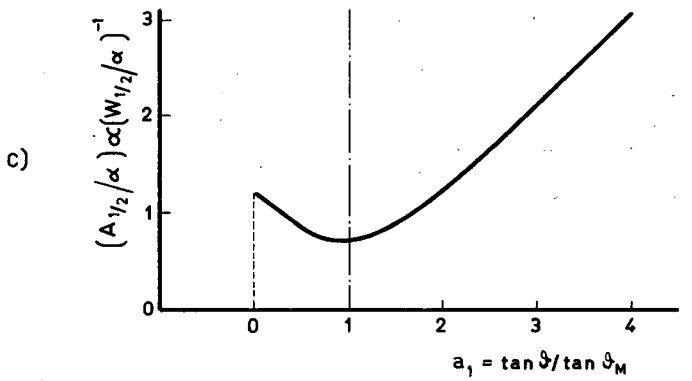

(c) The behaviour of the full width at half maximum $A_{\frac{1}{2}}$ of the elastic diffraction peaks, as a function of a_1

$A_{\frac{1}{2}}$ reaches a minimum at the focussing position.

spectrometer, especially where the focussing effects connected with the $\text{grad}_q\omega$ can be neglected.

5. CONCLUSIONS

The performance of a three-axis spectrometer in experiments of elastic diffraction of neutrons in solids and liquids is briefly discussed, and a detailed study on the energy resolution of this instrument in measurements of coherent elastic diffraction is presented.

In solids, the method of elastic neutron diffraction, allowing a reduction of the recorded thermal diffuse intensity beneath the Bragg reflections or even its elimination between them, offers the possibility of slightly improving accuracy in the determination of the Debye-Waller factor. Furthermore it is helpful to reduce the effects of the second-order wavelength contamination in the monochromatic beam. Finally, it may find interesting applications in the analysis of diffuse disorder scattering in crystals undergoing phase transitions or in alloys, since it offers the possibility of mapping the intensity of the elastically diffracted neutrons at any individual point of the reciprocal space. In fact, while the point-by-point control of the reciprocal space (though affected by the dynamical contributions associated with the possible energy transfers) is possible by X-ray diffraction techniques, this control cannot at all be exerted in conventional neutron diffraction [10].

In liquids, this method provides information on the local behaviour of the system during a time defined in terms of the energy resolution of the instrumental setup [5].

REFERENCES

[1] Inelastic Scattering of Neutrons in Solids and Liquids, IAEA, Vienna (1961) 651 pp.

[2] Inelastic Scattering of Neutrons in Solids and Liquids I and II, IAEA, Vienna (1963) 1310 pp.

[3] CAGLIOTI, G., Acta cryst. 17 (1964) 1202.
[4] BROCKHOUSE, B.N., Suppl. Nuovo Cim. 9 (1958) 45.
[5] CAGLIOTI, G. and ASCARELLI, P., Inelastic Scattering of Neutrons in Solids and Liquids I IAEA, Vienna (1963) 259-62.
[6] BORGONOVI, G., CAGLIOTI, G. and ANTONINI, M., "Recent results on the crystal physics of white tin", these Proceedings I.
[7] CAGLIOTI, G. and TOCCHETTI, D., Nucl. Instrum. Meth., to be published.
[8] de GENNES, F.P., Physica 25 (1959) 852.
[9] SAILOR, V.L., FOOTE, H.L. Jr., LANDON, H.H. and WOOD, R.E., Rev. Sci. Instrum. 27 (1956) 26.
[10] CAGLIOTI, G., C.N.E.N. Techn. Rpt RT/FI (1964) 20.

DISCUSSION

P. EGELSTAFF: What is the relative intensity of elastic diffraction as compared with normal diffraction?

G. CAGLIOTI: The relative intensity is of the order of eight. I would point out, however, that in the passage from conventional to elastic diffraction the intensity loss is accompanied by an improvement in resolution, as indicated, for example, in Fig. 5 of Ref. [7].

P. EGELSTAFF: It should be emphasized that while for solids the elastic peak is integrated by this method, in the case of liquids only a part of the quasi-elastic peak is obtained, because often it is broader than the instrumental resolution or it is not clearly separated from the inelastic background. This method is especially valuable for non-crystalline solids such as glasses. In this case there are no Bragg peaks, so that normal diffraction does not work properly and the improvement in elastic diffraction is very important.

G. CAGLIOTI: It might be appropriate to add that another important problem – to which Dr. Iyengar has drawn attention – could arise in the neutron diffraction analysis of crystals containing hydrogen. The fraction of the neutrons which are inelastically scattered in these crystals can reach particularly high values. It would then be of interest to investigate the differences in the data for this important category of crystals, depending on whether they were obtained by elastic or conventional diffraction analysis.

ПРИМЕНЕНИЕ МЕТОДА ВРЕМЕНИ ПРОЛЕТА К НЕЙТРОННО-ДИФРАКЦИОННЫМ ИССЛЕДОВАНИЯМ

И. СОСНОВСКА, Е. СОСНОВСКИ, С.В. КИСЕЛЕВ* и Р.П. ОЗЕРОВ*
ОБЪЕДИНЕННЫЙ ИНСТИТУТ ЯДЕРНЫХ ИССЛЕДОВАНИЙ, ДУБНА
СССР

(Представлено Ф.Л. Шапиро)

Abstract — Résumé — Аннотация — Resumen

APPLICATION OF THE TIME-OF-FLIGHT METHOD TO NEUTRON-DIFFRACTION STUDIES. The pulsed reactor of the Joint Institute for Nuclear Research was used to study neutron diffraction in polycrystalline samples. Using a fixed scattering angle, the authors measured the effect of neutron flight time, i. e. wavelength, on scattering intensity.

The method described was used successfully to investigate the crystalline and magnetic structures of $BiFeO_3$, studied earlier by the usual neutron diffraction method with poorer resolution. Splitting of a number of peaks was observed, caused by slight rhombohedral distortion of the cell. From this it could be determined that below zero point the magnetic moments of the Fe ions are oriented parallel to the [111] axis.

APPLICATION DE LA MÉTHODE DU TEMPS DE VOL AUX ÉTUDES SUR LA DIFFRACTION DES NEUTRONS. Les auteurs ont utilisé le réacteur à impulsions de l'Institut unifié de recherches nucléaires pour étudier la diffraction des neutrons dans des substances polycristallines. Pour un angle de diffusion donné, ils ont déterminé la relation entre l'intensité de la diffusion et le temps de vol du neutron, c'est-à-dire sa longueur d'onde.

La méthode décrite a été appliquée à l'étude de la structure cristalline et magnétique du composé $BiFeO_3$, étude qui avait été faite précédemment par la méthode habituelle de diffraction des neutrons (avec un moins bon pouvoir de résolution). Les auteurs ont observé une fragmentation de certains pics, due à une légère déformation rhomboédrique de la cellule. Ce fait a permis d'établir qu'au-dessous du point de Neel les moments magnétiques des ions Fe sont orientés parallèlement à l'axe [111].

ПРИМЕНЕНИЕ МЕТОДА ВРЕМЕНИ ПРОЛЕТА К НЕЙТРОННО-ДИФРАКЦИОННЫМ ИССЛЕДОВАНИЯМ. Импульсный реактор Объединенного института ядерных исследований был применен для изучения дифракции нейтронов на поликристаллических образцах. При фиксированном угле рассеяния измерялась зависимость интенсивности рассеяния от времени пролета нейтрона, т.е. от его длины волны.

Описанная методика была применена для исследования кристаллической и магнитной структуры соединения $BiFeO_3$, изученного ранее обычным нейтронно-дифракционным методом с худшим разрешением. Наблюдалось расщепление некоторых пиков, обусловленное небольшим рамбоэдрическим искажением ячейки. Это позволило установить, что ниже точки нееля магнитные моменты ионов Fe ориентированы параллельно оси [111].

APLICACIÓN DEL MÉTODO DEL TIEMPO DE VUELO A LOS ESTUDIOS SOBRE DIFRACCIÓN NEUTRÓNICA. Los autores emplearon el reactor pulsado del Instituto Central de Investigaciones Nucleares para estudiar la difracción neutrónica en muestras policristalinas. Con un ángulo de dispersión fijo, midieron la intensidad de dispersión en función del tiempo de vuelo del neutrón, es decir, su longitud de onda.

El método descrito se utilizó para investigar la estructura cristalina y magnética del compuesto $BiFeO_3$, estudiado anteriormente por el método usual de difracción neutrónica (con un poder de resolución menos elevado). Se observó una subdivisión de algunos picos, condicionada por pequeñas distorsiones romboédricas de la celda. Este hecho permitió establecer que por debajo del punto de Neel los momentos magnéticos de los iones Fe están orientados paralelamente al eje [111].

В Лаборатории нейтронной физики ОИЯИ в Дубне на импульсном быстром реакторе (ИБР) [4] были проведены эксперименты с целью выясне-

* Физико-химический институт им. Карпова, Москва, СССР.

ния возможностей реактора в области структурной нейтронографии [1–3]. Тепловые нейтроны рассеивались на поликристаллических образцах, и для фиксированного угла методом времени пролета измерялся энергетический спектр рассеянных нейтронов.

Схема опыта показана на рис.1. Вплотную к активной зоне (1) реактора помещен замедлитель (2) толщиной 40 мм. Пучок нейтронов проходил через стальной коллиматор (3) соллеровского типа (угол расхождения – 20', окно – 100 × 110 мм^2), помещенный в стене зала реактора, через вакуумный нейтроновод (10), окно водяной защиты (4) и рассеивался на образце (7). Рассеянный пучок проходил через второй, идентичный первому коллиматор (6), установленный под углом 90° к направлению прямого пучка и регистрировался сцинтилляционным детектором (8), окруженным слоем карбида бора (9) и водяной защитой. Вся установка была окружена защитой из бетонных блоков. Использованный сцинтилляционный детектор на обогащенном B^{10} площадью 300 см^2 описан в работе [5].

Экспериментальные данные обрабатывались по формуле интегральной интенсивности дифракционных максимумов, выведенной в работе [6]:

$$E_{hk\ell}(\lambda) = C(\lambda^4 J_\lambda j F^2)_{hk\ell} ,$$

где C – постоянная;
λ – длина волны;
J_λ – интенсивность спектра падающих нейтронов, отнесенная к единичному интервалу длин волн;
j – фактор повторяемости;
F – структурный фактор.

Как сообщалось в работах [1–3], для вышеуказанных образцов получено хорошее совпадение теоретических и экспериментальных результатов.

Описанный метод был использован для изучения магнитной и атомной структуры сегнетоэлектрика – антиферромагнетика $BiFeO_3$ [7, 8]. Необходимость этого возникла в связи с тем, что разрешающая способность нейтронного дифрактометра, использованного в [7, 8], слишком мала для того, чтобы проверить предположение В. Плахтия и др. [9] о существовании в $BiFeO_3$ атомной сверхструктуры.

Образец размером 120 × 80 × 8 мм^2 был синтезирован по обычной керамической технологии. Гомогенность образца проверялась рентгенографически. Нейтронограмма образца $BiFeO_3$ представлена на рис.2.

Из рис.2 видно, что разрешены не только все максимумы кубической элементарной ячейки (a = 3,963 Å), но и отчетливо проявляется очень малое ромбоэдрическое искажение ячейки (a = 3,963 Å, α = 89°24'). Это искажение позволило непосредственно установить ориентацию магнитных моментов в структуре. Действительно, в отсутствие расщепления в связи с ограничениями порошкового метода определить ориентацию моментов в кубическом кристалле невозможно [10]. Расщепление позволило приписать магнитному отражению индекс ($\bar{1}$11) (а не (111)), что соответствует ориентации моментов параллельно ромбоэдрической оси [111] (так как при такой ориентация для отражения (111) $q^2_{111} = 0$). Это же заключение может быть

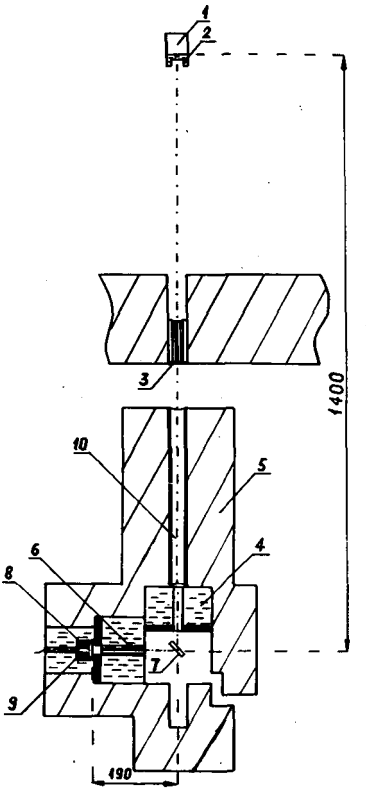

Рис.1

Схема установки для угла $2\theta = 90°$:

1 – активная зона;
2 – замедлитель;
3 – коллиматор;
4 – окно водяной защиты;
5 – корпус:
6 – коллиматор;
7 – образец;
8 – детектор;
9 – слой карбида бора;
10 – канал.

сделано на основании анализа полуширины магнитных отражений (311) и (333+511).

На рис.2 приведена также нейтронограмма при температуре 450°С (выше $T_N = 370°C$). На ней сохранились отражения (311) и (333+511). Это означает, что при этих температурах существует атомная сверхструктура, накладывающаяся на магнитную сверхструктуру при температурах ниже T_N. Это подтверждает упомянутое предположение работы [8], что в $BiFeO_3$ имеется атомная стуктура, по характеру совпадающая со сверхструктурой магнитной. Истинной – атомной и магнитной – является ромбоэдрическая элементарная ячейка с объемом, удвоенным по сравнению с объемом элементарного перовскитного куба с $a_R = a_k\sqrt{2}$ и углом $\alpha_R = 59°18'$ (индексы, соответствующие этой ячейке, указаны на рис.2 в скобках).

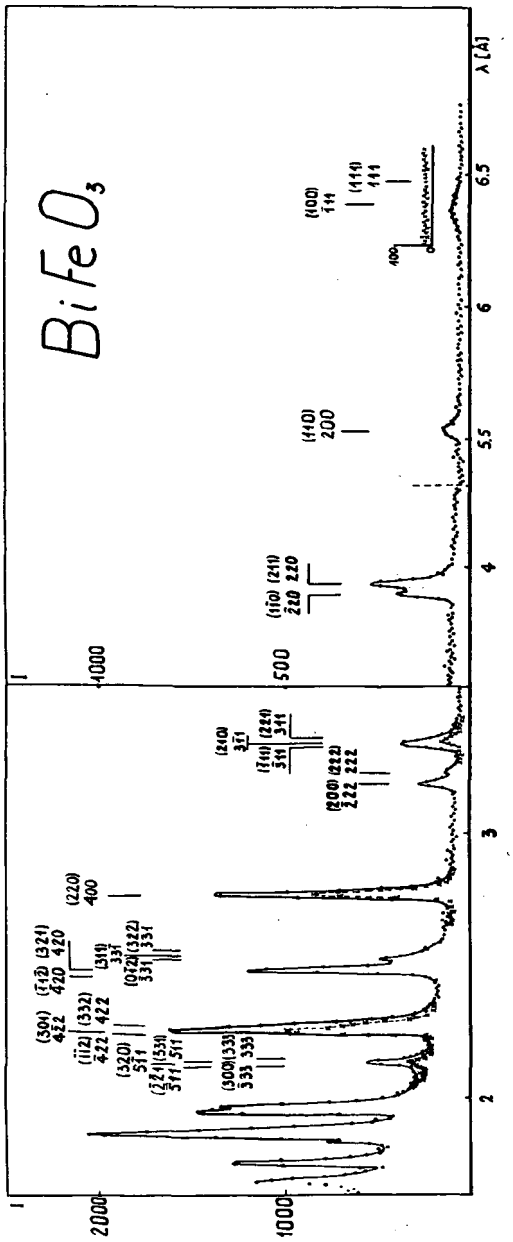

Рис.2

Нейтронограммы $BiFeO_3$ для комнатной температуры и T ≈ 450°C.
Приведены индексы ромбоэдрической ячейки $a'_R = 2a_k$, $\alpha'_R = 89°24'$ ($a_k = 3{,}963$ Å)
и истинной ромбоэдрической ячейки с $a_R = a_k\sqrt{2}$ и $\alpha_R = 59°18'$.

● ● ● T = 20°C × × × T = 450°C

ЛИТЕРАТУРА

[1] НИТЦ В.В., ПАПУЛОВА З.Г., СОСНОВСКА И., СОСНОВСКИ Е., ФТТ, 6, 1964, 1369.
[2] НИТЦ В.В., СОСНОВСКА И., СОСНОВСКИ Е., препринт ОИЯИ, 1964, 1614.
[3] BURAS B., LECIEJEWICZ J., NITC W.W., SOSNOWSKA I., SOSNOWSKI J., SHAPIRO F.L. Third United Nations International Conference on the Peaceful Uses of Atomic Energy A/Conf. 28/P/488.
[4] БЛОХИН Г.Е. и др., "Атомная энергия", 10, 1961, 437.
[5] ГОЛИКОВ В.В. и др., ПТЭ, 2, 59, 1963.
[6] BURAS B., Nukleonika, 8, 259 (1963).
[7] КИСЕЛЕВ С.В., ОЗЕРОВ Р.П., ЖДАНОВ Г.С., ДАН СССР, 145, 1962, 1255.
[8] КИСЕЛЕВ С.В., КШНЯКИНА А.Н., ОЗЕРОВ Р.П., ЖДАНОВ Г.С., ФТТ, 5, 1963, 3313.
[9] ПЛАХТИЙ В.П., МАЛЬЦЕВ Е.П., КАМИНКЕР Д.И., Известия АН СССР, 28, 1964, 436.
[10] SHIRANE G., Acta Cryst., 12, 282 (1959).

DISCUSSION

J.L. WARREN: We too have done measurements on bismuth* . At what temperature were the measurements carried out at Dubna?

F.L. SHAPIRO: The measurements reported were performed at room temperature.

W. GLÄSER: Is the thermal flux in your pulse higher or lower than the thermal flux of 7×10^4 n/cm^2 s soon to be available in the Brookhaven High-Flux Reactor? Can you give a rough figure for the ratio of these figures?

F.L. SHAPIRO: In a thick moderator, at the point of highest flux, the integrated thermal neutron flux is about 2×10^{11} n/cm^2 s and the corresponding peak flux at repetition frequency 3.3 cm^{-1} is about 3×10^{14} n/cm^2 s.

* IBM J. Res. Develop. 8 (1964) 234.

СПЕКТРОМЕТР ПО ВРЕМЕНИ ПРОЛЕТА С ФИЛЬТРОМ ПЕРЕД ДЕТЕКТОРОМ

А. БАЙОРЕК, Т.А. МАЧЕХИНА, К. ПАРЛИНЬСКИ и Ф.Л. ШАПИРО
ОБЪЕДИНЕННЫЙ ИНСТИТУТ ЯДЕРНЫХ ИССЛЕДОВАНИЙ, ДУБНА
СССР

Abstract — Résumé — Аннотация — Resumen

TIME-OF-FLIGHT SPECTROMETER WITH FILTER IN FRONT OF THE DETECTOR. The authors describe a time-of-flight neutron spectrometer with a filter in front of the detector, intended mainly for the measurement of incoherent neutron scattering. The spectrometer is designed for use with a pulsed fast reactor. Detailed studies are made of the neutron spectra produced by various moderators. Theoretical calculations of the resolving power of the apparatus in relation to various of its parameters are performed and agree with experimental data. The resolving power of the spectrometer in the inelastic region of the spectrum attains $\Delta t/t \sim 4\%$. The counting rate is quite high; for NH_4Cl (T = 90.5°K), with 85% transmission and resolution $\Delta t/t \sim 8\%$, the rate per channel is about 3200 counts/h at the rotational retardation peak and 1300 counts/h in the elastic region of the spectrum, with backgrounds of 170 and 100 counts/h, respectively.

SPECTROMÈTRE A TEMPS DE VOL COMPORTANT UN FILTRE AVANT LE DÉTECTEUR. Les auteurs décrivent un spectromètre à temps de vol comportant un filtre avant le détecteur, qui est essentiellement destiné à mesurer la diffusion incohérente des neutrons. Le spectromètre est rattaché à un réacteur à neutrons rapides pulsés. Les auteurs étudient en détail les spectres de neutrons obtenus avec différents ralentisseurs. En fonction des divers paramètres de l'installation, ils ont fait le calcul théorique de son pouvoir de résolution; ce calcul est en bon accord avec les données expérimentales. Plus particulièrement, le pouvoir de résolution du spectromètre dans la partie inélastique du spectre atteint $\Delta t/t \approx 4\%$. La vitesse de comptage de l'installation est assez grande: pour un échantillon de NH_4Cl (T = 90,5°K) (transmissibilité = 85% et pouvoir de résolution de $\Delta t/t \approx 8\%$), le comptage par canal représente environ 3200 imp/h au pic de rotation inhibée et 1300 imp/h dans la partie élastique du spectre, le bruit de fond étant respectivement de 170 et 100 imp/h.

СПЕКТРОМЕТР ПО ВРЕМЕНИ ПРОЛЕТА С ФИЛЬТРОМ ПЕРЕД ДЕТЕКТОРОМ. В докладе описан нейтронный спектрометр по времени пролета с фильтром перед детектором, предназначенный для измерения главным образом некогерентного рассеяния нейтронов. Спектрометр создан на базе импульсного быстрого реактора. Подробно изучены спектры нейтронов, даваемые различными замедлителями. Проведен теоретический расчет разрешающей способности установки в зависимости от различных ее параметров, который согласуется с данными эксперимента. В частности, разрешающая способность спектрометра в неупругой части спектра достигает $\Delta t/t \sim 4\%$. Скорость счета установки довольно велика: для образца NH_4Cl (T = 90,5° K) с пропусканием 85% и разрешением $\Delta t/t \sim 8\%$ счет на канал составляет примерно 3200 имп/час в пике заторможенного вращения и 1300 имп/час в упругой части спектра при фоне 170 имп/час и 100 имп/час соответственно.

ESPECTRÓMETRO DE TIEMPO DE VUELO, PROVISTO DE UN FILTRO DELANTE DEL DETECTOR. En la memoria se describe un espectrómetro neutrónico de tiempo de vuelo dotado de un filtro montado delante del detector; el aparato se destina esencialmente a medir la dispersión incoherente de neutrones y se utiliza en combinación con un reactor de neutrones rápidos pulsados. Se examinan en detalle los espectros neutrónicos obtenidos con diferentes moderadores. El poder de resolución del aparato se calcula en función de sus principales parámetros; los valores así obtenidos concuerdan con los datos experimentales. En especial, el poder de resolución del espectrómetro en la parte inelástica del espectro asciende a $\Delta t/t \sim 4\%$. La velocidad de recuento de la instalación es bastante elevada: para una muestra de NH_4Cl (T = 90, 5°K) con una transmisión de 85% y un poder de resolución $\Delta t/t \sim 8\%$, alcanza a unos 3200 imp/h por canal en el pico de rotación restringida y a 1300 imp/h en la parte elástica del espectro, siendo la actividad de fondo 170 imp/h y 100 imp/h, respectivamente.

I. ВВЕДЕНИЕ

Исследование угловых и энергетических распределений медленных нейтронов, рассеянных газами, жидкостями и твердыми телами, позволяет получить подробную информацию о микродинамике и структуре рассеивающих систем. Для проведения этих исследований используются разнообразные экспериментальные установки, среди которых выделяются работающие с пульсирующими пучками нейтронов, так как они позволяют одновременно вести анализ в широких пределах углов и энергий.

Применение в установках последнего типа импульсных источников нейтронов вместо механических прерывателей упрощает их конструкцию и дает возможность более эффективного использования нейтронов. В данной работе описывается нейтронный спектрометр, созданный на основе импульсного быстрого реактора (ИБРа) ОИЯИ в Дубне [17] и работающий по времени пролета в условиях так называемой обратной геометрии (метод фильтра перед детектором).

В обратной геометрии, впервые использованной в работах [2—4], измеряется энергия ϵ, передаваемая нейтронами образцу в процессе рассеяния, т.е. $\epsilon = E_0 - E'$. Энергия нейтронов после рассеяния E' определяется полосой пропускания фильтра, помещенного перед детектором. Начальная энергия нейтронов E_0, определяемая в работающих при реакторах постоянной мощности спектрометрах путем отражения от монокристаллов, в описываемой установке находится по времени пролета базы от замедлителя до детектора.

II. ОПИСАНИЕ УСТАНОВКИ

Расположение основных элементов аппаратуры представлено схематически на рис.1. Быстрые нейтроны, рождающиеся в активной зоне (1) реактора (ИБРа), попадают на замедлитель (2), установленный на расстоянии ≈ 40 мм от отражателя. Нейтроны, вышедшие из замедлителя, проходя через канал в защитной стене зала реактора, вакуумный нейтроновод (3), коллимирующее устройство (4), рассеиваются на образце (5), установленном в разрыве нейтроновода на расстоянии 20 или 30 м от активной зоны реактора. Угловая расходимость пучка нейтронов, падающего на образец, составляет $\pm 0{,}5°$.

Рядом с образцом под определенным углом ϕ относительно оси падающего пучка помещается криостат с фильтром (6), охлаждаемым до температуры жидкого азота. Фильтр размерами $20 \times 20 \times 24$ см^3 собран из кубиков бериллия (либо BeO или C), разделенных через 4 см вертикальными пластинами из кадмия толщиной 0,5 мм для коллимации пучка и уменьшения переноса нейтронов путем диффузии.

Нейтроны, рассеянные на образце, после фильтрации регистрируются сцинтилляционным детектором (7), расположенным непосредственно за криостатом. Детектор площадью 300 см^2 изготовлен на основе светосостава Т-1 [$ZnS(Ag) + B_2^{10}O_3$] [5]. Толщина слоя светосостава 1,5 мм, поверхностная плотность ≈ 150 мг/см^2. Зависимость эффективности детектора от энергии представлена на рис.2. В области энергии 140—50 мэв эффек-

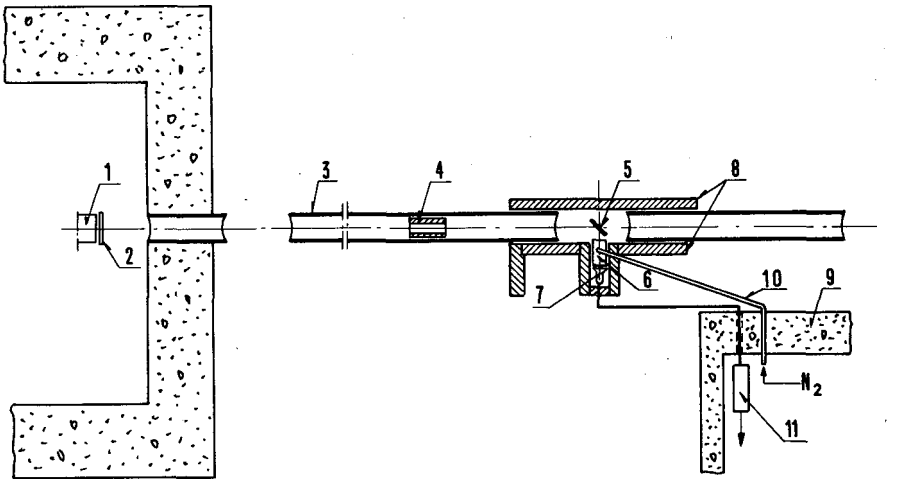

Рис.1

Схема установки:

1 – активная зона;
2 – замедлитель;
3 – вакуумный нейтроновод;
4 – коллиматор;
5 – образец;
6 – фильтр;
7 – детектор;
8 – защита;
9 – защита;
10 – трубка охлаждения;
11 – электронная аппаратура.

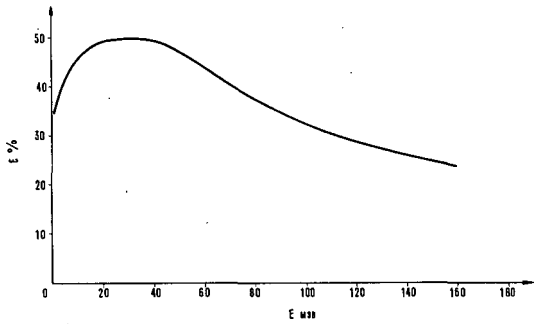

Рис.2

Эффективность детектора.

тивность меняется приблизительно по закону $1/V$. Максимум эффективности (около 50%) достигается в области энергий 40—20 мэв, а далее эффективность постепенно спадает до 35% при энергии 2 мэв. Уменьшение эффективности в области малых энергий объясняется поглощением сцинтиллятором световых вспышек, созданных в передних слоях светосостава. Во избежание перегрузки фотоумножителя и электронной аппаратуры во время импульса мощности реактора применяется блокировка фотоумножителя импульсом прямоугольной формы. Запирающий импульс с амплиту-

дой ≈ 250 в и длительностью 0,5—3 миллисек подается на первое фокусирующее кольцо фотоумножителя. Нормальный режим работы электронной аппаратуры после запирающего импульса восстанавливается в течение 300—500 мксек. Импульсы детектора после формирования и усиления поступают на многоканальный временной анализатор (256—2048 каналов) для анализа по времени пролета.

Криостат вместе с детектором может перемещаться, допуская изменение угла рассеяния в пределах 30° —120°; разброс угла рассеяния составляет ±7°. Расстояние образец—детектор может составлять 40—70 см в зависимости от используемого криостата. Для измерения спектра нейтронов, падающих на образец, в прямом пучке вместо образца устанавливался тонкий счетчик BF_3.

Для снижения фона стены нейтроновода выложены листами кадмия; криостат, детектор и разрыв нейтроновода окружены защитой из кадмия и смеси парафина с карбидом бора (8 на рис.1).

III. ХАРАКТЕРИСТИКИ СПЕКТРОМЕТРА

1. Импульсный источник нейтронов

Импульсный быстрый реактор генерирует быстрые нейтроны импульсами приблизительно гауссовой формы с частотой повторения 2—8 имп/сек. Ширина этих импульсов на половине высоты равна 36 мксек. Средняя интенсивность нейтронов при мощности 1 квт составляет $4{,}5 \cdot 10^{13}$ нейтр/сек. Начиная с 1964 года, реактор работает на мощности 3 квт. Тепловые нейтроны получаются замедлением быстрых.

Для подбора условий эксперимента было проведено сравнение различных замедлителей с точки зрения среднего времени жизни нейтронов и их выхода. Выход нейтронов определялся с помощью тонкого счетчика BF_3, помещенного на пролетном расстоянии 30 м. Время жизни определялось по наклону переднего фронта спектра нейтронов, профильтрованных слоем Be толщиной 16 см. Форма бериллиевой границы довольно хорошо описывается формулой:

$$N(T)dT = \left(\frac{T_0}{T}\right)^5 - \exp\left(-\frac{T - T_0}{\tau}\right), \qquad (1)$$

где T_0 — время пролета, соответствующее началу крутого подъема бериллиевой границы;

τ — время жизни нейтронов.

Результаты измерений представлены на рис.3 и в таблице. В таблице приводятся также значения параметра I/t^2 (где I — скорость счета на канал; $t = \tau +$ ширина вспышки быстрых нейтронов), определяющего скорость счета при измерениях по времени пролета с заданным энергетическим разрешением.

Из приведенных результатов следует, что лучшими характеристиками в области холодных нейтронов обладают охлажденные замедлители дырочный и с бериллиевым отражателем. В области тепловых нейтронов наи-

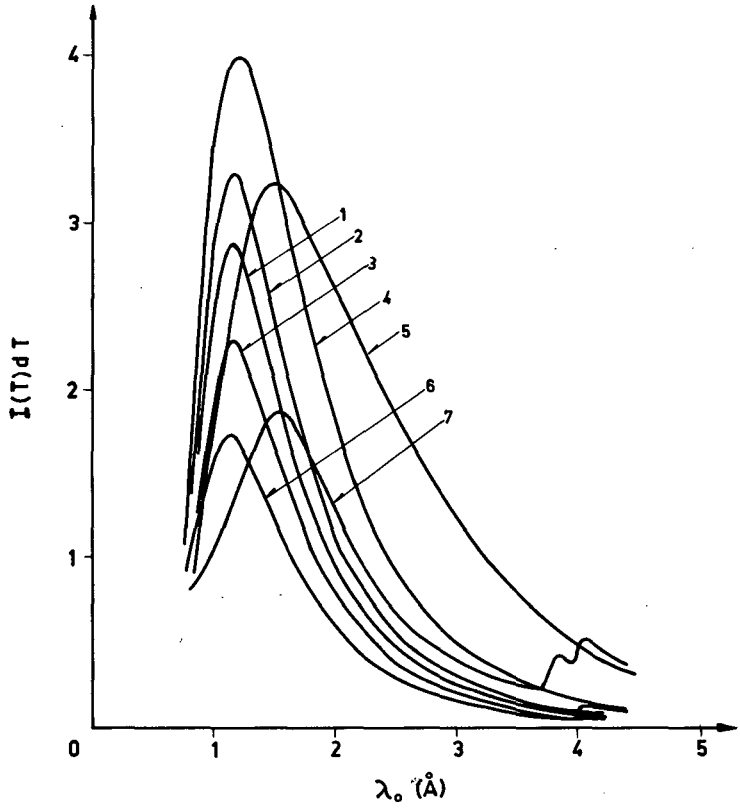

Рис.3

Выход нейтронов из разных замедлителей:

1 – 36 мм воды (T ≈ 300° K); 4 – дырочный замедлитель (T ≈ 300° K);
2 – 56 мм воды (T ≈ 300° K); 5 – дырочный замедлитель (T ≈ 90° K);
3 – 36 мм спирта (T ≈ 300° K); 6 – спирт + Be (T ≈ 300° K);
7 – спирт + Be (T ≈ 90° K).

больший выход дает дырочный замедлитель при комнатной температуре, а по величине параметра I/t^2 лучшим является водяной замедлитель толщиной 36 мм.

2. Бериллиевый фильтр

На рис.4 представлен спектр нейтронов, пропущенных сквозь фильтр (толщиной 24 см) из бериллия, охлажденного до температуры жидкого азота и помещенного непосредственно перед детектором т.е. в рабочем положении).

Пропускание фильтра $\Phi(E')$ в области энергий $E' < E_{гр} = 5{,}2$ мэв показано на рис.5. При энергии $E' > E_{гр}$ среднее пропускание составляет примерно $5 \cdot 10^{-5}$. Это приводит к ошибке в измерении сечения неупругого рассеяния нейтронов порядка $5 \cdot 10^{-5} \sigma_{упр}$, где $\sigma_{упр}$ – сечение упругого рассеяния нейтрона энергии E'. Обычно эта ошибка пренебрежимо мала по сравнению с сечением неупругого рассеяния в интервале энергий 0–5,2 мэв.

Таблица

ВРЕМЕНА ЖИЗНИ НЕЙТРОНОВ И ОТНОСИТЕЛЬНЫЕ ИНТЕНСИВНОСТИ НЕЙТРОНОВ РАЗЛИЧНЫХ ЭНЕРГИЙ ДЛЯ РАЗЛИЧНЫХ ЗАМЕДЛИТЕЛЕЙ

Замедлитель	вода 36 мм	вода 56 мм	спирт 36 мм	дырочный*	дырочный*	спирт** +Be	спирт** +Be
Температура	комн.	комн.	комн.	комн.	азот.	комн.	азот.
τ мксек	60	85	65	115	125	120	130
$\frac{I}{I_{36\,H_2O}}$ 5 мэв	1	1,2	0,8	2,3	6,9	1,7	7,6
$\frac{I}{I_{36\,H_2O}}$ 25 мэв	1	1,15	0,85	1,9	2,1	0,61	1,07
$\frac{I}{I_{36\,H_2O}}$ 50 мэв	1	1,15	0,85	1,75	1,2	0,60	0,69
$\frac{I}{(\tau+36)^2}$ 5 мэв	1	0,73	0,76	0,94	2,46	0,65	2,55
$\frac{I}{(\tau+36)^2}$ 25 мэв	1	0,77	0,73	0,77	0,75	0,23	0,35
$\frac{I}{(\tau+36)^2}$ 50 мэв	1	0,77	0,73	0,71	0,43	0,22	0,23

* Дырочный замедлитель – 36 мм спирта + 60 мм плексигласа с дырками ($\phi = 5$ мм), занимающими ≈ 50% площади замедлителя.

** Замедлитель из 36 мм спирта + 80 мм Be.

3. *Расчет разрешающей способности установки*

Нейтроны с энергией E_0, покидающие замедлитель в момент времени t, попадают на образец в момент $T_1 = t + \frac{\alpha L_1}{\sqrt{E_0}}$, где L_1 – длина пролетной базы замедлитель–образец. Потеряв при рассеянии на образце энергию $\epsilon = E_0 - E'$, такую, что $E' \leq E_{гр}$, нейтроны достигают детектора в момент

$$T = t + \frac{\alpha L_1}{\sqrt{E_0}} + \frac{\alpha L_2}{\sqrt{E'}} \qquad (2)$$

(L_2 – расстояние образец–детектор).

При фиксированной величине передаваемой энергии ϵ время регистрации нейтронов T испытывает некоторый разброс связанный в основном с неопределенностью времени выхода нейтронов из замедлителя (Δt), разбросом времени пролета рассеянными нейтронами базы

$$L_2\left[\Delta\left(\frac{\alpha L_2}{\sqrt{E'}}\right)\right],$$

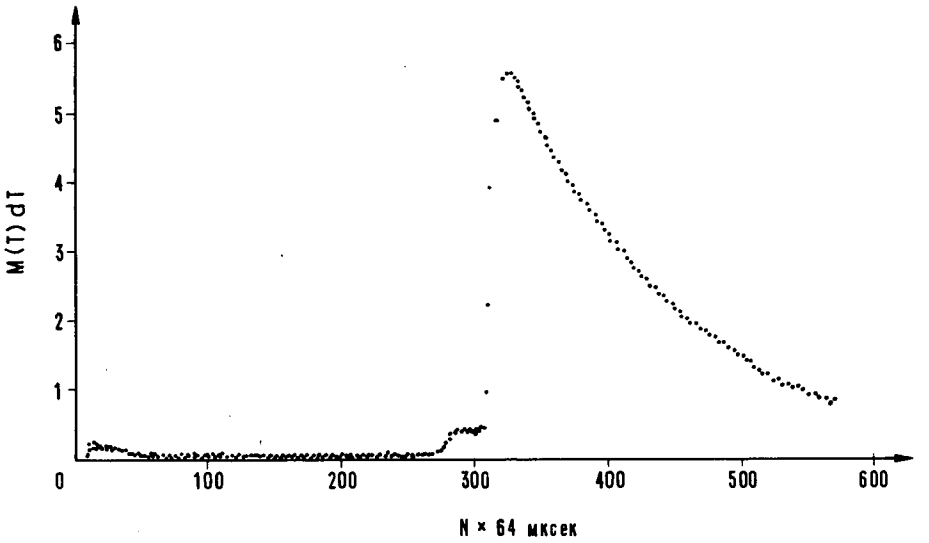

Рис.4

Спектр нейтронов, профильтрованных бериллиевым фильтром.

связанным с их немоноэнергетичностью, и соответствующим разбросом времени пролета базы первичным нейтроном

$$\left(\Delta \frac{\alpha L_1}{\sqrt{\epsilon + E'}}\right).$$

Функция распределения времени регистрации T в довольно хорошем приближении может быть записана в виде:

$$N(T)dT = dT\int_0^\infty dE_0 \int_0^\infty dE' \int_{-\infty}^{\infty} dt\rho(t)n(E_0)\Phi(E')\sigma(E_0, E', \phi)\delta\left(T - \frac{\alpha L_1}{\sqrt{E_0}} - \frac{\alpha L_2}{\sqrt{E'}} - t\right), \quad (3)$$

где $\rho(t)$ и $n(E_0)$ – соответственно временное и энергетическое распределения нейтронов, выходящих из замедлителя;

$\Phi(E')$ – эффективное пропускание фильтра (рис.5);

$\sigma(E_0, E', \phi)$ – дважды дифференциальное сечение рассеяния нейтронов на образце;

$\delta\left(T - \frac{\alpha L_1}{\sqrt{E_0}} - \frac{\alpha L_2}{\sqrt{E'}} - T\right)$ – условие регистрации нейтронов в момент T.

В выражении (3) не учитываются малые в данной установке разбросы времени регистрации, связанные с неопределенностями баз L_1 и L_2 и с конечной шириной канала временного анализатора.

При расчете разрешающей способности предполагается, что образец рассеивает нейтроны только некогерентно и его спектр частот имеет осо-

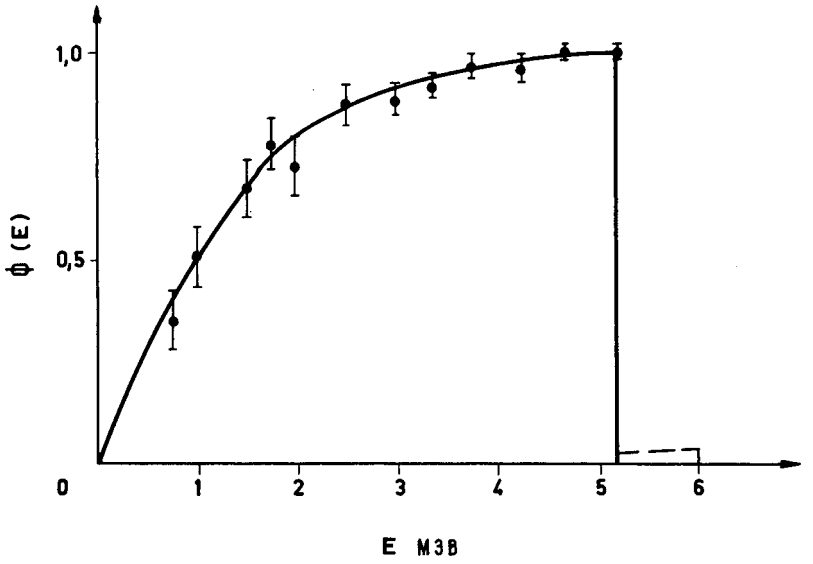

Рис.5

Пропускание бериллиевого фильтра.

бенность при энергии ϵ, заключающуюся в том, что $g(\omega) = \delta(\omega - \epsilon)$. Сечение $\sigma(E, E', \phi)$ бралось в однофононном приближении. Распределение $\rho(t)$ принималось в форме $\rho(t) = 0$ при $t < 0$ и $\rho(t) = e^{-\frac{t}{\tau}}$ при $t > 0$, т.е. ширина вспышки быстрых нейтронов и разброс времен замедления не принимались во внимание. Ошибка, вносимая этими допущениями, мала, пока среднее время жизни теплового нейтрона в замедлителе $\tau >$ длительности вспышки реактора. Спектр нейтронов $n(E_0)$ брался в соответствии с данными измерений (рис. 6)в форме максвелловского распределения с $kT'_{Максв} = 29{,}5$ мэв, исправленного на рассеяние нейтронов 9 метрами воздуха на пути пучка.

На рис.7 представлены вычисленные функции распределения времени регистрации для различных ϵ для установки с бериллиевым фильтром и параметрами $L_1 = 20$ м, $L_2 = 0{,}73$ м, $\tau = 120$ мксек (условия, соответствующие проведенному исследованию). Характерной чертой кривых является их сильная асимметрия с крутым передним фронтом. В некоторых случаях для определения величины передачи энергии и ее дисперсии можно пользоваться положением переднего края и изменением его наклона. Разрешающая способность в этом случае есть величина порядка $(\Delta T/T) \approx (\tau/T_K)$, где T_K – положение переднего края.

Если использование переднего фронта невозможно, мерой разрешающей способности является относительная полуширина кривых распределения, т.е.

$$\frac{\Delta T}{T} \approx \frac{(\Delta T)_{\frac{1}{2}}}{T_{макс}},$$

где $(\Delta T)_{\frac{1}{2}}$ – ширина на половине высоты, $T_{макс}$ – положение максимума кривой $N(T)$. Среднее значение ϵ можно определить из формулы (2), под-

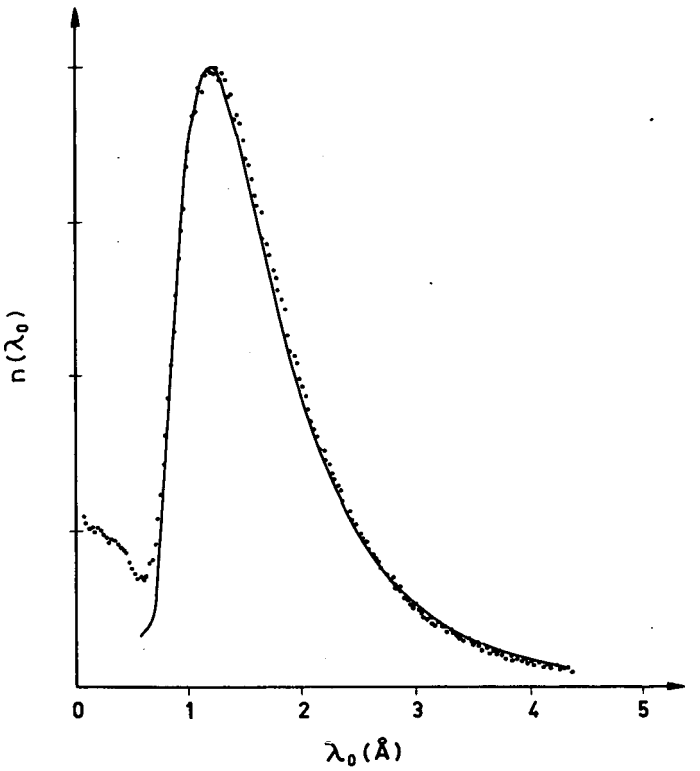

Рис.6

Спектр нейтронов $n(\lambda_0)$, падающих на образец в функции длины волны нейтронов λ_0. Сравнение максвелловского распределения с $T_{Максв} = 29{,}5$ мэв с экспериментальными данными.

ставляя вместо t $\bar{\tau}$ – среднее время жизни нейтронов в замедлителе и вместо E' $\bar{E}'$ – среднее значение энергии регистрируемых нейтронов. Зависимость относительной полуширины от параметров L_1, L_2, τ представлена на рис.8. Кривые с $L_1 = 0{,}01$ м даны для сравнения разрешающей способности описываемого спектрометра со спектрометрами, работающими на реакторах постоянной мощности в условиях $(\Delta\lambda_0/\lambda_0) \approx (\tau/T)$ (λ_0 – длина волны падающих нейтронов). При постоянных L_1 и пропускании фильтра разрешение улучшается с уменьшением параметров L_2 и τ, которые не могут быть выбраны очень малыми. Длительность импульса тепловых нейтронов τ даже в крайнем случае сильно отравленного замедлителя определяется шириной импульса быстрых нейтронов и временем замедления (в сумме 50 мксек). Расстояние L_2 задается поперечными размерами пучка падающих нейтронов и минимальной длиной фильтра, необходимой для обеспечения хорошей фильтрации ($\ell > 15-20$ см).

При расстоянии $L_2 > 40$ см фильтры с низкоэнергетической границей (например, графит) дают по сравнению с бериллием выигрыш в разрешении 50% только в области малых и средних значений ϵ (до ≈ 60 мэв); при больших ϵ разрешение ограничивается разбросом времени пролета расстояния

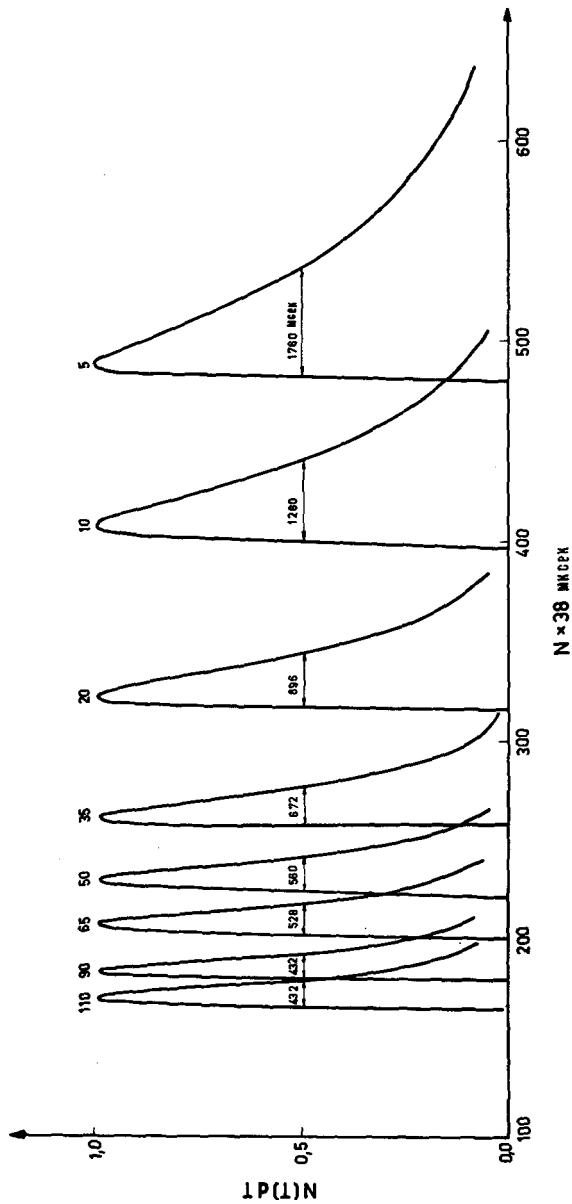

Рис. 7

Форма кривых разрешения.

$L_1 = 20$ м; $L_2 = 0{,}73$ м; $\tau = 120$ мксек, Be.

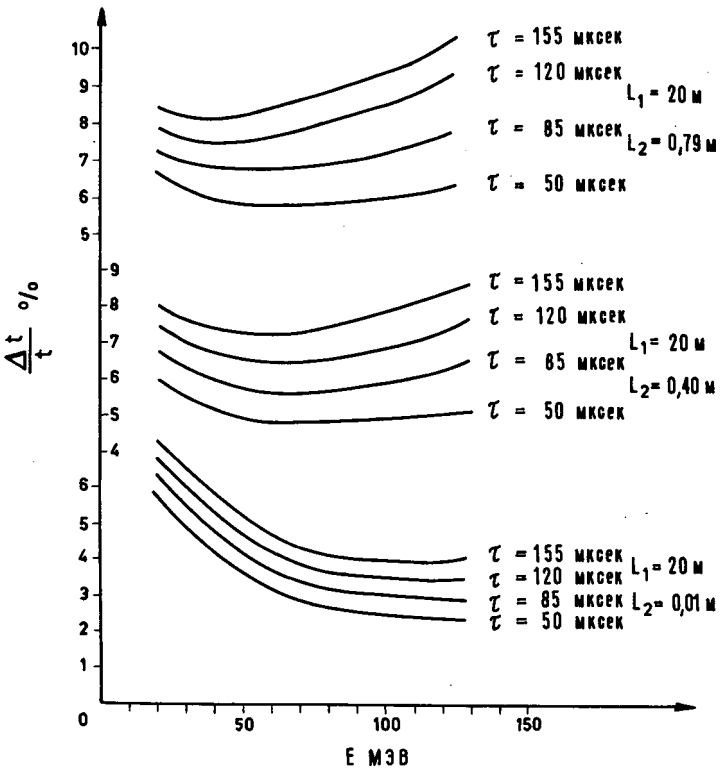

Рис.8

Зависимость относительной полуширины от параметров L_1, L_2, τ:

а) Зависимость ширины кривых разрешения от энергии передачи ϵ для $L_1 = 20$ м.

L_2, возрастающим при уменьшении E'. Поэтому значительно лучше использовать двойной фильтр Be—BeO, например, по схеме рис.9, имеющий примерно такую же ширину пропускания, как и графит, но более высокую среднюю энергию. Применение двойного фильтра может улучшить разрешающую способность установки в $\approx 2{,}2$ раза по сравнению с ее разрешающей способностью при использовании бериллиевого фильтра.

4. *Экспериментальные данные об интенсивности, фоне и разрешающей способности спектрометра*

На рис.10 и 11 представлены нейтронные спектры, полученные на данной установке с образцами H_2O и NH_4Cl. Для перехода от нейтронных интенсивностей к сечениям необходимо кривые рис.10 и 11 нормировать к падающему спектру нейтронов (рис.6), который, как уже отмечалось, измеряется с помощью борного счетчика, помещенного в позиции образца.

В случае NH_4Cl использовался порошкообразный образец размером 18×24 см^2 с пропусканием около 85%, помещенный в алюминиевую кассету со стенками толщиной 0,5 мм; применялся неохлаждаемый дырочный за-

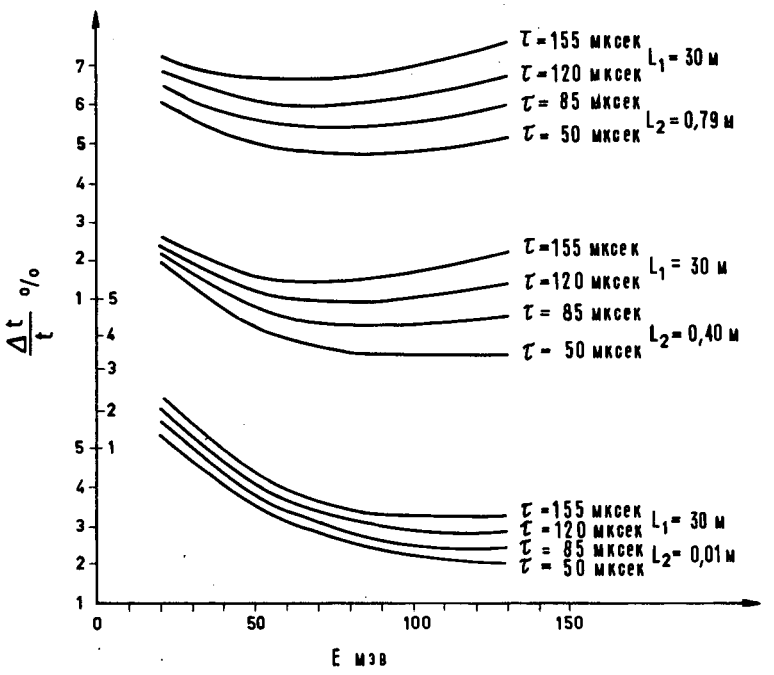

Рис.8

Зависимость относительной полуширины от параметров L_1, L_2, τ:

б) Зависимость ширины кривых разрешения от энергии передачи ϵ для $L_1 = 30$ м.

медлитель; реактор работал на мощности 2,5 квт. Как видно, скорость счета довольно значительна — 3200 и 1300 отсчетов/час в максимумах неупругого рассеяния соответственно. При необходимости скорость счета в низкоэнергетической части спектра можно увеличить в 3 раза путем охлаждения замедлителя (см. таблицу). Уровень фона, измерявшегося с пустой кассетой, изменялся в области от 3 мэв до 90 мэв со 100 до 170 отсчетов/час, т.е. составлял 5—7% от эффекта. Низкий фон является одним из важных преимуществ импульсного режима работы реактора. Острые пики на рис.11 соответствуют однофононному рассеянию нейтронов с возбуждением торсионных колебаний группы NH_4.

На рис.12 приведено сравнение измеренной формы пика (NH_4Cl; $\epsilon = 48{,}5$ мэв, $T' = 91°$ K) с рассчитанной по формуле (3). Полученное согласие свидетельствует о довольно узкой истинной ширине этого пика и о возможности применения принятых приближений к определению разрешающей способности установки.

IV. ЗАКЛЮЧЕНИЕ

Описанная установка обладает удовлетворительными характеристиками в отношении разрешающей способности, интенсивности и отношения эффект—фон при исследовании процессов упругого или квазиупругого рас-

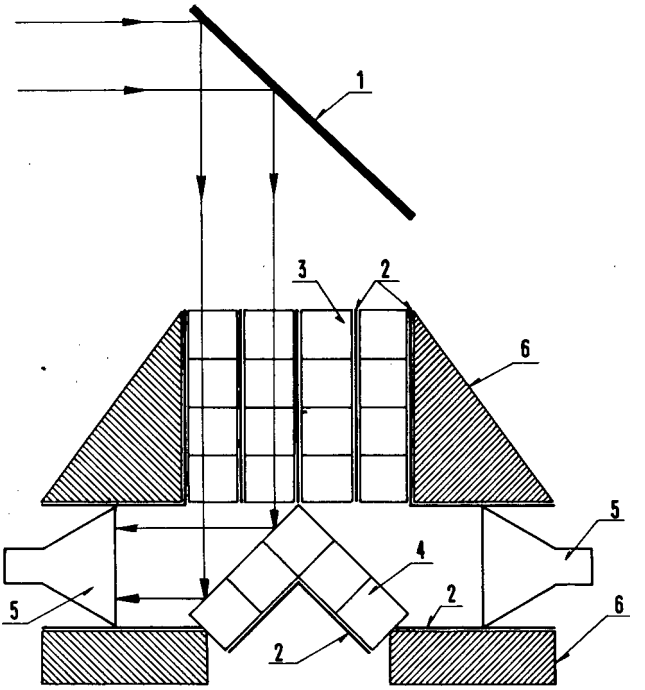

Рис.9

Схема двойного фильтра.

1 – образец,
2 – кадмий,
3 – бериллий,
4 – окись бериллия,
5 – детектор,
6 – защита.

сеяния холодных нейтронов и неупругого рассеяния нейтронов с передачей энергии до ≈130 мэв. В дальнейшем параметры установки могут быть улучшены путем одновременного измерения рассеяния на несколько углов, расширения диапазона углов, улучшения разрешения за счет сокращения времени жизни нейтрона в замедлителе и тому подобных мер.

Авторы благодарят коллектив Лаборатории нейтронной физики за помощь в проведении работы, а также Т. Залесского за разработку электроники детектора и профессора Е. Яника за полезные обсуждения.

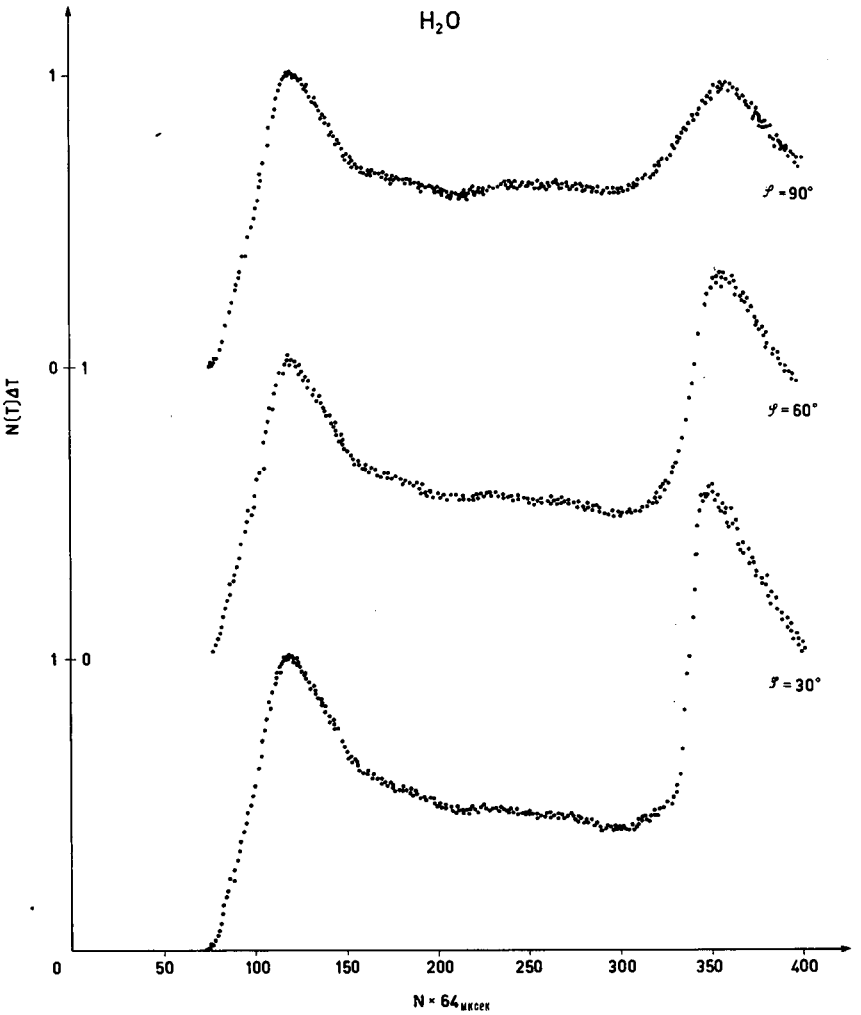

Рис.10

Спектр нейтронов, рассеянных на воде при комнатной температуре.

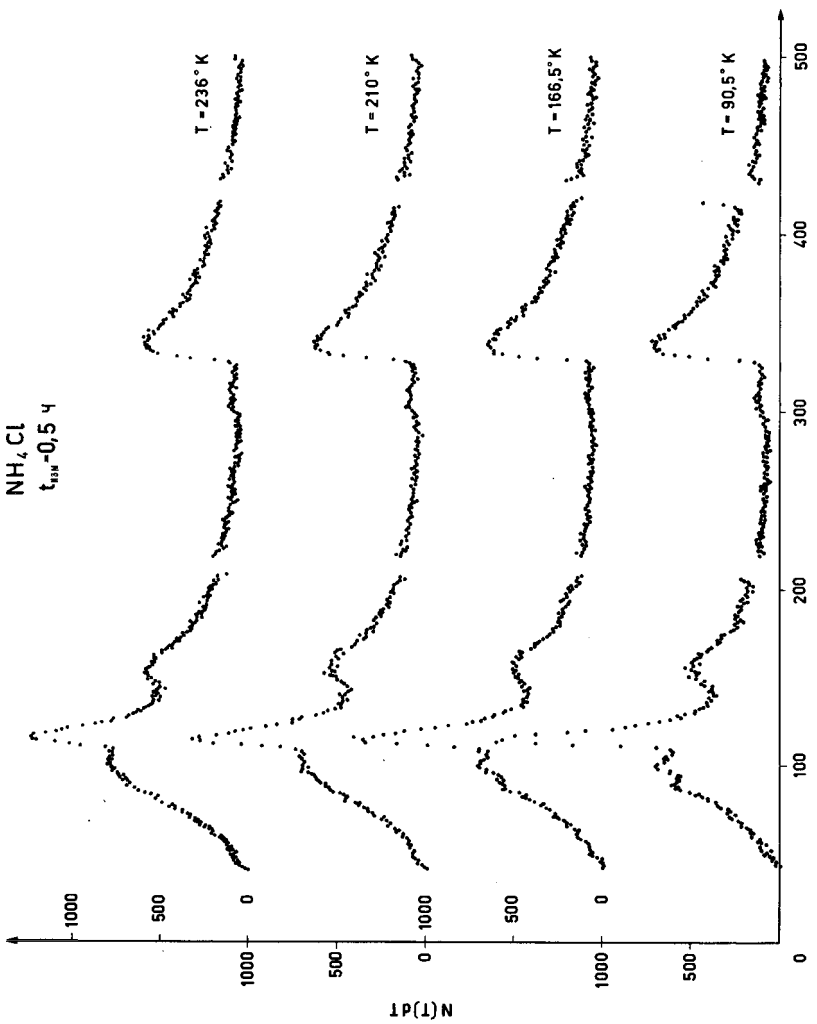

Рис. 11

Спектр нейтронов, рассеянных поликристаллическим NH_4Cl.

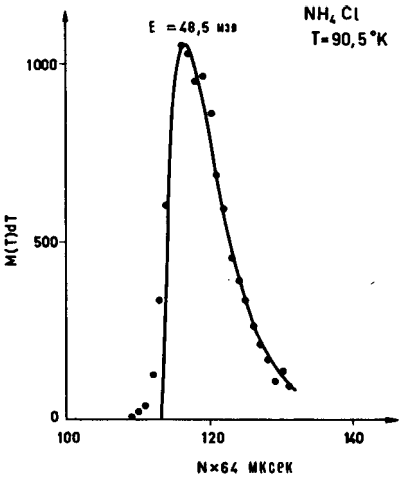

Рис.12

Сравнение рассчитанной формы кривой разрешения с формой измеренного пика при $\epsilon = 48{,}5$ мэв для NH_4Cl.

ЛИТЕРАТУРА

[1] БЛОХИН Г.Е. и др. "Атомная энергия", 10 (1961) 437.
[2] WOODS A.D.B., BROCKHOUSE B.N., SAKOMATA M., SINCLAIR R.N., Inelastic Scattering of Neutrons in Solids and Liquids. Proc. I.A.E.A. Vienna, 1961, p.487.
[3] STILLER H.H., DANNER H.R., Inelastic Scattering of Neutrons in Solids and Liquids. Proc. I.A.E.A. Vienna, 1961, p.363.
[4] МАЧЕХИНА Т.А., ОГЖЕВАЛЬСКИЙ З.И., ШАПИРО Ф.Л., Матриалы рабочего совещания по физике медленных нейтронов, 956, Дубна, 1962, 180.
[5] ГОЛИКОВ В.В., ШИМЧАК Г.Ф., ШКАТУЛА А.А., ПТЭ, 2, 59 (1963).

DISCUSSION

W. GLÄSER: Has there been any idea of using a chopper in phase with the pulse of the IBR (Dubna) reactor in order to get a shorter and perhaps more symmetrical thermal neutron pulse?

K. PARLINSKI: There is a mechanical interrupter in phase with the neutron pulse of the reactor in one of the reactor beams. This installation is described in the Proceedings of the IAEA Symposium on the Inelastic Scattering of Neutrons in Solids and Liquids*. The width of the thermal neutron pulse can be reduced by poisoning the moderator with boron.

R.E. SCHMUNK: I would like to ask Dr. Egelstaff how the method just described compares with that used by Dr. Webb with the RPI (Rensselaer Polytechnic Institute, Troy, N.Y.) linear accelerator?

---

* БОНДАРЕНКО И.И., ЛИФОРОВ В.Г., НИКОЛАЕВ М.Н., ОРЛОВ В.В., ПАРФЕНОВ В.А., СЕМЕНОВ В.А., СМИРНОВ В.И. и ТУРЧИН В.Ф., "ДВОЙНОЙ СПЕКТРОМЕТР МЕДЛЕННЫХ НЕЙТРОНОВ НА РЕАКТОРЕ ИБР", Inelastic Scattering of Neutrons in Solids and Liquids I IAEA, Vienna (1963) 127-37.

P. EGELSTAFF: Dr. F. J. Webb of our Laboratory worked at the linear accelerator of the RPI for a year on a similar experiment. However he was mainly interested in 0.1 - 1 eV neutron-energy transfers. The neutron burst was about 5μs, the incident path was 10 m and the scattered path 0.5 m. He used the BeO - Be filter-difference, by having two sets of detectors 180° apart and each at 90° to the beam. The detectors were alternated but the filters were cooled and fixed in position. Results were obtained on Zr and Ti hydrides in this range and the 1-, 2- and 3-phonon levels were clearly seen, while the fourth and higher levels were too broad to be observed.

DYNAMICS OF LIQUIDS AND SOLIDS BY OPTICAL SPECTROSCOPY

R. S. KRISHNAN
INDIAN INSTITUTE OF SCIENCE,
BANGALORE, INDIA

Abstract — Résumé — Аннотация — Resumen

DYNAMICS OF LIQUIDS AND SOLIDS BY OPTICAL SPECTROSCOPY. When a beam of monochromatic light traverses any medium, be it a liquid or a crystal, a portion of the radiation is scattered. This scattering of light arises from two distinct processes. One is the thermal scattering of light and the other is Raman effect. The former involves an interaction of the radiation with the optical stratifications in the medium associated with the thermally excited phonons of the acoustic type. The latter, on the other hand, arises from an interaction of the vibrations of the atoms and molecules of the medium with the radiation and is therefore closely linked with its optical vibration spectrum.

The theory of thermal scattering by Leon Brillouin (1922) ascribes the diffusion of light to the equispaced time periodic stratifications of density in the medium characteristic of acoustic waves and evisages a Doppler shift of frequency. The experimental observation of well-defined Doppler components in the interferograms of light scattered by liquids and amorphous solids is therefore of fundamental importance in understanding the mechanism of light scattering and the structure of liquids. The presence of such fine structure in the scattered light of liquids was established unequivocally in this laboratory by Rao, Venkateswaran and Sunanda Bai. An important outcome of their studies is the observation of a strong dependence of the intensity of the central component, the continuum and the Brillouin components on the viscosity of the medium and the inadequacy of Landau-Placzek theory. The results of their studies and those of Gross, Meyer, Ramm, Rank and co-workers are briefly discussed. The only case of an amorphous substance in which the Brillouin components have been successfully recorded by the author is fused silica.

A precise study of the second-order Raman spectra of alkali halides has great significance in view of the conflicting theories of vibration spectra of crystals due to Raman and Born. Hence with the powerful Rasetti technique the author initiated a systematic investigation of the Raman spectra of alkali halides and other simple crystals, such as diamond and alumina. The available data on the spectra of these crystals cannot be fully explained by Raman's theory based on the atomistic standpoint and according to which the observed spectrum is due to the finite number of allowed combinations and overtones of the discrete vibrations of the supercell. On the other hand, the occurrence of only a finite and relatively sharp maxima in the Raman spectra of alkali halides, which cannot be explained if the frequency distribution in each branch has only broad maxima in the Born's picture, has led to the concept of the critical points by Van Hove and their activity in optical processes has been worked out by Birman and Loudon. The experimental results in the case of the alkali halides will be discussed in the light of these theories and the Lyddane-Sachs-Teller relation.

ÉTUDE DE LA DYNAMIQUE DES LIQUIDES ET SOLIDES PAR LES MÉTHODES DE SPECTROMÉTRIE OPTIQUE. Lorsqu'un faisceau de lumière monochromatique traverse un milieu liquide ou cristallin, une fraction du rayonnement est diffusée. Cette diffusion est due à deux phénomènes distincts: la diffusion thermique et l'effet Raman. La diffusion optique implique une interaction du rayonnement et des stratifications optiques du milieu, associée aux phonons thermiquement excités du type acoustique. L'effet Raman provient d'une interaction des vibrations des atomes et molécules du milieu et du rayonnement; il est donc étroitement lié à son spectre de vibrations optiques.

La théorie de la diffusion thermique établie par Léon Brillouin (1922) attribue cette diffusion de la lumière aux stratifications périodiques équidistantes de la densité dans le milieu, qui sont caractéristiques des ondes acoustiques; elle envisage l'existence d'un déplacement de fréquence du type Doppler. L'observation expérimentale de composantes Doppler bien définies dans les interférogrammes de lumière diffusée par des liquides ou des solides amorphes est donc d'une importance fondamentale pour comprendre le mécanisme de la diffusion de la lumière et la structure des liquides. L'existence de cette structure fine dans la lumière diffusée par des liquides a été clairement démontrée dans le laboratoire de Bangalore par Rao, Venkateswaran

et Sunanda Bai. Leurs travaux ont notamment permis de constater que l'intensité de la composante centrale, le spectre continu et les composantes de Brillouin dépendaient étroitement de la viscosité du milieu et que la théorie de Landau-Placzek était insuffisante. Les renseignements fournis par ces études et celles de Gross, Meyer, Ramm, Rank et leurs collaborateurs font l'objet d'un bref examen critique. La silice fondue constitue l'unique substance amorphe dans laquelle l'auteur a pu nettement observer les composantes de Brillouin.

Une étude précise des spectres de Raman du deuxième ordre dans les halogénures alcalins revêt un grand intérêt, en raison des divergences entre les théories établies par Raman et par Born sur les spectres de vibrations des cristaux. Aussi l'auteur a-t-il fait appel à la méthode très efficace de Rasetti pour étudier systématiquement les spectres Raman relatifs aux halogénures alcalins et à d'autres cristaux simples tels que le diamant et l'alumine. Les données dont on dispose sur les spectres de ces cristaux ne peuvent pas être entièrement expliquées par la théorie de Raman dont la base est atomistique et selon laquelle le spectre observé serait dû au nombre fini de combinaisons et harmoniques possibles des vibrations discrètes de la supercellule. En revanche, l'existence d'un maximum fini et relativement accentué dans les spectres Raman des halogénures alcalins, qui ne saurait s'expliquer si la distribution des fréquences dans chaque branche ne présentait que des maxima larges comme dans la représentation du Born a conduit Van Hove à la notion de points critiques; le rôle de ces points dans les phénomènes optiques a été déterminé par Birman et Loudon. L'auteur discute les données expérimentales relatives aux halogénures alcalins en tenant compte de ces théories et de la relation de Lyddane-Sachs-Teller.

ИССЛЕДОВАНИЕ ДИНАМИКИ ЖИДКОСТЕЙ И ТВЕРДЫХ ТЕЛ С ПОМОЩЬЮ ОПТИЧЕСКОЙ СПЕКТРОСКОПИИ. При прохождении пучка монохроматического света через любую среду, будь то жидкость или кристалл, происходит его частичное рассеяние. Это рассеяние света объясняется двумя различными процессами. Одним из них является тепловое рассеяние света, а другим — рамановский эффект. Первый процесс связан с взаимодействием излучения с оптическими стратификациями в среде, связанными с возбужденными теплом фононами акустического типа. Второй же процесс объясняется взаимодействием колебаний атомов и молекул среды с излучением и поэтому тесно связан со спектром оптических колебаний.

Теория теплового рассеяния Леона Бриллуэна (1922 год) объясняет диффузию света периодическими стратификациями плотности в среде через равные промежутки времени, типичными для акустических волн, и предполагает допплеровское смещение частоты. Поэтому для понимания механизма рассеяния света и структуры жидкостей первостепенное значение имеет экспериментальное наблюдение совершенно определенных компонентов Допплера на интерферограммах света, рассеянного жидкостями и аморфными твердыми телами. Наличие такой тонкой структуры в рассеянном жидкостями свете было точно установлено в данной лаборатории Рао, Венкатесвараном и Баем. Важным результатом их исследований явилось обнаружение сильной зависимости интенсивности центрального компонента, непрерывного компонента и компонента Бриллуэна от вязкости среды, а также недостаточности теории Ландау-Плачека. Кратко рассматриваются результаты их исследований, а также исследований Гросса, Мейера, Рамма, Ранка и их коллег. Единственным аморфным веществом, в котором авторы смогли успешно зарегистрировать компоненты Бриллуэна, является расплавленная двуокись кремния.

Ввиду расхождения теорий колебательных спектров кристаллов, сформулированных Раманом и Борном, точное изучение рамановских спектров второго порядка для щелочных галоидов имело огромное значение. Поэтому с помощью эффективного метода Разетти автор начал систематическое изучение рамановских спектров щелочных галоидов и других простых кристаллов, например алмаза и глинозема. Имеющиеся данные по спектрам этих кристаллов не могут быть полностью объяснены с позиций теории Рамана, в основе которой лежит атомистическая концепция и согласно которой наблюдаемый спектр объясняется ограниченным числом разрешенных комбинаций и обертонов дискретных колебаний сверхячейки. С другой стороны, наличие только ограниченного числа и относительно резких максимумов в рамановских спектрах щелочных галоидов, которые не могут быть объяснены, если распределение частот в каждой ветви имеет только широкие максимумы в картине Борна, позволило сформулировать концепцию о критических точках Ван-Гове. Вопрос о их роли в оптических процессах был разработан Бирманом и Лоудоном. Экспериментальные результаты для щелочных галоидов будут рассмотрены в свете этих теорий и отношения Лиддана-Сахса-Теллера.

ESTUDIO DE LA DINÁMICA DE LOS LÍQUIDOS Y DE LOS SÓLIDOS POR ESPECTROSCOPIA ÓPTICA. Cuando un haz de luz monocromática atraviesa un medio líquido o cristalino, una parte de la radiación sufre una dispersión originada por dos procesos distintos: uno que consiste en la dispersión térmica de la luz y el otro

en el efecto Raman. El primero implica una interacción de la radiación con las estratificaciones ópticas del medio asociadas a los fonones de tipo acústico térmicamente excitados. El segundo, en cambio, tiene su origen en la interacción de las vibraciones de los átomos y moléculas del medio con la radiación y está, por lo tanto, estrechamente vinculado al espectro de vibraciones ópticas de dicho medio.

La teoría de la dispersión térmica, formulada por Léon Brilluoin en 1922 atribuye la difusión de la luz a las estratificaciones periódicas equidistantes de la densidad del medio, características de las ondas acústicas, y admite el desplazamiento de la frecuencia según el efecto Doppler. La observación experimental de componentes Doppler bien definidos en los interferogramas de luz dispersa por líquidos y sólidos amorfos es, pues, de fundamental importancia para conocer el mecanismo de dispersión de la luz y la estructura de los líquidos. La existencia de esta estructura fina en la luz dispersa por líquidos ha sido demostrada inequívocamente en este laboratorio por Rao, Venkateswaran y Sunanda Bai. Un resultado importante de esos estudios es la observación de una marcada influencia de la viscosidad del medio sobre la intensidad del componente central del continuo y de los componentes de Brillouin, así como las limitaciones de la teoría de Landau-Placzek. Se comparan brevemente los resultados de tales estudios con los de los efectuados por Gross, Meyer, Ramm, Rank y colaboradores. El único caso de sustancia amorfa en el que el autor ha logrado registrar los componentes de Brillouin es el de la sílice fundida.

El estudio minucioso de los espectros Raman de segundo orden de los haluros alcalinos tiene gran importancia en vista de las teorías contradictorias sobre los espectros de vibración de sustancias cristalinas, formuladas por Raman y Born. Por tanto, aplicando el útil procedimiento de Rasetti, el autor ha emprendido una investigación sistemática de los espectros Raman de los haluros alcalinos y de otros cristales simples, como el diamante y la alúmina. Los datos existentes sobre los espectros de estos cristales no pueden explicarse enteramente por la teoría atomística de Raman, según la cual el espectro observado se debe al número finito de combinaciones y armónicos superiores admisibles de las vibraciones discretas de la supercelda. En cambio, la existencia de sólo un máximo finito y relativamente acusado en el espectro Raman de los haluros alcalinos, que no puede explicarse si la distribución de frecuencias de cada rama presenta únicamente máximos aplanados conforme a la teoría de Born, ha dado origen al concepto de los puntos críticos de Van Hove, cuya actividad en los procesos ópticos ha sido analizada por Birman y Loudon. Los resultados experimentales obtenidos en el caso de los haluros alcalinos se examinan a la luz de estas teorías y de la relación de Lyddane-Sachs-Teller.

The optical methods generally employed for the elucidation of the internal structure and the dynamics of liquids and solids are based on the scattering of light including Raman effect, infrared absorption, luminescence and ultraviolet absorption. In the present survey I wish to confine myself to the information that can be obtained from the first and most important method, namely that based on the scattering of light.

The scattering of light observed in any medium is broadly of two different kinds. The first kind may be described as a scattering without change of frequency or unmodified scattering. Such a diffusion would necessarily arise if the structure of the medium presents static or quasi-static irregularities or imperfections. These are present in liquids, in amorphous substances and in certain types of crystals. The second kind of scattering is that which appears with a change of frequency and is ascribable to dynamic or time periodic variations in the structure of the medium. This again can be resolved into two distinct phenomena which differ both in their origin and their characteristics. We have in the first place the type of scattering recognized as the Raman effect. This exhibits frequency shifts identical with the characteristic infrared frequencies of the medium and arises by reason of the vibrations of atoms excited by the radiation traversing the crystal. The frequency shifts are sensibly independent of the frequency of the exciting radiation and of the angle of scattering and in the case of crystals they are independent of the crystal orientation with reference to the directions of

incidence and of scattering except in piezoelectric crystals. This aspect is dealt with further in the latter part of this paper. The other phenomenon is the scattering of light which arises from the presence in the medium of elastic waves of thermal origin.

The thermal scattering of light in material media was first observed by Lord Rayleigh who approached the problem from the individual molecular point of view. In 1922 BRILLOUIN [1] regarded the thermal scattering of light as a "coherent reflection" of light waves by the sound waves of thermal origin traversing the medium. It was further shown that the reflection should be accompanied by shifts of frequency in the nature of a Doppler effect which vary with the direction of observation of the scattered light with the frequency of the incident light. Such shifts of frequency are identical with the frequency of the sound waves which are effective in scattering along the particular direction of observation. Their magnitude is very much smaller than those associated with the infrared vibrations of the material and hence much more difficult to observe than the latter. The experimental proof of their existence followed rather than preceded the discovery of the Raman effect in 1928.

The conservation of energy in the collision process gives

$$h\nu_s = h\nu_i \pm h\nu_e, \tag{1}$$

where ν_s, ν_i, and ν_e are the frequencies of the scattered photon, of the incident photon and of the phonon, respectively. From the conservation of momentum we get the relation

$$\frac{\Delta\lambda}{\lambda e} = \sqrt{n_i^2 + n_s^2 - 2n_i n_s \cos\theta}, \tag{2}$$

where θ is the angle of scattering and n_i and n_s are the refractive indices of the medium along the directions of incidence and scattering. In the most general case of a birefringent crystal $n_i \neq n_s$. If θ_i and θ_s are the angles of incidence and scattering with reference to the elastic wave normal

$$n_i \cos\theta_i = n_s \cos\theta_s \tag{3}$$

and

$$\theta_i + \theta_s = \theta. \tag{4}$$

The Doppler shift of frequency is given by

$$\frac{\Delta\nu}{\nu_i} = \pm \frac{v_e}{c} \sqrt{n_i^2 + n_s^2 - 2n_i n_s \cos\theta}, \tag{5}$$

where v_e is the velocity of the elastic wave or phonon. Equations (2), (3), (4) and (5) are the fundamental ones required to analyse the characteristics of the scattered radiation. In case of a liquid or amorphous substance like glass, Eq. (5) reduces to

$$\frac{\Delta\nu}{\nu_i} = \pm \frac{2v_e}{c} n \sin\theta/2. \tag{6}$$

This is the same as the original Brillouin formula. Since the observed shift is only a fraction of a wave number, interferometric aids would be necessary for successfully recording the effect.

In 1930, using high resolving instruments, the existence of the effect contemplated by Brillouin was reported by GROSS [2] in the light scattered by liquids and by quartz. It was in the Physics Department of the Indian Institute of Science, Bangalore, that the appearance of the Doppler shifts in the light scattered by liquids was unequivocally established by RAO [3], VENKATESWARAN [4] and SUNANDA BAI [5]. Subsequently the subject of the Brillouin scattering by liquids has been extensively studied [6-10]. The main results of these investigations are summarized as follows:

(1) The scattered radiation is generally found to consist of three components; a central component of the same frequency as the original radiation and the other two components symmetrically placed on either side of the undisplaced line with a Doppler shift in accordance with Brillouin's formula (see Eq. [6]).

(2) At room temperature the Brillouin components and the central component are sharp and have half widths significantly greater than the incident radiation (CHIAO and STOICHEFF, [11]).

(3) The Brillouin components are strongly polarized in transverse scattering, but whether the polarization is complete is not definite.

(4) The central component exhibits a marked imperfection of polarization and the extent of imperfection is dependent however on the temperature and viscosity of the liquid and the anisotropy of the molecules.

(5) There is a general background superposed on the entire interferogram; the intensity of this background scattering is greater, the higher the depolarization of the total scattering of the liquid. The intensity however depends on the viscosity of the liquid, being less for liquids of higher viscosity.

(6) Besides this background scattering, there is a definite and conspicuous diffuse band spread between the central component and the two Brillouin components on either side (Cabannes-Daure effect).

(7) The intensity of the Brillouin components increases with temperature and the frequency shift diminishes slightly. Also the Brillouin components broaden out at temperatures close to the boiling point of the liquid. But the unmodified central component loses intensity as the temperature increases and the diffuse band between the components shows a corresponding increase in intensity.

(8) The relative intensity of the imperfectly polarized central component and the well polarized side components is controlled by two distinct factors, one being the viscosity of the liquid and the other the optical anisotropy of the molecule. The more viscous the liquid is the stronger is the central component relative to the outer component. A greater optical anisotropy has a similar effect.

The experimental facts outlined above are no doubt intimately connected with the ultimate structure of the liquid. An explanation for these experimental observations may be offered on the basis of a hole theory of the liquid state (FRENKEL [12]). At any given instant, the space distribution of molecules in a liquid is taken to be similar to that in a crystal, except for the fact that a large number of "lattice points" may be regarded as vacant. The

vacant sites or holes appear and disappear as a result of the fluctuations accompanying thermal motion. The translational and rotational motions of molecules in the liquid are of the same character as in solids and consist of vibrations of particles about an equilibrium position. But unlike in a solid, this equilibrium position is not invariant and each molecule after executing a large number of oscillations about the same position during a certain interval jumps to a new position of equilibrium. The mean time τ for which a molecule remains in the same position or the mean life of the sedentary state varies from 10^{-9} to 10^{-12} s for ordinary liquids. The translational vibrations involving a slight shift of the centre of gravity of the molecules due to the finite life of sedentary state lead to the density fluctuations and accompanying thermal waves which account for the Brillouin effect observed in liquids. But superimposed on the changes of density arising from pressure changes in the waves, an additional variation of density in the medium should exist as a result of local variations of temperature. This latter type of variation called "entropy fluctuations" leads to an additional density scattering and this part of the density scattering constitutes the polarized part of the central unmodified component and thus provides an explanation for a part of the observed intensity of the central component.

If we now consider the possible rotational oscillations of the molecule in a liquid, these may in a similar fashion give rise to "orientational waves". If the molecules are anisotropic their thermal motion will lead to an orientation scattering which consists of two parts: a purely angular part irrespective of the translational one and the other in which angular vibrations accompany translation motion also. The purely angular part of the orientation scattering is responsible for the general depolarized background superposed on the interferogram. The translational-angular part of the orientation scattering may be further subdivided into two parts corresponding to the longitudinal type of translational motion (LA-waves) and the transverse type of translational motion (TA-waves). The scattering from both these waves will be governed by the Bragg condition but the intensity caused by LA waves will be weak. The TA-waves will lead to intense scattering if the molecules are anisotropic. But as the frequency of these waves satisfying the Bragg condition has a period comparable with the relaxation time, these TA waves will be damped. This damping has a broadening effect and the Brillouin components arising from these waves are therefore broad. As in density scattering one can also expect orientation fluctuations from entropy changes to be possible. Hence a portion of the orientation scattering from TA waves will contribute to the intensity of the unmodified component. On account of the small velocity of the transverse waves, the broad Doppler components caused by the TA waves will be of smaller shift and obviously the intensity of these components will increase with the optical anisotropy of the molecules. Thus the diffuse band spread between the central component and the two Brillouin components may be qualitatively accounted for.

Although many attempts have been made to observe the Doppler shifts in amorphous solids and glasses, only in the case of used silica have they been successfully observed (KRISHNAN, [13]; FLUBACHER, et al. [14]).

In the case of crystals the presence of Doppler shifted components in the scattered light which were predicted by BRILLOUIN [1] was first repor-

ted by GROSS [15] in quartz. Subsequently using interferometers, work was done on this subject by RAMAN and VENKATESWARAN [16] and SIBAIYA [17]. However, several investigators including LEONTOWITSCH and MANDELSTAM [18], TAMM [19], MUELLER [20], GROSS [21], BHATIA and KRISHNAN [22], KASTLER [23] and THEIMER [24] have considered the theory of thermal scattering of light in crystals (BORN and HUANG, [25]). However, using the resonance radiation of mercury, 2536.5 Å wavelength, as the exciter, and the powerful Rasetti technique as developed in the author's laboratory, KRISHNAN [26] and his co-worker CHANDRASEKHARAN [27] have been able not only to establish unambiguously the physical reality of such Brillouin components without interferometric aid but also to study their dependence on crystal orientation, effect of temperature, etc. in diamond, alumina, quartz, calcite, alkali halides and other crystals. In the case of diamond the scattered spectrum shows two pairs of Doppler shifted components clearly resolved from each other, one pair resulting from the longitudinal sound waves and the other from the two sets of transverse waves which have nearly the same velocity. The observed shifts in diamond are not in very good agreement with the values calculated from the elastic constants, the transverse components having shifts definitely larger and the longitudinal components having shifts slightly smaller than the expected values. The significance of these results in relation to the current theories of elasticity has been discussed elsewhere [28]. None of the authors quoted earlier has specifically considered the effect of birefringence of the crystal on the Doppler shifts. When this is examined in detail as was done by CHANDRASEKHARAN [27] the remarkable result emerges that there should be in general not three but twelve Doppler components for a birefringent crystal. It can easily be seen from Eq. (5) that there should be in general twelve pairs of Doppler shifted components, since n_i and n_s can each take two values and there are three possible values for v_e for a given direction of elastic wave normal.

Let us now consider the case of scattering of light involving large frequency shifts or what is commonly called Raman effect. The optical effects due to the rotation of the molecules appear as a wing accompanying the Rayleigh line while the vibrations of the molecules appear as discrete lines with frequency shifts which are nearly the same as those for molecules in the gaseous state. The extent and intensity of the wing depend very much on the nature of the molecules and the nature of aggregation. It is often observed that a few peaks are superposed on the wing. A closer study of these peaks will give us some information concerning the structure of the liquid. In order to explain the observed spectrum one has to consider the individual particles in the medium as the responsible agents. The dynamics of such rotation and vibration is essentially a matter of individual behaviour of the molecules though they are influenced and partly modified by the interactions occurring between a molecule and its immediate neighbours.

Let us now come to the case of crystals. As the theoretical work on lattice dynamics has been confined to simple cubic crystals such as alkali halides, I shall restrict myself to the survey of results obtained on the Raman spectra of alkali halides. Because of the cubic symmetry of their lattice, the first-order spectrum is inactive in Raman effect. One can expect to re-

cord only their second-order Raman spectra in which overtones and combinations of all the frequencies including those from the acoustic branches can appear, satisfying the conservation of energy and momentum conditions. Hence the true nature of their vibration spectra is reflected by these optical studies.

Since the second-order spectra are of feeble intensity, one has to employ optically clear crystals with polished faces and truly monochromatic sources for excitation. All the investigators in this field have successfully used the 2537 resonance radiation of mercury from a low-pressure water-cooled magnetic controlled quartz mercury devised by RASETTI [29] and later perfected by KRISHNAN [30] for exciting the Raman spectrum of alkali halides. A filter of mercury in the path of scattered light suppresses the 2537 radiation thereby giving a clear background for the Raman spectrum to appear. The use of a suitable laser source for excitation, especially in the case of coloured crystals, may be expected to give more data on this topic.

While RASETTI [29] recorded for the first time the Raman spectrum of NaCl, a systematic study of the Raman spectra of alkali halides of NaCl and CsCl structures was undertaken by KRISHNAN and his co-workers [31]. Similar studies on a few halides (NaCl, NaBr, KCl, KBr and RbBr) were made by MENZIES and SKINNER [32]. GROSS, STEKHANOV and their co-workers [33] have studied the Raman spectra of NaCl, NaBr, KBr, CsBr, LiCl and their temperature dependence, Polarization studies are available for KI and CsBr from the work of NARAYANAN [34], STEKHANOV and KOROLKOV [35], and MENZIES and SKINNER [32]. A study of the intensity distribution in NaCl has been carried out by WELSH, CRAWFORD and STAPLE [36].

The main results are as follows: The frequency shifts of the prominent Raman lines or peaks in the Raman spectra of alkali halides reported by the various authors are collected in Table I. Except for CsBr and CsI which belong to the CsCl structure, the rest of the halides belong to the NaCl structure. The lines marked with an asterisk are found to be very sharp and intense and are depolarized while the rest of the spectrum is polarized in the case of all the alkali halides of NaCl structure, except for KCl and RbBr in which the entire spectrum is polarized. In the case of CsBr, the entire spectrum is depolarized, this being attributed to the high symmetry of the CsCl lattice.

Qualitatively, one can group the spectra of alkali halides into three classes:

(a) Those of KCl and RbBr where mass ratio of the cation and anion is nearly one exhibiting weak and completely polarized spectra,

(b) Those of CsBr and CsI exhibiting intense and evenly distributed lines with all of them depolarized, and

(c) The rest, exhibiting one strong and depolarized line (example: the 235 cm^{-1} line of NaCl) while the rest are polarized.

A comparative study of the spectra of the halides reveals the following:

(1) The highly individual character of the vibration spectrum of each halide is reflected in its Raman spectrum which shows marked variations in intensity distributions from halide to halide.

(2) The intensity of scattering increases as one goes from the chloride to iodide showing thereby that the electron shells of halogen atoms play a main role in the scattering, as they have large polarizability. The increased in-

TABLE I

RAMAN SPECTRA OF ALKALI HALIDES

LiCl	NaCl	NaBr	NaI	KCl	KBr	KI	RbBr	RbI	CsBr	CsI
49	85	31	19	122	46	63		55	25	19
86	135	64	42	212	84	89*		82*	40	22
116	140	116	58	237	126*	101		115	54	44
							50-180			
128	162	152*	88	257	146	102		125	75	61
147	184	181	103*	331	170	175		156	105	91
159	199	254	120	349	186	210		160	125	94
168	202		132		216	252		171	134	106
207	220		200		228				163	110
227	235*		225		232				176	124
274	258		340		242					137
292	270									155
298	276									181
307	286									
337	300									
357	314									
375	320									
405	326									
432	343									
444	350									
453										
472										
498										
522										
540										
558										
618										

tensity of scattering in caesium halides has been attributed to the scattering from the alkali ions since the ionic polarizability of caesium is close in magnitude to that of chlorine and is only 1.4 times smaller than that of bromine. The inability to record the spectra of LiF and NaF has therefore been attributed to the low polarizability of the fluorine ion.

(3) In the spectra of NaCl, the lines are bunched together and besides those given in Table I, there are five more weak lines in the region of 390 - 507 cm^{-1}. In the case of KBr and KI, the lines are evenly distributed even though the frequency shifts are smaller because of the large masses of the cation and anion. NaBr shows, besides the frequency shifts 118, 154 and 185 cm^{-1}, an unresolved band extending from 228 - 310 cm^{-1}. The spectra of KCl and RbBr are very weak and diffuse in character. In the case of NaI, the lines are bunched in the form of four bands, the second one exhibiting the strongest lines when studied under high dispersion. CsBr and CsI exhibit intense spectra with CsI exhibiting not less than a dozen lines of which the strongest at 20, 94 and 108 cm^{-1} are closely spaced doublets. These can be easily explained if one considers the effect of the mass ratio of the cation and anion on the dispersion curves for the halides.

Any proper theory of the Raman effect in crystals should explain the appearance of sharp peaks or lines in the observed spectra. Using the vibration spectrum of the NaCl lattice, BORN and BRADBURN [37] were the first to work out quantitatively the intensity distribution in the second-order Raman spectrum of NaCl. To simplify the problem, they had to reduce the thirty six narrow maxima representing the density maxima of the combinations in pairs of the six branches of frequency (three optical and three acoustic) of the exact theory to sixteen and to assume the same selection rule, as at the point L ($\frac{1}{2}$ $\frac{1}{2}$ $\frac{1}{2}$) in the reduced zone, to hold good for all points. Their results show that the second-order Raman spectrum of NaCl is of the nature of a continuum with superimposed peaks, corresponding to the high density of frequencies in some narrow frequency regions of the vibration spectrum of the lattice. These high densities of frequencies consequently lead to intensity maxima in the second-order spectrum. Recently, the method has been improved upon to take into account the selection rules at each point and the intensity distribution in the case of KBr and NaI have been worked out by COWLEY [38] with the help of their vibration spectra which gave good fit to the observed neutron scattering experiments. It is to be remarked here that the extreme sharpness of some of the lines found in the Raman spectra, such as the 235 cm-1 line of NaCl, and their high intensity cannot be satisfactorily accounted for by these theories. The failure of the continuously ranging frequencies and the continuous variation of the phases in such modes along the successive cells to account satisfactorily for the experimentally observed spectroscopic features led RAMAN [39] to postulate a new lattice dynamics. According to his theory, every crystal has, in addition to the (3p - 3) modes of internal oscillations of the group of p-non-equivalent atoms in the unit cell, 21 p modes of oscillation of the lattice in which the equivalent atoms in adjacent cells vibrate in opposite phases. This comes to the same problem as the vibrations of a supercell containing 8p atoms, i.e. one having twice the unit translation in each direction. The 21p modes may be pictured as oscillations, relative to each other, of the alternate planes of equivalent atoms in the crystal, these planes being the cubic and octahedral for the rock salt structure. Because of the opposite phases involved in these modes, they are forbidden to appear as fundamentals and can only manifest themselves as overtones and combinations. On account of the high symmetry of the lattice, these 42 modes reduce to eight degenerate modes for the rock-salt structure, the modes involving the oscillations of the cubic planes being three-fold degenerate while those of the octahedral planes are four-fold degenerate. A further increase in degeneracy to six and eight arises for the transverse modes. So, the second-order spectrum is expected to consist of nine octaves and thirty six combinations of these nine modes of the supercell. If we consider, for example, CsI which belongs to the CsCl structure, these overtones and combinational modes have frequencies ranging from 20-160 cm^{-1} and a large number of these therefore appear crowded in this region giving the appearance of a continuum with super-imposed peaks even on the Raman theory. Further, the presence of thermal broadening and perturbations can play their part in practically masking the details of the spectrum. The explanation of the observed Raman spectra on this model is based on certain qualitative selection rules based on the physical picture of the 24p modes and

the changes in the polarizability involved in them. The frequency shifts and the relative intensities have been found to be explainable fairly satisfactorily, on Raman's method for the halides.

The inadequacy of the Born lattice dynamics to explain the finer details of the Raman spectra made BIRMAN [40] and LOUDON and JOHNSON [41] extend the concept of critical points of VAN HOVE [42] and the activity of the phonon frequency branches from these in multiphonon optical processes. According to these authors, all the overtones and combinations of frequencies among themselves from the critical points L, X, W, K, etc. can appear in infrared and Raman spectra. Using the L and X critical point frequencies, LOUDON and JOHNSON [41] were able to give a satisfactory explanation of the observed Raman spectrum of diamond. With the L and X critical point frequencies as obtained from neutron scattering for KBr and NaI and calculated with a shell model for RbI and those from R, M and X for CsI calculated on a shell model, it has been possible to explain their observed spectra satisfactorily [43] .

Now, we see that this method of explaining the Raman spectra by considering the presence of singularities in the frequency spectra is exactly similar to the ideas of Raman in postulating supercell modes. Since the critical points L, X, for example, for NaCl structure and R, M and X for CsCl structures, are situated at the extremities of the dispersion curves along the [111], [100] or [110] directions, they involve a phase difference of π at least along one of the axes. The transverse and longitudinal phonon branches at these points correspond to the tangential and normal oscillation of these planes of atoms. A further subdivision into optical and acoustical branches is closely related to the physical picture of the supercell modes, their degeneracy being a consequence of the statistical weights of the critical points. Another point of interest is the invalidity of the rule of mutual exclusion as shown by VENKATARAYUDU [44] for the diamond supercell. The same conclusion has been arrived at by Birman for second-order processes from the critical point approach. Thus the Raman picture postulated in 1943 is an extremely practicable and simple method for explaining the second-order processes and has now received full justification from the critical point analysis of Birman and Loudon and Johnson. Expressions for the frequencies of the Raman modes are available [45] and the analysis is very simple even though the inclusion of polarizability and ionic character can improve the agreement between the observed and calculated frequencies. The expressions for the elastic constants, limiting frequencies along symmetry directions for diamond calculated on this model, agree well with those of SMITH [46] based on the conventional lattice dynamics of Born.

Finally, the extent of the second-order Raman spectra gives us an indication of the role of the Lyddane-Sachs-Teller [47] (L.S.T.) splitting of the triply-degenerate infrared active (polar) vibration. The second-order Raman spectra should terminate at a frequency corresponding to the octave of the maximum frequency of the lattice vibrations which is the limiting longitudinal optical frequency for $k = 0$. This frequency can be calculated using the L.S.T. relation with the limiting transverse optical frequency and the static and the high frequency dielectric constants. Table II clearly indicates that the observed extent and in particular the bands observed in the Raman

TABLE II

EXTENT OF THE SECOND-ORDER RAMAN SPECTRA

Name of the halide	ω_{TO} (cm^{-1})	ϵ_o	ϵ_∞	ω_{LO} (cm^{-1})	$2\omega_{LO}$ (cm^{-1})	Observed limit of the spectrum
LiCl	191	12	2.7	398	796	700
NaCl	164	5.9	2.25	264	528	520
NaBr	134	6.4	2.6	209	418	310
NaI	117	6.6	2.91	176	352	370
KCl	142	4.85	2.1	214	428	349
KBr	113	4.9	2.3	165	330	380
KI	101	5.1	2.7	139	278	252
RbBr	88	4.9	2.3	127	254	150
CsBr	73	6.5	2.8	112	224	230
CsI	62	5.65	3.0	85	170	190

spectra of NaI and NaBr can be satisfactorily explained by this rule. On this basis, the weaker continuum found beyond the limit of the spectrum postulated by this rule, has been explained as the result of third-order processes.

ACKNOWLEDGEMENTS

The author is grateful to Dr. P. S. Narayanan and Mr. N. Krishnamurthy for their help in the preparation of this article.

REFERENCES

[1] BRILLOUIN, L., Ann. Phys. 17 (1922) 88.
[2] GROSS, E., Nature 126 (1930) 201, 400.
[3] RAO, B. V. R., Proc. Ind. Acad. Sci. 1A (1934) 261, 473 and 765 and 2A (1935) 236.
[4] VENKATESWARAN, C. S., Proc. Ind. Acad. Sci. 15A (1942) 362 and 371.
[5] SUNANDA BAI, K., Proc. Ind. Acad. Sci. 15A (1942) 349.
[6] MEYER, E. H. and RAMM, W., Phys. Z. 33 (1932) 270.
[7] RAMM, W., Phys. Z. 35 (1934) 111.
[8] BIRUS, K., Phys. Z. 37 548 and 39 (1939) 80.
[9] RAFALOUSKI, I., Nature 128 (1931) 495.
[10] RANK, D. H., McCARTNEY, J. S. and SZASZ, G. J., J. opt. Soc. Amer. 38 (1948) 287.
[11] CHIAO, R. Y. and STOICHEFF, B. P., J. opt. Soc. Amer. 54 (1964) 1286.
[12] FRENKEL, J., in Kinetic Theory of Liquids, Oxford University Press, London (1946).
[13] KRISHNAN, R. S., Proc. Ind. Acad. Sci. 37A (1953) 377.

[14] FLUBACHER, P., LEADBETTER, A.J., MORRISON, J. A. and STOICHEFF, B. P., J. Phys. Chem. Solids 12 (1959) 53.
[15] GROSS, E., Z. Phys. 63 (1930) 685.
[16] RAMAN, C. V. and VENKATESWARAN, C. S., Nature 142 (1938) 250.
[17] SIBAIYA, L., Proc. Ind. Acad. Sci. 8A (1938) 393.
[18] LEONTOWITSCH, M. and MANDELSTAM, S., Phys. Z. Sowjet 1 (1931) 317, Z. Phys. 75 (1932) 350.
[19] TAMM, Ig., Z. Phys. 60 (1930) 345.
[20] MUELLER, H., Proc. roy. Soc. 166A (1938) 425.
[21] GROSS, E., Z. Phys. 63 (1930).
[22] BHATIA, A. B. and KRISHNAN, K. S., Proc. roy. Soc. 192A (1948) 181.
[23] KASTLER, A., J. Chim. phys. 46 (1949) 40.
[24] THEIMER, O., Proc. phys. Soc. 64 (1951) 1012, Proc. phys. Soc. 65 (1952) 38.
[25] BORN, M. and HUANG, K., in Dynamical Theory of Crystal Lattices, Clarendon Press, Oxford Press, Oxford (1954) 373.
[26] KRISHNAN, R. S., Proc. Ind. Acad. Sci. 22A (1945) 329, Proc. Ind. Acad. Sci. 26A (1947) 399 and 450, Nature 159 (1947) 740; KRISHNAN, R. S. and CHANDRASEKHARAN, V., Proc. Ind. Acad. Sci. 31A (1950) 427.
[27] CHANDRASEKHARAN, V., Proc. Ind. Acad. Sci. 32A (1950) 379, Proc. Ind. Acad. Sci. 33A (1951) 183, Curr. Sci. 19 (1950) 371, J. Ind. Inst. Sci. 34 (1952) 269, Proc. Natl. Inst. Sci. India 19 (1953) 547.
[28] KRISHNAN, R. S., Proc. Ind. Acad. Sci. 41A (1955) 91; KRISHNAN, R. S., CHANDRASEKHARAN, V. and RAJAGOPAL, E. S., Nature 182 (1958) 518.
[29] RASETTI, F., Phys. Rev. 34 (1929) 364.
[30] KRISHNAN, R. S., Proc. Ind. Acad. Sci. 18A (1943) 298.
[31] KRISHNAN, R. S., Nature 156 (1945) 267, Proc. roy. Soc. A87 (1946) 188, Proc. Ind. Acad. Sci. 26A (1947) 419 and 432; KRISHNAN, R. S. and NARAYANAN, P. S., Proc. Ind. Acad. Sci. 28A (1948) 296, Nature 163 (1949) 570, J. Ind. Inst. Sci. A34 (1957) 85; KRISHNAN, R. S. and KRISHNAMURTHY, N., Z. Phys. 175 (1963) 440; KRISHNAMURTHY, N. and KRISHNAN, R. S., Ind. J. pure appl. Phys. 1 (1963) 239; KRISHNAMURTHY, N., in publication (1964).
[32] MENZIES, A. C. and SKINNER, J., J. Phys. Radium 9 (1948) 93, C. N. R. S. Int. Colloquium, Bordeaux (1948) 60.
[33] GROSS, E. F. and STEKHANOV, A. I., Nature (Lond.) 160 (1947) 568; GROSS, E. F., PAVINSKII, P. P., and STEKHANOV, A. I., Dokl. Akad. Nauk, USSR 68 (1949) 27; STEKHANOV, A. I. and PETROVA, M. L., Soviet Phys. JETP 19 (1949) 1108; STEKHANOV, A. I., Soviet Phys. - JETP 20 (1950) 330; STEKHANOV, A. I., GABRICHIDZE, Z. A. and ELIASHBERG, M. B., Sov. Phys. sol. State 3 (1961) 964; STEKHANOV, A. I. and ELIASHBERG, M. B., Soviet Phys. sol. State 2 (1961) 2096; STEKHANOV, A. I. and ELIASHBERG, M. B., Opt. and Spectrosc. 10 (1961) 348.
[34] NARAYANAN, P. S., Proc. Ind. Acad. Sci. 42A (1955) 303.
[35] STEKHANOV, A. I. and KOROLKOV, Sov. Phys. sol. State 4 (1962) 945; STEKHANOV, A. I. and KOROLKOV, Sov. Phys. sol. State 4 (1963) 2311.
[36] WELSH, H. L., CRAWFORD, M. F. and STAPLE, W. J., Nature (Lond.) 164 (1949) 737.
[37] BORN, M. and BRADBURN, M., Nature 156 (1945) 567, Proc. roy. Soc. A188 (1947) 161.
[38] COWLEY, R. A., Proc. Phys. Soc. 84 (1964) 281.
[39] RAMAN, C. V., Proc. Ind. Acad. Sci. 18A (1943) 237.
[40] BIRMAN, L., Phys. Rev. 131 (1963) 1489.
[41] LOUDON, R. and JOHNSON, F. A., Royal Radar Establishment Memorandum No. 2054 (1964).
[42] VAN HOVE, L., Phys. Rev. 89 (1953) 1189.
[43] KRISHNAMURTHY, N., in publication (1964).
[44] VENKATARAYUDU, T., J. chem. Phys. 22 (1954) 1219.
[45] RAMAN, C. V., Proc. Ind. Acad. Sci. 54A (1961) 253, 281.
[46] SMITH, H. M. J., Phil. Trans. Roy. Soc. A241 (1948) 105.
[47] LYDDANE, R. H., SACHS, R. G. and TELLER, E., Phys. Rev. 59 (1941) 673-76.

DISCUSSION

K.-E. LARSSON: In your discussion of small energy transfers you mentioned that the central and the Brillouin components have a broad general background. Is the origin of this background known?

R.S. KRISHNAN: Yes. The background arises mainly from orientation scattering in the case of anisotropic molecules and extends over several wave numbers.

K.-E. LARSSON: In your discussion of large energy transfers you mentioned that for liquids the central line has broad wings with structure appearing on them. Is the origin of these wings and of this structure known? Also do these results refer to complex liquids only or have you seen similar effects for simple liquids?

R.S. KRISHNAN: The wings are due to the rotational oscillations of the molecules and the extent and intensity distribution depend on their anisotropy. The structure consists mainly of a couple of peaks in the intensity distribution and is found in the case of both complex and simple liquids. The simple liquids examined include water, aliphatic alcohols, etc. The peaks are attributed to inter-molecular oscillations and hindered rotations.

R.J. ELLIOTT: I feel that Dr. Krishnan has oversimplified the description of the role of critical points. These give discontinuities in the slope of the absorption coefficient and not necessarily peaks. They must occur at certain symmetry points where the energy bands have extrema or saddle points, but they can also occur at general points in the zone if the frequency spectrum is complicated enough. Thus, I think the analogy with the Raman frequencies calculated from a supercell is not very satisfactory.

R.S. KRISHNAN: I should like to ask Dr. Krishnamurthy to reply to this.

N. KRISHNAMURTHY: The main idea pointed out in the paper is that the critical points Γ, L and X for a face-centred cubic lattice give rise to phonon frequencies which correspond to the vibrations of the planes of atoms, like the (111) or (100) planes. These frequencies correspond to the Raman modes of the supercell. It is only the Raman frequency shifts that are explained using these critical point phonon frequencies. However, it is true that one has to consider all the critical points, Γ, L, X, K, W, Z, Q etc. as well as other points generated with the particular model used for the dynamics calculations. To simplify the evalutation of the critical points phonon combination selection rules, only Γ, L and X are considered.

P. EGELSTAFF: Could Dr. Krishnan repeat the explanation of the experimental result that $I_c/2I_B > \gamma - 1$?

R.S. KRISHNAN: Perhaps Dr. Narayanan would answer this question.

P.S. NARAYANAN: The Landau-Placzek relation $I_c/2I_B = \gamma - 1$ takes into account only the "entropy fluctuation" contribution to density scattering; the possible contributions due to fluctuations in orientation were not taken into account. When this is done on the basis of Frenkel's theory of liquids, one finds that the transverse type of translational-angular waves can contribute to the central component intensity in the case of liquids with anisotropic molecules. That is the reason why the observed value is always higher than that predicted by the Landau-Placzek relation.

J. MAHANTY: In three-dimensional lattice models the maxima in the frequency distribution function are not so sharp as those one gets in two-

dimensional or one-dimensional crystals. It is therefore not clear to me how one can use the Van Hove idea of critical points to explain the very sharp lines you have got.

R.S. KRISHNAN: The idea of the critical points is not to explain the width and intensity of the observed Raman lines but only their approximate frequency shifts. It explains the appearance of the octaves and combinations at the appropriate frequency shifts in the Raman spectrum.

R.K. ASUNDI: I have two comments to make regarding Dr. Krishnan's paper. The laser is no doubt a very powerful source of extremely monochromatic radiation of high coherence. However, when employing it to study Raman scattering phenomena it is necessary to bear in mind that higher order effects become operative, so that one should be prepared to encounter the situation whereby the phenomena observed with the new sources may become complicated. Stoicheff has in fact shown that stimulated Raman spectra have most remarkable properties compared with the corresponding normal Raman spectra.

My second comment is that optical absorption of fluorescence and normal Raman spectra of rare earth and similar ions forming part of crystal lattices are found to be capable of yielding information regarding observable properties (magnitude, intensity, polarization) of lattice vibrations, not only in the normal state of the ion but also in electronically excited states. Some work has been done in this direction, e.g. $LaCl_3$, $LaBr_3$, $PrCl_3$, etc., but the subject appears to merit greater attention.

SUMMARY OF THE SYMPOSIUM ON INELASTIC SCATTERING OF NEUTRONS

P. A. EGELSTAFF
ATOMIC ENERGY RESEARCH ESTABLISHMENT,
HARWELL, BERKS., ENGLAND

I expect that most of you are aware that at this time of year we suffer from fog in London, and it so happened that at the time of the meeting of the committee there was such a fog and my airplane was rather late. When I eventually arrived in Vienna I was met by a nice car-driver from the International Atomic Energy Agency who said to me, "Oh, the first day's meeting is now over; would you like to meet the others at a restaurant?" So of course I said, "yes". Off we set and duly arrived at a pleasant restaurant. On my arrival the other members looked at me and said, "We're very pleased to see you, because we've thought up just the job for you to do." And that is why I am here now.

Of course this job has various compensations. One is that I hadn't to prepare a paper before the meeting. Another is that I can say what I like about everybody else's paper without giving them the opportunity of asking me difficult questions. You may have noticed that I have been sitting in the front row taking notes during the sessions and I'm told I asked a lot of questions. This is entirely the result of taking notes, and I can merely recommend that you all take notes in future and then the discussion will be much more lively! I'm also told that the purpose of a summary is that the name of everybody who contributed to the Symposium may be quoted, and this makes them feel happy and go home delighted. So I counted the number of names I would have to read and it is 157. I believe this is a prime number, Mr. Chairman; you might like to correct me. I propose to take all these names as read; I hope you will leave just as delighted! However, before leaving the question of attendance of the Symposium, I would like to comment on the absentees. We are all extremely sorry that Professor Brockhouse was unable to come because of ill health and I understand that Dr. Pevsner is ill also. I am sure we would all like to wish them a swift recovery. These things are very sad, because it seems that ill health does affect neutron scattering people especially; perhaps some aspirin tablets are kept at this desk.

On looking through the papers and on hearing them too it is clear that the Chalk River group continue to present excellent papers and to make tremendous progress in this field. One tends to expect this of them. I think we would have been very disappointed at this Symposium if the papers from Chalk River had fallen below their usual high quality. However, looking to the future, we were struck during our visit to Trombay at the progress the group here has made in the last four years, and I am sure they are going to present extremely strong competition to the Chalk River group. Those of us who don't have a huge reactor hall packed with multiple-arm three-axis spectrometers are getting worried by that aspect.

My general impression of this Symposium is one of steady progress rather than outstanding developments. Consequently, I am not going to pick out any highlights; I am going to give my views on these developments and make one or two critical remarks in some of the fields. The field of inelastic neutron scattering is becoming markedly more mature. This is partly because techniques are now developed and people are concentrating on obtaining and interpreting the data, and partly because the technique is being more widely accepted by people in different fields. I think in these circumstances it is up to neutron people to exert a certain self discipline, particularly in their interpretation and presentation of their results.

The importance of neutron work has been shown by the recent conferences on lattice dynamics and magnetism. I think it is noticeable, particularly in the case of magnetism, that the work reported at these conferences has had an adverse effect on the amount of work reported here. This is likely to be a trend in the future. As neutron work becomes more widely recognized and its application to different fields more widely accepted, it will find a natural place in the conferences pertaining to such fields which will reduce the need for conferences on neutron scattering intended purely for the neutron people.

I was pleased, however, to notice that optical work had gained the status of an acceptable subject at a neutron conference. The Mössbauer effect also slid in sideways but no other techniques seemed to be popular here. More attention should be devoted to the combination of results from these differing techniques. Neutron scattering is frequently the most powerful of these techniques: it has a wider range of applications and a wider range of usage in the long run. But these other methods are extremely valuable in supplying checks on the neutron data and providing complementary results. There are a number of cases where several differing techniques should be used by one experimentalist (or group) on one material.

Turning now to the work that was discussed at this Symposium, I shall review it in the following way. First I shall consider the experimental questions and secondly look at the sessions on solids, liquids, molecules and magnetism in the order they appeared. I will not devote a special session to the papers from the USSR, but rather put them in the place they naturally fill. Because I come last, I have a slight advantage over the International Atomic Energy Agency in that respect.

EXPERIMENTAL EQUIPMENT

Considering then experimental equipment, one finds that only modest developments have occurred. At the last two symposia of this kind [1, 2] we saw progress - quite significant progress, I think - in neutron spectrometry, new instruments and new ways of using them being announced. This time, although there have been some useful improvements - I don't want to minimize the actual improvements which have been made and reported - it seemed to me there were no very large steps forward. On the other hand, two striking developments were reported. These concerned the new sources which are coming into use. Although we had heard of the IBR (pulsed fast

reactor) before, it was only at this Symposium that the large quantity of data produced with this machine was published. The full use of that instrument is an important development. We heard also about the high-flux beam reactor at Brookhaven which is nearing completion, and when it is in operation a great deal of new and better data will be obtained. These developments will produce two effects. First of all, they will spur on others like myself and many colleagues here who have nothing to match these sources. All we can hope is that we can think of "tricks" to match the brawn of the big boys! And therefore next time both better techniques and results on the better sources should be reported. Secondly the new data one can expect from these sources will help stimulate the theory, and so one can look forward to theoretical improvements following the improvement in resolution and quality of data.

It was interesting that we heard very little about detectors, electronic equipment, and data handling. These subjects were mentioned in one paper but only in a part of that paper and not elsewhere. The He^3 counter is now coming steadily into use and before long there will be other counter developments which will gradually transform the inelastic scattering field. Once again the new high-flux neutron sources will focus attention upon these developments. They will encourage people to think more about detectors, electronics and particularly about data handling.

As we tend to deal with more complex problems and the quantity of data we collect with more sophisticated spectrometers becomes greater, the whole question of data handling may well become one of the most important in our field.

SOLIDS

I'd now like to turn to the question of solids. The work on metals filled an entire session. Theoretical progress, both by the amateurs and the professionals, was to me quite encouraging. It seems that the effect of electrons in metals is becoming understood and that for most of the cases we study there are various models available. Even for the polyvalent metals a model can be used with which to analyse the data, and which is one of a series of such models covering most metals. Of course time will show whether these models are sufficient and it will also show whether the parameters which appear in the models can be calculated properly. But at the moment any type of deformity or anomaly in the dispersion curve seems to be acceptable to the theorists, and it is therefore up to the experimentalists to show whether the models are adequate.

The correlation of the data on the transition metals was impressive and showed one direction for the future. There was also the remarkable situation that no less than six laboratories were considering the subject of white tin. I wonder what the chances are that six laboratories work simultaneously on one material! At one time this probability would have been thought to be zero, but this Symposium has shown it to be finite!

For some time I've been disappointed that hexagonal close-packed metals are not properly understood. It seems that this is a case worth examining in detail, and I would like to encourage people working on phonons to take cases of this kind, study them thoroughly and try to understand them

completely. This is one point of discipline that should be observed now in the neutron field. Over the past few years a large amount of data on dispersion curves for different classes of crystals has been taken. Perhaps it's being a little severe, but nevertheless it's true to say that any one class is not properly understood partly because the experimental data is just not adequate. I would suggest that people, either by getting together or by using more extensive facilities, concentrate considerable effort in a small part of the field and try to understand it thoroughly.

Turning to the case of defects, we had papers on two types of effect: those concerned with the inelastic spectra and those concerned with elastic scattering. The work on elastic scattering is much better understood and more interpretable than that on inelastic. There were papers describing the theory of inelastic scattering by defects, the so-called defect modes, and in that field it is clear that the theory is well ahead of the experiment. This arises, I'm sure, because of the difficulty of finding good experimental cases to work with. But I feel that the first experiment on defect modes will completely alter this situation and then the experiment will be well ahead of the theory.

Phase transitions also received some attention, both theoretically and experimentally, and in the future this area is likely to command an increasing part of our attention. It was notable that certain special cases, such as diamond and UO_2, are now reasonable experimental subjects. The general field of solids seems to be getting rather diffuse, because in fact there are many kinds of solids. In the future people will try to group this work into the different classes of solids, which is perhaps a further reason why it becomes increasingly difficult to hold a conference covering every field.

A certain amount of work was reported on line widths; there were two theoretical papers and one experimental. One of the disappointments of this Symposium was the limited amount of experimental data on line widths. After the previous symposia [1, 2] many people had hoped that the measurement of line widths would develop into an important experimental field. That has not happened because of the difficulty of doing such experiments. Maybe next time the new sources and the new techniques about which I was prophesying earlier will have yielded good data on line widths. We can only hope about that.

My general impression of the "solid situation" is that the theoreticians are now creeping up on the experimentalist. For a long time the experimentalist seemed to dominate them, but they have counter-attacked and the experimentalist must now consider matters and confound them again! So I'm going to make five comments on possible things he might do, some of which, like the first one, (1) lack of line-width data, I've already mentioned. The second item is (2) off-symmetry direction data. None was reported at this Symposium. I know that a certain amount of off-symmetry data has been taken, but I think most of the experimentalists have set this to one side because of the difficulty in treating it. More work is needed on the significance of it and the methods of analysis. Another field where no measurements were reported was that of (3) the polarization vector. We had some discussion on this subject last time, but if you believe the results of this Symposim there has been no progress in the last two years. I'm sure that's not exactly true.

It is merely a statement of the fact that this measurement is experimentally rather difficult. My fourth point is that the choice of samples is still severely restricted by (4) the availability of materials. That limitation will be raised stepwise as time passes. My last point is (5) the variation in quality of the results. It is obvious that everyone should aim for high quality. But we saw some results with very small errors and other results with (apparently) much larger errors. I get the impression that there is no uniform opinion on how to interpret phonon data (I mean the raw data) and how to deduce the errors on the results. I would like to see a closer comparison of the techniques, techniques for measurement, for correction of the raw data and for analysis into phonon frequencies. This will help find out whether the good are as good as they claim and the bad are as bad as they say they are.

LIQUIDS

I would now like to turn to the session on liquids and to mention first the basic theory. It was pleasing to see papers on the basic theory because up till now a lot of the interpretation of liquid data has rested on models, and people who work out models are unpleasantly aware of the need to set the models on a reliable basis. Although the basic theoretical work is proceeding slowly and may never yield results which can be compared directly with experiment, it ought to be aimed at providing a reliable basis on which to construct models. I'm suggesting this as an initial aim, bearing in mind the longer-range aim of a proper theory of liquids.

It seemed to me that the experimental position on liquids became clearer and then more obscure. There were more data on liquids which established certain experimental facts better than we had known them before, but at the same time these facts revealed the need for more work and for better interpretations. Let us consider the incoherent quasi-elastic peak. For many hydrogenous liquids we get a result such as that shown in Fig. 1. The measurements of this kind which were shown here start at C and go to D. The measurements of the diffusion constant are at A and give the initial slope. There's a huge gap, of several orders of magnitude in ΔE, between A and C. If one extrapolates the slope at A the line ΔE is obtained. Now, an effective diffusion constant was discussed, obtained by joining C to the origin, and there was some controversy on the interpretation of this effective diffusion constant. For myself, I feel unhappy about this situation until somebody has discussed the region B. It's clear that there must be a large bend between A and C, and I would like to suggest that B which is not really accessible to experiment at the moment should be considered theoretically. After that, one should then try to reinterpret the data. I will make one remark on that score. If you take the curve ABCD of Fig. 1, and interpret it in terms of a spectral density $p(\beta)$, you get the results shown in Fig. 2. The letters ABCD in Fig. 2 correspond to the letters in Fig. 1. Thus on this interpretation, the region B gives rise to a large peak in the spectral density and this peak should be discussed theoretically. Perhaps some of the points which were made during the session on liquids could be given a more quantitative form.

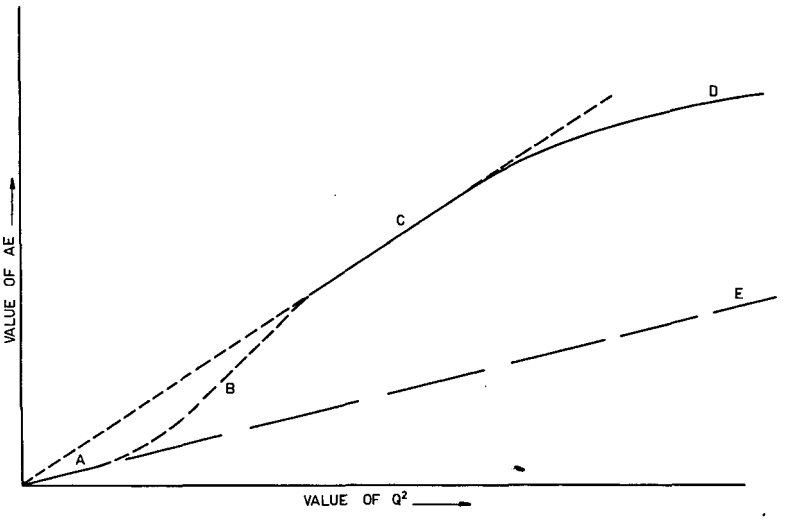

Fig. 1

Typical curve of width (Δ E) of quasi-elastic peak versus Q^2

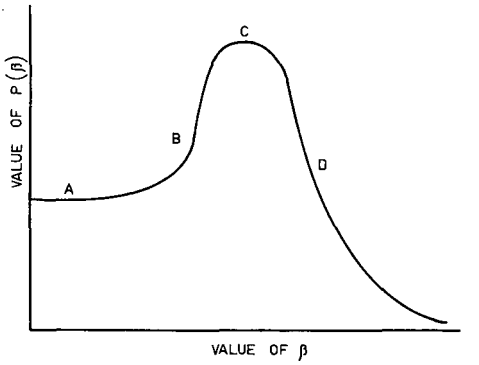

Fig. 2

Spectral density corresponding to curve shown in Fig. 1

But now I'd like to make an experimental remark on this question. If we have a p(β) curve such as Fig. 2 a multi-component diffusion model is needed. In this case can one feel very happy about the interpretations of the spectra taken with a beryllium-filtered spectrum? The normal method of interpretation seems to me quite applicable if one believes that the spectral shape is simple; but as soon as one has complex spectral shape, I think it's essential to use a line spectrum in the experiments. Consequently, it is pleasant to note that most experimental people are now going over to line spectra, although perhaps for other reasons.

I would also like to comment on the results obtained from the region D. This gives, as was shown, the delay time before diffusion sets in, and for many liquids at many temperatures; for example, for sodium between 100 and 200°C, for water between 25 and 75°C, for glycerol between 96 and 180°C, and even for argon at 84° K this delay time is between 1 and 2 x 10^{-12} s. The constancy of this number should be emphasized because it is a very interesting result which the neutron data have thrown up and which has not been adequately explained.

Coherent scattering from liquids was discussed quite extensively here, both inside and outside the main sessions. At the Chalk River meetings [2] we had a number of papers on coherent scattering and it was clear there that the field was just starting. And one can see by comparing the work reported here with the work reported at Chalk River that substantial progress has been made. It now seems to be clearly demonstrated that co-operative modes exist at least in liquid metals. The broadening near the main diffraction peak in liquid argon has been shown to be related to the velocity of sound, and this again suggests co-operative modes. In this field there is room for a lot of development, both experimental and theoretical.

There was some discussion on the question of using the same interatomic potential for the liquid and solid states. This is an important matter that could be considered from the point of view of the experiments one should do to check whether the same potential can really be used in both cases.

My disappointment about the liquid experiments was that no work on the liquid gas critical point was reported. I'm sure this is one area where experiment would be well justified and I'm sure also that most of the experimentalists know this quite well. It is again an illustration that many of the experiments are governed by practicability rather than physical interest.

MOLECULES

Consider now the subject of scattering by molecules. Infrared results figured large in this Symposium, and all molecular people know the significance of these data. But I think it is rather important to emphasize that each worker should consider how his results can improve the situation represented by the infrared data. I don't think enough attention is being paid to the special advantages of neutrons, of how to utilize these advantages to measure things that cannot be measured by infrared and to find ways of improving on knowledge which infrared data has made available. It is well known, for example, that the neutron resolution will always be much, much worse than the infrared resolution and that the large sequences of levels seen in infrared experiments will never be seen in the neutron experiments. Therefore one is starting at a disadvantage, and unless the special advantage of neutrons are exploited we shall not succeed in making a success of this field.

There was a lot of work reported on molecular systems. The field is obviously exciting and is expanding quite fast, but it is also in a state of flux. So I shall make a number of points, some of which you may feel are slightly critical.

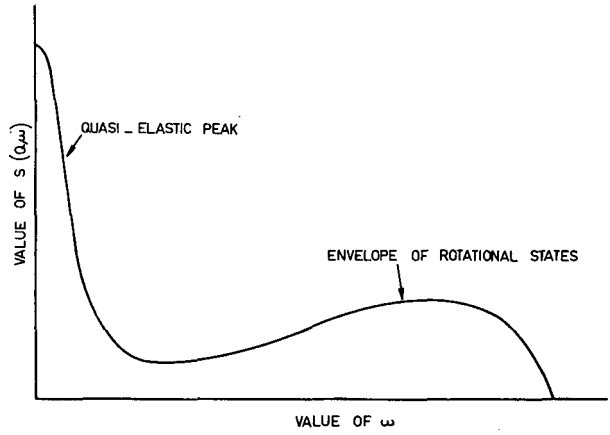

Fig. 3

Scattering law for a rotational system

First, there was some discussion of the Krieger-Nelkin theory about which I have a simple opinion, namely, that if you find your data fit the Krieger-Nelkin theory you have learned next to nothing and should try another experiment. The reason is that the Krieger-Nelkin treatment is a theory of neutron scattering when only certain averages over the molecular situation are important. Inasmuch as these averages give very little information you have learned little.

The second point I would like to make is not quite so severe. We had a discussion on methane, particularly liquid methane, and, for the purpose of these remarks, I have transposed it from the session on liquids to the session on molecules. After listening to the discussions in this session I was rather puzzled as to why the situation shown in Fig. 3 was not considered. This figure illustrates the intensity against energy for neutron inelastic scattering, showing an elastic peak and then a region of rotational levels. At high-energy transfers the level spacing Δ is very much less than the energy transfer and one can use a classical description. Consider the envelope of the level. This envelope is related to the frequency spectrum, which is given by:

$$p(\beta) = (\text{const.})\, \beta^3 \exp\left(-\tfrac{1}{2} I \beta^2\right),$$

where I is the moment of inertia. In the case of liquid methane and in some other materials it is worthwhile comparing the experimental data with an envelope of this kind, which merely expresses the level probability density, and the Boltzmann factor. If this result fits the data, one could assume that either many levels are involved or the damping is quite large. In either case one is hard put to it to learn a great deal, except for the value of I. The experimental value of I may differ from the free molecule value due to the hindrance of the rotation in the liquid state.

In the case of experiments where many peaks are seen in the data we hear phrases such as hindered translation, torsional oscillation, libration, free rotation, hindered rotation, and so on. These phrases are vague, be-

cause if you want a complete and proper statement you must turn these phrases into a theory which enables you to discuss the energy of the levels, the relative magnitude of the different peaks, the absolute magnitude of the peaks, the shape of the line, and whether the lines are single states or multiple states, etc. Experimental workers in this field should add measurements of the absolute magnitude of the cross-section to their present measurements, and theoreticians will have to calculate the things I listed above before we can talk adequately about these processes.

I made a remark earlier about the interpretation of complex spectra using a beryllium-filter method. This remark is less applicable, I think, to the molecular work, because the energy transfers are on the whole larger, but may still be applicable to some extent. Therefore the advent of line spectra in many laboratories will be a good thing for this field too. We had some remarks in one of the papers about the difference between time-of-flight spectra, cross-section curves and spectral density, where it was shown that some peaks were big in one plot but small or distorted in the others. This is important for the interpretation of molecular data, and in principle, one should convert to a spectral density before discussing the peaks.

The experimental work has obviously moved towards better resolution and significant variations in momentum transfer. I was interested in the small peaks which were seen in polymers, in water vapour and in some of the other measurements. The existence of small sharp peaks has always worried me and I would appeal to the theoreticians to try and relieve me of this worry and any future conference by presenting a paper on them.

Neutron scattering by molecules seems to be becoming a branch of physical chemistry, and I would like to warn physicists working on this subject that at any future Symposium they are likely to be swamped by chemists.

MAGNETISM

In the case of magnetic scattering it was notable that both at the Chalk River meeting and at this Symposium less work was reported than is actually being conducted. This time it was due to the fact that the Nottingham Conference on Magnetism absorbed most of the papers.

A wide range of work can of course be done as was indicated in the review papers, and attempts were made to try and combine one class of data with another although some limitations were pointed out. Spin-wave results should, I feel, receive more attention from two points of view. One is of course the point of view emphasized this morning of the interest to theories of magnetism. Another is the advantages to the experimentalists which have been overlooked too long. It is puzzling why manganese fluoride had to wait four or five years before it was studied, since it offers advantages to the experimentalist greater than those of the magnetic materials studied at an earlier stage. When one comes to study changes of dispersion laws with temperature, changes of line widths and phase transitions, there are enormous experimental advantages in spin-wave work over phonon work because the effects are all much larger and more within the experimental resolution of present-day equipment.

We didn't hear much about the critical point work on magnetic materials but this is a particularly interesting field. The data obtained at the magnetic critical point contrasts with the lack of data on the gas-liquid critical point and emphasizes again that it is accessibility which controls much of the work being done. There is great interest too in the data which is now available on coherent effects above the critical point of magnetic systems, and this is obviously a field which will be developed a lot in the next few years.

FINAL REMARKS

That brings me to my final remarks, in which I shall summarize some of the advice and forecasts given earlier. I feel that neutron people are slowly getting to grips with their problems. Most of us, I'm sure, realize what our problems are and therefore I have really nothing new to say here, but to emphasize the trends and directions in which we hope to move.

The experimentalist always wants high resolution. He wants high resolution in his ingoing and outgoing beams. He wants to vary Q. Lower values are needed in the study of the liquid state, and in the study of crystals he has to go to higher-order reciprocal lattice points. He wants good statistics but he never has sufficient patience to wait to get them. In the future the rates of data collection will be even higher than they have been in the past, and this implies a high rate of data reduction. The multiple-arm three-axis crystal spectrometers and computer-controlled time-of-flight machines will lead to substantially higher rates of data collection than hitherto, which will create serious problems for the experimentalist. If we want experimentalists who neither go mad nor present data without adequate analysis, then a lot of work will have to be done on this question of data reduction

Also, I'd like to emphasize the need for measurements of absolute intensity, to which I feel too few people are paying attention.

Turning lastly to the theoretician, I'm going to suggest that he should be stretched out in two directions. In both liquids and solids, the models seem to me to have gone almost as far as they should without further basic work, and therefore, on the one hand, he should concentrate on basic theory. I'm sure he wishes to do this and needs no encouragement from me. He needs ideas, which is a challenge to us all. On the other hand, the experimentalist needs help in analysis, interpretation and reduction of his data. What he needs most of all in this is the help of the theoretician. So in addition to the theoretician's being stretched in the basic direction, he must be pulled in the direction of data analysis.

I think the next few years will see a big change in the neutron scattering field. We will see more and more people trying to separate the wheat from the chaff in the huge array of neutron results. We shall also see those who work with colleagues in other fields doing some missionary work to give them a better understanding of what we are trying to do.

REFERENCES

[1] INTERNATIONAL ATOMIC ENERGY AGENCY, Inelastic Scattering of Neutrons in Solids and Liquids (Proc. Symp., Vienna, 1960), IAEA, Vienna (1961).

[2] INTERNATIONAL ATOMIC ENERGY AGENCY, Inelastic Scattering of Neutrons in Solids and Liquids (Proc. Symp., Chalk River, 1962) IAEA, Vienna (1963) 2 vols.

SYMPOSIUM ON INELASTIC SCATTERING OF NEUTRONS

HELD AT BOMBAY, 15-19 DECEMBER 1964

CHAIRMEN OF SESSIONS

Session I	R. RAMANNA	Atomic Energy Establishment Trombay, Bombay
Session II	H. HAHN	Kernforschungsanlage Jülich
Session III	B. BURAS	Institute of Nuclear Research, Swierk
Session IV	H. PALEVSKY	Brookhaven National Laboratory, New York
Session V	D. CRIBIER	Commisariat à l'énergie atomique, Saclay
Session VI	N. POPE	Royal Military College of Canada
Sessions VII and VIII	F. L. SHAPIRO	Joint Institute for Nuclear Research, Dubna
Session IX	W. COCHRAN	University of Edinburgh

SECRETARIAT OF THE SYMPOSIUM

Scientific Secretaries:	G. R. KEEPIN	Division of Research and Laboratories
	D. W. MAGNUSON	Division of Research and Laboratories
Administrative Secretary:	H. H. STORHAUG	Division of Scientific and Technical Information
Editor:	M. M. BROWN	Division of Scientific and Technical Information
Records Officer:	D. J. MITCHELL	Division of Languages

LIST OF PARTICIPANTS

Name	Institution	Nominating State or Organization
Akcasu, Z.	Nuclear Engineering Department, University of Michigan, Ann Arbor, Mich.	United States of America
Asundi, R.K.	Atomic Energy Establishment Trombay, Bombay	India
Bhandari, R.C.	University of Rajasthan, Jaipur	India
Boccara, N.	Centre d'études nucléaires de Saclay, Gif-sur-Yvette (S et O)	France
Bose, M.	Saha Institute of Nuclear Physics, Calcutta	India
Boutin, H.	United States Army, Picatinny Arsenal, Dover, N.J. and Brookhaven National Laboratory, Upton, N.Y.	United States of America
Buras, B.	Institute of Nuclear Research, Laboratory II, Swierk	Poland
Caglioti, G.	Comitato Nazionale per l'Energia Nucleare, Centro Comune Ricerche, Ispra (Varese)	Italy
Chandra, G.	Tata Institute of Fundamental Research, Colaba, Bombay	India
Chari, S.L.N.G.K.	Atomic Energy Establishment Trombay, Bombay	India
Cochran, W.	University of Edinburgh, Edinburgh, Scotland	United Kingdom
Cribier, D.	Centre d'études nucléaires de Saclay, Gif-sur-Yvette (S et O)	France
Dasannacharya, B.A.	Atomic Energy Establishment Trombay, Bombay	India
Dayal, B.	Banaras Hindu University, Varanasi	India
Dharmatti, S.S.	Tata Institute of Fundamental Research, Colaba, Bombay	India
Dolling, G.	Chalk River Nuclear Laboratories, Chalk River, Ontario	Canada
Dorner, B.	Kernforschungsanlage Jülich	Federal Republic of Germany

Name	Institution	Nominating State or Organization
Egelstaff, P.	Atomic Energy Research Establishment Harwell, Berks.	United Kingdom
Elliott, R.J.	Clarendon Laboratory, Parks Road, Oxford	United Kingdom
Fatehally, R.	Tata Institute of Fundamental Research, Colaba, Bombay	India
Ghatak, A.K.	University of Delhi	India
Ghose, A.M.	Bose Institute, Calcutta	India
Gläser, W.	Kernforschungszentrum Karlsruhe	Federal Republic of Germany
Govil, G.	Tata Institute of Fundamental Research, Colaba, Bombay	India
Hahn, H.	Kernforschungsanlage Jülich	Federal Republic of Germany
Iyengar, P.K.	Atomic Energy Establishment Trombay, Bombay	India
Iyer, R.N.	Atomic Energy Establishment Trombay, Bombay	India
Janik, J.A.	Institute of Nuclear Physics, Cracow	Poland
Joshi, S.K.	Allahabad University, Allahabad	India
Kanekar, C.R.	Tata Institute of Fundamental Research, Colaba, Bombay	India
Khubchandani, P.G.	Atomic Energy Establishment Trombay, Bombay	India
Kosály, G.	Hungarian Academy of Sciences, Central Research Institute for Physics, Budapest	Hungary
Krishnamurthy, N.R.	Indian Institute of Science, Bangalore	India
Krishnan, R.S.	Indian Institute of Science, Bangalore	India
Kroó, N.	Hungarian Academy of Sciences, Central Research Institute for Physics, Budapest	Hungary

Name	Institution	Nominating State or Organization
Larsson, K.-E.	Royal Institute of Technology, Institute of Reactor Physics, Stockholm	Sweden
Low, G.	Atomic Energy Research Establishment, Harwell, Berks.	United Kingdom
Mackintosh, A.R.	Iowa State University, Ames, Iowa	United States of America
Mahanty, J.	Indian Institute of Technology, Kanpur	India
Manohar, C.	Atomic Energy Establishment Trombay, Bombay	India
Marsongkohadi	Institute of Atomic Energy Bandung, Indonesia	International Atomic Energy Agency
Møller, H.B.	Atomic Energy Commission Research Establishment, Risø, Roskilde	Denmark
Narasimham, N.A.	Atomic Energy Establishment Trombay, Bombay	India
Narayanan, P.S.	Indian Institute of Science, Bangalore	India
Nielsen, P.	University of Copenhagen	Denmark
Nimwanadon, T.	Office of the Atomic Energy for Peace, Bangkok, Thailand	International Atomic Energy Agency
Padmanabhan, V.M.	Atomic Energy Establishment Trombay, Bombay	India
Palevsky, H.	Brookhaven National Laboratory, Upton, N.Y.	United States of America
Parfenov, V.A.	Institute of Physics and Power, Obninsk	Union of Soviet Socialist Republics
Parlinski, K.	Joint Institute for Nuclear Research, Dubna, Union of Soviet Socialist Republics	Joint Institute for Nuclear Research
Patankar, A.V.	Tata Institute of Fundamental Research, Colaba, Bombay	India
Pelah, I.	Israel Atomic Energy Commission, Soreq Research Establishment, Yavne	Israel

Name	Institution	Nominating State or Organization
Pope, N.	Royal Military College of Canada, Kingston, Ontario	Canada
Pryor, A.W.	Australian Atomic Energy Commission, Sutherlands, N.S.W.	Australia
Radhakrishnan, V.	Tata Institute of Fundamental Research, Colaba, Bombay	India
Raghavacharyulu, I.V.V.	Annamalai University, Annamalai Nagar	India
Ramanna, R.	Atomic Energy Establishment Trombay, Bombay	India
Rao, K.R.	Atomic Energy Establishment Trombay, Bombay	India
Roy, A.P.	Atomic Energy Establishment Trombay, Bombay	India
Rush, J.J.	National Bureau of Standards, Washington, D.C.	United States of America
Satya Murthy, N.S.	Atomic Energy Establishment Trombay, Bombay	India
Saxena, S.C.	Rajasthan University, Jaipur	India
Schmatz, W.	Laboratorium für Technische Physik der Technischen Hochschule, Munich	Federal Republic of Germany
Schmunk, R.E.	Phillips Petroleum Company, Atomic Energy Division, Idaho Falls, Idaho	United States of America
Shapiro, F.L.	Joint Institute for Nuclear Research, Dubna	Union of Soviet Socialist Republics
Siddiq, A.	Dacca University, Dacca	Pakistan
Sigmar, D.J.	Institute for Theoretical Physics, Technical University of Vienna	Austria
Singh, R.P.	Indian Institute of Technology, Powai, Bombay	India
Singwi, K.S.	Argonne National Laboratory, Argonne, Ill.	United States of America
Sinha, K.P.	National Chemical Laboratory, Poona	India

Name	Institution	Nominating State or Organization
Sinha, S.K.	Cavendish Laboratory, Cambridge University, Cambridge	United Kingdom
Sjölander, A.	Chalmers University of Technology, Gothenburg	Sweden
Song, J.	Iri Nam Sung High School, Iri, Korea	International Atomic Energy Agency
Spano, A.H.	Division of Nuclear Power and Reactors, Department of Technical Operations	International Atomic Energy Agency
Srinivasan, R.	Indian Institute of Technology, Madras	India
Srivastava, P.L.	Banaras Hindu University, Varanasi	India
Stedman, R.	AB Atomenergi Studsvik, Nyköping	Sweden
Subramanian, R.	Atomic Energy Establishment Trombay, Bombay	India
Thosar, B.V.	Tata Institute of Fundamental Research, Colaba, Bombay	India
Toya, T.	Research Institute for Catalysis, Hokkaido University, Sapporo	Japan
Umakantha, N.	Karnatak University, Dharwar	India
Venkataraman, B.	Tata Institute of Fundamental Research, Colaba, Bombay	India
Venkataraman, G.	Atomic Energy Establishment Trombay, Bombay	India
Verma, G.S.	University of Allahabad, Allahabad	India
Vijayaraghavan, P.R.	Atomic Energy Establishment Trombay, Bombay	India
Vijayaraghavan, R.	Tata Institute of Fundamental Research, Colaba, Bombay	India
Wallér, I.	University of Uppsala, Institute for Theoretical Physics, Uppsala and AB Atomenergi, Studsvik, Nyköping	Sweden

Name	Institution	Nominating State or Organization
Warren, J.L.	Los Alamos Scientific Laboratory of the University of California, Los Alamos, N. Mex.	United States of America
Whittemore, W.	General Atomic Division of General Dynamics Corp., San Diego, Calif.	United States of America
Yagodin, G.A.	Department of Technical Operations	International Atomic Energy Agency
Yip, S.	Department of Engineering Physics and Material Science, Cornell University, Ithaca, N.Y.	United States of America
Zemlyanov, M.G.	Institute of Atomic Energy "I.V. Kurchatov", Moscow	Union of Soviet Socialist Republics

AUTHOR INDEX

(Including participants in discussions)

Roman numerals are volume numbers.
Arabic numerals underlined refer to the first page of a paper by the author concerned.
Other Arabic numerals denote the page numbers of discussion comments.
Literature references have not been indexed.

IAEA SALES AGENTS

Orders for Agency publications can be placed with your bookseller or any of our sales agents listed below:

ARGENTINA
Comisión Nacional de
Energía Atómica
Avenida del Libertador
General San Martin 8250
Buenos Aires - Suc. 29

AUSTRALIA
Hunter Publications,
23 McKillop Street
Melbourne, C.1

AUSTRIA
Georg Fromme & Co.
Spengergasse 39
Vienna V

BELGIUM
Office international de librairie
30, avenue Marnix
Brussels 5

BRAZIL
Livraria Kosmos Editora
Rua do Rosario, 135-137
Rio de Janeiro

Agencia Expoente Oscar M. Silva
Rua Xavier de Toledo, 140-1° Andar
(Caixa Postal No. 5.614)
São Paulo

BYELORUSSIAN SOVIET SOCIALIST REPUBLIC
See under USSR

CANADA
The Queen's Printer
Ottawa, Ontario

CHINA (Taiwan)
Books and Scientific Supplies Service, Ltd.,
P.O. Box 83
Taipei

DENMARK
Ejnar Munksgaard Ltd.
6 Nörregade
Copenhagen K

FINLAND
Akateeminen Kirjakauppa
Keskuskatu 2
Helsinki

FRANCE
Office international de
documentation et librairie
48, rue Gay-Lussac
Paris 5e

GERMANY, Federal Republic of
R. Oldenbourg
Rosenheimer Strasse 145
8 Munich 8

ISRAEL
Heiliger and Co.
3 Nathan Strauss Street
Jerusalem

ITALY
Agenzia Editoriale Internazionale
Organizzazioni Universali (A.E.I.O.U.)
Via Meravigli 16
Milan

JAPAN
Maruzen Company Ltd.
6, Tori Nichome
Nihonbashi
(P.O. Box 605)
Tokyo Central

MEXICO
Libraria Internacional
Av. Sonora 206
Mexico 11, D.F.

NETHERLANDS
N.V. Martinus Nijhoff
Lange Voorhout 9
The Hague

NEW ZEALAND
Whitcombe & Tombs, Ltd.
G.P.O. Box 1894
Wellington, C.1

NORWAY
Johan Grundt Tanum
Karl Johans gate 43
Oslo

PAKISTAN
Karachi Education Society
Haroon Chambers
South Napier Road
(P.O. Box No. 4866)
Karachi, 2

POLAND
Ośrodek Rozpowszechniana
Wydawnictw Naukowych
Polska Akademia Nauk
Pałac Kultury i Nauki
Warsaw

SOUTH AFRICA
Van Schaik's Bookstore (Pty) Ltd.
Libri Building
Church Street
(P.O. Box 724)
Pretoria

SWEDEN
C.E. Fritzes Kungl. Hovbokhandel
Fredsgatan 2
Stockholm 16

SWITZERLAND
Librairie Payot
Rue Grenus 6
1211 Geneva 11

TURKEY
Librairie Hachette
469, Istiklâl Caddesi
Beyoğlu, Istanbul

UKRAINIAN SOVIET SOCIALIST REPUBLIC
See under USSR

UNION OF SOVIET SOCIALIST REPUBLICS
Mezhdunarodnaya Kniga
Smolenskaya-Sennaya 32-34
Moscow G-200

UNITED KINGDOM OF GREAT BRITAIN AND NORTHERN IRELAND
Her Majesty's Stationery Office
P.O. Box 569
London, S.E.1

UNITED STATES OF AMERICA
National Agency for
International Publications, Inc.
317 East 34th Street
New York, N.Y. 10016

VENEZUELA
Sr. Braulio Gabriel Chacares
Gobernador a Candilito 37
Santa Rosalía
(Apartado Postal 8092)
Caracas D.F.

YUGOSLAVIA
Jugoslovenska Knjiga
Terazije 27
Belgrade

IAEA publications can also be purchased retail at the United Nations Bookshop at United Nations Headquarters, New York, at the news-stand at the Agency's Headquarters, Vienna, and at most conferences, symposia and seminars organized by the Agency.

In order to facilitate the distribution of its publications, the Agency is prepared to accept payment in UNESCO coupons or in local currencies.

Orders and inquiries from countries where sales agents have not yet been appointed may be sent to:

Distribution and Sales Unit, International Atomic Energy Agency,
Kärntner Ring 11, Vienna I, Austria

INTERNATIONAL
ATOMIC ENERGY AGENCY
VIENNA, 1965

PRICE: USA and Canada: US $11,50
Austria and elsewhere: S 241,50
(£3.9.0; F.Fr. 46,-; DM 40,25)